Cracking risk of concrete structures in the hardening phase: Experiments, material modeling and finite element analysis

Guomin Ji

Doctoral Thesis

Department of Structural Engineering
The Norwegian University of Science and Technology
Trondheim, Norway

May 2008

Acknowledgement

The work in this thesis has been carried out under the supervision of Professor Terje Kanstad, and Dr.ing Øyvind Bjøntegaard at the Department of Structural Engineering, Norwegian Science and Technology University (NTNU), Norway. I would like to express my deepest gratitude for their patience, guidance and support during the course of my study. Their invaluable guidance and outstanding knowledge of concrete structures has truly been a great inspiration to the author. Their numerous suggestions for the improvement of the manuscript and their patience and kindness have made this study an enjoyable and memorable experience. Without their professional support and permanent encouragement, this work would not have been possible.

The work was part of a comprehensive research program, namely NOR-CRACK, and the financial support from the Norwegian Research Council (NFR) is gratefully acknowledged. The Norwegian industrial partners in the project were: Selmer Skanska AS, Elkem ASA Materials, Norcem AS, Fesil AS and the Directorate of Public Roads.

I am also grateful to my colleagues at the Department of Structural Engineering, especially to Professor Erik Sellevold for the fruitful discussion. Most of the laboratory work has been performed with great skill and care by research technician Helge Rødsjø. I wish to express my most heartily appreciation to him. I would also like to thank all the other personnel of the Concrete group, and the laboratory team of the Department of structural engineering at NTNU for the pleasant and friendly environment.

Finally, I would like to thank my family and all other persons who in some way have supported me during this project.

Trondheim, April 2008

Guomin Ji

Abstract

This thesis deals with prediction of early age cracking caused by restrained thermal dilation and autogenous deformation. The purpose of the present work is to provide new and extend the existing knowledge of material properties, especially thermal dilation, autogenous shrinkage, mechanical properties and viscoelastic behavior, of high performance concrete at early age and their contribution to the generation of self-induced stresses in concrete structures during hardening.

The major features of hardening concrete are described and mathematical descriptions of the phenomena are given within a thermodynamic framework. The maturity concept (equivalent time) was introduced to describe the development of material properties, and all material properties may be considered as maturity dependent. It is shown that the simple maturity based model for the heat of hydration development can describe temperature development in the concrete structure with good accuracy. A modified CEB equation for E-modulus and compressive and tensile strength development is implemented. The different isothermal temperature influence on creep is taken into account by the maturity concept, and the influence of the change of temperature on creep is considered by introducing a transient thermal creep term.

The concrete compositions and test methods to characterize the following material properties were described in detail and a series of comprehensive tests were performed to independently determine the material parameters:

- The temperature sensitivity (activation energy)
- Heat of hydration
- Volume change (Coefficient of Thermal Expansion (CTE), and Autogenous Deformation (AD))
- Mechanical properties (E-modulus, compressive strength, tensile strength)
- Creep/relaxation properties under compressive and tensile loading
- Transient thermal creep

First the influence of mineral additives such as fly ash (FA) and blast furnace slag (BFS) on the development of material properties of young concrete is studied. The replacement of cement with the mineral additives such as FA and BFS significantly reduces the hydration heat. The replacement of cement with BFS does not have significant influence on the development of autogenous deformation, while the replacement of cement with FA has a considerable influence on the development of autogenous deformation. The replacement of cement with FA or BFS has significant influence on the development of the compressive strength. In general, the higher the mineral additives content the lower the compressive strength. The replacement of cement with FA or BFS has moderate influence on the 28-days elastic modulus, but the elastic modulus development at very early age (less than 1 day) is considerably affected by the slow development of the pozzolanic reaction, and the higher the content of FA is, the lower is the elastic modulus. The 28 day splitting tensile strength is significantly reduced by the replacement of cement with FA or BFS.

The comparison of the test results of the compressive and tensile creep tests show that at loading ages before 4 days the magnitude and rate of compressive creep is higher than that of tensile creep for a period of time, while afterwards the rate of compressive creep decreases more

rapidly than the rate of tensile creep. This leads to higher tensile creep a few days after loading. The development of compressive and tensile creep is more similar for age of loading beyond 7 days. The amount of cement replaced with FA or BFS substantially influences the compressive and tensile creep relation as well as the creep magnitude. The results show that high creep in the concrete containing FA or BFS can accelerate the stress relaxation and therefore be beneficial in reducing the risk of cracking at early ages. This effect would then add to the more obvious and well-known positive effect of using such concrete, namely the reduced hydration heat.

Furthermore the transient thermal creep was investigated for Basic 5 concrete. For hardened concretes, the test results showed that not only during heating, but also during cooling, the compliance functions increase dramatically due to temperature changes during these two periods. The calculated compliance functions are in good agreement with the measured results, the improvement of the modeling by including the transient thermal creep term is significant. For young concrete, the test results for young concrete under compression show low increase of compliance function due to transient creep during the cooling period, and the test results for young concrete under tension show that the transient thermal creep exists during the heating and cooling period. The analytical model of transient thermal creep gives an acceptable prediction of the test results for the young concretes and the maturity concept is able to describe the major part of the temperature influence on the creep strain development. But it seems that it is not enough to take into account the temperature effect on the creep by only using the maturity concept when large temperature increase or decrease happens in a short period, and it gives more reliable prediction if the transient thermal creep term is added. The parameter ρ is similar in hardened and young concrete under either compressive or tensile load condition, but it is higher in compressive loading than in tensile loading.

The total experimental test program also involves restraint stress measurements in a Temperature-Stress Test Machine (TSTM) under realistic temperature histories and full or partial restraint conditions. A field test of wall structure was also carried out in 2004. The wall structure is comparable to a submerged tunnel that will be constructed in Oslo, and a part of NOR-CRACK is devoted to this project. First the test data of material properties was directly used as input to calibrate the temperature and stress development in the TSTM, and then the well documented material models were applied in 3-D numerical analysis performed with DIANA to predict temperature and strain development in two of the instrumented sections of the field test. Deviation between calculated and measured temperature is within range of ±3ºC. Deviation between calculated and measured strains in the middle part of both walls (0.6 – 1.2 m above the slab) is about ±50 μ. When all uncertainties in material modeling and measuring methods are considered it is concluded that results of the simulation are satisfying.

The last part of the work was to evaluate the crack risk for five types of concretes mixes: ordinary Norwegian concrete (SV 40*), two types of concretes containing 40% and 60% FA by weight of cement (40% and 60% FA*), and two types of concretes containing 40% and 60% BFS by weight of cement (40% and 60% BFS), in the design phase of the Bjørvika submerged tunnel in Oslo, and thus to provide valuable recommendation in the process of selecting concrete composition. Both thermal and mechanical properties of five types of concretes were investigated in the test program to identify material parameters. Material models were checked in the TSTM under realistic temperature histories. 3D analyses were performed with DIANA to calculate the temperature and stress/strain development in Bjørvika submerged tunnel for these five types of concretes. The analysis showed that the 60% FA* concrete has both the lowest maximum temperature (42.2 ºC) and the lowest stress/strength ratio (0.74) for the outer wall.

Table of content

Notation and Abbreviations

Notation

α_T	coefficient of thermal expansion (CTE)
ξ	the degree of hydration
f_c	compressive strength
f_t	tensile strength
f_{ts}	splitting tensile strength
E_c	compressive E-modulus
t_0	the time when the significant mechanical properties develops
σ	stress tensor
ε	strain tensor
ε_{ttc}	transient thermal creep
ε_{el}	elastic strain
ε_c	creep strain
ε_{tol}	total strain
ε_{th}	thermal dilation
ε_{sh}	autogenous shrinkage
φ	intrinsic dissipation
S	entropy
T	temperature
Ψ	Helmholtz free energy
$\boldsymbol{\varepsilon}^p$	plastic strain tensor
χ	hardening/softening variable
m	skeleton mass
E_a	hydration activation energy
R	idea gas constant
C	heat capacity per unit volume
Q	internal heat source associated to hydration reaction
H	external heat source
q	heat flux
k	thermal conductivity

Abbreviations

AD	autogenous shrinkage
TD	thermal dilation
CTE	coefficient of thermal expansion
TSTM	temperature stress testing machine
BFS	blast furnace slag
FA	fly ash
OPC	ordinary Portland cement
HPC	high performance concrete
HSC	high strength concrete
LVDT	Linear Variable Differential Transducer
SVV	Norwegian road administration
Basic 5	w/b=0.4, 5% silica fume
Reference	w/b=0.45, 5% silica fume
SV 40	ordinary Norwegian bridge concrete (w/b=0.4, 5% silica fume)
%	percentage represents the ratio of weight between mineral additives and cement in the concrete composition
40% BFS	w/b=0.45, 5% silica fume, containing 40% blast furnace slag by weight of cement
60% BFS	w/b=0.45, 5% silica fume, containing 60% blast furnace slag by weight of cement
100% BFS	w/b=0.45, 5% silica fume, containing 100% blast furnace slag by weight of cement
40% FA	w/b=0.45, 5% silica fume, containing 40% fly ash by weight of cement
60% FA	w/b=0.45, 5% silica fume, containing 60% fly ash by weight of cement
100% FA	w/b=0.45, 5% silica fume, containing 100% fly ash by weight of cement
NL-slag	w/b=0.45, 2% silica fume, containing 74% NL-slag by weight of binder

1. Introduction

1.1.Background

Cracking of concrete structures during the hardening phase often seriously compromises not only structure integrity, but also durability and long-term service life. The problem arises from the fact that concrete experiences complex chemical and physical changes and interacts with its environment at early ages. During the hardening process (first 1-2 weeks), volumetric changes due to thermal dilation and autogenous deformation occur simultaneously in the concrete structures. Thermal dilation is caused by the temperature changes due to heat of hydration. Autogenous deformation is a result of continuing water consumption in the hydration reactions, leading to self-desiccation (unlike drying shrinkage, which is due to water loss from the concrete). The mechanical properties such as elastic modulus and tensile strength are developed quickly during the hardening phase. Consequently, self-induced stresses will be generated in structural members subjected to restrained conditions. Cracking of young concrete is mainly caused by restrained thermal deformation and autogenous shrinkage, which may induce a severe state of stress beyond the material strength development.

High-strength concretes (HSC) and high-performance concretes (HPC) with low water/binder ratio are increasingly used for structures where their superior mechanical properties and durability performance provide an override advantage. However, the increased use of such concretes was accompanied by concern regarding their early age cracking sensitivity. In these concretes considerable deformation due to combination of autogenous shrinkage and thermal dilation can develop and lead to early sensitivity to cracking in restrained conditions. The cracking of early age concrete increases the permeability and permits ingress of external harmful agents into the concrete more easily, such as penetration of chlorides, carbonation, damage due to freezing, and sulphate attack etc..

The pozzolanic (e.g. fly ash, silica fume) and cementitious materials (e.g. ground blast-furnace slag) are used extensively as mineral additives in production of high-strength and high-performance concretes in the last decades due to significant cost and energy savings. A pozzolan is defined as a siliceous or siliceous and aluminous material which in it self possesses little or no cementing property but will in a finely divided form and in the presence of moisture chemically react with calcium hydroxide at ordinary temperature to form compounds possessing cementitious properties. The reaction between a pozzolan and calcium hydroxide is called the pozzolanic reaction. The engineering benefits, likely to be derived from the use of mineral additives in concrete, include improved resistance to thermal cracking because of lower heat of hydration, enhancement of ultimate strength and impermeability due to pore refinement, and (as a result of reduced alkalinity) a better durability to chemical attacks such as by sulfate water and alkali-aggregate expansion.

Traditionally, the risk of cracking in early age concrete structures were evaluated based on temperature criteria. A temperature criterion can be applied by limiting the maximum temperature difference between newly cast concrete and old concrete or ambient environment. Temperature criteria are often unreliable as they reflect only a fraction of the influencing factors, and an important reason for this uncertainty is that the zero-stress temperature is usually different over the cross-section of a member. Especially for large massive structures where

stresses are built up during the heating period the temperature criteria have shown some limitations, and therefore a more accurate analysis of the stress development at early age is needed. (Springenschmidt, R. et al., 1994)

Early age cracking has been subject of extensive research in last decades. In recent years, more realistic insights have been gained through various research efforts in related fields, as for example, thermal cracking in concrete at early age by RILEM proceeding 25 and early age cracking in cementitious systems by RILEM technical committee TC 181-EAS. On the other hand, the even-growing number of application of high-strength concrete and massive concrete structures makes essential to establish comprehensive methodology to prevent cracking of early age concrete.

The amount of stress generated by thermal dilation and autogenous shrinkage in a given time interval depends on the degree of restraint which is imposed by the surrounding structures, the development of mechanical properties, especially elastic modulus and tensile strength, and the creep/relaxation properties of the concrete at early age. Making reliable cracking risk assessment involves experimental testing and advanced modeling of the time and temperature dependent behavior of the properties mentioned above, the restraint conditions of the structure as well as the external environmental conditions. The cracking risk at given time is determined by comparing the (measured or calculated) maximum tensile stress or strains in concrete structure to the tensile strength or ultimate tensile strain of concrete at that time.

1.2.Objective and scope of research

The present PhD project is a part of the Norwegian project NOR-CRACK, which was financially supported by the Research Council of Norway and the concrete industry. The main objective of the present work is to provide new and extend the existing knowledge of material properties, especially thermal dilation, autogenous shrinkage, mechanical properties and viscoelastic behavior, of high performance concrete at early age and their contribution to the generation of self-induced stresses in structures during hardening. Furthermore to provide better understanding and better prediction of temperature, strain and stress development in concrete structures at early age in engineering practice, and to improve the applicability and reliability of advanced curing technology in design and production of concrete structures.

The main scope is defined as follows:

- To review the existing knowledge of material properties of high strength/performance concrete at early age in the literature
- To further develop material models and determine model-parameters for early age concrete behavior by taking the temperature effects into account, and to clarify the viscoelastic behavior of early age concrete in compression and tension and their influence on self-induced stresses
- To perform comprehensive experimental programs to investigate the influence of mineral additives such as fly ash and blast furnace slag on the development of material properties of young concrete, and the viscoelastic behavior of concrete in compression and tension at early age
- To conduct a transient thermal creep test in the updated Temperature-Stress Test Machine (TSTM), and study the influence of temperature variation on the creep behavior

- To simulate the temperature and strain development in field tests, and to examine to what extent the different parameters affect the calculation results
- To determine the early age cracking risk of a structural element in the Bjørvika submerged tunnel, and to evaluate the cracking risk of several types of concretes with different mineral additives

1.3.Organization of the thesis

The doctoral thesis is organized in eight chapters. It starts with an introductory chapter, where the background of the problem concerning cracking in hardening concrete structure is described. The objective and scope are given, together with its significance to engineering practice.

In chapter 2, the main features of young concrete behavior are described. The driving forces generating self-induced stresses in concrete structure at early age are discussed, and the development of material properties in the hardening phase is briefly described. Experimental results from the literature on the viscoelastic behavior of young concrete in compression and tension are presented and the main factors influencing creep/relaxation properties at early age are discussed. The material models and numerical solution used to assess the cracking risk of early age concrete are also briefly discussed.

In chapter 3, the comprehensive experimental programs to investigate the viscoelastic property in compression and tension of young concretes containing mineral additives are presented. The test apparatus for thermal and mechanical properties as well as for viscoelastic properties (tensile and compressive creep rig) are briefly described. The test equipment for restraint stress development (TSTM) and free deformation (dilation rig) under realistic temperature histories is also presented and the test procedure of transient thermal creep in the updated TSTM is discussed in detail. In addition, the field test of a "double-wall" structure carried out in 2004 is described.

In chapter 4, the material models and the numerical solution used in the finite element analysis are described. The most commonly used models for material properties of young concrete such as hydration heat, elastic modulus, tensile strength, are briefly described, and the modeling of viscoelastic behavior are discussed in detail. The relatively simple approach used in the present study is introduced and it is described how the temperature effect on the creep/relaxation property is taken into account in the creep model. The solution method for 1-D analysis of restraint stress development in TSTM is given briefly, and furthermore mathematical formulations governing temperature and stress development and their numerical solution in 3-D finite element analysis of hardening concrete structures are presented.

In chapter 5, the results of the experimental program involving thermal properties, mechanical properties, viscoelastic properties in compression and tension, transient thermal creep behavior and restraint stress measurements in TSTM are presented. The influence of mineral additives on the material properties (mainly thermal, mechanical and viscoelastic) is discussed and the viscoelastic behavior in compression and tension is compared for each concrete. A simple model is applied to fit the creep data in compression or tension under 20ºC and sealed conditions. The modeling of viscoelastic behavior under realistic temperature histories is then discussed by taking the temperature effect into account through the maturity concept. The creep parameters in compression and/or tension are implemented in the restraint stress analysis of the TSTM, and

their influence on the prediction of self-induced stress in TSTM is further discussed. The relative importance of transient thermal creep in the prediction of cracking risk of early age concrete is discussed based on the test results.

In chapter 6, numerical analysis of the field test and the parameter study are presented. The well-documented material models are used in the finite element program Diana to simulate the temperature, stress and strain development in the field test of the wall structure. The influence of parameters such as hydration heat, autogenous shrinkage and creep properties on the stress development is further investigated.

In chapter 7, the advanced curing technology is applied in the design phase of Bjørvika submerged tunnel to evaluate the crack risk, and to provide valuable information on the cracking risk for several types of concretes. The concrete with high content of fly ash showed lowest cracking sensitivity in the analysis.

Finally, in chapter 8, the summary and conclusion are given together with suggestions for further research.

2. Literature study

2.1.Introduction

Immediately after mixing concrete behaves as a liquid, and within the first hours stiffening takes place due to cement hydration, then a matrix termed the cement gel is formed and the material properties develop. During the hydration process the chemical reactions between water and cement particles liberate heat and consume water, and chemical shrinkage occur due to a reduction of the volume of the reaction products compared to the reactants, it leads to self-desiccation in high performance concrete with low water/cement ratio. The thermal dilation and the autogenous deformation caused by the self-desiccation are the two main causes of the volume changes in early age concrete. No stress is generated if the concrete is free to expand and contract. However, a newly cast concrete element is always restrained to some degree, either externally by adjoining structures or internally due to steel reinforcement or temperature profiles. Therefore stresses are built up and normally compressive stresses develop in the first hours during the heating period and they are turned to tensile stresses in the following cooling period. The typical situation appearing in a newly cast concrete structure is shown in Figure 2-1 for specimen tested in the Temperature Stress Testing Machine (TSTM).

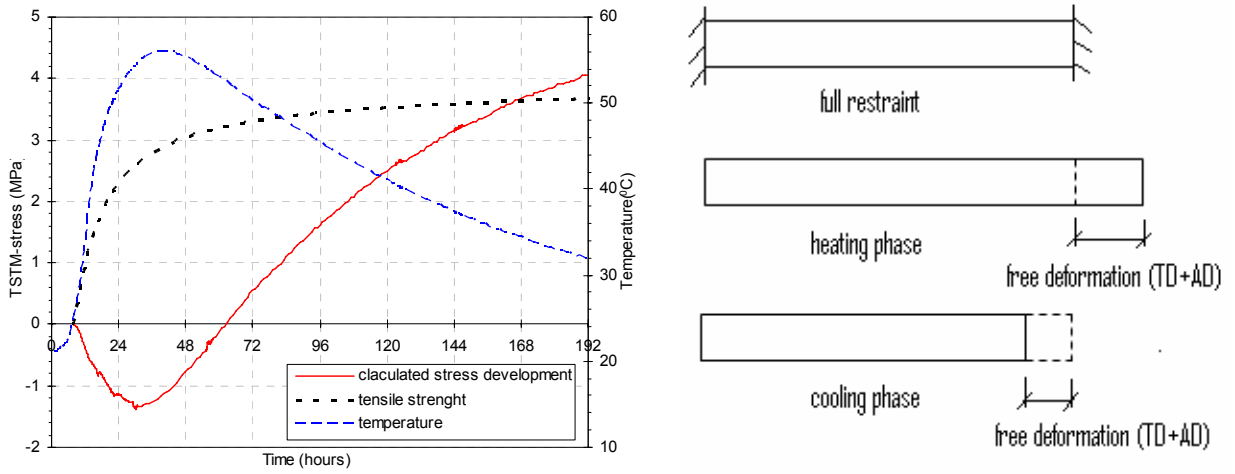

Figure 2-1 Temperature and stress development of concrete specimen in TSTM

The stresses that cause cracking of early age concrete are, in case of absence of external loading, induced by the restraint of deformation. It is usually difficult but essential to evaluate the effective level of restraint, which depends on the ratio between the local stiffness of the concrete and that of the surrounding concrete or adjoining structure elements. The restraint level is a key factor for predicting crack initiation in early age concrete. The creep/relaxation properties reduce a given stress increment over time. During hardening the different parts of concrete structure experience compressive and tensile stresses in different periods. And in the present study, the creep/relaxation properties in compression and tension are investigated. This is an area in which there is clearly a lack of knowledge today.

Mineral additives such as silica fume (SF), blast furnace slag (BFS) and fly ash (FA) have been used extensively in production of High Performance Concrete in the last decades. It is well known that replacement of cement with pozzolanic materials such as FA and BFS can significantly reduce the hydration heat. Most previous research on the influence of mineral additives had been focus on the mechanical properties such as compressive strength, tensile strength and elastic modulus, whereas the visco-elastic behavior of young concrete containing mineral additives is covered only to a small extent, which is unsatisfactory since it is important regarding the stress development in the hardening phase.

2.2.Mechanisms and driving force

2.2.1. Volume change

Restraint stress which arises in early age concrete is mainly associated with three types of deformation: autogenous deformation, thermal dilation, and drying shrinkage. Drying shrinkage is well accepted as being a volume deformation induced by evaporation of water from concrete to the surrounding atmosphere, and is therefore negligible in sealed condition for the large cross section in the early ages.

The concrete goes through a natural heating-cooling cycle during the first few days in realistic cases, and the total deformation, i.e. the sum of thermal dilation (TD) and autogenous deformation (AD), is easily and accurately measured in the laboratory for given temperature history. However the result is only valid for that particular temperature history and it is difficult to evaluate the relative importance of the two parts because they always occur simultaneously. From the structural analysis point of view, this is unsatisfactory because a stress calculation procedure applicable to any temperature development requires a general model for each mechanism to avoid too many costly and time-consuming experiments (Bjøntegaard, 1999). At present there are no generally accepted models for TD and AD under realistic temperature histories. Determination of TD depends on the assumptions that are made about AD and vice versa.

$$\varepsilon_{tot} = \varepsilon_{TD} + \varepsilon_{AD} \tag{2.1}$$

$$\varepsilon_{TD} = \alpha_T \cdot \Delta T \tag{2.2}$$

ε_{tot} is the total deformation, ε_{TD} is the thermal dilation, ε_{AD} is the autogenous deformation, α_T is the coefficient of thermal expansion (CTE) and ΔT is the temperature change.

The following two strategies are often used to separate AD and TD during variable temperature:

1) AD is directly measured at 20 ºC isothermal conditions, and then it is transferred to AD under realistic temperature by using the maturity concept, which thereby makes it possible to calculate TD. (Emborg M., 1989) (Hedlund, 2000)
2) Another strategy is to assume that the coefficient of thermal expansion (CTE) is constant and makes it possible to calculate AD. (Tazawa et al., 1977) (Dilgner et al, 1996)

Both of the above methods are regarded as rough approximations. For the first approach, the use of simple maturity transformation on AD between different isothermal temperatures and realistic temperatures has been found to be questionable (Bjøntegaard, 1999), and it is discussed in detail

in the following section. For the second one, several experimental results showed that the CTE of concrete varies during the hydration process. (Bjøntegaard, 1999)

Bjøntegaard (1999) proposed a test method to measure CTE of early age concrete directly by superimposing "saw-toothed" temperatures for some hours following the background realistic temperature regime closely. A model is used to describe the development of CTE:

$$CTE(t_e) = CTE(t_0) + \left[CTE(t_{28}) - CTE(t_0)\right] \bullet \left\{ \exp\left[s_{CTE} \bullet \left(1 - \sqrt{\frac{28}{t_e - t_0}} \right) \right] \right\}^{n_{CTE}} \quad (2.3)$$

Where t_e is the equivalent time, $CTE(t_0)$ and $CTE(t_{28})$ are the calculated CTE at t_0 and 28 days, s_{CTE} and n_{CTE} are model parameters which can be determined by fitting the curve to the directly measured CTEs.

In the present study, the test method proposed by Bjøntegaard (1999) is applied to separate the TD and AD during the hardening phase. In the standard procedure of the test, the TSTM and the Dilation Rig run in parallel to produce "compatible data" for re-calculations of the restraint stress development measured from the TSTM. The Dilation Rig is run with a "saw-toothed" temperature history, and the parameters of the CTE model are determined by the directly measured CTEs. The total deformation in the TSTM is then separated into thermal dilation and autogenous shrinkage.

2.2.1.1. Autogenous shrinkage

ACI 116R defines autogenous deformation as "change in volume produced by the continued hydration of cement, exclusive of the effects of applied load and change in either thermal condition or moisture content. Autogenous deformation is a consequence of chemical shrinkage: the absolute volume of hydration products is less than the total volume of the reactants (cement and water). The volumetric balance shows a deficit of the order of 10% of the volume of the hydrates formed. Once the solid skeleton is formed, chemical shrinkage results in the formation of pores in hydrating paste structure, in the absence of external source of water hydration reactions continue through the consumption of capillary water. Successive emptying of the pore structure is essentially a self-desiccation process. According to the Kelvin equation, self-desiccation gradually increases the tensile stresses in the pore water through the formation of menisci. The effect of the capillary tension on the matrix clearly prevails over the other mechanical effects, and is therefore in fact the origin of autogenous shrinkage. The extent of self-desiccation is related to the changes in the internal relative humidity, and the build-up of internal capillary stress results in a contraction of the hardening concrete.

Autogenous shrinkage depends mainly on the water/binder ratio and on the mineral composition of the binder. The w/b ratio effect is very clear – autogenous deformation increases with decreasing w/b ratio (Tazawa, 1997) (Toma et al, 1999) (Schieβl, 2000). Autogenous shrinkage remains less than 100 μm/m in concrete of which the w/c ratio is greater than 0.45, but it increases quickly when this ratio falls below 0.40, as shown in Figure 2-2. This is simply an effect of pore size: the tension stresses in the liquid phase vary inversely with the pore size at interface with the gaseous phase. High-strength concretes with low water-cement ratio (w/c) are prone to significant autogenous shrinkage. For example, Bjøntegaard (2001) reported that

autogenous deformation of super-high performance concretes (w/b=0.23 and 20% silica fume) containing 32 l/m^3 superplasticizer reaches 800 μm/m at 1 day after setting.

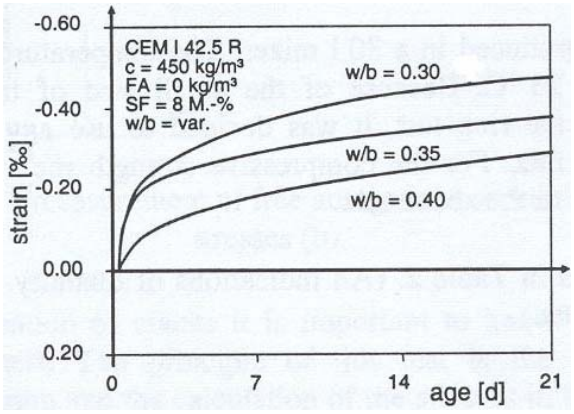

Figure 2-2 Influence of w/b ratio on autogenous shrinkage of concrete (20ºC isothermal curing) (Schieβl, 2000).

The effect of mineral additives such as silica fume, fly ash and blast furnace slag on autogenous shrinkage of early age concrete was investigated by several researchers under isothermal condition (Tazawa, 1995, 1997) (Schieβl, 2000) (Brooks, 1998) (Lura, 2001, 2002) (Bjøntegaard, 1999).

In general, it is concluded that silica fume increases autogenous shrinkage in young concrete, as shown in Figure 2-3. Silica fume acts as pure pozzolan due to its high activity and high content of amorphous silica. The product (C-H-S) of pozzolanic reaction between silica fume and calcium hydroxide has the refinement effect on the pore system in the matrix.

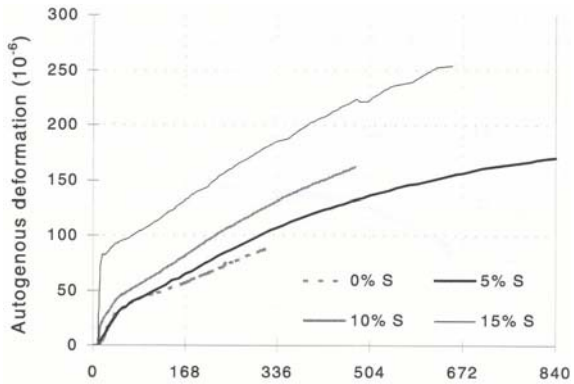

Figure 2-3 Autogenous deformation for concrete with 0, 5, 10 and 15% silica fume at 20ºC isothermal curing, t_0=11 hours. (Bjøntegaard, 1999)

As shown in Figure 2-4, the replacement of cement by fly ash generally reduces the autogenous shrinkage of young concrete, and the higher the fly ash content, the lower the autogenous shrinkage is. The fineness of fly ash also has significant influence on the autogenous shrinkage. The lower the fineness of fly ash, the more the autogenous shrinkage is reduced. (Schieβl, 2001)

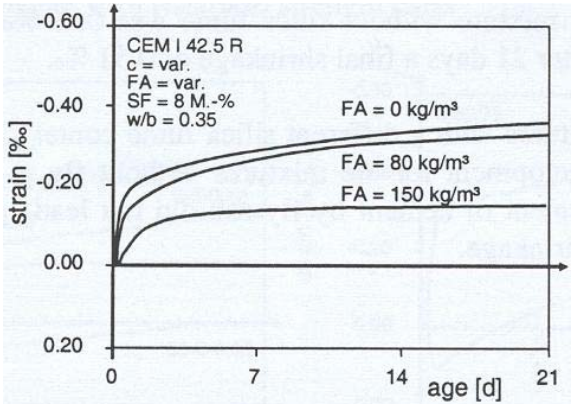

Figure 2-4 Effect of fly ash content on autogenous shrinkage of concrete (20ºC isothermal curing) (Schieβl, 2001)

The investigation of Tazawa (1997), as shown in Figure 2-5, indicated that the fineness of BFS has a significant effect on the development of autogenous shrinkage because the activity of BFS mainly depends on its fineness. In low fineness case, the fineness of BFS is less than that of ordinary Portland cement (OPC, 3520 cm^2/g), and the BFS cement paste shows lower autogenous shrinkage compared to the OPC cement paste. But, in the case with higher fineness, the higher reactivity of BFS leads to higher autogenous shrinkage.

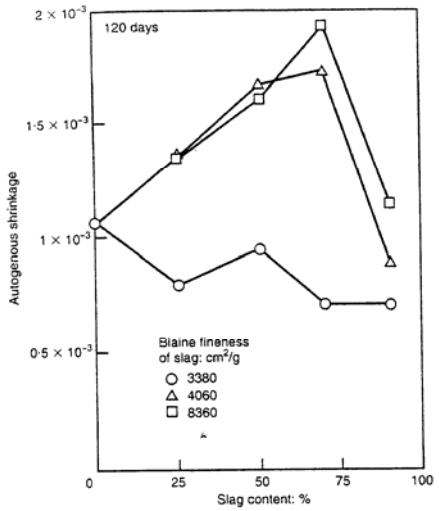

Figure 2-5 Influence of BFS on autogenous shrinkage of cement paste at 120d (Tazawa, 1997)

The effect of different isothermal curing temperature on the development of autogenous shrinkage was investigated by Bjøntegaard (1999) and Lura et al. (2001, 2002). Bjøntegaard (1999) measured the development of AD for a concrete ("basic 5", w/b=0.4 and 5% silica fume by weight of cement) under four isothermal curing temperature (5, 13, 20, 45ºC). The AD developments are shown in Figure 2-6. The t_0 is defined as the time when the stresses start to develop in the TSTM. Lura et al. (2001, 2002) measured the development of AD under four isothermal curing temperature (10, 20, 30, 40ºC) for Portland cement (CEM I 52.5 R) and BFS cement (CEM III/B 42.5 LH HS) concretes with w/b ratio of 0.35 and 5% silica fume by weight of binder. The AD developments for mixture A (Portland cement), and B (BFS cement) under four curing temperatures are shown in Figure 2-7. The both results shown that the effect of different isothermal curing temperature on the development of AD is unsystematic, and it seem

that higher temperature do not necessarily lead to higher deformation rates, and then the use of maturity transformation to predict AD under different isothermal temperature is questionable.

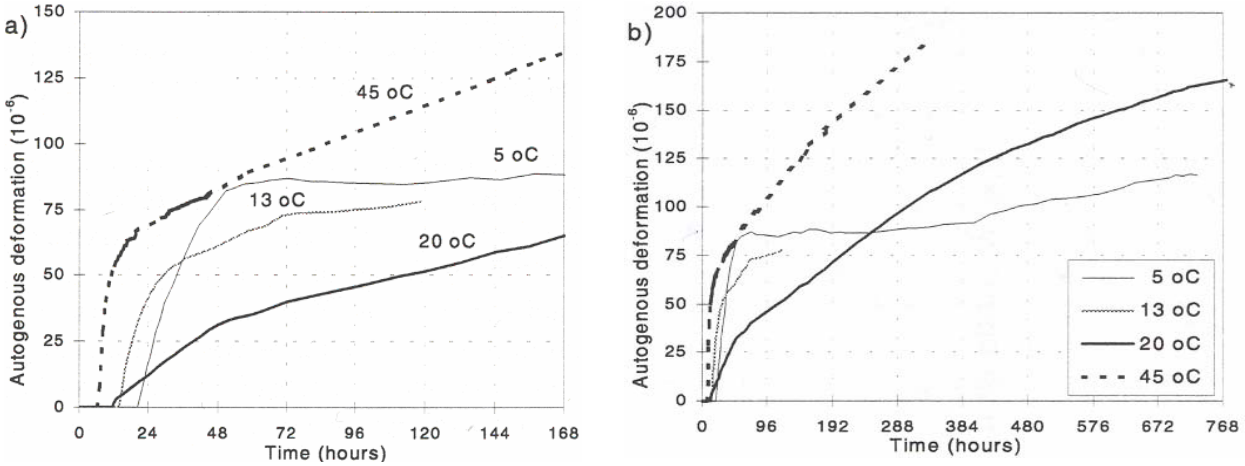

a) the first week b) 1 month

Figure 2-6 Autogenous shrinkage of "Basic 5" concrete under 5, 13, 20, and 45ºC isothermal tests, the results zeroed at t_0 (Bjøntegaard, 1999)

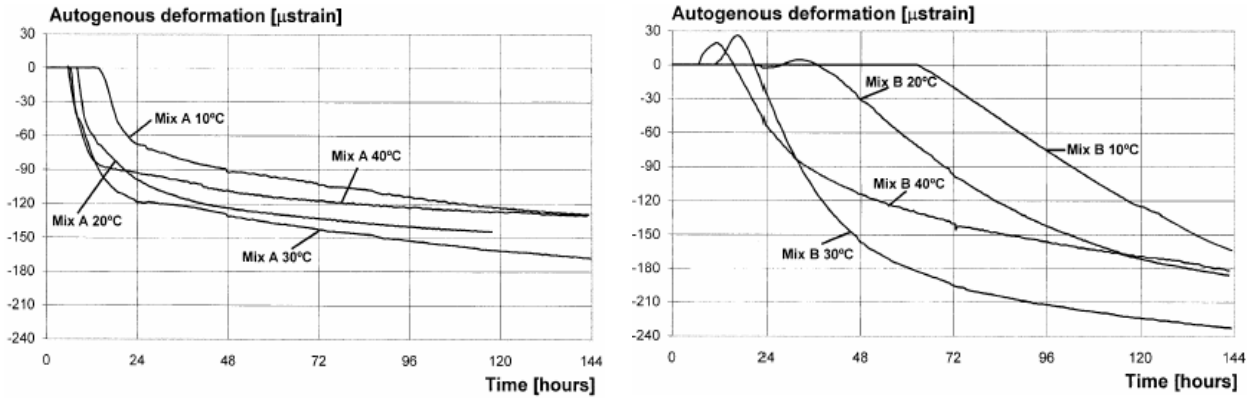

Figure 2-7 Autogenous deformation of mixture A, and B cured at 10, 20, 30, and 40ºC, AD was zeroed at t_0. (Lura, 2001)

Autogenous shrinkage under realistic temperature histories was studied by Bjøntegaard (1999). The CTE of the early age concrete is directly measured by imposing "saw-toothed" temperatures histories, and the AD under such temperature histories is then deduced by subtracting the TD from measured total deformation in each step. The step-wised temperatures and calculated AD for a concrete ("basic 5", w/b=0.4) are shown in Figure 2-8. The behavior of the AD depends strongly on the imposed temperature regime, and the AD has shown to be reduced during cooling in the realistic temperature tests ending up in autogenous expansion after 3 days for the temperature histories with 62 ºC maximum temperature. The attempt to generalize the behavior of AD for this concrete based on isothermal tests was therefore impossible as the behavior of AD is changed fundamentally when the concrete is subjected to the heating/cooling, especially the maximum temperature over about 50 ºC.

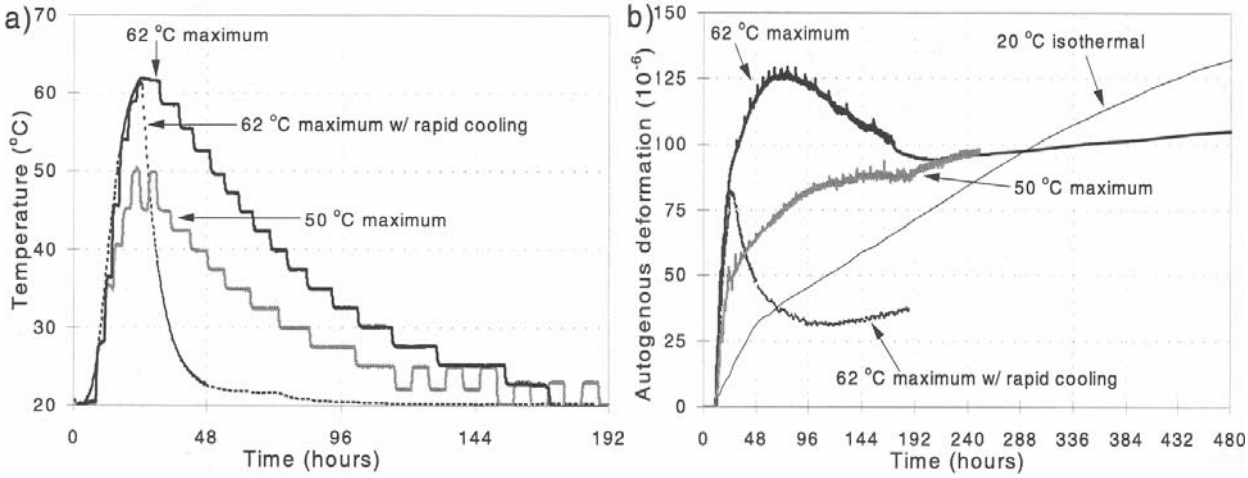

Figure 2-8 The imposed saw-toothed temperature histories and calculated AD of "Basic 5" concrete, AD are zeroed at t_0=11h (Bjøntegaard, 1999)

Bjøntegaard (1999) investigated the influence of silica fume on the cracking risk of concrete structure, and the free deformations of concretes containing different percentage of silica fume are measured under realistic temperature history, and the deduced AD is shown in Figure 2-9, and the increase of silica fume content results in higher AD under similar temperature history.

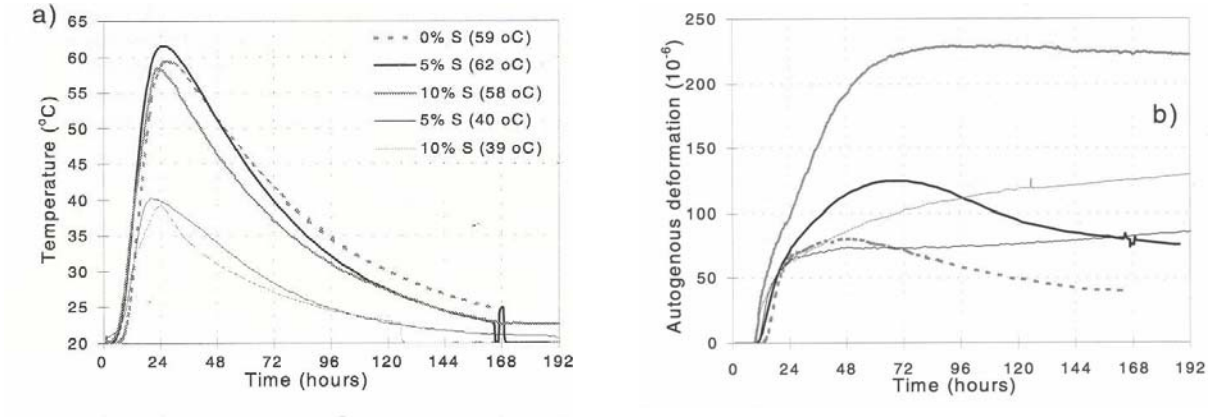

a) Imposed temperature b) Autogenous deformations are zeroed at t_0

Figure 2-9 Deduced autogenous deformation during realistic temperature tests (Bjøntegaard, 1999)

Autogenous shrinkage of concretes containing different percentage of mineral additives, such as BFS, and FA, under realistic temperature histories was studied by Bjøntegaard (2003) for Nor-Crack project, and the results are presented in Chapter 5.

2.2.1.2. Thermal dilation

The thermal dilation is induced by the temperature rise caused by hydration reactions and is proportional to the coefficient of thermal dilation (CTE). The thermal dilation is in most cases the most important factor when it comes to build up of restraint stresses in concrete structures at early ages, and it is therefore somewhat surprising that relatively little experimental data is available on the development of the CTE during the hardening phase.

Bjøntegaard (1999) measured CTE of early age concrete directly by superimposing saw-toothed temperature step following the realistic temperature history. The experiments were carried out on Norcem Anleggsement (CEM I-52.5 LA) concrete (Basic 5) with w/b ratio of 0.40 in 3 series - all with initial temperature of 20ºC, see Figure 2-10 a): A saw-toothed isothermal series (20-series) where temperature steps of either 6ºC or 2ºC were superimposed on 20ºC constant temperature, and two realistic temperature series (47- and 60-series) where temperature steps of different amplitudes were superimposed on the realistic temperature development. A systematic observation in Figure 2-10 b) is that the CTEs of the three series drop from a high value (about 20×10^{-6}/ºC) to a minimum value (about 7×10^{-6}/ºC) around the final setting, and thereafter gradually increase with a rate which depends on the temperature history. The reduction is due to the fact that at the early age stages the free water is continuous while as the setting is approached a solid skeleton is being built up and disrupts this continuity. After setting, self-desiccation (reduction of the degree of capillary saturation, DCS) causes an increase in the thermal dilation coefficient. Based on the test data, a CTE model, given in equation (2-3), is proposed by Bjøntegaard (2003) to describe the development of CTE during hardening phase.

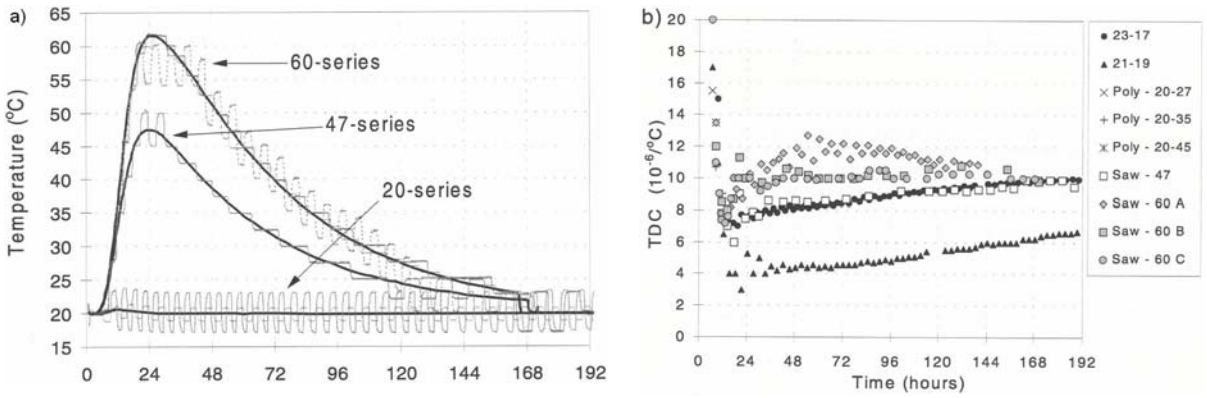

Figure 2-10 a) Imposed saw-toothed temperature histories including series with 20, 47, and 60ºC maximum temperature, b) deduced coefficient of thermal expansion (CTE). (Bjøntegaard, 1999)

After several weeks sealed curing the CTE of the same concrete was measured again after immersing the specimen in water, and results shown in Figure 2-11 indicate that the development of CTE in hardening concrete is dependent on the moisture state. The CTEs were reduced to a minimum around the final setting, and thereafter they increased gradually. When the concrete is immersed in water a few weeks later, by re-saturating the pore system the CTE was immediately reduced to a level which is close to the observed minimum occurring at about the setting time. Bjøntegaard (1999, 2001)

The moisture state clearly influences not only the autogenous shrinkage but also the thermal dilation, and control of the moisture content at a given time may significant reduce the volume change during hardening phase. In this regard, two important benefits will be obtained by supplying an internal water source during curing such as part replacement of natural aggregate with light weight aggregate: the autogenous deformation is reduced or eliminated due to a lower self-desiccation and CTE is minimized due to a wet state.

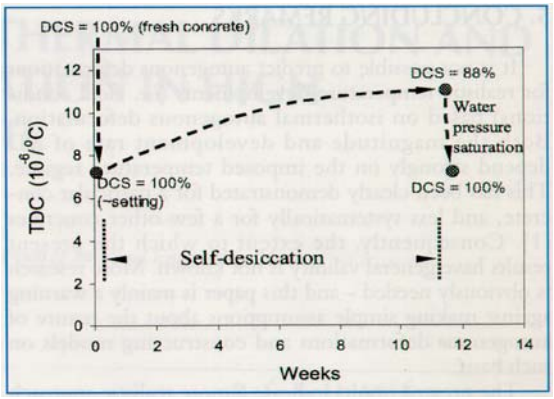

Figure 2-11 Effect of the degree of capillary saturation (DCS) on CTE, concrete with w/b=0.4 and 5% silica fume. (Bjøntegaard, 2001)

Bjøntegaard (1999, 2003, and 2004) also measured the CTEs of concretes containing different percentage of BFS or FA for Nor-Crack project, and the results are discussed in chapter 5.

2.3. Thermal and mechanical properties of early age concrete

The accuracy of numerical analysis of strain and restraint stress development in concrete structures at early age depends primarily on how accurately the required material properties are described. In additional to the volume changes, the main material properties are the thermal properties and the mechanical properties.

2.3.1. Thermal properties

The thermal properties are the thermal conductivity, k, the specific heat capacity, c, and the heat of hydration. The hydration heat depends on the chemical composition of the cement – it increases with the C_3S and C_3A content – and on the fineness of grinding.

Mineral additives, such as SF, BFS, and FA, have significant influence on the heat of hydration. Increasing percentage of BFS or FA content reduces amount of heat of hydration significantly. As shown in Figure 2-12, when the 50% of OPC is replaced by slag, the heat of hydration is decreased by 28% and the maximum temperature rise is reduced from 24 ºC to 16 ºC. (Thomas, 1994)

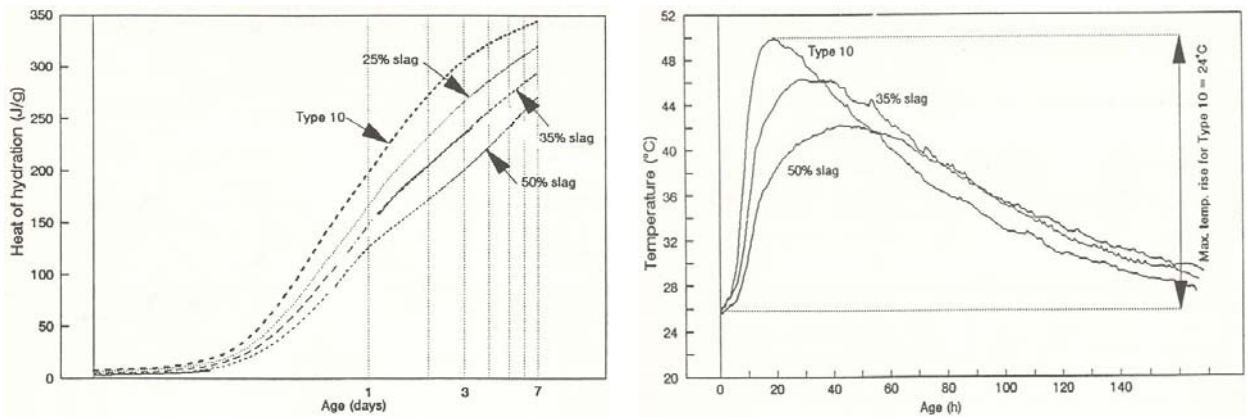

Figure 2-12 Heat of hydration- calorimetry tests on cement paste and temperature rise of concrete cylinders (Thomas, 1994)

The heat of hydration can be determined by either isothermal or adiabatic calorimetry both of which can only be performed by using advanced, expensive equipment. As an alternative, semi-adiabatic calorimeter is used at NTNU, and this simple, easily achievable type of equipment produces the same type of information with an acceptable accuracy and lower cost. The hydration heat and adiabatic temperatures of concretes containing different percentage of mineral additives, such as BFS, and FA are measured or deduced in present study.

2.3.2. Mechanical properties

The most important mechanical properties in analysis of young concrete are modulus of elasticity E, tensile strength f_t, ultimate strain capacity ε_{ult}, and the viscoelastic behavior, and all these properties develop rapidly during the first few days as the cement (and pozzolanic) reactions proceeds. The relative development of E-modulus, compressive and tensile strength of a concrete (w/b=0.4, 5% silica fume) is shown in Figure 2-13, and at very early age (<48 h) the E-modulus develops at highest rate, and the compressive strength develops at lowest rate. The development of the tensile strength is very important in early age cracking evaluation, and higher rate of development (<48 hours) is beneficial to the prevention of cracking. The relative development of the E-modulus, compressive and tensile strength of concretes containing different percentage of mineral additives, such as BSF and FA, is investigated in the present study, and is discussed in chapter 5.

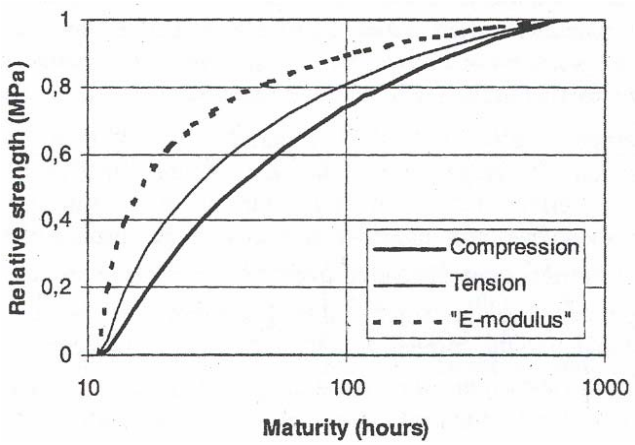

Figure 2-13 Relative developments of E-modulus, compressive and tensile strength (Kanstad, 1999)

The influence of temperature on strength growth is discussed in many investigations. High curing temperature may lead to a lower final strength. The extent to which elevated temperatures influence the mechanical properties of concrete depends on the concrete composition, the moisture state and the drying conditions of the concrete. In particular, it has been found that HPC is less sensitive to the negative effects of elevated curing temperatures than normal strength concrete. The developments of E-modulus of a HPC (w/b=0.4, 5% SF) under isothermal and realistic temperature histories are shown in Figure 2-14, and the model based on the maturity concept gives good agreement with the test data. (Kanstad, 2003) In present study, the temperature effect on the E-modulus and strength development is taken into account by using the maturity concept.

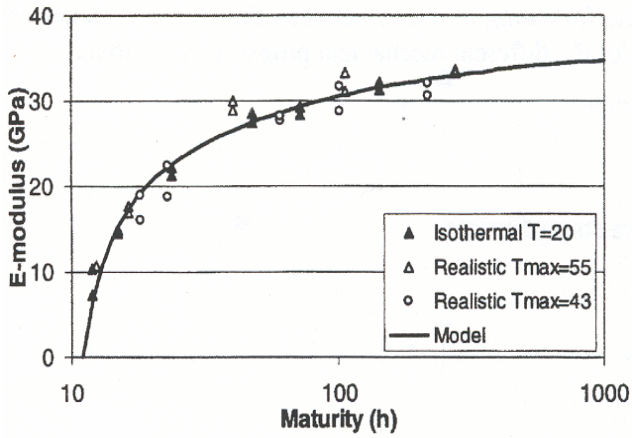

Figure 2-14 Development of E-modulus vs. maturity for different temperature histories (Kanstad, 1999)

When Portland cement is partially replaced by FA or BFS, the rate of strength development is retarded at early age, but the ability of mineral additive to react at normal temperature with calcium hydroxide present in the hydrated Portland cement paste and to form additional calcium silicate hydrate (C-S-H) can lead to significant reduction in porosity of both the matrix and the transition zone. Consequently, considerable improvements in ultimate strength and water tightness can be achieved by incorporation of mineral additives in concrete. Silica fume generally improves the mechanical and durability properties of concrete.

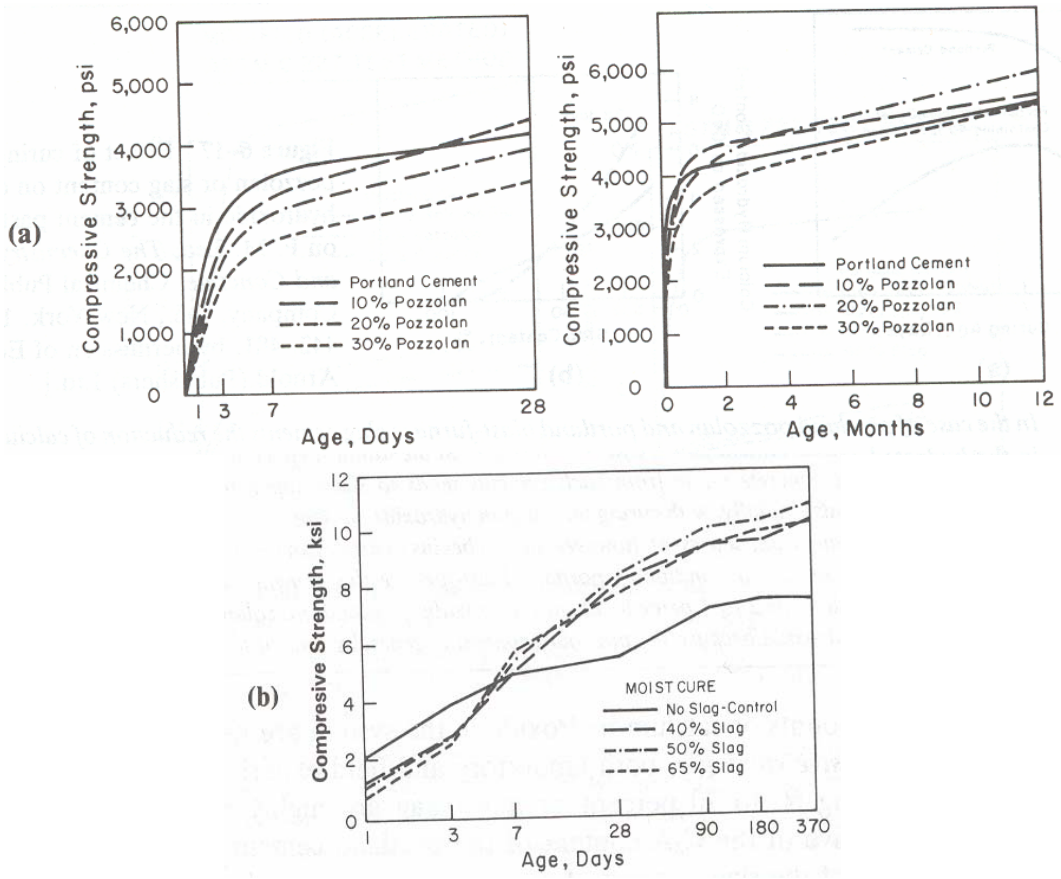

Figure 2-15 Compressive strength development of blended Portland cement containing a pozzolan or a blast furnace slag (Mehta P.K., 1993)

Rostasy (2000) investigated the mechanical properties of specimens cast in the laboratory and specimens extracted from real structure with similar temperature curing history for early age concrete. The following relations between in situ effective values and laboratory test values were found:

$$f_{cte} \approx 0.75 f_{ct} \quad \text{(Tensile strength)}$$
$$f_{ce} \approx 0.85 f_{c} \quad \text{(Compressive strength)}$$
$$E_{ce} \approx E_{c} \quad \text{(E-modulus)}$$

Where f_{cte}, f_{ce}, and E_{ce} are the in situ effective values, and f_{ct}, f_{c}, and E_{c} are the laboratory test values.

In the present study, the crack-index, defined as the ratio between tensile stress ($\sigma(t)$) and tensile strength ($f(t)$), is used to assess whether or not cracking will occur in the concrete element, and several studies indicated that cracking occurs at a ratio in the range between 50% and 75%.

2.4. Viscoelastic behavior of early age concrete

Due to relaxation, restraint stresses induced by thermal dilation and autogenous shrinkage can be significantly reduced. In many cases a reduction of restraint stresses by 30-40% due to stress relaxation in hardening concrete has been reported. (Bosnjak, 2001, Schutter, 2004, Atrushi, 2003)

2.4.1. Factors affecting the creep and relaxation properties

Creep of the concrete depends on many factors, intrinsic and external, and the intrinsic factors represent the material characteristic which are dictated by the concrete mixture, and the external ones are those, which can vary after casting, such as the temperature and moisture conditions, age of loading, load duration, type of loading (tension or compression), level of loading etc.. Creep of hardening concrete is an even more complicated issue due to the effect of varying temperature and humidity content. In many investigations, the influence of the following factors on the creep/relaxation properties of the early age concrete is investigated:

- Age of loading
- Water/binder ratio
- The linearity of applied stress and induced strain under different load/strength ratio
- The temperature history prior to loading and the temperature development during and after loading

High creep at early loading age, the influence of the temperature and humidity content on the creep and creep under tensile stress are some of the most relevant aspects for cracking risk assessment in young concrete. A relatively small numbers of tests that investigated these aspects were reported in literatures. And within the present study, the focus is mainly on the influence of the following three factors on the creep property of early age concrete:

- Type of load (tension or compression)
- Replacement of amount of cement with mineral additives, such as FA and BFS

- Temperature variation during the hardening process, including the influence of different isothermal temperature, and transient thermal creep induced by elevated temperature

2.4.2. Experimental data on creep/relaxation of early age concrete

2.4.2.1. Creep and relaxation properties under compression

Compressive creep has been studied by a large number of researchers, and large amount of experimental data was available in the literatures. (Nevile et. 1983) Only some of the investigations are referenced here. Westman (1995) performed compressive creep tests of high performance concrete (w/b=0.3, SF/C=0.05) and normal concrete (w/b=0.4, SF/C=0.05) at loading age from 13 hrs to 7 days under 20ºC temperature. The results indicated that high creep appears at very early age, and then turns into a stiffer response. As shown in Figure 2-16, the HPC exhibits higher creep compliance than the normal concrete at very early age (<2 days).

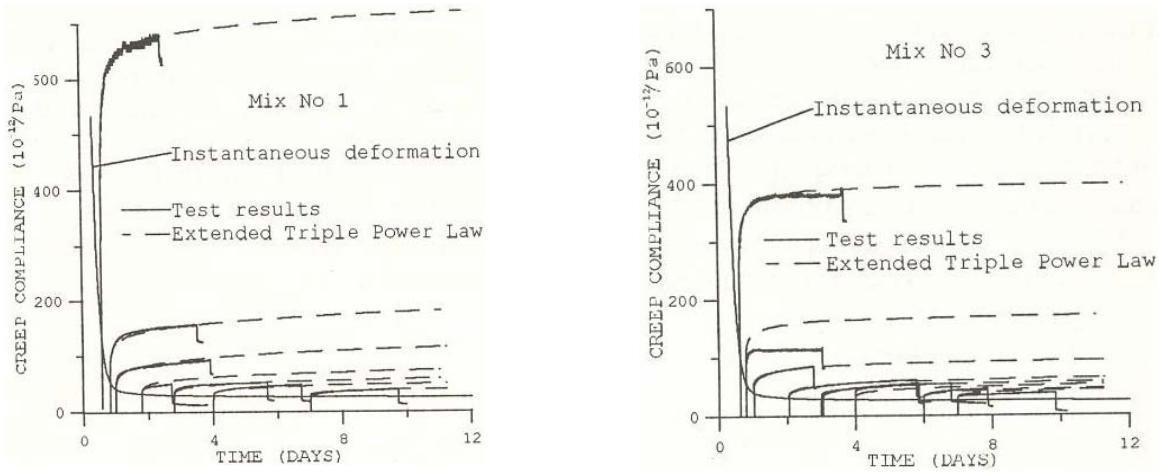

Figure 2-16 Creep test results of HPC (Mix No 1) and normal concrete (Mix No 3) (Westman, 1995)

Schutter (1996, 2000, 2002) conducted compressive creep tests for blast furnace slag concrete (CEM III/B 32.5) with w/c ratio of 0.5 under 20ºC and sealed condition, the test results were shown in Figure 2-17. The loading age varied from 12 hrs to 14 days, and the stress/strength ratio at loading was 20% and 40% respectively. The test results indicated a high nonlinearity of creep at early age, and based on the experimental results a basic creep model was developed for hardening concrete with the evolution of the degree of hydration as the main parameter.

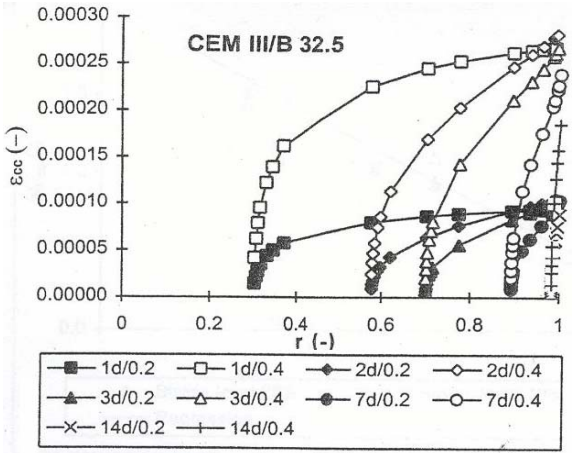

Figure 2-17 Creep strain versus degree of hydration at different loading age/stress level (Schutter, 2000)

Another problem is the increase of creep due to temperature change, regardless of cooling and heating, so-called transitional thermal creep. The phenomenon was discovered by Hansen and Erikson in 1966, but Illston and Sanders (1973) were first to report it in details, and called it "transitional thermal creep". Hauggaard (1997, 1999) carried out two experiments to investigate the temperature influence on creep properties in compression at early age, the imposed temperature histories and the measured strains were shown in Figure 2-18. The concrete had w/b ratio of 0.38. The first specimen was loaded 12 h after mixing with 1.5 MPa corresponding to 24% of the compressive strength at that time. The second specimen was loaded 16 h after mixing with 2.9 MPa corresponding to 29% of the compressive strength. One dummy followed each loaded specimen to compensate for shrinkage and thermal deformation. The measured temperature history in the center of the specimens and the elastic plus creep strain are showed in Figure 2-18. The elastic modulus at loading is 35×10^3 and 40×10^3 MPa for 20 ºC and 40 ºC series respectively. Due to the different maturity age at loading, and different temperature development after loading as well as different magnitude of load applied on the specimens, it is difficult to directly evaluate the temperature effect from total strain shown in Figure 2-18. The estimated compliance function (elastic plus creep strain/stress) for two cases still shows that the temperature have certain influence on the creep properties at early age, and the creep strain is increased due to the temperature change during load duration in the 40 ºC series.

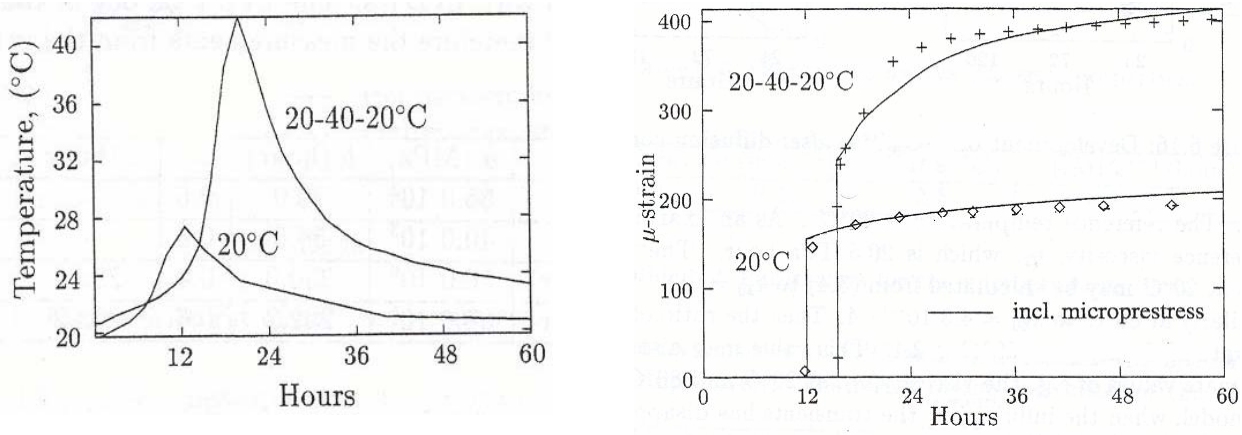

Figure 2-18 Development of temperature and creep of concrete subjected to thermal gradients (Hauggaard, 1997)

Concluding marks

- Loading age
  The compliance function in compression is sensitive to the age of loading, and the earlier the loading is, the higher the compliance function
- Stress level
  The linearity between compressive creep strain and stress is valid up to 60% of the compressive strength. (Nevile et. 1983) But nonlinearity of the creep at early age is reported by Schutter (2000). Due to the fact that the compressive stress level in hardening concrete is normally very low, the compressive creep can be regarded as linear.
- Temperature
  Generally, the changes of the properties in early age concrete are assumed to be governed by the hydration process. High temperature accelerates the hydration reactions and the increase of the maturity age of the concrete at loading, which reduces the rate of creep, but at the same time, the high thermal activation reduces the viscosity, and this results in an increase of creep rate. Usually the latter prevails and then the overall effect of temperature rise is an increase in creep.

2.4.2.2. Creep and relaxation properties under tension

Contrary to creep in compression, the available experimental data on the tensile creep of early age concrete are limited. The difficulties related to the accurate measurement of creep properties in tension partly explains why little attention has paid to tensile creep. The capacity of concrete to deform in tension, especially its creep potential, could help to prevent shrinkage or/and temperature induced cracking, and thus improve the durability of concrete structure, and an increasing amount of research has recently focused on this issue.

Bissonnette and Pigeon (1995) carried out tensile creep tests under drying and sealed conditions to investigate the viscoelastic behavior of repair concrete under 20 ºC temperature. The influence of most basic parameters was studied: w/c ratio (0.35 and 0.55), the type of cement (normal Portland cement and silica fume cement), and the age of loading (1 and 7 day). The test results indicated that the tensile creep increases significantly with the w/c ratio, decreases with the age of loading. Silica fume seems to enhance creep as well as drying shrinkage, but the effect is relatively small.

Hauggaard (1997) studied non-linearity of creep in tension for a concrete with w/b ratio of 0.38 under 20 ºC temperature condition. The loading history and measured elastic plus creep strain, which are the raw data compensated for shrinkage and thermal deformations, are presented in Figure 2-19. The results indicated that the response is linear below a stress/strength ratio of 60%, while non-linearity appears in the interval 0.6 to 0.8 times the tensile strength.

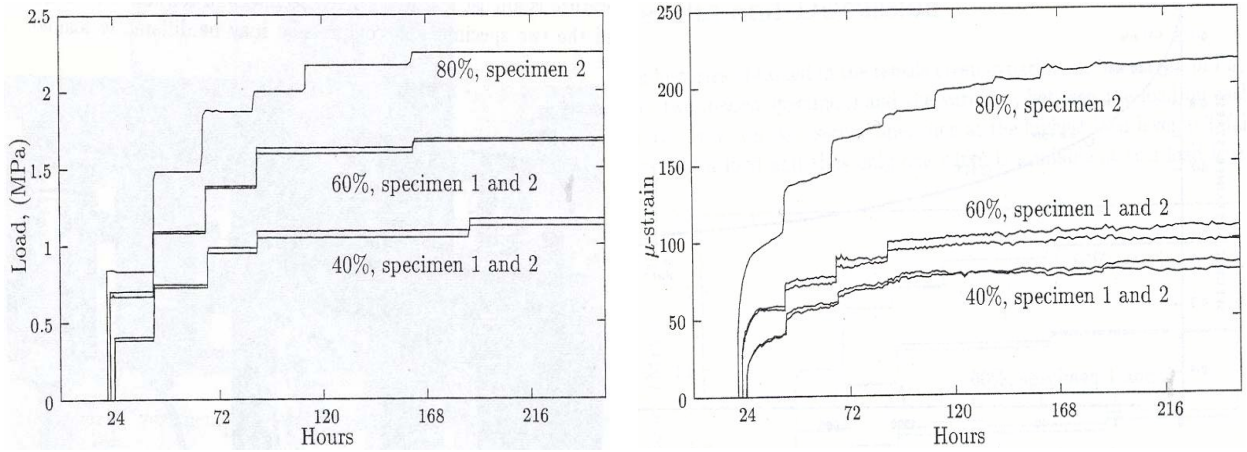

Figure 2-19 load history and measured creep in tension (Hauggaard, 1997)

Atrushi (2003) also investigated the non-linearity in tensile creep, and tensile creep tests were performed for high-performance concrete with w/b ratio of 0.40 at age of 3 days and five initial stress/strength levels 0.2, 0.3, 0.4, 0.6, 0.7 and 0.8 under 20 ºC temperature. The results indicated that the creep response is proportional to initial stress/strength level up to about 70% as shown in Figure 2-20.

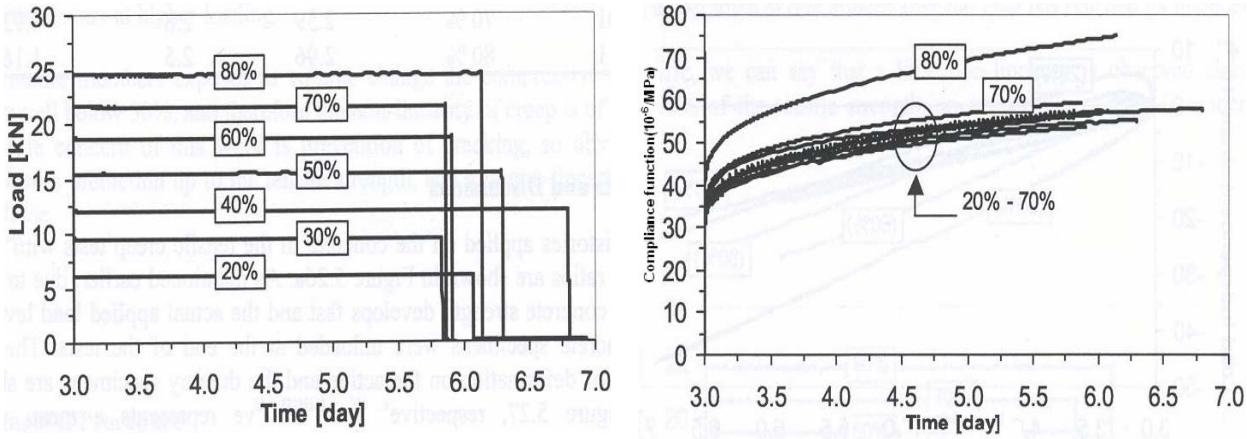

Figure 2-20 load histories with the initial stress/strength ratio and compliance function (Atrushi, 2003)

Altoubat *et al.* (2001) performed a so-called Discretized Restrained Shrinkage (DRS) test to investigate the tensile creep and shrinkage behavior of normal and high performance concrete at early age. In usual experimental tests, sealed concrete is used to measure basic creep, but sealing will not eliminate internal drying (self-desiccation) during early age. Especially for concrete with low w/c ratio, the measured creep of sealed specimen will include interaction with autogenous shrinkage. In the experimental program performed by Altoubat *et al.*, tensile creep and shrinkage were measured under three different curing conditions: moist-cover (specimens constantly surround with wet cover), sealed and drying. The drying creep mechanisms (Pickett effect) are separated into two components: stress-induced shrinkage and microcraking. Testing concrete under moist-cover condition gives basic creep because the early-age autogenous shrinkage is eliminated; and tests under sealed condition provide data of basic creep and stress-induced shrinkage, while testing under drying condition determines the sum of basic creep, stress-induced shrinkage and microcracking. The test results were shown in Figure 2-21, and Altoubat *et al.* revealed that both internal and external drying play a significant role. The free

shrinkage of normal concrete and HPC in the first days after casting is significant, and may induce high tensile stresses that fractures the concrete samples. The tensile creep is a very significant phenomenon which plays an important role in reducing the stress due to restrained shrinkage. The results also indicated that the stress induced shrinkage is a major mechanism of the Pickett effect.

The test procedure used by Altoubat *et al.* depends on the effectiveness of the moist-cover curing in suppressing the autogenous shrinkage. Two other important things must be taken into account when comparison of the test results from Altoubat *et al.* with other creep data in the literatures. The first one is the curing condition in measuring of basic creep. Altoubat *et al.* measured the basic creep under moist-cover curing, and most of the basic creep data in the literatures were measured under sealed condition. The second one is that creep strain measured in the Discretized Restrained Shrinkage (DRS) test is under the generated shrinkage stress condition as shown in Figure 2-21 a), and is not under constant loading condition as the conventional creep tests.

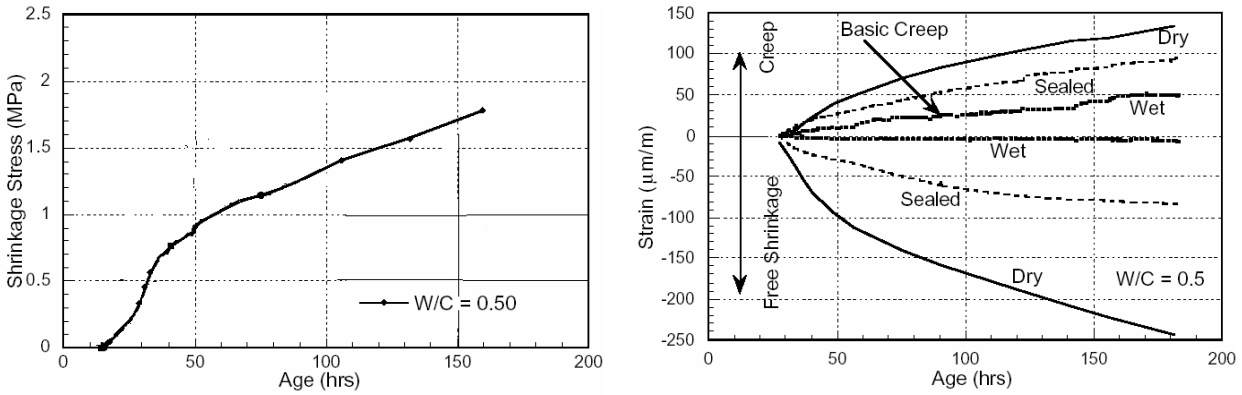

Figure 2-21 a) shrinkage stress b) Creep and shrinkage under different curing condition (Altoubat *et al.*, 2001)

Østergaard *et al.* (2001) conducted basic tensile creep tests for early age concrete under constant load, 20 ºC temperature and water curing condition (supposed to eliminate the autogenous shrinkage). The experiments investigated the influence of age at loading (0.67, 1, 3 and 5 days), initial stress/strength ratio (25% and 45%) and w/b ratio (mix A 0.50, mix B 0.40 and mix C 0.32) on basic creep property in tension. The results showed that concrete exhibits high tensile creep strain when it is loaded at an age less than 1 day. The response is far stiffer when the loading age is beyond 3 days as shown in Figure 2-22. The study also indicted that the creep response is not proportional to the applied initial stress/strength level when loading applied at 1 day.

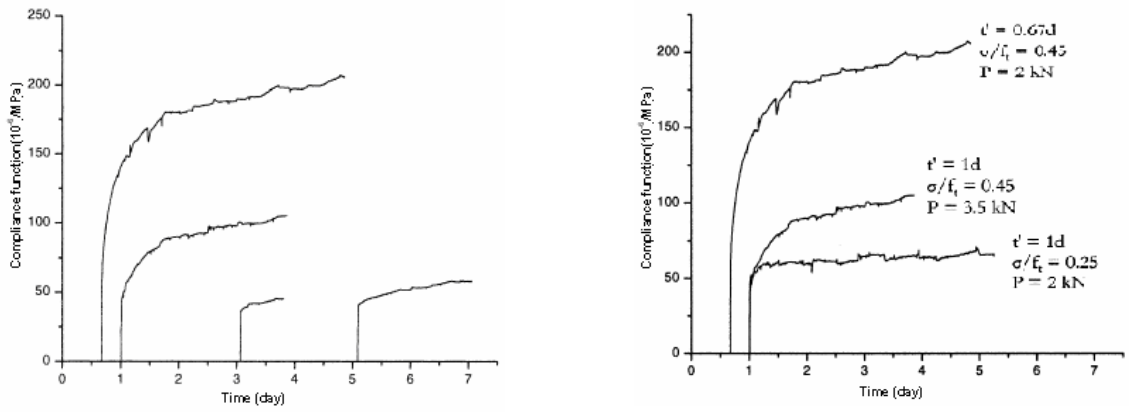

Figure 2-22 tension creep tests of young concrete (Østergaard, 2001)

Igarashi (2001) investigated the development of restrained stresses induced by autogenous shrinkage in high-strength concrete at early ages. Restrained shrinkage test was performed on ordinary Portland cement concrete and silica fume concrete (10% binder weight) with w/b ratio of 0.25 under 18ºC isothermal and sealed or water-cured condition, and the effect of silica fume on the stress development was evaluated. It is well known that the hardened high-strength concrete with silica fume exhibits smaller creep deformation than the concrete without silica fume. (Nevile et. 1983) The lower creep potential in silica fume concrete results from the higher strength and the denser microstructure at the time of loading. However, test results from Igarashi showed that the hardening silica fume concrete exhibits a higher creep potential than the concrete without silica fume when loaded at very early ages.

Pane and Hansen (2002) performed tensile creep tests for four types concrete, including ordinary Portland cement, and three mixes containing OPC plus different mineral additives: 25% FA, 25% BFS, and 10% SF (*the percentage of the weight of OPC*). The w/b ratio is 0.45, and each mix contains 350 kg/m^3 binder. Prior to testing, specimen were cured in lime-saturated water at room temperature (22-23 ºC), then sealed with plastic sheets to prevent the moisture loss during the test. The loading was applied at approximately 24, 72, 168 and 336 h after mixing. The elastic strain and specific creep for OPC and 25% FA concrete are shown in Figure 2-23, and the relaxation modulus at age of 72 hours for four mixes is shown in Figure 2-24. It can be seen that the mineral additives such as fly ash, silica fume and blast furnace slag influence the creep properties at early age, the development rate of the specific creep of concrete with 25% FA is higher than that of OPC at very early age (<2 days), replacement of cement with FA can accelerate the stress relaxation and then be beneficial in reducing the risk of cracking at early ages.

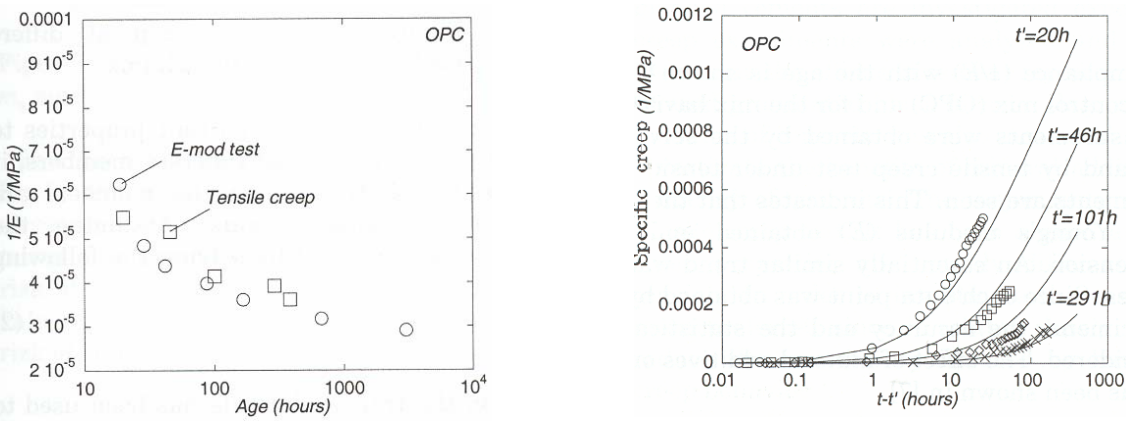

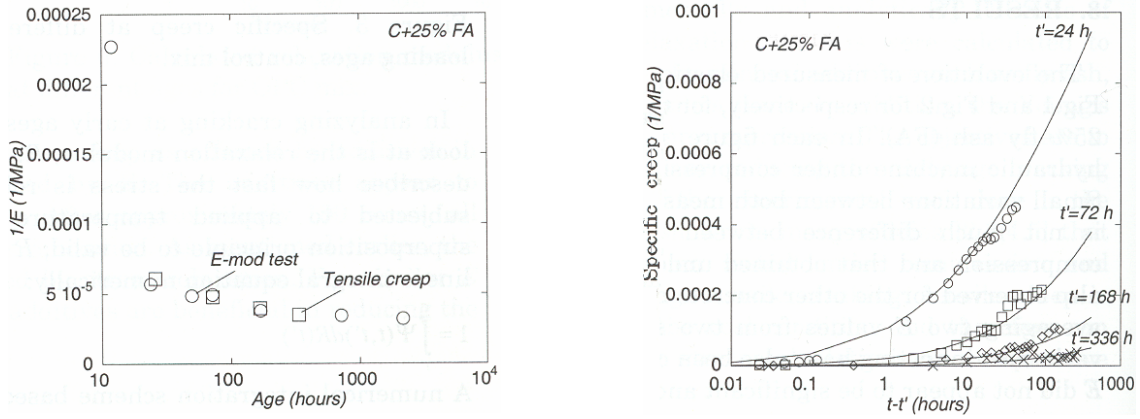

Figure 2-23 Elastic strain and specific creep of OPC and 25% FA concrete (Pan and Hansen, 2002)

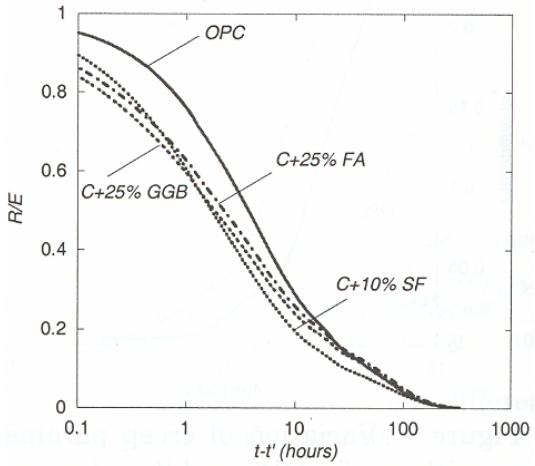

Figure 2-24 Relaxation modulus at age of 72 hours for four (Pane and Hansen, 2002)

Concluding marks

- w/b ratio
  The tensile creep increase significantly with the increase of w/b ratio
- Loading age
  The compliance function in tension is shown to be very sensitive to the age of loading, especially when the load is applied at age less than 2 days, and the earlier the loading is, the higher the compliance function is.
- Stress level
  The several researches showed that the linearity between the tensile creep strain and the stress is valid up to 60-70% of the tensile strength
- Composition: silica fume, BFS, and FA
  Silica fume moderately increase the creep strain of hardening concrete, and the mineral additives, such as FA and BFS have more pronounced influence on the creep properties, and significantly increase the creep strain in tension.

2.4.2.3. Comparison of creep/relaxation properties in compression and tension

The creep properties in compression and tension were previously considered equal to each other. Performing creep test in tension is in general more difficult than making compressive test,

especially at early ages, and the comparable experimental data of compressive and tensile creep for same concrete is very scarce in the literature, and the results from several researchers are not consistent.

Hagihara *et al.* (2000) carried out a comprehensive study of the early age mechanical properties and creep behavior of high-strength concrete (100N/mm^2). The compressive and tensile creep experiments were conducted parallel under sealed and 20 ºC temperature condition in two series. In the first series, concrete with w/b ratio of 0.22 was tested under different age of loading (1 or 3 days) and different initial stress/strength ratio (20% or 40%) with the same load duration. In the second series, mix proportion (w/b ratio of 0.19, 0.22 and 0.25) was the test parameter. The test procedure of compressive and tensile creep is similar; and compliance function is the difference between measured strain from loaded specimen and free autogenous shrinkage from unloaded specimen. Due to the different magnitude of applied load, the measured strain in compression is far larger than the free autogenous shrinkage. However, the measured strain in tension is of the same order as the free autogenous shrinkage, and the calculated tensile creep consequently are strongly influenced by the amount of autogenous shrinkage. The test results shown in Figure 2-25 indicate that specific tensile creep strain (not include the elastic part) is about 75% of the specific compressive creep strain. The elastic strain of early age concrete is also important, and the E-modulus in tension is about 15% higher than the E-modulus in compression.

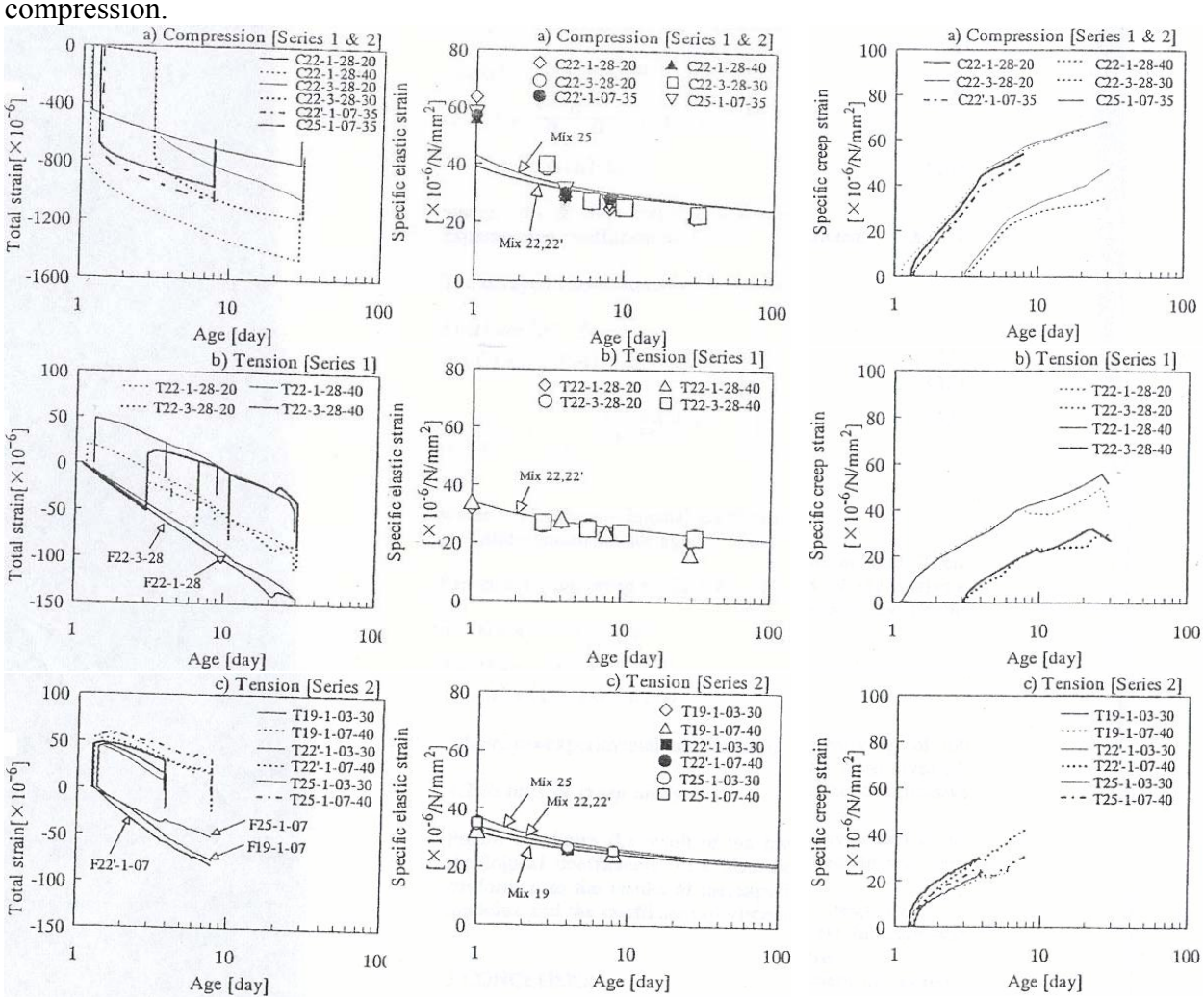

Figure 2-25 Measured strain in loaded and unloaded specimen, specific elastic strain, and specific creep strain (Hagihara *et al.*, 2000)

Gutsch (2000, 2001, and 2002) reported results of a comparative study on the compressive and tensile creep behavior of early age concrete with w/b ratio of 0.53. The initial stress/strength ratio varied between $0.5 \le \sigma / f_t \le 0.9$ in the tensile creep tests, and between $0.13 \le \sigma / f_c \le 0.2$ in the compressive creep tests. Both tests were performed under 20ºC and sealed conditions. The results of compressive creep tests are shown in Figure 2-26 together with the shaded scatter band of tensile creep function from about 25 creep tests. The test results revealed that the creep functions for compression are within the scatter band of the creep function for tension, and the tensile creep function is smaller than the compressive creep function at the first day after loading. Tensile creep tests were also performed under 20ºC, 40ºC isothermal and realistic temperature history as well. The test results were shown in Figure 2-27. Creep of early age concrete is accelerated under temperature higher than 20ºC during time under load. Based on experimental data a creep function model was presented taking into account the aging effect prior to loading and the temperature effect during loading.

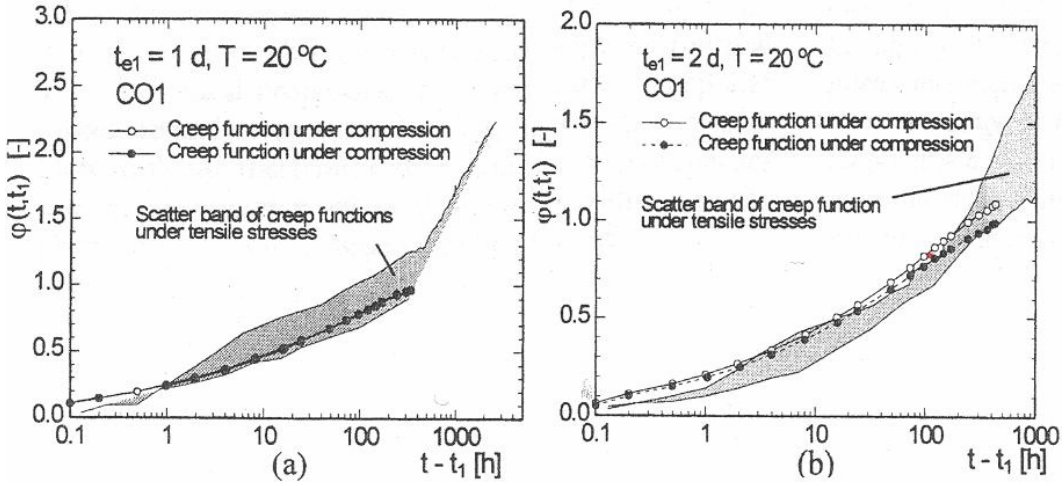

Figure 2-26 Creep function under compression and scatter band of creep function under tension Gutsch (2000)

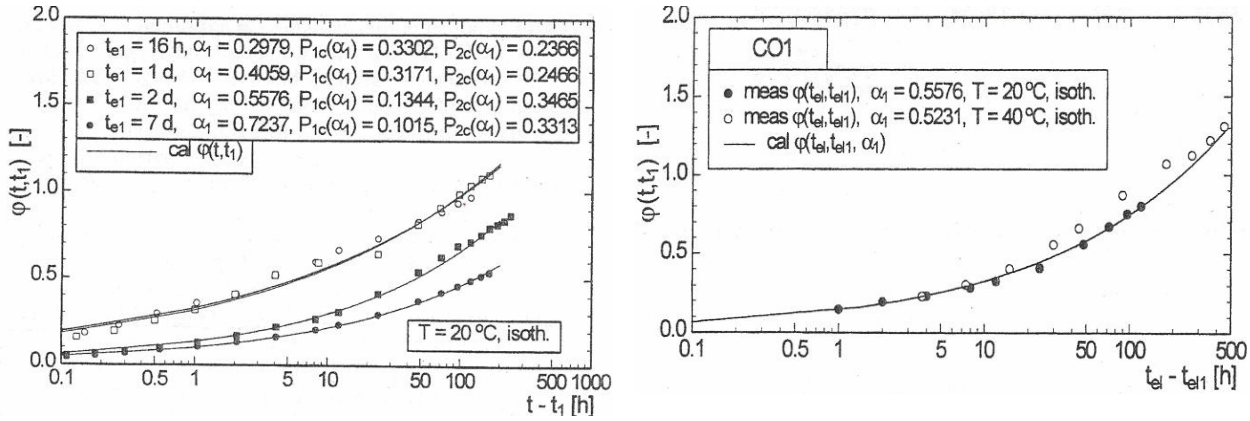

Figure 2-27 Creep function for different temperature (isothermal 20ºC, 40ºC) (Gutsch, 2002)

Atrushi (2003) performed a comprehensive experimental program to investigate the viscoelastic behavior of early age concrete in both compression and tension. The compressive and tensile creep tests were conducted for high-performance concrete with w/b ratio of 0.40 and 5% SF of cement weight, and the test results, as shown in Figure 2-28, indicated that:

- Instantaneous deformation in tension is lower than in compression, and the elastic modulus in tension is about 11% higher than that in compression for the investigated concrete mixes.
- Immediately after loading and within approximately the first 24 hrs the rate of compressive creep is higher than the rate of tensile creep. Afterwards, the creep rates decreases continually with time, but the decrease in tensile creep is much less pronounced than in compressive creep. This leads to a higher tensile creep than compressive creep a few days after loading.

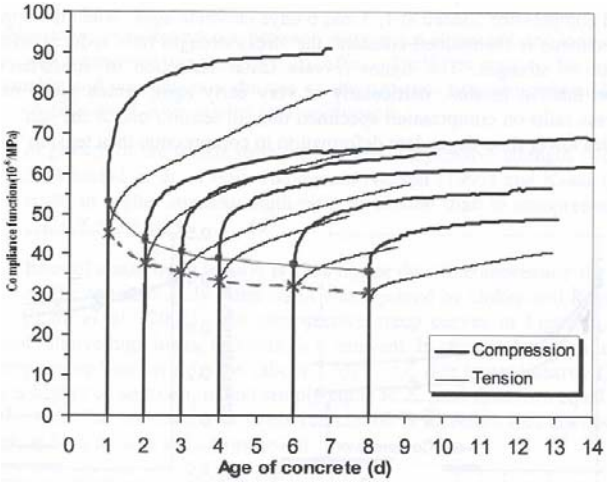

Figure 2-28 Comparison of compliance functions under compression and tension (Atrushi, 2003)

Tensile creep tests were conducted at different isothermal temperature (20, 34, 40, 57, and 60 ºC) for high-performance concrete with w/b ratio of 0.40 and 5% SF of cement weight (Basic-5) by Atrushi (2003). For the test at 34 ºC, the temperature was increased 3 hrs before loading. For the other test (40, 57, and 60 ºC) the temperature was increased to the desired level one day before loading. The imposed temperature histories and the test results were shown in Figure 2-29. An important observation was that the maturity takes the temperature effect well into account, and is good enough to use for different isothermal temperatures. Note however the results are only for loading ages of more than 3 days maturity.

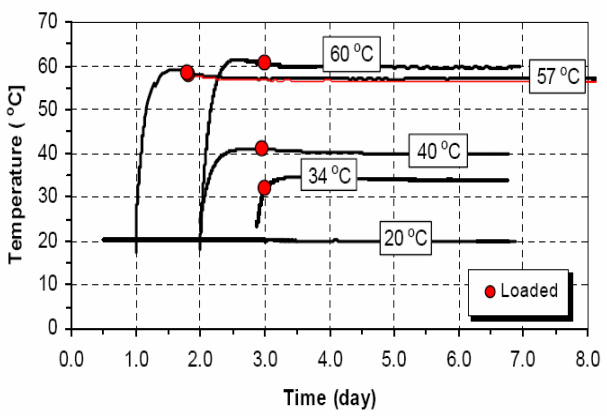

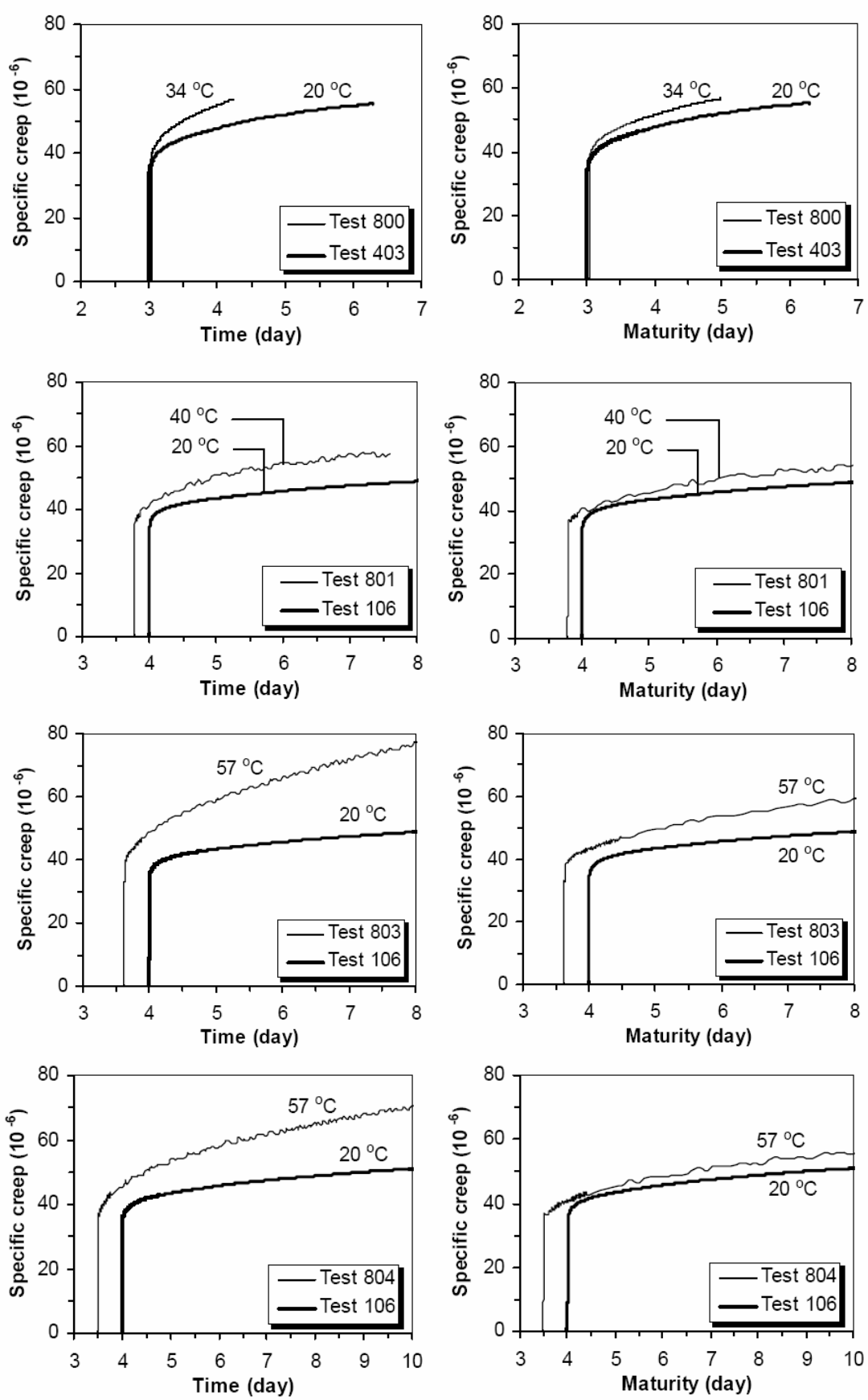

Figure 2-29 Tensile creep tests at different isothermal temperature (Atrushi, 2003)

Morimoto *et al.* (1994) conducted a comparative study on stress relaxation in both compression and tension. Two series of relaxation tests were performed under sealed conditions. In the first series the effects of initial stress level (30, 60 and 80%) and loading age (1, 3, 7, 14 and 21 day) on compressive and tensile relaxation were investigated for a concrete with w/c ratio of 0.50. In the second series compressive relaxation tests were conducted at 3 different temperatures 20, 40, and 60ºC for concrete with w/c ratio of 0.59. In the test programs, Morimoto *et al.* suggested that due to the high w/c ratio, the autogenous shrinkage is so small and its effect on test results was not taken into account in all the tests. The results as shown in Figure 2-30 indicated that the compressive and tensile relaxations are proportional to the initial stress up to 80%, and that stress relaxation depends on the loading age. The tensile relaxation is much smaller and terminates in a shorter period than compressive relaxation as shown in Figure 2-31. The effects of temperature are marginal in the range of 60ºC. The last two findings are doubtful and in contrast to the findings in creep properties. As discussed before, the autogenous shrinkage has small effect on the calculated compressive creep, but has a dominate influence on the calculated tensile creep, the higher stress in present tensile relaxation tests is probably due to the autogenous shrinkage, even its magnitude is small.

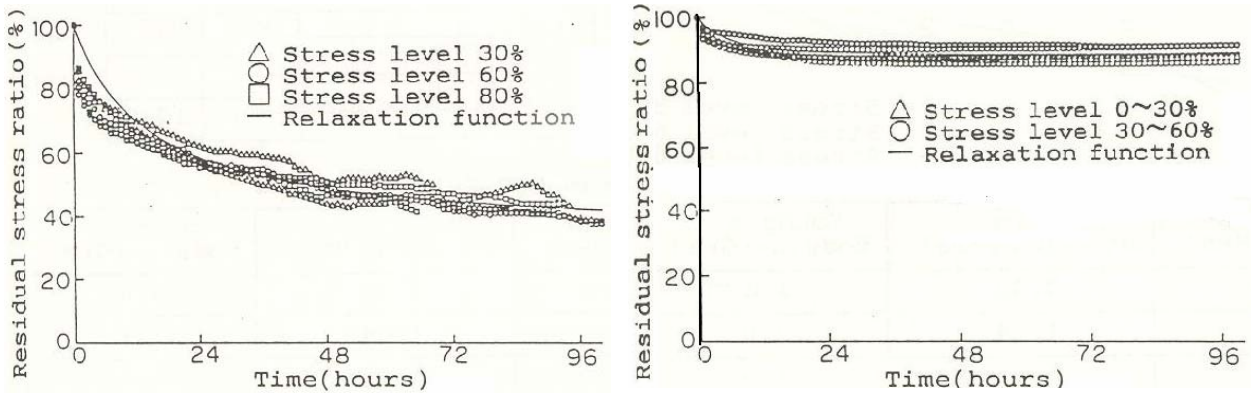

Figure 2-30 Compressive and tensile relaxation curve with loading age of 3 days (Morimoto *et al.*, 1994)

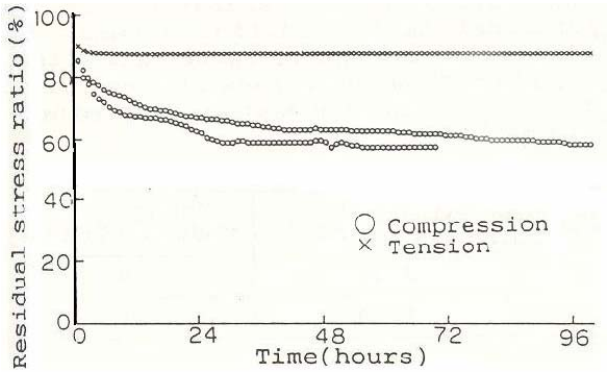

Figure 2-31 Comparison of compressive and tensile relaxation with loading age of 3 days (Morimoto *et al.*, 1994)

2.4.2.4. Conclusion

It can be seen from experimental data mentioned above, that the research results on creep data both in compression and tension are often not consistent, and the main reasons might be due to

the differences in treatment of specimen before and during test, test procedures, and measurement devices. But the following conclusion still can be made:

- Creep test in compression and tension
  The test procedure of compressive and tensile creep is similar; and the compliance function is the difference of measured strain of loaded specimen and free deformation of a dummy specimen. But the influence of the autogenous shrinkage on the calculated compressive or tensile creep compliance is quite different. Due to the different magnitude of applied load, the measured strain in compression is far larger than the free autogenous shrinkage. However, the measured strain in tension is of the same order as the free autogenous shrinkage, and the calculated tensile creep consequently are strongly influenced by the amount of autogenous shrinkage.
- Loading age
  The compliance function in both compression and tension is shown to be sensitive to the age of loading, and the earlier the loading is, the higher the compliance function is.
- Stress level
  The linearity between the tensile creep strain and stress is valid up to 60% of the tensile strength, and similar results were reported on the linearity between compressive creep strain and stress.
- Creep properties in compression and tension
  The comparison of the creep properties in compression and tension are still not clarified. Although the available creep data indicated that the trend of creep under compression and tension is similar, the experimental results of the rate and magnitude of creep development under compression and tension are not consistent.
- Composition: silica fume, BFS, and FA
  Silica fume have moderate influence on the creep properties of early age concrete, and the mineral additives, such as fly ash and blast furnace slag have significant influence on the creep properties, and increase the creep strain in both compression and tension.
- Temperature
  The creep compliance in both compression and tension are accelerated when the isothermal temperature is higher than 20ºC, and the influence of different isothermal temperature history on creep properties is normally taken into account by using maturity or hydration degree as the main parameters in creep model.

In the present study, the influence of the last three factors on creep properties is investigated further through a comprehensive experimental program.

2.5. Material models

2.5.1. Hydration process and hydration heat

Analytical models for simulating the cement hydration process can broadly be classified into three categories according to the scale at which the hydration process is defined. The first type, categorized as a microscopic model, can simulate point by point the random hydration of each chemical component constituting the cement particles. The second type, referred to as meso-model, directly simulates the growth of cement particles as the hydration process evolves to form a skeleton structure of the hardened cement paste. The third type, known as macro-model,

considers the progress of hydration reaction as material variances without considering individual particle explicitly.

Bentz et al. (1996) developed a method to directly represent the chemical components constituting the cement microstructure as image data by relating them to each image element, thereby to simulate the random hydration reaction occurring at each image element point by point, an initial 3-D image for a cement with w/c=0.4 are shown in Figure 2-32. Since this model allows study of the hydration process and the subsequent formation of microstructure, as well as representation of the growth behavior of void structure, the modeling results can also be used to simulate the strength development and volume change during hardening phase.

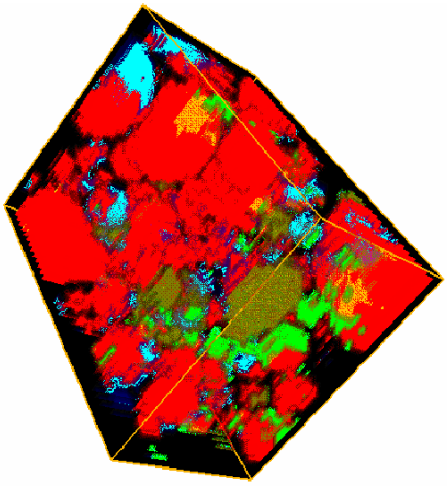

Figure 2-32 Portion of initial 3-D image for a cement with w/c=0.4 (Bentz et al., 1996)

Van Breugel (1991) developed a meso-model to directly represent the cement particles by considering the random distribution of particles in various sizes. Hydration product is formed and expanded around larger cement particle, which then takes in smaller particles along with their hydration products, creates hydration clusters and consolidates them. The cross-linked particles represent the level of consolidation inside the cement pastes, which has close correlation with the development of strength and elastic modulus. The sketch of the modeling of cement hydration were shown in Figure 2-33 and Figure 2-34.

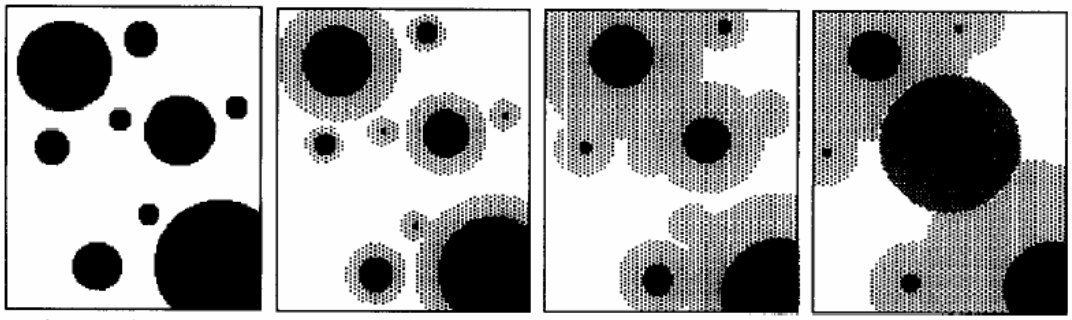

a) initial stage b) early hydration c) "clusters" first embedding d) "bridge" between clusters

Figure 2-33 Formation of load-bearing microstructure in hardening cement paste (Breugel, 1991)

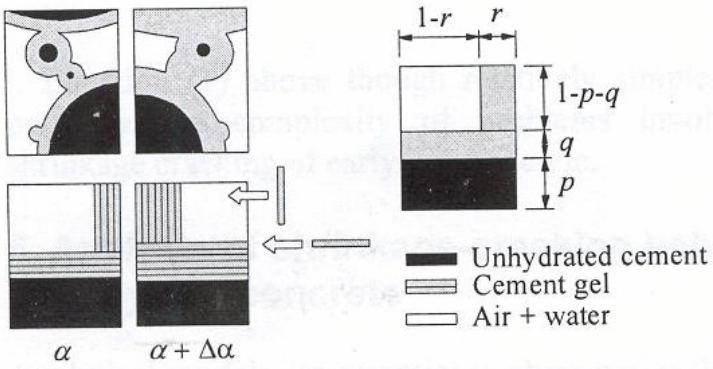

Figure 2-34 Meso-level of modeling of cement hydration (Lokhorst and Van Breugel, 1997)

Most empirical models are macro-model, and the hydration degree or maturity is used as material variances to directly describe the hydration process. The degree of hydration is the ratio between the amount of cement that have reacted and the amount of cement added to the concrete initially. Another way to characterize the progress of hydration is the maturity age. Using degree of hydration or maturity concept the hydration processes at different temperature histories can be compared. The coupled thermo-chemo-mechanical analysis of young concrete based on the theory of reactive porous media within thermodynamic framework was proposed by Ulm and Coussy (1995, 1996) and Ulm (1998), and the main features of the model are described in chapter 4. In the present study, the approach based on the macro scale is used to model the hydration heat and mechanical properties, and the hydration degree or maturity age is the main parameter in the analytical models discussed in the following section.

- Hydration heat

Isothermal or adiabatic hydration heat test is usually performed in laboratory, and then analytic models are used to describe the hydration heat development at various temperature regimes.

For the isothermal hydration test, the rate of heat production at temperature T according to the same hydration degree at 20ºC reference temperature (Schutter, 1995) is given as:

$$q(\xi,T) = q_{T_0}(r) \bullet \exp\left\{-\frac{E}{R} \bullet \left(\frac{1}{T} - \frac{1}{T_0}\right)\right\} = q_{\max,20} \bullet g(\xi) \bullet \exp\left\{-\frac{E}{R} \bullet \left(\frac{1}{T} - \frac{1}{T_0}\right)\right\} \tag{2.4}$$

Where q_{T_0} is the heat generation rate at reference isothermal temperature T_0 , $q_{\max,20}$ is the maximum rate of heat production at isothermal temperature 20ºC, $g(\xi)$ is the normalized heat production rate depending on the degree of reaction.

For an adiabatic hydration test, the rate of hydration heat q can be calculated with:

$$q = \dot{Q} = C\dot{T}_{ad} \tag{2.5}$$

Where T_{ad} is the adiabatic temperature rise measured in the adiabatic test.

The degree of hydration is also defined as the ratio of the amount of heat liberated at time t to the amount of heat at complete hydration, and then the development of degree of hydration in adiabatic test is described as:

$$\xi = \frac{Q(t)}{Q_{\max}} = \frac{T(t) - T_0}{T_{\max} - T_0} \tag{2.6}$$

Under a temperature regime different from that under which the adiabatic temperature T_{ad} is measured, the degree of hydration ξ can be calculated with:

$$\xi = \exp\left[-\left(\frac{\tau}{t_e} \right)^{\alpha} \right] \tag{2.7}$$

And then the heat of hydration is expressed in the simple three parameter equation, which is commonly used in engineering practice (Freiesleben, 1977):

$$Q = Q_{\infty} \cdot \xi(t) = Q_{\infty} \bullet \exp\left(-\left(\frac{\tau}{t_e} \right)^{\alpha} \right) \tag{2.8}$$

The rate of the hydration degree $\dot{\xi}$ under variable temperature regime can be calculated according to:

$$\dot{\xi} = \frac{d\xi}{dt_e} \bullet \frac{dt_e}{dt} = \alpha \tau^{\alpha} \frac{\exp\left[-\left(\frac{\tau}{t_e} \right)^{\alpha} \right]}{t_e^{\alpha+1}} \exp\left[-\frac{E}{R}\left(\frac{1}{T} - \frac{1}{T_{ref}} \right) \right] = \frac{\alpha \tau^{\alpha} \xi}{t_e^{\alpha+1}} \exp\left[-\frac{E}{R}\left(\frac{1}{T} - \frac{1}{T_{ref}} \right) \right] \tag{2.9}$$

In the present study, the hydration heat is measured in the semi-adiabatic hydration heat tests, and the simple three parameter model as expressed in equation (2.8) is used to calculate the hydration heat.

2.5.2. Mechanical properties

The development of mechanical properties of the hardening concrete like compressive strength, E-modulus and tensile strength can be described by the degree of hydration (Schutter, 1996),

$$X_i(\xi) = X_i(\xi = 1) \bullet \left(\frac{1 - \xi}{1 - \xi_0} \right)^{n_i} \tag{2.10}$$

With ξ, degree of hydration; ξ_0, degree of hydration at transition into solid state; $X_i(\xi)$, mechanical property at α; $X_i(\xi = 1)$ mechanical property at $\xi = 1$; n_i, parameter of the mechanical property.

Kanstad (1999) used the modified version of CEB-FIP MC 1990 to describe the development of the compressive strength, tensile strength and modulus of elasticity, and t_0 was introduced in the equations to identify the start of significant mechanical properties development. This method is applied in the present study, and the details are discussed in Chapter 4.

2.5.3. Viscoelastic properties

2.5.3.1. The theory of linear viscoelastic

Linear viscoelastic behavior means that the strain is proportional to the applied stress. If the assumption of linearity should be applicable several restrictions must be fulfilled (Bažant, 1982):
1) The stress is less than about 40% of the (compressive) strength
2) The strains do not decrease in magnitude (but the stresses may)
3) There is no significant drying during creep
4) There is no sudden large increase of the stress magnitude after initial loading

During the hardening phase, the main concern is the tensile stresses induced in the structure members, and its magnitude may be up to the tensile strength after 1 or 2 weeks, and the non-linearity may have influence on the stress development. Several investigations (Hauggaard, 1997), (Atrushi, 2003) have revealed that the linearity is kept below a stress/strength ratio of 60% in tensile creep test, while the non-linearity appears in the interval 0.6 t 0.8 times the tensile strength. The linear viscoelastic theory overestimates the creep recovery under unloading conditions compared to the experimental results. (Atrushi, 2003)

2.5.3.2. Integral and differential formulation

According to the linear viscoelastic theory, the strain at time t caused by constant stress σ applied at time t' is given by:

$$\varepsilon(t,t') = J(t,t')\sigma \tag{2.11}$$

For variable stress history, the total strain is calculated with the principle of superposition, originally formulated by Maslov and McHenry (Neville 1983): strain produced at any time t by a stress increment applied at age $t' < t$ is independent of the effects of any stress applied earlier or later that time. The general integral formulation becomes:

$$\varepsilon(t) = \int_{t_0}^{t} J(t,t')\, d\sigma(t') + \varepsilon^0(t) \tag{2.12}$$

or

$$\sigma(t) = \int_{t_0}^{t} R(t,t')\, d\varepsilon(t') + \sigma^0(t) \tag{2.13}$$

In the differential formulation, the creep behavior is represented by rheological models composed of elastic (spring) and viscous (dashpot) elements placed together in a series and/or parallel coupling. The main advantage of the differential formulation is that differential equation can be resolved step-by-step, which means that the strain state at any time t is defined by the state from the previous step and the change during the last time increment, without the storage of the complete stress history, which is necessary if integral formulation are being used.

2.5.3.3. Rheological models

In rheological models, material properties influencing the creep behavior are associated to elastic (spring) and viscous (dashpot) elements placed together in a series and/or parallel coupling.

The age-dependent aspects of basic creep are mathematically handled by considering the material parameters involved in the creep model as empirical functions of the age. Nakamura *et al.* (2002) simulated the rapid changes in material properties in accordance with the progress of hydration reaction by using Burger's model, on the assumption that each parameter of the spring and dashpot elements changes with age, and the schematic representation of Burgers model is shown in Figure 2-35. One of the special characteristics of this model is that it allows adjusting each model component's function to actual creep behavior of early age concrete. In specific terms, Maxwell's spring element and Maxwell's dashpot element bear the reversible instant elastic deformation and irreversible delayed elastic deformation, respectively. The reversible delayed elastic deformation is born by the Voigt model, in which the spring and dashpot elements are connected in series. Thus, it is possible to quantify each model parameter by performing inverse-analysis on experimental results.

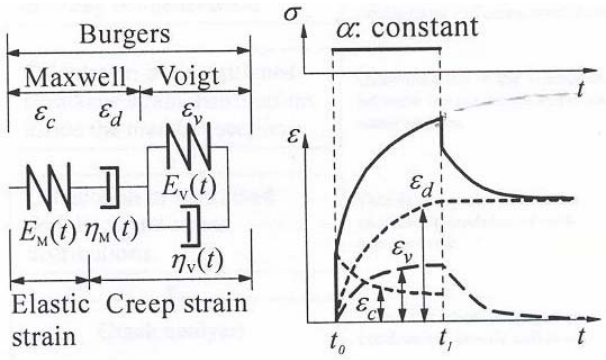

Figure 2-35 Schematic representation of Burgers model (Nakamura *et al.*, 2002)

2.5.3.4. Creep function

Based on tensile creep and relaxation test results, Gutsch (2001, 2002) showed that the maturity principle is applicable for basic creep behavior of early age concrete. The creep function $\varphi(t-t_1,t_1)$ under 20ºC isothermal condition, which is the ratio of the creep strain $\varepsilon_{cr}(t-t_1,t_1)$ to the elastic strain at loading $\varepsilon_{el}(t_1)$, is modelled by:

$$\varphi(t-t_1,t_1)=\frac{\varepsilon_{cr}(t-t_1)}{\varepsilon_{el}(t_1)}=P_{1c}(\alpha_1)\left[\frac{t-t_1}{t_c}\right]^{P_{2c}(\alpha_1)} \tag{2.14}$$

The creep equivalent time under load $t_{el}-t_{el1}$ was introduced on the basis of the Arrhenius – equation to take into account the temperature effect on the viscoelastic behavior. Creep and relaxation curve under elevated temperatures can be transformed into curves under 20ºC isothermal conditions, provided the degree of hydration at loading is identical.

$$\varphi(t_{el}-t_{el1},t_{el1})=\frac{\varepsilon_{cr}(t,t_1,\alpha_1,T(t,t_1))}{\varepsilon_{el}(t_1)}=P_{1c}(\alpha_1)\left[\frac{t_{el}-t_{el1}}{t_c}\right]^{P_{2c}(\alpha_1)} \tag{2.15}$$

Schutter (1996, 2001) introduced a basic creep model for hardening concrete with the evolution of the degree of hydration as the main parameter for the evolution of basic creep strain:

$$\varepsilon_{cc}(\alpha,\alpha_b,\eta_b)=\varepsilon_{c0}(\alpha_b,\eta_b)\cdot\varphi_c(\alpha,\alpha_b) \tag{2.16}$$

in which $\varepsilon_{c0}(\alpha_b,\eta_b)$ is the instantaneous deformation due to the stress level η_b at loading, α_b is the degree of hydration at loading, α is the degree of hydration, and

$$\varphi_c(\alpha,\alpha_b) = c_1(\alpha_b)\left(\frac{\alpha-\alpha_b}{1-\alpha_b}\right)^{c_2(\alpha_b)} \tag{2.17}$$

The temperature influence is implemented automatically through the temperature influence incorporated in the hydration model.

2.5.3.5. Creep compliance

- Double and triple power law

The creep of concrete at constant moisture and thermal state may be well described by power curves of load durations $t-t'$, and by inverse power curves of age t' at loading. This leads to the most well known compliance function: Double-Power law, Bažant and Panula (1978)

$$J(t,t') = \frac{1}{E_0} + \frac{\varphi_1}{E_0}\left(t'^{-m}+\alpha\right)\left(t-t'\right)^n \tag{2.18}$$

Compared with long term test data, the slopes of the power curves of load duration $t-t'$ have been observed to be too high for long load durations. When converting creep into relaxation it will get negative stress at long time relaxation curves. Bažant and Chern (1985) proposed Log-double power to avoid this problem.

$$J(t,t') = \frac{1}{E_0} + \frac{\psi_0}{E_0}\ln\left[1+\psi_1\left(t'^{-m}+\alpha\right)\left(t-t'\right)^n\right] \tag{2.19}$$

The long time creep is better described when the Double power law is extended to the triple power law (Bažant and chem., 1985a)

$$J(t,t') = \frac{1}{E_0} + \frac{\varphi_1}{E_0}\left(t'^{-m}+\alpha\right)\left[\left(t-t'\right)^n - B\left(t,t_0,n\right)\right] \tag{2.20}$$

The Double and triple power law is originally proposed for hardened concrete. They were modified to describe the creep property of early age concrete by taking into account the aging characteristics of young concrete:

$$J(t,t') = \frac{1}{E(t')}\left[1+\varphi_0 \bullet \left(t'\right)^{-d}\left(t-t'\right)^p\right] \tag{2.21}$$

- Creep under various isothermal temperatures

Temperature exerts a significant influence on the concrete creep. Heating of concrete accelerates creep but it also accelerates hydration which tends to reduce creep. Creep of sealed specimen at various isothermal temperatures is generalized by introducing the equivalent time at loading and the equivalent creep duration. (Bažant, 1988) The details are discussed in Chapter 4.

- Transient creep under temperature changes

Thelandersson (1987) suggested that the transient thermal creep is the interdependence between temperature response and mechanical response, and the thermal strain rate should be made dependent on the current stress state:

$$\Delta\varepsilon = \alpha_T \Delta T \bullet \left(1 + \rho \bullet \frac{\sigma}{f_c'}\right) \tag{2.22}$$

Bažant (1985a) assumed that the creep rate depends on the micro diffusion of water between the macropores and the micropores in the cement gel. Since the microdiffusion is driven by a humidity- and temperature gradient, the rate depends on pore humidity $\dot{h}$ and temperature $\dot{T}$. Bazent proved mathematically that this theory is equivalent to the assumption about stress-induced shrinkage and stress-induced thermal strain.

$$\Delta\varepsilon_T = \alpha_T \Delta T \bullet \left(1 + \rho \bullet \frac{\sigma}{f_t'} \bullet sign(\Delta H)\right) \tag{2.23}$$

$$\Delta\varepsilon_h = k\Delta h \bullet \left(1 + r \bullet \frac{\sigma}{f_t'} \bullet sign(\Delta H)\right) \tag{2.24}$$

$$\Delta H = \Delta h + c\Delta T \tag{2.25}$$

This model is applied in the present study to determine the parameter ρ by calibrating of the transient thermal creep test.

2.6. Crack risk assessment

2.6.1. Temperature criteria

In the past, prediction of the early age cracking was almost exclusively based on temperature criteria. The temperature development in the young concrete was calculated and cracking predicted from the maximal temperature difference in a structure. To avoid cracking, limitations were applied to maximum temperature, temperature difference between the surface and the center of the structure, and between the new and the older adjoining structure. These limitations were based on practical experience and experience from the laboratory.

The "cracking frame", originally developed in Germany in the 1960s, had been employed as method for the thermal stress measurement of early age concrete. Springenschmid et al. (1985) developed an improved frame, named "temperature stress testing machine" (TSTM), to provide 100% restraint and temperature control formwork. In the frame an electronically controlled step motor moves one of the crossheads in order to keep the distance between gauge marks at the center of specimens constant. A load cell registers the restraint force. Twin specimens were used, one of them was restrained and the other free to deformation. The stress induced due to restrained deformation is recorded, while the strain in the other specimen undergoing free shrinkage is also measured. They use a criterion, T_{crack}, to characterize the cracking tendency directly from each test. An example of such test was shown in Figure 2-36.

The main drawback of the temperature based crack risk estimation is that the other important factors in stress calculation are not considered: restraint conditions, material properties and shrinkage. Several researcher, (Emborg, 1989) and (Bernander 1994) have shown that there is no general correlation between stresses and temperature. Whether young concrete will crack or not, depends very much on restraint conditions and material properties.

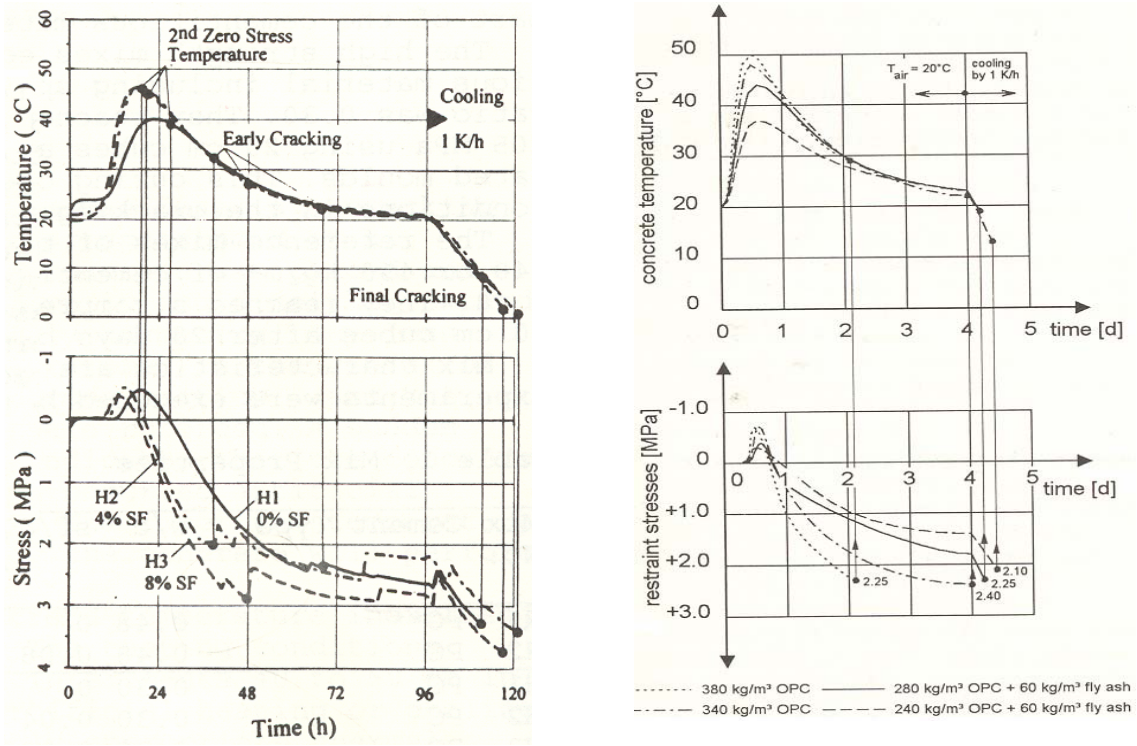

Figure 2-36 The stress measurement in the cracking frame (I. Schrage, Th. Summer, 1994)

2.6.2. Advanced numerical simulation

For reliable crack perdition at early ages strain-strain criteria must be applied. This calls for well-documented material models. In recent years an increased interest in cracking of hardening concrete has led to extensive research on this subject. A large number of material models for young concrete have been presented and implemented in computer programs for the simulation of stress development. Simulation of the hardening structure in general has to take into account temperature development due to hydration, development of material properties, and restraint conditions of the particular structure. Today there exist several commercially available computer programs capable of calculating the temperature and stress development in hardening concrete structure. Within the IPACS project a Round Robin calculation has been performed, and five different programs have been used to simulate temperature and stress development in two examples of hardening concrete structure, the results were shown in Figure 2-37. All calculations were based on same set of laboratory test results describing specific concrete properties. (Bosnjak, 2000)

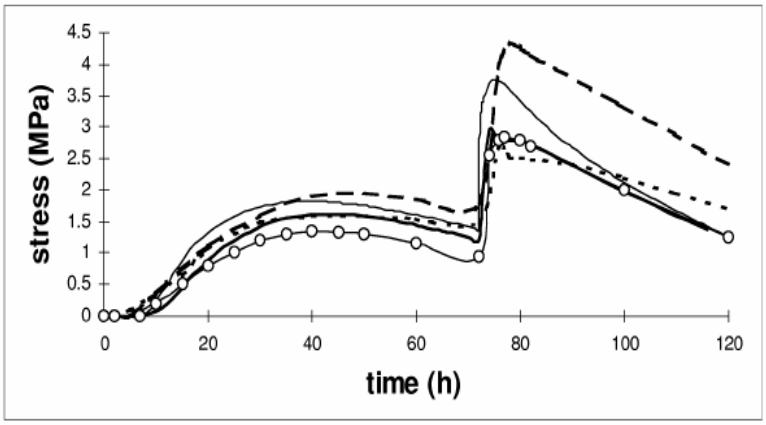

Figure 2-37 Stress development in hardening concrete slab calculated with different programs (J. Olafsson, M. Uhlán, 2000)

The deviation between the results obtained by different programs may be explained by differences in material modeling, modeling of geometry and restraint conditions. The deviations were considerable even in the case of stress simulation of hardening specimen in the TSTM with well defined temperature and restraining conditions, i.e. the material modeling was the only reason for disagreement. The different material models were calibrated to the same experimental data, but in simulation of total behavior of a structure they gave different results. The comparison gave rise several questions. What kinds of tests are most appropriate for characterization of different material properties? Although different material models are able to describe material properties separately, is the combination of the models able to describe the total behavior of hardening concrete structure, or do the different material models match with each other?

It is obvious that a thorough understanding of modeling of hardening concrete behavior is lacking, and that more research is necessary to bridge the gap between mathematical description of different phenomena on one hand, and their application in practical design on the other hand. (Bosnjak, 2000)

3. Experimental program

3.1. Introduction

Advanced testing methods combined with suitable modeling of material properties and accurate numerical analysis techniques are necessary for solid understanding and effective control of early age cracking.

During the hardening phase, the hydration reaction is constantly progressing and accompanied by volume changes due to thermal dilation and autogenous shrinkage, as well as the development of mechanical properties due to the changes in microstructure. Although all the processes occur simultaneously and are affected by diverse interacting factor, the determining material properties can still be identified, if carefully performed experiments are used in conjunction with appropriate analytical models.

The following material properties are main factors which influence the sensitivity of concrete to cracking at early age, and are required for a full evaluation of cracking risk in hardening concrete structures:

- The temperature sensitivity (activation energy)
- Heat of hydration
- Coefficient of Thermal Expansion (CTE)
- Autogenous Deformation (AD)
- Mechanical properties (E-modulus, compressive strength, tensile strength)
- Creep/relaxation properties

- Restraint Stress development in a TSTM (the test result is the net effect of the properties listed above)

All above listed material properties are determined by tests performed in the present study, and the test methods and procedures are described in detail in the following sections. In addition, a field test of a "double-wall" structure was carried out in 2004 by the Norwegian Public Road Administration (SVV), and this wall is comparable to the walls in the Bjørvika submerged tunnel which is under construction in Norway.

The test data of material properties is used directly as input for temperature and stress calculations of the wall. The calculations were first compared to the stress development in the TSTM, and then the material models are applied in 3-D numerical analysis of the field test to predict temperature, strain and stress development in real concrete structures.

3.2. Concrete composition

The concretes studied in the present investigation were divided into two series. The first series include 8 types of concretes: "Basic 5" for a trial test, "reference concrete", three types of

concretes containing 40%, 60% and 100% blast furnace slag, and three types of concretes containing 40%, 60% and 100% fly ash (FA and BFS contents are given as percentage of cement weight). The detailed composition is presented in Table 3.1. In the first series, the influence of mineral additives, such as FA and BFS, on the cracking risk of young concrete is generally investigated, and based on the test results, Norwegian Road Administration suggested a further investigation for FA concrete, and the second series were carried out. The second series include four types of concrete: "SV 40" concrete (a typical Norwegian high performance concrete mix for bridges), Dutch (NL) slag cement concrete, and two concretes containing 40% and 60% fly ash. The detailed composition is presented in Table 3.2. Note that all concretes contain 5% silica fume of cement weight, and that the water/binder ratio is 0.45, except for "Basic 5" and SV 40 concrete which have water/binder ratio=0.40.

Table 3.1 Concrete compositions (first series)

Materials	Concrete fraction (Kg/m^3), Nominal values							
	REF	40% BFS	60% BFS	100% BFS	40% FA	60% FA	100% FA	Basic 5
NORCEM Anleggsement (c)	359.5	263.4	232.5	188.2	263.7	232.9	188.2	367
Silica fume (s)	18.0	13.2	11.6	9.4	13.2	11.6	9.4	18.0
Fly ash (FA)	-	-	-	-	105.5	139.6	188.2	-
Blast furnace slag (BFS)	-	105.4	139.5	188.2	-	-	-	-
Water (w)	178							154
Norstone 0-8 mm	1002	995	994	988	965	958	935	
Norstone 8-16 mm	880							
Sikament 92	1.9	1.9	1.9	1.9	1.9	1.9	1.9	
Measured values: Fresh concrete								
Air (%)	1.8	1.6	1.6	1.1	1.4	1.1	0.9	
Density (Kg/m^3)	2430	2410	2410	2400	2410	2370	2350	
Slump (mm)	125	125	140	200	150	160	200	
Binder composition (ratio and volumes)								
s/c ratio	0.05	0.05	0.05	0.05	0.05	0.05	0.05	0.05
FA or BFS/c ratio	-	0.40	0.60	1.00	0.40	0.60	1.00	-
FA or BFS/(c+s+FA+BFS) ratio	-	0.276	0.364	0.488	0.276	0.364	0.488	-
Binder and water volume (ltr)	301	305	306	307	316	321	327	280
w/(c+2s+FA+BFS) ratio	0.450	0.450	0.450	0.450	0.450	0.450	0.450	0.40

Note: 40% BFS - FA or BFS contents are given as percentage of cement weigh

Table 3.2 Concrete compositions (second series)

Materials	Concrete fraction (Kg/m^3), Nominal values				
	40% FA*	60% FA*-1	60% FA*-2	SV 40*	NL Slagcement*
NORCEM Anleggsement (c) NL Slaggsement (c)	263.7	232.9		404.1	 382.1
Silica fume (s)	13.2	11.6		20.2	6.7
Fly ash (FA)	105.5	139.7		-	-
Blast furnace slag (BFS)	-	-		-	-
Water (w)	178	178		178	178
Norstone 0-8 mm	912	899		910	948
Norstone 8-16 mm	880	879		880	877
Visco-Crete 140	0.57	0.58		0.48	0.39
SIKA BV-40	1.91	1.92		2.13	1.94
AER-S (1:9)	2.01	2.56		0.36	0.33
Scancem demper	0.08	-		-	-
Measured values: Fresh concrete					
Air (%)	4.7	5.8	6.1	4.3	3.4
Density (Kg/m^3)	2320	2260	2260	2370	2340
Slump (mm)	170	165	215	70	200
Binder composition (ratio and volumes)					
s/c ratio	0.05	0.05		0.05	0.02
FA or BFS/c ratio	0.40	0.60		-	0.74/0.26=2.85
FA or BFS/(c+s+FA+BFS) ratio	0.276	0.364		-	0.74
Binder and water volume (ltr)	316	321		317	304
w/(c+2s+FA+BFS) ratio	0.450	0.450		0.400	0.450

Note: In order to distinguish with the first series, all the concretes tested in the second series marked with a prefix *

3.3. Test method

3.3.1. Hydration heat

The heat of hydration was determined by a semi-adiabatic calorimeter at SVV and NTNU. The test setup used at NTNU is according to Norwegian Standard NS3657, and consists of a box made of plywood, with an internal volume of 15 liters surrounding with lining of 100 mm EPS. The concrete sample is cast into the box immediately after mixing, afterwards the box is closed. The temperature development in the sample is recorded by the use of thermal-couples and a data logger, see Figure 3-1. The equipment used in SVV is similar in principle.

The total heat evolvement is defined to be the sum of the heat corresponding to the temperature increase and the heat loss to the surroundings due to the imperfect insulation. The heat flux from box is assumed to be proportional to the temperature difference between concrete and the ambient air. Heat loss can be characterized by temperature transmission coefficient which is deduced by the assuming a certain low rate of temperature increase at the end of the adiabatic curve, see Figure 3-2. The adiabatic temperature development can be converted to equivalent

isothermal heat evolvement. The calculation principle is described in Smeplass and Maage (1990).

Figure 3-1 Semi-adiabatic heat calorimeter

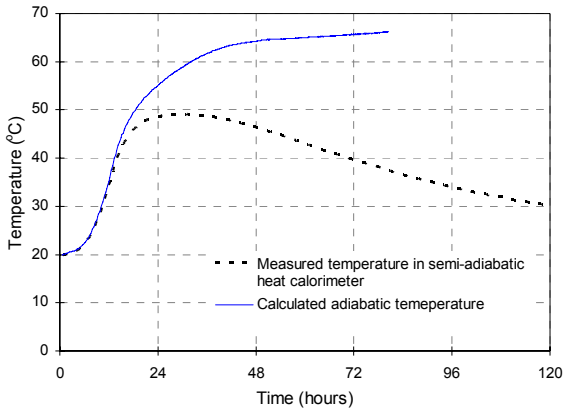

Figure 3-2 Measured semi-temperature and calculated temperature

3.3.2. Elastic modulus and compressive strength

Compressive strength tests were performed on 100×100 mm cubes according to Norwegian Standard NS3656 at SVV and NTNU. The activation energy (temperature sensitivity factor) of a given concrete was determined from compressive strength tests on specimens cured at 5, 20, and 50ºC isothermal temperatures from right after mixing.

The elastic modulus in compression is measured on 150×300 mm cylinders according to NS 3676, which is based on ISO 6784-1982. The test procedure includes two preloading cycles:

(1) Loading to 45% of ultimate load. Resting period 90 sec. Unloading followed by a new 90 sec resting period.
(2) Loading to 30% of ultimate load. Resting period 60 sec. Unloading followed by a new 60 sec resting period.
(3) Loading to 30% of ultimate load. Resting period 90 sec. Unloading followed by a new 90 sec resting period.

The modulus of elasticity is determined from the unloading part of step 3 (including the subsequent 90 sec resting period). The loading rate is 0.8 MPa/sec and the deformation is measured over the 120 mm mid section using 3 displacement transducers. The test setup is shown in Figure 3-3.

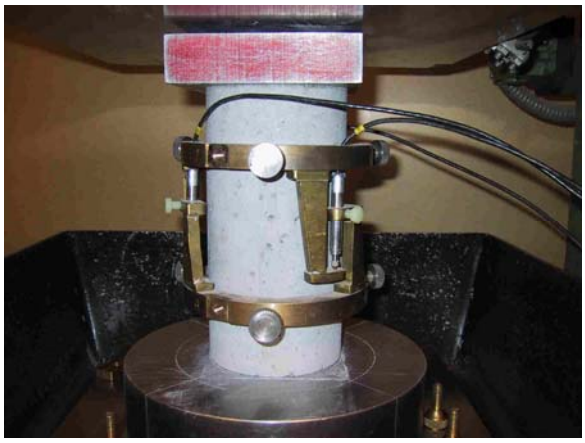

Figure 3-3 Elastic modulus test in compression

The E-modulus in the creep tests is determined from the first loading, and is slightly higher than the E-modulus measured by above test procedure.

3.3.3. Tensile strength

The tensile strength was determined both by direct tensile tests and by tensile splitting tests at NTNU, while it was only determined by tensile splitting tests at SVV. The unixial tensile strength test is measured on the 90×100×600 prismatic specimen in TSTM after the restraint stress test under realistic temperature histories for several types of concretes, and the data well represents the direct tensile stress in massive concrete structure experienced a heating-cooling temperature cycle.

Tensile splitting test have been widely used because of the difficulties in performing the direct tensile test. The tensile splitting strength was usually measured on 100×100 mm cubes, and the load is applied along two opposite generatrices, as shown in Figure 3-4. According to linear elastic theory a stress-field with tensile stresses normal to the load direction is established, the tensile splitting strength, f_{ts}, at failure is found as:

$$f_{ts} = \frac{2P}{\pi D^2} \tag{3.1}$$

P=the failure load, D=cube length

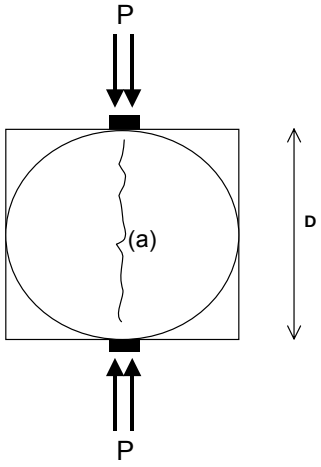

Figure 3-4 Tensile splitting test: principal set-up

3.3.4. Creep rig test

3.3.4.1. Compressive creep rig

Five compressive creep rigs, originally designed for long-term creep testing of mature concrete, were used in the present creep test for hardening concrete after the measurement system was updated from electrical strain gauge to the displacement transducer of the type Linear Variable Differential Transformer (LVDT) to improve the stability and accuracy of testing. The details of the compressive creep rig were described by Tomazewicz (1988). Each rig is equipped with a hydraulic jack and a spherical bearing plate to ensure uniform distribution of imposed load over the specimen. Hydraulic pressure in jacks was individually measured and controlled by a central hydraulic system, which included oil pressure accumulators.

The compressive creep tests can be performed only at room temperature (e.g. 20 ºC ±1 ºC). Three specimens were used in each compressive creep test. Two active specimens were loaded to measure the load-dependent deformation and the third passive one was kept unloaded to measure the load-independent deformation simultaneously, which represents autogenous shrinkage in this case. After the mixing, the concrete is cast in five moulds, and stored under 20 ºC in the temperature control room. All five specimens are demoulded at 2 days, and covered with aluminum foil immediately to prevent evaporation of water. Three of them are used to conduct creep test at 2 days, and other two are used to conduct the creep test at 7 or 8 days.

In the old measuring system, the deformation was measured by using a set of three TLM electrical strain gauges (type PL-60-11), glued on each of the 150×300 mm cylindrical specimens with 120º distance. During the first few trial tests, it was found that the moisture content of concrete specimens at very early age was too high for the glue to fix the strain gauges on the surface of the specimens, and sometimes specimens had to be set in dry condition for 1-2 hours to wait for the glue to solidify. The moisture condition is essential for the development of autogenous shrinkage at early age, and moisture exchange with environment during the test procedure introduces a measuring error (drying creep and drying shrinkage). Therefore, the new LVDT-based measuring system was made to avoid the problem. Each specimen is equipped with three strain measurement devices (LVDT), which are mounted with 120º distance on the surface of the specimens.

Figure 3-5 Compressive creep rigs equipped with oil pressure accumulators (Note: old measurement system)

3.3.4.2. Tensile creep rig

The tensile creep rig was recently developed and built in the NTNU laboratory, and was described in detail by Atrushi (2003), see Figure 3-6 and Figure 3-7. The rig consists of two parts: the creep frame, which is a vertical steel frame, and a horizontal loading frame. The tensile load is applied on the "active" specimen through a lever arm system by changing the position of a dead weight on the arm. Load-independent strain (i.e. thermal dilation and autogenous shrinkage) is always measured simultaneously on an unloaded (dummy) specimen. Both specimens are covered with aluminum foil during testing in order to prevent evaporation of water.

Each specimen is equipped with three strain measurement devices (LVDT), which are mounted with 120º distance on the surface of the specimen. Both the loaded and the dummy specimen are placed in temperature-controlled chambers, and the test can be performed under different isothermal temperature conditions. For each tensile creep test two specimens with dimension of 103×425 mm are used. One specimen is loaded at each loading time, and one dummy specimen is used simultaneously to measure free deformation. The creep strains are determined by subtracting the strains of the dummy specimen from the strains of the active.

Difficulties in tensile creep test were discussed by Atrushi (2003). The reproducibility tests performed by Atrushi showed that under variable temperature conditions the instability of the measuring system seriously affects the reliability of the strain output, and therefore only tests under different isothermal temperature conditions was carried out in his investigation. Another concern in the measuring system is that two measuring frames were fastened to the 150 mm mid section of the specimen by six bolts. Pores or sand may exist right under the surface layer of the concrete specimen, and if some bolts meet them, the frames would not be perfectly fixed on the specimen. When the specimen is under loading, independent movement may be induced in the frames and LVDT during test.

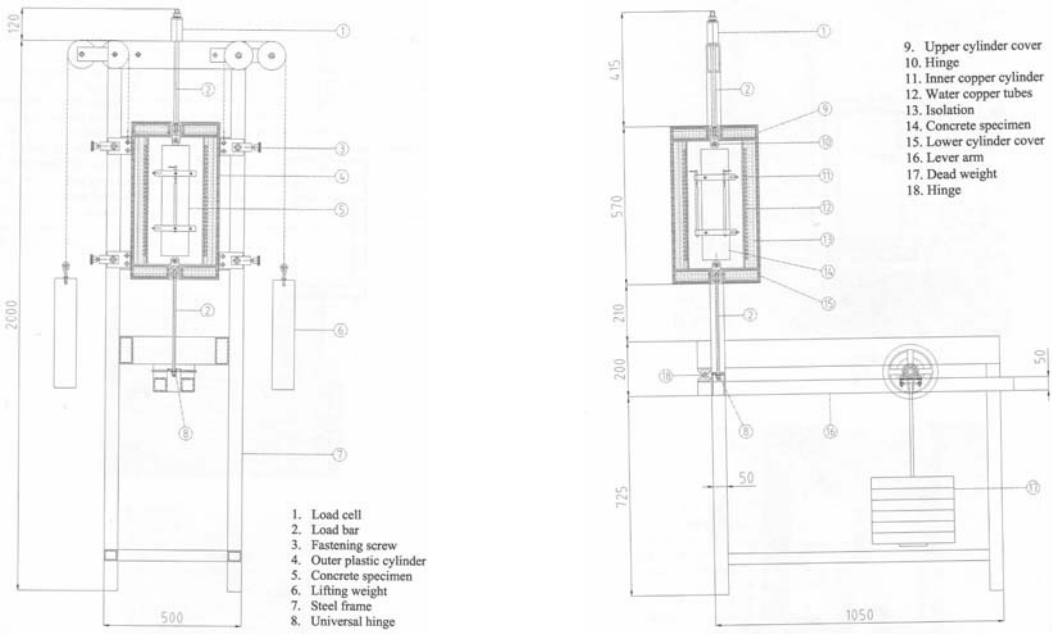

Figure 3-6 Tensile creep rig: principle sketch

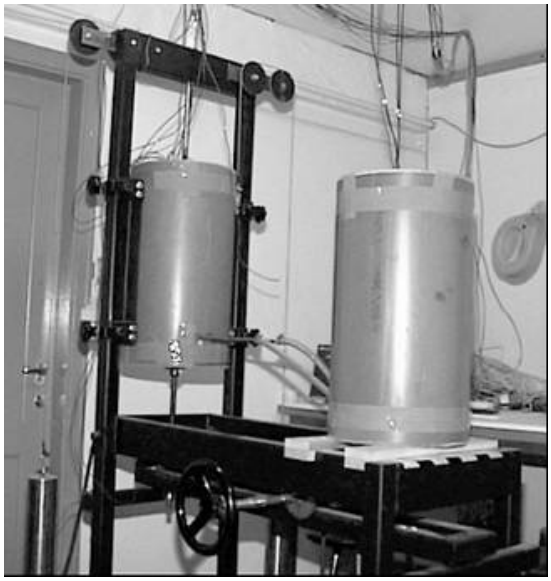

Figure 3-7 Tensile creep rig with dummy specimen (right)

3.3.5. Free deformation test in Dilation Rig

The Dilation Rig is constructed to measure free deformation of concrete, i.e. thermal dilation and autogenous shrinkage, from about 1 hour after mixing. In the present study, the specimen is sealed with an aluminum plastic foil impermeable to moisture, and drying shrinkage is avoided to occur. The rig is equipped with a temperature control system, which allows the tests to be performed under any desired temperature history.

The cross section of the specimen is 100×100 mm and the length is 500 mm. The length change is measured by inductive displacement transducer at each end of the specimen. Each signal is

recorded separated and added to obtain the total length change. A thermal couple measures the temperature in the center of the specimen. The test setup is shown in Figure 3-8.

In the standard procedure the TSTM and the Dilation Rig run in parallel to produce "compatible data" for re-calculations of the restraint stress development from TSTM. The Dilation Rig test is run with a stepwise temperature history, and such procedure allows us to separate the deformation into thermal dilation (CTEs are calculated at each step) and autogenous deformation (AD is measured directly during every isothermal period), as shown in Figure 3-9.

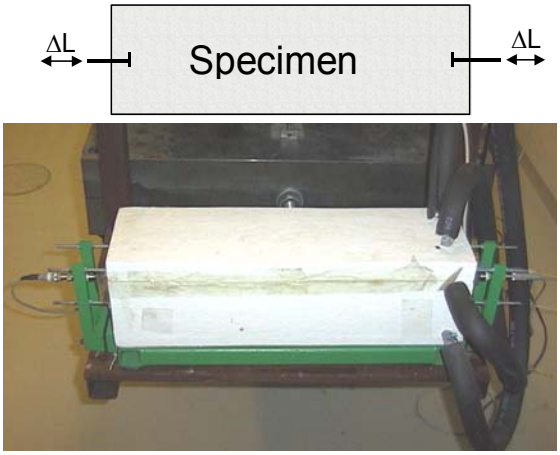

Figure 3-8 Dilation rig measuring free deformation

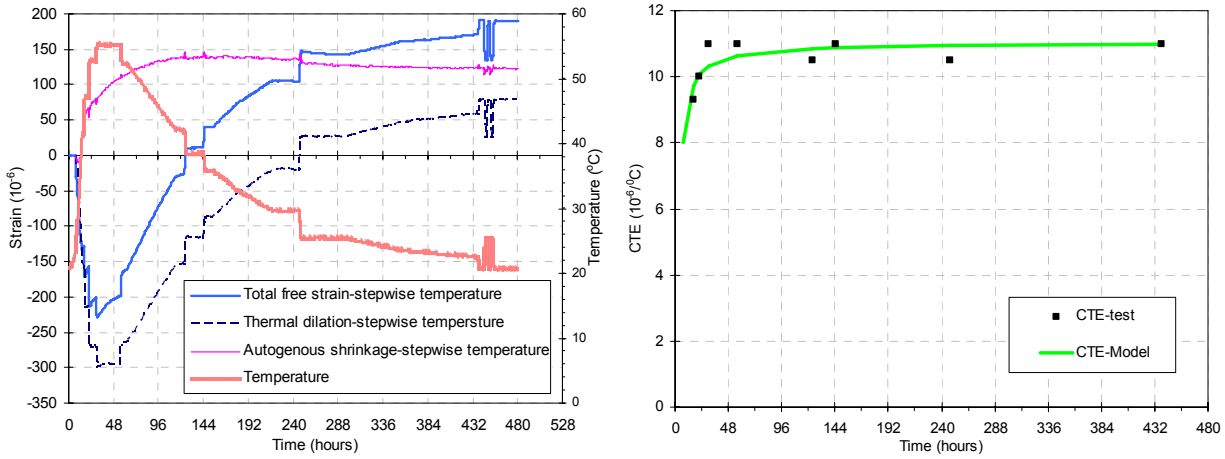

a) Imposed temperature and free deformation b) Calculated CTE

Figure 3-9 Example from Dilation Rig test

3.3.6. Restraint stress test in TSTM

The systems of the special designed Temperature Stress Test Machine (TSTM) as shown in Figure 3-10 is essentially a closed loop servo system that can be operated either in load or deformation control mode. The main part of the system is the servo controller with the operator, and it controls the balance between the desired and the actual value of load or position which provides the driving signal for a Lenze servo drive. This in turn consists of an amplifier and a motor driving the loading screw with a pitch of 1 mm through a 1:70 reduction gear.

The servo controller is of conventional design where the demand set on the balance pot and read on the little DVM (3 digits "+" for tension, "-" for compression) is subtracted by the actual value from the load or position transducer and the difference, amplified if necessary, is the input to the Lenze servo drive. When the desired load or position has been reached the difference is zero and the motor stops and from then on makes small correcting movements to maintain the desired load or position.

The cross section of the specimen is 90×100 mm and the total prismatic length is 1000 mm, and at the both ends the dimensions are increased in crossheads forming the anchorage. The temperature control system of the TSTM is similar to that of the Dilation Rig. In the present study, the specimen is sealed with an aluminum plastic foil impermeable to moisture, and drying shrinkage is thus avoided.

The TSTM is operated in deformation control mode. Tests can be performed under full (100%) or partial restraint. The full (100%) restraint condition is provided by an electronic feedback system that moves the left anchoring head of the specimen to compensate for the any length change in the 700 mm mid section of the specimen. A load cell, connected to the right anchoring head, records the restraining force. A partial restraint situation is obtained simply by deactivating the feedback system, meaning that the restraint against deformation is provided by the stiff steel frame of the rig and the anchorage of the specimen (hence, the restraint degree may vary from test to test, but it is generally around 40% (Bjøntegaard, 1999)).When partial restraint is used, the deformation of the 700 mm section is recorded as well as the restraining force. The advantage with the partial restraint situation is that an early tensile failure of the specimen is avoided during variable temperature development.

The stress development measured in the TSTM is the net effect of all the parameters acting to produce restraint stresses in hardening concrete (*i.e.* thermal dilation, autogenous deformation, elastic modulus, and creep/relaxation properties). The TSTM results are used directly for cracking risk comparison of different types of concretes and/or to calibrate the material models by re-calculating the restraint stress development in the TSTM.

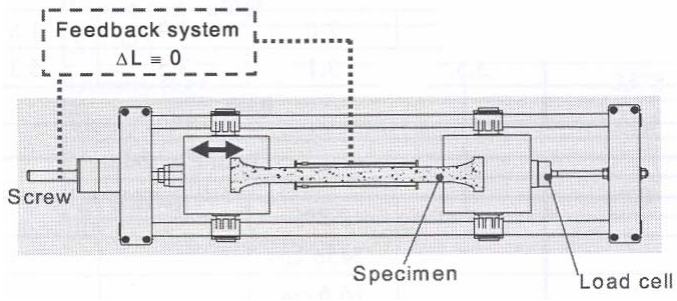

Figure 3-10 Temperature stress test machine

3.3.7. Creep test in modified TSTM

As part of the present study the TSTM was modified to perform creep test in compression or tension, and the main improvement include a new voltmeter added on the front panel and some adjustments of the feedback system. The input of the feedback system now can be easily switched between the LVDT-signal (deformation controlled relaxation mode, *i.e.* self-induced stress measurement) and the load cell signal (load controlled creep mode, *i.e.* creep test) according to choice.

Creep testing in the modified TSTM, as shown in Figure 3-11, operates according to following procedure: at the start of a creep test, the desired load (tension or compression) is set as a given voltage on the voltmeter and the feedback system is switched on in load control mode. The loading is applied in the following way: initially the rate of loading is relatively rapid, and then it decreases as the "actual load" approaches the "set load". The desired load is reached within one minute. From then on the load is kept constant by the feedback system. In the present study, the creep test in tension was performed in the modified TSTM and in either the tensile or compressive creep rig in parallel for comparison.

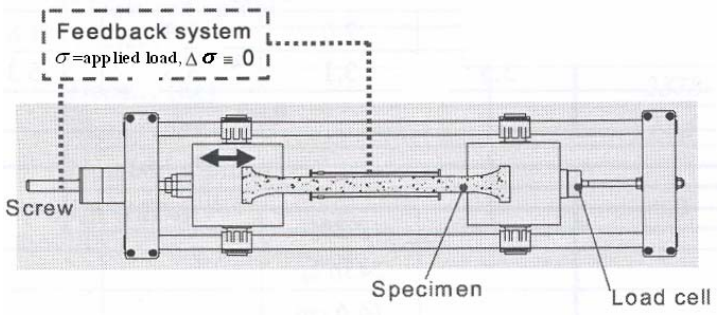

Figure 3-11 Modified TSTM for creep test

3.3.8. Transient thermal creep test in TSTM

Under variable temperature conditions, while the concrete is under load, an additional creep component, the so-called transient thermal creep, develops during the temperature change. The advantage of the temperature control system in the modified TSTM and the Dilation Rig makes it possible to perform creep test under variable temperature conditions at constant load. And in the present study, the transient thermal creep tests were performed for young and hardened "basic 5" concrete.

Transient thermal creep $\varepsilon_{ttc}(T,\sigma)$ during heating/cooling under constant stress can be determined indirectly from the total strain $\varepsilon_{tol}(T,\sigma)$ given by the following expression:

$$\varepsilon_{tol}(T,\sigma)=\varepsilon_{ttc}(T,\sigma)+\varepsilon_{el}(T,\sigma)+\varepsilon_{c}(T,\sigma)+\varepsilon_{th}(T,0)+\varepsilon_{sh}(T,0) \quad (3.2)$$

$$\varepsilon_{v}(T,\sigma)=\varepsilon_{el}(T,\sigma)+\varepsilon_{c}(T,\sigma) \quad (3.3)$$

$$\varepsilon_{free}(T,0)=\varepsilon_{th}(T,0)+\varepsilon_{sh}(T,0) \quad (3.4)$$

Where $\varepsilon_{v}(T,\sigma)$ is the viscoelastic strain under variable temperature and constant load condition, and $\varepsilon_{free}(T,0)$ is the free strain measured under same variable temperature condition.

3.3.8.1. Hardened concrete

The concrete specimens were sealed by watertight aluminum and stored in a temperature control room (20 ±0.5 ºC) for more than two months, and then two specimens were placed in the modified TSTM and the Dilation Rig respectively under 20ºC and free restrain condition, and they were set there for several days to release any possible initial restraint and load.

The uniaxial load (compression or tension) was then applied in the TSTM, at a rate of 0.2 MPa/s, until the required loading level was reached. The maximum load capacity (compression and tension) of modified TSTM is about 9 MPa, and the applied constant load was about 10% of compressive strength or about 20% of tensile strength measured at 20ºC.

One day after the loading, the specimens in the TSTM and the Dilation Rig were heated from 20 to 65ºC simultaneously at a constant rate of 0.2ºC/min, and the time of heating is estimated to be 3-4 hours, then the temperature level of about 65ºC were maintained constant for 1-2 days to ensure the stabilisation of internal temperatures. At the end of the heating cycle, the specimens were then cooled down from 65 to 20ºC at a rate of 0.2ºC/min. After a delay of at least a week at 20ºC temperature condition, some specimens were submitted to a second identical heating–cooling cycle. The sketch of the test process including the temperature and loading history is shown in Figure 3-12.

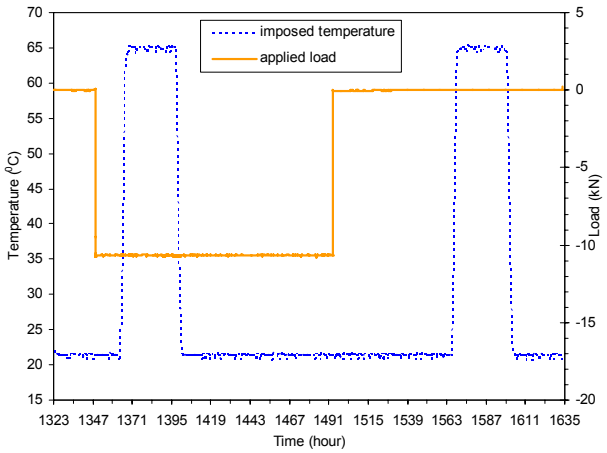

Figure 3-12 Temperature and loading history of transient thermal creep test in tension

During the test, the elastic strain at 20ºC temperature was instantaneously recorded when the load is applied, and the measured strain in modified TSTM is the sum of the elastic and creep

stain when temperature is constant, and the additional thermal dilation and transient thermal creep is developed while the temperature is changed. To determine the transient thermal creep, it was also necessary to measure the free (unloaded) deformation of sealed mature concrete, i.e. thermal strain in this case. It is measured by imposing a similar heating–cooling cycle without load in the Dilation Rig or TSTM. The magnitude of transient thermal creep is then calculated by subtracting the elastic, creep and thermal strain from the total strains measured in modified TSTM in the load condition:

$$\varepsilon_{ttc}(T,\sigma) = \varepsilon_{tol}(T,\sigma) - \varepsilon_{el}(T,\sigma) - \varepsilon_{c}(T,\sigma) - \varepsilon_{th}(T,0) \tag{3.5}$$

3.3.8.2. Young concrete

A similar test procedure was also applied for young concrete. The fresh concrete was cast in the TSTM and the Dilation Rig respectively after mixing, and then they were cured under 20ºC, sealed and free restraint condition for 1 day before the load was applied in the TSTM.

The uniaxial load (compression or tension) was only applied on the TSTM, at a rate of 0.2 MPa/s, until the required loading level was reached. The maximum load capacity of modified TSTM is about 9 MPa, and the applied initial load was about 20% of compressive strength or about 30% of tensile strength measured at loading time under 20ºC curing temperature.

The specimens in the TSTM and the Dilation Rig were heated from 20 to 65ºC simultaneously at a constant rate of 0.2ºC/min at 12 hours after loading, and the time of heating process is estimated to be 3-4 hours, then the temperature level of about 65ºC were maintained constant for 1-2 days to ensure the stabilisation of internal temperatures. At the end of the heating cycle, the specimens were then cooled down from 65 to 20ºC at a rate of 0.2ºC/min. The sketch of the test process including the temperature and loading history is shown in Figure 3-13.

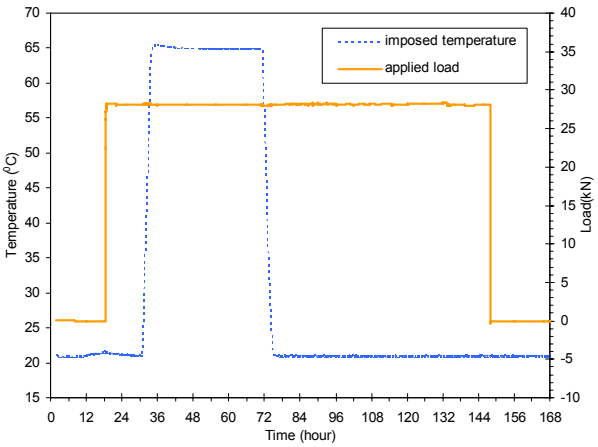

Figure 3-13 Temperature and loading history of transient thermal creep test in compression

The free (unloaded) deformation measured in young concrete is the combination of thermal dilation and autogenous shrinkage. Transient thermal creep $\varepsilon_{ttc}(T,\sigma)$ during heating/cooling under constant stress is determined indirectly by subtracting the elastic, creep and free deformation from the total strain $\varepsilon_{tol}(T,\sigma)$ in the load condition:

$$\varepsilon_{ttc}(T,\sigma) = \varepsilon_{tol}(T,\sigma) - \varepsilon_{el}(T,\sigma) - \varepsilon_{c}(T,\sigma) - \varepsilon_{th}(T,0) - \varepsilon_{sh}(T,0) \tag{3.6}$$

3.4. Test program

3.4.1. Laboratory test

Experimental tests on semi-adiabatic hydration heat and mechanical properties, such as compressive strength, elastic modulus and tensile strength, were conducted both at SVV in Oslo and at NTNU. Creep tests in compression and tension were performed by Ji (2005) at NTNU, and Dilation rig tests measuring thermal dilation and autogenous deformation and TSTM tests were carried out parallel by Bjøntegaard (2002, and 2003) at NTNU. The overview of the test program is shown in Table 3.3. Therefore, well documented material models based on experimental data will be implemented in 1D-calculations (re-calculation of restraint stress development in TSTM) and 3D cracking risk analysis of concrete structures.

The overview of the concrete specimens used in creep rig is given in Table 3.4, and the complete test programs including the loading age and the duration of the creep test are presented in Table 3.5. Totally 14 compressive and 15 tensile creep tests were conducted covering several types of concretes. The concretes were loaded roughly after 2 days and 1 week respectively after mixing, and the duration of each test varied from 5-42 days. In the present study, both the creep rig in compression and tension are placed under $20 \pm 0.5^{\circ} C$ in a temperature control room.

One tensile creep test was performed in parallel in the creep rig and modified TSTM for reference concrete at age of 2 days. Two transient thermal creep tests were performed for hardened concrete, test No.183 is under compression and test No.173-2 is under tension. Four transient thermal creep tests were performed for young concrete, and among them test No. 172 is under compression, and test No. 173 is under tension. The overview of the transient thermal creep test is presented in Table 3.6.

Table 3.3 Test program overview

Test / Concrete	Activation energy(1)	Hydration heat	Elastic modulus	Tensile strength	Creep		Dilation Rig		TSTM
					tensile	compressive	CTE	AD	
Basic 5						(N)			
Ref		(S, N)(2)	(S, N)	(S, N)	(N)	(N)	(N)	(N)	(N)
40% FA		(S, N)	(S, N)	(S, N)			(N)	(N)	(N)
60% FA		(S, N)	(S)	(S)			(N)	(N)	(N)
100% FA		(S, N)	(S, N)	(S, N)		(N)	(N)	(N)	(N)
40% BFS		(S, N)	(S, N)	(S, N)		(N)	(N)	(N)	(N)
60% BFS		(S, N)	(S, N)	(S, N)	(N)	(N)	(N)	(N)	(N)
100% BFS		(S, N)	(S, N)	(S, N)	(N)		(N)	(N)	(N)
SV 40*	(S)	(S, N)	(N)	(N)	(N)	(N)	(N)	(N)	(N)
NL Slagcement*	(S)	(S, N)	(N)	(N)	(N)		(N)	(N)	(N)
40% FA*	(S)	(S, N)	(N)	(N)	(N)	(N)	(N)	(N)	(N)
60% FA*	(S)	(S, N)	(N)	(N)	(N)	(N)	(N)	(N)	(N)

(1) Activation energy is determined from compressive strength tests at 5, 20, and 50ºC isothermal temperatures
(2) S - test is performed at SVV, N - test is performed at NTNU

Table 3.4 Concrete specimens used in creep rig and standard compressive strength test

Number of specimens	Dimension (mm)	Test	Use of specimen
3	150x300 (cylinder)	Compressive creep	2 Loaded (active) 1 Unloaded (dummy)
2	103x425 (cylinder)	Tensile creep	1 Loaded (active) 1 Unloaded (dummy)
3	100x100x100 (cubic)	Compressive strength	3

Table 3.5 Overview of the creep testing: loading age and the duration of test

Concrete	Compressive creep rig		Tensile creep rig		
	loading(duration)	loading(duration)	loading(duration)	loading(duration)	loading(duration)
Basic 5*	2d(5d)	7d(14d)			
SV 40*	2d(7d)	9d(20d)	2d(7d)		9d(12d)
40% FA*	3d(5d)	8d(9d)	2d(20d)		8d(9d)
60% FA*	4d(46d)	7d(8d)	2d(5d)	4d(42d)	7d(9d)
FA 100%		7d(8d)			
NL Slagcement*			2d(5d)	3d(10d)	8d(15d)
Reference		7d(9d)	2d(5d)		7d(8d)
40% BFS	2d(5d)	7d(7d)			
60% BFS	2d(5d)	7d(7d)	2d(5d)		7d(7d)
100% BFS			2d(5d)		

Table 3.6 Overview of transient creep test

Test No.	TSTM				Dilation Rig
	Load (KN)		Loading age	Loading duration	
	compression	tension			
183	53.4		1.2 year	16 days	yes
173-2		10.6	60 days	6 days	yes
170(1)	yes (under unloaded condition and specified temperature history)				yes
171	failed				yes
172	28.0		18.7 hours	130.3 hours	yes
173		4.7	30.2 hours	117.1 hours	yes

(1) For Test No. 170, free deformations were measured in both the TSTM and the Dilation Rig under similar temperature histories to verify the reproducibility of the test methods

3.4.2. Field test

As part of the "Bjørvika Submerged Tunnel Project", a great deal of R&D work has been carried out by the Norwegian Public Roads Administration (SVV) in order to develop a "low-heat" concrete with a minimal risk of early age cracking. The project involved the first submerged concrete tunnel in Norway designed for traffic, and was constructed crossing the harbour of Oslo. Focus has been set on building a crack-free and water tight structure.

In order to evaluate the crack risk of the "low-heat" concrete, a field investigation on a specially designed structure with relevant dimensions was carried out in the summer 2004 in Oslo, Norway. It was essential to compare the cracking risk of "low-heat" concrete with that of "SV 40" concrete which is commonly used in Norway. The "double-wall" structure was tested in the field – one wall for each type of concrete and the slab with "SV 40". The dimensions of the walls and the slab were chosen to represent the approximate restraint conditions of the submerged tunnel, see Figure 3-14. The length of the structure is 15m. The slab was about 2 ½ weeks old when both walls were cast at same time.

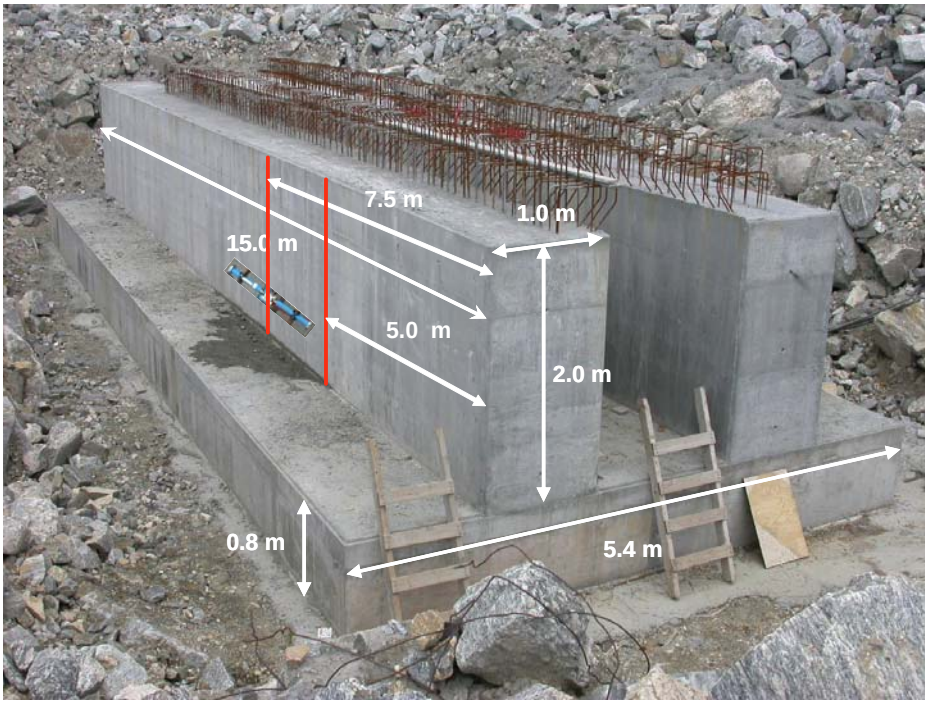

Figure 3-14 Field test

A total of 26 strain gauges of the vibrating-wire type (GEOKON VCE-4200) were installed prior to casting. These strain gauges measure simultaneously both temperature and strain in the same position. Hence, concrete strains can be calculated by compensating temperature strain of the strain gauges. 24 strain gauges were installed in two sections of the structure – 5.0 and 7.5 meters from the south end, all longitudinal with respect to the length-axis of the structure. For each section 4 gauges were installed in each wall (8 in total) and 4 gauges in the slab (2 under each wall), as can be seen in Figure 3-15. In addition, for each wall one strain gauge was installed transverse to the length-axis 0.75m from the south end of the structure to measure the approximated free-deformation (no stresses) strains. Numerical simulations were performed by Diana to compare the calculated results with the measurements as described later in Chapter 6.

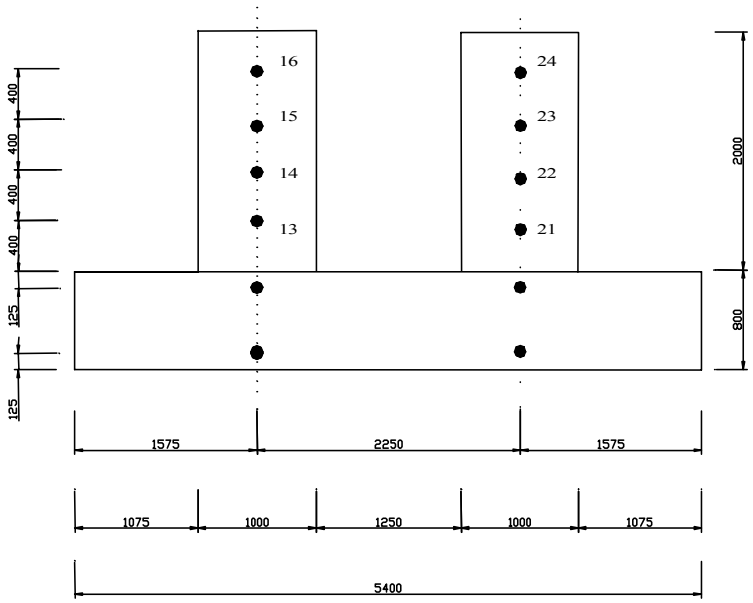

Figure 3-15 Middle cross-section of the "double-wall" structure and the positions of the strain gauges (black dots). (Dimensions in mm)

4. Material model and solution method

The coupled thermo-chemo-mechanical analysis of young concrete based on the theory of reactive porous media within thermodynamic framework was carried out by Ulm and Coussy (1995, and 1996) and Ulm (1998). The constitutive relation of macroscopic model described by chemo-mechanical cross-effect and chemo-thermal cross-effect is further simplified and used in the analysis of the young concrete structure.

4.1. Constitutive relation of macroscopic model based on theory of reactive porous media within thermodynamic framework

Within the framework of reactive porous media, concrete is considered as a porous medium composed of a skeleton and some fluid phases saturating the macro-porous space (capillary pores the width of which are larger than 1 μm). The solid part of the medium is formed of unhydrated cement and hydrates. The hydration process is viewed as a chemical reaction in which the free water is a reactant phase that diffuses through the layers of hydrates to the unhydrated cement and forms chemically and/or physically combined water in the new hydration product. The diffusion of water is considered as the dominant mechanism regulating the reaction kinetics.

For the sake of clarity, the system is considered as closed with respect to external flow (no external supply of water mass during hydration); and the water phase in the porous medium is only involved in the liquid-solid phase change of the hydration reaction. Applying standard thermodynamics, the intrinsic dissipation of the closed system reads:

$$\varphi = \boldsymbol{\sigma} : \dot{\boldsymbol{\varepsilon}} - S\dot{T} - \dot{\Psi} \geq 0 \tag{4.1}$$

where a dot denotes time derivation; $\boldsymbol{\sigma}$ and S are stress tensor and entropy. They are the thermodynamic forces associated to the rate of strain tensor $\boldsymbol{\varepsilon}$ and absolute temperature T respectively. Ψ is Helmholtz free energy, and is a function of the external state variables (absolute temperature T and strain tensor $\boldsymbol{\varepsilon}$) and of the internal state variables (plastic strain tensor $\boldsymbol{\varepsilon}^p$ and hardening/softening variable χ, associated with the irreversible skeleton deformation (for instance micro-cracking), and skeleton mass m involved in the hydration reaction). Free energy Ψ is assumed formally:

$$\Psi = \Psi\left(T, \boldsymbol{\varepsilon}, \boldsymbol{\varepsilon}^p, \chi, m\right) = \psi\left(\boldsymbol{\varepsilon} - \boldsymbol{\varepsilon}^p, T, m\right) + U\left(\chi, m\right) \tag{4.2}$$

where $U\left(\chi, m\right)$ is the part of free energy associated with plastic hardening/softening phenomena in the material. Then, using (4.1) and (4.2) yields:

$$\varphi = \left(\boldsymbol{\sigma} - \frac{\partial \Psi}{\partial \boldsymbol{\varepsilon}}\right) : \dot{\boldsymbol{\varepsilon}} - \left(S + \frac{\partial \Psi}{\partial T}\right)\dot{T} - \frac{\partial \Psi}{\partial \boldsymbol{\varepsilon}^P} : \dot{\boldsymbol{\varepsilon}}^P - \frac{\partial \Psi}{\partial \chi}\dot{\chi} - \frac{\partial \Psi}{\partial m}\dot{m} \geq 0 \tag{4.3}$$

In the case of no skeleton mass change ($\dot{m} = 0$), and no plastic evolutions occur ($\dot{\boldsymbol{\varepsilon}}^p = 0$, $\dot{\chi} = 0$), inequality equation (4.3) leads to following state equations:

$$\boldsymbol{\sigma} = \frac{\partial \psi}{\partial \boldsymbol{\varepsilon}} \; ; S = -\frac{\partial \psi}{\partial T} \tag{4.4}$$

Equation (4.4) still holds in the case of a reactive porous material and when plastic evolutions occur, and equation (4.3) then reads:

$$\varphi = \boldsymbol{\sigma} : \dot{\boldsymbol{\varepsilon}}^{p} + \zeta\dot{\chi} + A_m\dot{m} \geq 0 \tag{4.5}$$

with state equations:

$$\boldsymbol{\sigma} = \frac{\partial\psi}{\partial\boldsymbol{\varepsilon}}; \zeta = -\frac{\partial U}{\partial\chi}; A_m = -\frac{\partial\Psi}{\partial m} = -\frac{\partial\left(\psi + U\right)}{\partial m} \tag{4.6}$$

where A_m is affinity of the chemical reaction which expresses the thermodynamic imbalance between the free water and the water combined in the solid phase, and is the driving force of the microdiffusion process governing the hydration reaction. ζ is hardening force, which account for the evolution of the plastic threshold within the plastic criterion $f = f\left(\boldsymbol{\sigma}, \zeta\right) \leq 0$.

From the standpoint of constitutive modeling, the chemo-mechanical, chemo-thermal and chemo-plastic couplings can be derived from Maxwell-symmetries on the free energy. Since:

$$\frac{\partial\boldsymbol{\sigma}}{\partial m} = -\frac{\partial A_m}{\partial\boldsymbol{\varepsilon}} = \frac{\partial^2\psi}{\partial\boldsymbol{\varepsilon}\partial m}; \frac{\partial \mathrm{S}}{\partial m} = \frac{\partial A_m}{\partial T} = -\frac{\partial^2\psi}{\partial T\partial m}; \frac{\partial\zeta}{\partial m} = \frac{\partial A_m}{\partial\chi} = -\frac{\partial^2 U}{\partial\chi\partial m} \tag{4.7}$$

Differentiating the preceding state equations (4.4) and (4.6) leads to the incremental state equations:

$$d\boldsymbol{\sigma} = \frac{\partial^2\psi}{\partial\boldsymbol{\varepsilon}^2} : \left(d\boldsymbol{\varepsilon} - d\boldsymbol{\varepsilon}^{p}\right) + \frac{\partial^2\psi}{\partial\boldsymbol{\varepsilon}\partial T}dT + \frac{\partial^2\psi}{\partial\boldsymbol{\varepsilon}\partial m}dm \tag{4.8}$$

$$dS = -\frac{\partial^2\psi}{\partial T^2}dT - \frac{\partial^2\psi}{\partial T\partial\boldsymbol{\varepsilon}} : \left(d\boldsymbol{\varepsilon} - d\boldsymbol{\varepsilon}^{p}\right) - \frac{\partial^2\psi}{\partial T\partial m}dm \tag{4.9}$$

$$d\zeta = -\frac{\partial^2 U}{\partial\chi^2}d\chi - \frac{\partial^2 U}{\partial\chi\partial m}dm \tag{4.10}$$

$$dA_m = -\frac{\partial^2\Psi}{\partial m\partial\boldsymbol{\varepsilon}} : \left(d\boldsymbol{\varepsilon} - d\boldsymbol{\varepsilon}^{p}\right) - \frac{\partial^2\Psi}{\partial m\partial T}dT - -\frac{\partial^2\Psi}{\partial m\partial\chi}d\chi - \frac{\partial^2\Psi}{\partial m^2}dm \tag{4.11}$$

4.1.1. Chemo-mechanical cross-effect

The product of hydration reaction leads to stiffening of the concrete, which – at the macro-level of material description – appears as a variation of the elasticity modulus in time. At a micro-level of material description, this aging elasticity may be regarded as a change in the concentration of the non-aging constituents, i.e. the hardened cement gel.
Inverting state equation in (4.8) leads to:

$$d\boldsymbol{\varepsilon} - d\boldsymbol{\varepsilon}^{p} = \boldsymbol{C}^{-1} : d\boldsymbol{\sigma} + \mathrm{a}dT + \mathrm{b}dm \tag{4.12}$$

where $\boldsymbol{C} = \partial^2\psi / \partial^2\boldsymbol{\varepsilon}$ is elastic stiffness tensor, which depends on the hydration mass m [i.e. $\boldsymbol{C} = \boldsymbol{C}\left(m\right)$]; The second order tensors $\mathrm{a} = -\boldsymbol{C}^{-1} : \partial^2\psi / \partial\boldsymbol{\varepsilon}\partial T$ and $\mathrm{b} = -\boldsymbol{C}^{-1} : \partial^2\psi / \partial\boldsymbol{\varepsilon}\partial m$ are, respectively, the tensor of thermal dilation coefficient, which relates the temperature variation dT to strain increment of the thermal origin, and the tensor of chemical dilation coefficient, which relates the increases in hydration mass m to the strains of chemical origin. State equation (4.12) can be inverted into:

$$d\boldsymbol{\sigma} = \boldsymbol{C}\left(m\right) : \left(d\boldsymbol{\varepsilon} - d\boldsymbol{\varepsilon}^{p} - d\boldsymbol{\varepsilon}^{th}\left(T\right) - d\boldsymbol{\varepsilon}^{shr}\left(m\right)\right) \tag{4.13}$$

4.1.2. Chemo-thermal cross-effect

From the first and second principle of thermodynamics, the thermal field equation can be written in its entropy rate form as:

$$T_0 \dot{S} = Q + \varphi \tag{4.14}$$

where S is the internal entropy, $Q/T_0 = \left(R - \mathrm{div}\boldsymbol{q}\right)/T_0$ is the rate of external entropy supply provided by heat exchange with the exterior, in form of volume heat sources R and heat conduction ($-\mathrm{div}\boldsymbol{q}$, with heat flux vector $\boldsymbol{q} = -\boldsymbol{K}\mathrm{grad}T$ when adopting a linear isotropic conduction law). While φ/T_0 is the rate of internal entropy production due to dissipation φ. Using state equation (4.9) in (4.14), the thermal equation reads:

$$C_\varepsilon \dot{T} - T_0 \boldsymbol{A} : \left(\dot{\boldsymbol{\varepsilon}} - \dot{\boldsymbol{\varepsilon}}^P\right) - L_m \dot{m} = Q + \varphi \tag{4.15}$$

where $C_\varepsilon = -T_0 \partial^2\psi/\partial T^2$ is volume heat capacity per unit of volume; $T_0\boldsymbol{A} = T_0 \partial^2\psi/\partial T \partial \boldsymbol{\varepsilon}$ is the latent heat per unit of deformation $d\boldsymbol{\varepsilon} - d\boldsymbol{\varepsilon}^p$, due to the small order of magnitude of elastic strains in cementitious material, it can be considered negligible with respect to the hydration heat generation; $L_m = T_0 \partial^2\psi/\partial T \partial m$ is the latent heat of the hydration reaction per unit of solidification mass dm .The heat released by hydration reaction is due to latent heat effects ($L_m > 0$ due to the exothermic nature of the hydration reaction), as well as due to the hydration dissipation φ (i.e. $A_m \dot{m} \geq 0$), even though the latter can be considered as negligible with respect to the hydration heat. Then, heat equation (4.15) simplifies to:

$$C_\varepsilon \dot{T} = Q + L_m \dot{m} \tag{4.16}$$

4.1.3. Hydration kinetics

The diffusion of water through the layers of hydrates is considered as the rate-determining process of the hydration kinetics. Mass rate $\dot{m}$ can be viewed as measure of this diffusion rate. Thermodynamic considerations of chemically reactive porous media lead to postulate that the hydration of concrete is governed by two constitutive laws under sealed condition.

The first law links the mass rate $\dot{m}$ of the current hydrate to the affinity A_m of the reaction. Diffusion rate of water is controlled by the thermodynamic imbalance (affinity A_m) between free water and water combined in the solid phase, and amplified by thermal activation when the free water combined with unhydrated cement to form new hydrates. The kinetics law is assumed to be given as:

$$A_m = \eta(m)\frac{dm}{dt}\exp\left(\frac{E_a}{RT}\right) \tag{4.17}$$

Where E_a is hydration activation energy; R is idea gas constant. The factor $\exp\left(E_a/RT\right)$ accounts for the thermally activated character of the reaction according to the Arrhenius concept, while the factor $\eta(m)$, an increasing function of m, accounts for the increase of the thickness of the hydrates layers, which increases the micro-diffusion time of the free water to reach the unhydrated cement.

The second constitutive law is the state equation which relates the hydration affinity A_m to the current hydrate mass m. As described in state equation(4.11), affinity A_m may as well dependent on strain $\boldsymbol{\varepsilon}$ and $\boldsymbol{\varepsilon}^p$, temperature T, and hardening variable χ. As a first approximation, the affinity is assumed to depend significantly only on hydrate mass m, while the coupling of stress, temperature and plastic hardening/softening may be considered as weak and the effects of them are assumed to be negligible. Applying this weak coupling hypothesis to (4.11) and integrating leads to:

$$A_m \cong A_0 - a(m) \tag{4.18}$$

with $$a(m) = \int \frac{\partial^2 \Psi}{\partial m^2} dm$$

The affinity A_m decreases progressively from its initial value A_0, which depends on the characteristics related to the concrete mix design. At thermodynamic equilibrium, the reaction stops and affinity $A_m = 0$, using (4.18) it follows:

$$A_0 = a(m_\infty) \tag{4.19}$$

Where m_∞ is the asymptotic hydrate mass. The affinity is same for two identical concrete samples, provided the same initial affinity A_0. Therefore, for a given composition, the hydration degree can be intrinsically defined in following way:

$$\xi(t) = \frac{m(t)}{m_\infty} \qquad 0 \le \xi \le 1 \tag{4.20}$$

Furthermore, definition (4.20) together with (4.18) and (4.19) allows one to rewrite the kinetics law (4.17) in the form:

$$\tilde{A}(\xi) = \frac{d\xi}{dt} \exp\left(\frac{E_a}{RT}\right) \; ; \; \frac{d\xi}{dt} = \tilde{A}(\xi) \cdot \exp\left(\frac{E_a}{RT}\right) = g(\xi) \cdot f(T) \tag{4.21}$$

where $\tilde{A}(\xi)$ can be considered as normalized affinity [$\tilde{A}(\xi) \sim A_m(\xi)/\eta(\xi)$], which accounts for the thermodynamic nonequilibrium $A_m(\xi)$, as well as for the nonlinear diffusion process, expressed by $\eta(\xi)$, of free water through the increasing layers of hydrates already formed. The rate of hydration at a given degree of hydration is a function of temperature only.

It may be useful to introduce the maturity M, widely used to describe the effect of hydration kinetics on the evolution of the mechanical properties of concrete. It is defined as:

$$M(t) = t_e = \int_0^t \exp\left[-\frac{E}{R}\left(\frac{1}{T} - \frac{1}{T_{ref}}\right)\right] dt \tag{4.22}$$

Using (4.22) in (4.21) reduces the kinetics law to an ordinary differential equation:

$$\frac{d\xi}{dM} = \exp\left(-E_a / RT_0\right) \bullet \tilde{A}(\xi) \tag{4.23}$$

And it reveals the existence of unique relation between the maturity M and hydration degree ξ.

Hydration kinetics can be followed only indirectly through the effects the phenomenon induces, i.e. through its cross-effects with heat generation, strength evolution or autogenous shrinkage. The hydration kinetic can be determined by exploring the Maxwell-symmetries of the modeling, provided that the order of coupling is known. The data of adiabatic calorimetric experiments and isothermal strength evolution tests is used to determine the hydration kinetic.

4.2. Temperature development

The temperature distribution can be obtained by applying the thermodynamic energy conservation to space and time domain of interest, and convert from equation(4.16):

$$C\dot{T} = \dot{Q} + \dot{H} - div(q) \tag{4.24}$$
$$q = -k\nabla T$$

Where C denotes the heat capacity per unit volume, Q is the internal heat source associated to hydration reaction, H is the external heat source, q is the heat flux. k is the thermal conductivity.

Boundary condition:

- A boundary with prescribed temperature A_T
- A boundary with prescribed heat flux A_f, $q_n = q^T n = h$
- A convection boundary A_c, $q_n = \alpha(T - T_\infty)$
- Heating or cooling pipe L_{c_i}, $q = \beta(T - T_w)$

The heat of hydration is expressed in the simple three parameter equation, which is commonly used in engineering practice (Freiesleben 1977):

$$Q = Q_\infty \cdot \xi(t) = Q_\infty \bullet \exp\left(-\left(\frac{\tau}{t_e}\right)^\alpha\right) \tag{4.25}$$

4.3. Mechanical model: elastic modulus and tensile strength

In the present study, the modified version of CEB-FIP MC 1990 is used to describe the development of the compressive strength, tensile strength and modulus of elasticity (Kanstad, 1999):

$$f_c(t_e) = f_c(28) \bullet \left\{\exp\left[s \cdot \left(1 - \sqrt{\frac{28}{t_e - t_0}}\right)\right]\right\} \tag{4.26}$$

$$f_t(t_e) = f_t(28) \bullet \left\{\exp\left[s \cdot \left(1 - \sqrt{\frac{28}{t_e - t_0}}\right)\right]\right\}^{n_t} \tag{4.27}$$

$$E_c(t_e) = E_c(28) \bullet \left\{\exp\left[s \cdot \left(1 - \sqrt{\frac{28}{t_e - t_0}}\right)\right]\right\}^{n_E} \tag{4.28}$$

t_0 is introduced to identify the start of significant mechanical properties development, and it might be determined from a TSTM test, it is the time at which stiffness achieves value high enough to produce measurable stresses. The parameter s was determined from the compressive strength development, whereas parameters n_t and n_E were determined from the tensile strength and E-modulus tests, respectively.

4.4. Viscoelastic properties

4.4.1. Creep compliance

- Double power law

The creep of concrete at constant moisture and thermal state may be well described by power curves of load durations $t-t'$, and by inverse power curves of age t' at loading. This leads to the most well known compliance function: Double-Power law, Bažant and Panula (1978)

$$J\left(t,t'\right)=\frac{1}{E_0}+\frac{\varphi_1}{E_0}\left(t'^{-m}+\alpha\right)\left(t-t'\right)^n \tag{4.29}$$

The Double power law is originally proposed for hardened concrete. It was modified to describe the creep property of early age concrete by taking into account the aging characteristics of young concrete:

$$J\left(t,t'\right)=\frac{1}{E\left(t'\right)}\left[1+\varphi_0\bullet\left(t'\right)^{-d}\left(t-t'\right)^p\right] \tag{4.30}$$

- Creep under various isothermal temperatures

Temperature exerts a significant influence on the concrete creep. Heating of concrete accelerates creep but it also accelerates hydration which tends to reduce creep. Creep of sealed specimen at various isothermal temperatures is generalized by introducing the equivalent time at loading and the equivalent creep duration, which are calculated with (Bažant, 1988):

$$t_e'=\int_0^{t'}\beta_T\left(\tau\right)d\tau \qquad\qquad t-t_e'=\int_{t'}^{t}\beta_T'\left(\tau\right)d\tau \tag{4.31}$$

Based on activation energy theory:

$$\beta_T\left(t\right)=\exp\left\{\frac{U_h}{R}\left(\frac{1}{T_0}-\frac{1}{T\left(t\right)}\right)\right\} \tag{4.32}$$

$$\beta_T'\left(t\right)=\exp\left\{\frac{U_c}{R}\left(\frac{1}{T_0}-\frac{1}{T\left(t\right)}\right)\right\} \tag{4.33}$$

Where T =absolute temperature, T_0 =reference temperature, U_h and U_c = activation energies of cement hydration and creep, respectively. The equivalent hydration period at the moment of loading, t_e', represents the period needed at reference temperature T_0 to achieve the same degree of cement hydration as that achieved at actual temperature T during the actual time period t' up to the moment of loading. The equivalent creep duration $t-t_e'$ represents the creep duration at reference temperature T_0 that gives the same creep strain as that obtained after load duration $t-t'$ at actual temperature T. In present study, it is assumed that $U_h=U_c$.

- Transient creep under temperature changes

Bažant (1985a) assumed that the creep rate depends on the micro diffusion of water between the macropores and the micropores in the cement gel. Since the microdiffusion is driven by a

humidity- and temperature gradient, the rate depends on pore humidity $\dot{h}$ and temperature $\dot{T}$. Bazent proved mathematically that this theory is equivalent to the assumption about stress-induced shrinkage and stress-induced thermal strain.

$$\Delta\varepsilon_T = \alpha_T \Delta T \bullet \left(1 + \rho \bullet \frac{\sigma}{f_t'} \bullet sign(\Delta H)\right) \tag{4.34}$$

$$\Delta\varepsilon_h = k\Delta h \bullet \left(1 + r \bullet \frac{\sigma}{f_t'} \bullet sign(\Delta H)\right) \tag{4.35}$$

$$\Delta H = \Delta h + c\Delta T \tag{4.36}$$

Jonasson (1994) first applied this theory to young concrete. Assuming that for young concrete the temperature change dominates:

$$sign(\Delta H) = sign(\Delta T) \tag{4.37}$$

And the stress-induced thermal strain is:

$$\Delta\varepsilon_T = \alpha_T \Delta T \bullet \rho \bullet \frac{\sigma}{f_{ct}} \bullet sign(\Delta T) \tag{4.38}$$

Where f_{ct} is tensile strength dependent on maturity. The equation (4.38) is applied in the analysis of the test results of transient thermal creep, and the parameter ρ is determined for hardened and young concrete.

4.5. 1-D analysis of restraint stress development in the TSTM

Thermal dilation and autogenous deformation occur simultaneously in the concrete specimens in the stress rig and the dilation rig. The amount of stress generated by thermal dilation and autogenous shrinkage in a given time interval depends on the degree of restraint in the stress rig, the elastic modulus, and the creep/relaxation properties of the concrete. Figure 4-1 illustrates the interplay of these factors in a TSTM test, each of which changes with time.

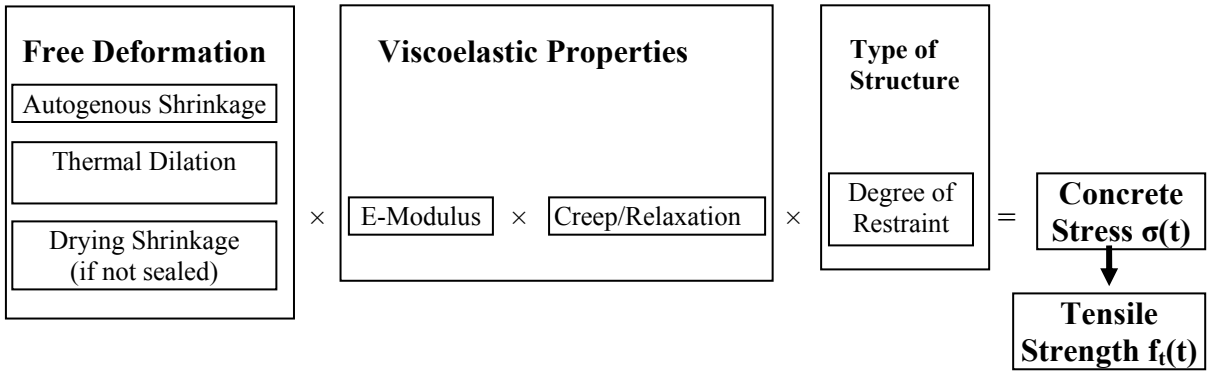

Figure 4-1 The main factors inducing restraint stress in TSTM test

The integral type of formulation which is used in the 1-D analysis of the restraint stress development in the TSTM is given as:

$$\varepsilon(t) = \int_{t_0}^{t} J(t,t')\, d\sigma(t') + \varepsilon^0(t) \tag{4.39}$$

To describe the stress and strain histories according to the principle of superposition, the time history is subdivided into time intervals:

$$\varepsilon(t_n) = \sum_{j=1}^{n} J(t_n, t_j) \cdot \Delta\sigma_j + \varepsilon^0(t_n) \tag{4.40}$$

For continuously varying strain, the second order algorithm (Bažant and Najjar, 1973), which is based on approximating the integral by the trapezoidal rule, is used to calculate the stress due to a strain increment (or decrement) $\Delta\varepsilon_j$ occurring during the time Δt_j, and a good accuracy can be achieved. The stress increment $\Delta\sigma_j$ is assumed applied in the middle of the j th interval (at time $t_{j-1/2}$). The total loaded induced strain at the end of the j th interval is the sum of the strains due to stress increments, $\Delta\sigma_j$, applied during all the previous increments.

$$\varepsilon_{el}(t_j) + \varepsilon_{cr}(t_j) = \sum_{i=1}^{j} J(t_j, t_{i-1/2}) \cdot \Delta\sigma_j \tag{4.41}$$

Where $$t_{i-1/2} = \frac{1}{2}(t_i - t_{i-1})$$

The constitutive behavior of young concrete in stress rig (TSTM) is defined by equation as proposed by the CEB-FIP (1991), the strain rate $\Delta\varepsilon_j$ at time t_j may be composed to thermal-, autogenous- and creep- and transient thermal creep strains.

$$\Delta\varepsilon(t_j) = \Delta\varepsilon_{th}(t_j) + \Delta\varepsilon_{sh}(t_j) + \Delta\varepsilon_{el}(t_j) + \Delta\varepsilon_{cr}(t_j) + \Delta\varepsilon_{ttc}(t_j) \tag{4.42}$$

with $$\Delta\varepsilon_{el}(t_j) + \Delta\varepsilon_{cr}(t_j) = \sum_{i=1}^{j} J(t_j, t_{i-1/2}) \cdot \Delta\sigma_i - \sum_{i=1}^{j-1} J(t_{j-1}, t_{i-1/2}) \cdot \Delta\sigma_i \tag{4.43}$$

$$\Delta\varepsilon_{th}(t_j) = \varepsilon_{th}(t_j) - \varepsilon_{th}(t_{j-1}) \tag{4.44}$$

$$\Delta\varepsilon_{sh}(t_j) = \varepsilon_{sh}(t_j) - \varepsilon_{sh}(t_{j-1}) \tag{4.45}$$

$$\Delta\varepsilon_{ttc}(t_j) = \alpha_T \left|\Delta T_j\right| \rho \bullet \frac{\sigma(t_j)}{f(t_j)} \tag{4.46}$$

Where ε =measured strain in TSTM; ε_{th} =thermal dilation; ε_{sh} =autogenous shrinkage; ε_{el} = elastic strain; ε_{cr} =creep strain; ε_{ttc} = transient thermal creep strain.

Free deformation measured in Dilation rig under different temperature are the sum of ε_{th} and ε_{sh}, and is directly used in the stress calculation. Stress increment at time t_j can be determined as:

$$\Delta\sigma_j = \frac{1}{\left(J(t_j, t_{j-1/2}) + \alpha_T \left|\Delta T_j\right| \rho / f(t_j)\right)} \cdot \left\{ \Delta\varepsilon(t_j) - \left[\Delta\varepsilon_{th}(t_j) + \Delta\varepsilon_{sh}(t_j) + \sum_{i=1}^{j-1} \left(J(t_j, t_{i-1/2}) - J(t_{j-1}, t_{i-1/2}) \right) \cdot \Delta\sigma_i + \alpha_T \left|\Delta T_j\right| \rho \frac{\sigma(t_{j-1})}{f(t_j)} \right] \right\} \tag{4.47}$$

4.6. 3- D finite element model of concrete structure

In a numerical analysis concrete is treated as a homogeneous material, therefore the calculated stresses are not representative for e.g. the boundary zones around aggregate, but represent only regions with a size larger than some characteristic dimension, e.g. the maximum aggregate size.

4.6.1. Solution of the thermal problem

The finite element equations are formulated using the Galerkin weighting procedure, and this procedure extends the equilibrium to a finite volume,

$$\int_V v div(q)\, dV + \int_V v\rho c\dot{T} dV = \int_V vQdV \tag{4.48}$$

Where v is the scalar weighting function and V is the volume of the structure.
Use of the Green-Gauss theorem and introduction of the boundary conditions gives:

$$\begin{aligned} &\int_V (\nabla v)^T k\nabla T dV + \int_V v\rho c\dot{T} dV = -\int_{A_T} vq_n dA - \int_{A_f} vhdA \\ &-\int_{A_c} v\alpha (T - T_\infty) dA - \int_{L_{c_i}} v\beta (T - T_w)\, dL + \int_V vQdV \end{aligned} \tag{4.49}$$

In the finite element method the structure is divided into discrete element. The temperature field and the temperature gradient are approximated as the linear function of the nodal temperature.

$$T = NT \qquad \nabla T = \nabla NT = BT \tag{4.50}$$

Where N is the matrix of temperature interpolation function and T is the vector of nodal temperature. Application of equation(4.50) to each finite element gives:

$$\left(K + K_c + K_{c_i}\right)T + C\dot{T} = R \tag{4.51}$$

Where $K = \int_V B^T kBdV$ is the thermal conductivity matrix,

$K_c = \int_{A_c} \alpha N^T NdA$ is the convection matrix, $K_{c_i} = \int_{L_{ci}} \beta N^T NdL$ is the internal convection matrix,

$C = \int_V \rho c N^T NdV$ is the specific heat capacity matrix,

$R = -\int_{A_f} N^T hdA - \int_{A_T} N^T q_n dA + \int_{A_c} N^T \alpha T_\infty dA + \int_{L_{ci}} N^T \beta T_w dL + \int_V N^T QdV$ is the load vector.

4.6.2. Solution of the mechanical problem

The starting point for numerical analysis of the development of stresses in time is the incremental formulation of the principle of virtual work,

$$\int_V \delta\varepsilon^T \sigma dV = \int_V \delta u^T g dV + \int_A \delta u^T t dA \tag{4.52}$$

The displacements are approximated by interpolation of the nodal displacement:

$$u = Nv \qquad \varepsilon = \Delta u = \Delta Nv = Bv \tag{4.53}$$

$$\delta v^T \int_V B^T \sigma dV = \delta v^T \left(\int_V N^T g dV + \int_A N^T t dA\right) = \delta v^T r \tag{4.54}$$

$$\int_V B^T \sigma dV = r \tag{4.55}$$

The constitutive relation for aging viscoelastic material is given via creep compliance or relaxation compliance, and can be solved by integral or differential formulation. (Bosnjak, 2001)

$$\varepsilon(t) = \int_{t_0}^{t} J(t,t')\bar{C} d\sigma(t') + \varepsilon^0(t) \tag{4.57}$$

$$\sigma(t) = \int_{t_0}^{t} R(t,t')\bar{D} d\varepsilon(t') + \sigma^0(t) \tag{4.58}$$

$\bar{C}$ and $\bar{D}$ are dimensionless matrix that relate the three-dimension deformation state to the one-dimensional creep or relaxation function by using Poisson's ratio v.

$$\bar{C} = \begin{bmatrix} 1 & -v & -v & 0 & 0 & 0 \\ -v & 1 & -v & 0 & 0 & 0 \\ -v & -v & 1 & 0 & 0 & 0 \\ 0 & 0 & 0 & 2(1+v) & 0 & 0 \\ 0 & 0 & 0 & 0 & 2(1+v) & 0 \\ 0 & 0 & 0 & 0 & 0 & 2(1+v) \end{bmatrix}, \quad \bar{D} = \bar{C}^{-1} \tag{4.56}$$

The temperature gradient depends on the total quantity of hydration heat, boundary conditions, thermal properties, and discontinuity in geometry and material properties. The stress gradient depends on temperature distribution, mechanical properties, restraint conditions, discontinuity in geometry and material properties, etc.

In thermal stress analysis the element model must permit same level of complexity for the strain field as for the temperature field. Since the stresses are less accurate than displacements and temperatures, stress calculations need finer mesh than temperature calculations, and the order of the element in stress analysis has to be of higher order than the element in temperature analysis. If the same element model is used in both analyses, the requirements of stress analysis are usually decisive.

5. Test results, modelling and discussion

The results of comprehensive experimental work are described in this chapter. With regard to various properties, the analysis of the results is divided into six parts. In the first part, the influence of mineral additives on the volume change of early age concrete under realistic temperature is investigated, and the relative importance of TD and AD is evaluated. In the second part, the influence of mineral additives on the hydration heat and mechanical properties such as modulus of elasticity, compressive strength and tensile strength are studied. The results of creep tests in compression and tension are presented in the third part and the influence of mineral additives on the creep properties and comparison of viscoelastic properties in compression and tension is also discussed in this part. In the fourth part, the results of transient thermal creep tests are presented and the temperature influence on the creep properties is further discussed. The test results of restraint stress measurement in TSTM are described in the fifth part. In the last part, the compressive or/and tensile creep data is applied in the restraint stress analysis, and their influence on the stress development is investigated, and temperature effects are further studied by different approaches based on the maturity concept.

5.1. Volume changes

The free deformations of concrete specimen under sealed conditions and realistic temperature history, *i.e.* thermal dilation and autogenous deformation, are measured in the Dilation Rig, as shown in Figure 5-1 and Figure 5-3. Because the test is performed with a stepwise temperature history the coefficient of thermal expansion can be calculated within each temperature step, and the total deformation separates into thermal dilation and autogenous deformation. (Bjøntegaard, 1999) The test results for each concrete, based on the tests performed by Bjøntegaard (2003), are presented in Appendix A.

The calculated CTEs and autogenous deformations are shown in Figure 5-2 and Figure 5-4 for concrete containing different percentage of mineral additives, such as FA and BFS (*FA and BFS contents are given as percentage of cement weight*). The calculated CTEs show that CTEs gradually increase from the time of setting, and after 2-3 days the value of CTEs becomes approximately constant. The replacement of cement with FA or BFS reduces the CTE, and the higher percentage of replacement, the lower the calculated CTE is, but the influence of FA on CTE is more pronounced than that of BFS, for example, the calculated CTE of 100% BFS is 9.40×10^{-6}/ºC at 318 hours after casing, and it is 8.80×10^{-6}/ºC for 100% FA at the same time.

The CTE is then modeled by using equivalent time (Bjøntegaard and Sellevold, 2002):

$$CTE(t_e) = CTE(t_0) + \left[CTE(t_{28}) - CTE(t_0)\right] \bullet \left\{ \exp\left[s_{CTE} \bullet \left(1 - \sqrt{\frac{28}{t_e - t_0}} \right) \right] \right\}^{n_{CTE}} \tag{5.1}$$

Where t_e is the equivalent time, $CTE(t_0)$ and $CTE(t_{28})$ are the calculated CTE at t_0 and 28 days, s_{CTE} and n_{CTE} are model parameters which can be determined from experimental data.

The CTE model gives good agreement with the calculated results, except for the NL-slag concrete, as shown in Figure 5-5, the calculated CTE of NL slag concrete was 10.0×10^{-6}/ºC at 23 hours after casting, and it dramatically decreased to 7.5×10^{-6}/ºC at 27 hours, and then increased to 10.0×10^{-6}/ºC at 68 hours. Comparison of the autogenous deformation deduced by using modeled CTE and calculated CTE for NL-slag concrete is also shown in Figure 5-5, although the CTE model can not take into account the measured dramatic decrease of CTE from 23 hours to 27 hours, the maximum difference during the expansion period between two separated autogenous deformations is about 18μ.

Table 5.1 Parameters of CTE Model

Concrete	$CTE(t_0)$	$CTE(t_{28})$	s_{CTE}	n_{CTE}	t_0 (hours)
Reference	8.00	11.00	0.59	0.15	8.0
SV 40*	7.50	10.70	0.17	0.71	8.0
40% FA*	7.00	9.50	0.31	0.69	9.5
60% FA*	7.00	9.00	0.58	0.43	10.5
100% FA	8.00	8.80	1.46	1.33	11.0
40% BFS	7.50	10.40	0.28	0.75	8.8
60% BFS	8.00	10.20	0.31	0.75	8.8
100% BFS	7.50	10.00	0.45	0.78	9.0
NL-slag*	8.00	10.50	0.71	0.30	16.0

The replacement of cement with BFS did not have significant influence on the development of autogenous deformation. Except for NL-slag concrete, a large volume of expansion appears during the first 2 days, and the reason for this phenomenon is not clear. The replacement of cement with FA have certain influence on the development of autogenous deformation, and expansion deformation appears in 40% and 60% FA* concrete.

The total deformation is then separated into TD and AD, and the details are presented in Appendix A for each concrete, and two examples performed in parallel in the dilation rig and the TSTM are shown in Figure 5-6 for the reference and the 100% FA* concrete. The strain developments in the Dilation rig and the TSTM are almost same. The main part of the autogenous shrinkage is developed during first 2-4 days, and then the thermal shrinkage during the cooling period is the dominating part of the free deformation.

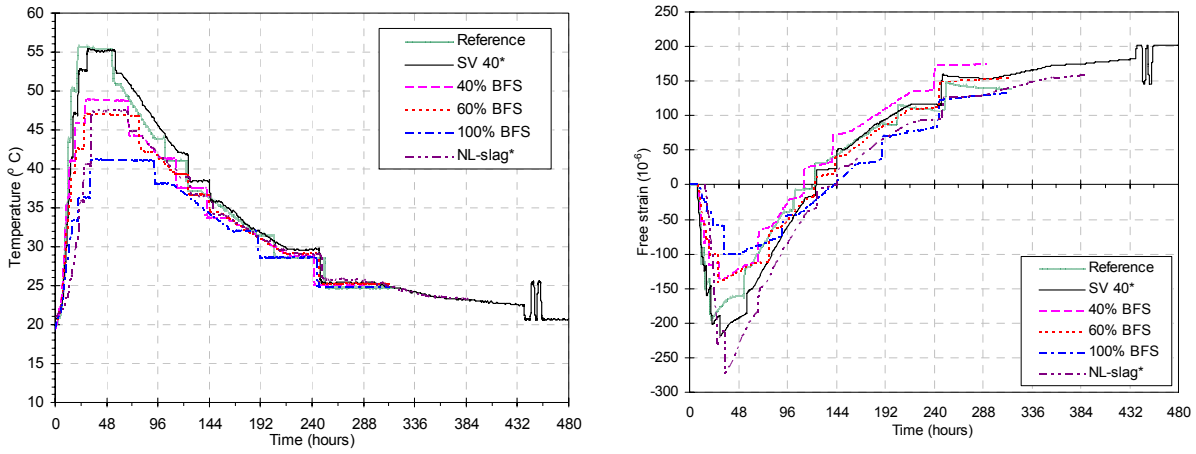

Figure 5-1 Temperature and free strain in the Dilation Rig for concretes containing BFS (free strains are zeroed at t_0 as shown in Table 5.2)

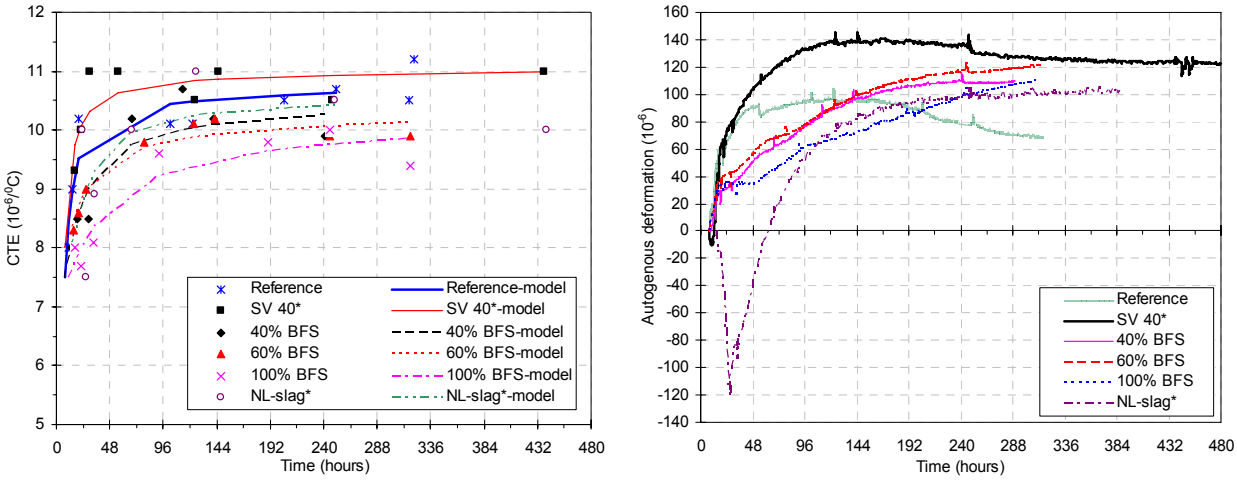

Figure 5-2 Calculated CTE and autogenous deformation for concretes containing BFS (Autogenous deformation are zeroed at t_0 as shown in Table 5.2)

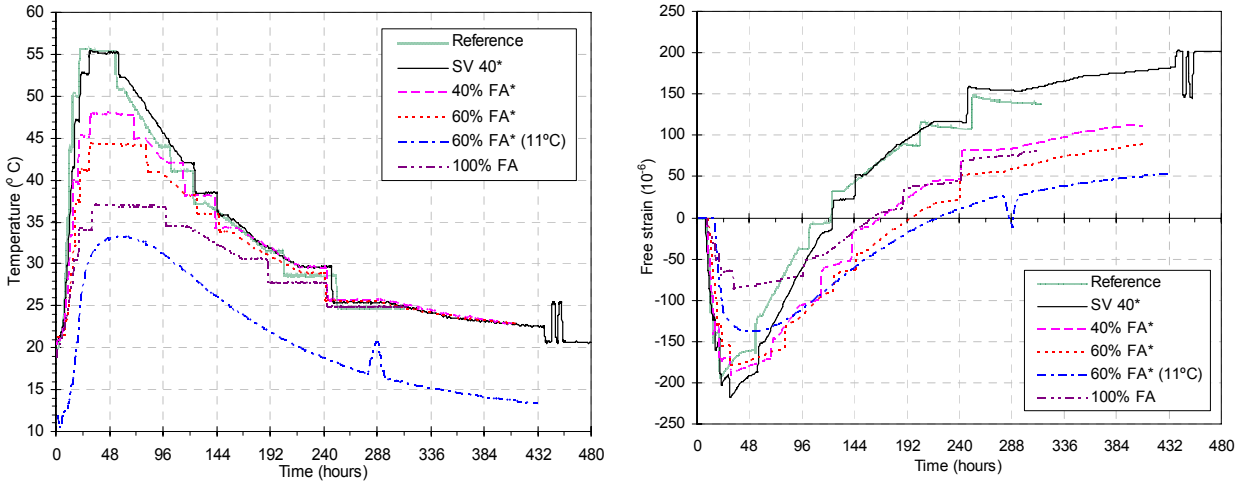

Figure 5-3 Temperature and free strain in dilation rig for concretes containing FA (free strains are zeroed at t_0 as shown in Table 5.2)

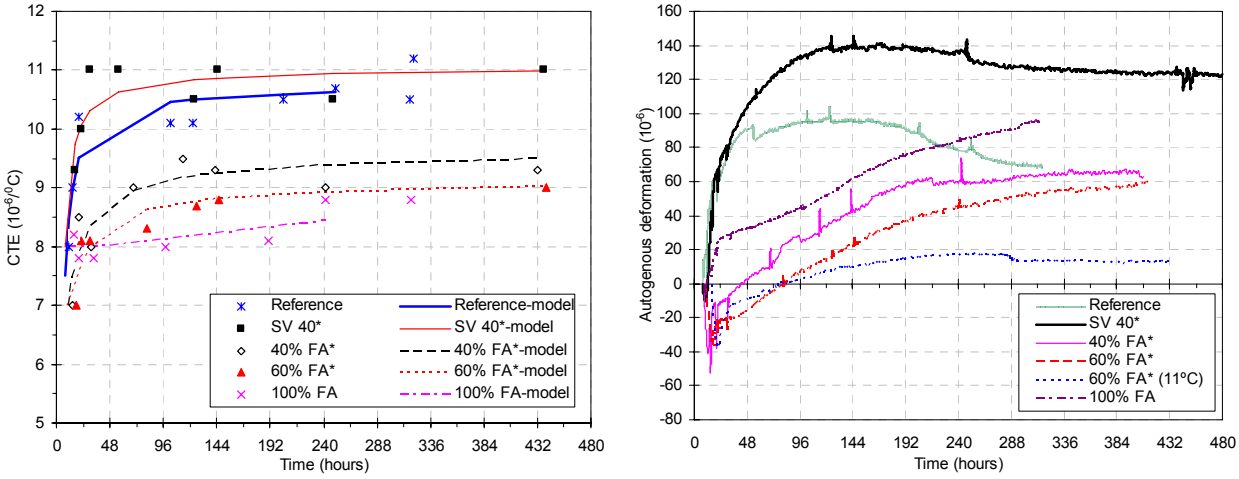

Figure 5-4 Calculated CTE and autogenous deformation for concretes containing FA (Autogenous deformation are zeroed at t_0 presented in Table 5.2)

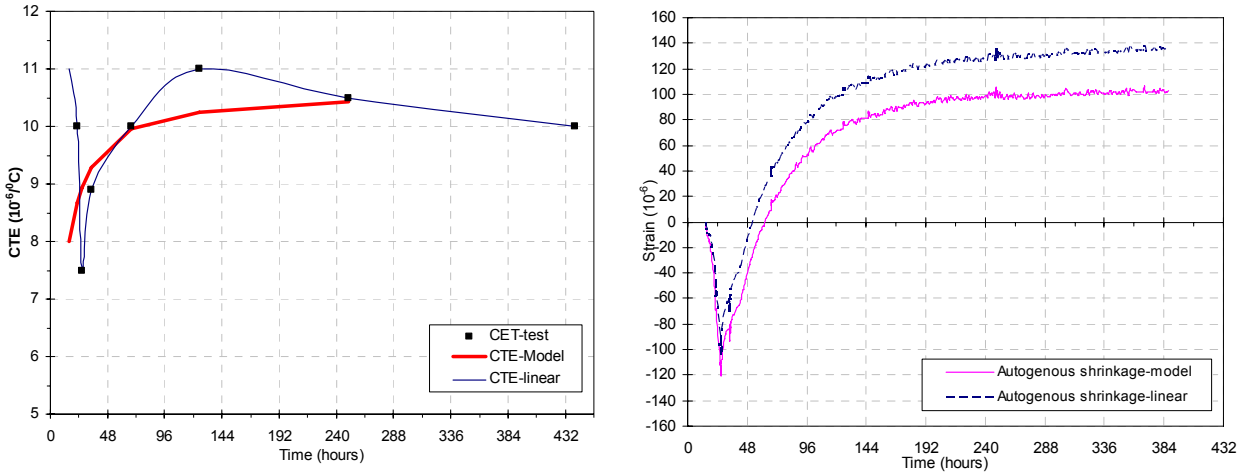

Figure 5-5 Calculated and modeled CTE and separated autogenous deformation (NL-slag*)

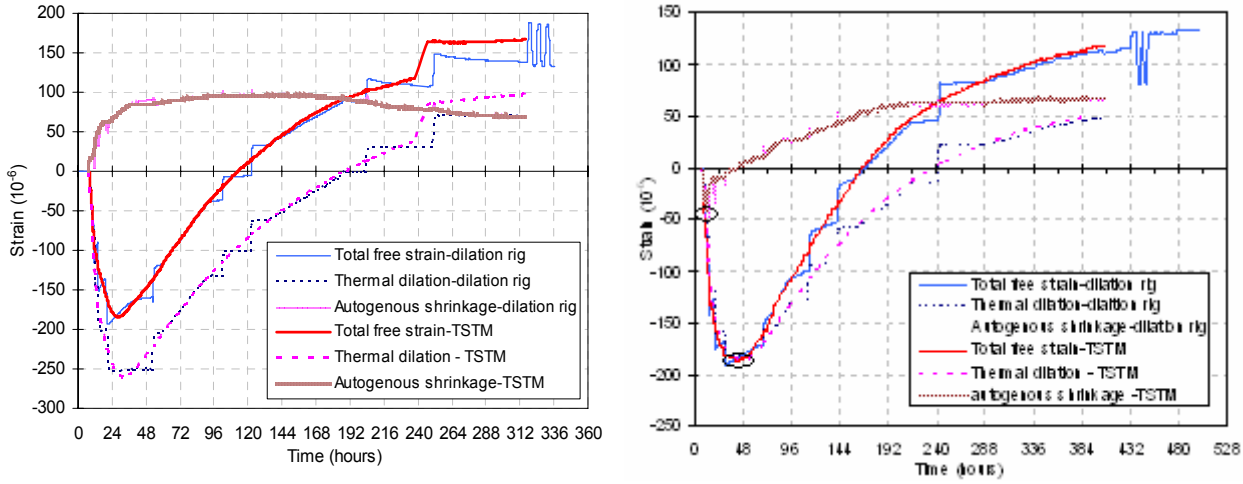

a) Reference concrete b) 100% FA concrete

Figure 5-6 Separation of total deformation into TD and AD based on the modeled CTEs

5.2. Influence of mineral additives on material properties

The detailed experimental data of hydration heat and mechanical properties, such as compressive strength, modulus of elasticity, splitting tensile strength and direct tensile strength are presented in the appendix B.

The semi-adiabatic hydration heat for all the concretes were measured at the concrete laboratories at both NTNU and SVV. The compressive strength and E-modulus tests were performed at SVV at several ages under 20ºC conditions. In most of the cases, only 28-day compressive strength and E-modulus were measured at NTNU. Splitting tensile strength tests were performed at NTNU and SVV at different ages, and then splitting strength were transferred to the uniaxial tensile strength by empirical function proposed by Kanstad (1999). Several direct tensile strength tests were carried out in the TSTM after the restraint stress tests under realistic temperature histories. The data is presumably close to the development of direct tensile stress in real concrete structures, and gives valuable information in the prediction of the cracking risk.

5.2.1. Hydration heat

The hydration heat development versus maturity is shown in Figure 5-7, and the adiabatic temperature is shown in Figure 5-8. The replacement of cement with the mineral additives such as FA and BFS significantly reduces the hydration heat. The increase of maximum adiabatic temperature of 100% BFS reduces 28% compared to that in reference concrete, for the 100% FA mix the reduction is 34%.

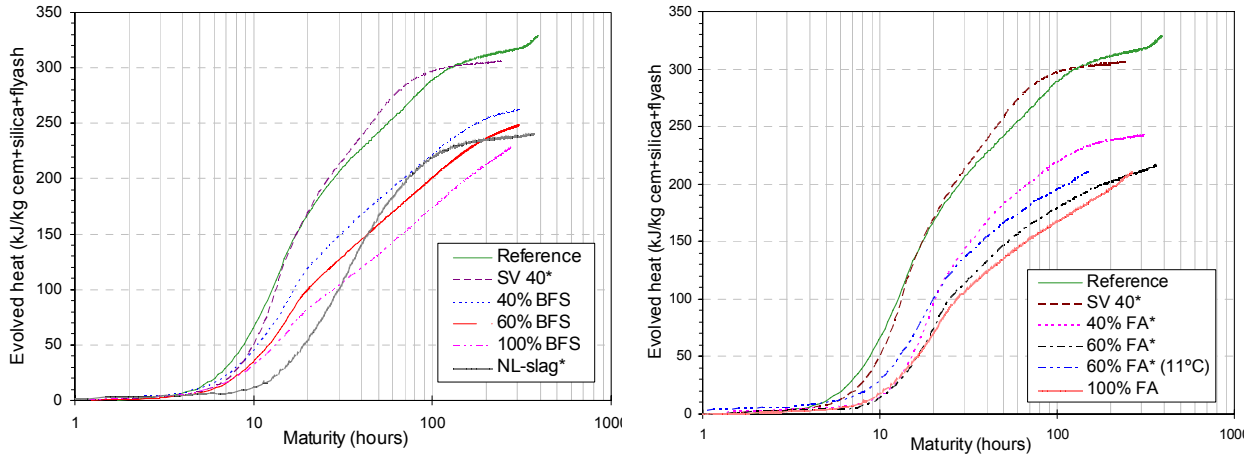

Figure 5-7 Hydration heat developments of concretes containing BFS and FA

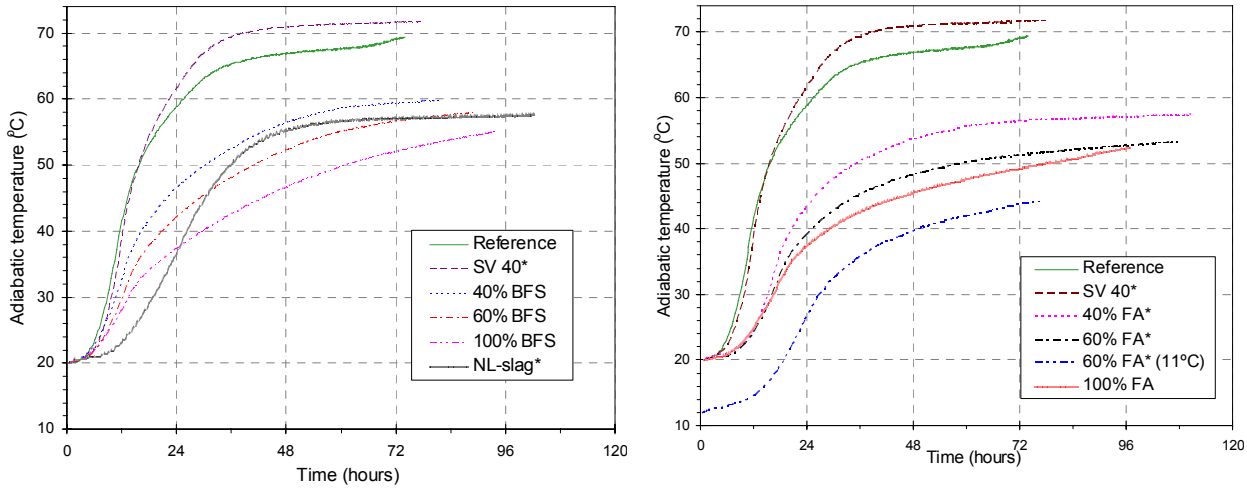

Figure 5-8 Adiabatic temperature developments in BFS and FA concretes

Table 5.2 Adiabatic temperature

concrete	$T_{initial}$ (ºC)	$T_{Maximum}$ (ºC)	ΔT(ºC)	$(\Delta T_{reference}-\Delta T)/\Delta T_{reference}$
Reference	20	69.0	49.0	
SV 40*		71.7	51.7	
40% FA*		57.5	37.5	23%
60% FA*		53.3	33.3	32%
60% FA*(11ºC)	11	44.3	33.3	32%
100% FA	20	52.3	32.3	34%
40% BFS		59.8	39.8	19%
60% BFS		57.4	37.4	24%
100% BFS		55.0	35.0	28%
NL-slag*		57.6	37.6	23%

The heat production is described by the frequently used three-parameter equation originally proposed by Freiesleben-Hansen (1977) at Ålborg University:

$$Q(t_e) = Q_\infty \bullet \exp\left[-\left(\frac{\tau}{t_e}\right)^{\alpha}\right] \tag{5.2}$$

Where Q_∞ is the asymptotic value of the produced heat, while τ and α are model parameters, which are determined from experimental data, see Table 5.3 below. The activation energy is determined by strength development at several isothermal temperature histories. For temperature calculation the most important input parameters, in addition to the produced heat and heat capacity, are the heat conductivity and the boundary conditions (connectivity and ambient air temperature) at the various surfaces of the structure.

Table 5.3 Parameters of thermal properties

Concrete type	Heat production				Activation energy (1/ºK)		Thermal conductivity kJ/ms°C	Specific heat J/kg°C
	Binder[(1)] kg/m³	Q_∞ (kJ/kg binder)	τ (h)	α	A	B		
Reference	378	336	14.00	1.03	33500[(2)]	1400[(2)]	0.0022[(2)]	1.04[(2)]
Basic 5	391	323	17.18	1.56	25000	1470	0.0026	1.04
Recipe D-40%BFS	382	286	18.95	0.84			0.0024	
Recipe E-60%BFS	384	274	21.97	0.78			0.0024	
100%BFS	386	292	33.05	0.60				
Recipe C-40%FA*	382	244	20.12	1.39	26574	1030	0.0024	1.07
Recipe B-60%FA*	384	215	21.86	1.17	36192	1136	0.0024	1.07
60%FA*(11ºC)	382	222	17.34	1.15			0.0024	
100%FA	386	202	21.12	1.10				
Recipe A-SV40*	424	319	15.04	1.34	21966	2699	0.0026	1.06
NL slag*	389	263	28.01	1.32	33648	2680		1.06

(1) Binder=Cement + Silica fume + Fly ash + Blast furnace slag
(2) The default value used in the analysis if the test data are not available

5.2.2. Modulus of elasticity and compressive strength

The measured compressive strength of the reference concrete and the concretes containing 40, 60 and 100% FA or BFS are shown in Figure 5-9 and Figure 5-10 (*FA and BFS contents are given as percentage of cement weight*). The replacement of cement with FA or BFS has significant influence on the development of the compressive strength, and the 28-day compressive strength of 100% FA concrete is only 55% of that of reference concrete at 20ºC curing condition. In general, the higher the mineral additives content the lower the compressive strength.

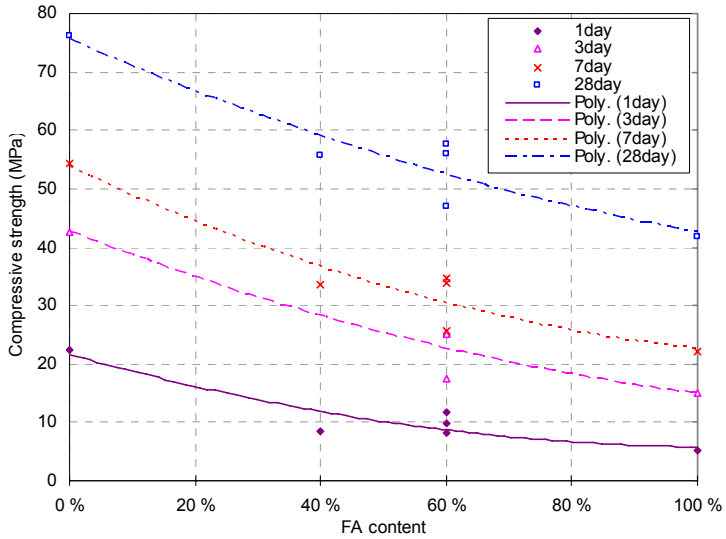

Figure 5-9 Compressive strengths of reference and 40, 60 and 100% FA concrete (SVV)

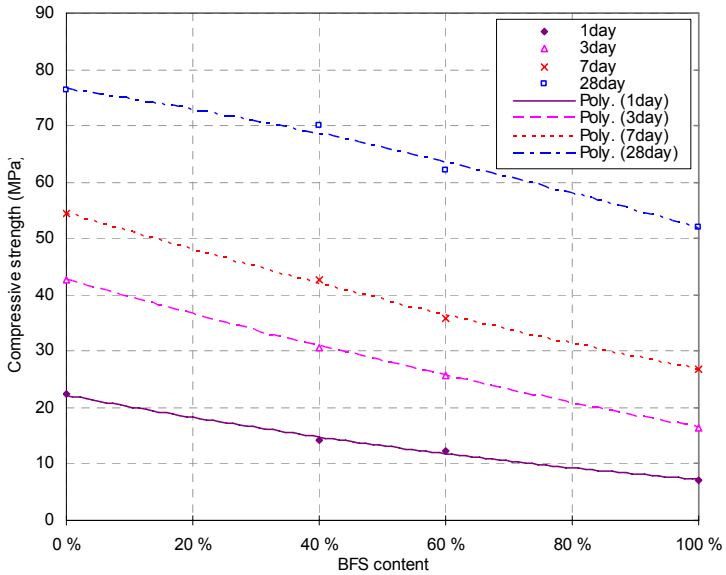

Figure 5-10 Compressive strengths of reference and 40, 60 and 100% BFS concrete (SVV)

The elastic modulus of the reference concrete and the concretes containing 40, 60 and 100% FA or BFS are shown in Figure 5-11 and Figure 5-12. The replacement of cement with FA or BFS has moderate influence on the 28-days elastic modulus, but the elastic modulus development at

very early age (less than 1 day) is considerably affected by the slow development of the pozzolanic reaction, and the higher the content of FA is, the lower is the elastic modulus at early ages.

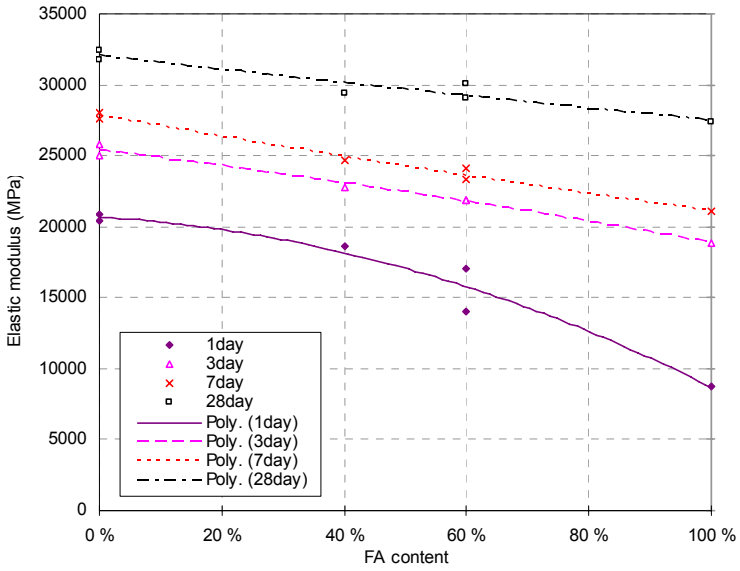

Figure 5-11 Elastic modulus of reference and 40, 60 and 100% FA concrete (SVV)

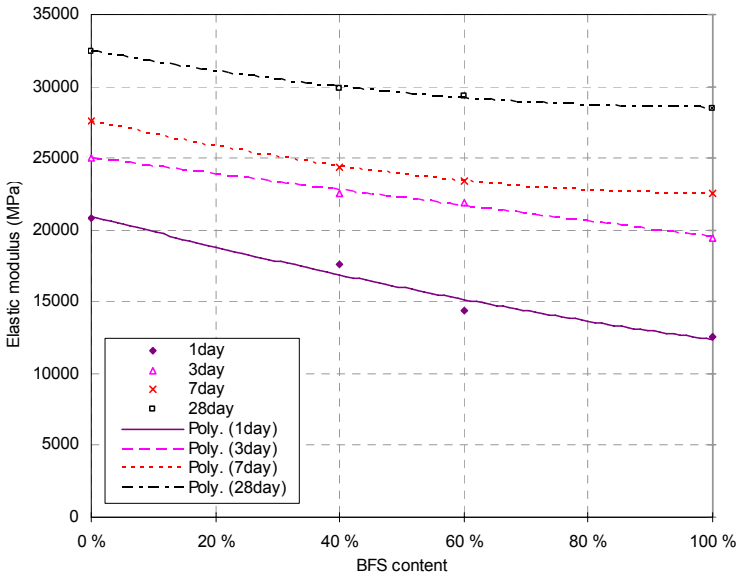

Figure 5-12 Elastic modulus of concretes containing 0, 40, 60 and 100% BFS

5.2.3. Tensile strength

The tensile strength has been determined based on a large number of tests. In general splitting tensile tests (cylinders) have been carried out by SVV, while both splitting tensile tests (100 mm cubes) and the uniaxial tests have been performed at NTNU. Although the test program is comprehensive, the evaluation is complicated due to the influence of test methods, test specimen, loading age and temperature history.

The measured splitting tensile strengths development of concretes containing 0, 40, 60 and 100% FA and BFS are presented in Figure 5-13. The development of splitting tensile strength is significantly affected by the replacement of cement with FA or BFS. The 28-day splitting tensile strength of 100% FA concrete is 3.5 MPa while the value reaches 5.5 MPa for reference concrete at 20ºC curing condition.

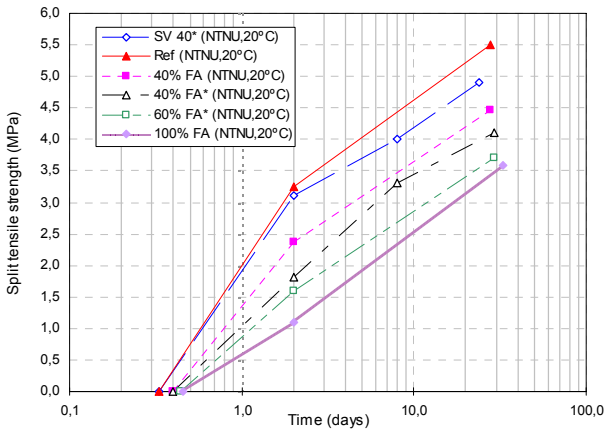

a) concretes containing 0, 40, 60 and 100% FA

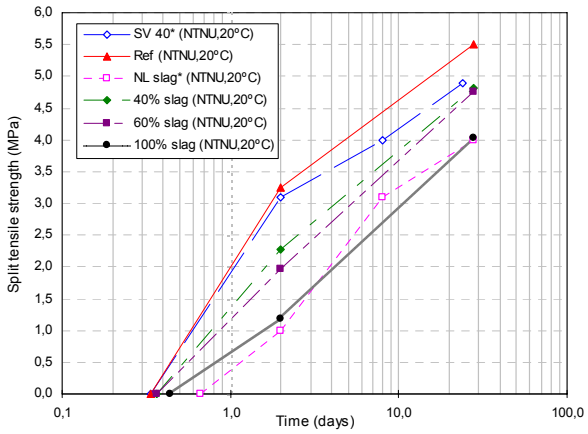

a) concretes containing 0, 40, 60 and 100% BFS

Figure 5-13 Splitting tensile strength of concretes containing different percentages of FA and BFS

The following relation was applied to determine the uniaxial tensile strength from splitting tensile strength of cubes (Kanstad, 1999):

$$f_t = 0.76 \bullet f_{ts} + 0.20$$

The results are presented in Appendix B, and used to determine model parameters for the tensile strength development.

The mechanical properties such as E-modulus, compressive and tensile strength are usually modeled as function of maturity age or degree of hydration. The limitation of this approach is that the direct influence of temperature on the final values of material properties is not taken into account, for example the fact that high curing temperatures may result in lower final compressive strength. The recent observations (Kanstad, 1999) have shown different temperature sensitivities for the E-modulus, compressive and tensile strength. It was also found that the loss of the final strength and E-modulus is less pronounced for high performance concrete under realistic temperature histories than under constant temperatures. The modified version of CEB-FIP MC 1990 (Kanstad, 1999) is then used to describe the development of the compressive strength, tensile strength and modulus of elasticity:

$$f_c(t_e) = f_c(28) \bullet \left\{ \exp\left[s \cdot \left(1 - \sqrt{\frac{28}{t_e - t_0}} \right) \right] \right\} \tag{5.3}$$

$$f_t(t_e) = f_t(28) \bullet \left\{ \exp\left[s \cdot \left(1 - \sqrt{\frac{28}{t_e - t_0}} \right) \right] \right\}^{n_t} \tag{5.4}$$

$$E_c(t_e) = E_c(28) \bullet \left\{ \exp\left[s \cdot \left(1 - \sqrt{\frac{28}{t_e - t_0}} \right) \right] \right\}^{n_E} \tag{5.5}$$

A concept of t_0 is introduced to identify the start of significant development of mechanical properties. t_0 is the time at which stiffness achieves value high enough to produce measurable stresses, and it is suggested by Bjøntegaard (1999) that for practical reason it can be determined from TSTM test as the time when the stress reaches 5% of the maximum compressive stress under full restraint. The parameter s was determined from the compressive strength tests, whereas the parameters n_t and n_E were determined from the tensile strength and E-modulus tests, respectively.

The data of compressive strength and E-modulus measured at different ages at the SVV laboratory were used to determine parameters s and n_E, but the 28-day compressive strength and elastic modulus were directly determined by the test results from NTNU. Splitting tensile strength measured at the NTNU laboratory was transferred to uniaxial tensile strength to determine the parameter n_t, while the 28-days value f_{t28} was determined from the most relevant test which is the uniaxial test of specimens after restraint stress test in TSTM under realistic temperature histories.

Table 5.4 Model parameters for mechanical properties

Concrete	$f_{c28}(MPa)$	$f_{t28}(MPa)$	$E_{c28}(MPa)$	s	n_E	n_t	t_0 (hrs)
Reference	62.9	3.88	35000	0.256	0.312	0.629	8.0
Basic 5	81.0	4.44	34300	0.173	0.394	0.658	8.0
Recipe D-40% BFS	54.8	3.89	33700	0.368	0.300	0.605	8.8
Recipe E-60%BFS	52.8	3.34	32200	0.433	0.327	0.604	8.8
100%BFS	41.0	2.91	32200	0.549	0.291	0.618	10.5
Recipe C-40%FA*	47.2	3.32	32900	0.363	0.253	0.623	9.5
Recipe B-60%FA*	41.2	3.20	33360	0.418	0.251	0.561	10.5
100%FA	35.0	2.85	27100	0.564	0.325	0.560	11.0
Recipe A-SV40*	65.1	3.86	31700	0.197	0.421	0.722	8.0
NL slag*	47.4	3.30	34600	0.430		0.766	16.0

(1) f_{c28} and E_{28} is directly determined from test results from NTNU

(2) The data for Basic 5 is from previous tests conducted in NTNU

The modeling of mechanical properties for concrete mixes with different BFS content is presented in Figure 5-14 to Figure 5-16. The development of E-modulus and tensile strength versus compressive strength development, as shown in Figure 5-17, is similar for the reference and BFS concretes with same w/b ratio, the parameters n_E and n_t are rather invariant for those concretes as shown in Table 5.4. This implies that the development of mechanical properties of concretes containing different percentage of BFS with same w/b ratio can be derived from test of one BFS concrete, but more experimental data is needed to verify this relation which is useful in engineering practice. Due to the difference of w/b ratio between the SV 40* concrete and the reference and BFS concretes, the SV 40* concrete shows relatively slow development in E-modulus and tensile strength.

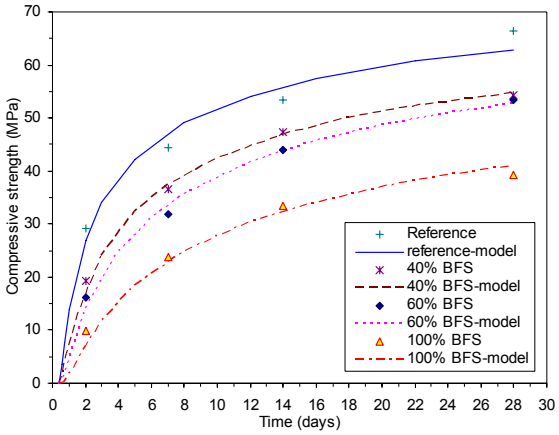

a) Compressive strength

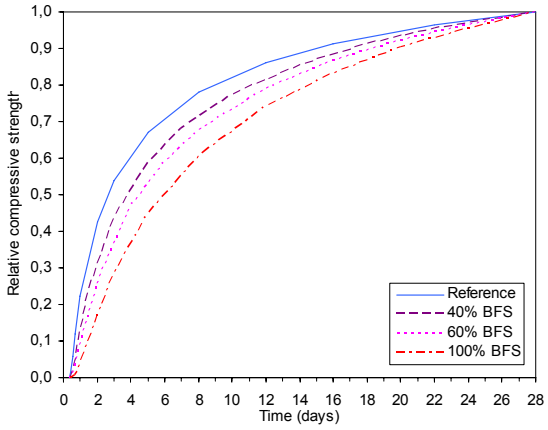

b) Relative compressive strength

Figure 5-14 Development of compressive strength for concretes with different BFS content

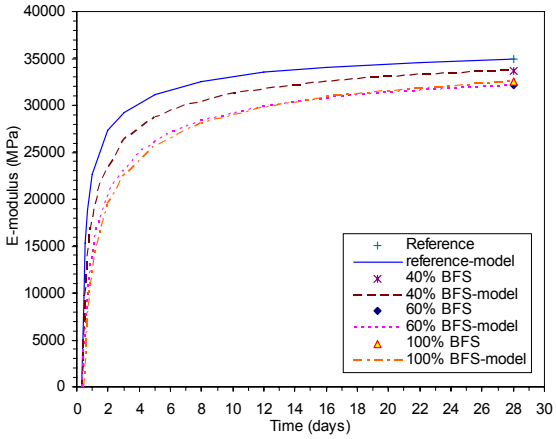

a) E-modulus

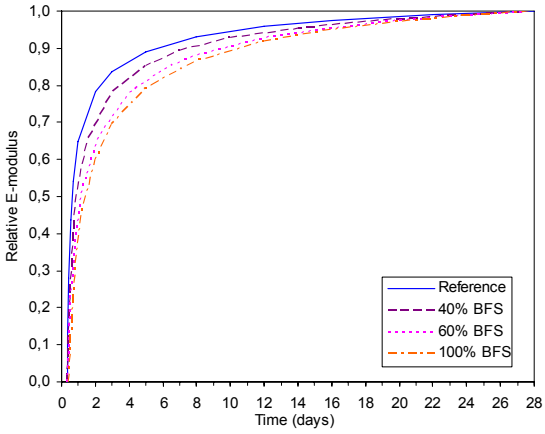

b) Relative E-modulus

Figure 5-15 Development of E-modulus for concretes with different BFS content

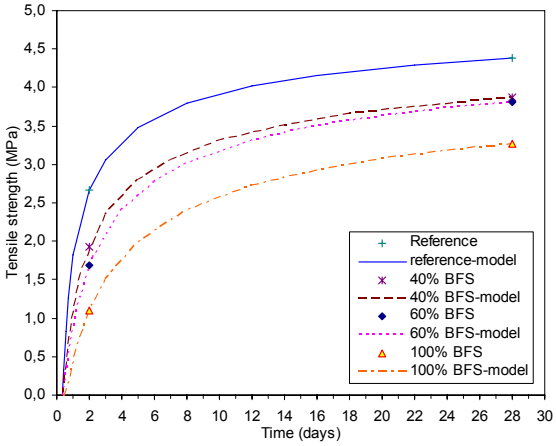

a) Tensile strength

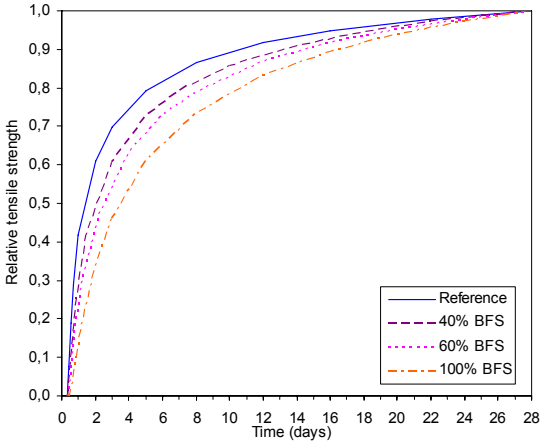

b) Relative tensile strength

Figure 5-16 Development of tensile strength for concretes with different BFS content

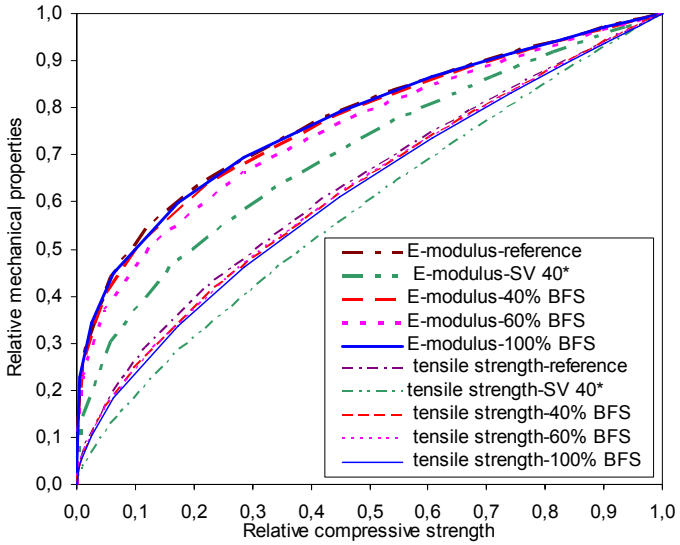

Figure 5-17 Development of mechanical properties versus compressive strength development for concretes with different BFS content

The modeling of mechanical properties for concrete mixes with different FA content is presented in Figure 5-18 to Figure 5-20. It is surprising that the E-modulus of the concrete mixes with 60% FA and 40% FA are 10% higher than that of the SV40 concrete at 28 days after casting. Only one set of E-modulus test was performed for the 40% FA, 60% FA, and the SV40 concrete, the uncertainty due to the variation of the test results is not take into account in the model. The development of E-modulus and tensile strength versus compressive strength development is shown in Figure 5-21, and the relation is slightly different for the reference and the FA concretes with same w/b ratio. The w/b ratio has similar effect on the development of relative mechanical properties between the SV* 40 concrete and the FA concretes.

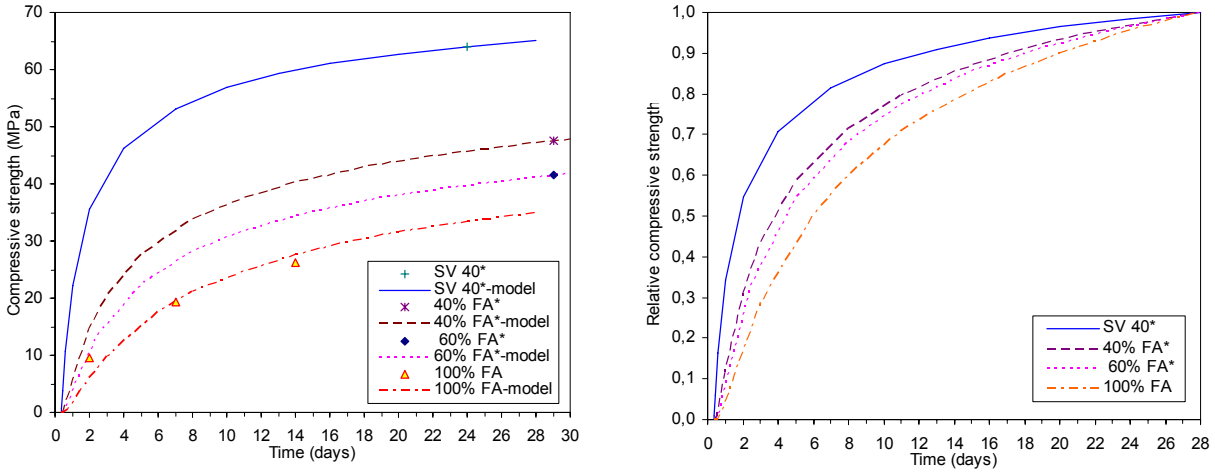

a) Compressive strength b) Relative compressive strength

Figure 5-18 Development of compressive strength for concrete with different FA content

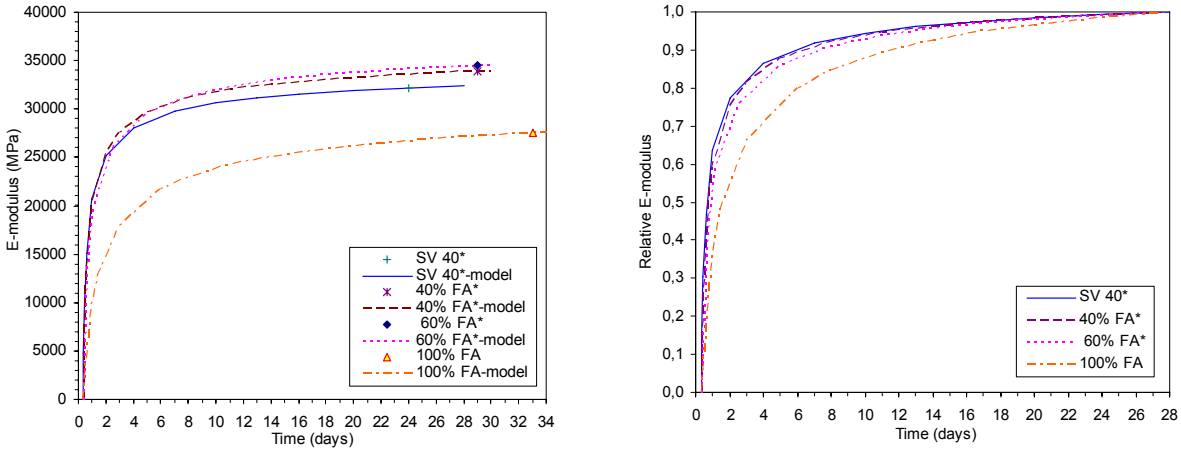

a) E-modulus b) Relative E-modulus

Figure 5-19 Development of E-modulus for concrete with different FA content

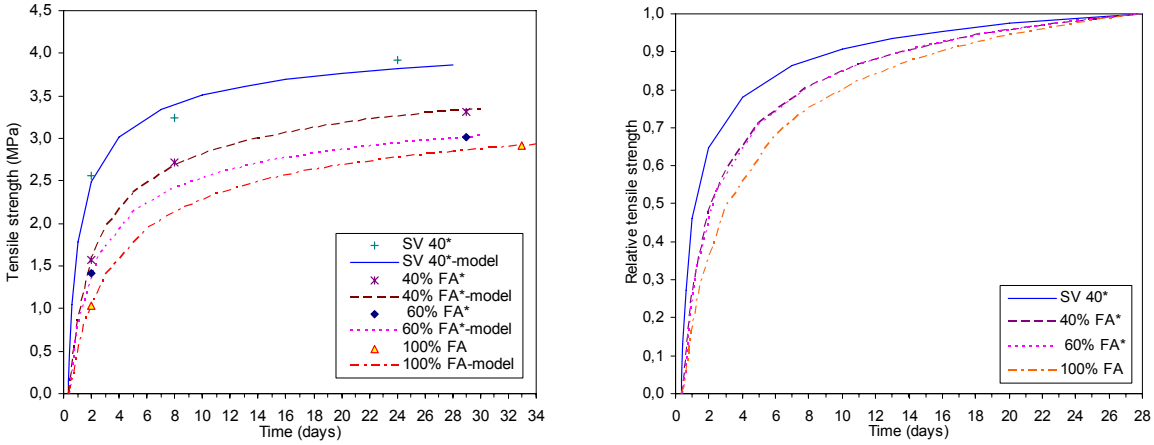

a) Tensile strength b) Relative tensile strength

Figure 5-20 Development of tensile strength for concrete with different FA content

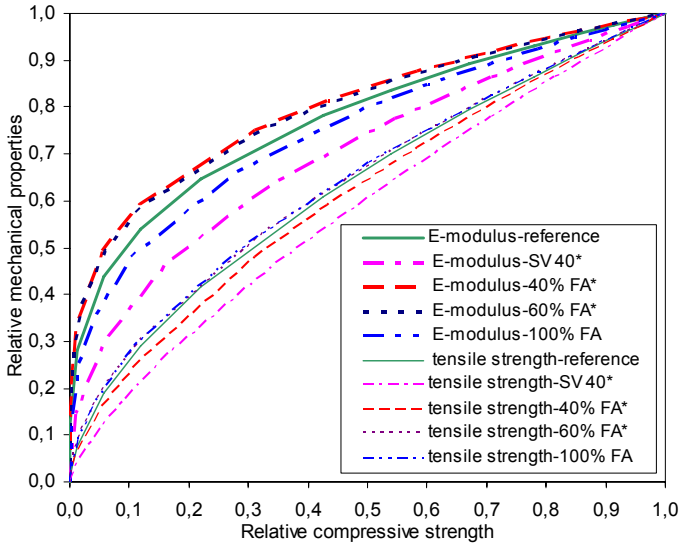

Figure 5-21 Development of mechanical properties versus compressive strength development for concrete with different FA content

5.3. Viscoelastic properties

The measured creep under sealed conditions is traditionally defined as basic creep. But for HPC/HSC the sealed condition can not eliminate the internal drying during the hardening process due to low water/cement ratio. The term sealed creep is therefore used to characterize the creep occurring under sealed conditions.

As described in the previous chapter, totally 14 compressive and 15 parallel tensile creep tests have been performed in the creep rigs under nearly the same conditions, and the measured strain developments of the loaded and dummy specimens are fully shown in Appendix C. One tensile creep test was performed both in the creep rig and in the modified TSTM at age of 2 days for the reference concrete to check the consistency.

In this section, the results of creep tests in both tension and compression are presented and the influence of mineral additives on the creep properties is studied, and the comparison of the tensile and compressive creep is also discussed.

5.3.1. Creep tests in compression

For each type of concrete, five specimens are cast and stored under 20 ºC in the temperature control room. All five specimens are demoulded at 2 days, and covered with aluminum foil immediately to prevent evaporation of water. Three of them (two loaded specimens and one dummy) are used to conduct creep test at 2 days age, and the other two (two loaded specimens) are used to conduct the creep test at 7 or 8 days.

The temperature and humidity history in the test room during the compressive creep test are shown in Figure 5-22 for the SV 40* concrete and the measured deformations in three specimens (two loaded and one dummy) are shown in Figure 5-23. The load was applied at 2 days and was about 30% of the compressive strength at loading time. Although the measured strains in the three LVDT's have large scatter in the loaded specimen, the average strains in two specimens are similar and are about 800 μ after one week of loading. The autogenous shrinkage measured in the dummy specimen is only about 50 μ, and is relatively small compared to the measured strain of the loaded specimen. The elastic plus creep strain is calculated by subtracting the autogenous shrinkage from the measured strain of the loaded specimen, and then it is divided by the average stress to obtain the compliance function (strain per unit stress), as shown in Figure 5-23 e).

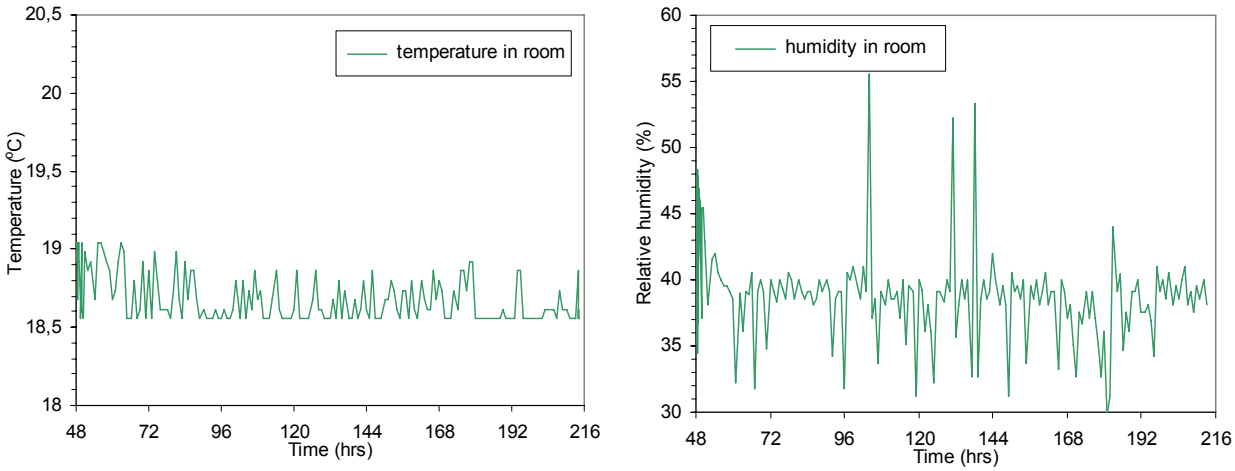

Figure 5-22 Recorded temperature and humidity development in room during creep test (SV 40*)

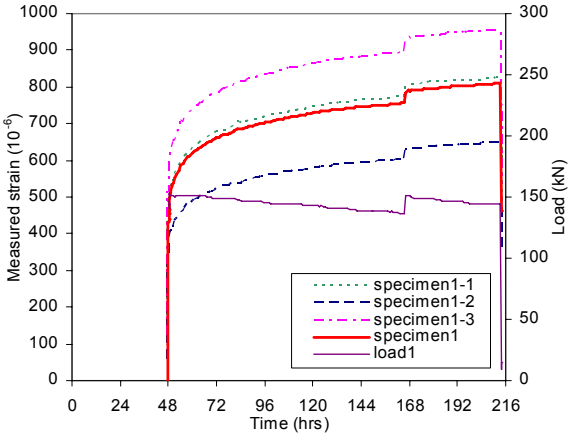

a) Load and measured strain (specimen no.1)

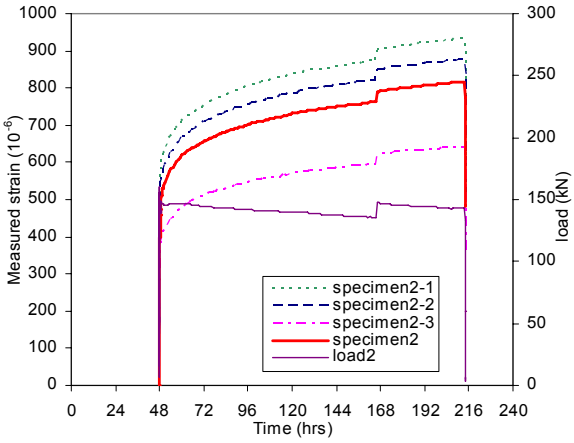

b) Load and measured strain (specimen no.2)

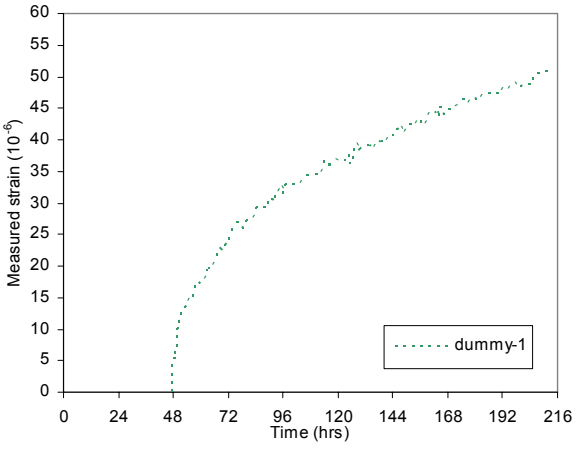

c) Load-independent strain (Dummy specimen)

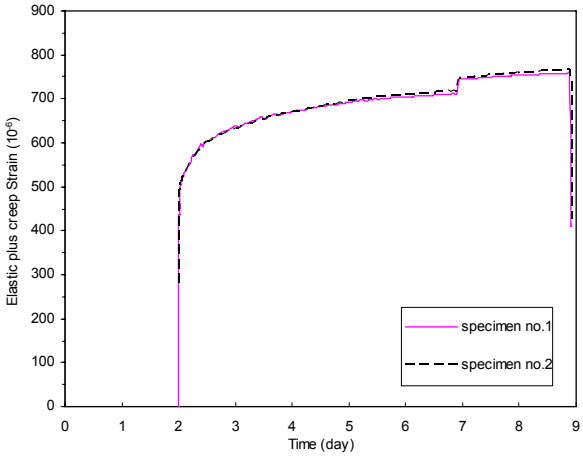

d) Elastic plus creep strain

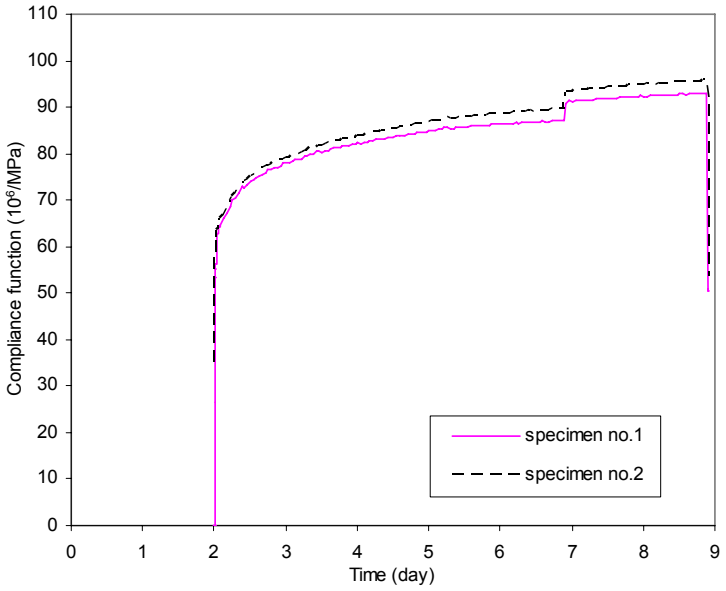

e) Compliance function

Figure 5-23 The results from compressive creep test on SV 40* concrete at loaded 2 days

The results of the creep tests in compression are presented in Figure 5-24 to Figure 5-31 for the different concretes. The calculated elastic compliance (1/E) is also given. It can be seen that the earlier the age of loading is, the higher the magnitude of creep. The influence of the concrete composition is discussed in a subsequent section.

The simplified version of the Bažant-Panula model (Double Power Law) is used to model the creep behavior in the present work. The BP-model follows the principle of linear superposition, and the compliance function (elastic and creep compliance) at reference temperature (20ºC) is:

$$J(t,t') = \frac{1}{E_c(t')}\left[1+\varphi \bullet t'^{-d}\left(t-t'\right)^{p}\right] \tag{5.6}$$

Where $J(t,t')$: Compliance function

t': Concrete age at loading (day)

t: Concrete age (day)

$E_c(t')$: Modulus of elasticity at loading time

φ, d and p: Creep model parameters

When the duration of the loading is same ($t_2 - t_1' = t_4 - t_3'$) for two creep tests performed at different loading age, the equation below can be derived from equation(5.6):

$$\frac{\left[J(t_2,t_1')E_c(t_1')-1\right]}{\left[J(t_4,t_3')E_c(t_3')-1\right]} = \left(\frac{t_1'}{t_3'}\right)^{-d} \tag{5.7}$$

The parameter d is determined from equation (5.7) and presented in Table 5.5, and then the other parameters of the creep model are determined by minimizing the quadratic sum of the deviation from the test data. The results show that the DPL is suitable to fit the compressive creep data of early age concrete very good for loading ages beyond 2 days.

Table 5.5 Creep parameters in DPL for the compressive creep tests

Concrete	Creep model parameters		
	φ	d	p
Basic 5*	1.15	0.18	0.18
SV 40*	0.98	0.18	0.19
FA 40%*	1.23	0.28	0.30
FA 60%*	1.47	0.24	0.24
Slag 40%	1.05	0.30	0.32
Slag 60%	0.77	0.30	0.32

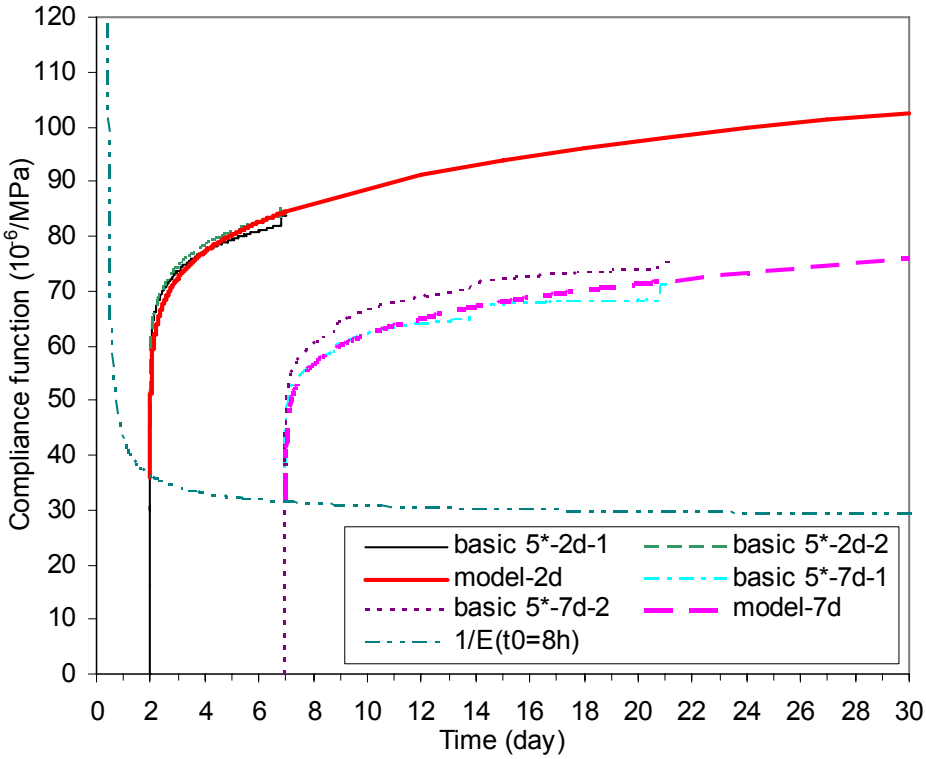

Figure 5-24 Compliance function from compressive creep tests at 20ºC (Basic 5*)

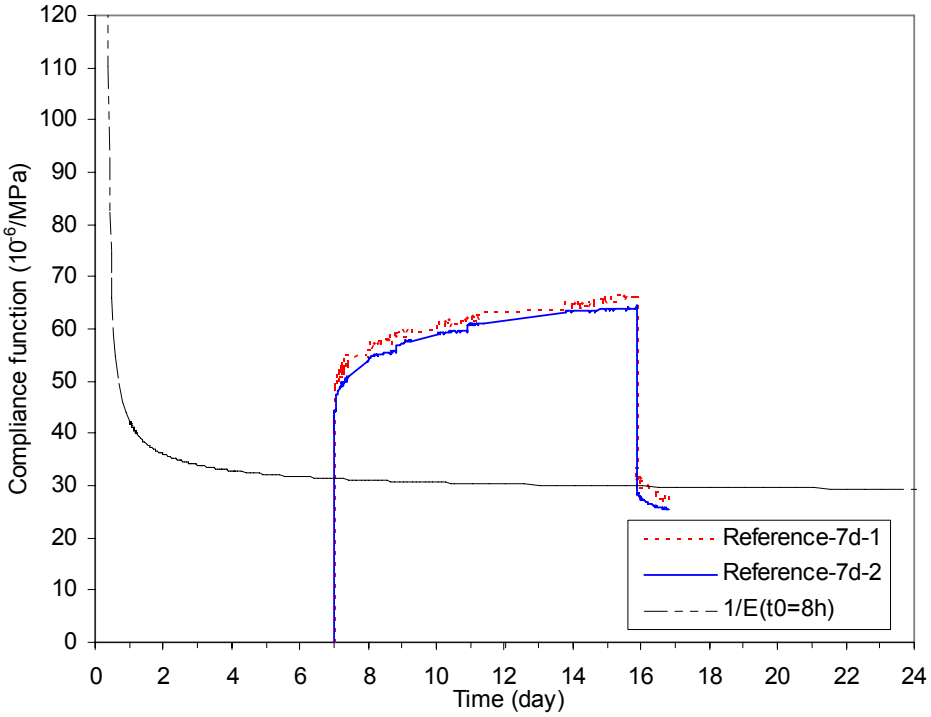

Figure 5-25 Compliance function from compressive creep tests at 20ºC (reference concrete)

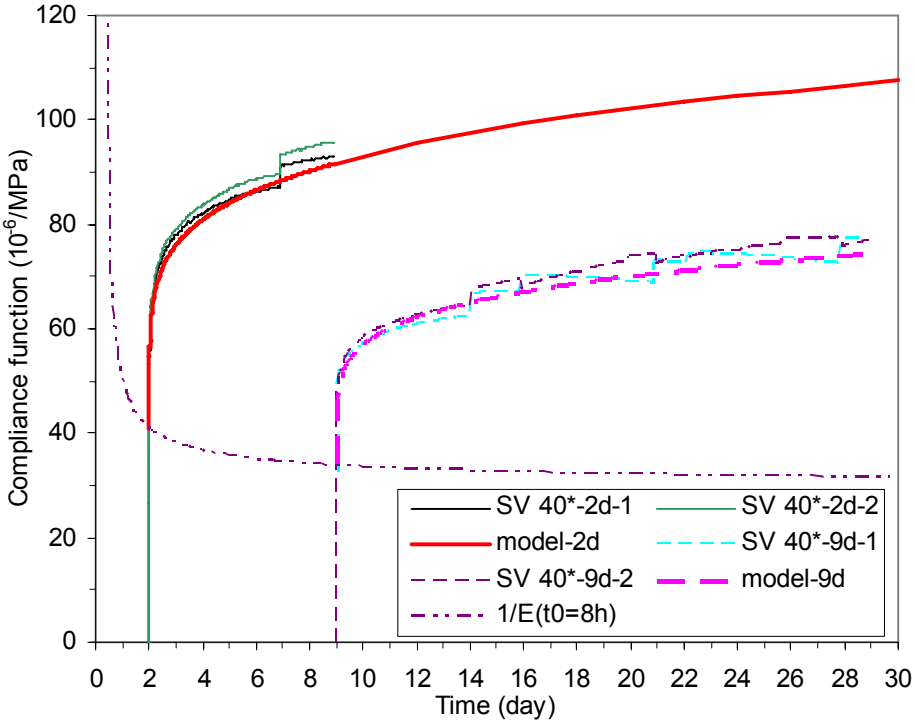

Figure 5-26 Compliance function from compressive creep tests at 20ºC (SV 40*)

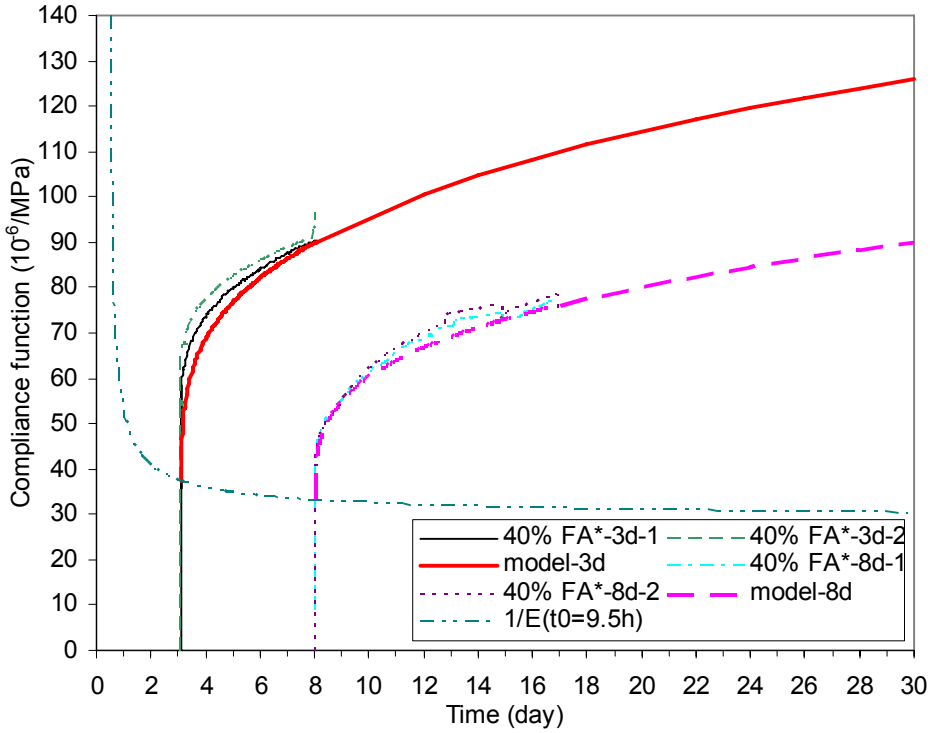

Figure 5-27 Compliance function from compressive creep tests at 20ºC (40% FA*)

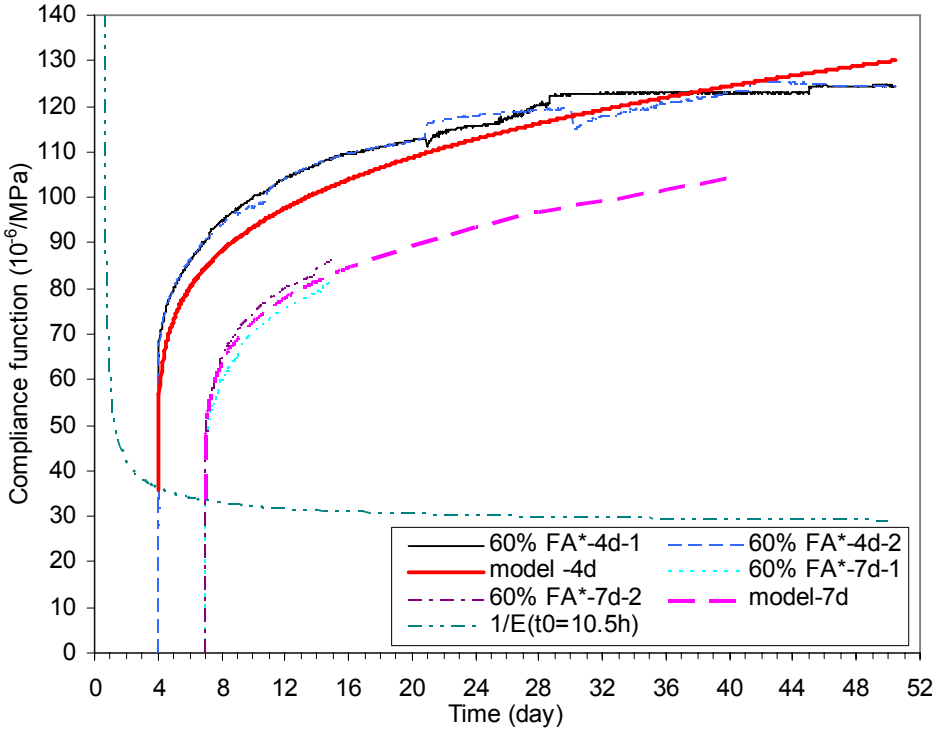

Figure 5-28 Compliance function from compressive creep tests at 20ºC (60% FA*)

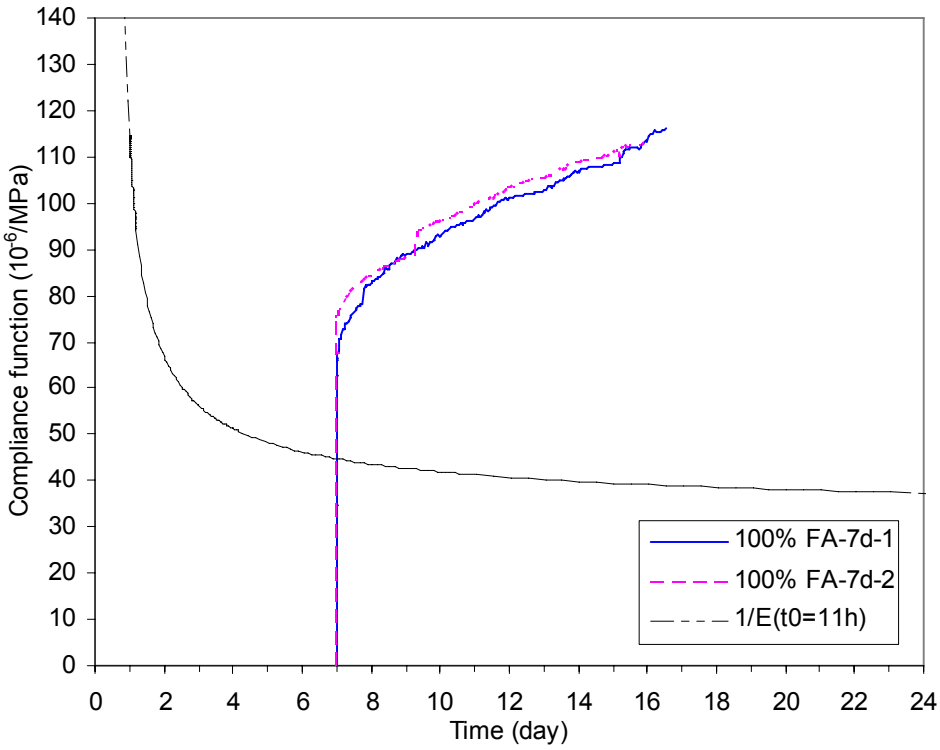

Figure 5-29 Compliance function from compressive creep tests at 20ºC (100% FA)

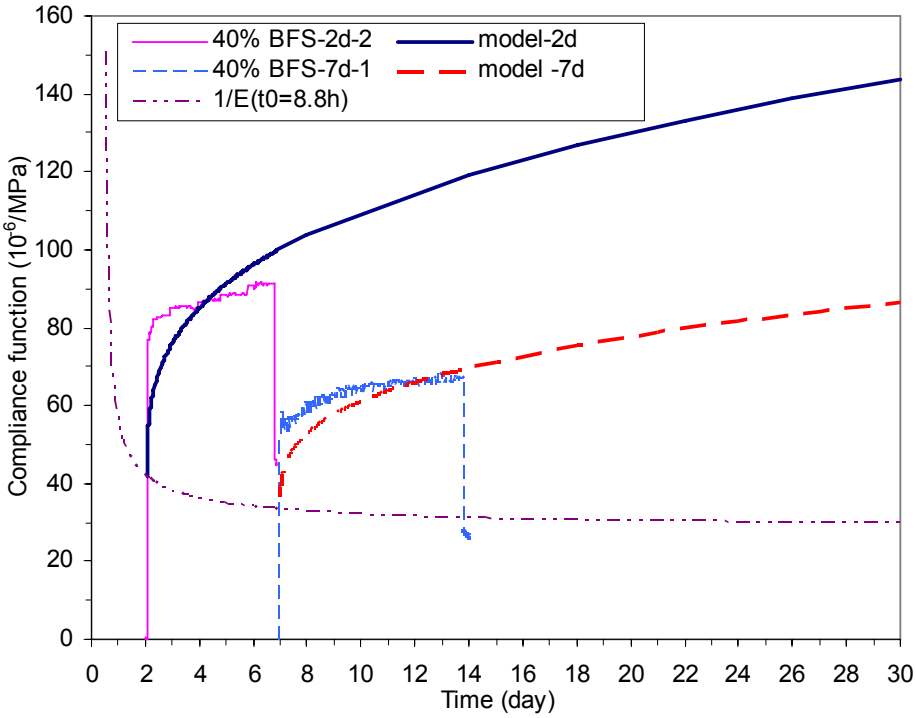

Figure 5-30 Compliance function from compressive creep tests at 20ºC (40% BFS)

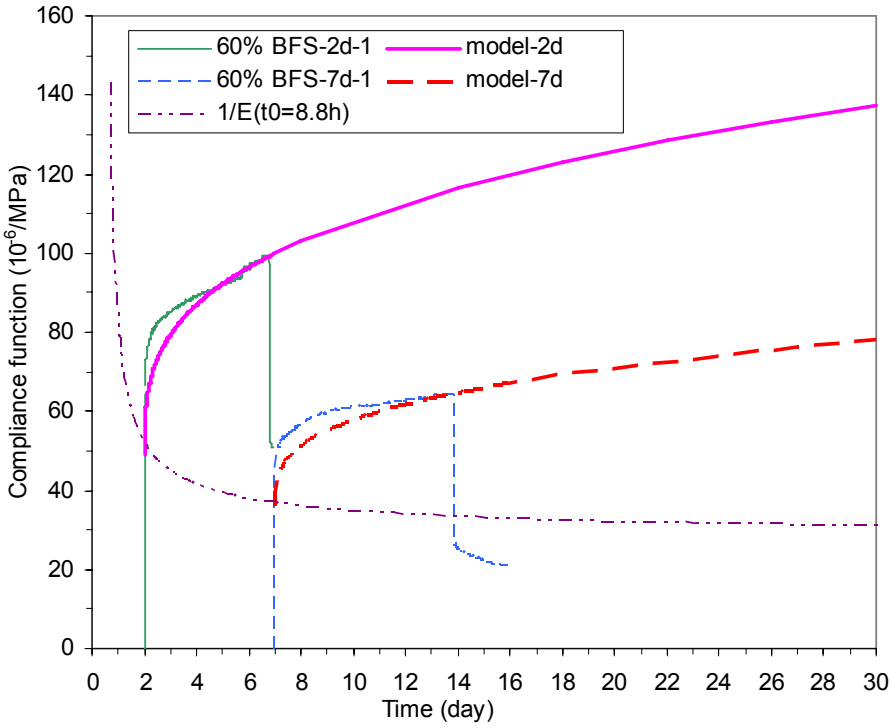

Figure 5-31 Compliance function from compressive creep tests at 20ºC (60% BFS)

5.3.2. Creep tests in tension

5.3.2.1. Comparison of tensile creep test in modified TSTM and creep rig

Tensile creep tests for the reference concrete were performed in parallel in the tensile creep rig and the modified TSTM at a loading age of 2days. The comparison of measured strain in loaded and dummy specimen in the parallel tests is shown in Figure 5-32. Although both the measured strains in the loaded specimens and the autogenous shrinkages in the dummy specimens are different for the parallel tests, the elastic plus creep strain in the creep rig and the modified TSTM are quite similar. Furthermore the compliance function in the TSTM test is slightly higher than that in the creep rigs the first few days, while they become quite close to each other after several days of loading.

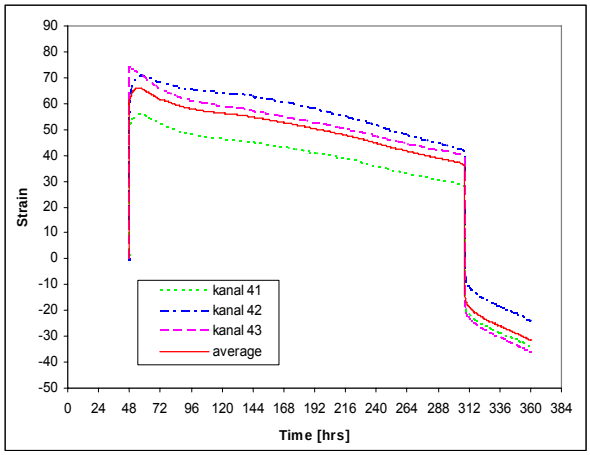

a) Loaded specimen in the creep rig

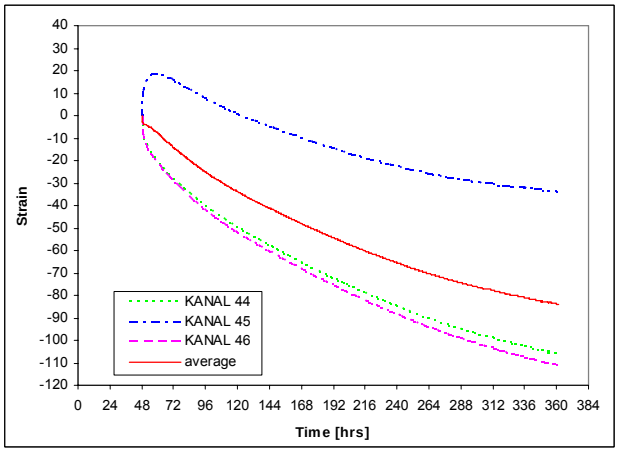

b) Dummy specimen in the creep rig

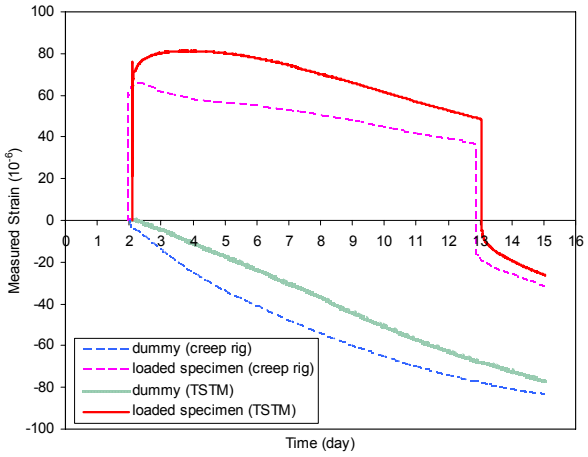

c) Comparison of measured strain in the creep rig and the TSTM

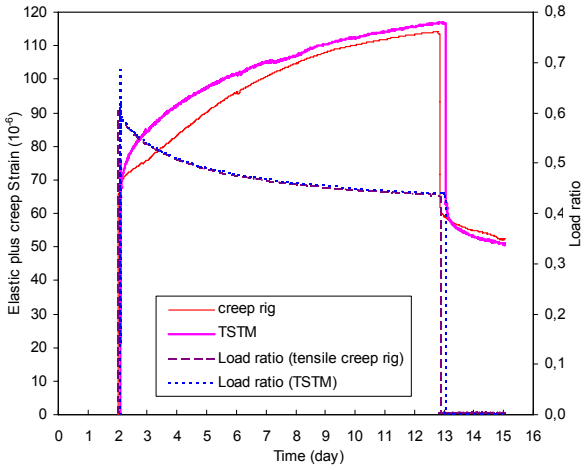

d) Elastic plus creep strain for both test methods

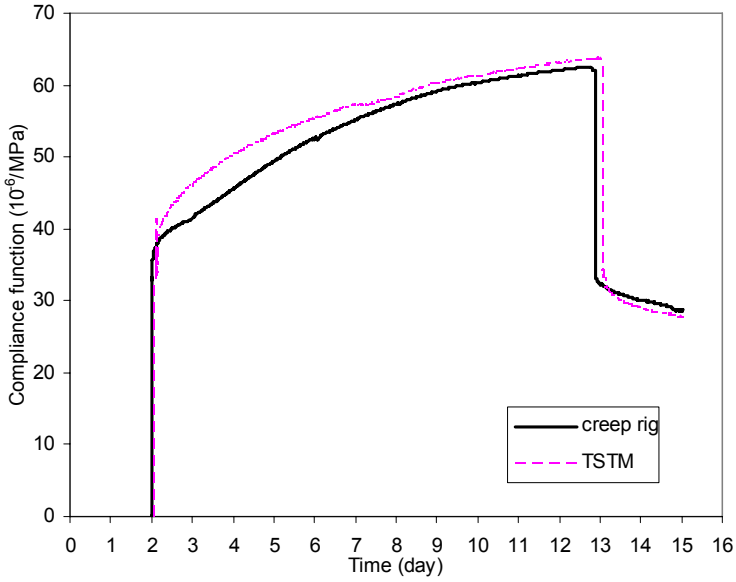

e) Compliance function of the reference concrete

Figure 5-32 The results from parallel tensile creep tests in the tensile creep rig and the modified TSTM

5.3.2.2. Tensile creep rig

The measured deformations in the two specimens (one loaded and one dummy) are shown in Figure 5-33 for the 60% FA* concrete. The load was applied at 7 days and the stress level was about 40% of the tensile strength at loading time. The measured strains in the loaded specimen in the three LVDTs have some scatter, and the strain instantly increases at loading, but the tension load is small and the strain declines during the loading period due to the effect of autogenous shrinkage. The strain in the loaded specimen is about 40 μ after 10 days of loading, and the autogenous shrinkage measured in the dummy specimen is in the same order of magnitude, and has a dominant influence on the calculated compliance function. The elastic plus creep strain is calculated by subtracting the autogenous shrinkage from the measured strain of the loaded specimen; afterwards it is divided by the tensile stress to obtain the compliance function, as shown in Figure 5-33 d).

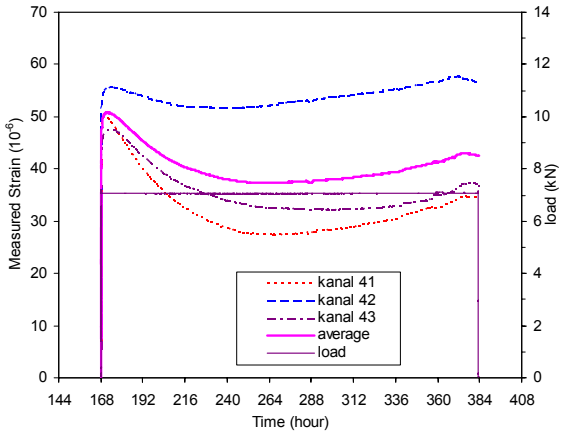

a) Loaded specimen

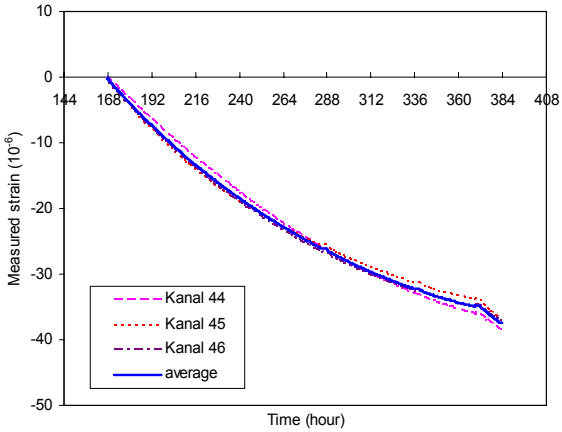

b) Dummy specimen

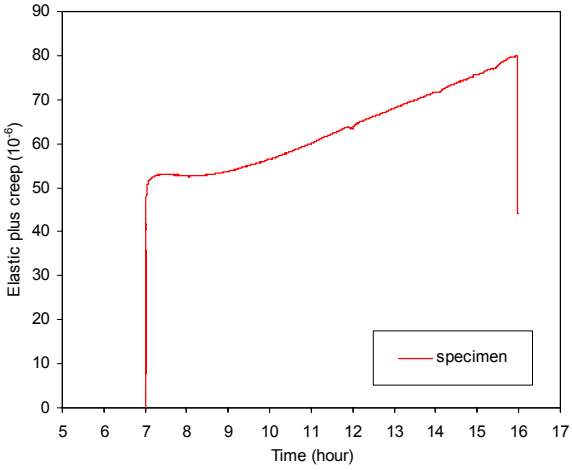

c) Elastic plus creep strain

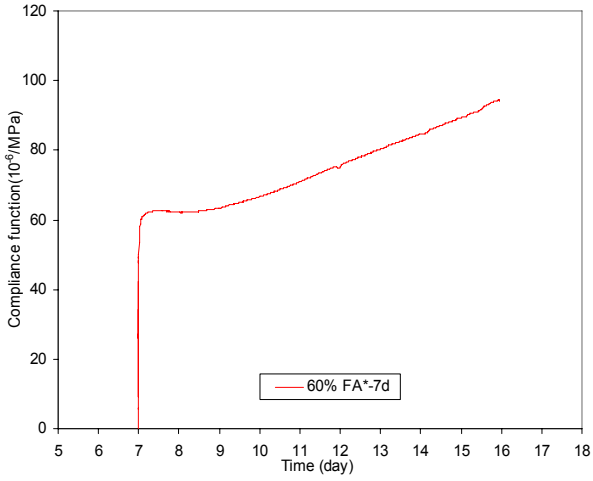

d) Compliance function

Figure 5-33 The results from tensile creep test on 60% FA* concrete loaded at 7 days

The results of the creep tests in tension for all the concretes are presented in Figure 5-34 to Figure 5-40. The calculated elastic deformations (1/E) are also given. The age of loading obviously also has major influence on the development of tensile creep. As discussed above, the tensile strength of the specimen at the loading age is very small, and the measured strain in

loaded specimen is in same order as the autogenous shrinkage in the dummy. The uncertainty of the tensile creep test at very early age is therefore larger than that of the compressive creep test, and some of the test results are even physical unreasonable, for example the compliance function of the 60% FA* concrete loaded at 4 days, which decreases 14 days after loading. As a result, the DPL model has some difficulties to achieve good agreement with the tensile creep test results. However, in order to compare the influence of the compressive creep and the tensile creep on the stress development in TSTM, the Double Power Law is applied to model the tensile creep data, and the tensile creep parameters determined by minimizing the quadratic sum of the deviation from the test data are presented in Table 5.6.

Table 5.6 Creep parameters in DPL for the tensile creep tests

Concrete	Creep model parameters		
	φ	d	p
Reference	0.68	0.26	0.24
SV 40*	0.97	0.20	0.20
FA 40%*	1.45	0.44	0.36
FA 60%*	2.10	0.50	0.30
NL slag*	1.38	0.40	0.27
Slag 60%	0.80	0.40	0.40

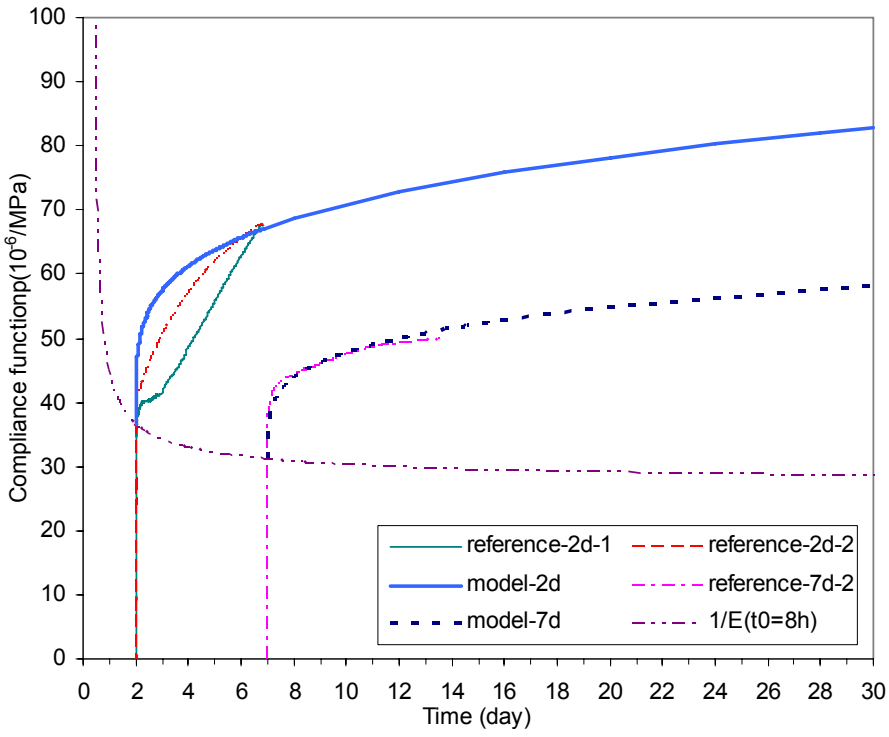

Figure 5-34 Compliance function of tensile creep tests at 20ºC (Reference concrete)

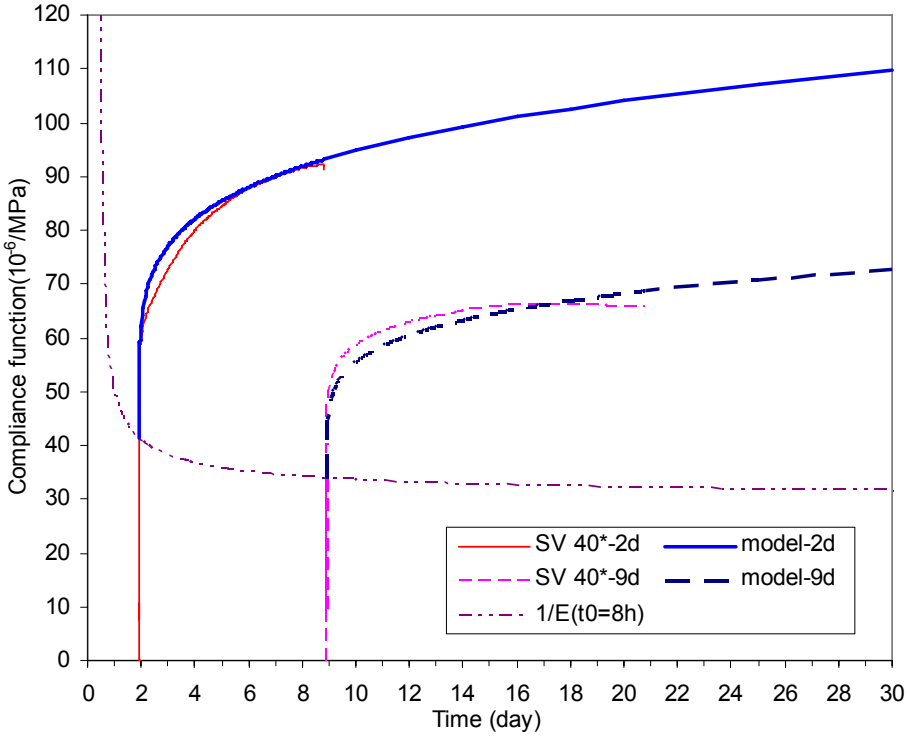

Figure 5-35 Compliance function of tensile creep tests at 20ºC (SV 40*)

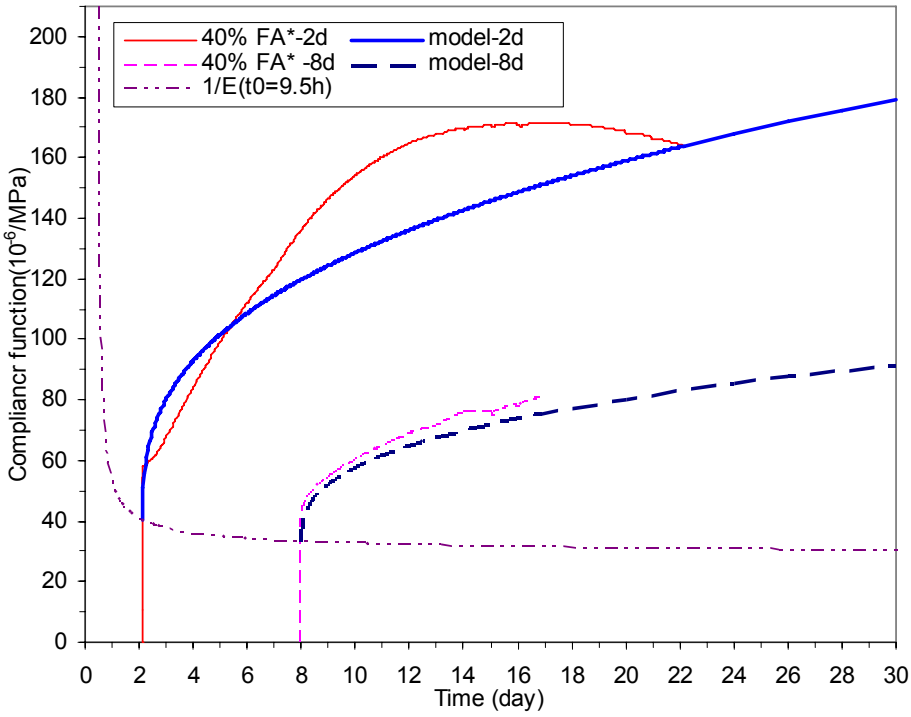

Figure 5-36 Compliance function of tensile creep tests at 20ºC (40% FA*)

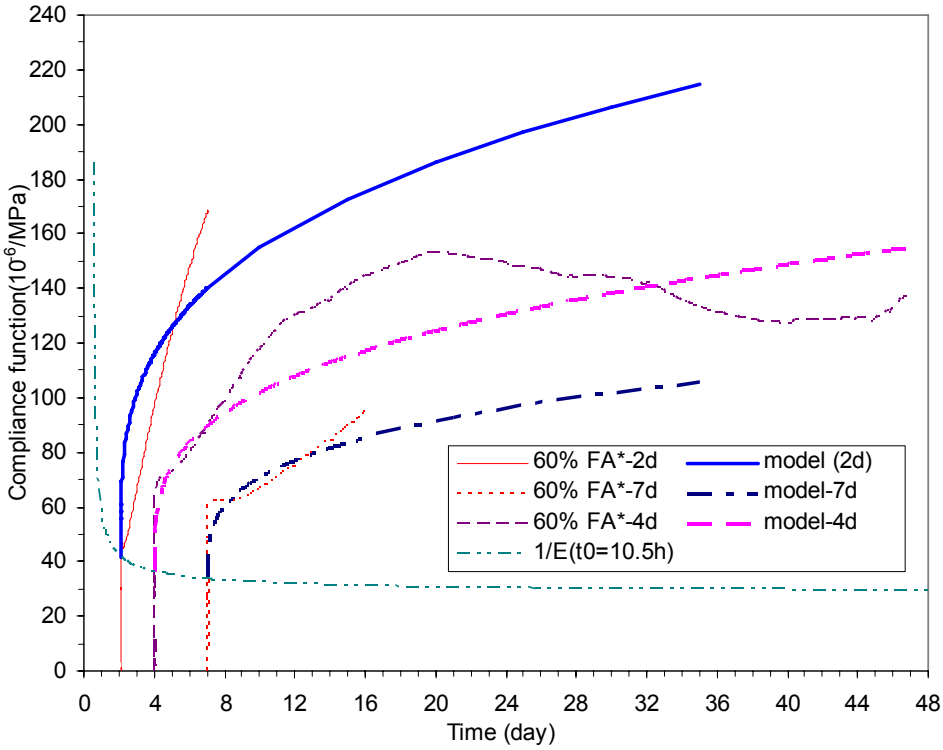

Figure 5-37 Compliance function of tensile creep tests at 20ºC (60% FA*)

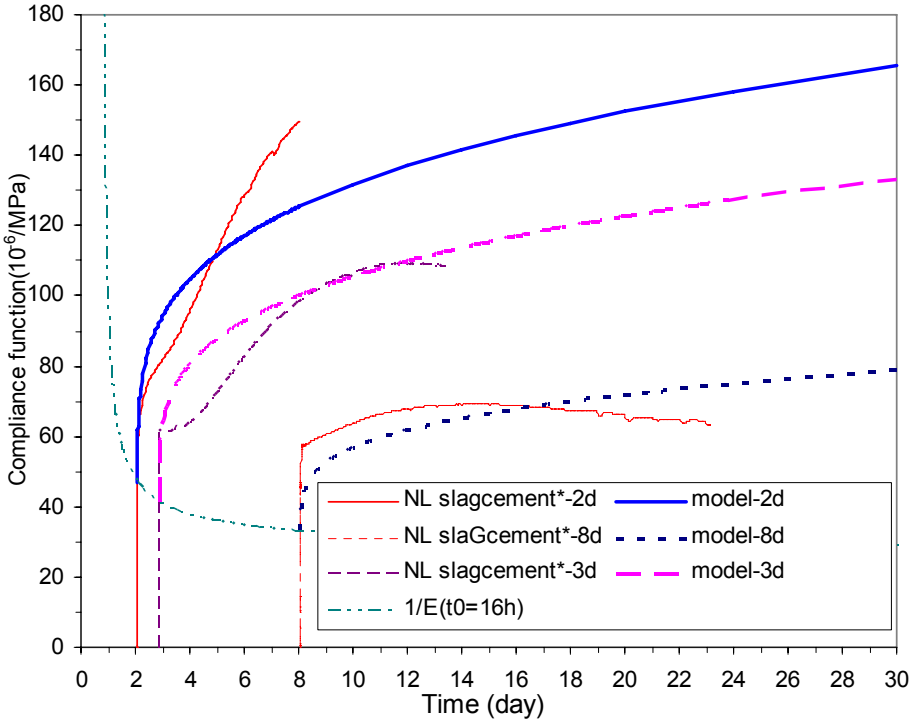

Figure 5-38 Compliance function of tensile creep tests at 20ºC (NL Slag*)

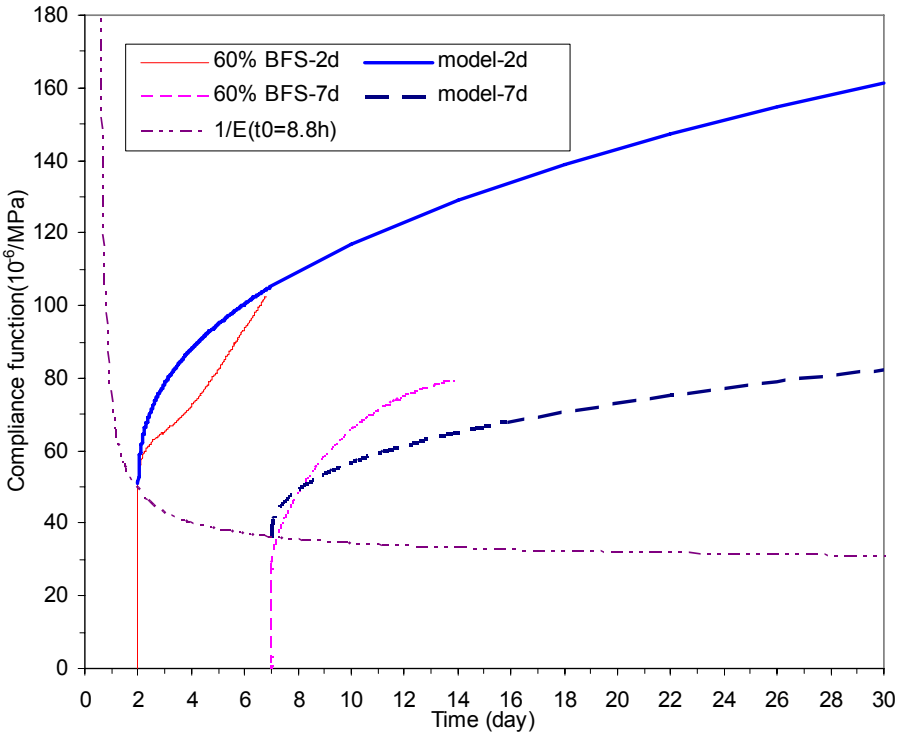

Figure 5-39 Compliance function of tensile creep tests at 20ºC (60% BFS)

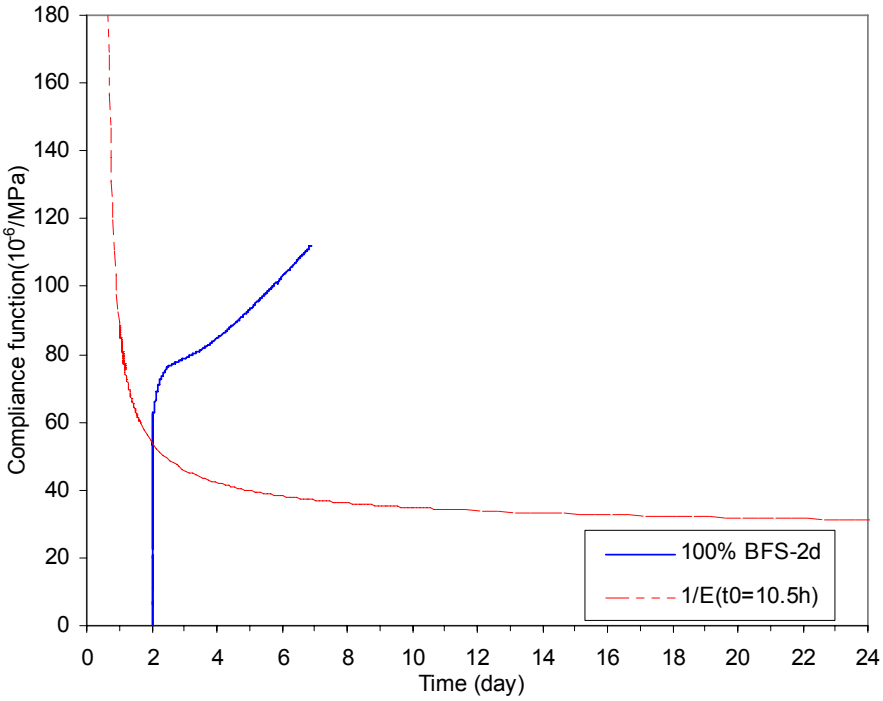

Figure 5-40 Compliance function of tensile creep tests at 20ºC (100% BFS)

Two different sets of creep parameters were obtained by fitting the creep model to the compressive and tensile test data, and due to the different curvature of the compressive and tensile creep data it can be seen that the DPL expresses the former ones considerably better than the latter ones.

5.3.3. Influence of mineral additives on the creep properties at early ages

5.3.3.1. Creep properties in compression

The development of the compliance functions in compression for concrete mixes with different BFS or FA content are presented in Figure 5-41 and Figure 5-42. The replacement of cement with BFS does not have significant effect on the development of the compliance function in compression, and the compliance functions of concrete mixes with 40% or 60% BFS content are only slightly higher than those of the reference concrete.

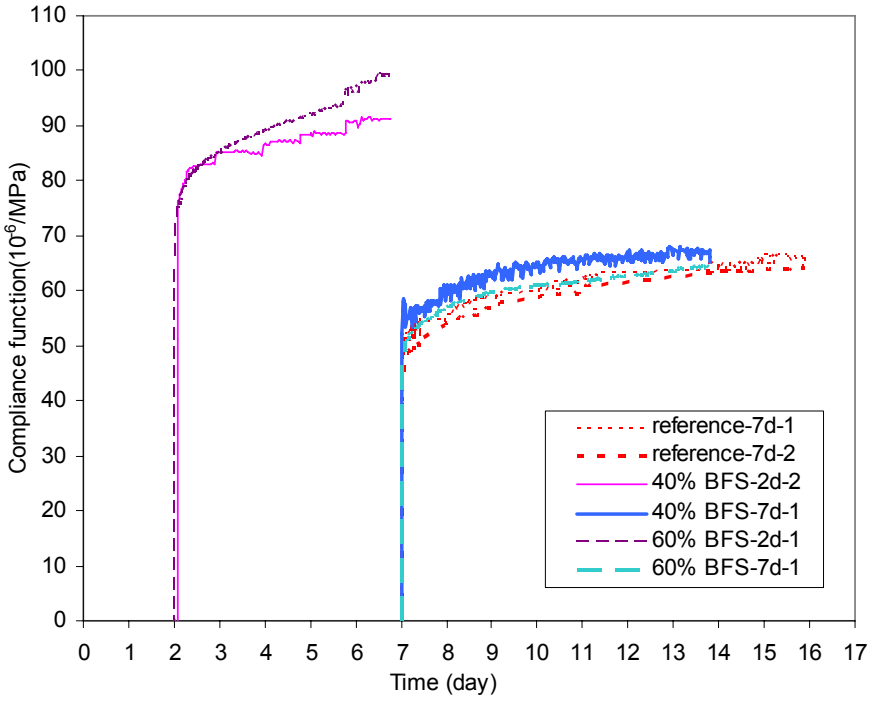

Figure 5-41 Compressive compliance function of concretes containing 0, 40, and 60% BFS

On the other hand, the replacement of cement with FA significantly influences the development of the compliance function in compression. As expected, the higher percentage of fly ash the concrete contains, the higher is the compliance function when the load is applied at very early ages, while the difference of the compliance function between the concrete mixes with different FA content seems to reduce with increasing loading ages.

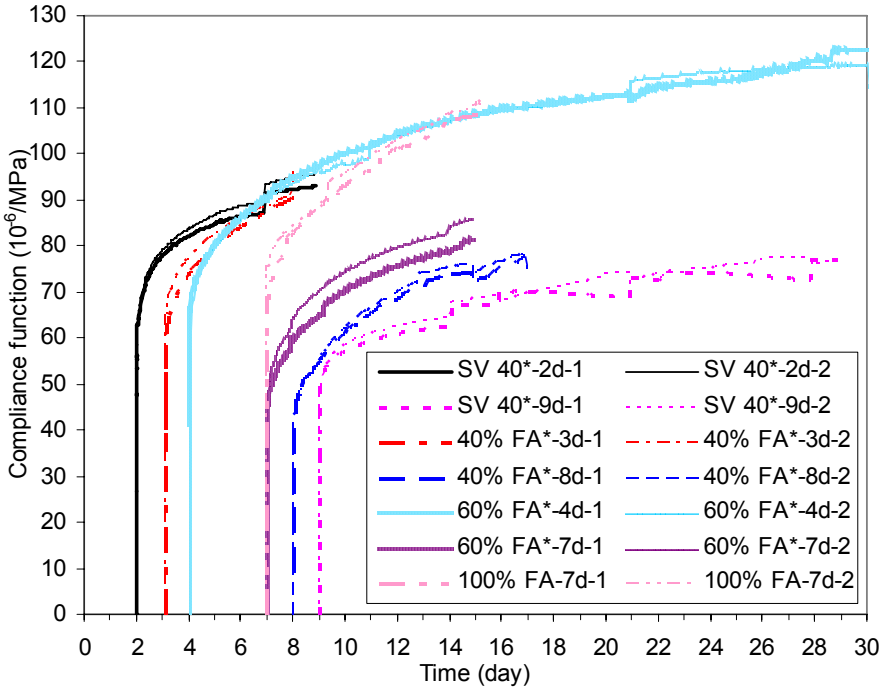

Figure 5-42 Compressive compliance function of concretes containing 0, 40, 60, 100% FA

5.3.3.2. Creep properties in tension

The development of the compliance functions in tension for concrete mixes with different BFS or FA content is presented in Figure 5-43 and Figure 5-44. The results reveal that the replacement of cement with BFS or FA has more pronounced effects on the development of compliance function in tension than in compression. The higher the BFS content is, the higher the compliance function is, and the compliance function increases systematically with the increase of BFS content when the load was applied at 2 days, and the trend is similar when the loading age is 7 days. Note that the NL-slagcement consists of 74% slag and 26% cement; hence it has clearly the highest BFS content and consequently the highest compliance function among the tested concretes in Figure 5-43.

The compliance functions of concrete mixes with FA are lower than that of SV 40* concrete the first day when the load is applied at 2 days, but they develop more rapidly and becomes significantly higher than that of SV40* concrete after several days of loading. It reaches 150 $\mu m/m{\bullet}MPa$ for the concrete with 40% FA after 7 days load duration (at age of 9 days), while the corresponding compliance function of the SV40* concrete is only 90 $\mu m/m{\bullet}MPa$. With the slow reaction of FA/BFS, they are expected to have high compliance functions at early ages.

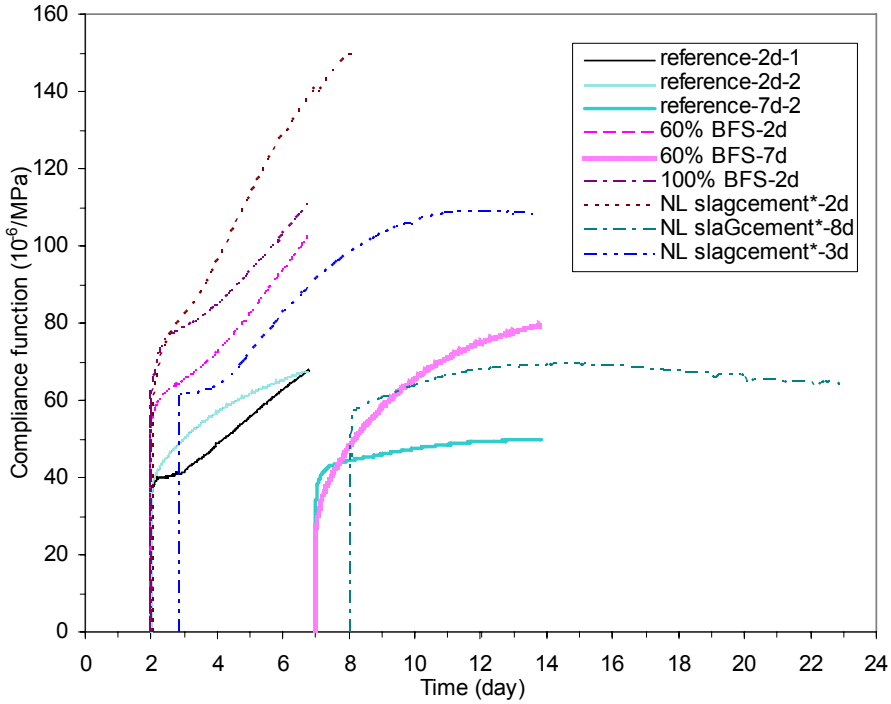

Figure 5-43 Tensile compliance functions of concretes containing different percentage of BFS

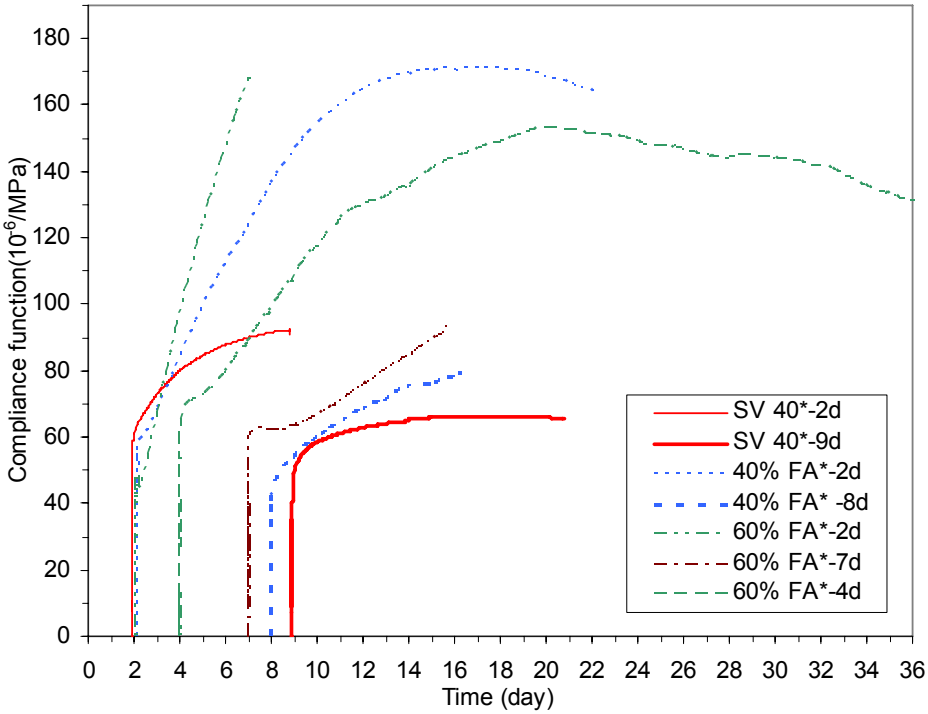

Figure 5-44 Tensile compliance functions of concrete containing 0, 40, and 60% FA*

5.3.4. Comparison of creep in compression and tension

The creep test procedures in compression and tension are similar. Both creep tests in compression and tension contain one loaded (active) specimen and one unloaded specimen (passive). The passive specimen measures the effect of autogenous shrinkage, which results from a gradual self-desiccation of the concrete during hydration. The time-dependent strain measured in the active specimen results from both creep and autogenous shrinkage. Then the time dependent strain measured in the active specimen is compensated for the autogenous shrinkage from the passive one in order to determine the creep strain over time, hence it is assumed that the two phenomena are independent.

An important point to note in this regard is that the relative importance of the compensation is very different in compressive and tensile creep tests. During the tensile creep tests, the applied load is small, hence the creep strains (expansion) are quite small and often in the same order of magnitude as the autogenous shrinkage from the dummy. Consequently, the compensation (autogenous shrinkage) from the dummy is significant compared to the phenomenon under study (creep). In compressive creep tests this is not the case, since the loaded specimen is subjected to considerably higher stresses and, hence, the relative importance of autogenous shrinkage is much less.

For example, the comparison of measured strains in compressive and tensile creep tests for the 60% FA* concrete is shown in Figure 5-45. The load is applied at 7 days, and the magnitude of compressive load is 95KN and is much higher than the tensile load (7 KN), but the compressive stress/strength ratio is similar as the tensile stress/strength ratio at the loading time. The measured strain in the compressive loaded specimen is about 480 μ, which is about 10 times the strain in the tensile loaded specimen.

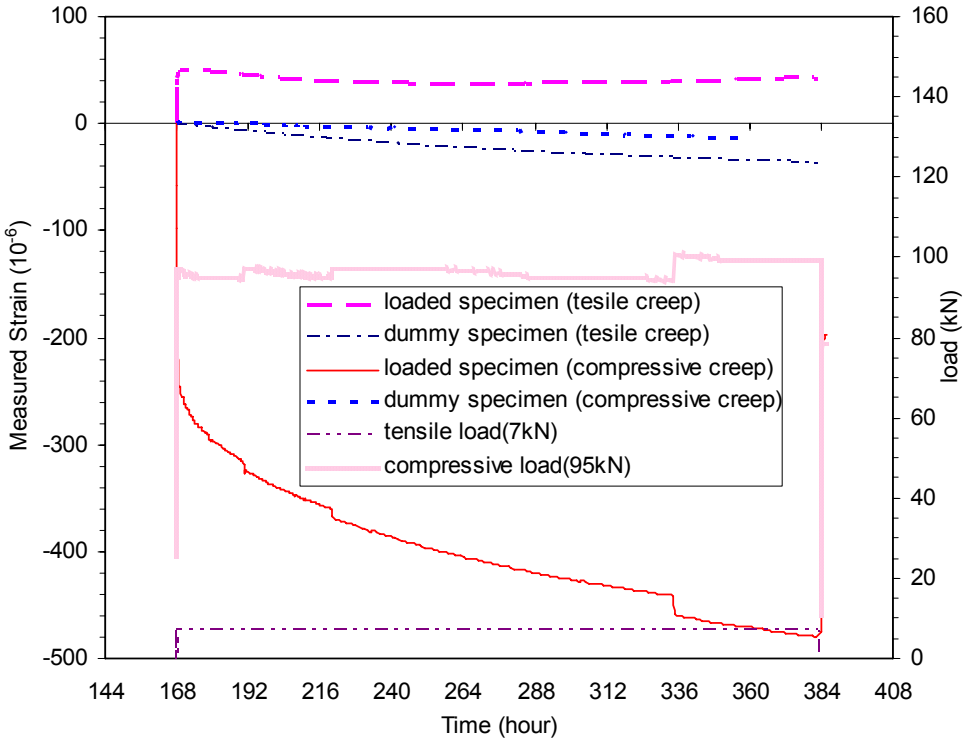

Figure 5-45 Comparison of measured strains in compressive and tensile creep test

The results of the parallel creep tests in both tension and compression for four types of concretes: SV40*, 40% FA*, 60% FA*, and 60% BFS, are presented in Figure 5-46 to Figure 5-49.

The compliance function of the SV40* concrete is fairly similar in compression and tension, as shown in Figure 5-46. But the compliance functions for the concretes with BFS or FA show larger differences in compression and tension, as shown in Figure 5-47 and Figure 5-48, especially when the load is applied at very early age. For 60% FA* concrete, the instantaneous deformation under tension is lower than that under compression, and the compliance function in compression is higher than that in tension within several days after loading. However the rate of the compliance function in compression decreases strongly shortly after loading and the difference between two compliance function curves reduces by time, and then the total compliance function in tension becomes higher than the one in compression. A similar trend is also observed in the concrete with 60% BFS.

The creep behavior in compression and tension for early age concretes containing mineral additives as we have just seen is quite different. The reason why compressive and tensile creep appears to be so different at early age is presently unclear, but the results presented here confirms earlier work from the concrete laboratory at NTNU (Atrushi, 2003).

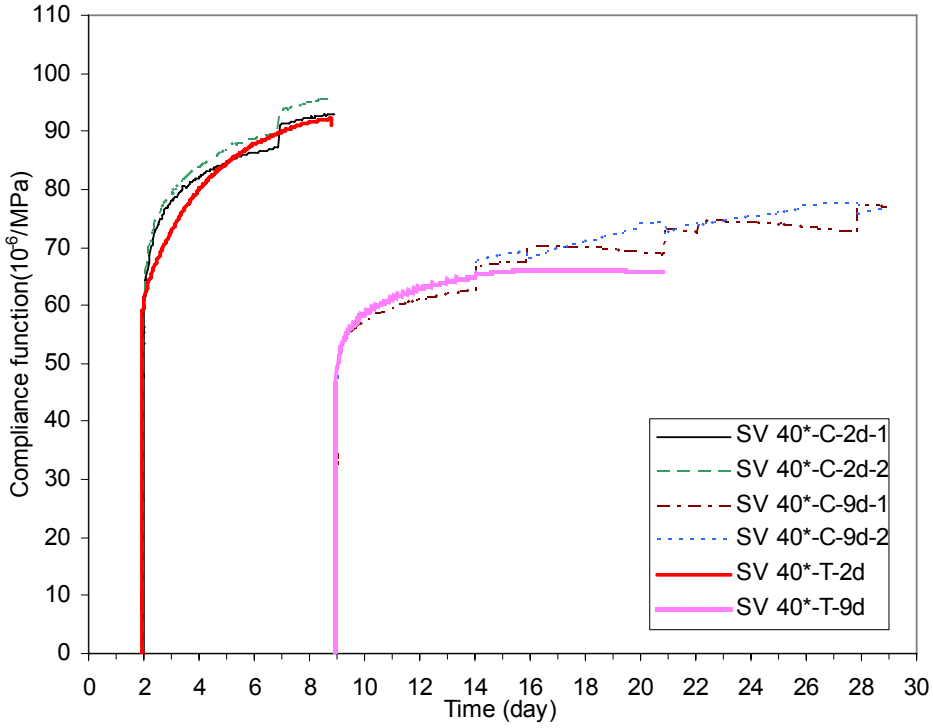

Figure 5-46 Comparison between compliance function in tension and compression, SV 40*

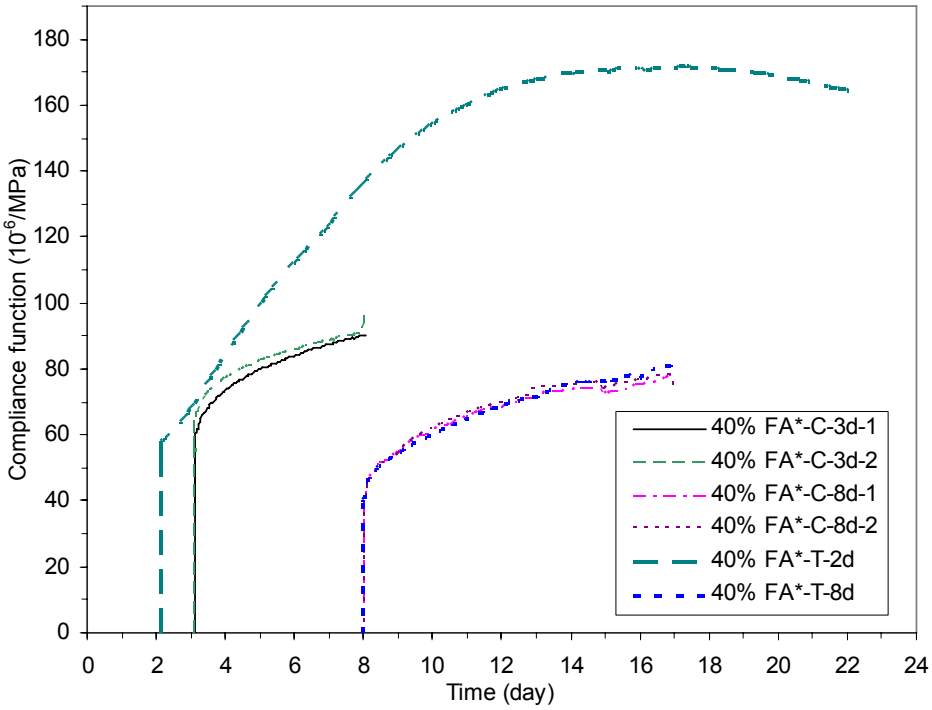

Figure 5-47 Comparison between compliance function in tension and compression, 40% FA*

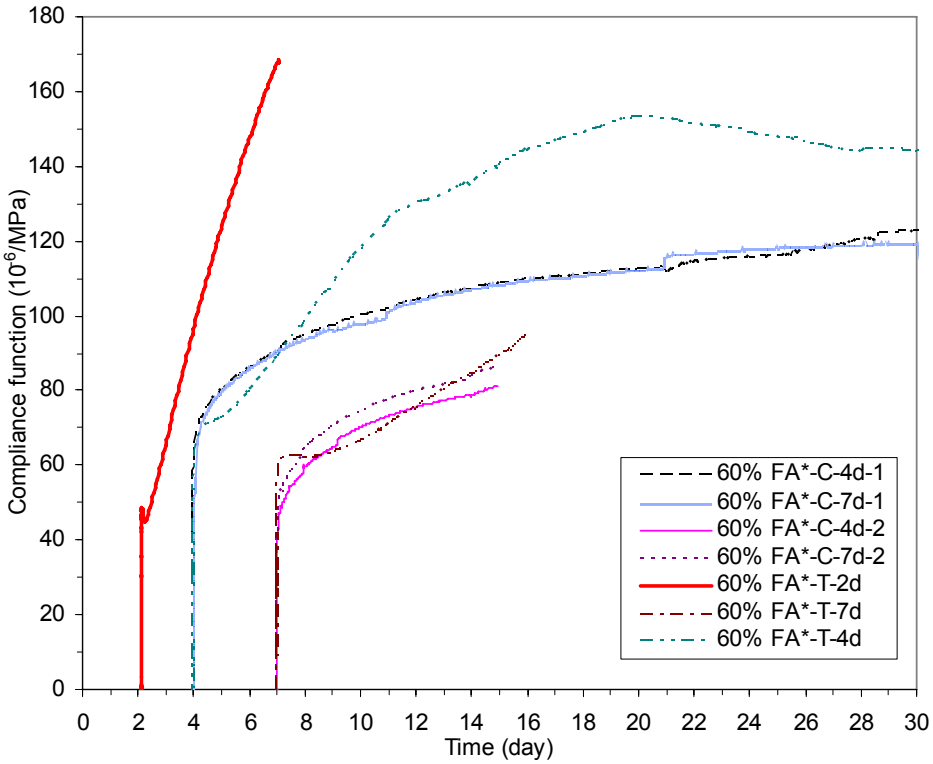

Figure 5-48 Comparison between compliance function in tension and compression, 60% FA*

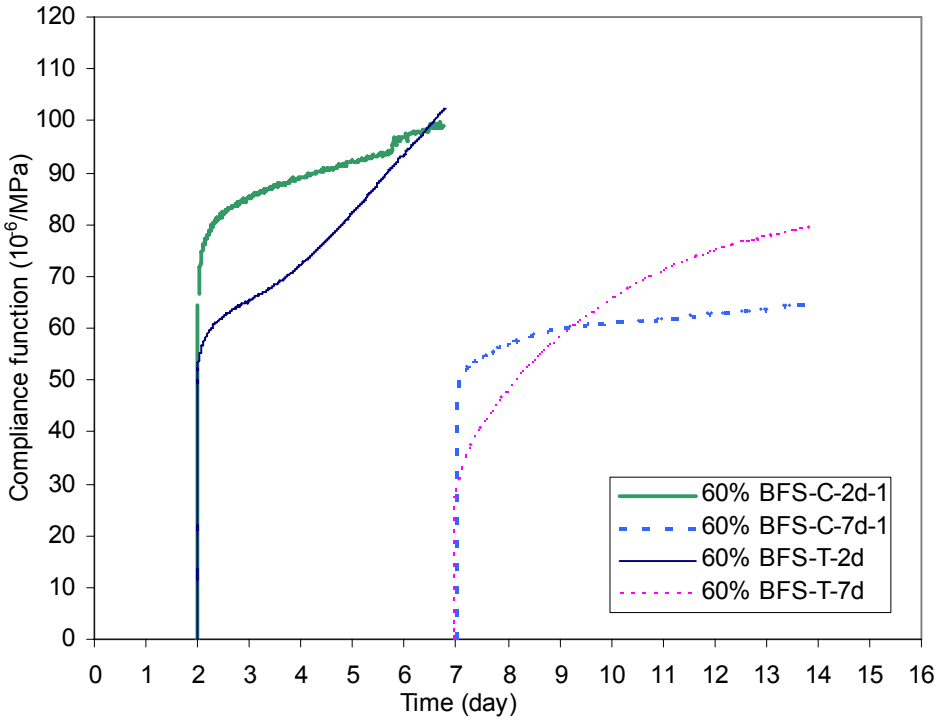

Figure 5-49 Comparison between compliance function in tension and compression, 60% BFS

5.4. Transient thermal creep

Transitional thermal creep is described as the increase of creep due to temperature change, regardless of cooling and heating. The test method of transient thermal creep is previously discussed in Chapter 3.

The results of transient thermal creep tests for hardened and young concrete (Basic 5) are presented in this part. The free strain measured in the dilation rig and the TSTM tests under similar temperature histories with heating-cooling cycles have been compared, and the reproducibility between the dilation rig and the TSTM test is discussed. Then the temperature effect on the strain development is determined by subtracting the relevant free strain from the total strain measured in the TSTM under the same temperature and constant load condition. An analytical method is then used to analyse the test data, and its applicability is further discussed.

5.4.1. Test results of hardened concrete

To determine the transient thermal creep, it is necessary to know the free deformation strain under variable temperature history. The autogenous shrinkage is negligible for mature hardened concrete under sealed conditions, and the free deformation during heating-cooling cycles at different times can therefore be measured in the same specimen either in the Dilation Rig or in the unrestrained TSTM. The reproducibility in either rig under variable temperature history has been verified by comparison of the free strain development in successive cycles with the exactly same temperature histories. The changes of the temperature have been moderate, because high

temperature will alter the structure of the mature concrete. The temperature histories applied in the TSTM and the Dilation Rig are as similar as possible, and the results from parallel specimens in the Dilation Rig and the TSTM during the same cycle are also compared. Finally the relevant free strain applied to calculate transient thermal creep is determined.

Parallel tests (No.183, Basic 5 concrete, age=1.2 year) were performed in the TSTM and the Dilation Rig with the same three cycles of heating-cooling. Compressive load was applied to the specimen in the TSTM during the second cycle. The temperature history for the TSTM and the Dilation Rig and the compressive load in the TSTM are shown in Figure 5-50, while the measured strain development of the two parallel specimens are presented in Figure 5-51.

The measured free strains in the dilation rig develop quickly under heating, but the expansive behaviour changes into contraction during the following isothermal period. This phenomenon is so called delayed thermal deformation, and it is presumably related to the water redistribution to match thermodynamic equilibrium. The phenomenon is less pronounced when the temperature is kept constant after cooling. The delayed thermal deformation is also observed in the TSTM test, but its magnitude during the first and the third heating-cooling cycle in the TSTM is smaller than the magnitude in the dilation rig, and this is possibly due to the restraint in the two end heads of the TSTM specimen. The compressive load which is applied during the second heating-cooling cycle increases the contraction strain in the TSTM as expected.

Particular attention is paid to the rapid strain evolution at high rate of temperature changes (approximate 15ºC/hr), and the relationship between strain development and temperature increase/decrease is plotted in Figure 5-52. The free strain developments in the dilation rig and the TSTM test during the first temperature increase are quite similar, and the measured strain in the TSTM under compressive load is apparently lower than the free strain when the temperature increases second time from 20ºC to 65 ºC. The existence of transient thermal strains is clearly shown by using the experimental technique of changing temperature stages under constant load.

It is shown in Figure 5-52 that the reproducibility in both the dilation rig and the TSTM is good. The free strain measured during the first heating-cooling cycle and the total strain measured during the second cycle under compressive load from the same specimen in the TSTM is applied to calculate the transient thermal creep, as shown in Figure 5-53, and the elastic plus creep strain and the compliance function are presented in Figure 5-54. It can be seen from Figure 5-50 that the applied compressive load had a sudden decrease when the temperature was reduced from 65ºC to 20ºC, and the effect of the reduction of the load was included in the elastic plus creep strain in Figure 5-54 a), and it was divided by the reduced stress to obtain this part of compliance function.

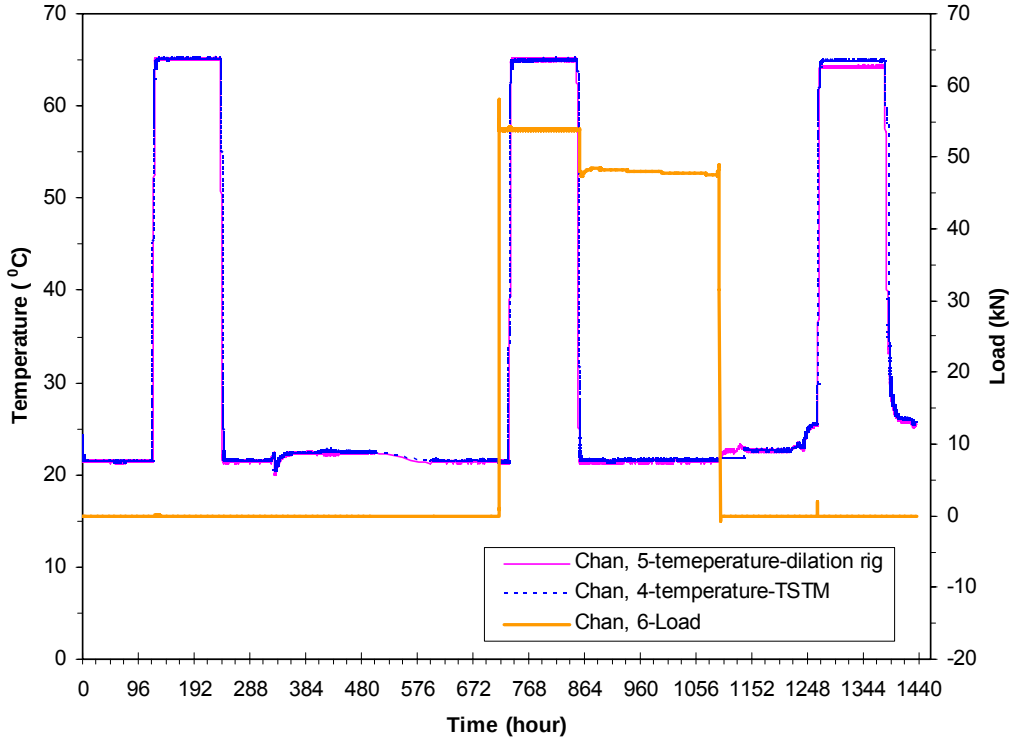

Figure 5-50 Temperature and loading history in the TSTM and the dilation rig (No. 183, compressive stress)

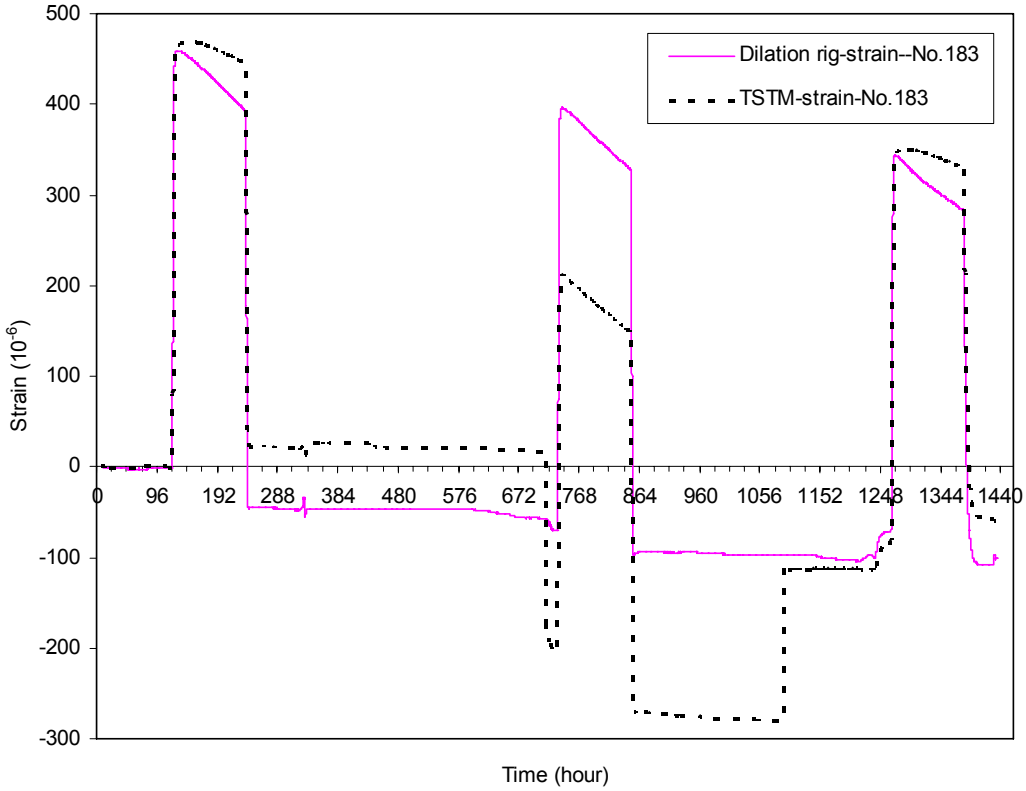

Figure 5-51 Total strain development in the TSTM and the dilation rig (No. 183) Compressive load

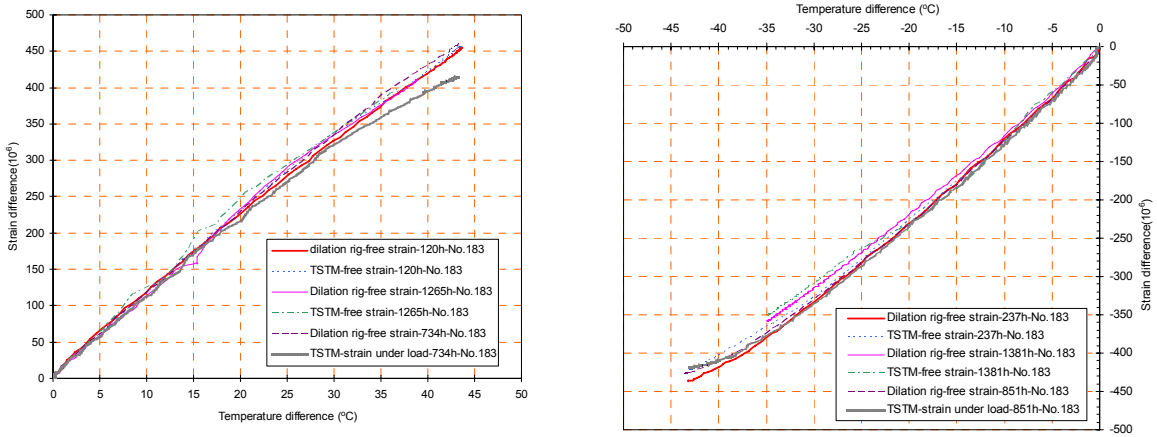

a) Temperature increase b) Temperature decrease

Figure 5-52 Strain developments in the TSTM and the dilation rig during temperature increase/decrease

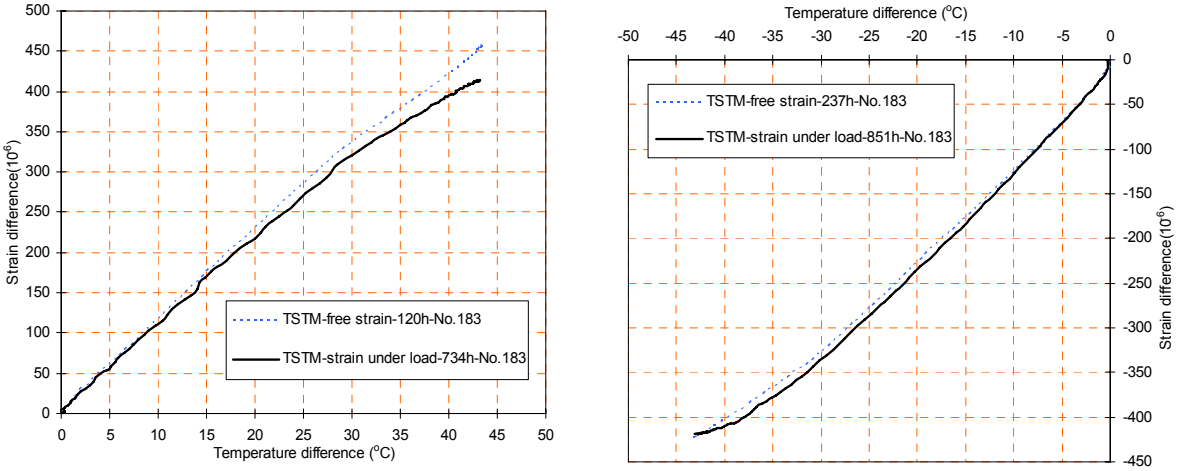

a) Temperature increase b) Temperature decrease

Figure 5-53 Free strain and total strain applied to calculate the transient thermal creep (No.183)

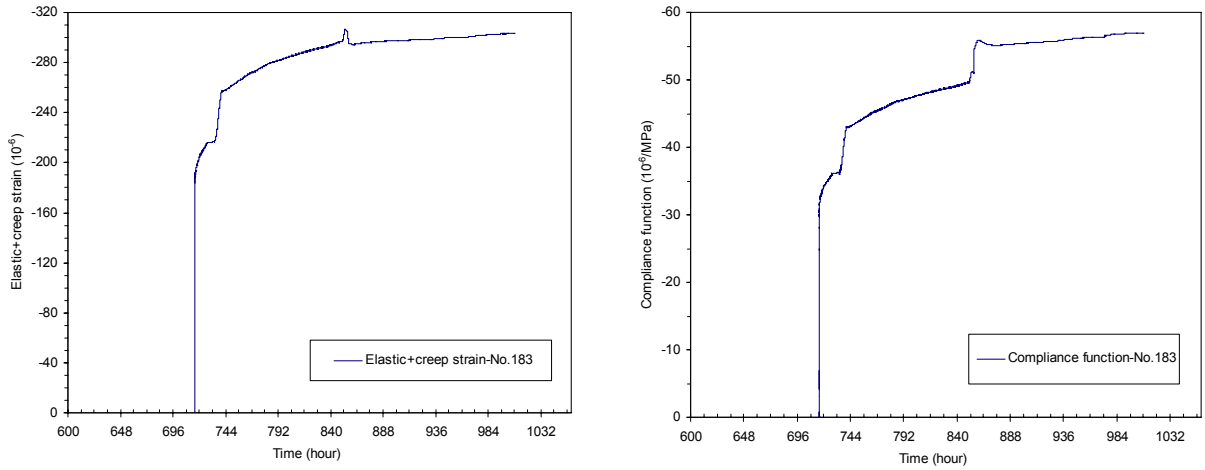

a) Elastic plus creep strain b) Compliance function

Figure 5-54 Transient thermal creep test (No.183, compressive stress)

Another parallel test (No. 173-2, age=60 days) was performed in the dilation rig and the TSTM with two cycles of heating-cooling. This time tensile load was applied to the specimen in the TSTM during the first cycle. The temperature history of the TSTM and the dilation rig tests and the tensile load of the TSTM test are shown in Figure 5-55, and the measured strain development of the tests are presented in Figure 5-56.

The measured free strains of the specimen in the dilation rig during two cycles are almost the same, hence the reproducibility in the dilation rig is good for hardened concrete, but comparison of the measured free strains of parallel specimens in the dilation rig and the TSTM during second cycle shows that the free strain in the TSTM is apparently smaller than that in the dilation rig. This was also discussed for the previous test, and the size effect and different restraint conditions in the dilation rig and the TSTM may contribute to the difference. The deviation of measured free strain in the dilation rig and the TSTM is also observed in the tests for young concrete as shown later.

The measured free strain in the dilation rig is about 40 μm/m higher than that in the TSTM when the temperature increases from 20 ºC to 64ºC, which is in the same order of magnitude of difference between total strain measured in the TSTM under tension and free strain measured in TSTM without load. Which of these two free deformation strains is used in the determination of transient thermal creep will show different temperature effect on creep. It is seen from Figure 5-57 that the reproducibility in the dilation rig is good, and then it is assumed the reproducibility in the TSTM also is good. In this case, the free strain from the TSTM test under second heating-cooling cycle is used to calculate the transient thermal creep, as shown in Figure 5-58, and the elastic plus creep strain and compliance function are presented in Figure 5-59.

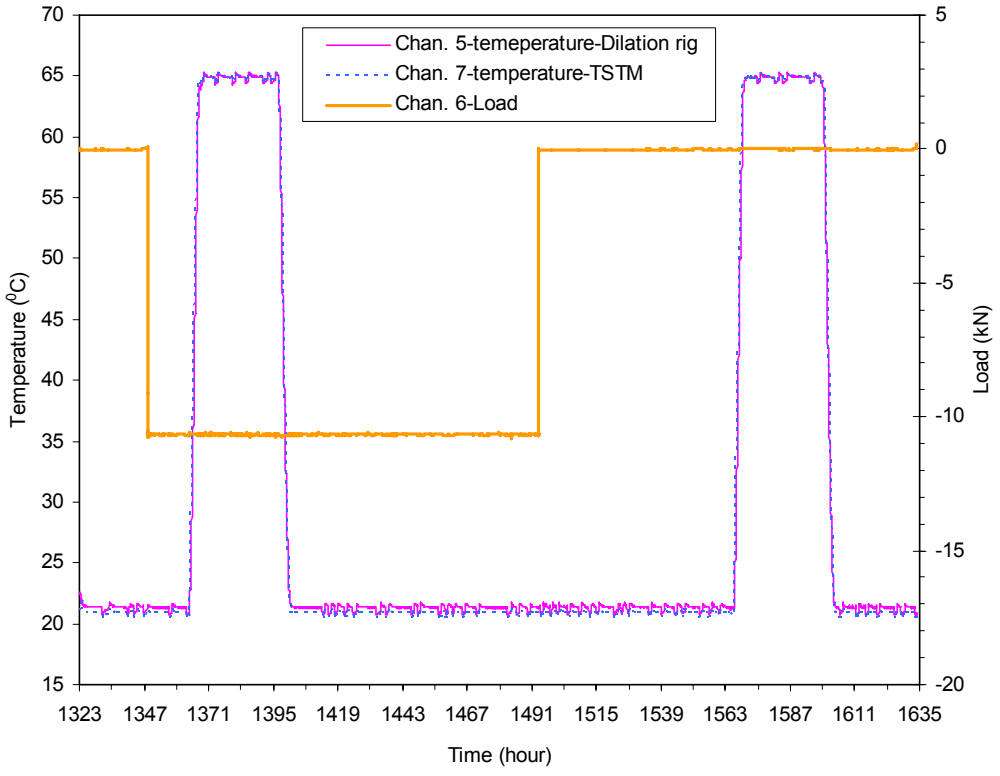

Figure 5-55 Temperature and loading history in the TSTM and the dilation rig (No. 173-2, tensile stress)

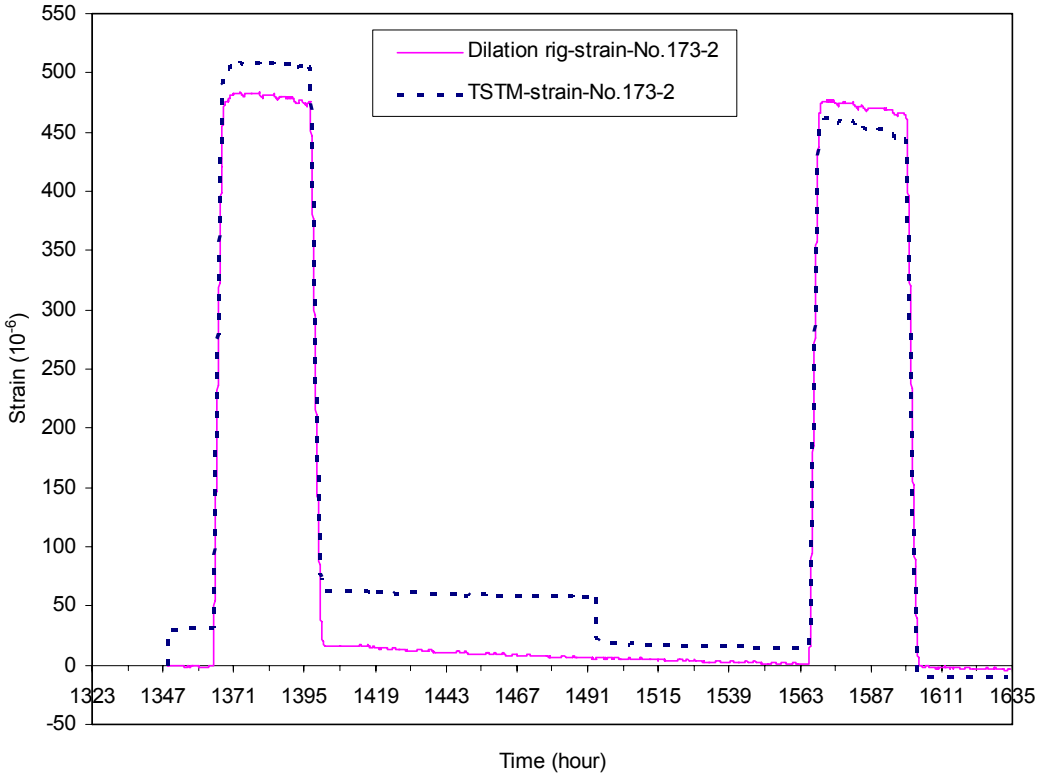

Figure 5-56 Total strain development in the TSTM and the dilation rig (No. 173-2)

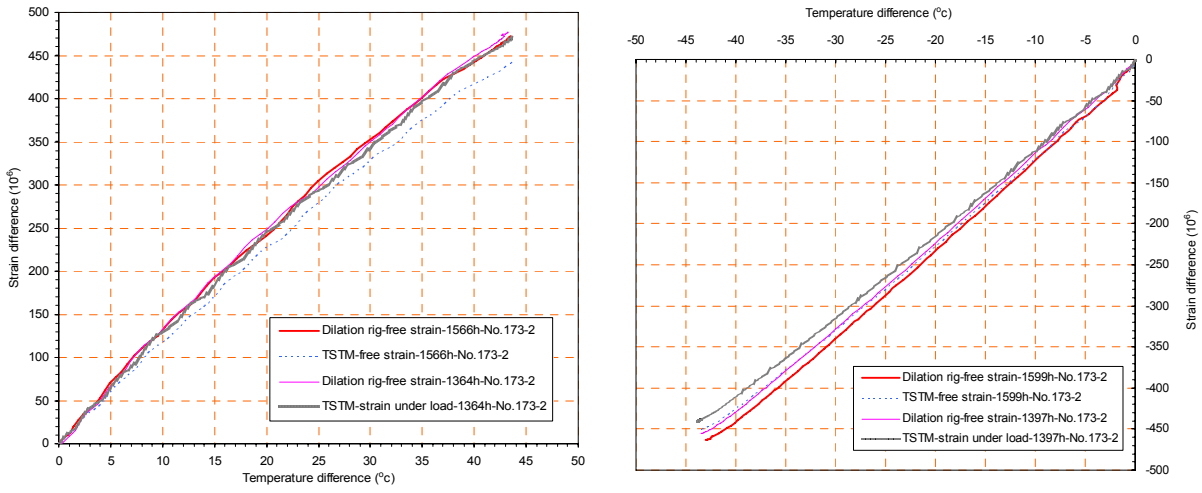

a) Temperature increase b) Temperature decrease

Figure 5-57 Strain developments in the TSTM and the dilation rig during temperature increase/decrease

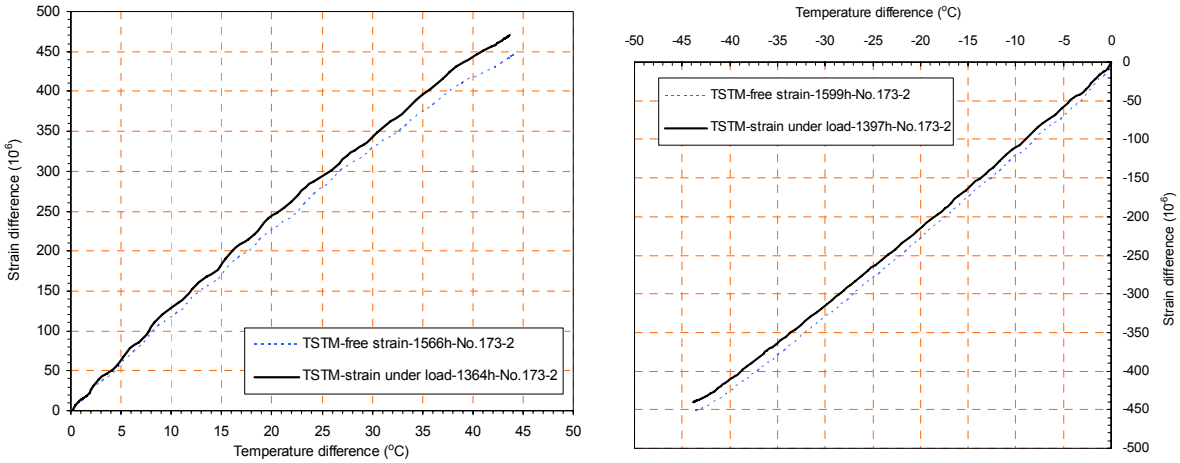

a) Temperature increase b) Temperature decrease

Figure 5-58 Free strain and total strain applied to calculate the transient thermal creep (No.173-2)

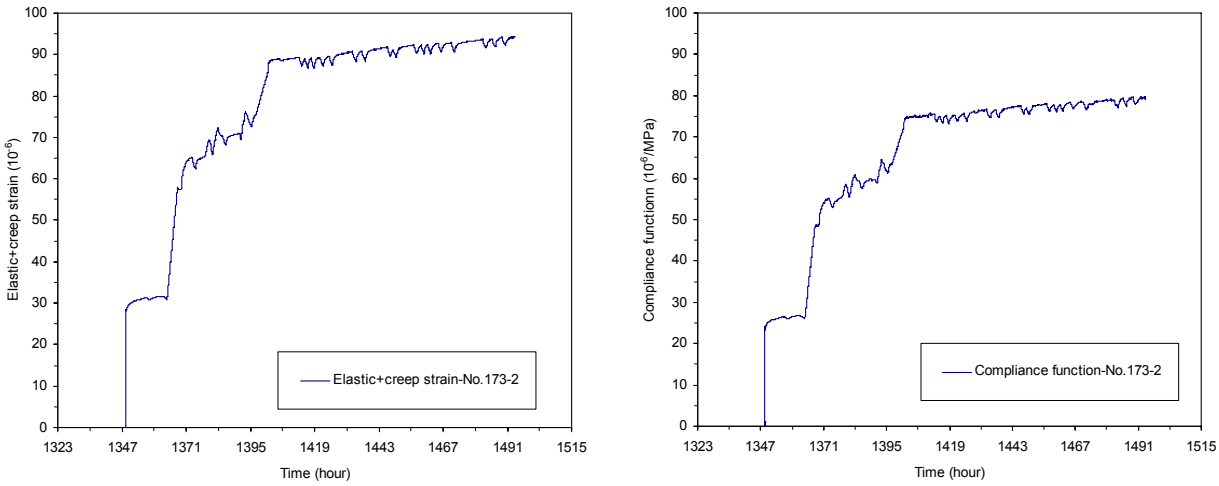

a) elastic plus creep strain b)Compliance function

Figure 5-59 Transient thermal creep test (No.173-2, tensile stress)

As shown in Figure 5-54 b) and Figure 5-59 b), the transient thermal creep apparently exists in both heating and cooling phase for compressive and tensile loading, and the compliance functions increase significantly due to temperature changes.

5.4.2. Test results of early age concrete

The evaluation of the temperature effects on creep is even more complex for early age concrete than for hardened concrete. The free deformation measured in the hardened concrete under sealed condition represents only the thermal dilation, and the free strains are measured in the same specimen in the TSTM during heating-cooling cycles at different times and then they are used to determine the temperature effect on the creep properties. But the free deformation measured in the young concrete includes not only thermal dilation but also autogenous shrinkage, and the mechanical properties, which strongly depend on time and develop rapidly at early age. Tests in the dilation rig and the TSTM with the same temperature at the same age are

repeated, and the reproducibility can only be verified by comparison of test results from different specimens in the dilation rig or the TSTM.

The free deformation is measured in several specimens either in the dilation rig or in the TSTM with the same temperature at same age, and the free strain developments of the different specimens in the dilation rig or the TSTM during the same cycle is used to verify the reproducibility in the dilation rig or the TSTM under variable temperature history. The free strain measured in parallel specimens in the dilation rig and the TSTM during same cycle is also compared, and the relevant free strain used in determination of transient thermal creep is further discussed.

Four parallel tests were performed for young concrete. In the first parallel test (No. 170), the free strains were measured in the dilation rig and the TSTM with two similar cycles of heating-cooling, and the temperature and free strain developments are presented in Figure 5-60 and Figure 5-61. In the second parallel test (No. 171), the TSTM test under compressive load was not performed because the motor failed during the application of loading, and only the free deformation in dilation rig with one cycle of heating-cooling was recorded. The temperature and free strain are presented in Figure 5-62 and Figure 5-63. The TSTM test under compressive load was repeated in the third parallel test (No. 172), and the temperature and total strain development are shown in Figure 5-65 and Figure 5-66. In the last parallel test (No. 173), the TSTM test under tensile load was conducted, and the temperature and total strain development are shown in Figure 5-70 and Figure 5-71.

The results show that the free deformation measured in the TSTM and the dilation rig under similar temperature history are different for the early age concrete. The mechanical properties develop rapidly during the hardening process and different restraint conditions are possibly induced in the TSTM and the dilation rig due to different specimen size and test apparatus. The measured free strain in the dilation rig is higher than the free strain in the TSTM during the same cycle, which indicates that the restraint in the TSTM is higher than the restraint in the dilation rig. The difference is about 50 μ when the temperature increases from 20ºC to 65ºC, as shown in Figure 5-64. Which free deformation is used in the process of calculation of transient thermal creep is of course very important for the result.

The free strain developments in the three dilation rig tests (No.170, 171, 172) are quite similar, as shown in Figure 5-64 and Figure 5-67, demonstrating that the reproducibility in the dilation rig is quite good for young concrete. The measured free strain in the unrestrained TSTM, which has the same specimen geometry and temperature history as the TSTM test under load condition, is considered most appropriate to be applied in the calculation of transient thermal creep for the young concrete. It is therefore used even if the documentation of reproducibility is lacking.

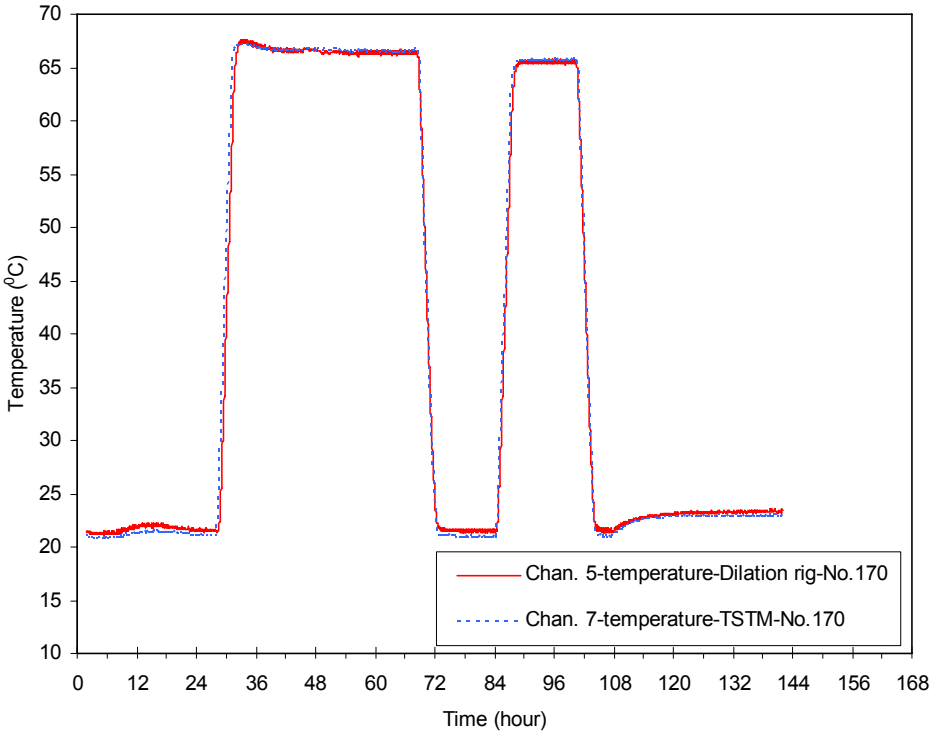

Figure 5-60 Temperature history in the TSTM and the dilation rig (No. 170)

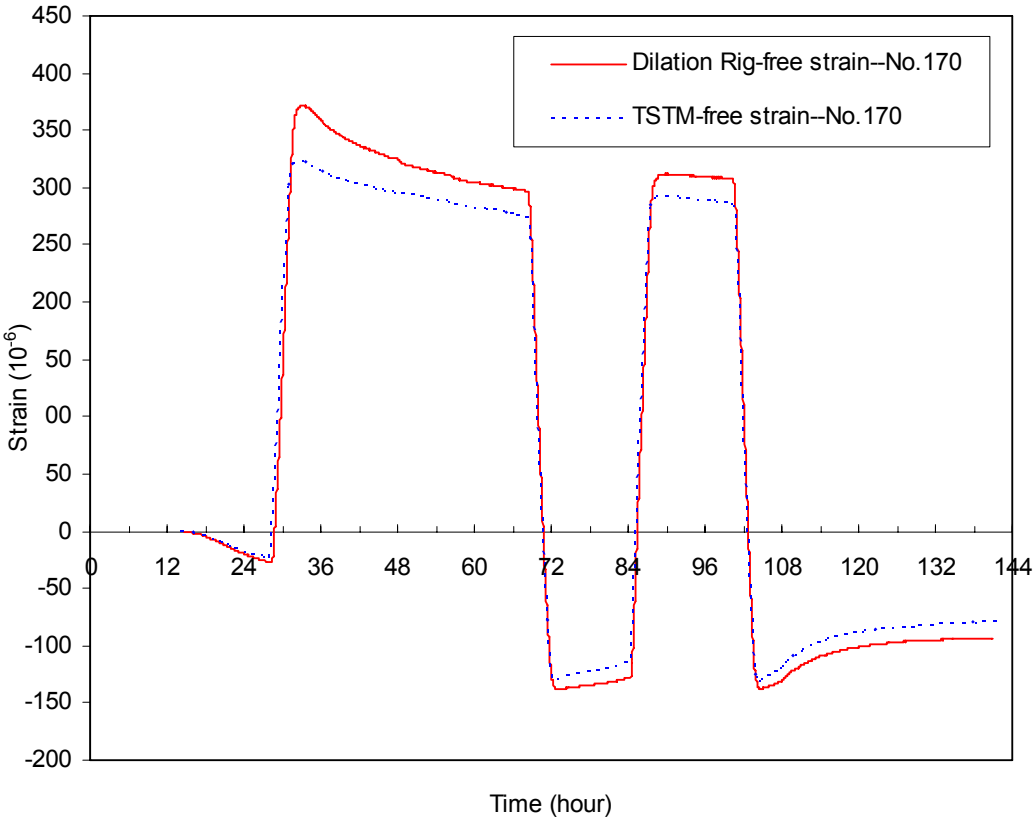

Figure 5-61 Total strain developments in the TSTM and the dilation rig (No. 170)

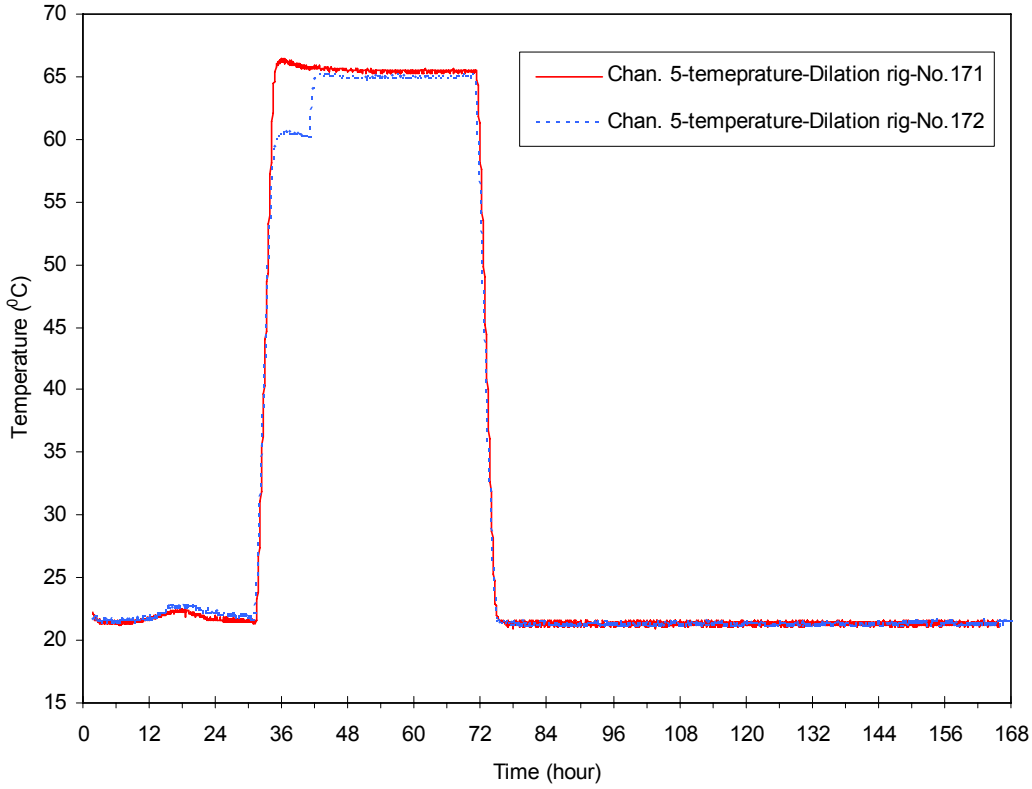

Figure 5-62 Temperature histories in the dilation rig (No. 171 and 172)

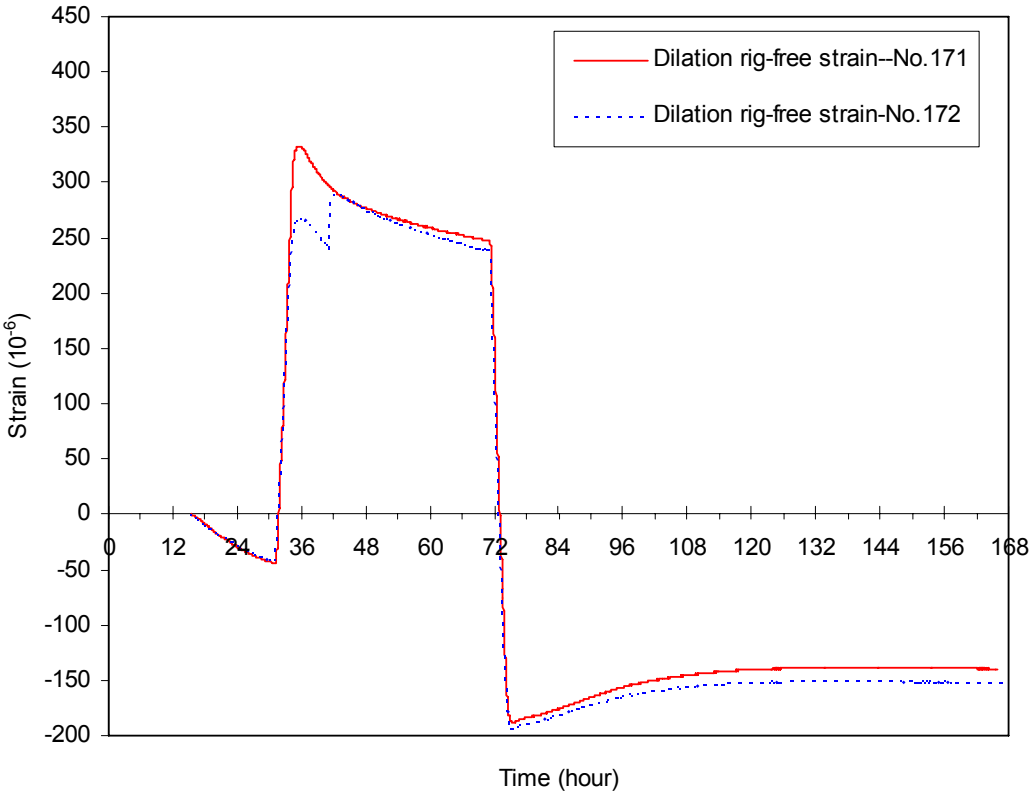

Figure 5-63 Free strain developments in the dilation rig (No. 171 and 172)

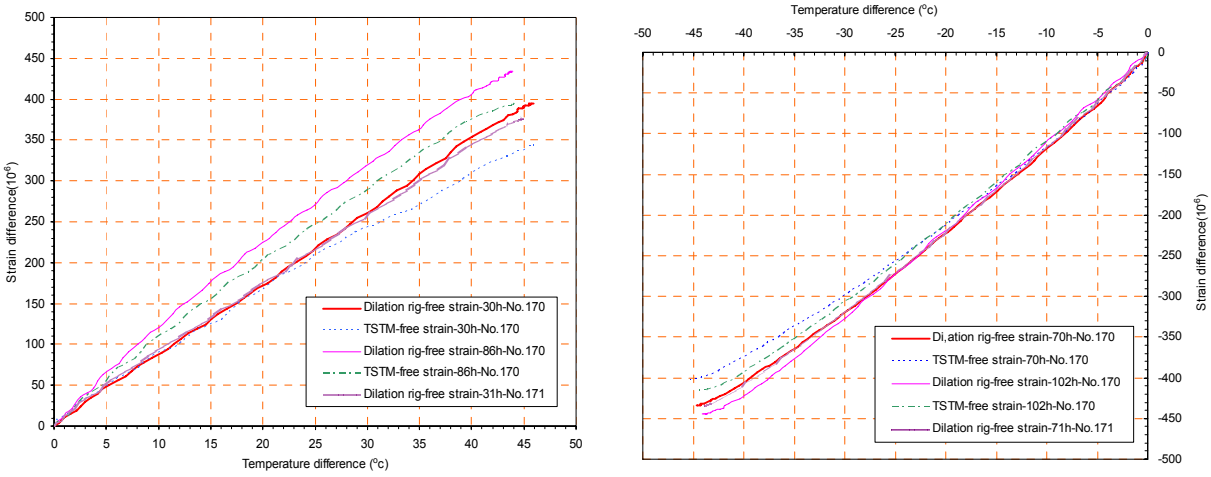

a) Temperature increase b) Temperature decrease

Figure 5-64 Free strains in TSTM and dilation rig during temperature increase/decrease

The temperature effect on the strain development under compressive load is evaluated by subtracting free strain measured in the TSTM test (No.170) from the total strain measured in the TSTM test (No. 172), as shown in Figure 5-68, and the elastic plus creep strain and the compliance function are presented in Figure 5-69.

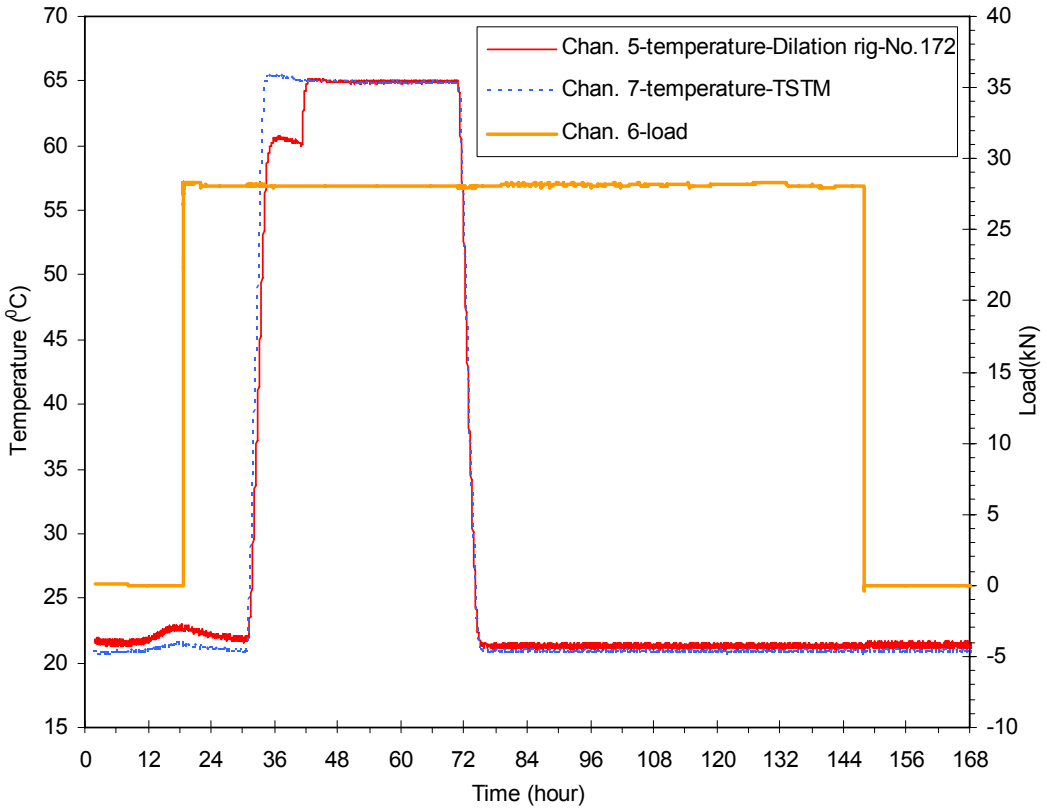

Figure 5-65 Temperature and loading history in the TSTM and the dilation rig (No. 172, compressive stress)

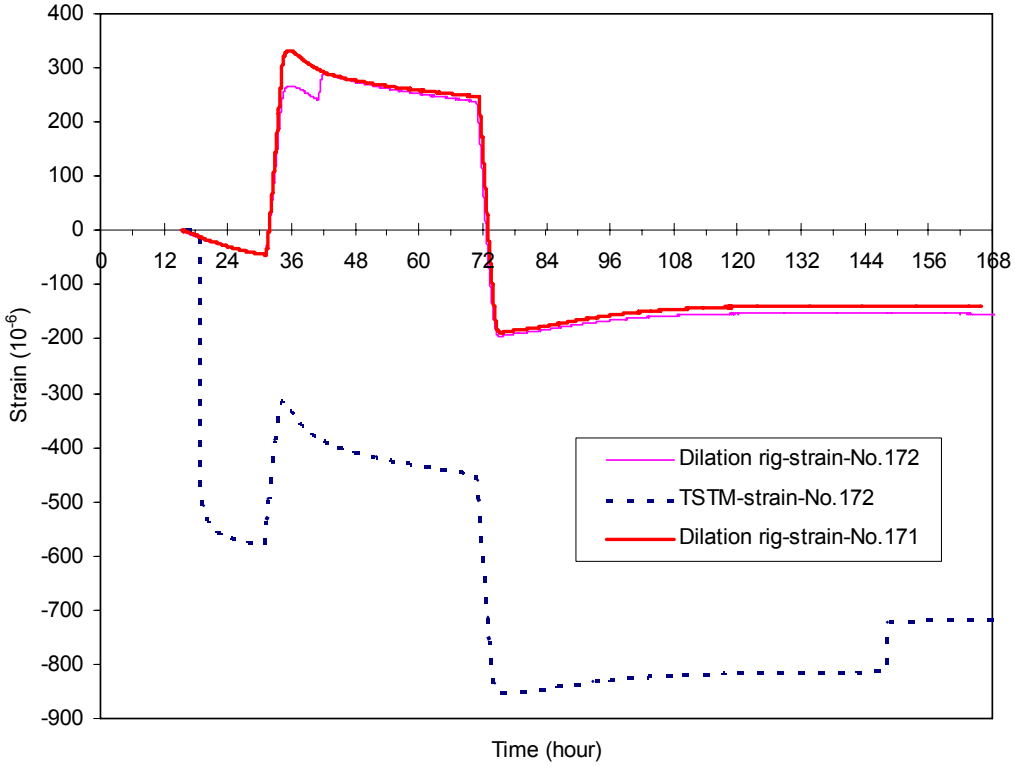

Figure 5-66 Total strain developments in the TSTM and the dilation rig (No. 172 and 171, compressive stress)

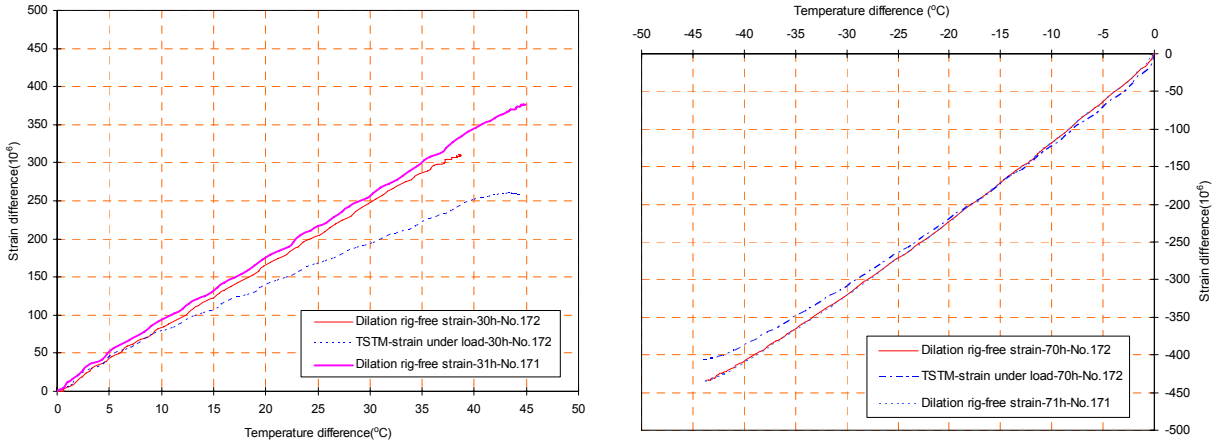

a) Temperature increase b) Temperature decrease

Figure 5-67 Strain developments in TSTM and dilation rig during temperature increase/decrease

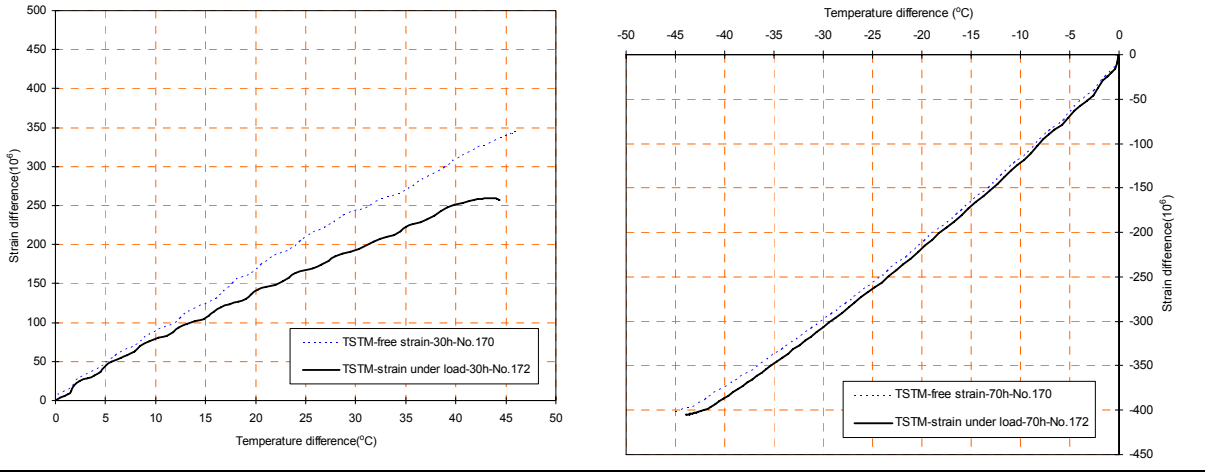

a) Temperature increase b) Temperature decrease

Figure 5-68 Free strain (No.170) and total strain (No.172) applied to calculate the transient thermal creep

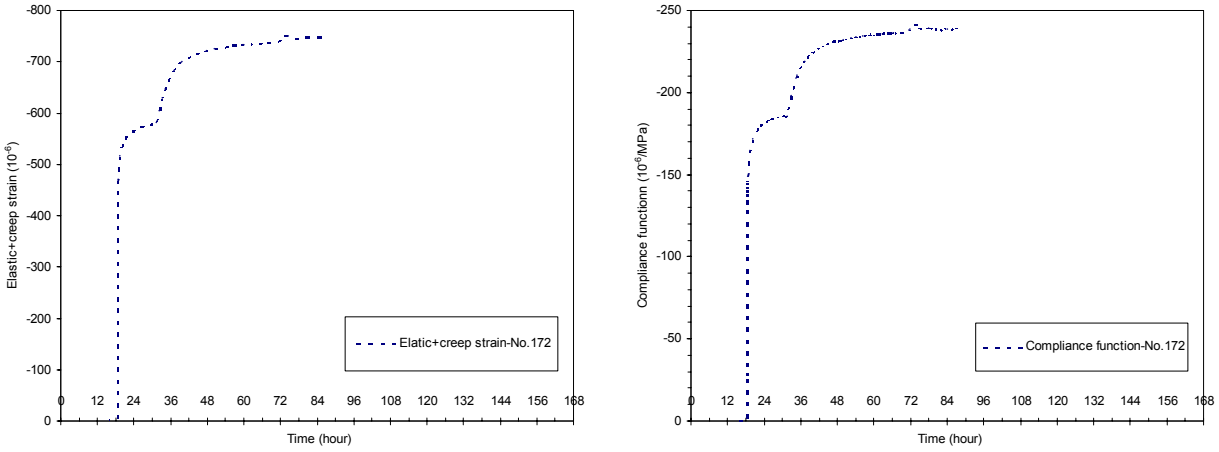

a) Elastic plus creep strain b) compliance function

Figure 5-69 Transient thermal creep test (No.172, compressive stress)

A simple relationship between free deformation strains measured in the TSTM and the dilation rig during same cycle may be introduced, and then the free deformation measured in dilation rig can be transferred to predict free deformation in the TSTM, which can be used as an alternative in calculation of transient thermal creep if the free deformation in TSTM test is not available. This procedure is applied in another case (No.173) to evaluate the temperature effect on strain development under tensile load, as shown in Figure 5-73, and the elastic plus creep strain and the compliance function are presented in Figure 5-74.

As shown in Figure 5-69 b) and Figure 5-74 b), the transient thermal creep exists in the heating phase for compressive and tensile loading, but not in the cooling phase, which is in contradiction to hardened concrete.

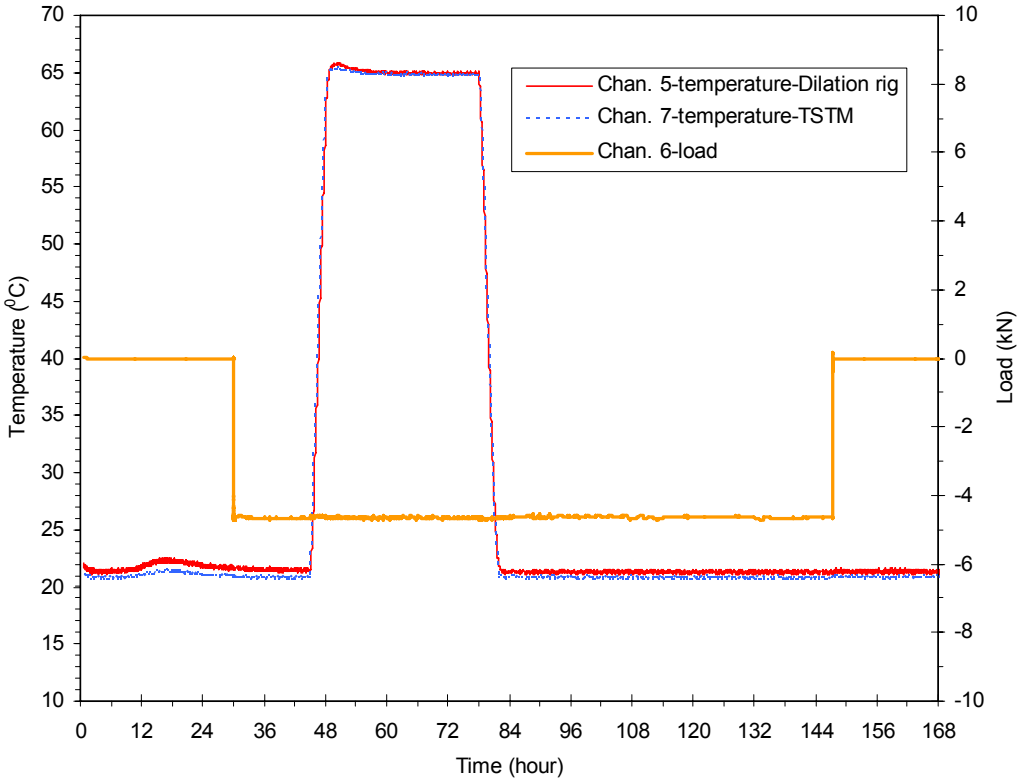

Figure 5-70 Temperature and loading history in the TSTM and the dilation rig (No. 173, tensile stress)

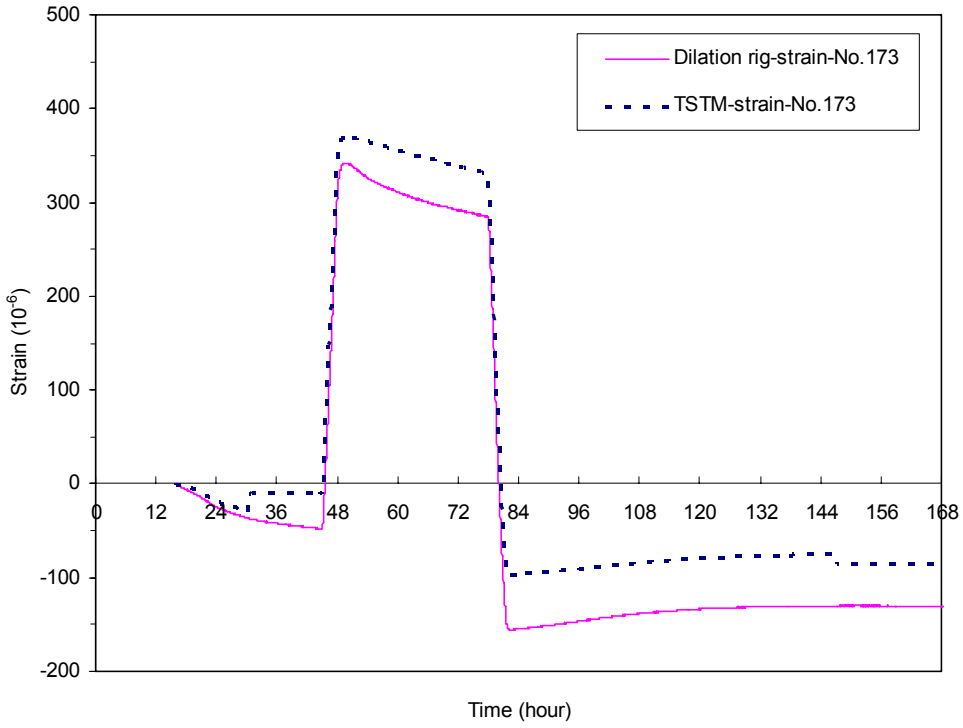

Figure 5-71 Total strain developments in the TSTM and the dilation rig (No. 173)

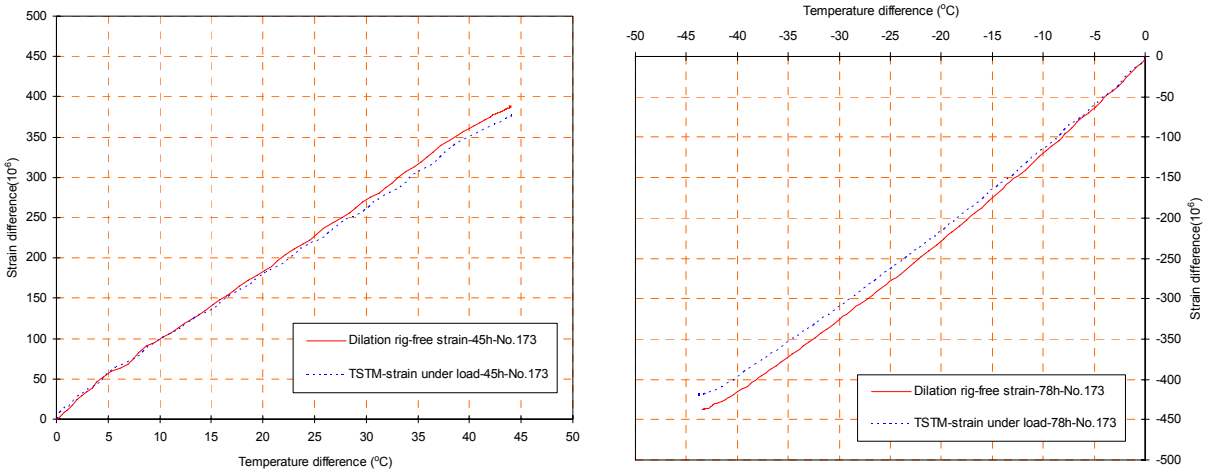

a) Temperature increase b) Temperature decrease

Figure 5-72 Strain developments in the TSTM and the dilation rig during temperature increase/decrease

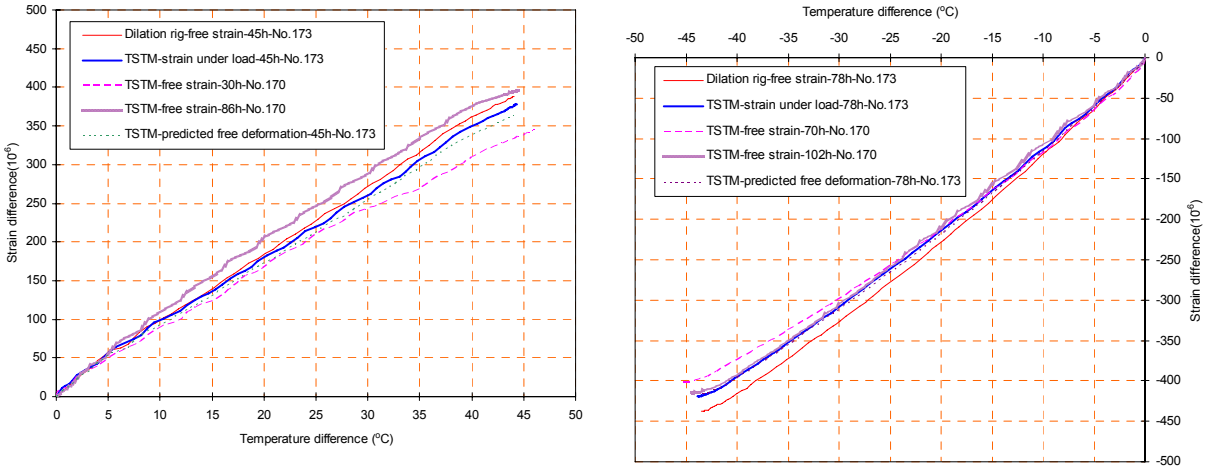

a) Temperature increase b) Temperature decrease

Figure 5-73 Predicted free strain and total strain applied to calculate the transient thermal creep (No.173)

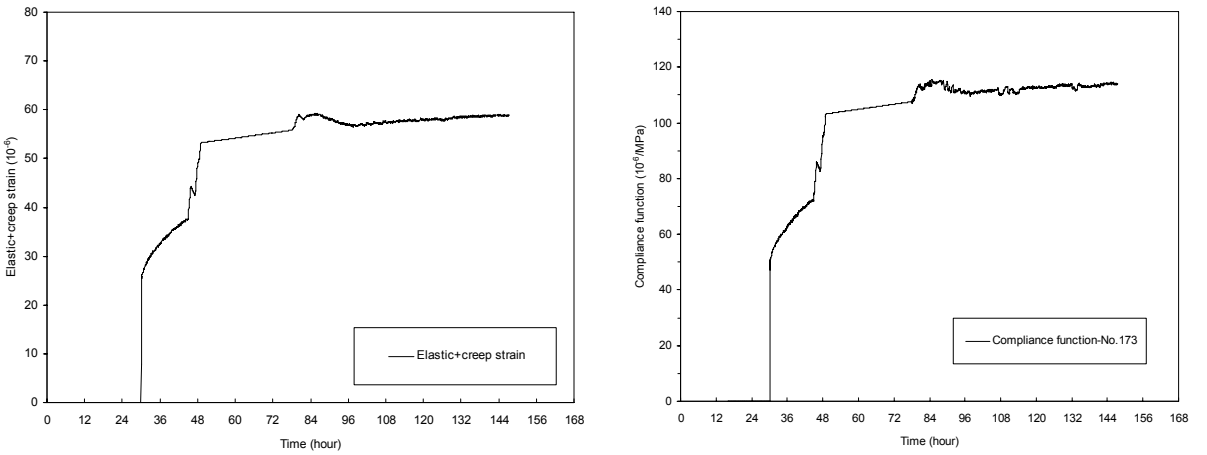

a) elastic plus creep strain b)Compliance function

Figure 5-74 Transient thermal creep test (No.173, tensile stress)

5.4.3. Discussion of transient thermal creep

As discussed in chapter 4, several approaches have been proposed to take into account the temperature effect on creep in structural analysis. The analytical approach proposed by Bažant (1985a) and further developed by Thelandersson (1987) and Jonasson (1994) is quite simple as applied in engineer practice. In this part, the analytical approach is used to model the test data, and its applicability is further discussed.

The strain development in the TSTM during a heating-cooling cycle under constant load and sealed condition can be decomposed as follow:

$$\varepsilon_{tot}\left(t,\sigma\right)=\varepsilon_{e}\left(t',\sigma\right)+\varepsilon_{c}\left(t,t',\sigma\right)+\varepsilon_{th}\left(\Delta T\right)+\varepsilon_{sh}\left(t\right)+\varepsilon_{ttc}\left(\Delta T,\sigma\right) \tag{5.8}$$

The viscoelastic strain can be expressed by compliance function:

$$\varepsilon_{vis}\left(t,\sigma\right)=\varepsilon_{e}\left(t',\sigma\right)+\varepsilon_{c}\left(t,t',\sigma\right)=J\left(t,t'\right)\sigma=\left[\frac{1+\varphi\left(t_{e}'\right)^{-d}\left(t_{e}-t_{e}'\right)^{p}}{E\left(t_{e}'\right)}\right]\sigma \tag{5.9}$$

And the free strain is measured in unloaded specimen:

$$\varepsilon_{free}\left(t\right)=\varepsilon_{th}\left(\Delta T\right)+\varepsilon_{sh}\left(t\right) \tag{5.10}$$

The autogenous shrinkage can be neglected for hardened concrete and the transient thermal strain is modeled by:

$$\varepsilon_{ttc}=\alpha_{T}\Delta T\bullet\rho\bullet\frac{\sigma}{f\left(t_{e}\right)}\bullet sign\left(\Delta T\right) \tag{5.11}$$

Where $f\left(t_{e}\right)$ is compressive strength under compression or tensile strength under tension.

The parameter ρ is not always directly determined by transient thermal creep test, but can be found by adjusting the value of ρ to achieve the best curve fitting of the measured stress development in TSTM under variable temperature history. The parameter values $\rho=0.1$ and $\rho=0.4$ were used by Westman (1999) in thermal stress calculation for two types of Swedish concrete. The test results of TSTM for Base concrete were calibrated by Bosnjak (2000), and the parameter ρ was found to be 0.27.

The creep parameters determined by creep rig tests described in previous sections are used to calculate the viscoelastic strain under constant loading, and the only unknown parameter is the ρ in the transient thermal creep term, and it can then be deduced by fitting model to the test data. All other parameters used in analyses and the results of the parameter ρ are presented in Table 5.7. The parameter ρ is similar in hardened and young concrete under either compressive or tensile load condition, but it is higher in compressive loading than in tensile loading. The explanation might be due to the low stress/strength ratio applied in the compressive test.

Test results from the hardened concretes show that transient thermal creep apparently exists. Not only during heating, but also during cooling, the compliance functions increase dramatically due to temperature changes during these two periods. The calculated compliance functions are in good agreement with the measured results, the improvement of the modeling by including the

transient thermal creep term is significant and therefore the transient thermal creep should be considered in structural analysis considering variable temperature histories.

For young concrete, the compressive and tensile strength develop rapidly which has considerable influence on the transient thermal creep compliance. The test results for young concrete under compression show low increase of compliance function due to transient creep during the cooling period. As the compressive strength develops, the ratio between the applied constant stress and the compressive strength declines from 0.12 at initial loading to 0.04 at the age of 4 days for case No.172, and the calculated transient thermal creep compliance is only 4μ/MPa.

As shown in Figure 5-75 to Figure 5-78, the analytical model gives an acceptable prediction of the test results for young concretes and the maturity concept is able to describe the major part of the temperature influence on the creep strain development. But it seems that it is not enough to take into account the temperature effect on the creep by only using the maturity concept when large temperature increase or decrease happens in a short period, and it gives more reliable prediction if the transient thermal creep term is added. The influence of transient thermal creep on the restraint stress development in TSTM under realistic temperature histories is further discussed in the subsequent section.

Table 5.7 Parameters used in analytic model

Parameters	Compressive loading		Tensile loading	
	Hardened concrete (No.183)	Young concrete (No.172)	Hardened concrete (No.173-2)	Young concrete (No.173)
ρ	0.80	0.65	0.21	0.07
φ	1.15		0.97	
d	0.18		0.20	
p	0.18		0.20	
$E(t_e')$ (MPa)	36200	15000(1)	43500	26000(1)
α_T (10^{-6}/ºC)	10.0			
t_e' (day)	582	0.83	119	1.33
$\sigma / f(t_e')$	0.07	0.12	0.26	0.18

(1) The elastic modulus is determined by the stress and strain ratio measured in the TSTM at loading time

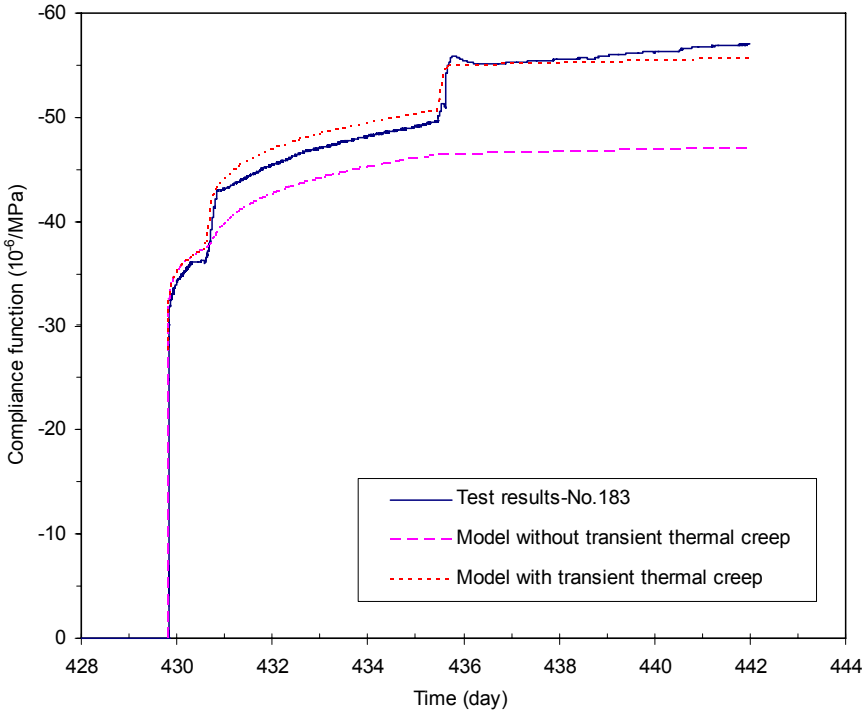

Figure 5-75 Modeled and measured compliance function (No.183, compressive load, hardened concrete)

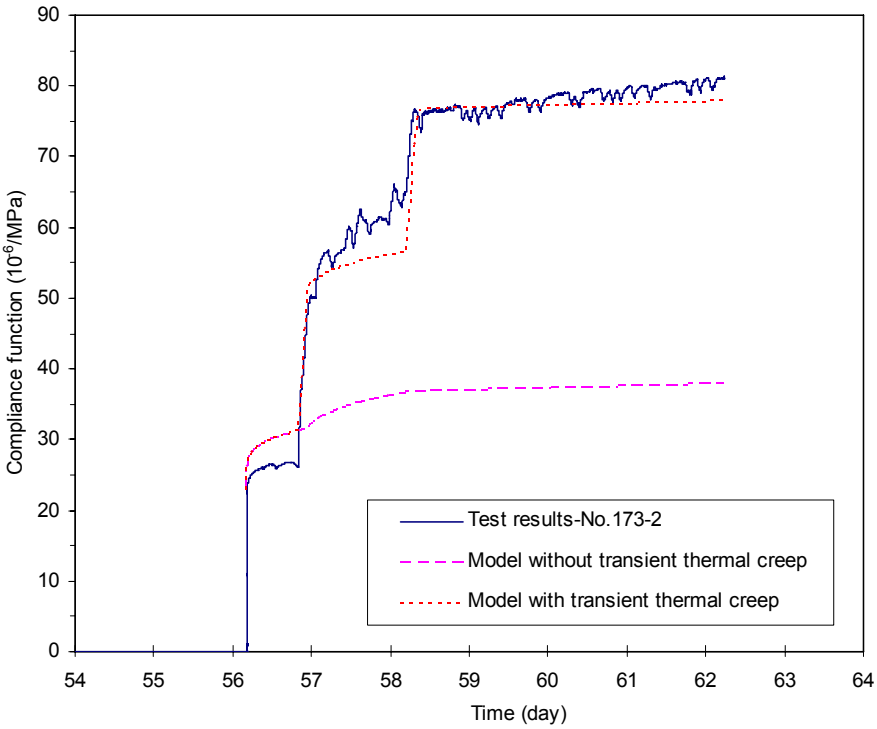

Figure 5-76 Modeled and measured compliance function (No.173-2, tensile load, hardened concrete)

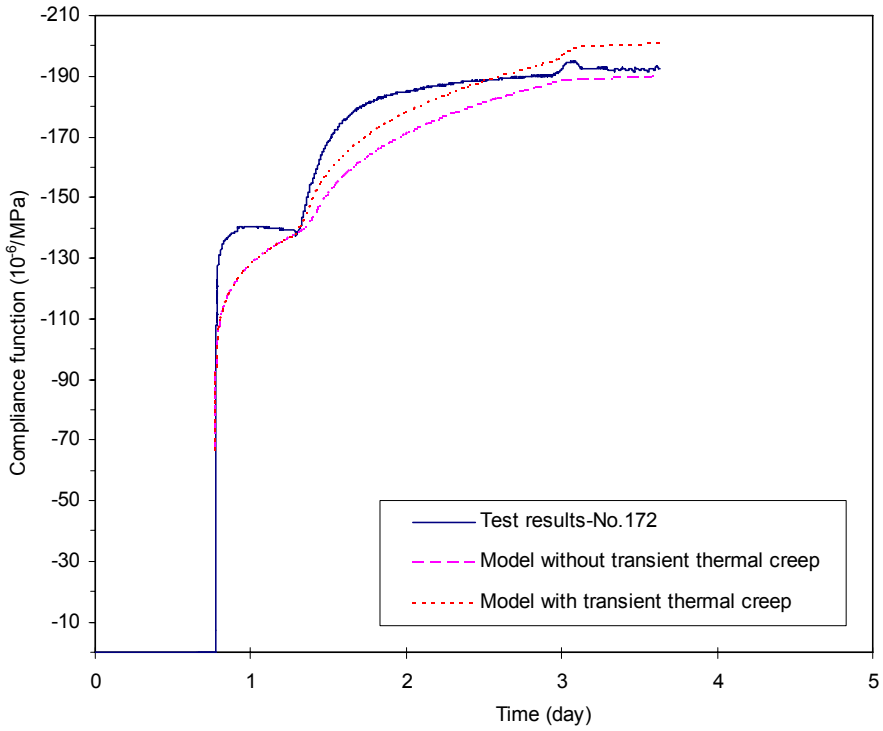

Figure 5-77 Modeled and measured compliance function (No.172, compressive load, young concrete)

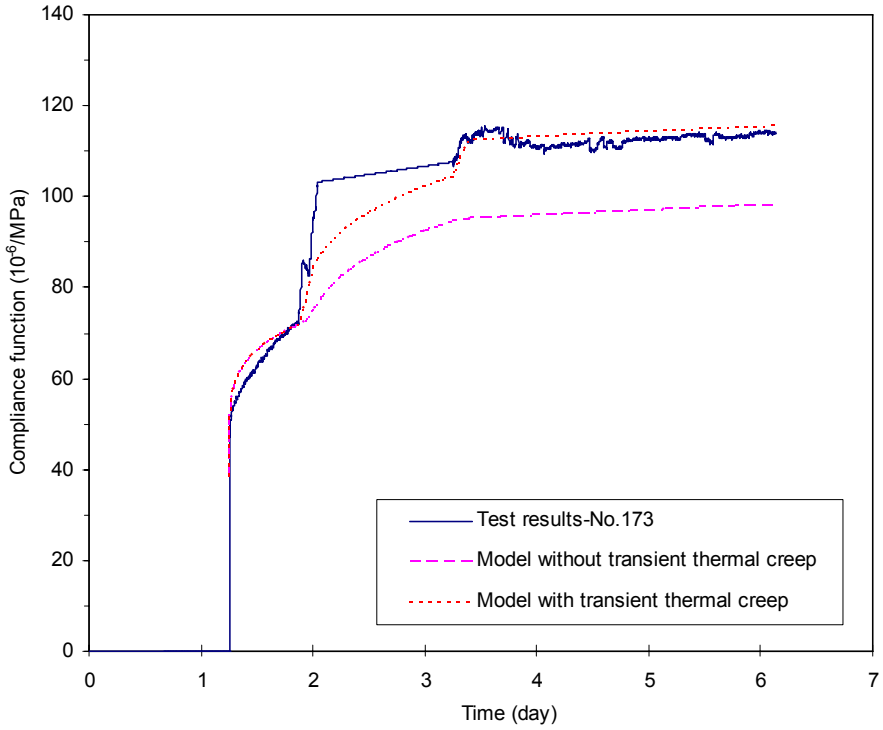

Figure 5-78 Modeled and measured compliance function (No.173, tensile load, young concrete)

5.5. Restraint stress development in TSTM

In the standard procedure, the dilation rig and stress rig are run in parallel. The TSTM measures the development of self-induced stress in sealed specimen under well defined temperature and restraint conditions in a uniaxial stress state, and simultaneously the dilation rig measures the free deformation in another sealed specimen, *i.e.* thermal dilation and autogenous deformation, with same temperature history. The test methods are described in detail by Bjøntegaard (1999).

The stress development measured in the TSTM is the net effect of all the parameters acting to produce stresses in hardening concrete (*i.e.* thermal dilation, autogenous deformation, E-modulus and creep/relaxation properties), and the TSTM is a suitable tool to investigate the stress development in hardening concrete under realistic temperature conditions and to further optimize the concrete mix to reduce the cracking risk. The experimental data can also be used as valuable information to verify the material models.

The test results presented in Figure 5-79 to Figure 5-84 show that the replacement of cement by slag or fly ash reduces the maximum tensile stress in the TSTM. Cracking did not occur in the TSTM tests of 60 % FA* with initial temperature 11ºC under 100% restraint condition.

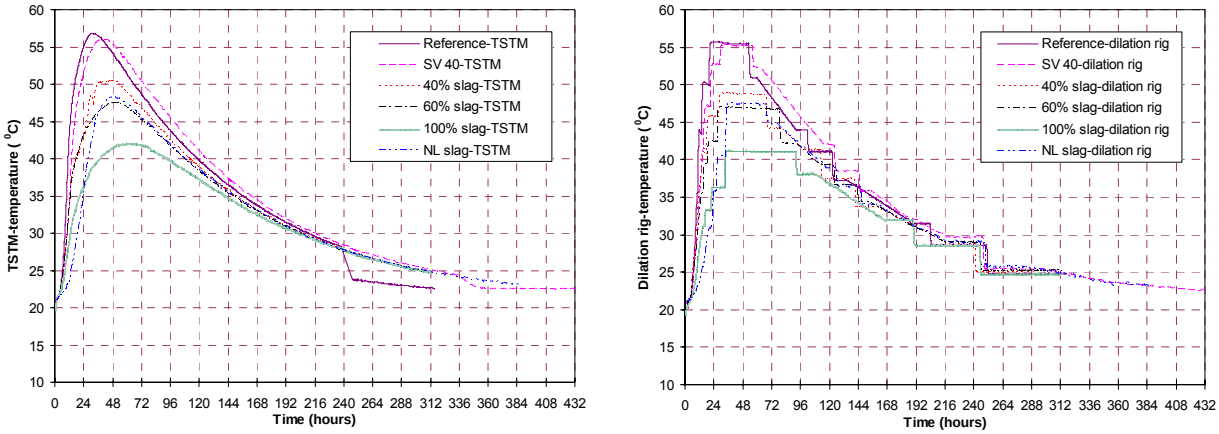

Figure 5-79 Smooth temperature in TSTM and stepwise temperature in dilation rig

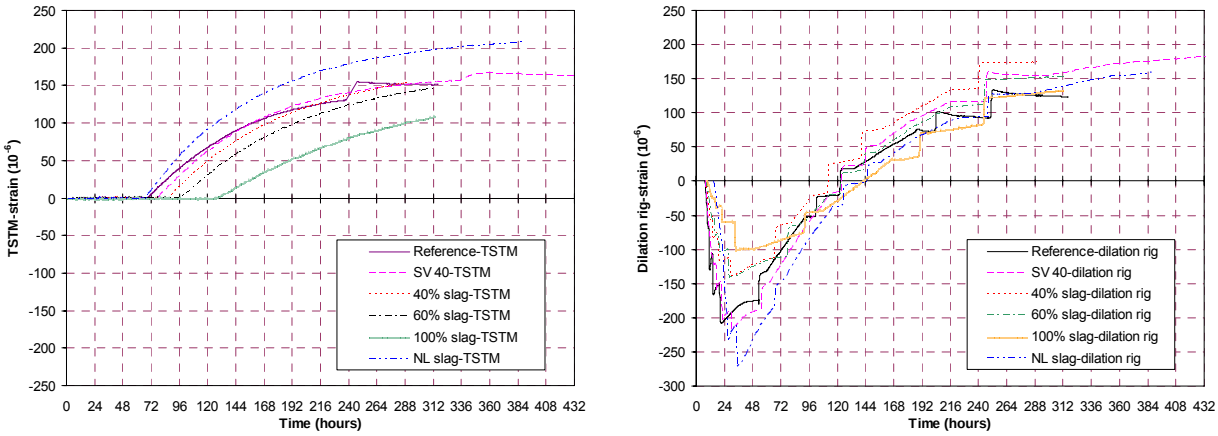

Figure 5-80 Strain in TSTM under partial restrained condition and free strain in dilation rig

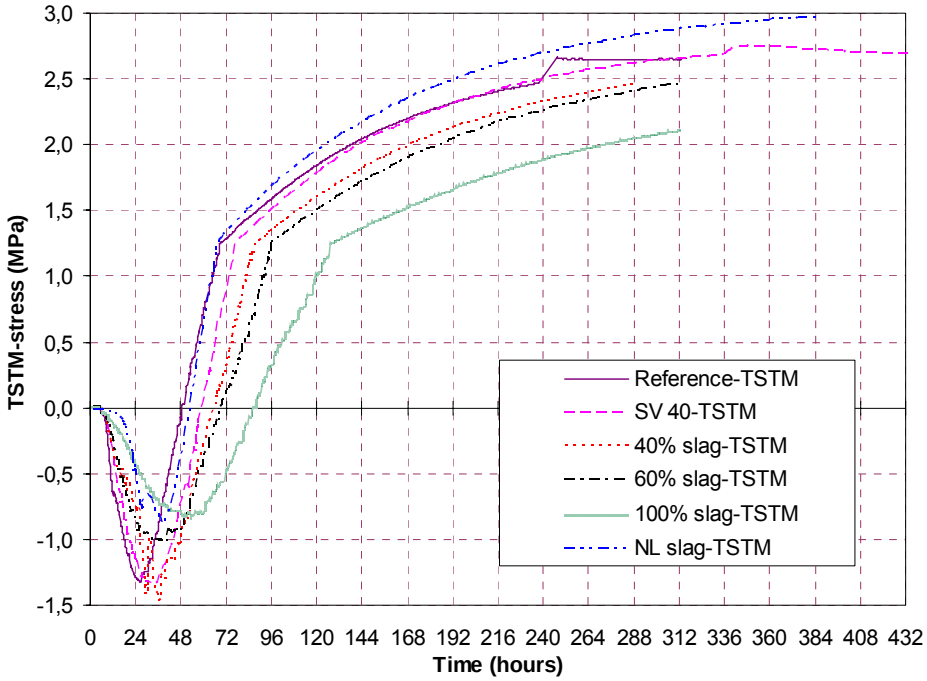

Figure 5-81 Measured restraint stress development in TSTM

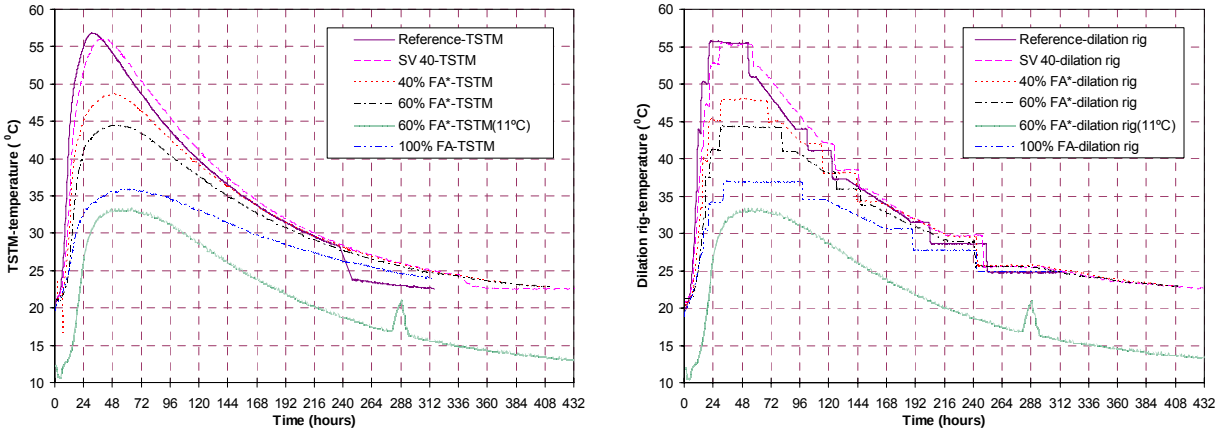

Figure 5-82 Smooth temperature in TSTM and stepwise temperature in dilation rig

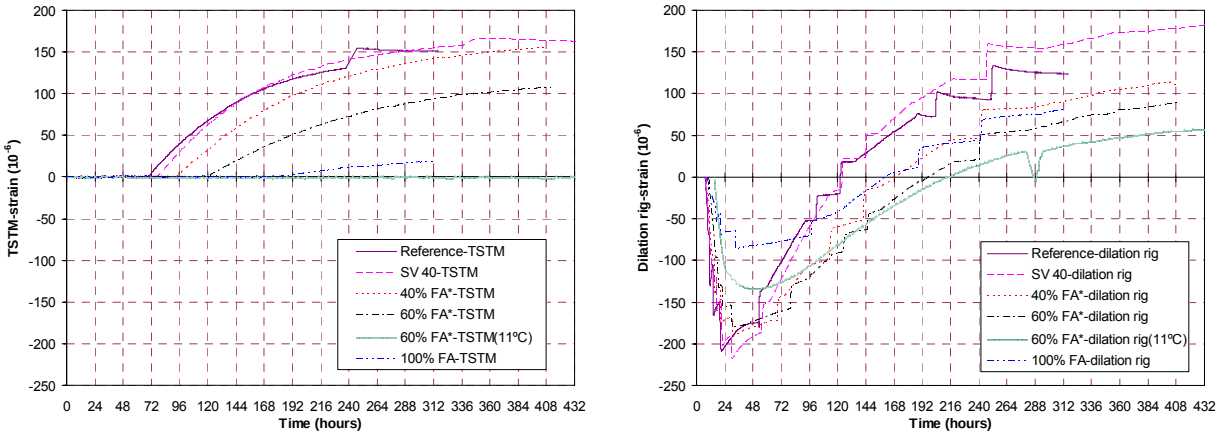

Figure 5-83 Strain in TSTM under partial restrained condition and free strain in dilation rig

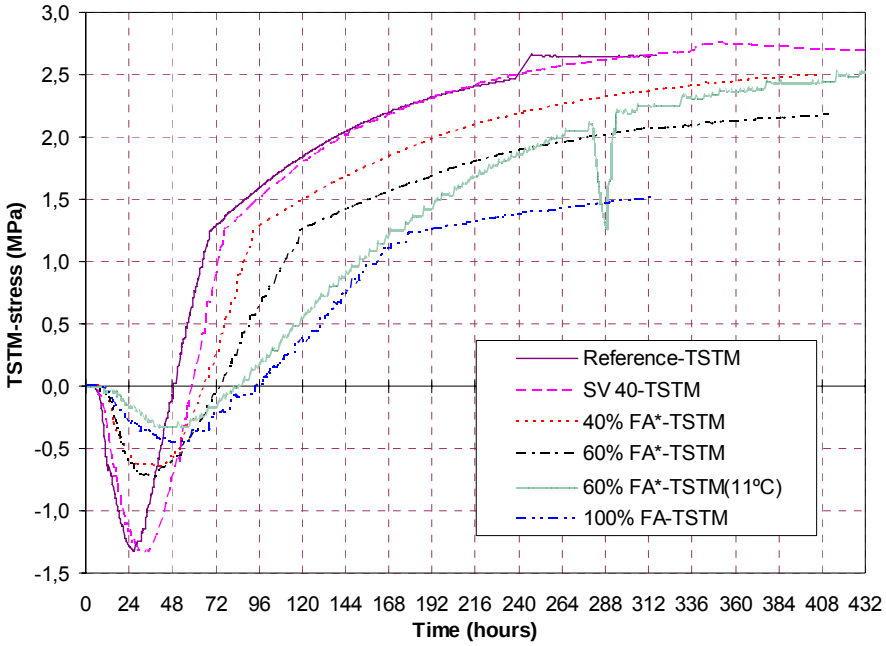

Figure 5-84 Measured restraint stress development in TSTM

5.6. Restraint stress analysis of TSTM-results

In the description of the constitutive behavior of young concrete it is assumed that the strain rate in the TSTM may be decomposed as follows:

$$\Delta\varepsilon = \Delta\varepsilon_{el} + \Delta\varepsilon_{cr} + \Delta\varepsilon_{th} + \Delta\varepsilon_{sh} + \Delta\varepsilon_{ttc} \tag{5.12}$$

$$\varepsilon_{free} = \varepsilon_{th} + \varepsilon_{sh} \tag{5.13}$$

$$\varepsilon_{ve} = \varepsilon_{el} + \varepsilon_{cr} = \int_{t_1}^{t} J(t,t')\,d\sigma(t') \tag{5.14}$$

Where Δ represents increments, and ε_{free} is the measured free deformation in the dilation rig, ε_{el} is the elastic strain, ε_{cr} is the creep strain and ε_{ttc} is the transient thermal creep component which takes into account the change in creep rate during changes in temperature.

5.6.1. Compressive or/and tensile creep data

The DPL is used to fit the compressive and tensile creep data, and due to the different curvature of the compressive and tensile creep data it can be seen that the DPL expresses the former ones better than that latter. Nevertheless, the two sets of parameters in the DPL are applied in restraint stress calculation for the TSTM tests in three different combinations:

a) Only compressive creep parameters,

b) Only tensile creep parameters,

c) A combination where the compressive parameters are used during the initial compressive stress period in the TSTM specimen and the tensile parameters are used during the later part when the specimen develops tensile stresses.

The temperature effect on the creep property is taken into account by the maturity concept and the transient thermal creep adjustment.

$$\Delta\varepsilon = \Delta\varepsilon_{el} + \Delta\varepsilon_{cr} + \Delta\varepsilon_{th} + \Delta\varepsilon_{sh} + \Delta\varepsilon_{ttc} \tag{5.15}$$

$$J(t_e, t'_e) = \frac{1}{E_c(t'_e)}\left[1 + \varphi \bullet t'^{-d}_e \left(t_e - t'_e\right)^p\right] \tag{5.16}$$

The calculated stress development for seven types of concretes are shown in Figure 5-85 to Figure 5-92, and the comparisons of maximum compressive and tensile stresses between test and calculation are shown in Table 5.8 and Figure 5-93. The fictive stress shown in the figures is defined as the calculated elastic stress development without taking into account the creep and transient thermal creep in the calculation.

The influence of creep on the self-induced stresses in the TSTM is twofold, creep in the early compression phase directly reduces the compressive stresses, but indirectly increases the later tensile stress, and secondly creep in the tension phase reduces the tensile stresses. These two effects are competing and the final effect is their summation. (Bosnjak, 2001) Because of this complicated influence of creep on the risk of through-cracking, it is difficult to give general rules – the creep influence on the cracking risk varies from case to case and depends on the concrete situation, i.e. temperature, shrinkage and restraint conditions. In general terms, creep is a very important factor in simulation of hardening concrete, and correct prediction of creep during the whole period of hardening is necessary for reliable prediction of cracking risk.

The results presented in Table 5.8 show that using combined compressive and tensile DPL-parameters gives good correspondence with the measured stress developments in the TSTM tests. Moreover, using only the compressive DPL-parameters give better agreement with the test results than using only the tensile DPL-parameters. A reason for this may be that early tensile and compressive creep are different especially for concretes containing mineral additives (see Figure 5-43 and Figure 5-44), and the fact that the compressive phase in the TSTM tests (and also in field situations) last typically from setting up to 2-4 days, which means 4-10 days in maturity time. Hence, in order to determine the most relevant creep data (at 20ºC test conditions) one should perform compressive creep measurements at early loading ages (from setting to 4-10 days), and tensile creep tests at later loading ages. The results also show that both creep increases and the hydration heat decreases with the FA content are positive effect with regard to reducing the stress generation.

Table 5.8 The influence of creep data on the stress calibration of TSTM test

Concrete	TSTM result		Compressive creep		Tensile creep		Combined compressive and tensile creep	
	$\sigma_{c,\max}$ (MPa)	$\sigma_{t,\max}$ (MPa)	$\sigma_{c,\max}$ (MPa)	$\sigma_{t,\max}$ (MPa)	$\sigma_{c,\max}$ (MPa)	$\sigma_{t,\max}$ (MPa)	$\sigma_{c,\max}$ (MPa)	$\sigma_{t,\max}$ (MPa)
SV 40*	-1.34	2.75	-1.33	2.64	-1.32	2.74	-1.32	2.74
FA 40%*	-0.64	2.50	-0.62	2.35	-0.48	3.03	-0.62	2.35
FA 60%*	-0.72	2.17	-0.60	2.07	-0.39	2.89	-0.60	2.19
FA 60%* (11ºC)	-0.33	2.52	-0.29	2.50	-0.20	2.89	-0.28	2.51
NL slag*	-0.88	2.98			-1.32	3.28		
Reference	-1.32	2.47	-1.46	2.24	-1.48	2.54		
Slag 40%	-1.46	2.46	-1.02	2.24				
Slag 60%	-1.01	2.47	-0.56	2.30	-0.50	2.66	-0.56	2.30

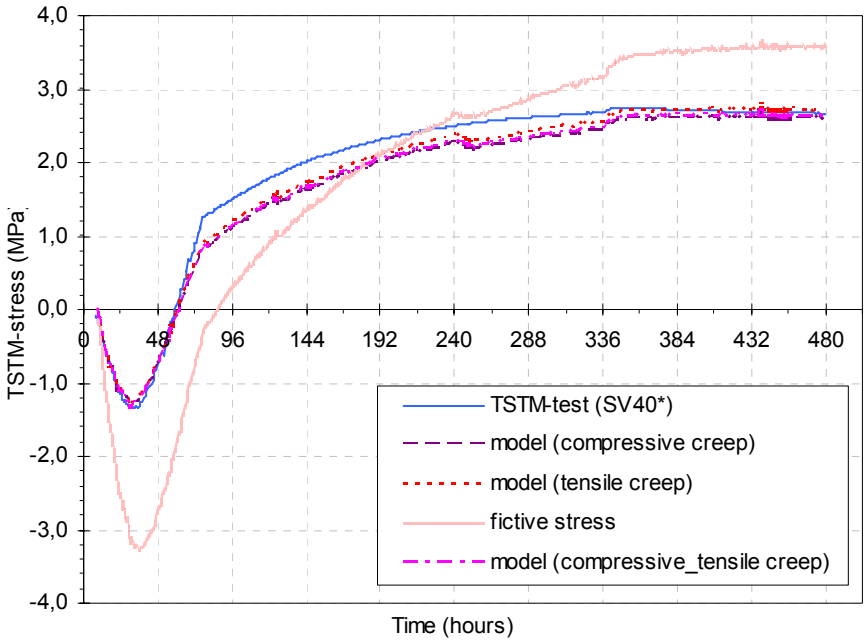

Figure 5-85 Calculated and measured stress development in hardening concrete (SV 40*)

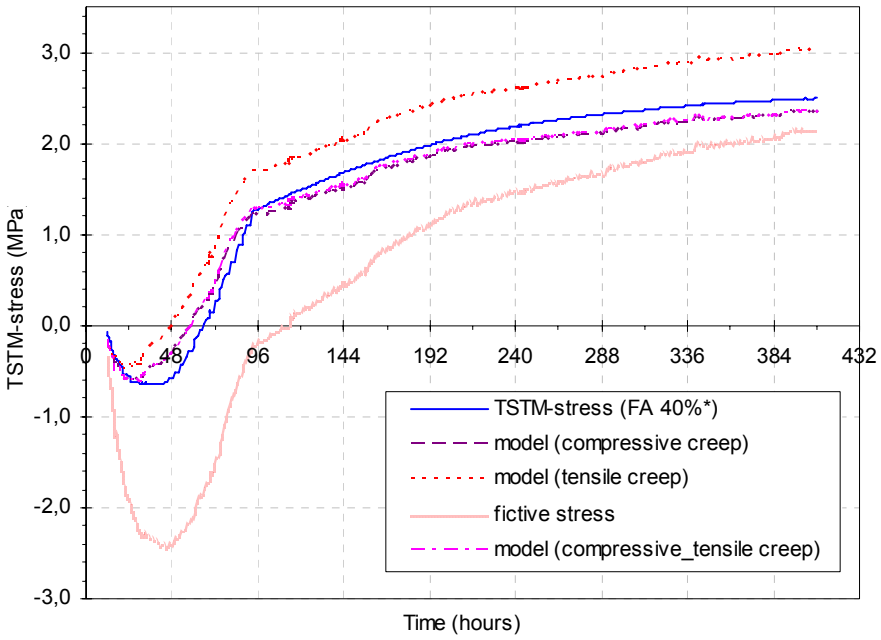

Figure 5-86 Calculated and measured stress development in hardening concrete (40% FA*)

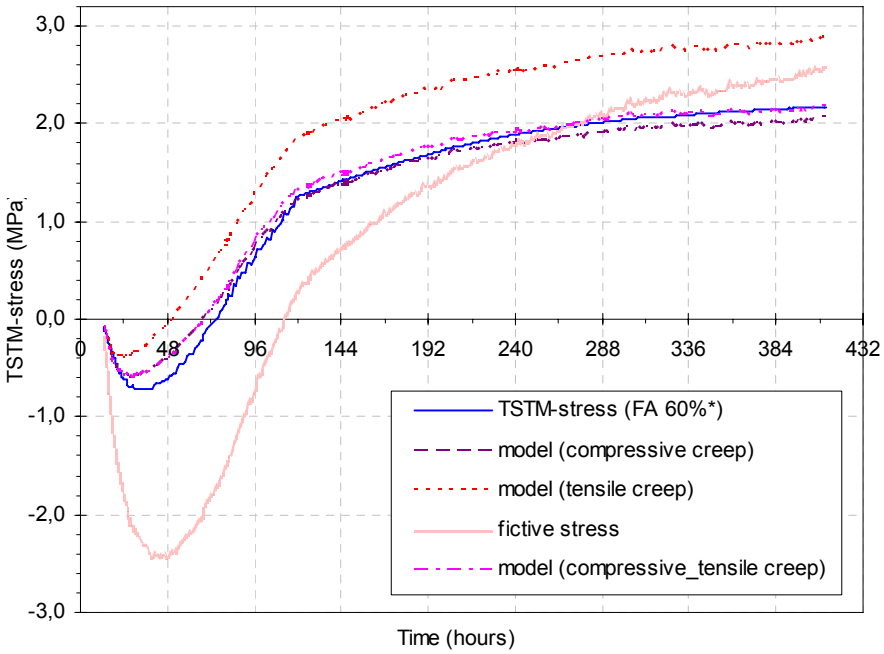

Figure 5-87 Calculated and measured stress development in hardening concrete (60% FA*)

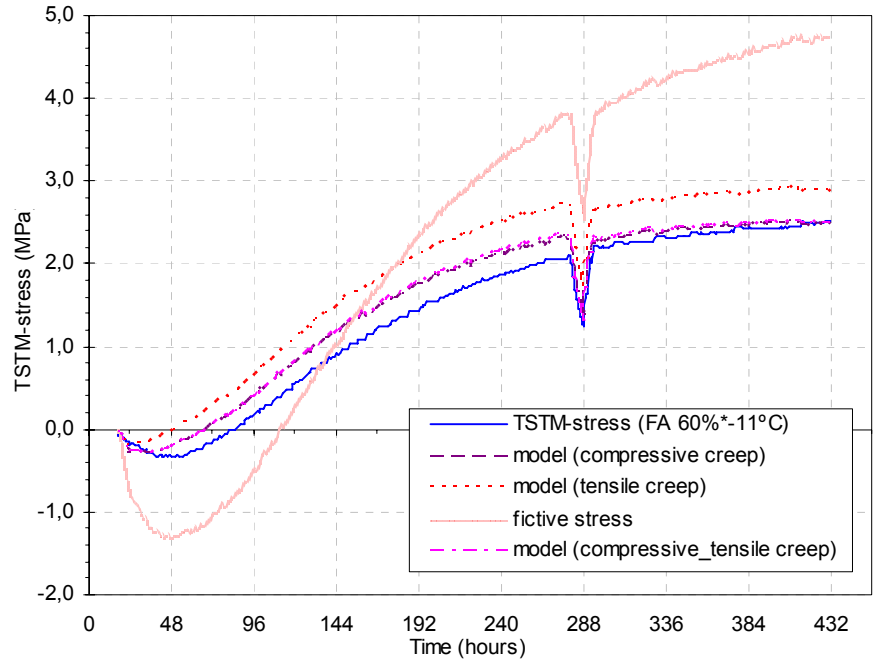

Figure 5-88 Calculated and measured stress development in hardening concrete (60% FA*-Initial temperature 11°C)

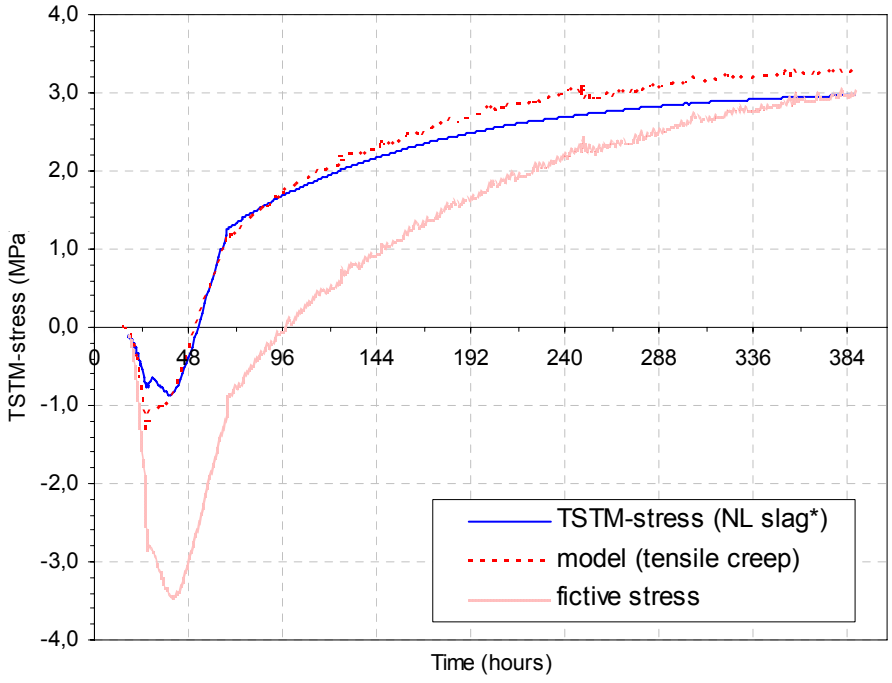

Figure 5-89 Calculated and measured stress development in hardening concrete (NL Slag*)

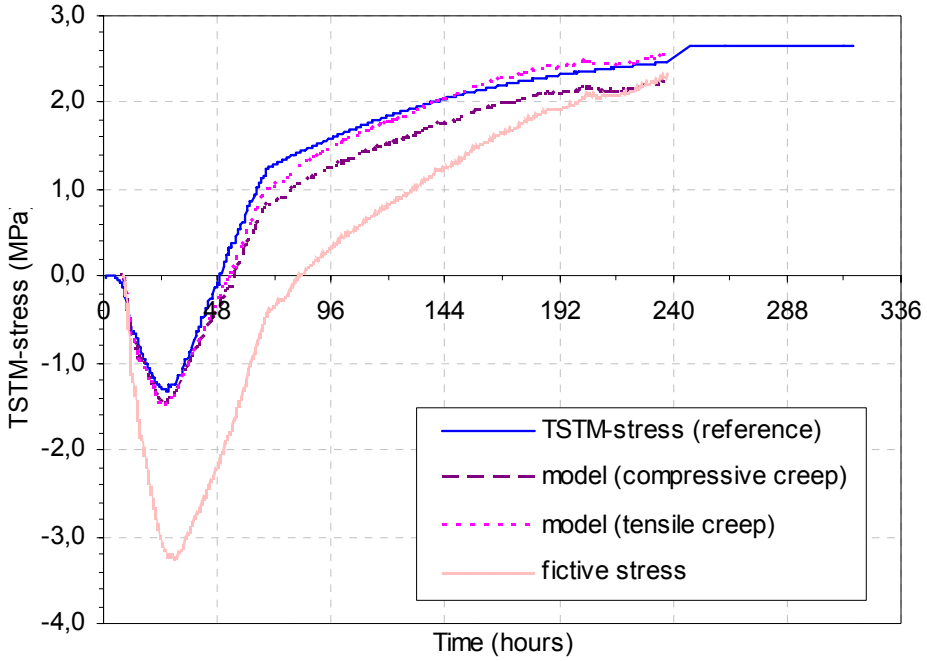

Figure 5-90 Calculated and measured stress development in hardening concrete (Reference)

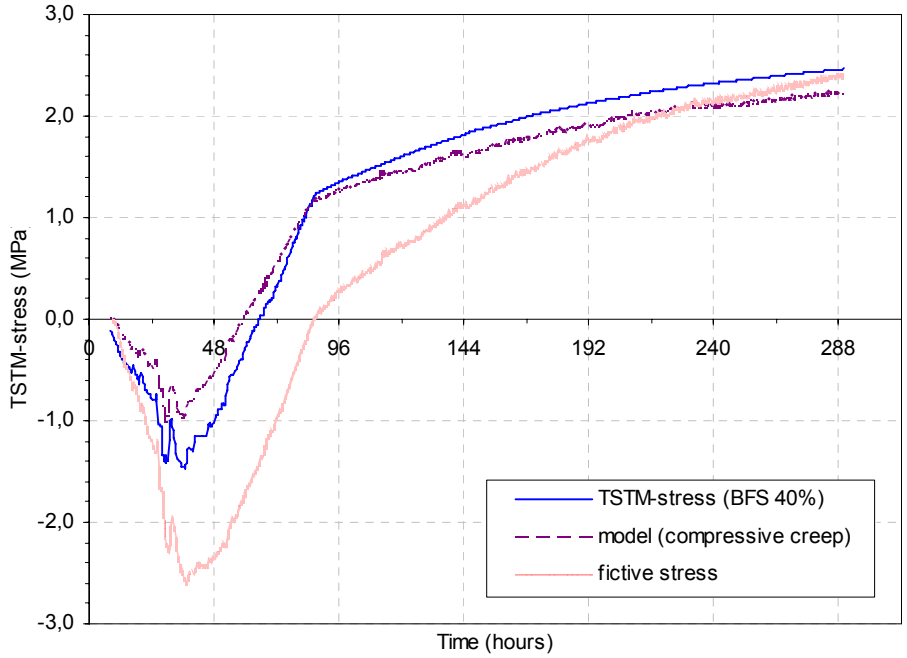

Figure 5-91 Calculated and measured stress development in hardening (40% BFS)

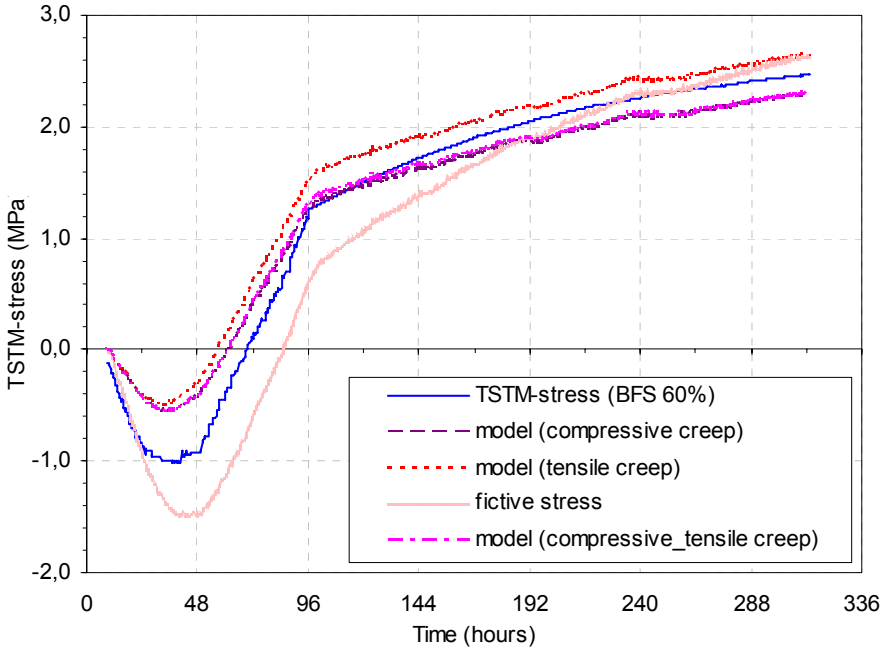

Figure 5-92 Calculated and measured stress development in hardening (60% BFS)

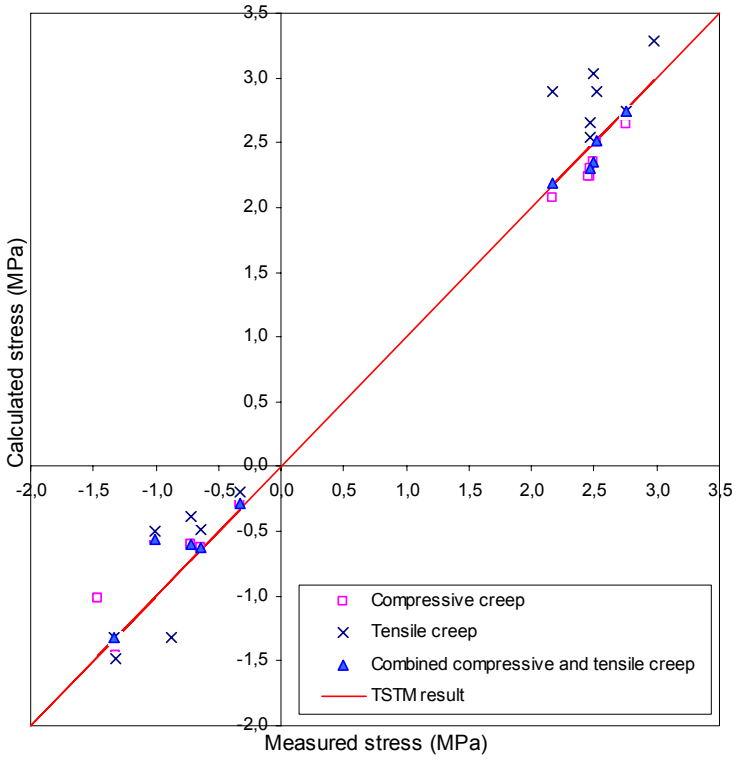

Figure 5-93 Comparison of calculated and measured maximum compressive and tensile stresses

5.6.2. Temperature effect

Temperature affects creep in two ways: directly, influencing the creep rate, and indirectly, influencing aging and maturity of concrete. The higher temperature tends to increase the creep rate, but in young concrete the effect is offset by the fact that a temperature increase also accelerates hydration, which in turn reduces creep. The former effect is usually larger than the latter one, but this depends on the concrete age.

Three different approaches are used in the calculation of the stress development in TSTM under realistic temperature histories, and based on the results the temperature effect on creep is further discussed.

In the first approach, the stress development in the TSTM is calculated by the Diana program, and the effect of temperature on the aging is taken into account by the maturity dependence of the E-modulus:

$$J(t,t') = \frac{1}{E_c(t'_e)}\left[1+\varphi \bullet t'^{-d}\left(t-t'\right)^p\right] \tag{5.17}$$

Compressive creep data is applied in the analysis.

In the second approach, maturity is used in creep model by replacing concrete age with the equivalent age in the term, and the loading duration $(t-t')$ replaced by the equivalent loading duration $(t_e - t'_e)$. The stress development in the TSTM is analyzed by a program made by the author based on Visual Basic:

$$J(t_e,t'_e) = \frac{1}{E_c(t'_e)}\left[1+\varphi \bullet t'^{-d}_e\left(t_e-t'_e\right)^p\right] \tag{5.18}$$

In the third approach, the visual basic program is still used and the transient thermal creep is considered in the constitutive behavior:

$$\Delta\varepsilon = \Delta\varepsilon_{el} + \Delta\varepsilon_{cr} + \Delta\varepsilon_{th} + \Delta\varepsilon_{sh} + \Delta\varepsilon_{trc} \tag{5.19}$$

$$\varepsilon_{ttc} = \alpha_T \Delta T \bullet \rho \bullet \frac{\sigma}{f(t_e)} \bullet sign(\Delta T) \tag{5.20}$$

In the last two methods, the combined compressive/tensile creep data is used in the simulation, i.e. the one corresponding to the actual condition in the TSTM. The results of calculation are shown in Figure 5-94 to Figure 5-100.

As presented in Table 5.9, the results from Diana show that the maximum compressive stresses are underestimated for BFS concretes, but they are overestimated for the other concretes, and the maximum tensile stresses are overestimated for all concretes except 60%FA*. The replacement of concrete age with maturity age at loading time reduces the creep compliance, at the same time replacement of loading duration with equivalent time duration increases the creep compliance, and these two effects are competing with each other. In the present cases, the application of maturity age increases the creep compliance in compression phase, and reduces the maximum compressive stresses for all concretes compared to the results from Diana, but its influence on maximum tensile stresses is more complex and the maximum tensile stresses are increased in the SV40* and the FA concretes, but decreased in the reference and the BFS concretes. The consideration of transient thermal creep reduces both maximum compressive and tensile stresses compared to the results from only taking into account maturity age. It can be

concluded that the calculated maximum compressive and tensile stresses in all three approaches give reasonable agreement with the measured ones in TSTM.

Table 5.9 Calibration of the stress development in TSTM test

Concrete	TSTM result		Diana		Maturity age		Maturity and transient thermal creep	
	$\sigma_{c,\max}$ (MPa)	$\sigma_{t,\max}$ (MPa)	$\sigma_{c,\max}$ (MPa)	$\sigma_{t,\max}$ (MPa)	$\sigma_{c,\max}$ (MPa)	$\sigma_{t,\max}$ (MPa)	$\sigma_{c,\max}$ (MPa)	$\sigma_{t,\max}$ (MPa)
SV 40*	-1.34	2.67	-1.63	2.78	-1.38	2.85	-1.32	2.66
FA 40%*	-0.64	2.50	-0.93	2.67	-0.61	2.76	-0.62	2.36
FA 60%*	-0.72	2.17	-0.83	2.16	-0.63	2.53	-0.58	2.19
FA 60%* (11ºC)	-0.33	2.52	-0.40	2.73	-0.31	3.02	-0.29	2.55
Reference	-1.32	2.47	-1.84	2.61	-1.55	2.48	-1.46	2.24
Slag 40%	-1.46	2.46	-1.18	2.57	-1.00	2.49	-0.97	2.24
Slag 60%	-1.01	2.47	-0.76	2.67	-0.56	2.60	-0.56	2.30

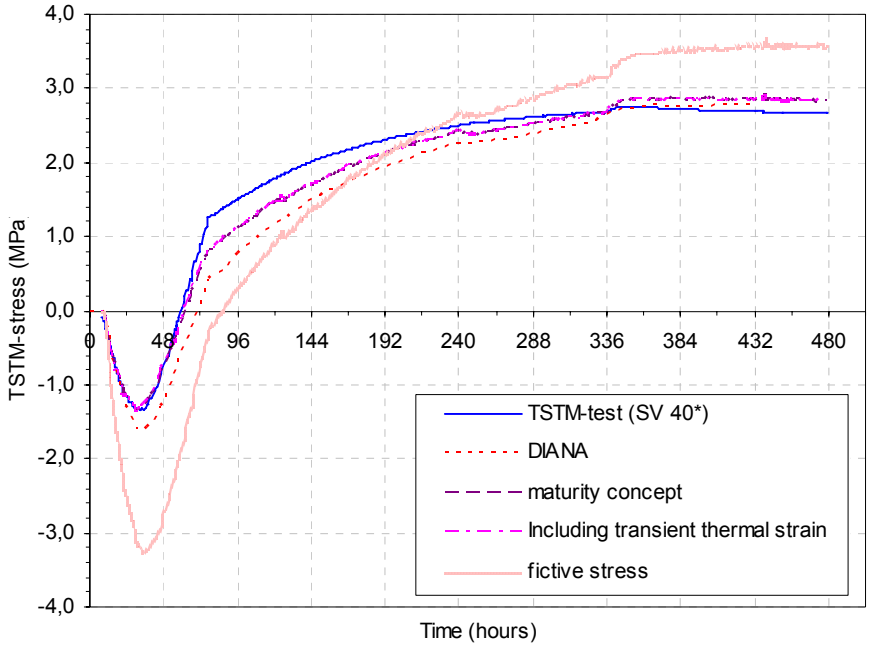

Figure 5-94 Stress developments in hardening concrete (SV 40*)

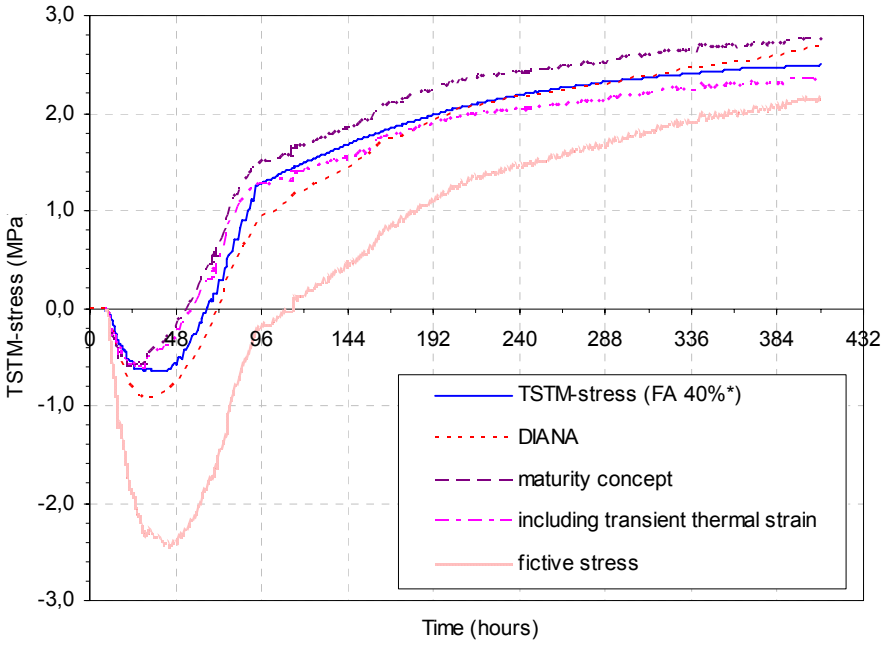

Figure 5-95 Stress development in hardening concrete (40% FA*)

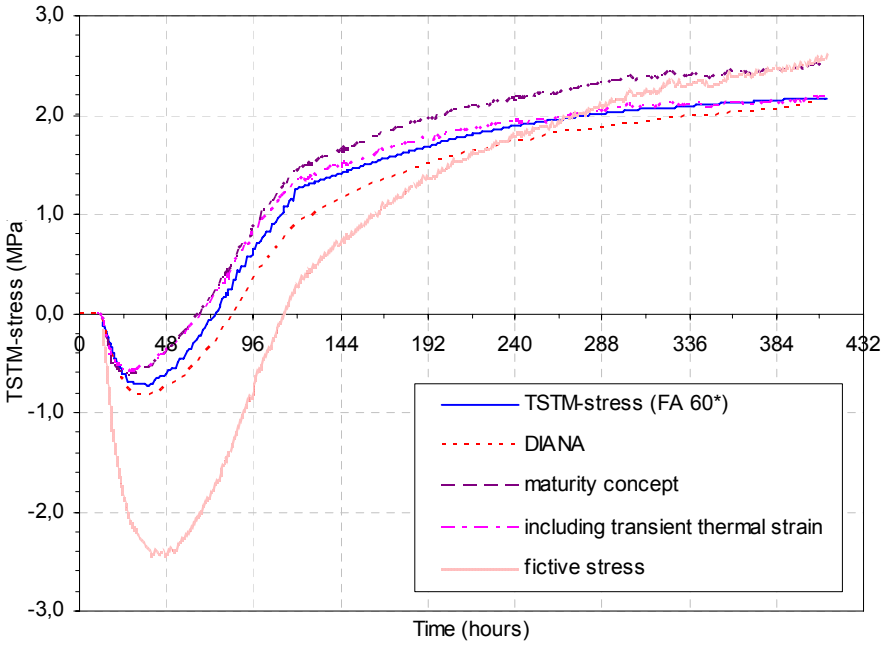

Figure 5-96 Stress development in hardening concrete (60% FA*)

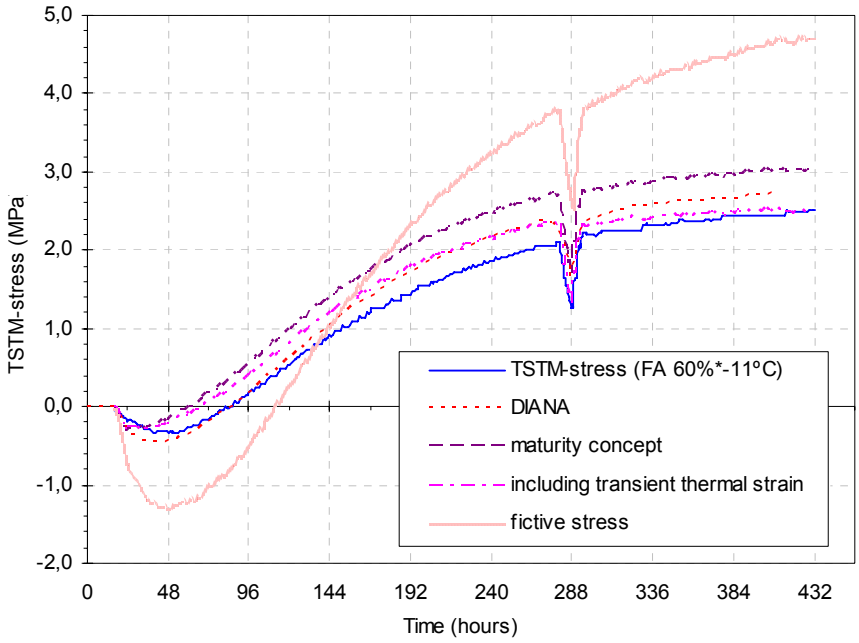

Figure 5-97 Stress development in hardening concrete (60% FA*-initial temperature 11ºC)

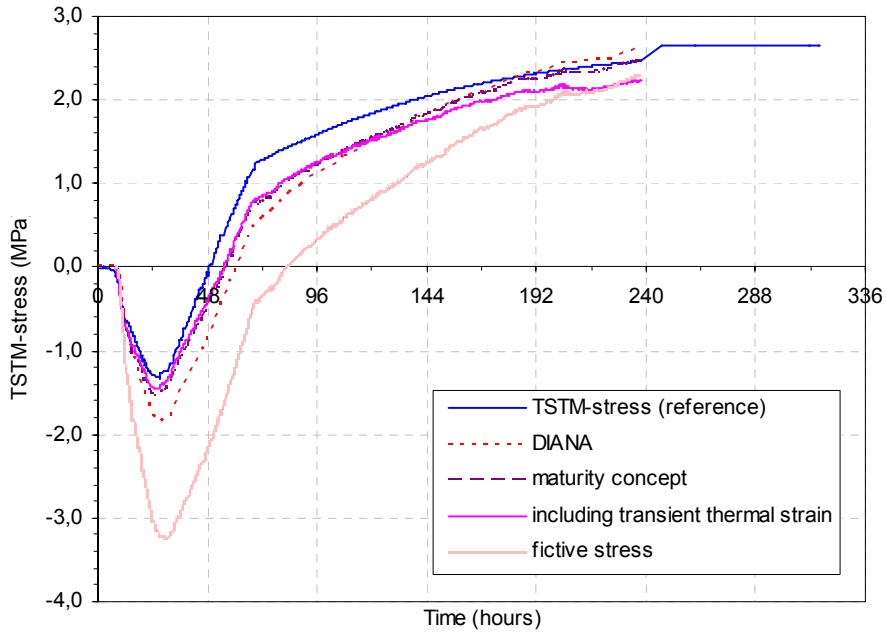

Figure 5-98 Stress development in hardening concrete (Reference concrete)

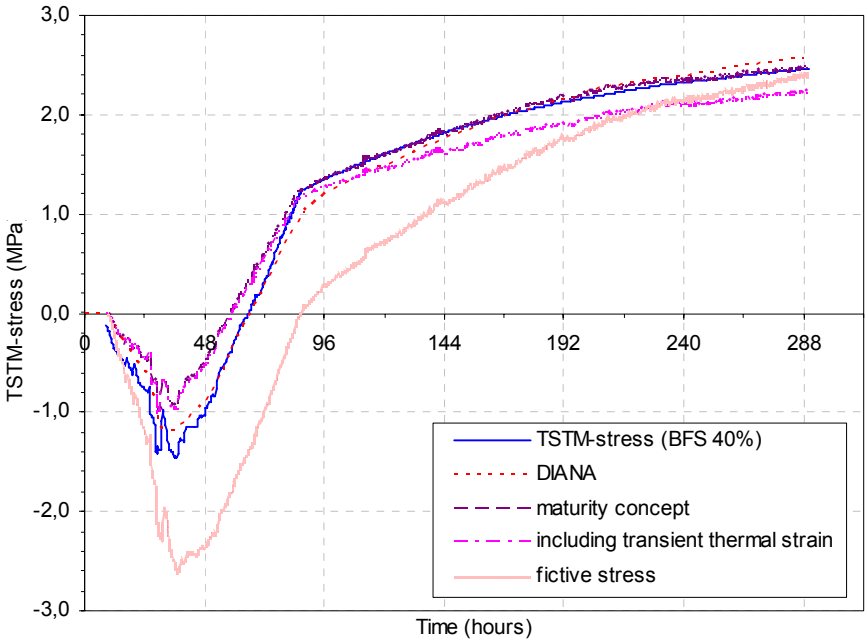

Figure 5-99 Stress development in hardening concrete (40% BFS)

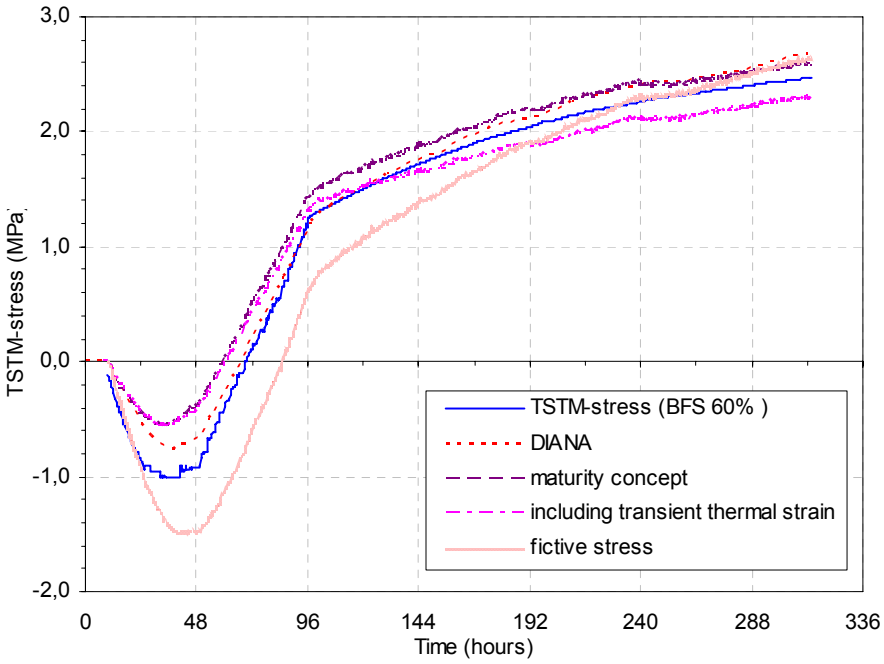

Figure 5-100 Stress development in hardening concrete (60% BFS)

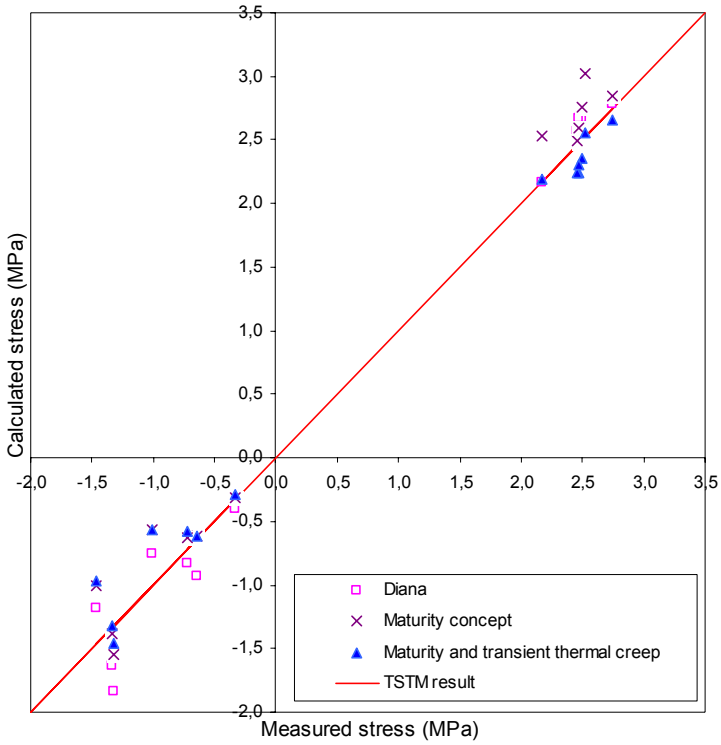

Figure 5-101 Comparison of calculated and measured maximum compressive and tensile stresses

6. Numerical analysis of a field test

6.1. Introduction

In this chapter the numerical analysis of a field test is discussed. The material properties used in the analysis were determined from laboratory tests as previously described, and the material model was checked in the TSTM for a realistic temperature history. Within the NOR-CRACK project, the Norwegian Directorate of roads carried out a field instrumentation programme to measure the temperature and strain development in a "double-wall" structure. 3D analysis of the structure was performed by DIANA and the calculated and measured temperature and strain in the structure were compared. Furthermore, the influence of three major factors: hydration heat, creep and autogenous shrinkage, on the stress development in the structure are investigated by parameter studies.

The field test of the "double-wall" structure previously described in Chapter 3 was carried out in 2004, and the wall is comparable to the submerged tunnel that will be constructed in Bjørvika, Oslo, and a part of NOR-CRACK is devoted to this project. The concrete containing 60% Fly ash was used in one wall and the SV 40 concrete was used in another. Temperature and strain development in 26 different positions were measured in two different sections in the structure.

6.2. Material properties

6.2.1. Concrete composition

The "SV 40" concrete is a typical high strength concrete used in bridges and tunnels in Norway, and it has a water-binder ratio (w/b) of 0.42 with 5% silica fume (percentage of OPC weight). The "low-heat" concrete has w/b of 0.46 and contains 36% FA of binder weight (60% of OPC weight) in addition to 5% silica fume (percentage of OPC weight). The composition of the two concretes is presented in Table 6.1.

Table 6.1 Concrete composition, all values in kg/m^3

Concrete	OPC (Norcem Anleggsement)	Fly ash	Silica fume	Coarse aggregate (8-16 mm)	Fine aggregate (0-8 mm)	Total water
SV 40	404	-	20	880	910	178
"Low-heat"	233	140	12	879	899	178

In the laboratory relevant concrete properties were measured, i.e. heat of hydration, coefficient of thermal expansion, autogenous shrinkage, mechanical properties, creep and restraint stress in the TSTM, and the detailed test program is previously described in chapter 3. Test results of mechanical properties are presented in Appendix B, and three specimens were used at each age. All properties are discussed below and implemented in the structural analysis.

6.2.2. Mechanical properties

The modified version of the CEB-FIP MC 1990 equations, as shown in equation (5.3), (5.4) and (5.5), is used to model the development of the compressive strength, tensile strength and modulus of elasticity.

It is surprising that the compressive E-modulus of the "low-heat" concrete at 28 day is higher than that of the "SV40" concrete. This is possibly due to the uncertainty of the test results, and only one compressive E-modulus test was performed for the "low-heat" concrete. Nevertheless, the parameters shown in Table 6.2 will be used in the numerical analysis of the "double wall" structure.

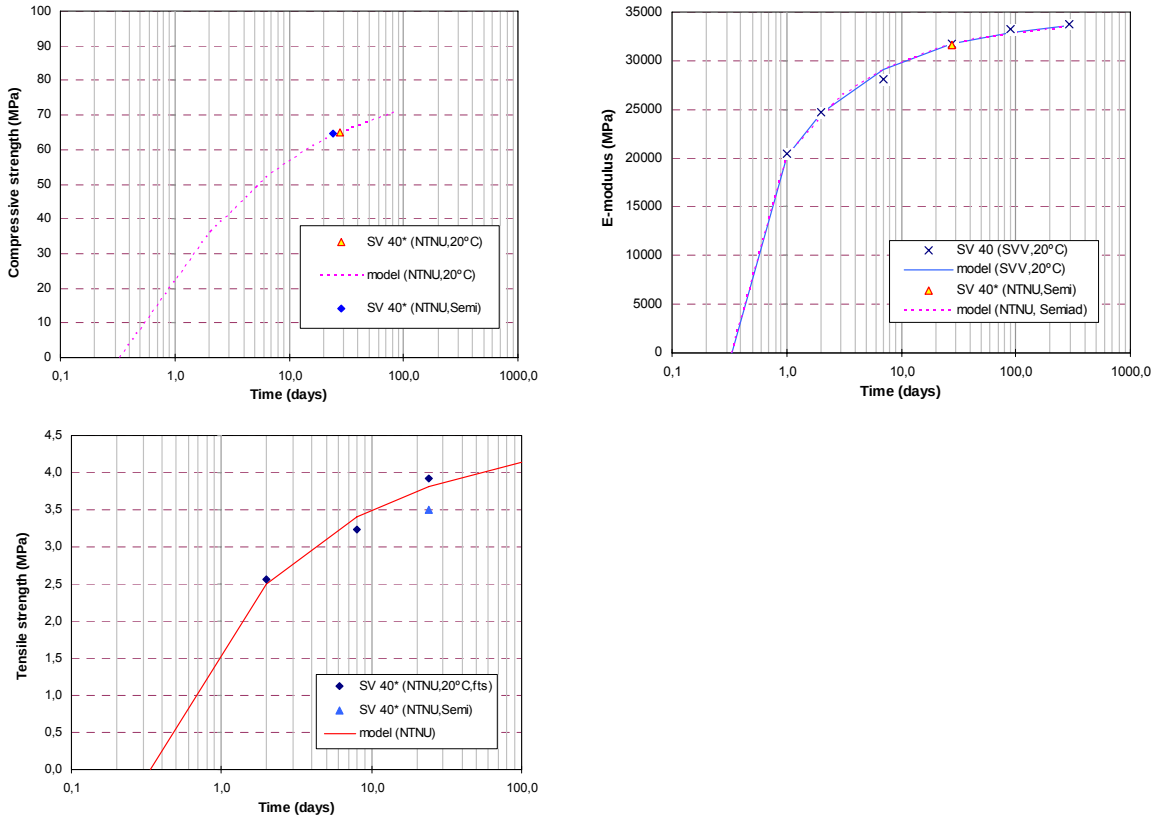

Figure 6-1 Compressive strength, E-modulus and tensile strength of SV 40 concrete

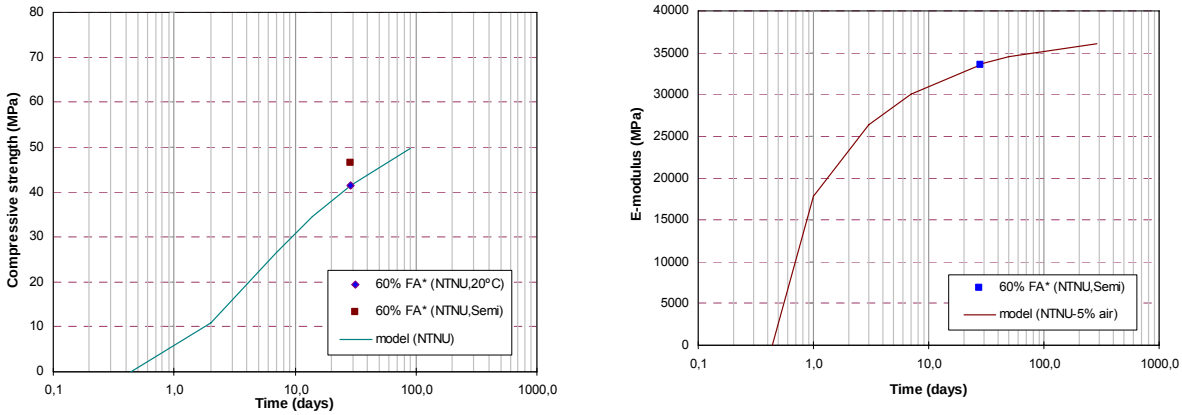

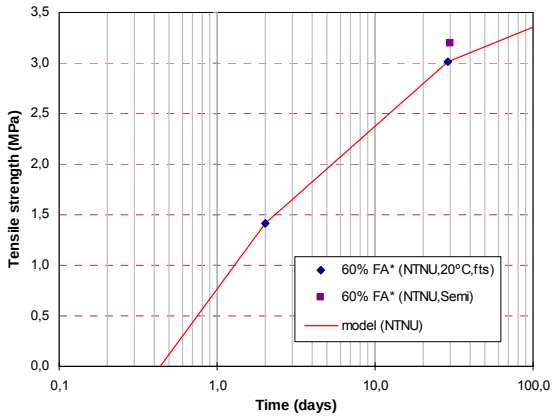

Figure 6-2 Compressive strength, E-modulus and tensile strength development of the "low heat" concrete

Table 6.2 Mechanical Properties of the "SV40" and "low-heat" concrete

Concrete	$f_c(28)$(MPa)	$f_t(28)$(MPa)	$E_c(28)$(GPa)	s	n_t	n_E	t_0 (h)
SV40	65.11	3.86	31700	0.197	0.722	0.421	8.0
"Low-heat"	41.20	3.20	33360	0.418	0.561	0.251	10.5

6.2.3. Thermal properties

The simple approach based on maturity age was used in the modeling of the heat development, as shown in equation(5.2).

The parameters of the activation energy were determined according to the Norwegian Code (NS3656). The results from isothermal tests at three temperature levels: 5, 20 and 50°C were plotted against equivalent time. Then the activation energy was found by fitting results at a level of 40% of maximum strength.

At first the heat development of the "low-heat" concrete tested in the laboratory was used in the analysis, but as discussed later in the parameter study, the calculated maximum temperature is about 10°C lower than the measured maximum temperature. Unfortunately, the hydration heat development of this particular concrete mixture used in the field test was not measured, and the input of the hydration heat, as shown in Figure 6-3, is adjusted to get better agreement with the measured temperature development in the field test. The heat development applied in the temperature and strain analysis was about 35% higher than that of the "low-heat" concrete tested in the laboratory. (Larsen and Ji, 2004)

It was later confirmed (personal communication with Skanska and Unicon) that for this particular field experiment the concrete manufacturer had put fly ash into a silo previously used to store silica fume, but unfortunately the silo was not completely cleaned, and probably some silica fume left at the bottom entered the mixture used in this field test.

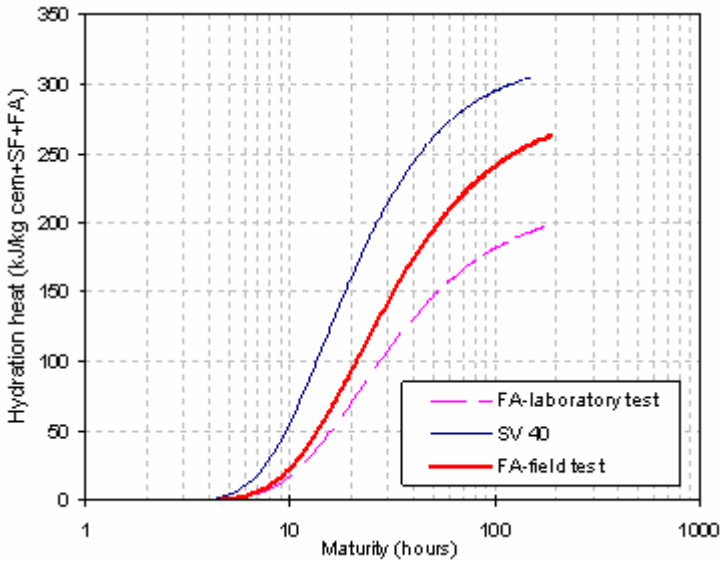

Figure 6-3 Heat evolutions of SV 40 and "low-heat" concrete

Table 6.3 Thermal properties of "SV40" and "low-heat" concrete

Concrete	Q_∞ (kJ/kg cem.)	τ	α	Thermal expansion coefficient (10^{-6}/°C)	Arrhenius constant (K)	Thermal conductivity (kJ/^{0}Cms)	Thermal capacitance (kJ/^{0}Cm^3)
"SV40"	319	15.04	1.34	10.54	2645.7	0.0026	2512.2
"Low-heat" (laboratory)	215	17.75	1.20	8.35	4353.1	0.0026	2482.4
"Low-heat" (field test)	290	17.75	1.20	8.35	4353.1	0.0026	2482.4

6.2.4. Volume change (Autogenous shrinkage and thermal dilation)

The free deformation was measured in the Dilation Rig with a stepwise realistic temperature history for both concretes in the NTNU laboratory. The maximum temperature for "SV 40" and "low-heat" concrete is 56 and 45ºC with initial temperature 20ºC, while the maximum temperature for "low-heat" concrete is 33ºC with initial temperature 11ºC. The autogenous shrinkage is then separated from the thermal dilation by assuming a constant value for the thermal dilation coefficient. The autogenous shrinkage curves of the "SV 40" and "low-heat" (60% FA) concrete are shown in Figure 6-4.

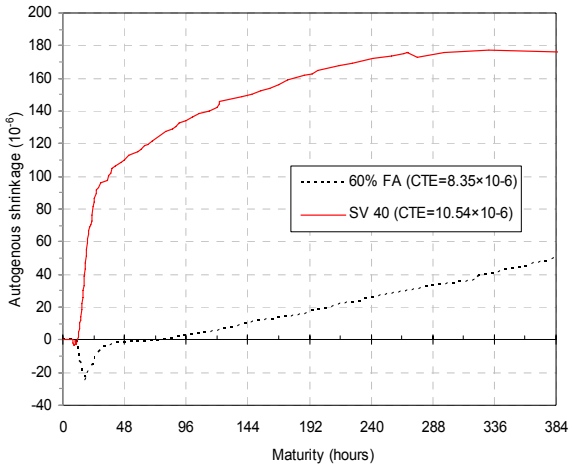

Figure 6-4 Autogenous shrinkage versus maturity time

6.2.5. Creep

Compressive creep tests for both concretes were performed at different ages at 20ºC and under sealed conditions, and the results are shown in Figure 6-5. The Double power law is used to model the creep behaviour in the numerical simulations, and the compliance function becomes:

$$J(t,t') = \frac{1}{E(t'_e)}\left(1+\varphi\cdot(t')^{-d}(t-t')^{p}\right) \tag{6.1}$$

Where t is the concrete age, t' is the concrete age at loading, $E(t'_e)$ is the E-modulus at loading age, φ, d, p are creep model parameters. In general two creep tests were performed for each of the loading ages. For the "SV 40" concrete, the creep tests were carried out at 2 and 9 days respectively, and as shown in Figure 6-5 a), the model is in good agreement with the experimental results. For the "low-heat" concrete, the creep tests were carried out at 4 and 7 days respectively, and it is seen from Figure 6-5 b) that the estimated the creep strain is slightly lower than the test results.

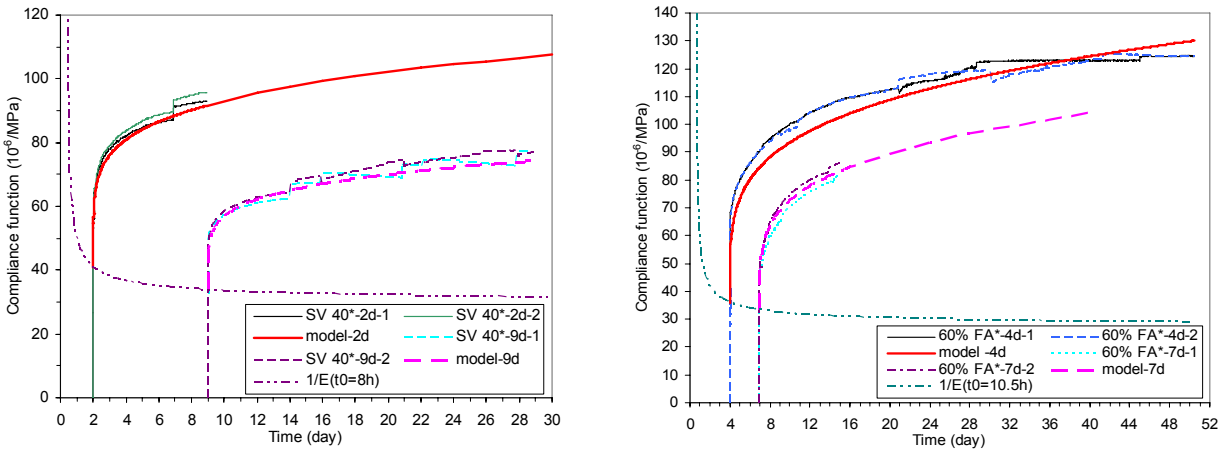

a) SV 40 concrete b) low-heat concrete

Figure 6-5 Double power law and results of compressive creep tests

Table 6.4 Creep parameters for "SV 40" and "low-heat" concrete

Concrete	d	p	φ
"SV 40"	0.18	0.18	1.10
"Low-heat"	0.26	0.22	1.60

6.3. TSTM results

The imposed temperature histories and measured stress developments in the TSTM for "SV 40" and "low-heat" concrete are shown in Figure 6-6 a), Figure 6-7 a) and Figure 6-8 a), and the strain developments in Dilation Rig and TSTM are shown in Figure 6-6 b), Figure 6-7 b) and Figure 6-8 b). For the "SV 40" concrete, the maximum temperature increase is about 36ºC from 20ºC to 56ºC, and the feedback system is deactivated at 76 hours, and the full restraint condition is then changed to the partial restraint condition to prevent break of the specimen during the test. For the "low-heat" concrete, the TSTM test was first performed at initial temperature 20ºC, and the maximum temperature rise is 25ºC, and the full restraint condition is changed to the partial restraint condition at 120 hours. Another TSTM test was carried out at the initial temperature 11ºC, which represented the approximate air temperature in the field test, under full restraint condition, and the maximum temperature rise is about 22ºC.

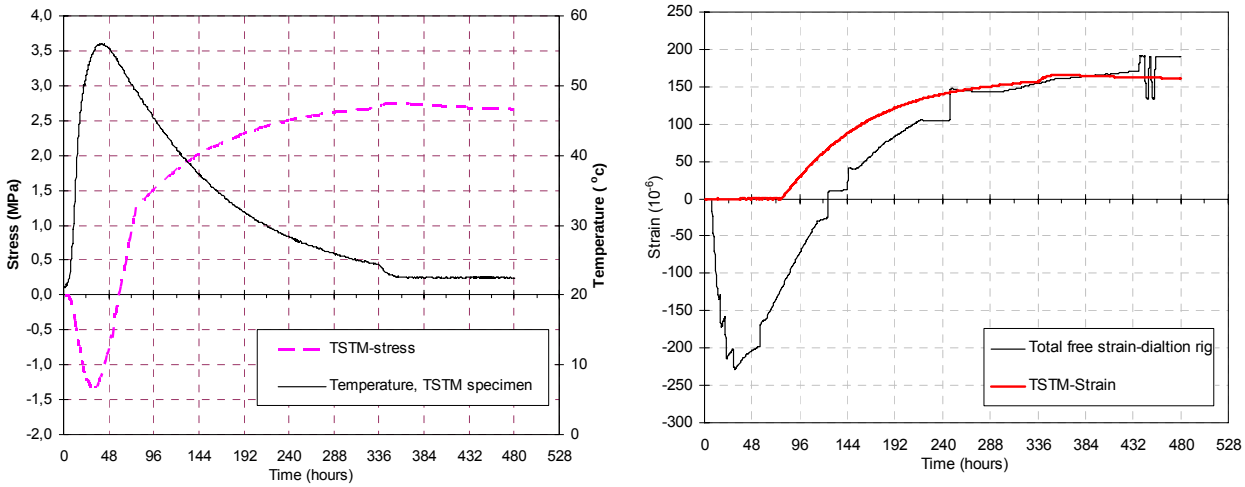

a) Temperature and stress in TSTM b) Deformation in Dilation Rig and TSTM

Figure 6-6 Test results of TSTM and Dilation Rig for "SV 40" concrete

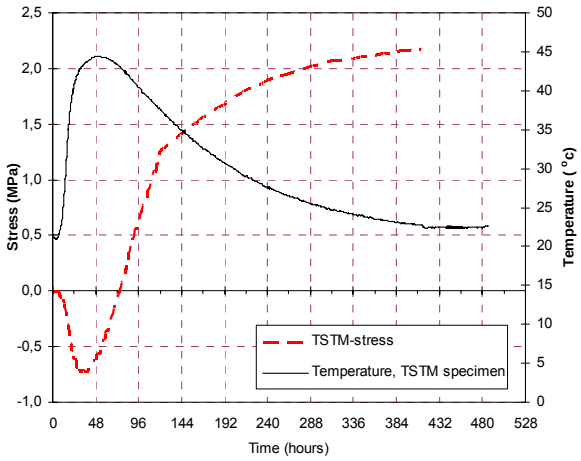

a) Temperature and stress in TSTM

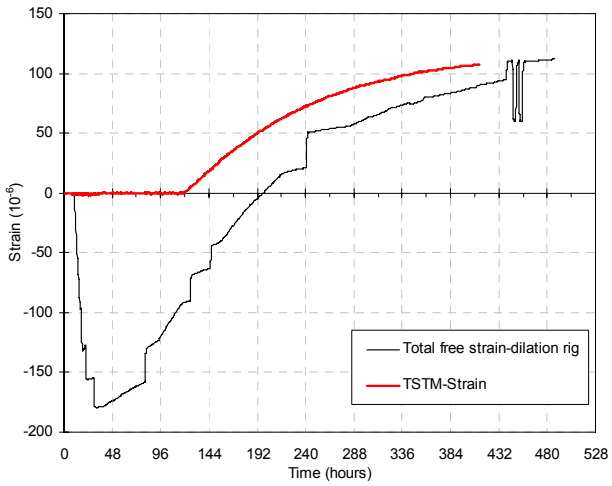

b) Deformation in Dilation Rig and TSTM

Figure 6-7 Test results of TSTM and Dilation Rig for "low-heat" concrete with initial temperature 20 ºC

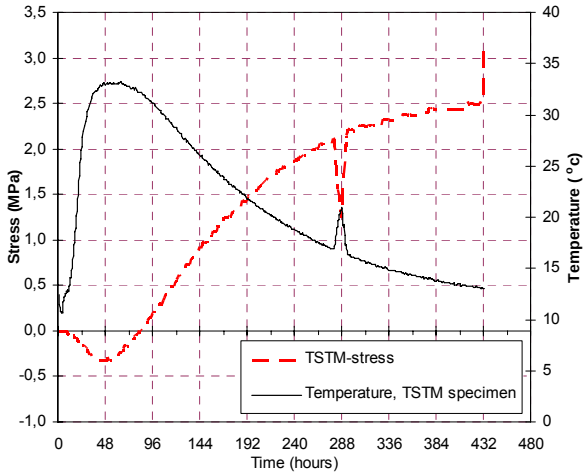

a) FA 60% -initial temperature 11ºC

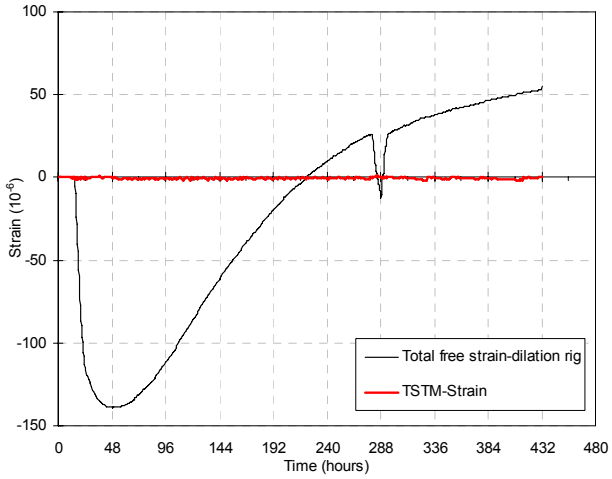

b) Deformation in Dilation Rig and TSTM

Figure 6-8 Test results of TSTM and Dilation Rig for "low-heat" concrete with initail temperature 11 ºC

The comparisons of calculated and measured stress development for "SV 40" concrete are shown in Figure 6-9, and the development of the compressive stress in the first 2 days is in good agreement with the test results, but the development of the tensile stress afterwards is lower than the test results. As mentioned early, the E-modulus of "SV 40" concrete at 28 day is lower than that of "low-heat" concrete; the low E-modulus of "SV 40" concrete significantly reduces the calculated tensile stress development. The calculated and measured stress developments of the "low-heat" concrete with 20ºC initial temperature are shown in Figure 6-10, and the development of the compressive stress in first 3 days is in good agreement with the test results, and the development of the tensile stress afterwards is slightly lower than the test results. The stress development of the "low-heat" concrete with 11ºC initial temperature is shown in Figure

6-11, and the development in both compressive and tensile stress is slightly higher than the test results.

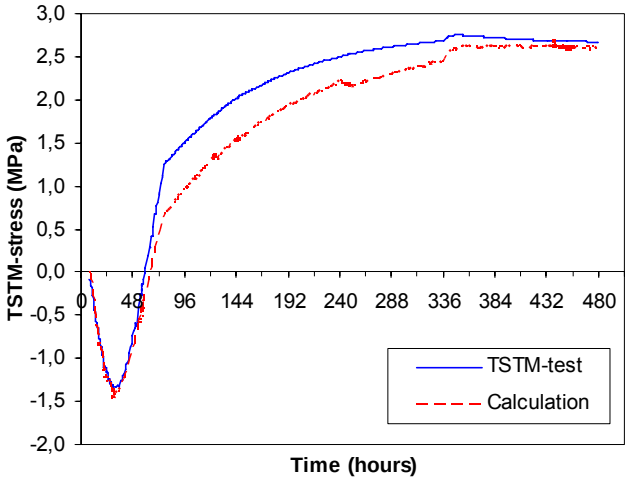

Figure 6-9 Stress development in TSTM for "SV 40" concrete

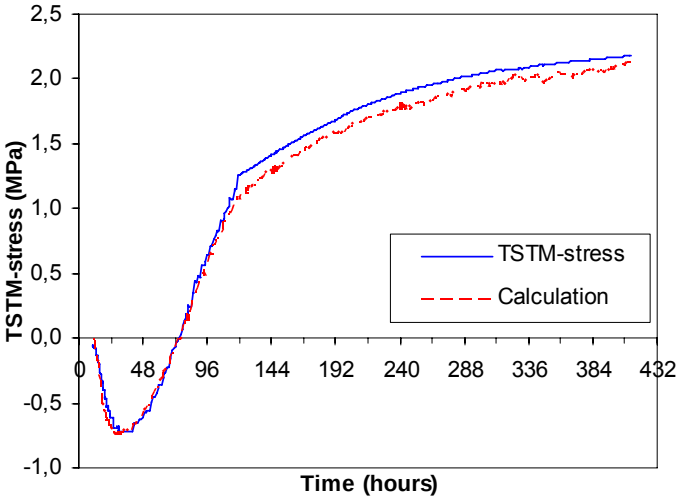

Figure 6-10 Stress development in TSTM for "low-heat" concrete with initial temperature 20°C

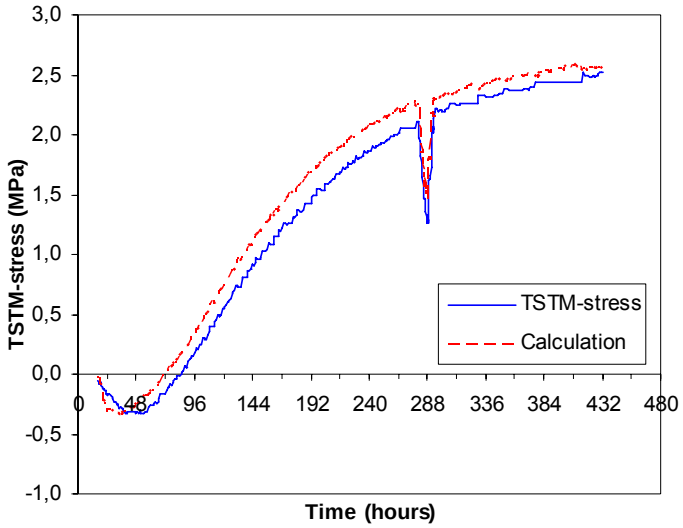

Figure 6-11 Stress development in TSTM for "low-heat" concrete with initial temperature 11ºC

6.4. Boundary conditions and finite element model

The actual external conditions on the field site are used for structural analysis. The plastic foil on top of the wall and the formwork on the side of the wall were removed 216 hours (9 days) after casting. The wind velocity is assumed to vary from 0 to 2 m/s, and the following convection coefficients are used:

Concrete-plastic foil-air convection coefficient=0.0040 kJ/°Cm^{2}s
Concrete-formwork-air convection coefficient=0.0026 kJ/°Cm^{2}s
Concrete-air convection coefficient=0.0133 kJ/°Cm^{2}s

The air temperature was recorded and is shown in Figure 6-12. The fresh concrete temperature for the "low-heat" concrete was about 23.0ºC (rather high) and for "SV 40" about 21.5ºC.

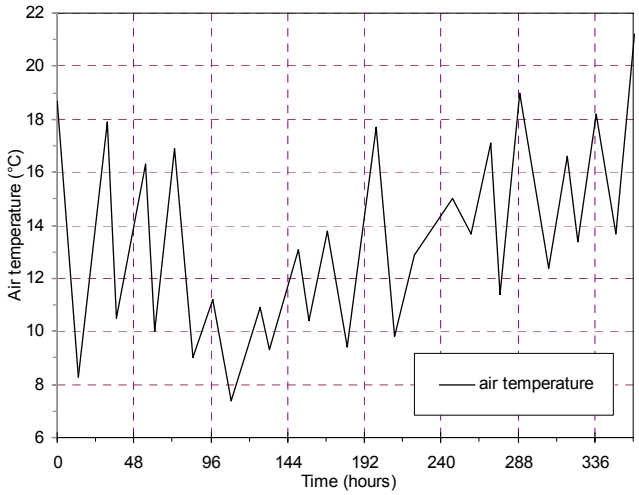

Figure 6-12 Temperature history of ambient air

In the analysis, the subgrade reaction modulus method is used to model the deformability of the ground, and the vertical modulus of subgrade reaction is $k_v = 250MN/m^3$ for compression, $k_v = 0MN/m^3$ for tension, and the horizontal modulus of subgrade reaction is $k_h = 60MN/m^3$.

The finite element mesh of the structure used in the program Diana is shown in Figure 6-13 c). The 20-node solid element CHX60 is used to model the concrete, and the element is automatically converted to 8-node HX8HT in the heat analysis. The 4-node boundary element BQ4HT is used to model the boundary conditions in the heat analysis.

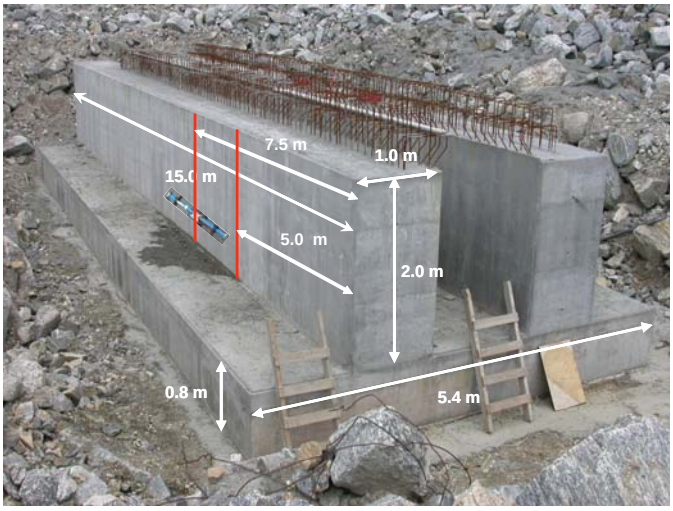

a) Picture of field test walls

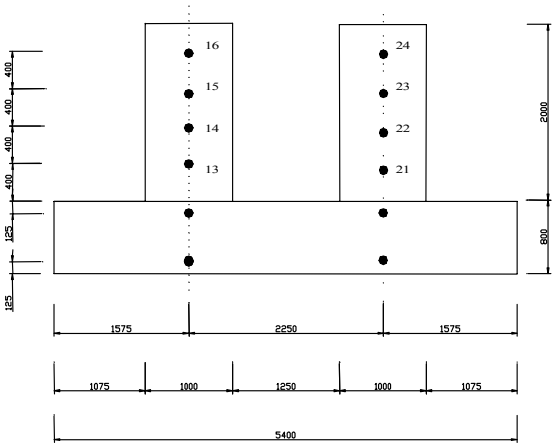

b) Measuring points at the middle section

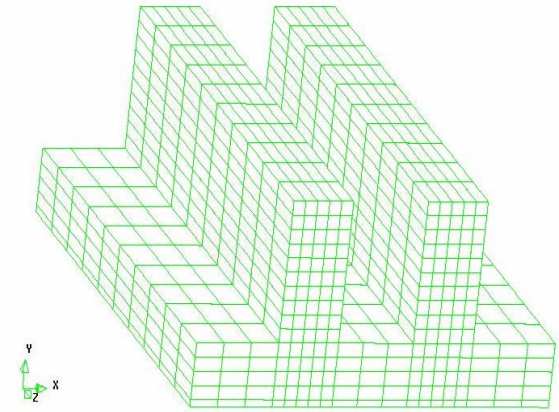

c) Finite element model

Figure 6-13 The double-wall structure

6.5. Analysis results

6.5.1. Temperature analysis

The measured and calculated temperature developments at the middle section (points 13-16 for the "SV 40", and points 21-24 for the "low-heat" concrete, as shown in Figure 6-13 b)) are shown in Figure 6-15 and Figure 6-16. The calculated temperature developments have a good agreement with the test results, and the deviation of the calculated and measured maximum

temperature is in the range of ±1.5°C for both the "SV 40" and the "low-heat" concrete, and the maximum temperatures in both concretes are presented in Table 6.5.

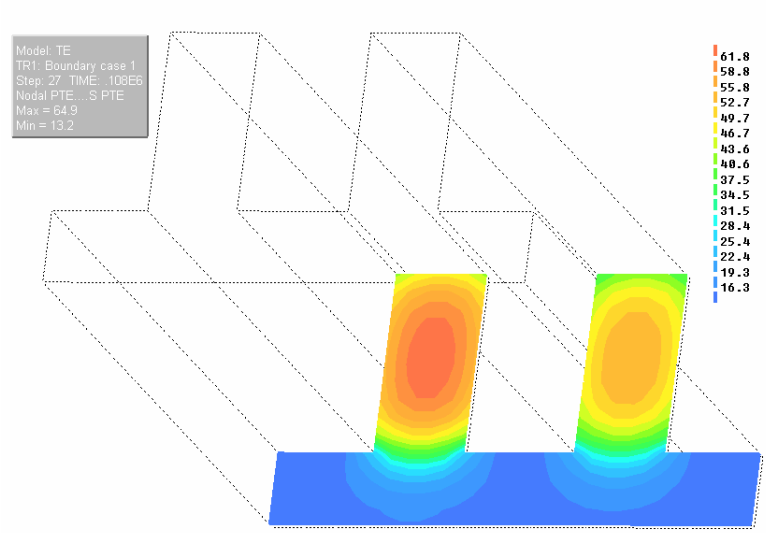

Figure 6-14 Temperature contour in the middle section of wall

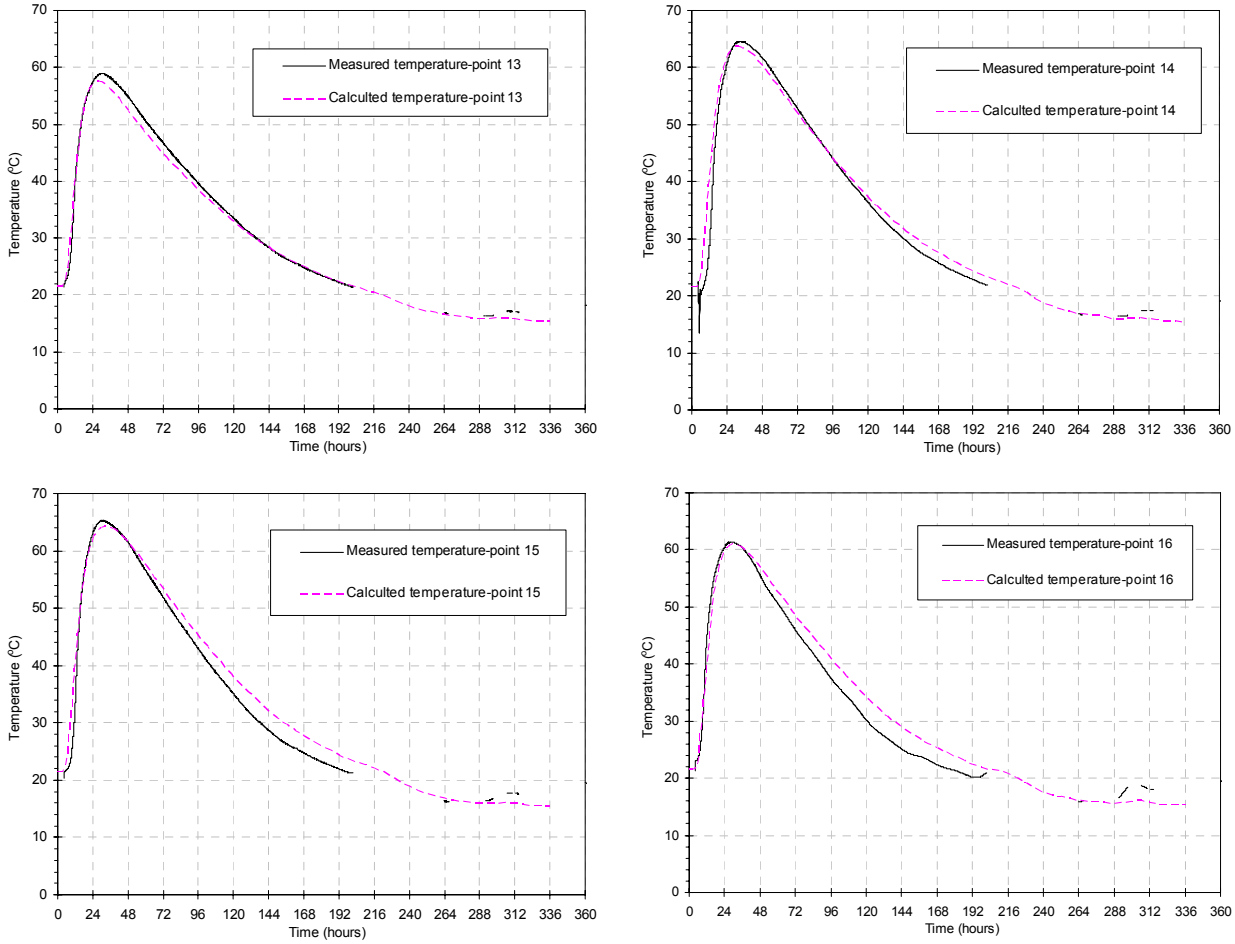

Figure 6-15 Calculated and measured temperature in the middle section (SV 40)

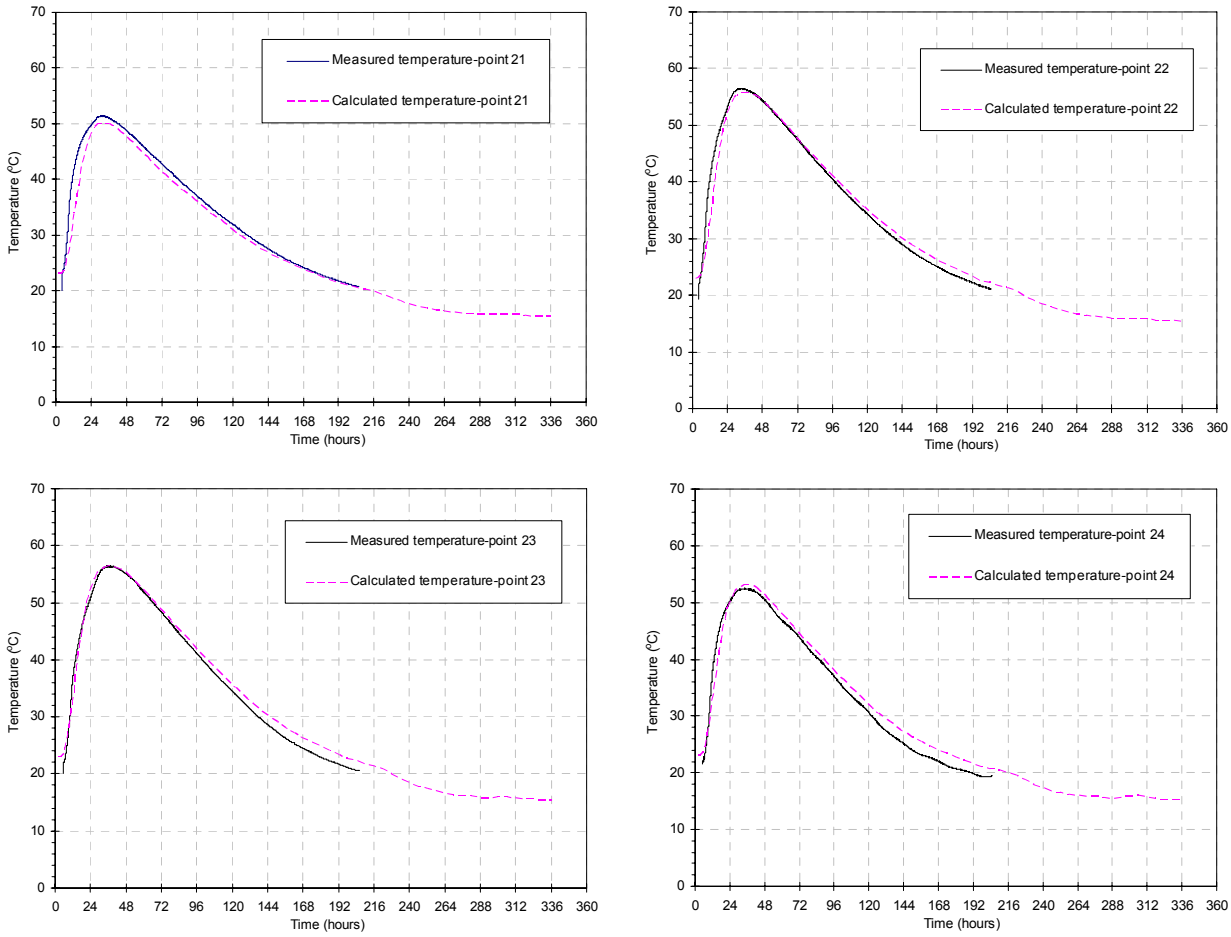

Figure 6-16 Calculated and measured temperature in the middle section (low-heat concrete)

Table 6.5 Maximum temperature in concrete

Concrete	Calculated temperature (°C)	Measured temperature (°C)
"SV 40"	64.16	65.25
"Low-heat"	56.40	56.47

6.5.2. Strain development

The simulated and measured total strain developments in the concrete wall (the middle section of SV-40 and 5.0 m section of low-heat concrete, as marked in Figure 6-13 a)) are shown in Figure 6-17 and Figure 6-18 respectively. In the SV 40 concrete wall, the calculated strain is underestimated for the lowest point (point 13, 0.4 m above slab) with maximum deviation of about 50 μ. They are in good agreement with the measured strains for the two middle points (point 14, 15), and it is overestimated for the top point (point 16, 1.6 m above slab) with a maximum deviation of about 100 μ. The strain developments of the four points at the middle section are similar, and it indicates that the rotation of the middle section is quite small, and the simulated wall rotates more than the experimental test. Similar result is obtained by Bosnjak (2000) in the analysis of a wall structure made of "basic 5" concrete. It means the restraint from foundation in the field test model is higher than the simulated model. Cracks are observed in the

wall after the remove of the framework, and according to the measurements they probably appear ca 7 and 9 days after casting, and the crack increases the strain in the two bottom points (point 13, and 14).

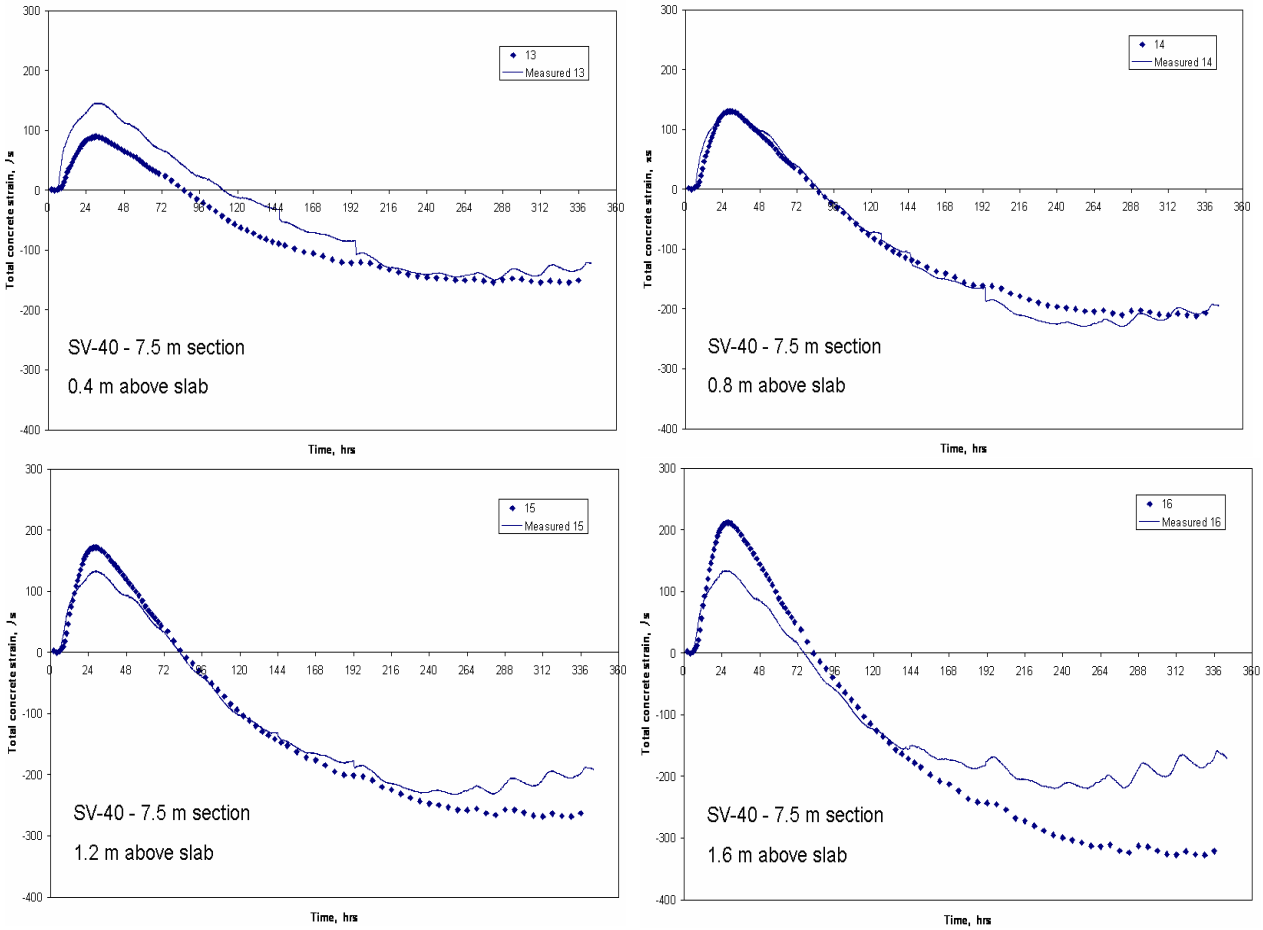

Figure 6-17 Simulated and measured total strain development in the middle section of the "SV-40" wall

In the low-heat concrete wall, the calculated strains of the bottom three points (point 17, 18, and 19) agree well with the measured ones, only the calculated strain of the top point (point 20) is higher than the measured one about 50 µ. Some difficulties were experienced in the recording, and the results in point 17, 18, 19 and 20 failed at about 7.5 days.

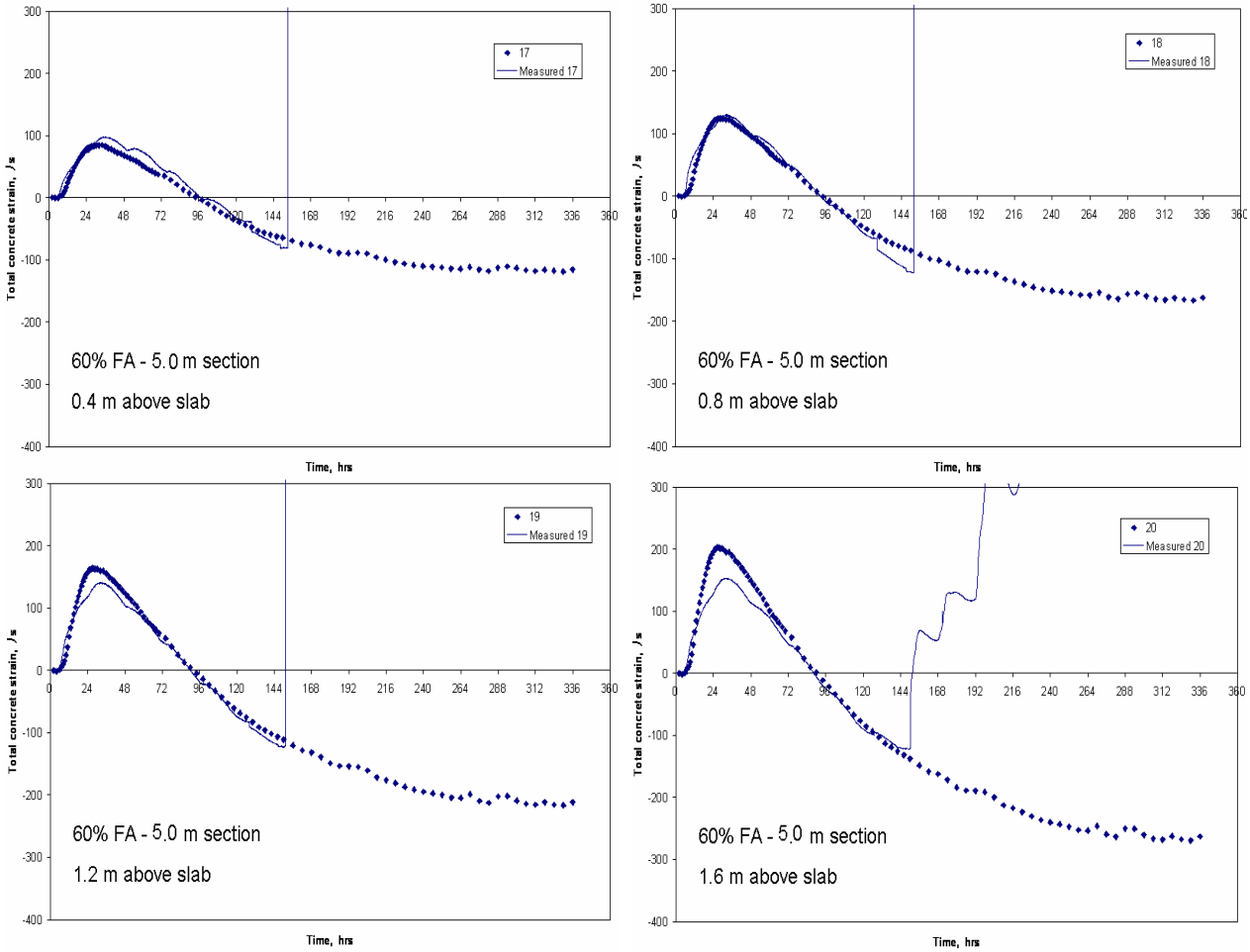

Figure 6-18 Simulated and measured total strain development in the 5.0 m section of the "low-heat" concrete

6.5.3. Stress development

The calculated stress development in element 98 and 648 and the comparison with the tensile strength development are shown in Figure 6-20 for SV 40 and low-heat concrete respectively. The crack-index, defined as the ratio between tensile stress ($\sigma(t)$) and tensile strength ($f(t)$), has also been determined, and the crack index is shown in Figure 6-21. The maximum stress and corresponding cracking index in both concretes is presented in Table 6.6.

For "SV 40" the maximum crack-index is about 0.97, and according to the measurement the first crack occurs at about 6 days, and the corresponding crack-index is 0.73 as shown in Figure 6-21. The maximum crack-index for the "low-heat" concrete is 0.75, and the first crack occurs at about 7 days, and the corresponding crack-index is 0.55. The observation on site showed that the cracking in "SV 40" concrete is more severe than the cracking in "low-heat" concrete.

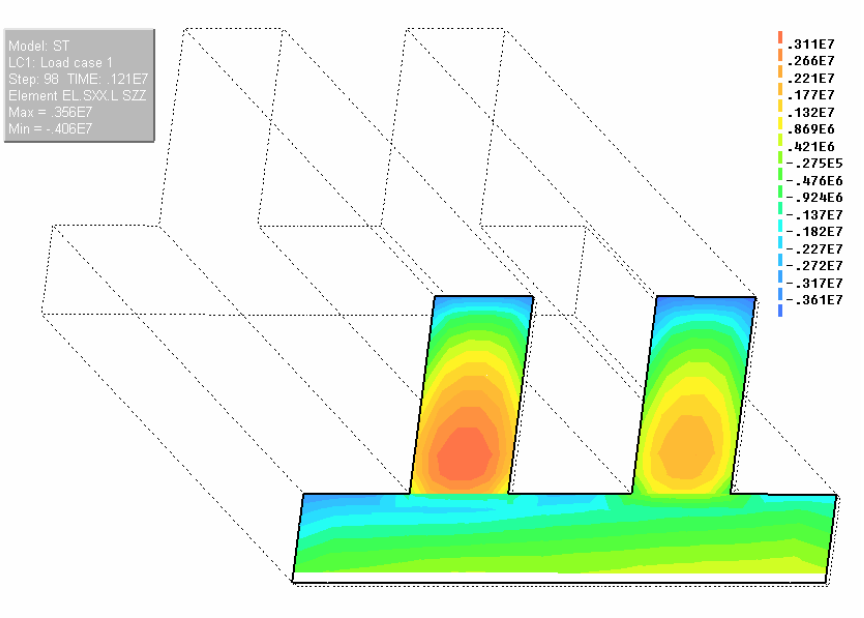

Figure 6-19 Stress contour in the middle section of wall

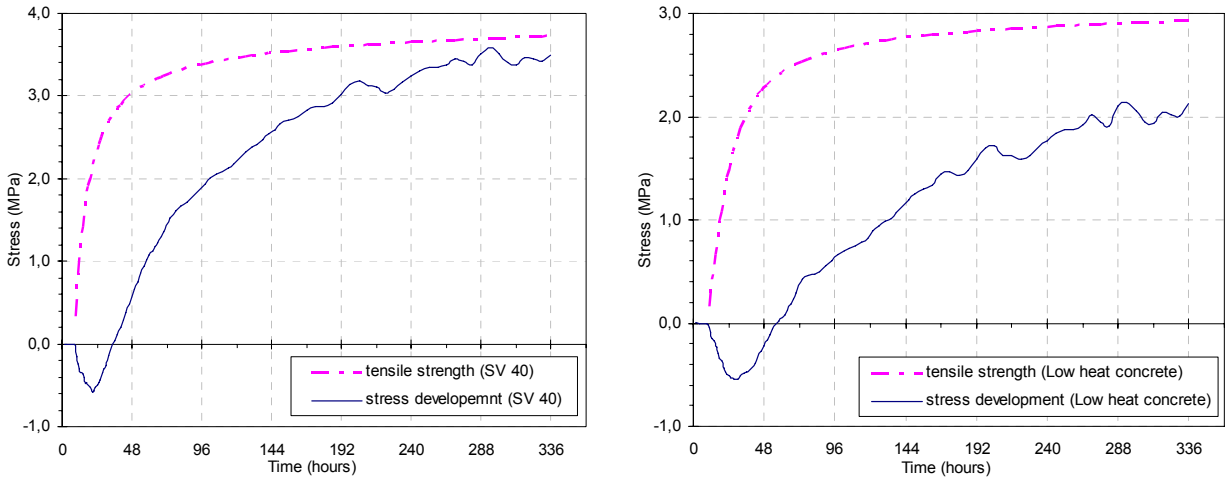

Figure 6-20 Stress and tensile strength developments in SV 40 and "low-heat" concrete

Table 6.6 Maximum stress and cracking risk index

Concrete	Tensile stress (MPa)	Maturity (hours)	Tensile strength (MPa)	Cracking index
SV 40	3.58	406	3.70	0.97
"Low-heat"	2.19	533	2.91	0.75

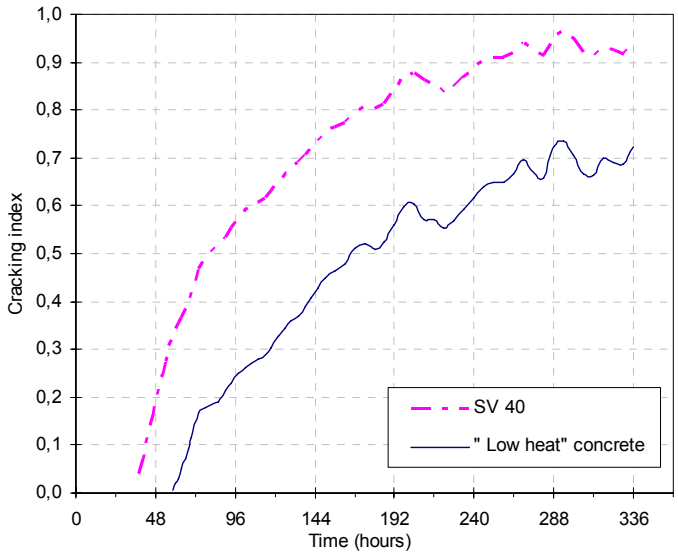

Figure 6-21 Cracking index in SV 40 and "low-heat" concrete

6.5.4. Conclusions and discussion

The calculated temperatures are in good agreement with the measured results, and the deviation between calculated and measured maximum temperature is in range of ±1.5°C for both SV 40 and "low-heat" concrete, and the maximum difference between calculated and measured temperature during the first 2 weeks is about 3°C.

The calculated strains in the middle part of both walls (0.6 – 1.2 m above the slab) where the maximum stresses occur are in good agreement with the measured ones. This will ensure that the predicted crack-indexes are reliable – as verified by occurring severe cracks in SV 40 concrete and fewer cracks in the low-heat concrete.

The cracking index at the first crack is 0.73 and 0.55 for SV 40 concrete and the low-heat concrete mixture used in the field test. The "low-heat" concrete with fly ash seems to have a lower probability to crack under the given conditions.

6.6. Parameter study

6.6.1. Hydration heat

The hydration heat of the "low-heat" concrete tested in the laboratory, as shown in Figure 6-3 and Table 6.3, is also applied in the structural analysis, and the calculated temperature in the middle section (point 21-24) is shown in Figure 6-22. The maximum calculated temperature in the low-heat concrete wall is about 45.9°C which is about 10°C lower than the measured maximum temperature. The additional silica fume left in the bottom of silo which entered the mix used in the field test increases the temperature in the concrete.

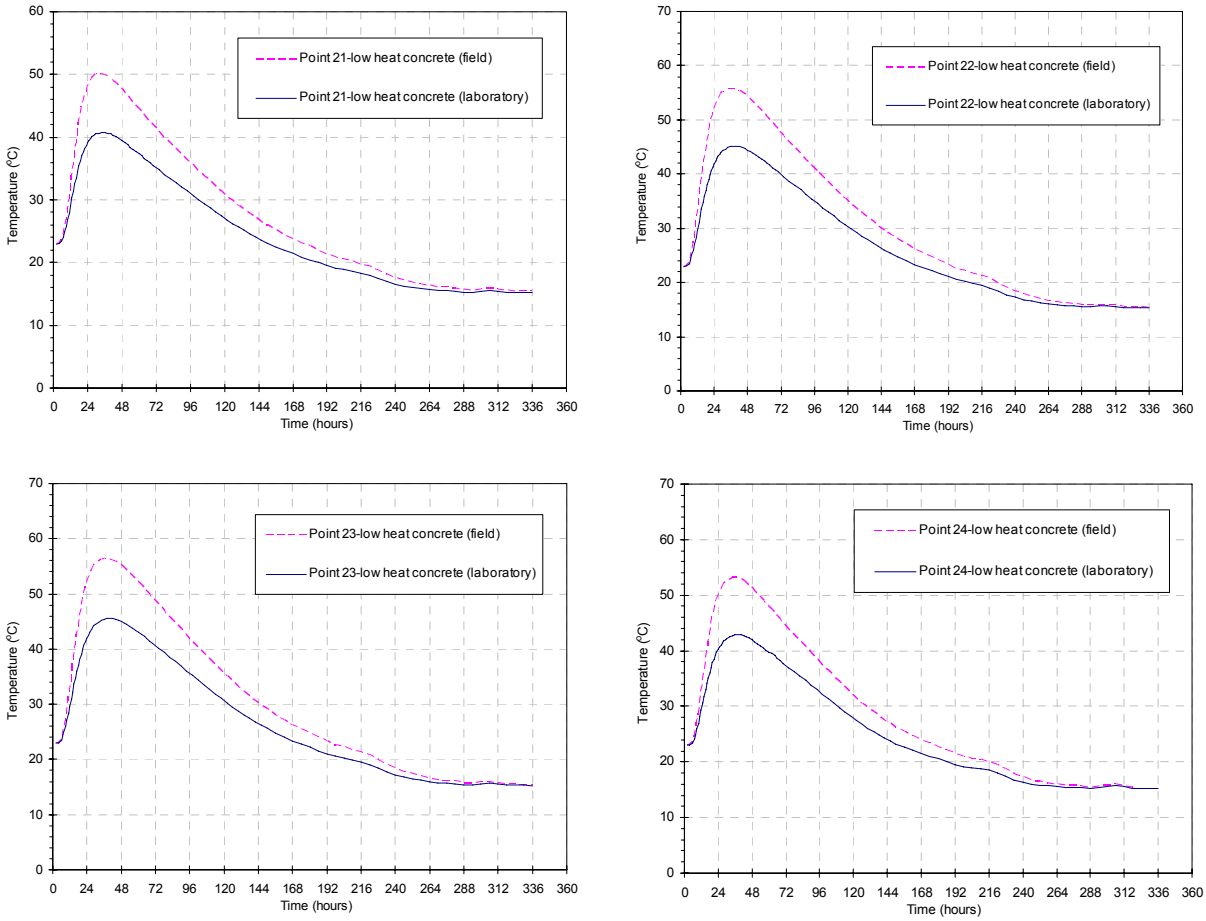

Figure 6-22 Calculated temperature developments for two different hydration heat input

The maximum calculated tensile stress of the concrete mix tested in the laboratory is as expected lower than that of the concrete mix applied in the field test, and consequently the crack-index is also lower. If the fly ash had not been polluted with silica fume in the field test, the measured temperature development would be lower, and the cracking-index would be around 0.58, and in this case the "low-heat" concrete would most likely not crack.

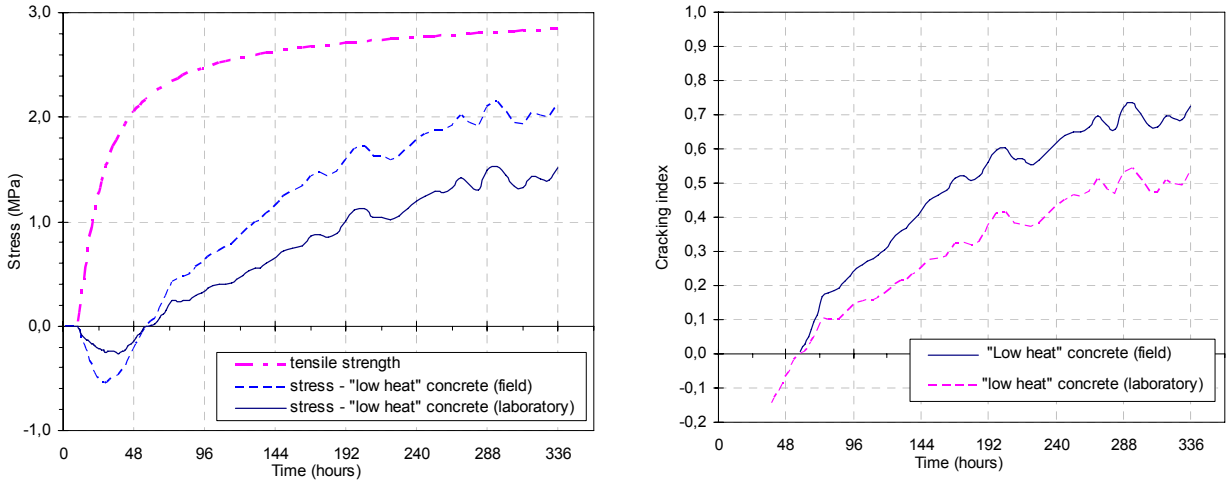

Figure 6-23 Stress and tensile strength development and cracking index (two different heat input)

Table 6.7 Maximum stress and cracking risk index

Concrete	Tensile stress (MPa)	Maturity (hours)	Tensile strength (MPa)	Cracking index
"Low-heat" (field)	2.19	533	2.91	0.75
"Low-heat" (laboratory)	1.63	426	2.81	0.58

6.6.2. Creep property

Creep is a very import factor reducing the restraint stresses in the order of 40-50% compared to the elastic case, and creep data during the whole period of hardening (heating and cooling) is necessary for reliable prediction of cracking risk.

The creep compliance is increased or decreased by 50%, and then applied in the analysis of the "double wall" structure. It can be seen from Figure 6-24 that 50% increase of the creep compliance leads to 15% and 20% decrease in the restraint stress for "SV 40" and "low-heat" concrete respectively. Higher creep in the early period reduces compressive stresses, and consequently increases the tensile stress, while increased creep in cooling period decreases tensile stresses. These two effects are competing and the final effect is their summation. The 50% decrease of creep compliance have more influence on the stress development, and leads to 26% and 30% increase in the restraint stress for "SV 40" and "low-heat" concrete respectively. Due to the higher creep compliance, the "low-heat" concrete is more sensitive to the creep increase/decrease.

Table 6.8 Creep parameters

Parameter	SV 40*			60% FA*		
	Test	Creep (+50%)	Creep (-50%)	Test	Creep (+50%)	Creep (-50%)
d	0.18			0.24		
p	0.19			0.24		
φ	0.98	1.47	0.49	1.47	2.205	0.735

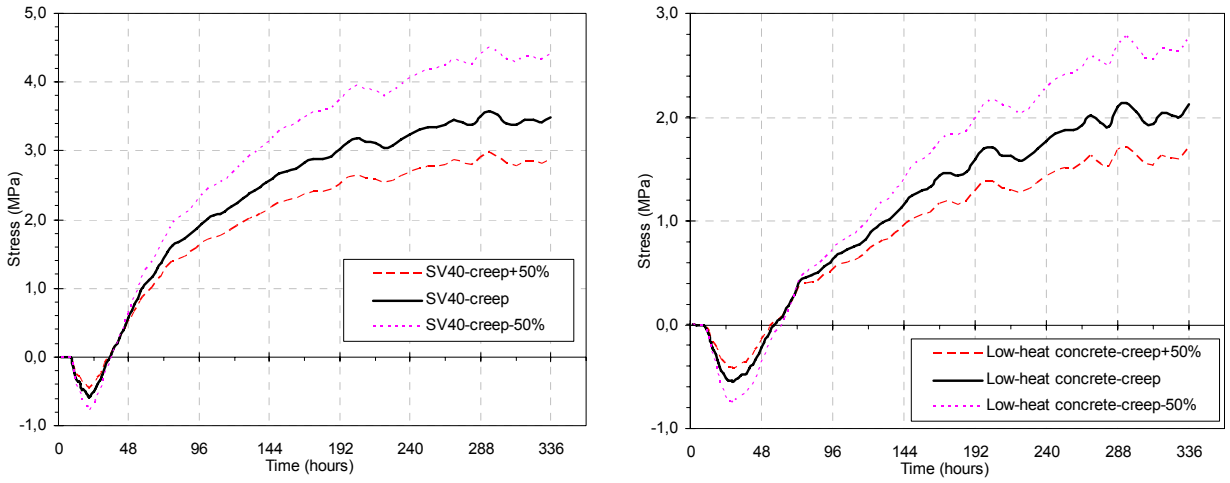

Figure 6-24 Calculated stress developments with 50% increase/decrease in creep compliance

6.6.3. Thermal dilation (TD) and autogenous deformation (AD)

As discussed in chapter 2, two strategies in the literature are often used to separate AD and TD during variable temperature, and the validation of those two strategies is investigated for the "basic 5" concrete. Bjøntegaard (1999) carried out experiments on Norcem Anleggsement (CEM I-52.5 LA) concretes with w/b ratio of 0.40 and 5% SF (Basic 5) under 20ºC isothermal, three saw-toothed series (29ºC, 47ºC and 60ºC series), and three similar smooth temperature histories.

According to the first strategy, the measured autogenous shrinkage of "basic 5" concrete under 20º C isothermal conditions is transferred to the AD under realistic temperature by maturity concept. The predicted autogenous shrinkage is used as input in the analysis with two different constant CTEs: 8.5×10^{-6} or 10.0×10^{-6}/ºC, then the results are compared with the stress development calculated with input of measured total deformation from 60ºC series.

As shown in Figure 6-25, the total deformations in the two cases with two different constant CTEs are different from the measured total deformation, and consequently the calculated stress development in those two cases can not represent the stress development in the structure. It means that only measuring autogenous shrinkage under isothermal condition is not sufficient, and with the assumed constant CTE it cannot ensure that the input total deformation represents the total deformation under realistic temperature history.

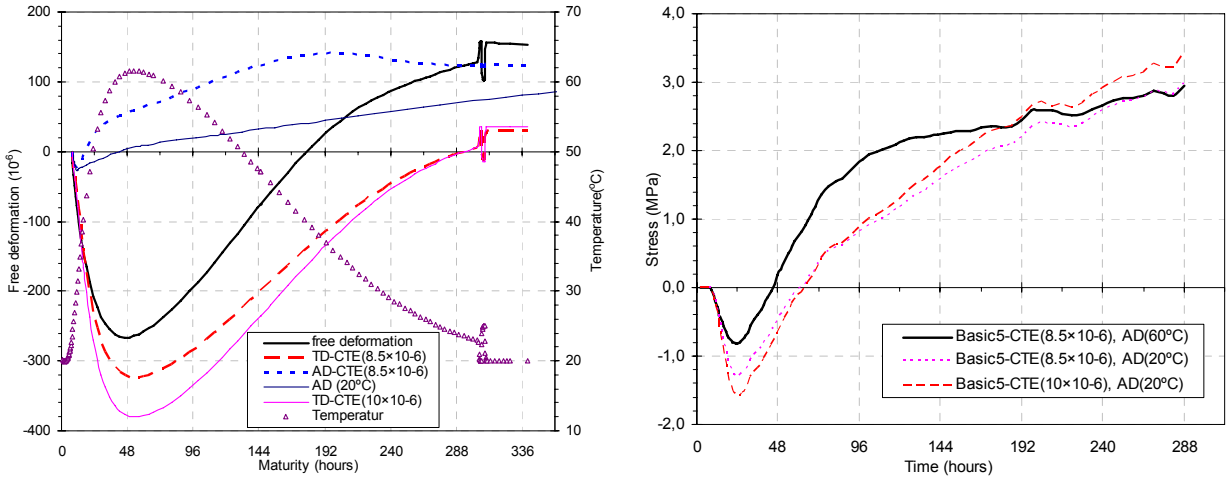

Figure 6-25 The different input of total deformation and stress development

According to the second strategy, the total deformation measured in the Dilation Rig under 60ºC series is used as input in the analysis, and it is separated by different assumed constant CTEs: 8.5×10^{-6} or 10.0×10^{-6} / ºC, as shown in Figure 6-26. It can be seen that the difference between the induced stresses at 7 days is about 10%, and as long as the input of total deformation is the same the induced stress is not significantly affected by different separation.

If the total deformation under realistic temperature history is available, although the CTE of the concrete in the early ages varies during the hydration process, the second strategy appears to be more robust since the CTE does not vary as much as AD.

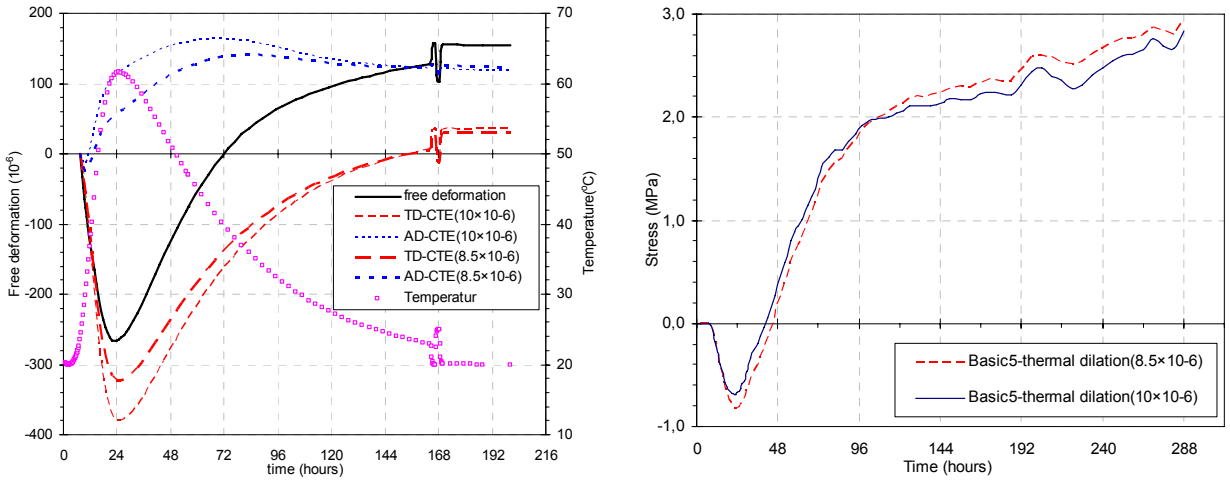

Figure 6-26 Different separation of free deformation and stress development

In the TSTM test, the temperature is approximately uniform in the specimen, but in a real structure, the temperature varies from point to point. In the lack of models for AD and TD the total deformation measured from 56 ºC series is used for the whole "SV 40" wall in the analysis. The experimental data of the total deformations for "SV 40" concrete under various temperature histories is not available, and in stead the basic 5 is used to investigate the effect of different total deformation input for different temperature ranges on the stress development.

The measured total deformations of basic 5 concrete under variable temperature histories with maximum temperature 29ºC, 47ºC and 60ºC respectively are separated into autogenous shrinkage and thermal dilation by assuming constant CTE (8.5×10^{-6} / ºC), and then the autogenous shrinkage under different temperature histories is applied as input for the different slices in the concrete wall, as shown in Figure 6-27.

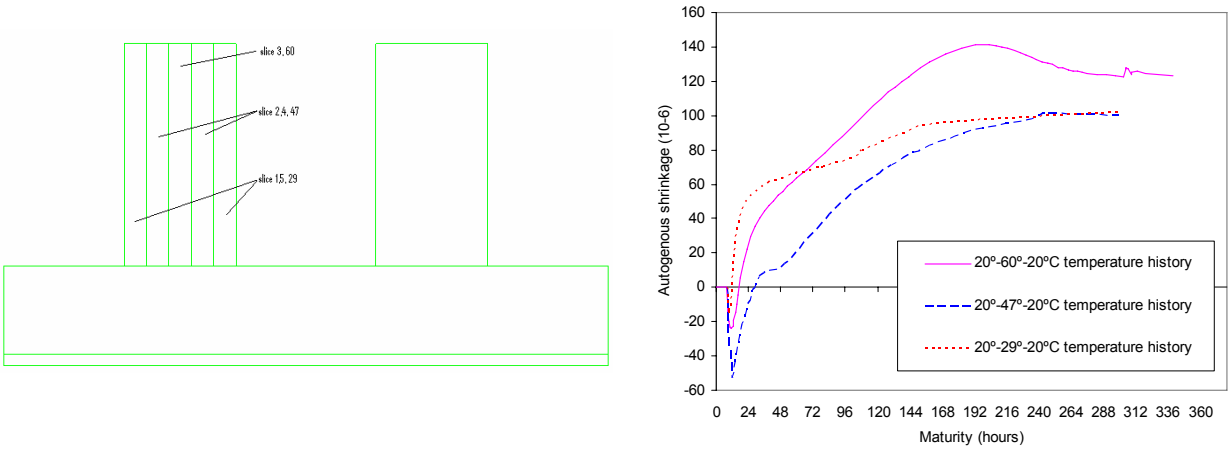

Figure 6-27 Different Autogenous shrinkage input for different slices in the concrete wall

The result is compared with another case, in which only one autogenous shrinkage data from 60ºC series is applied in the whole wall. The stress development in middle slice of the wall is similar in those two cases, as shown in Figure 6-28, but the location of maximum tensile stress is different, for the case with different autogenous shrinkage input for different slices the maximum tensile stresses occur in the second and fourth slices with autogenous shrinkage data

from 47ºC series, and do not occur in the middle of the concrete wall, and for another case, the maximum tensile stresses occur in the middle of the concrete wall. The maximum tensile stress with different autogenous shrinkage input is 10% higher than that with one autogenous shrinkage input, the autogenous deformation in 60ºC series appears apparent expansion from 8 days after casting, and it will reduce the development of the tensile stress.

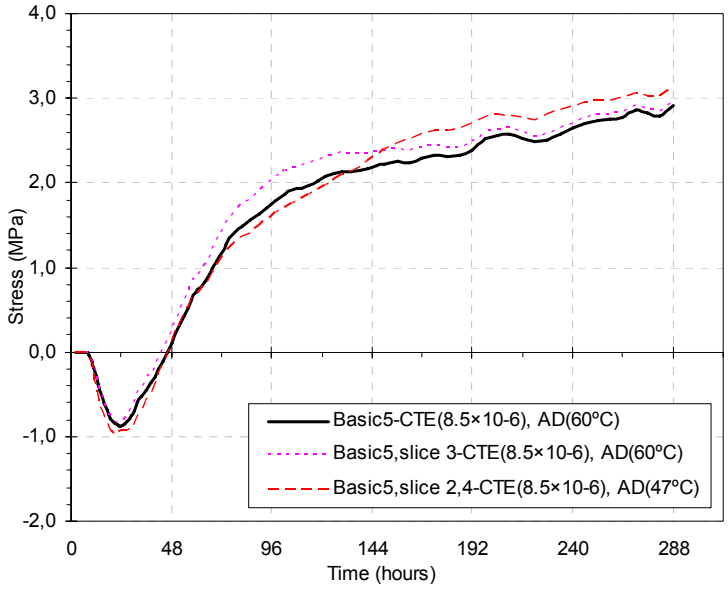

Figure 6-28 Stress developments in the concrete wall

6.6.4. Discussion

Prediction of crack-index (or crack risk assessment in general) should be based on well defined (measured) concrete properties, and the three most important groups of factors in prediction of early age cracking are:

- Hydration heat
- Volume change: thermal dilation and autogenous shrinkage
- Material properties: E-modulus, creep/relaxation

The hydration heat is the most important parameter in determining the temperature development in the concrete structure. The composition of cement and mineral additives has dominant influence on the hydration heat, as experienced in field test, the impropriate mixture containing amount of residual silica fume results in a 35% increase in the hydration heat, and consequently the cracking index of the "low heat" concrete increases about 30% from 58% to 75%, and cracks appeared in the wall structure. In order to control the quality of concrete mixes in the field, semi-adiabatic temperature tests may be performed at site when a new batch of cement or mineral additives is used.

The volume changes of early age concrete is the driving force of the cracking risk, and the sum of thermal dilation and autogenous deformation can be measured in realistic temperature histories in laboratory. As long as the total volume change is accurate, the separation into different TD and AD would not have significant influence on the structural analysis. In the present work, the volume change under stepwise temperature is used to directly calculate the

CTE, and to deduce the autogenous shrinkage. When the volume changes are calculated by autogenous deformation measured under isothermal temperature conditions and assumed constant CTE, one should be aware that this volume change may not be a close approximation for that in realistic temperature history because the temperature effect on AD is quite uncertain especially under temperature histories with high maximum temperature. The input of measured volume changes under various temperature histories, which closely represent the temperature distribution in the concrete structure, will give more reliable prediction of cracking risk in early age concrete structure.

Creep has two opposite of effect on tensile stress development in concrete. Creep in the early period decreases compressive stresses, and consequently increase the tensile stress, while creep in cooling period decreases tensile stresses. These two effects are competing and in general the latter effect prevails in most situations, and the creep/relaxation properties significantly reduce the restraint stresses in concrete structure.

7. Case study - Bjørvika submerged tunnel

7.1. Introduction

The concrete tunnel is presently being built in Bjørvika in Oslo, and the total length is about 1110 meters with three traffic lanes in each direction, and 675 meter of it (30 sections) is submerged under the seawater, see Figure 7-1, and the length of each section is 22m. The cross section of the tunnel is not exactly symmetric, and the width between left side and middle wall is slightly different from the width between right side and middle wall. In the current study, the cross section is treated as symmetric, only half of the section as shown in Figure 7-2 is used in the analysis, and it is considered that the simplification reduces the elements used in the FEM analysis by 50%, and analysis results is still accurate enough to the current purpose.

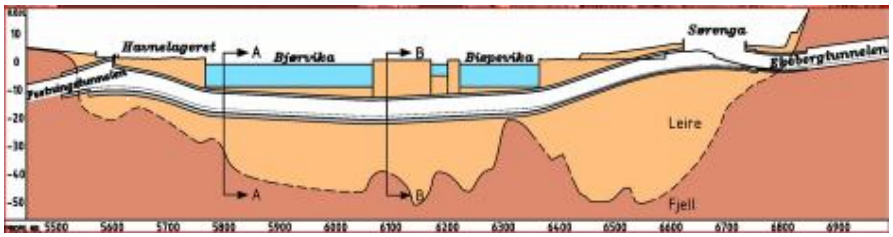

Figure 7-1 Plan view and vertical section of the Bjørvika submerged tunnel

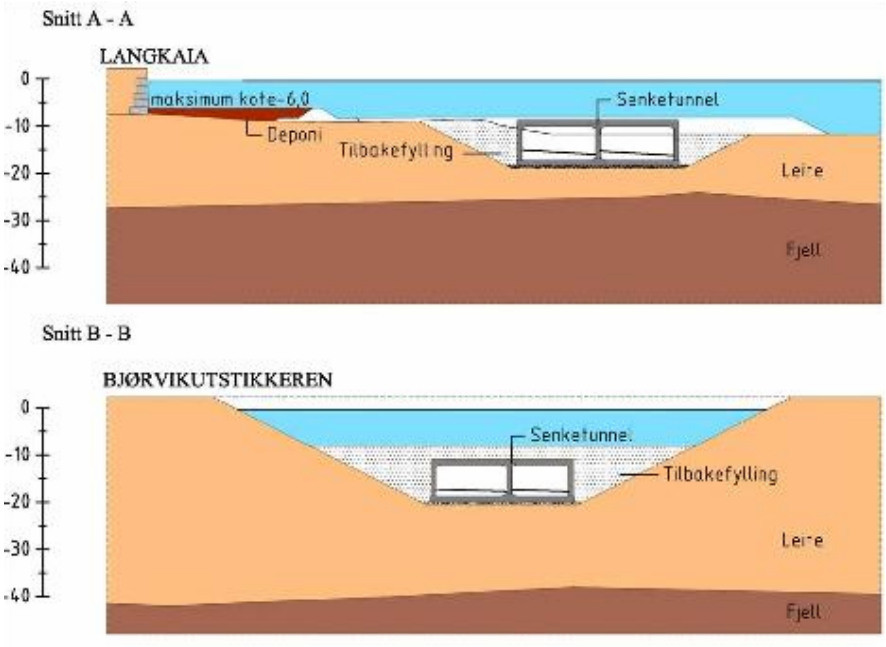

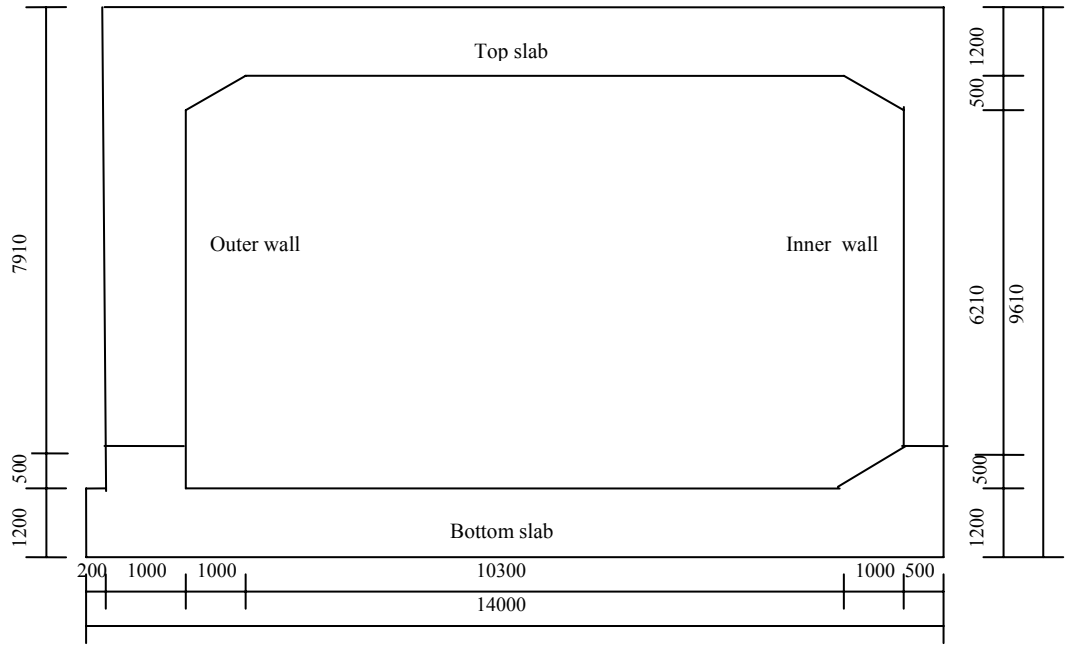

Figure 7-2 Geometry of the submerged tunnel (half of the cross section treated as symmetric).

The temperature and stress development have been analyzed by the FE program Diana to assess the risk of through cracking in the hardening phase. In the FE analyses, the temperature problem is solved first, and these results are used as input for the subsequent stress calculation.

7.2. Concrete properties

As explained in the previous chapter 3 and 5, the model parameters have been identified from a comprehensive test program performed at SVV and NTNU. Thermal and mechanical properties (semi-adiabatic temperature test, the E-modulus, and tensile strength test), volume changes (Dilation Rig) and stress development in restraint specimens exposed to realistic temperature histories (TSTM) have been tested for several concretes with varying content of fly ash and slag, and five concretes listed in the following were selected for further studies:

Recipe A: SV40 *("ordinary bridge concrete")
Recipe B: 40%FA* (40% by weight of cement, 28% by weight of binder)
Recipe C: 60%FA* (60% by weight of cement, 36% by weight of binder)
60%FA with initial temperature 11ºC
Recipe D: 40% BFS (40% by weight of cement, 28% by weight of binder)
Recipe E: 60% BFS (60% by weight of cement, 36% by weight of binder)

The composition of the five concretes was presented in detail in chapter 3, and the hydration heat and mechanical properties are described in chapter 5. The creep data in compression are applied in the FEM analysis. As discussed in Chapter 5, combined compressive and tensile DPL-parameters give best correspondence with the measured stress developments in the TSTM tests, and using only the compressive DPL-parameters gives better agreement with the test results than using only the tensile DPL-parameters. In the FEM program Diana, only one DPL-parameter can be specified in the input file, and then the compressive creep will be used in the analysis.

7.2.1. Volume change

The thermal dilation and the autogenous deformation, which are the driving forces to the restraint stress, were determined from the Dilation Rig test. The sum of the two properties is measured directly, and then separated into TD and AD. But this separation is only valid for that particular temperature history. The practical solution is simply to assume that the thermal dilation coefficient is a constant, and then the autogenous deformation is determined by subtracting thermal dilation from the total deformation measured under one realistic temperature history. Although the temperature distribution varies in the structure, as discussed in chapter 6, using only one autogenous shrinkage corresponding to that realistic temperature history has only a small effect on the calculated maximum tensile stress.

The imposed temperatures and measured total deformations for five concretes are shown in Figure 7-3. The constant CTEs are presented in Table 7.1, and the separated AD and TD are shown in Figure 7-3. The maximum temperature and autogenous deformation (AD) at 12 days are also presented in Table 7.1.

During the first 1 or 2 days, the temperature increases dramatically, and the specimen experiences expansion after the autogenous shrinkage is compensated by the high thermal dilation, and afterwards the temperature decreases gradually, and the specimen undergoes contraction induced by the thermal and autogenous shrinkage together. The maximum temperature is highest for the "SV 40" concrete, and lowest for the 60% FA* concrete. The total deformation of the "SV 40" is highest in both the expansion and contraction period, the expansion of the BFS concrete is lower than that of the FA concrete, but the contraction of the BFS is higher than that of the FA concrete.

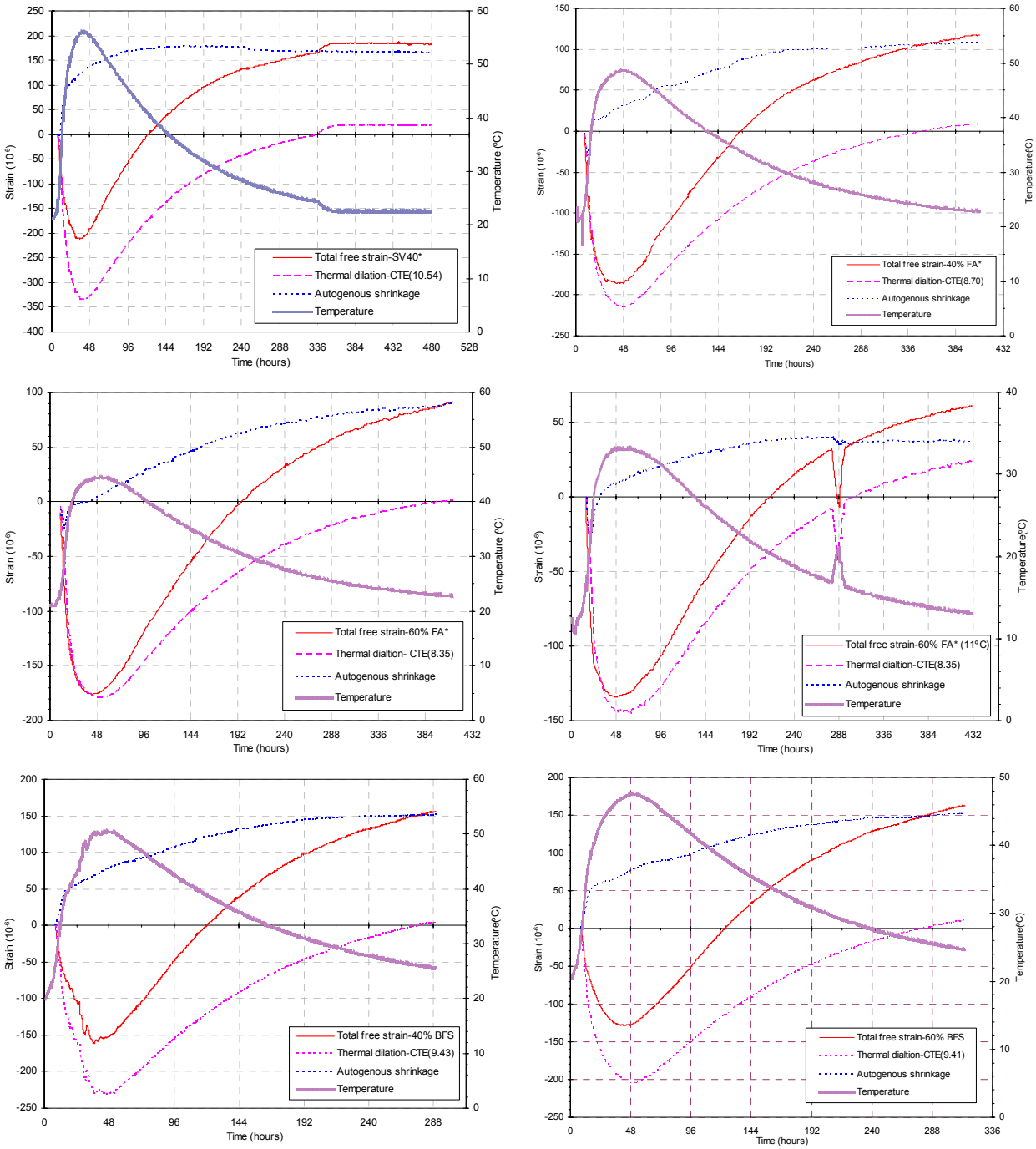

Figure 7-3 Free deformation and separated thermal dilation and autogenous deformation

Table 7.1 Thermal dilation coefficients and autogenous deformation after 12 days

Concrete type	Maximum temperature(^{o}C)	CTE (10^{-6})	AD (10^{-6})
SV40*	56.0	10.54	150
40% FA*	48.7	8.70	100
60% FA*	44.4	8.35	80
60% FA*- 11ºC	33.0	8.35	38
40% BFS	50.4	9.43	152
60% BFS	47.5	9.41	150

7.3. Numerical simulation

7.3.1. Verification of the calculation methods towards the TSTM-tests

The TSTM-tests were carried out for all the five concretes in the present test program, and the test results have been analysed by both Diana and a Visual basic program (1-D calculation, as discussed in chapter 5), and the results are shown in Figure 7-4.

It can be seen that the calculated stress developments of concretes containing 40% and 60% BFS have very good agreement with the test results, and that the maximum deviation in compression and tension is about 0.2 MPa. The calculated compressive stress of the concretes containing 40% and 60% FA with 20 ºC initial temperature is higher than the measured ones, and the calculated tensile stress of the 60% FA concrete is lower than the test results, while the calculated tensile stress of the 40% FA concrete is lower than the test results at first 10 days, and afterwards it becomes higher than the test results. The calculated compressive and tensile stress of the 60% FA concrete with 11ºC initial temperatures is higher than the test results. The calculated compressive stress of the SV 40 concrete is higher than the test results, and the calculated tensile stress is lower than the test results until 14 days.

All the model parameters used in the analysis were determined from independent tests as described in chapter 3, and no parameters are adjusted to achieve better fit with the test results. It can be concluded the model parameters used in the analysis make a reasonably accurate prediction of the stress development for the concretes containing different percentage of FA and BFS, but the deviation for the SV 40 concrete is high especially for the tensile stress at 3days, this is probably due to the low E-modulus of the SV 40 concrete. The maximum compressive and tensile stresses are summarized in Table 7.2 with the maximum deviation of compressive and tensile stress. The deviation between the calculated and measured maximum stress after 12-17 days is less than 12%, and in most cases the calculations overestimate the maximum tensile stresses.

Table 7.2 Calculated and measured stresses in the TSTM-tests

Concrete type	Maximum compresive stress (MPa)			Maximum deviation in compression (MPa)	Maximum tensile stress (Mpa)			Maximum deviation in tension (Mpa)
	TSTM	Diana	Ratio (TSTM/ Diana)		TSTM	Diana	Ratio (TSTM/ Diana)	
SV40*	1.27(1.5d)	1.60(1.6d)	0.79	-0.32(1.5d)	2.75(15d)	2.72 (15d)	0.99	0.80(3d)
40% FA*	0.62(1.5d)	0.92(1.5d)	0.67	-0.30(1.5d)	2.50(17d)	2.67 (17d)	1.07	0.30(4d)
60% FA*	0.70(1.6d)	0.82(1.6d)	0.85	-0.08(1.6d)	2.17(17d)	2.16 (17d)	1.00	0.30(5d)
60% FA*- 11ºC	0.30(2d)	0.45(2d)	0.67	-0.15(2d)	2.44(17d)	2.73(17d)	1.12	-0.30(17d)
40% BFS	1.50(1.5d)	1.25(1.5d)	1.20	0.25(1.5d)	2.46(12d)	2.57(12d)	1.04	-0.11(12d)
60% BFS	1.0(1.7d)	0.80(1.7d)	1.25	0.20(d)	2.47(13d)	2.67(13d)	1.08	-0.20(13d)

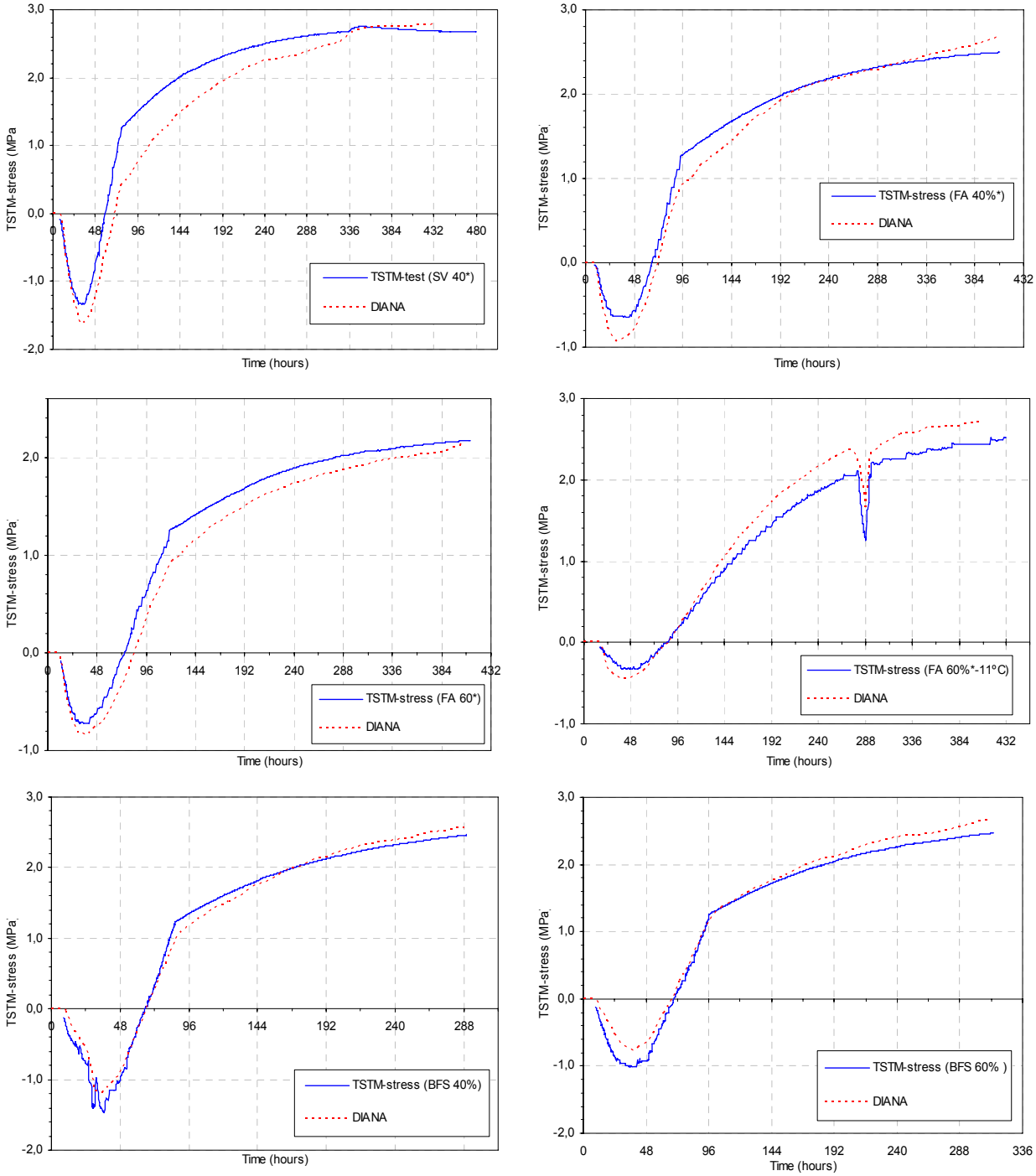

Figure 7-4 Calculated and measured stress development for the TSTM-tests

7.3.2. 3D structural analysis

7.3.2.1. Finite element modelling

The element mesh of the 3D model used in the analyses is shown in Figure 7-5. Due to symmetry conditions only one fourth of the structure between the dilation joints is modelled.

The bottom slab is modelled as hardened concrete, while it is assumed that the walls and top slab are cast in one operation.

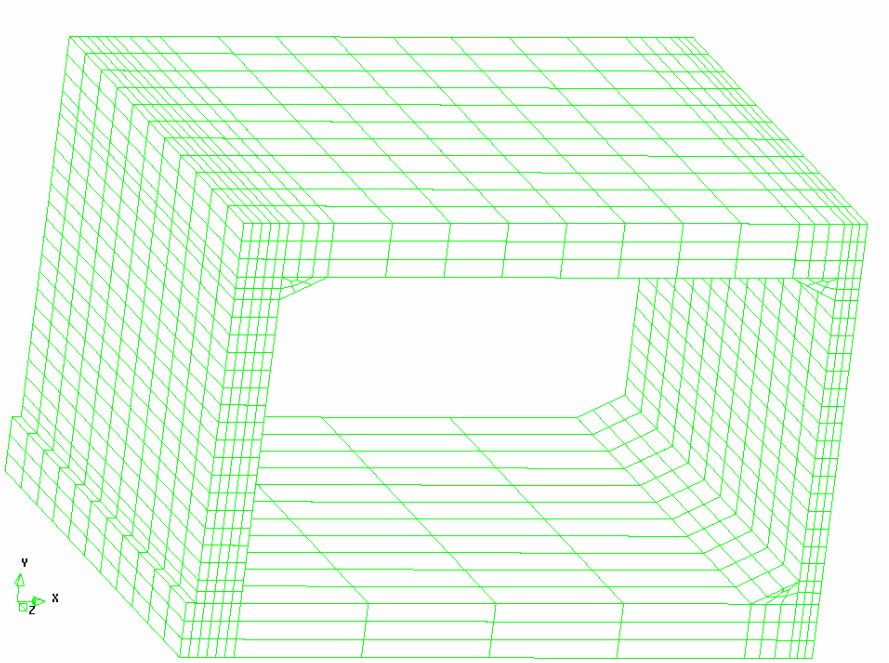

Figure 7-5 3D finite element model of ¼ of the tunnel structure
Geometry data: Bottom slab thickness: 1.2m, wall thickness 1.0m, top slab thickness 1.2m, tunnel width 28.0m, tunnel length (between dilation joints) 22.5m. The symmetry-line is in the mid-plane of the inner wall (to the right).

7.3.2.2. Boundary conditions and external factors

Fresh concrete temperature: 20^{o}C
Ambient air temperature: 20^{o}C
Wind velocity: 1m/s
Vertical walls (21mm plywood formwork, and convectivity: 0.0033kJ/m^{2}s^{o}C)
Top slab (plastic foil, and convectivity: 0.0076 kJ/m^{2}s^{o}C)
Time for formwork and plastic foil removal: 7 days (Convectivity: 0.0133 kJ/m^{2}s^{o}C)

7.3.3. Analysis Results

The temperature and stress contour in the middle section of the tunnel is shown in Figure 7-6-Figure 7-17. The maximum temperature appears at the corner between the wall and the top slab, while the critical locations, regarding the risk of through cracking determined as the ratio between maximum tensile stress and tensile strength, are in the middle of the wall (length direction) and approximately 0.6-1.2m above the foundation slab. Consequently, the temperatures in those locations, in addition to the maximum temperatures in the whole structure, are reported and discussed. It is seen that concrete with 60% FA* achieves both the lowest maximum temperature (42.2^{o}C / temperature rise 22.2^{o}C) and the lowest risk of cracking (0.74) in the outer wall. The temperature rise at the critical location of outer wall during hardening for

the other concretes are 40.7°C for the SV40* concrete, 26.5°C for the 40%FA* concrete, 25.6°C for 40%BFS concrete and 24.9°C for 60%BFS concrete. Furthermore it is seen that the reduction in fresh concrete temperature from 20 to 11°C results in a reduction of maximum temperature of 5.7°C, while the stress/strength ratio is reduced from 0.74 to 0.52.

The calculated maximum temperatures, tensile stresses after 2 weeks, and corresponding stress/strength-ratios are summarized in Table 7.4 below for the five types of concretes.

Table 7.3 Maturity and tensile strength in critical position at 14 days after cracking

Concrete	f_{t28} (N/mm^2)	Maturity time at 14 days	Tensile strength in critical position at critical time (N/mm^2)
SV40*	3.86	22.2 days	3.79
40%FA*	3.32	20.7	3.19
60%FA*	3.00	22.5	2.91
60%FA*-11ºC	3.00	19.7	2.86
40%BFS	3.89	20.7	3.74
60%BFS	3.34	21.0	3.20

Considering the calculated stresses in the outer wall, it is 3.91 N/mm^2 for the SV40* concrete while it is 2.14 for the 60% FA* concrete. The corresponding stress/strength ratios are 1.04 and 0.74 respectively. All the calculations show that the risk of cracking is about 12% higher in the inner wall compared to the outer wall due to the higher degree of restraint, but the consequences of through cracking are most serious in the outer wall which therefore should have to meet the crack criterion.

Table 7.4 Calculated temperatures and stress/strength ratio of the critical location in the wall

Concrete	T_{max} (°C)	Outer wall		Inner wall		Tensile strength	σ_t/f_t outer wall	σ_t/f_t inner wall
		$\sigma_{tensile,max}$	T_{max}	$\sigma_{tensile,max}$	T_{max}			
SV40*	69.0	3.91	60.7	4.40	60.3	3.79	1.04	1.18
40%FA*	53.1	2.69	46.5	2.99	46.2	3.19	0.86	0.96
60%FA*	48.4	2.14	42.2	2.38	41.9	2.91	0.74	0.82
60%FA*-11ºC	41.3	1.49	36.5	1.66	36.4	2.86	0.52	0.58
40%BFS	53.8	3.35	45.6	3.71	45.2	3.74	0.90	1.01
60%BFS	50.6	3.19	44.9	3.60	44.7	3.20	1.00	1.13

a) b)

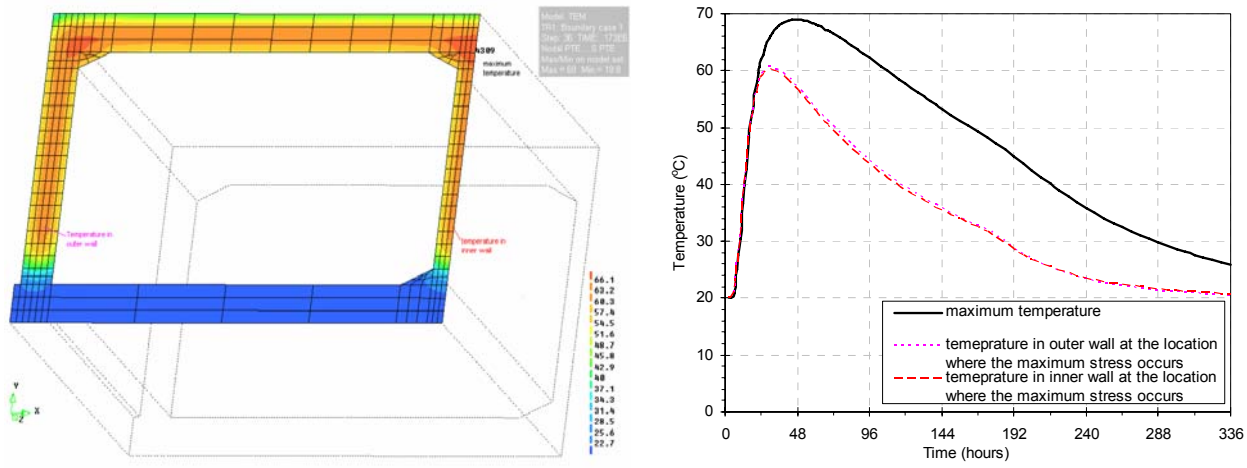

Figure 7-6 Calculated temperatures developments of SV40* concrete (a) Temperature contour (48h after casting), (b) Maximum temperature in the structure and temperature developments in the inner and outer wall

a) b)

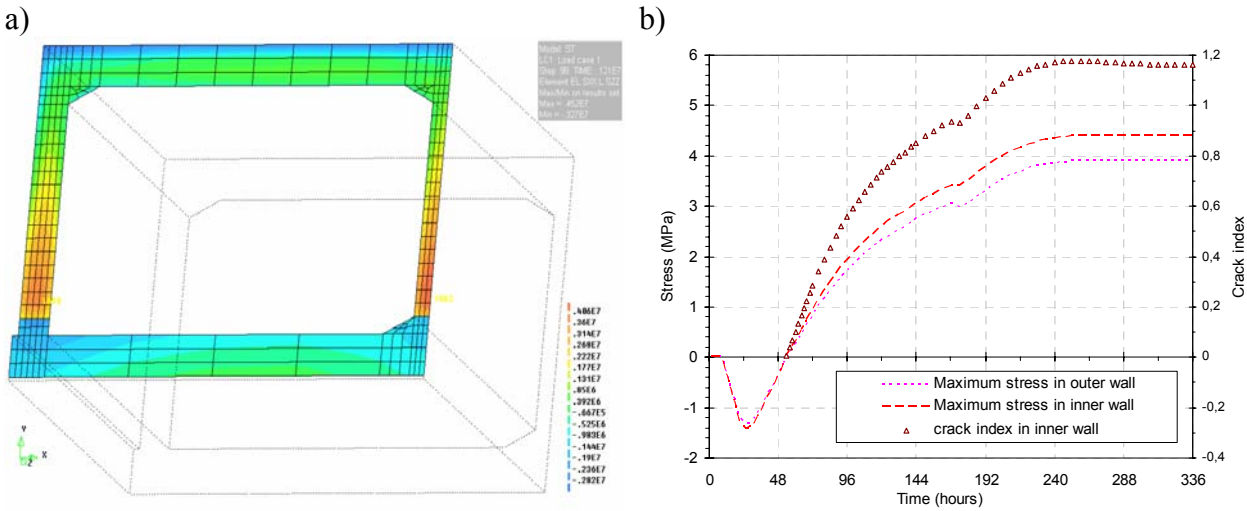

Figure 7-7 Calculated stress developments of SV40* concrete (a) Stress contour (336h after casting), (b) Stress developments in the inner and outer wall

a) b)

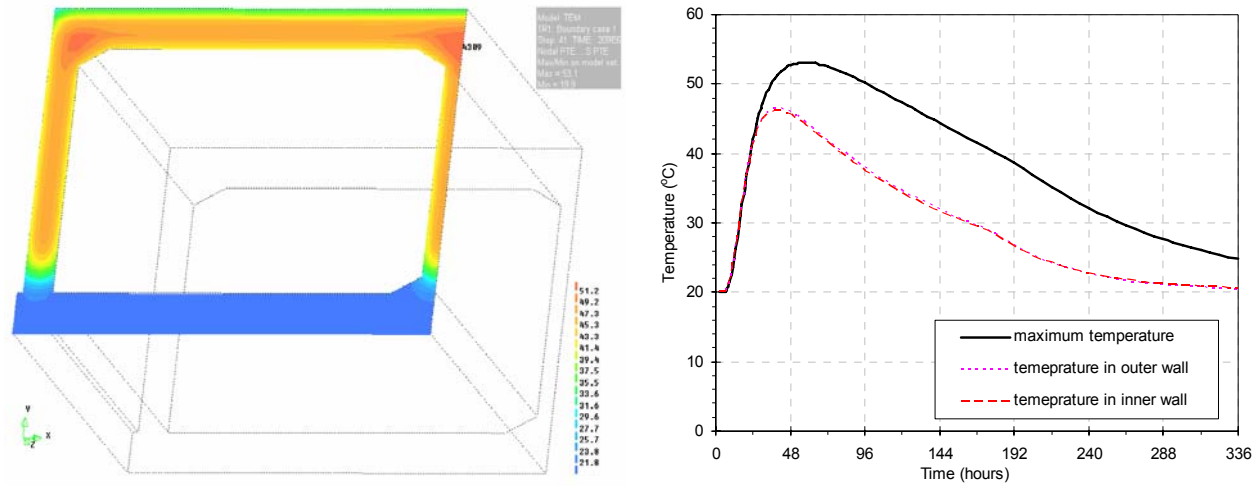

Figure 7-8 Calculated temperatures developments of 40% FA* concrete (a) Temperature contour (58h after casting), (b) Maximum temperature in the structure and temperature developments in the inner and outer wall

a) b)

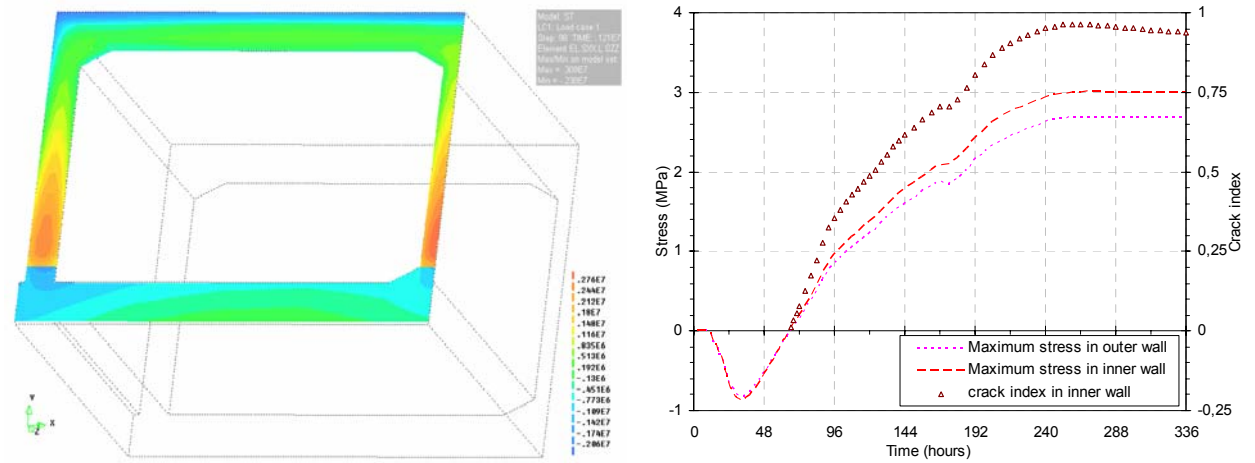

Figure 7-9 Calculated stress developments of 40% FA* concrete (a) Stress contour (336h after casting), (b) Stress developments in the inner and outer wall

a) b)

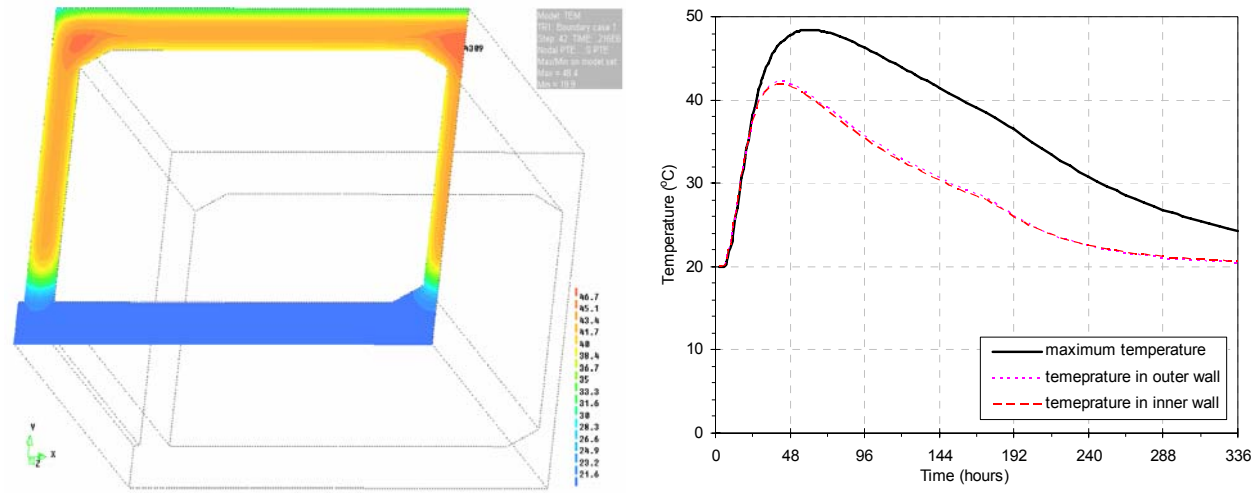

Figure 7-10 Calculated temperatures developments of 60% FA* concrete (a) Temperature contour (60h after casting), (b) Maximum temperature in the structure and temperature developments in the inner and outer wall

a) b)

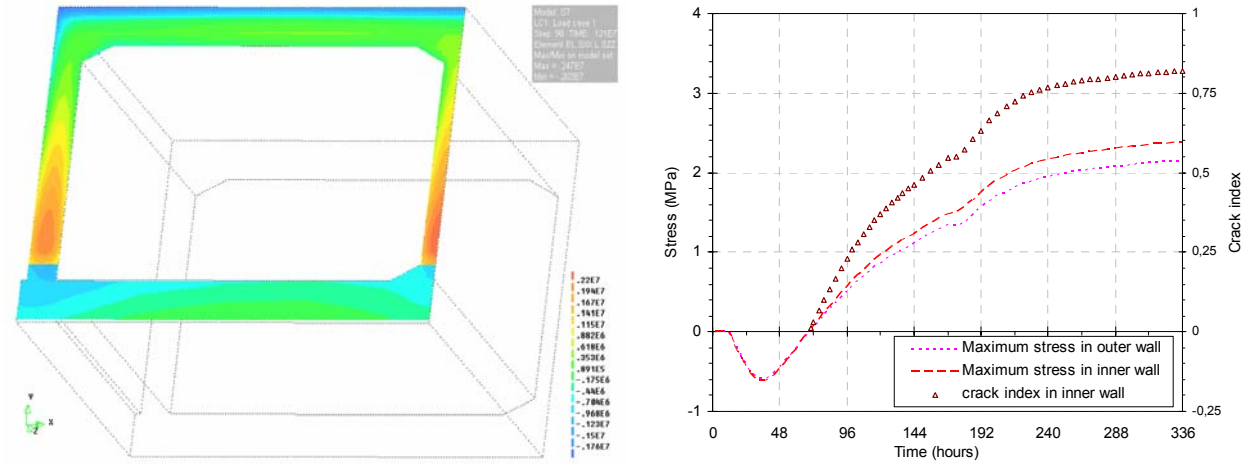

Figure 7-11 Calculated stress developments of 60% FA* concrete (a) Stress contour (336h after casting), (b) Stress developments in the inner and outer wall

a) b)

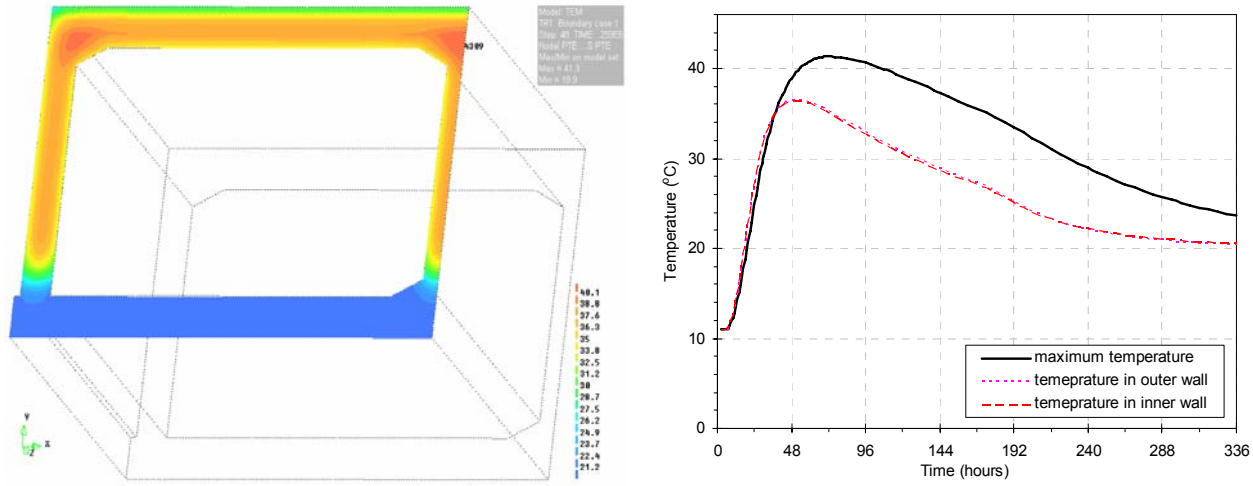

Figure 7-12 Calculated temperatures developments of 60% FA* concrete with initial temperature 11ºC (a) Temperature contour (72h after casting), (b) Maximum temperature in the structure and temperature developments in the inner and outer wall

a) b)

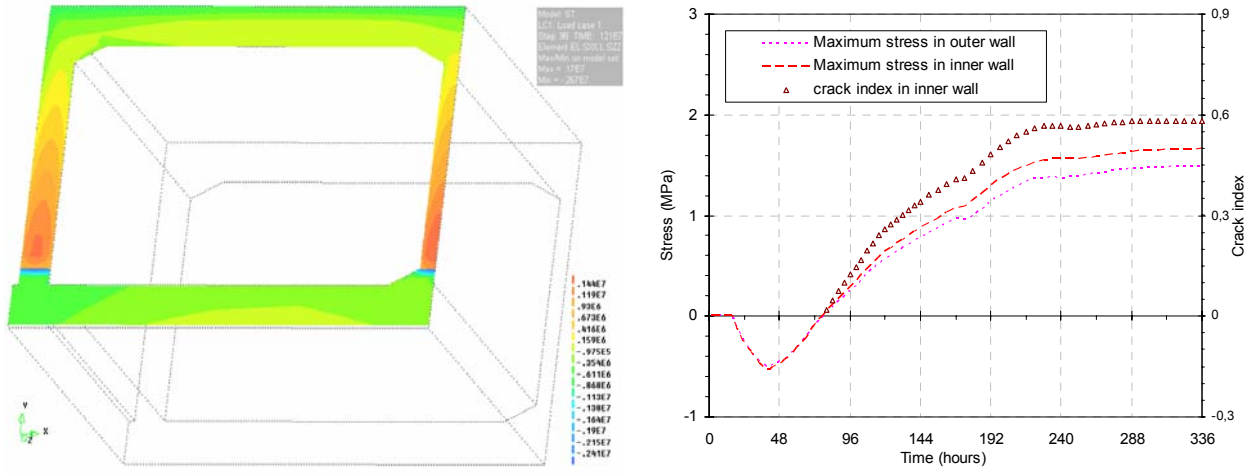

Figure 7-13 Calculated stress developments of 60% FA* concrete with initial temperature 11ºC (a) Stress contour (336h after casting), (b) Stress developments in the inner and outer wall

a) b)

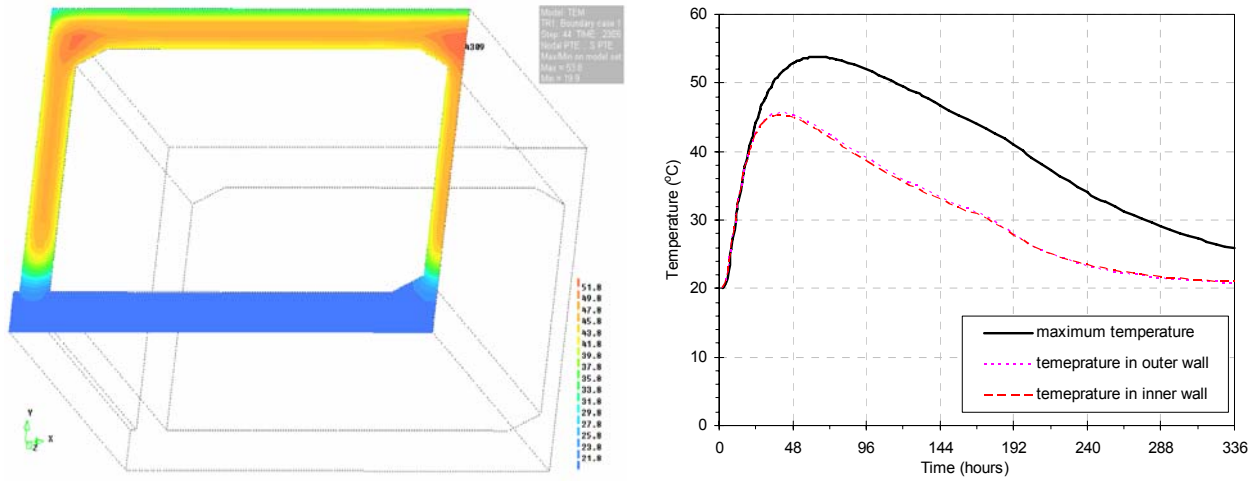

Figure 7-14 Calculated temperatures developments of 40% BFS concrete (a) Temperature contour (64h after casting), (b) Maximum temperature in structure and temperature developments in the inner and outer wall

a) b)

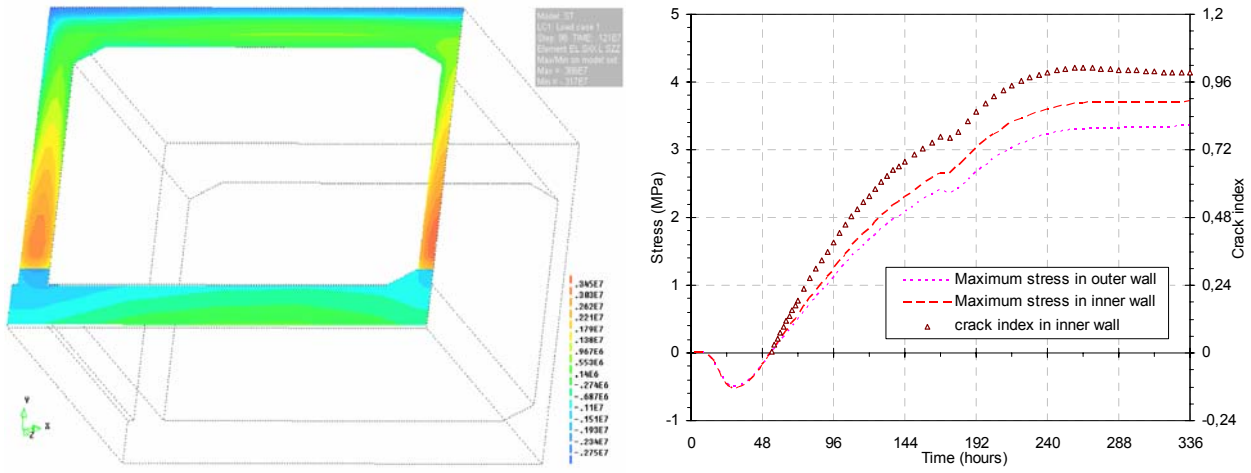

Figure 7-15 Calculated stress developments of 40% BFS concrete (a) Stress contour (336h after casting), (b) Stress developments in the inner and outer wall

a) b)

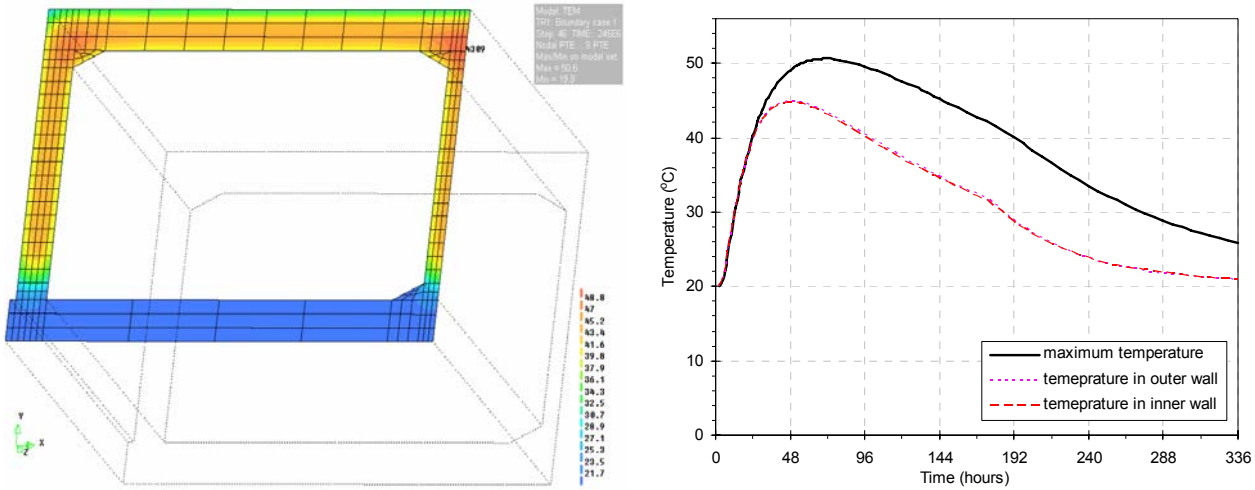

Figure 7-16 Calculated temperatures developments of 60% BFS concrete (a) Temperature contour (68h after casting), (b) Maximum temperature in the structure and temperature developments in the inner and outer wall

a) b)

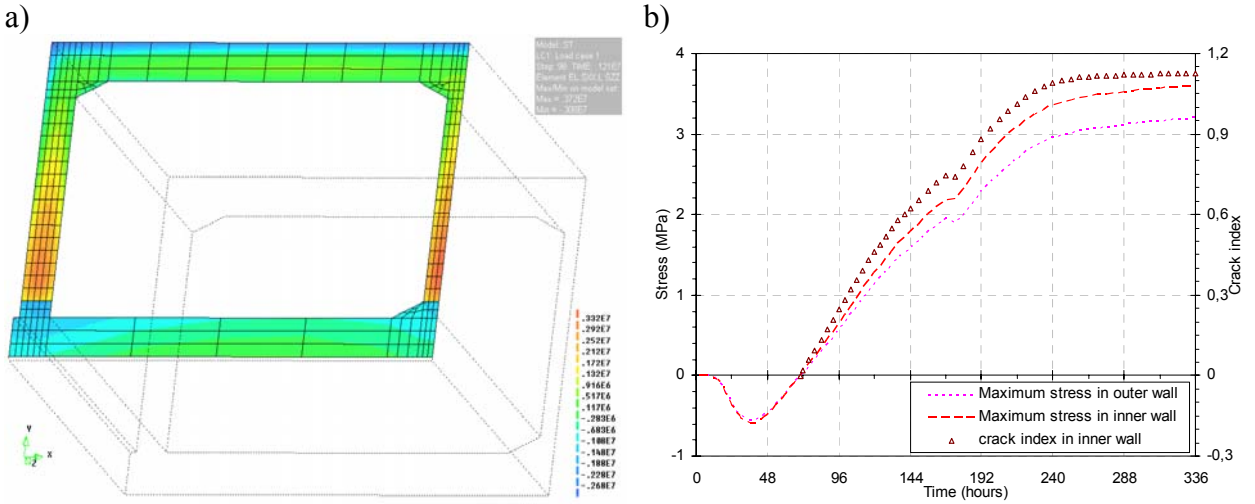

Figure 7-17 Calculated stress developments of 60% BFS concrete (a) Stress contour (336h after casting), (b) Stress developments in the inner and outer wall

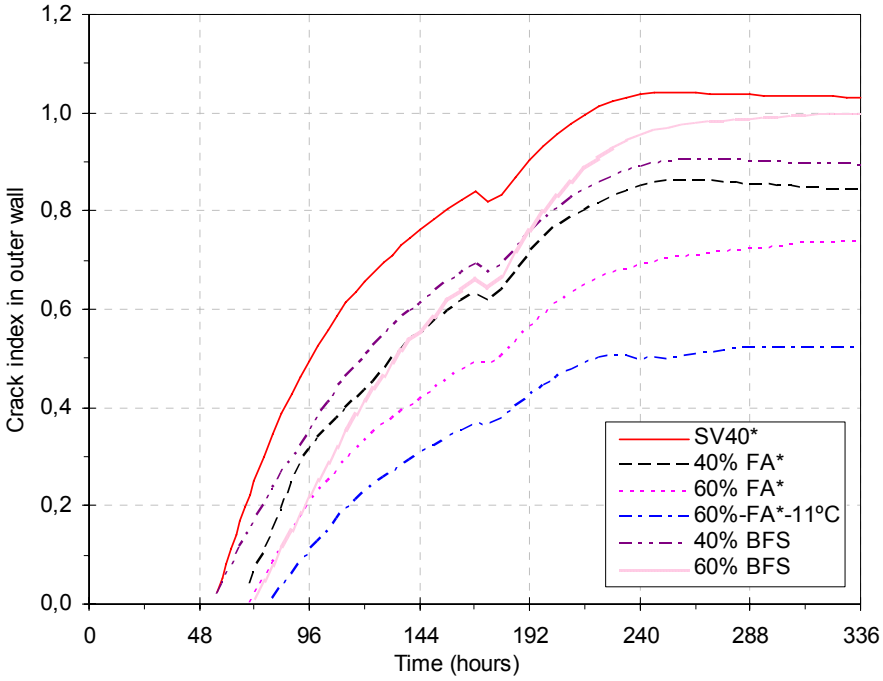

Figure 7-18 Crack index in the outer wall for the different concretes

7.4. Conclusion

The risk of through cracking (stress/strength ratio) for the Bjørvika tunnel is determined for five types of concrete mixes denoted: SV 40*, 40% FA*, 60% FA*, 40% BFS and 60% BFS concrete.

The temperature development is similar in the critical locations of the inner and outer walls, but the stresses and the risk of cracking is 12% higher in the inner walls due to larger degree of restraint. However, only the outer wall will experience water pressure, and therefore the results of outer wall are given most attention. The 60% FA* concrete has both the lowest maximum temperature (42.2 ºC) and the lowest stress/strength ratio for the outer wall (0.74).

8. Conclusions and suggestions for further work

8.1. Summary and conclusion

The following material properties are main factors which influence the sensitivity of concrete to cracking at early age, and which therefore are required for a full evaluation of cracking risk in hardening concrete structures:

- The temperature sensitivity (activation energy)
- Heat of hydration
- Coefficient of Thermal Expansion (CTE)
- Autogenous Deformation (AD)
- Mechanical properties (E-modulus, compressive strength, tensile strength)
- Creep/relaxation properties

A comprehensive experimental program was performed to investigate the influence of mineral additives such as FA and BFS on the development of all above listed material properties of young concrete.

The replacement of cement with the mineral additives such as FA and BFS significantly reduces the hydration heat. The increase of maximum adiabatic temperature in 100% BFS reduces 28% compared to that in the reference concrete, while for the 100% FA mix the corresponding reduction is 34%.

The replacement of cement with BFS does not have significant influence on the development of autogenous deformation. Except for the NL-slag concrete, a large volume of expansion appears during the first 2 days. The replacement of cement with FA have a certain influence on the development of autogenous deformation, and expansion deformation appears in the 40% and 60% FA* concrete.

The replacement of cement with FA or BFS has significant influence on the development of the compressive strength, and the 28-day compressive strength of 100% FA concrete is only 55% of that of reference concrete at 20ºC curing condition. In general, the higher the mineral additive content is the lower the compressive strength is. The replacement of cement with FA or BFS has moderate influence on the 28-days elastic modulus, but the elastic modulus development at very early age (less than 1 day) is considerably affected by the slow development of the pozzolanic reaction, and the higher the content of FA is, the lower is the elastic modulus. The development of splitting tensile strength is significantly affected by the replacement of cement with FA or BFS. The 28-day splitting tensile strength of 100% FA concrete is 3.5 MPa while the value reaches 5.5 MPa for reference concrete at 20ºC curing condition.

Although the test procedures for tensile creep and compressive creep are similar, an important point to note is that the relative importance of the compensation from the dummy specimen is very different. The comparison of the results of the compressive and tensile creep tests show that at loading ages below 4 days the magnitude and rate of compressive creep is higher than

the magnitude of tensile creep for a period of time, afterwards the rate of compressive creep decreases more rapidly than the rate of tensile creep. This leads to higher tensile creep a few days after loading. The development of compressive and tensile creep is more similar when time of loading is beyond 7 days. The amount of cement replaced with FA or BFS substantially influences the compressive and tensile creep relation as well as the creep magnitude. The results show that high creep in the concrete containing FA or BFS can accelerate the stress relaxation and therefore be beneficial in reducing the risk of cracking at early ages. This effect would then add to the more obvious and well-known positive effect of using such concrete, namely the reduced hydration heat.

Furthermore the transient thermal creep was investigated for the Basic 5 concrete. For hardened concretes, the test results showed that transient thermal creep apparently exists. Not only during heating, but also during cooling, the compliance functions increase dramatically due to temperature changes during these two periods. The calculated compliance functions are in good agreement with the measured results, the improvement of the modeling by including the transient thermal creep term is significant.

For young concrete, the compressive and tensile strength develop rapidly which has considerable influence on the transient thermal creep compliance. The test results for young concrete under compression show low increase of compliance function due to transient creep during the cooling period. As the compressive strength develops, the ratio between the applied constant stress and the compressive strength declines from 0.12 at initial loading to 0.04 at the age of 4 days for case No.172, and the calculated transient thermal creep compliance is only 4μ/MPa. The analytical model of transient thermal creep gives an acceptable prediction of the test results for the young concretes and the maturity concept is able to describe the major part of the temperature influence on the creep strain development. But it seems that it is not enough to take into account the temperature effect on the creep by only using the maturity concept when large temperature increase or decrease happens in a short period, and it gives more reliable prediction if the transient thermal creep term is added. The parameter ρ is similar in hardened and young concrete under either compressive or tensile load condition, but it is higher in compressive loading than in tensile loading.

The modeling of compressive and tensile creep (20ºC isothermal creep test) for different types of concretes shows that the curvature of the Double Power Law is more suitable to express the compressive creep data than tensile creep data. Furthermore, when comparing TSTM results with stress calculations the combined compressive and tensile creep data appears to be most promising. This is logic because the concrete specimens in TSTM develop compressive stresses during the heating phase and tensile stresses during the subsequent cooling phase. Moreover, using only the compressive DPL-parameters give better agreement with the test results than using only the tensile DPL-parameters. A reason for this may be that early tensile and compressive creep are different especially for concretes containing mineral additives, and the fact that the compressive phase in the TSTM tests (and also in field situations) last typically from setting up to 2-4 days, which means 4-10 days in maturity time. Hence, in order to determine the most relevant creep data (at 20ºC test conditions) one should perform compressive creep measurements at early loading ages (from setting to 4-10 days), and tensile creep tests at later loading ages.

Based on the measurements of the thermal and mechanical properties of young concretes containing different percentages of mineral additives, the measured stresses (the net effect of the

properties listed above) from the TSTM have been compared to stress calculations using the proposed material models for the different properties. It can be concluded that the model parameters used in the analysis make a reasonably accurate prediction of the stress development for the concretes containing different percentage of FA and BFS, but the deviation for the SV 40 concrete is high especially for the tensile stress at 3days, this is probably due to the measured low E-modulus of the SV 40 concrete. The deviation between the calculated and measured maximum stress after 12-17 days is less than 12%, and in most cases the calculations overestimate the maximum tensile stresses.

The finite element program Diana with well-documented material models is used to simulate the temperature, stress and strain development in the field test of the wall structure. The calculated temperature developments have a good agreement with the test results, and the deviation of the calculated and measured maximum temperature is in the range of ±1.5°C for both "SV 40" and "low-heat" concrete, and the maximum difference between calculated and measured temperature during the first 2 weeks is about 3°C. The calculated strains in the middle part of both walls (0.6 – 1.2 m above the slab) where the maximum stresses occur are in good agreement with the measured ones. This will ensure that the predicted crack-indexes are reliable – as verified by occurring severe cracks in SV 40 concrete and fewer cracks in the low-heat concrete. The maximum cracking index is about 0.97 for SV 40 concrete, and about 0.75 for the low-heat concrete mixture used in the field test. The "low-heat" concrete with fly ash has a lower probability to crack under the given conditions.

The finite element analysis is also applied in the design phase of the Bjørvika submerged tunnel to evaluate the crack risk for several types of concretes, and thus provide valuable input in the process of selecting concrete composition. The risk of through cracking (stress/strength ratio) for the tunnel is determined for five types of concrete mixes denoted: SV 40*, 40% FA*, 60% FA*, 40% BFS and 60% BFS concrete. The maximum temperature appears at the corner between the wall and the top slab, while the critical locations, regarding the risk of through cracking determined as the ratio between maximum tensile stress and tensile strength, are in the middle of the wall (length direction) and approximately 0.6-1.2m above the foundation slab. The temperature development is similar in the critical locations of the inner and outer walls, but the stresses and the risk of cracking is 12% higher in the inner walls due to larger degree of restraint. However, only the outer wall will experience water pressure, and therefore the results of outer wall are given most attention. It is seen that concrete with 60% FA* has both the lowest maximum temperature (42.2^{o}C / temperature rise 22.2^{o}C) and the lowest risk of cracking (0.74) in the outer wall. The temperature rise during hardening for the other concretes are 30.7^{o}C for the SV40* concrete, 26.5^{o}C for the 40%FA* concrete, 25.6^{o}C for 40%BFS concrete and 24.9^{o}C for 60%BFS concrete. Furthermore it is seen that the reduction in fresh concrete temperature from 20 to 11^{o}C results in a reduction of maximum temperature of 5.7^{o}C, while the stress/strength ratio is reduced from 0.74 to 0.52.

8.2. Recommendation for further research

In the present section some suggestions for more research and further improvement of modelling of concrete at early ages are given. They are based on the results and the limitations of the present work.

General thermal dilation and autogenous deformation model

Thermal dilation and autogenous deformation are major driving force to the stress generation in hardening concrete. However, there are no generally accepted models for thermal dilation coefficient and autogenous deformation. In the present work, the CTEs of early age concrete are directly measured by superimposing "saw-toothed" temperatures in the dilation rig test, and the parameters of the proposed CTE model are determined by the measured CTEs, and then the total deformation in the TSTM is separated into thermal dilation and autogenous deformation. Therefore it is a clear demand for more research on this topic, especially on the relationship between the change of relative humidity and the development of autogenous deformation during early age.

Coupling of shrinkage and creep in tensile creep test

As mentioned in Chapter 5, the commonly used procedure to define creep is simply to subtract the measured autogenous shrinkage of an unloaded dummy specimen from the total deformation measured on the loaded specimen, and it is assumed that the autogenous deformation and creep are two independent phenomena. In hardening concrete autogenous deformation takes place independently on the environmental conditions and can not be influenced from the exterior, so simultaneous creep and shrinkage are always present. In contrast to the compressive creep tests, the free deformations in the tensile creep tests are at least of the same order of magnitude as the load-dependent deformations. Consequently the load independent strains always have a large influence on both the magnitude and the rate of the creep development in tensile tests. More research is necessary to clarify whether this approach is valid for determination of tensile creep and to what extent the shrinkage and creep interacts with each other in the early ages.

Creep at variable temperature

Creep and its associated relaxation are very important properties in stress simulation of early age concrete. In the present work, transient thermal creep is investigated by a few experimental tests. Further creep test under different isothermal temperatures, and under other variable temperature histories, should be performed as basis for further improvement of the material modeling and understanding of the topic.

Materials development

Within the concrete industry, new materials as cement types and additives are continuously being developed. Furthermore, the requirements to the materials are also changing due to durability, aesthetics, and work environment etc. It is therefore important that the early age properties of the new concretes are being continuously investigated.

Reference

ACI Committee No. 209 (1992): Prediction of Creep, Shrinkage and Temperature Effects in Concrete Structures, Report No. ACI 209R-92.

Acker, P., Swelling, shrinkage and creep: a mechanical approach to cement hydration, Materials and Structures / Concrete Science and Engineering, Vol. 37, May 2004, pp 237-243

Acker, P., Ulm F.-J., Creep and shrinkage of concrete: physical origins and practical measurements, Nuclear engineering and design, Volume 203, Issues 2-3, January 2001, pp. 143-158

Altoubat S. A., Lange D. A., Shrinkage, and cracking of restraint concrete at early age, ACI Material Journal, V. 98, No. 4, July-August 2001

Altoubat S. A., Lange D. A., Tensile basic creep: measurements and behaviour at early age, ACI Material Journal, V. 98, No. 5, September-October 2001

Atrushi, D. S., Tensile and Compressive Creep at Early Age Concrete: Testing and Modeling, Department of Structural Engineering, the Norwegian University of Science and Technology (NTNU), Trondheim, Norway, 1999, ISBN 82-7984-002-8.

Bažant, Z. P., Mathematical modeling of creep and shrinkage of concrete, John Wiley and Sons, 1988

Bažant, Z. P., Prediction of concrete creep and shrinkage: past, present and future, Nuclear engineering and design, Volume 203, Issue 1, January 2001, Pages 27-38

Bažant, Z. P., Chern, J.C. (1985a), Concrete Creep at variable humidity, Journal of Engineering Mechanics, 18(103).

Bažant, Z. P., Chern, J.C. (1985b): Concrete creep at variable humidity: constitutive law and mechanism, Materials and Structures (RILEM), Vol.18.

Bažant, Z. P., Cusatis, G., and Cedolin, L., Temperature Effect on Concrete Creep Modeled by Microprestress-Solidification Theory, Journal of Engineering Mechanics, Vol.130, No.6, pp. 691-699, June, 2004

Bažant, Z. P., Hauggaard, A. B., Baweja, S., and Ulm F.-J., Microprestress-Solidification Theory for Concrete Creep. I: Aging and Drying Effects, Journal of Engineering Mechanics, Vol.123, No.11, November, 1997

Bažant, Z. P., Hauggaard, A. B., and Baweja, S., Microprestress-Solidification Theory for Concrete Creep. II: Algorithm and Verification, Journal of Engineering Mechanics, Vol.123, No.11, November, 1997

Bažant, Z. P., Kim J.-K., Panula L., Improved prediction model for time-dependent deformation of concrete: Part 1-shrinkage, Material and structures, 1991, 24, pp 327-345

Bažant, Z. P., Kim J.-K., Improved prediction model for time-dependent deformation of concrete: Part 2-Basic creep, Material and structures, 1991, 24, pp 409-421

Bažant, Z. P., Kim J.-K., Improved prediction model for time-dependent deformation of concrete: Part 3-Creep at drying, Material and structures, 1992, 21-28

Bažant, Z. P., Kim J.-K., Improved prediction model for time-dependent deformation of concrete: Part 4-Temperature effects, Material and structures, 1992, 84-94

Bažant, Z. P., Panula, L. (1978a): Simplified Prediction of Concrete Creep and Shrinkage From Strength and Mix, Structural Engineering Report, No. 78-10/6403, Department of Civil Engineering, Technological Institute, Northwestern University, Illinios, pp. 24

Bažant, Z. P., Panula, L. (1978b): Practical prediction of time dependent deformations of concrete, Materials and Structures, Part I and II: Vol. 11, No. 65, pp. 307-328

Bažant, Z. P., Panula L., Kim J.-K., Xi Y. P., Improved prediction model for time-dependent deformation of concrete: Part 6-Simplified code-type formulation, Material and structures, 1992, 219-223

Bažant, Z. P. and Wittman, F.H., Creep and Shrinkage in Concrete Structures, Wiley & Sons, New York, 1982

Bentz, D.P., Three-dimensional computer simulation of cement hydration and microstructure development, Journal of the American Ceramic Society, volume 80, Issue 1, 1997, pp. 3–21

Bernander, S., and Emborg, M., Risk of Cracking in Massiv Concrete Structures - New Development and Experiences, 'Thermal Cracking in Concrete at Early Ages', Proc. of the RILEM International Symposium, Edited by R. Springenschmid, E & FN Spon, London, 1994, pp. 385-392

Bissonnette B., Pigeon M., Tensile creep at early ages of ordinary, silica fume and fiber reinforced concretes, Cement concrete research, Vol. 25, No. 5, pp 1075-1085, 1995

Bjøntegaard, Ø., Thermal Dilation and Autogenous Deformation as Driving force to Self-Induced Stresses in High Performance Concrete, Doctor Thesis, Department of Structural Engineering, NTNU, Trondheim, Norway, 1999, ISBN 82-7984-002-8

Bjøntegaard Ø., Hammer T. A. and Sellevold E. J., On the measurement of free deformation of early age cement paste and concrete, Cement and Concrete Compositions, Volume 26, Issue 5, July 2004, Pages 427-435

Bjøntegaard, Ø., Kanstad T., Sellevold E. J., and Hammer A., Stress-inducing deformations and mechanical properties of high performance concrete at very early ages, Proc. of the 5th

International Symposium on Utilization of High-strength/High-performance concrete, Sandefjord, Norway, 1999

Bjøntegaard Øyvind, Kjell Tore Fosså, Dawood Atrushi, Erik J. Sellevold, Terje Kanstad, Tor Arne Hammer and Sverre Smeplass, Stress development and cracking tendency in hardening concrete: Test methods at NTNU, NOR-CRACK-report 2.1, Subtask 2 – Fundamental studies, 2003

Bjøntegaard Ø. and Sellevold E.J., Autogenous and thermal deformations, 'State-of-the-Art report: RILEM report 25 Early Age Cracking in Cementitious Systems', Editor: A. Bentur, RILEM Publications, Sarl, 2003, ISBN 2-912143-33-0

Bjøntegaard, Ø. and Sellevold E. J., Interaction between thermal dilation and autogenous deformation in high performance concrete, Materials and structures, Vol. 34, June 2001

Bjøntegaard Ø, Sellevold EJ, Thermal and Autogenous Deformation, IPACS-report, TU Luleå, Sweden, 2001, ISBN 91-89580-20-6

Bjøntegaard Ø., Sellevold E.J., Kanstad T., Deformation properties and crack sensitivity in young concrete: Experience and guidelines from a 4-year Norwegian R&D project, Proc. of the XIX Nordic Concrete Research Meeting, Sandefjord, Norway, 2005

Bosnjak, D., Self-Induced Cracking Problems in Hardening Concrete Structure, Doctor Thesis, Department of Structural Engineering, NTNU, Trondheim, Norway, 2001, ISBN 82-7984-151-2.

Brooks, J. J., Cabrera, J. G. and Johari, M. M., Factors affecting the autogenous shrinkage of silica fume high strength concrete, Proc. Autogenous Shrinkage of Concrete JCI (E. Tazawa, ed.), Hiroshima, 1998, pp 195–202

CEB-FIB (1990): High Strength Concrete - State-of-the-Art report, CEB Bulletin D'information No. 197, 61 pp

Cervera M., Faria R., Olover J., Prato T., Numerical Modeling of Concrete Curing, Regarding Hydration and Temperature Phenomena, Computers and Structure 80, 2002

Charron J.P., Zuber B., Marchand J., Bissonnette B., Pigeon M., Influence of temperature on the early–age behavior of concrete, International RILEM Symposium on Concrete Science and Engineering: A Tribute to Arnon Bentur, 2004

Claus K. L., Ji G.M., Crack risk modelling of restrained walls – is it possible? -a comparison between measured and computer modelled strains, Nordic Seminar, Trondheim, 2005

Dilgner W.H., Wang C. and Niitani K., Experimental study on shrinkage and creep of High performance concrete, the 4th int. Symposium on 'Utilization of High Strength/High Performance Concrete', May, Paris(1996), pp 311-319

Emborg, M., Development of mechanical behaviour at early ages, in 'Prevention of Thermal Cracking in Concrete at Early Ages', R. Springenschmid, editor, E&FN SPON, 1998, pp. 77-148

Emborg, M., Models and Methods for Computation of Thermal Stresses, in 'Prevention of Thermal Cracking in Concrete at Early Ages', RILEM Report 15, R. Springenschmid, ed., E&FN Spon, London, UK, 1998, pp. 179-230

Emborg, M., Thermal stresses in concrete structures at early ages, Doctoral thesis, Luleå University of Technology, 1989

Giesecke, J., Qin, M. H., Marx W., Realistic and Computational Efficient Evaluation of Temperature and Stress Development in Large RCC Dams, German Dam Research and Technology, Number 4, 2002, p 29

Gutsch, A., Influence of elevated temperature on creep and relaxation of early age concrete, IPACS report, 2000

Gutsch A., Properties of early age concrete – Experiments and modelling, Material and structures, Vol. 35, March 2002, pp 76-79

Gutsch, A., Properties of Early Age Concrete - Experiments and Modelling. RILIM International Conference on 'Early Age Cracking in Cementitious Systems' (EAC'01), Haifa, 2001, pp. 11-18

Gutsch, A and Rostasy, F.S., Mechanical models of the stress-strain behaviour of young concrete in axial tension and compression, IPACS report, 2000

Gutsch, A., and Rostasy, F. S., Young Concrete Under High Tensile Stresses-Creep, Relaxation and Cracking, 'Thermal Cracking In Concrete at Early Age', Proceedings of the International RILEM Symposium, R. Springenschmid, ed., Munich, Germany, 1994, pp. 111-118

Hagihara S., Nakamura S., Masuda Y., Uenishi T., Okihashi T., and Kono M., Mechanical properties and creep behavior of high-strength concrete in early age, Proceedings of the international workshop, Sendai, Japan, 2000

Hammer TA, Bjøntegaard Ø, Sellevold EJ. Measurement methods for testing of early age autogenous strain. In: Kovler K, Bentur A, editors. Proceedings of the RILEM Int. Conf.: Early Age Cracking in Cementitious Systems, Haifa, Israel, March 12–14, 2001, pp. 217–228

Hauggaard-Nielsen, A. B., Mathematical modeling and experimental analysis of early age concrete, Department of structural engineering and materials, technical university of Denmark, series R, No. 35, 1997

Hauggaard, A. B., Damkilde, L., and Freiesleben Hansen, P., Transitional Thermal Creep of Early Age Concrete, Journal of Engineering Mechanics, Vol.125, No.4, April, 1999

Hauggaard, A. B., Damkilde, L., and Freiesleben Hansen, P., Hougaard Hansen, J., Nielsen, A., and Christensen, S.L., HETEK, Control of early age cracking in concrete, phase 3: Creep in concrete, Department of Structural Engineering and Materials, Technical University of Demark, 1997

Hauggaard, A. B., Damkilde, L., and Freiesleben Hansen, P., Pedersen, E. S., and Nielsen, A., HETEK, Control of early age cracking in concrete, phase 4 and 5: Material modeling, Continuum approach, Department of Structural Engineering and Materials, Technical University of Demark, 1997

Hedlund H., Hardening Concrete – measurement and evaluation of non-elastic deformation and associated restraint stresses, Ph.D. thesis, Division of structural engineering, Luleå University of technology, Sweden, 2000

Igarashi S., Kawamura M., Efects of microstructure on restrained autogenous shrinkage behaviour in high strength concrete at early ages, Materials and structures, VOL. 35, March 2002, pp 80-84

Igarashi S., Bentur A., Kovler K., Autogenous shrinkage and induced restraining stresses in high-strength concretes, Cement and concrete research 30, 2000

Ji G.M., Bjøntegaard Ø., Kanstad T, Finite element analysis and material modelling of hardening concrete, Proc. of the XIX Nordic Concrete Research Meeting, Sandefjord, Norway, 2005

Ji G.M., Bjøntegaard Ø., Atrushi D., Kanstad T., and Sellevold E. J., Compressive and tensile creep of young concrete with mineral additives, Creep, shrinkage and durability mechanics of concrete and other quasi-brittle materials, Proc. of the seventh international conference, Nantes, France, 2005

Ji G.M., Kanstad T., Bjøntegaard Ø., Analysis of the SVV Double Wall Field Test Related to the Bjørvika Tunnel Project, Report nr. R-7-04, NTNU, Trondheim, Norway, 2004

Kanstad T., Ji G.M., Bjørvika Submerged Concrete Tunnel, Phase 2: Evaluation of the Risk of Cracking in the Hardening Phase, Report nr. R-6-04, NTNU, Trondheim, Norway, 2004

Kanstad T., Bjøntegaard, Ø., Sellevold, E.J., Hammer, T.A. and Fidjestøl, P., Effect of silica fume on early age crack sensitivity of high performance concrete,Concrete International, The Magazine of the American Concrete Institute 23 (12), 2001, pp 53-59

Kanstad, T., Hammer, T.A., Bjøntegård, Ø. and Sellevold, E.J., Mechanical properties of young concrete: Evaluation of test methods for tensile strength and modulus of elasticity. Determination of model parameters, SINTEF-report no. STF22 A99762, Trondheim, 1999

Kanstad, T, Hammer, T.A., Bjøntegaard, Ø., Sellevold, E.J., Mechanical properties of young concrete: Part 1:Experimental results related to test method and temperature effects, Materials and Structures, Volume 36, Number 4, May, 2003, pp 218-225

Kanstad, T, Hammer, T.A., Bjøntegaard, Ø., Sellevold, E.J., Mechanical properties of young concrete: Part 2:Determination of model parameters and test program proposals, Materials and Structures, Volume 36, Number 4, May, 2003, pp 226-230

Krauß, M.; Rostásy, F.S.; Gutsch, A.: Modeling of Degree of Hydration on Basis of Adiabatic Heat Release. IPACS, Luleå University of Technology, Sweden, August 2000

Lokhorst, S.J., and Van Breugel, K., Experimental and numerical analysis of stress development in hardening concrete, Progress in Concrete Research, Delft University of Technology, Faculty of Civil Engineering, Vol. 4, 1995

Lokhorst S.J., van Breugel K., Simulation of the effect of geometrical changes of the microstructure on the deformational behaviour of hardening concrete, Cement and concrete research, VOL. 27, No. 10., pp. 1465-1479, 1997

Loukili A.,Khelidj A., Richard P., Hydration kinetics, change of relative humidity, and autogenous shrinkage of ultra-high-strength concrete, Cement and Concrete Research 29, 1999

Lura, p., van Breugel, K., and Maruyama, I., Autogenous and drying shrinkage of high strength lightweight aggregate concrete at early ages – the effect of specimen size, in PRO23, Early age cracking in cementitious systems – EAC01, Proceedings of the International RILEM Conference, 2002, pp 335-342

Lura P., van Breugel K., Maruyama I., Effect of curing temperature and type of cement on early-age ahrinkage of high-performance concrete, Cement and concrete research 31, 2001

Metha, P.k. and Monteriro, P.G.M., concrete: structure, properties, and methods, 2nd ed., New Jersey, Prentice Hall, ISBN: 0 13 175621 4, 1993

Mihashi, H. and B. Leite, J. P. de, State-of-the-Art Report on Control of Cracking in Early Age Concrete, Journal of Advanced Concrete Technology, Vol.2, No. 2, pp. 141-154, June 2004

Morimoto H. and Koyanagi W., Estimation of stress relaxation in concrete at early ages, in *Thermal cracking in concrete at early ages*, Proc. of the International RILEM Symposium, Munich, October, 1994

Neville, A.M., Properties of concrete, Longman Group Limited, Harlow Essex England and John Wiley & Sons, New York

Neville, A. M., Dilger, W. H., and Brooks, J.J., Creep of plain and structural concrete, Construction Press, 1983

Olofsson, J., Uhlán M., Round Ronbin Simulation – Ground Slab Examples, Skanska Teknik AB, Sweden 2000, ISBN 91-89580-54-0

Pane, I., and Hansen, W., Early age creep and stress relaxation of concrete containing blended cement, Materials and Structures, Volume 35, Number 2, 2002

Rostasy F.S., Laube M., Experimental and analytical planning tools to minimize thermal cracking of young concrete, RILEM Int. Workshop: "Testing during concrete construction", 1990

Rostasy F.S., Krauss, M. and Gutsch, A., Computation of stresses and cracking criteria for early age concrete – methods of IBMB, IPACS report, 2000

Schachinger I., Schmidt K., Heinz D., Schieβl P., Early-age cracking risk and relaxation by restrained autogenous deformation of ultra high performance concrete, Proc. of the 6th International Symposium on Utilization of High-strength/High-performance concrete, Leipzig, June, 2002, p 1341-1354.

Schieβl P., Plannerer M., Brandes Chr., Influence of binders and admixtures on autogenous shrinkage of high performance concrete, International RILEM workshop on shrinkage of concrete, 2000

Schrage, I., and Summer, T., Factors Influencing Early Cracking of high-strength Concrete, 'Thermal Cracking in Concrete at Early Ages', R. Springenschmid, ed., E&FN Spon, London, UK, 1994, pp. 237-244

Schutter G. D., Apllicability of degree of hydration and maturity method for thermo-viso-elastic behavior of early age concrete, Cement & Concrete Composites, Vol. 26, Issue 5, July 2004, pp. 437-443

Schutter G. D., Fundamental study of early age concrete behaviour as a basis for durable concrete structures, Materials and structures, Vol. 35, Jan-Feb 2002, pp 15-21

Schutter G. D., Hydration and temperature development of concrete made with blast-furnace slag cement, Cement and concrete research, Volume 29, Issue 1, January 1999, Pages 143-149

Schutter G. D., Taerwe, L, Degree of hydration-based description of mechanical properties of early age concrete, Materials and structures, Vol. 29, 1996

Schutter G. D., Taerwe, L., Fictitious degree of hydration method for the basic creep of early age concrete, Materials and structures, Vol. 33, July 2000, pp 370-380

Sellevold EJ, Bjøntegaard Ø, Thermal expansion coefficient (CTE) of cement paste and concrete: Effect of Moisture Content. In: Lange D, Scrivener KL, Marchand J (Eds) Advances in cement and concrete IX: volume changes, cracking, and durability, ECI, USA, Copper Mountain, Colorado, 2003, pp 27–37

Song H.W., Cho H.J., Park S.S., Byun K.J., Maekawa K., Early-age cracking resistance evalution of concrete structures, Concrete Science and Engineering 3 (2001), pp. 62–72

Springenschmidt, R., Breitenbucher, R., and Mangold, M., "Development of the Cracking Frame and Temperature Stress Testing Machine," Thermal Cracking in Concrete At Early-Age, Ed. R. Springenschmid, EF Spon London 1994, pp. 137-44

Springenschmidt, R., Gierlinger, E., and Kernozycki, W., (1985) "Thermal Stress in Mass Concrete: A New Testing Method and the Influence of Different Cements", Proceedings of the 15th International Congress For Large Dams, Lausanne, R4,
pp. 57-72

Tazawa E. I. and Miyazawa S., Experimental study on mechanism of autogenous shrinkage of concrete. Cement and Concrete Research, Vol. 25, No.8, 1995, pp. 1633-1638

Tazawa E. I. and Miyazawa S., Influence of constituents and composition on autogenous shrinkage of cementitious materials, Magazine of concrete research, 1997

Thelandersson, S., Modelling of combined thermal and mechanical action in concrete, Journal of Engineering Mechanics, Vol. 113, Issue 6, 1987

Toma G., Pigeon M., Marchand J., Bissonnette B. and Bercelo L., Early-age autogenous restrained shrinkage: stress build up and relaxation. Persson B. and Fagerlund G., Editors, 'Self-Desiccation and Its Importance in Concrete Technology', Lund University, ISBN 91-630-8230-6, 1999, pp. 61–72

Thomas M.D.A., Mukherjee P.K., The effect of slag on thermal cracking in concrete, Thermal cracking in concrete at early ages, ISBN: 0 419 18710 3, 1994

Tomaszwicz, A., High Strength Concrete Subjected to Long-Term, Sustained Loads, SINTEF Report 1.4, Norway, 1988

Ulm F.-J., Couplings in early age concrete: from material modeling to structural design, Int. J. Solid Structures, Vol. 35., Nos 31-32, pp. 4295-4311, 1998

Ulm F.-J., Coussy O., Modeling of thermal chemo mechanical coupling of concrete at early ages, Journal of engineering mechanics, July 1995, pp. 785-794

Ulm F.-J., Coussy O.,Strength growth as chemo-plastic hardening in early age concrete, Journal of engineering mechanics, December 1996, pp. 1123-1132

Ulm F.-J., Coussy O., What is a "massive" concrete structure at early ages? Some dimensional arguments, Journal of engineering mechanics, May 2001, pp.512-522

Umehara H., Uehara T., Iisaka, T., and Sugiyama A., Effect of creep in concrete at early ages on thermal stress, in *Thermal cracking in concrete at early ages*, Proc. of the International RILEM Symposium, Munich, October, 1994

Van Breugel, K., "Simulation of Hydration and Formation of Structure in Hardening Cement-Based Materials," Ph. D. Thesis, Delft University of Technology, Delft, The Netherlands, pp. 228, 1991

Van Breugel, K., Numerical simulation of hydration and microstructural development in hardening cement-based materials, Heron, 37

Waller V., d'Aloia L., Cussigh F., Lecrux S., Using the maturity in concrete cracking control at early age, Cement & Concrete Composites, Vol. 26, Issue 5, July 2004, Pages 589-599

Westman G., Basic creep and relaxation of young concrete. In: R. Springenschmidt, Editor, *Thermal Cracking in Concrete at Early Ages, Proceedings of the International RILEM Symposium*, E&FN Spon, London, 1995, pp. 87–94.

Westman G., Creep and relaxation of high performance young concrete, Proc. of the 4th International Symposium on Utilization of High-strength/High-performance concrete, Paris, 1996

Østergaard L., Lange D. A., Altoubat S. A., and Stang H., Tensile basic creep of early –age concrete under constant load, Cement and concrete research 31, 2001

Appendix A: Test results of hydration heat and the mechanical properties

Semi-adiabatic temperature and hydration heat

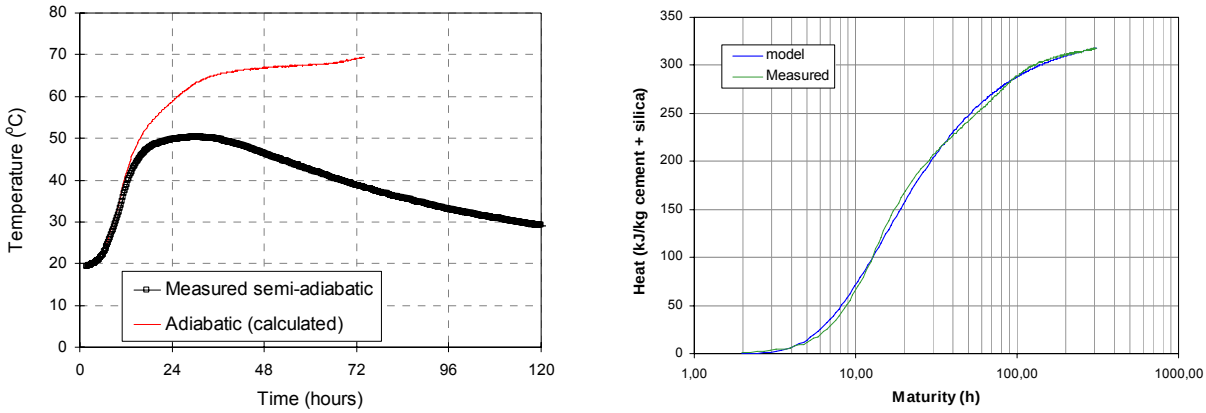

Figure A.1 Adiabatic temperature and hydration heat of Reference concrete

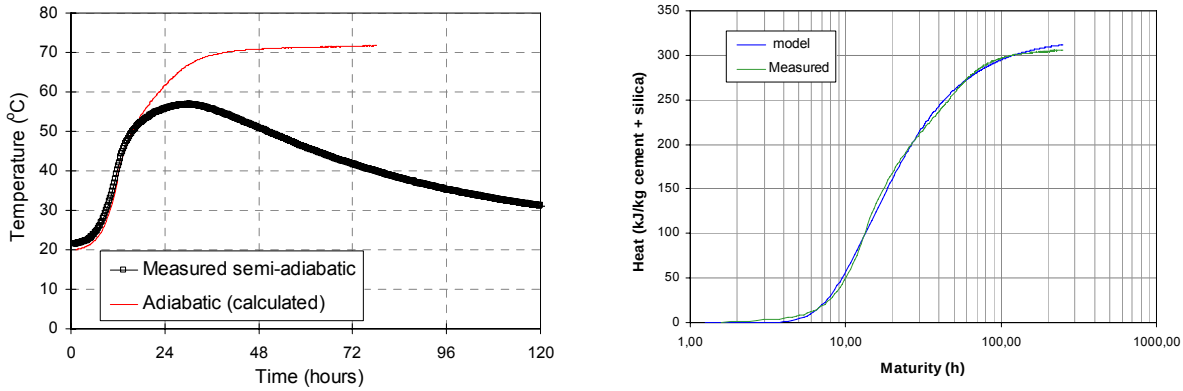

Figure A.2 Adiabatic temperature and hydration heat of "SV 40*" concrete

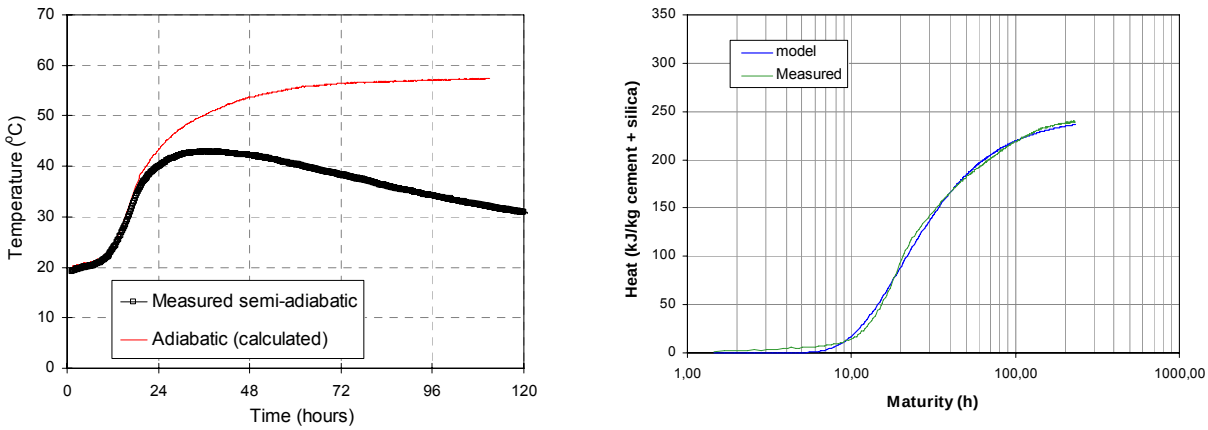

Figure A.3 Adiabatic temperature and hydration heat of 40% FA* concrete

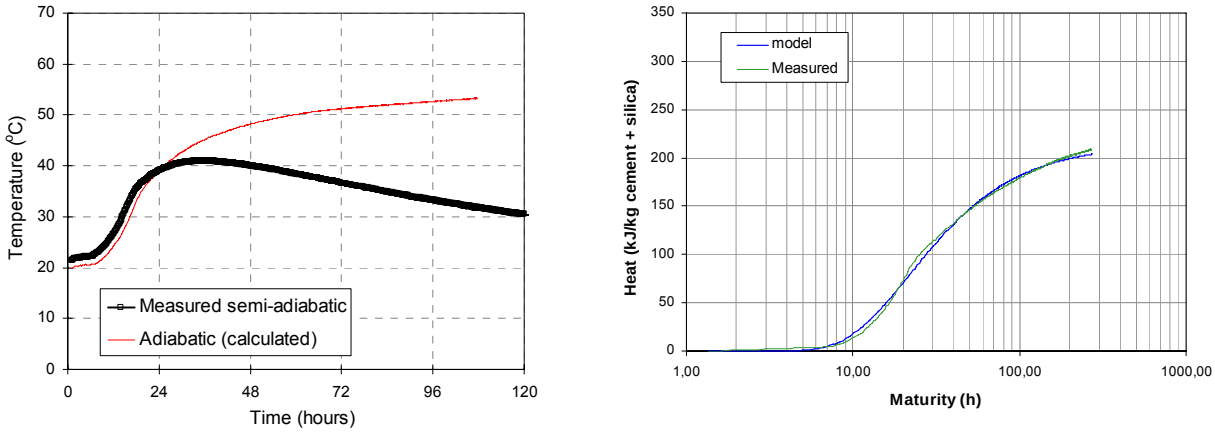

Figure A.4 Adiabatic temperature and hydration heat of 60% FA* concrete with initial temperature 20 ºC

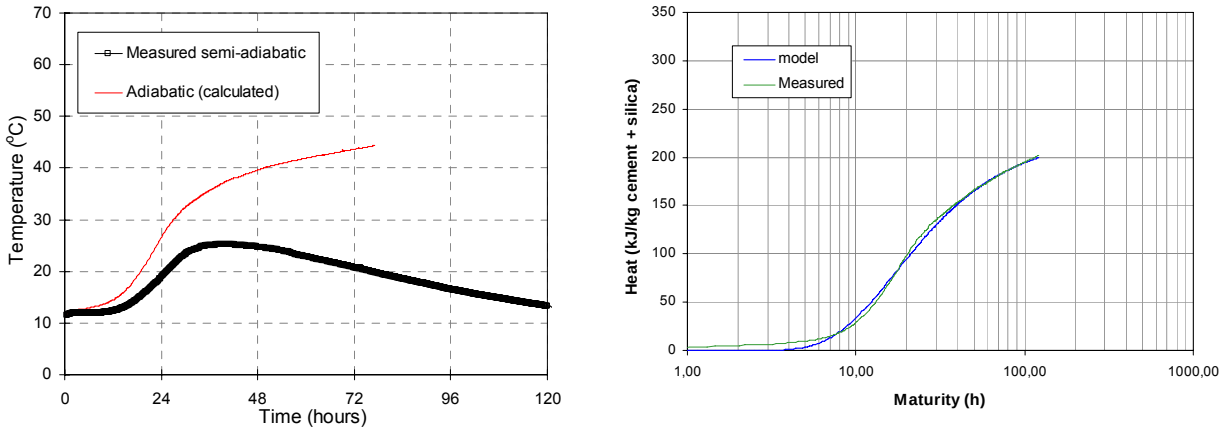

Figure A.5 Adiabatic temperature and hydration heat of 60% FA* concrete with initial temperature 11 ºC

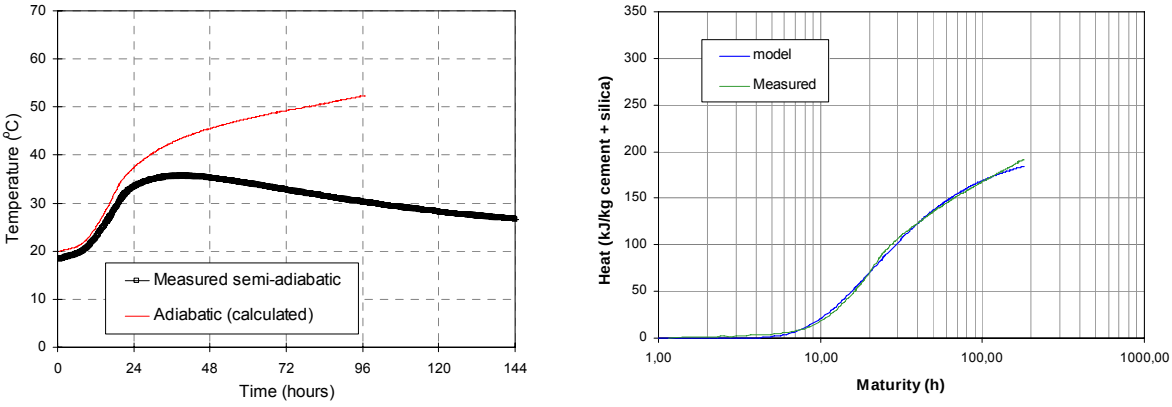

Figure A.6 Adiabatic temperature and hydration heat of 100% FA concrete

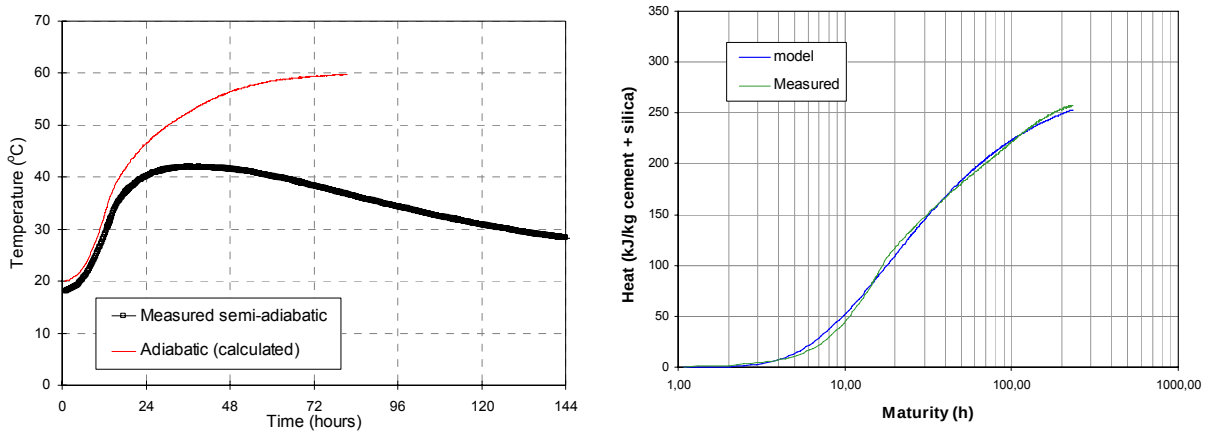

Figure A.7 Adiabatic temperature and hydration heat of 40% BFS concrete

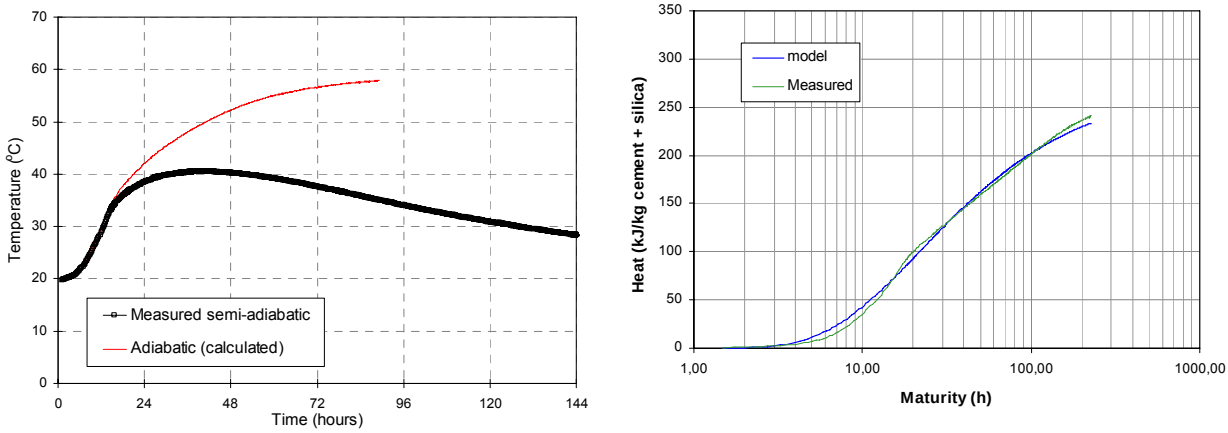

Figure A.8 Adiabatic temperature and hydration heat of 60% BFS concrete

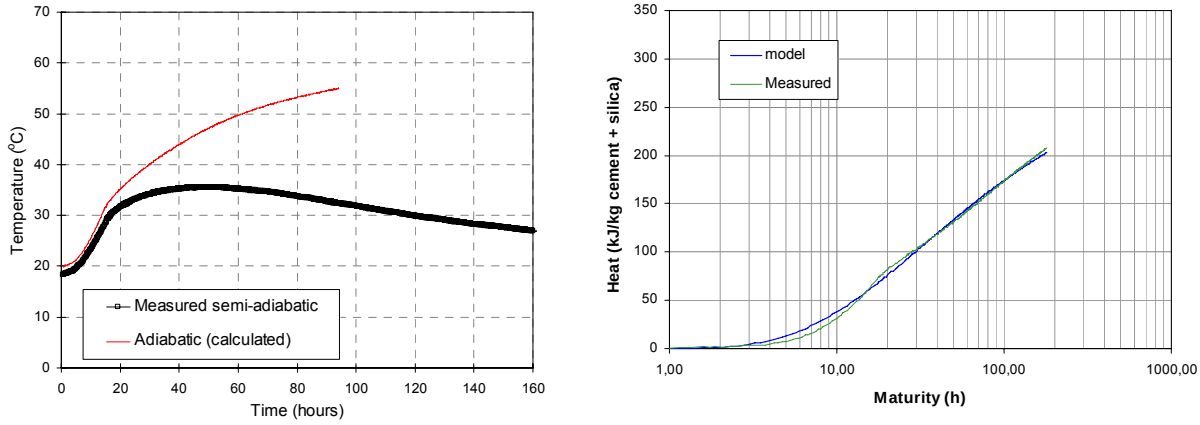

Figure A.9 Adiabatic temperature and hydration heat of 100% BFS concrete

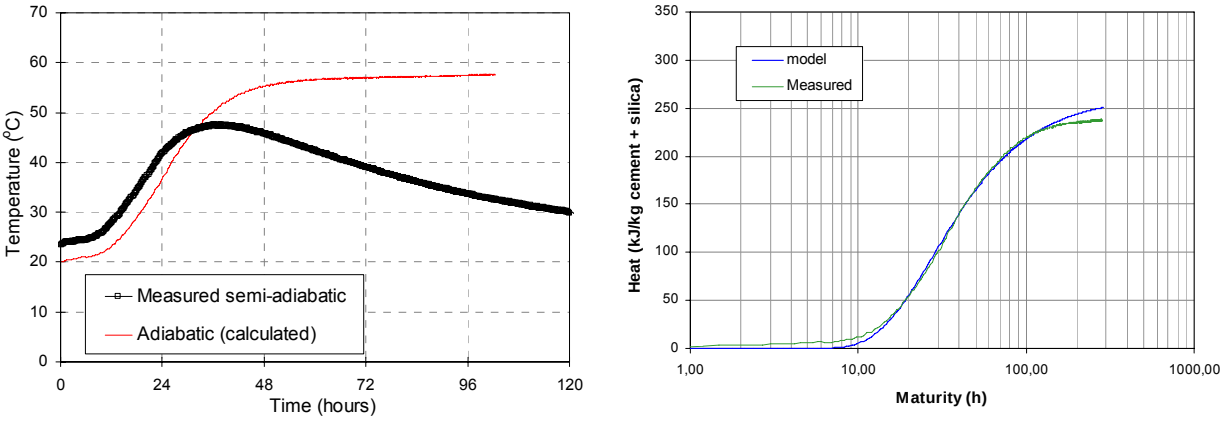

Figure A.10 Adiabatic temperature and hydration heat of NL slag concrete

Table A.1 Parameters for thermal properties

Concrete	Heat production $Q(t_{eq}) = Q_\infty \cdot \exp\left[-\left(\frac{\tau}{t_{eq}}\right)^{\alpha}\right]$				Parameters of activition energy		Thermal condutivity	Specific heat
	binder	Q_∞	τ	α	A	B	KJ/msºC	J/kgºc
Ref-0,45 (SVV)	378	336	14,00	1,03	33500**	1400**	0,0022**	1,04**
Ref-0,45 (NTNU)	378	310	16,34	1,10				
40% BFS (SVV)	382	313	17,04	0,81				
40% BFS (NTNU)	382	286	18,95	0,84				
60% BFS (SVV)	384	316	20,49	0,72				
60% BFS (NTNU)	384	274	21,97	0,78				
100%BFS (SVV)	386	322	33,98	0,58				
100%BFS (NTNU)	386	292	33,05	0,60				
40% FA (SVV)	382	281	16,84	0,97				
40% FA (NTNU)	382	251	17,07	1,11				
60% FA (SVV-a,b)	384	248	17,35	1,02				
60% FA (NTNU)	384	215	17,75	1,20				
100% FA (SVV)	386	215	23,52	0,86				
100% FA (NTNU)	386	202	21,12	1,1				
40% FA* (SVV)					26574	1030		
40% FA* (NTNU)	382	244	20,12	1,39				1,07
60% FA* (SVV)					36192	1136		
60% FA* (NTNU)	384	215	21,86	1,17				1,07
60% FA* (NTNU-initial temperature 10ºC)	382	222	17,34	1,15				1,07
SV40* (SVV)					21996	2699		
SV40* (NTNU)	424	319	15,04	1,34				1,06
NL slag* (SVV)					33648	2680		
NL slag* (NTNU)	389	263	28,01	1,32				1,06

* Second series

** The default value used in the analysis if the test data are not avaiable

Mechanical properties: Compressive strength, E-modulus and tensile strength

Table A.2 Compressive strength (Norwegian Public Road Administration (SVV))

concrete	fc (MPa)(20ºC)								fc (MPa) (Semi)
	1day	2day	3day	7day	14day	21day	28day	90day	28 day
SV40	30.2		52.4	61,6			80.9	90.7	
SV40*	17.44	33.03		47.79(6d)	57.06(15d)		67.15		61.91
Reference	22.3		42.7	54.4			76.2	87.3	
40% FA	13.3		29.5	39.5			64.4	78.5	
40% FA*	7.48(0.8d)	16.14(1.9d)		33.58	44.8(14.9d)	51.7	55.75		
60% FA (a)	11.7		27.5(4d)	33.9			55.9	71.9	
60% FA (b)	9.7		27.0(4d)	34.7			57.6	74.0	
60% FA*	8.86(1.3d)	13.3	17.39	23.74(6d)	34.64		46.96		
100% FA	5.1		14.9	22.0			41.9	58.6	
40% BFS	14.3		30.7	42.6			70.1	83.2	
60% BFS	12.3		25.8	35.8			62.0	80.1	
100% BFS	7.2		16.4	26.9			52.1	68.0	
NL slagcement*	8.0(1.4d)	12.35	18.1	32.2	44.3		53.45		

Note: *- Test data for second series including four types of concretes
(6d)- The value in the parentheses is the age at test
20ºC – Test performed at isothermal 20ºC temperature
Semi – Test performed at semi-adiabatic temperature history

Table A.3 Compressive strength (NTNU)

concrete	fc (MPa) (20ºC)				fc (MPa) (Semi)
	2day	7day	14day	28day	28 day
SV40*				64.1(24d)	64.5(24d)
Reference	29.2	44.5	53.3	66.3	63.9
40% FA	20.2	36.7	41.9	57.4	64.5
40% FA*				47.5(29d)	53.8(29d)
60% FA					
60% FA*				41.5(29d)	46.5(29d)
100% FA	9.6	19.4	26.2	36.9(33d)	43.6(33d)
40% BFS	19.3	36.5	47.4	54.4	60.6
60% BFS	16.1	31.8	44.0	53.4	63.0
100% BFS	9.9	23.7	33.5	39.3	50.9
NL slagcement*				47.4	51.1

Note: *- Test data for second series including four types of concretes
(24d)- The value in the parentheses is the age at test
20ºC – Test performed at isothermal 20ºC temperature
Semi – Test performed at semi-adiabatic temperature history

Table A.4 Elastic modulus (Norwegian Public Road Administration (SVV))

concrete	Ec (MPa)(20ºC)					
	1day	3day	7day	28day	90day	290day
SV40	20415	24774(2d)	28088	31750	33297	33726
SV40*						
Reference	20836	25055	27631	32469	32470	32457
40% FA	18653	22823	24707	29409	31129	32235
40% FA*						
60% FA (a)	17027	22854(4d)	24099	29021	31342	32362
60% FA (b)	14058	22911(4d)	23301	30088	31417	31293(343d)
60% FA*						
100% FA	8766	18820	21072	27353	29786	30889
40% BFS	17599	22519	24389	29873	32234	33075
60% BFS	14437	21917	23440	29258	32386	33672
100% BFS	12508	19469	22515	28483	32401	32368
NL slagcement*						

Note: *- Test data for second series including four types of concretes
(2d)- The value in the parentheses is the age at test
20ºC – Test performed at isothermal 20ºC temperature
Semi – Test performed at semi-adiabatic temperature history

Table A.5 Elastic modulus (NTNU)

concrete	Ec (MPa) (20ºC)	Ec (MPa) (Semi)
	28day	28 day
SV40*		32200
Reference	35000	
40% FA	32680(27d)	
40% FA*		33900(29d)
60% FA		
60% FA*		34500(29d)
100% FA	27500(33d)	
40% BFS	33700	
60% BFS	32190	
100% BFS	32500	
NL slagcement*		35500(21d)

Note: *- Test data for second series including four types of concretes
(27d)- The value in the parentheses is the age at test
20ºC – Test performed at isothermal 20ºC temperature
Semi – Test performed at semi-adiabatic temperature history

Table A.6 Split tensile strength (Norwegian Public Road Administration (SVV))

concrete	Split tensile strength fts (MPa) (20ºC)	
	1day	290day
SV40	2.8	5.8
SV40*		
Reference	2.4	5.6
40% FA	1.5	6.0
40% FA*		
60% FA (a)	1.1	4.7
60% FA (b)	0.9	5.8
60% FA*		
100% FA	0.4	5.3
40% BFS	1.6	5.5
60% BFS	1.1	5.0
100% BFS	0.7	5.1
NL slagcement*		

Note: 20ºC – Test performed at isothermal 20ºC temperature

Table A.7 Split and uniaxial tensile strength (NTNU)

concrete	Split tensile strength (MPa)				Uniaxial tensile strength(MPa)				
	fts (20ºC)			fts (Semi)	ft (20ºC)	ft (Semi)	TSTM (Realistic temperature)		
	2day	8day	28day	28day	28day	28day	ft	Time (d)	Maturity(d)
SV40*	3.16	3.96	4.9(24d)	5.1(24d)		3.5(24d)			
Reference	3.25		5.5	5.13	3.88	3.59			
40% FA	2.38		4.46	5.44	3.26	3.75	3.43	12.08	25.67
40% FA*	1.81	3.31	4.1(29d)	5.0(29d)		3.3			
	1.98								
60% FA							3.24	13.08	26.00
60% FA*	1.6		3.7(29d)	4.6(29d)		3.2(30d)	3.10**	18.00**	19.83**
	1.35	2.25							
100% FA	1.09		3.58(33d)	4.14(33d)	2.49(33d)	3.13(33d)	3.03	13.08	20.58
40% BFS	2.28		4.82	5.2	3.89	3.78	3.73	12.08	25.67
60% BFS	1.96		4.76	5.32	3.34	3.61	3.82	13.04	26.00
100% BFS	1.19		4.04	5.12	2.91	3.4	3.20	13.04	23.83
NL slagcement*	1.0	3.08	4.0	4.3		3.3			

Note: **- Initial temperature 11ºC
*- Test data for second series including four types of concretes
(24d)- The value in the parentheses is the age at test
20ºC – Test performed at isothermal 20ºC temperature

Semi – Test performed at semi-adiabatic temperature history

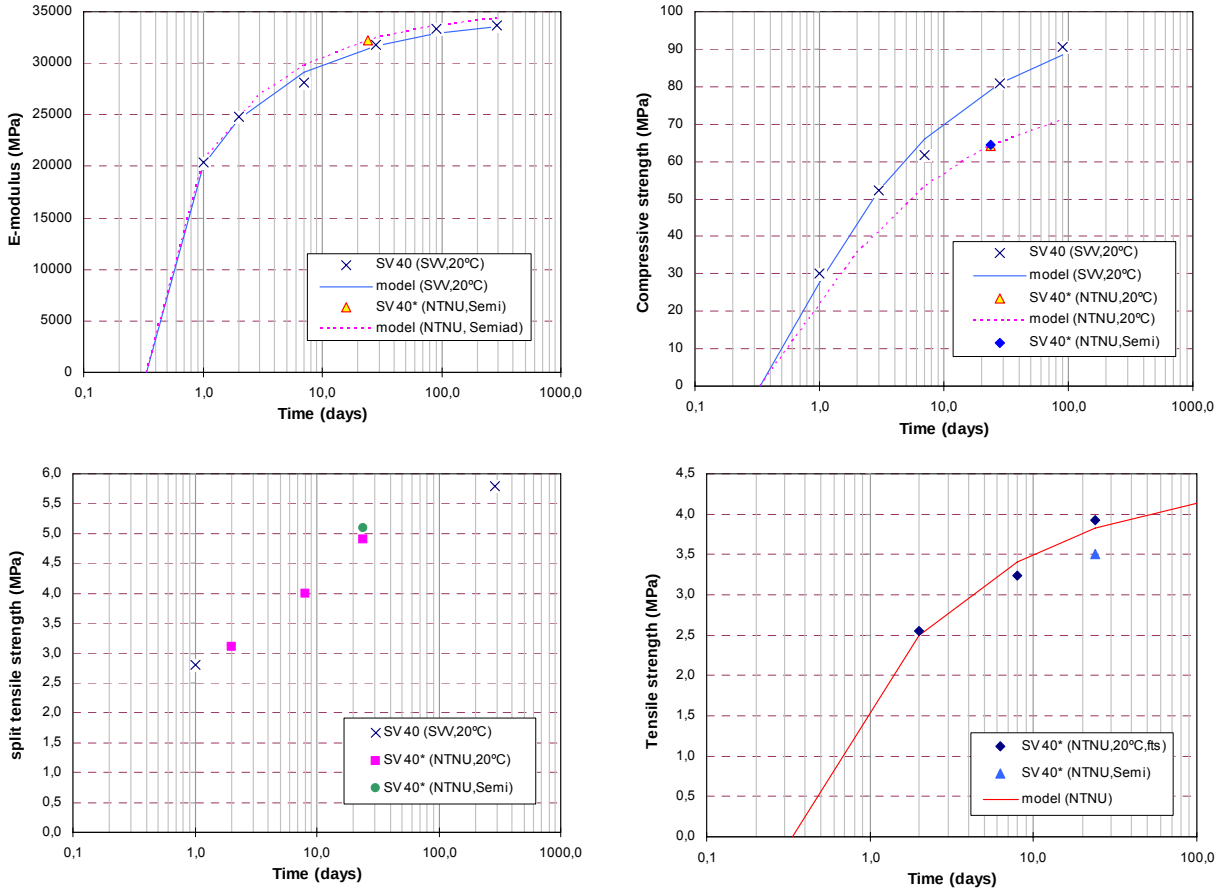

Figure A.11 Mechanical properties of SV 40 and SV 40* concretes

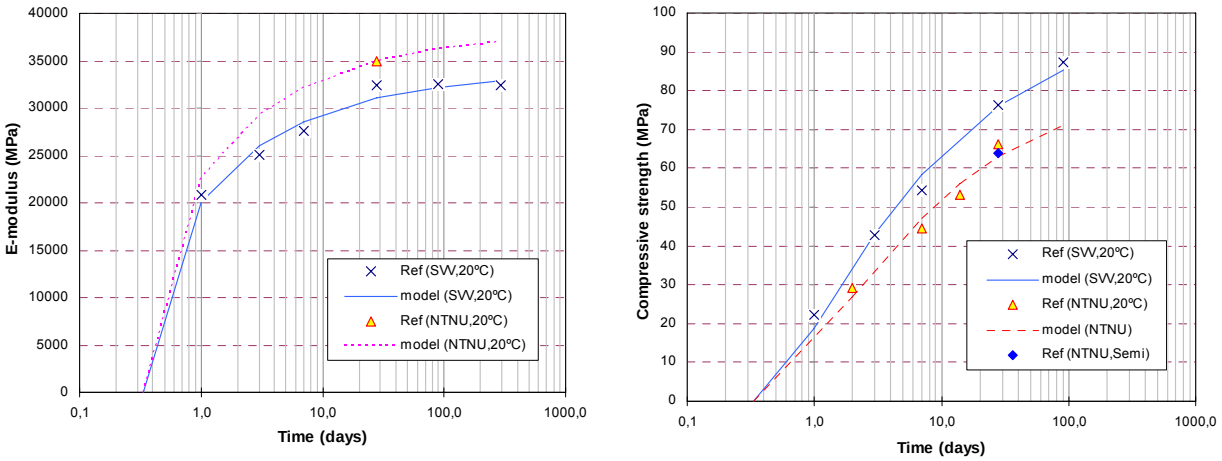

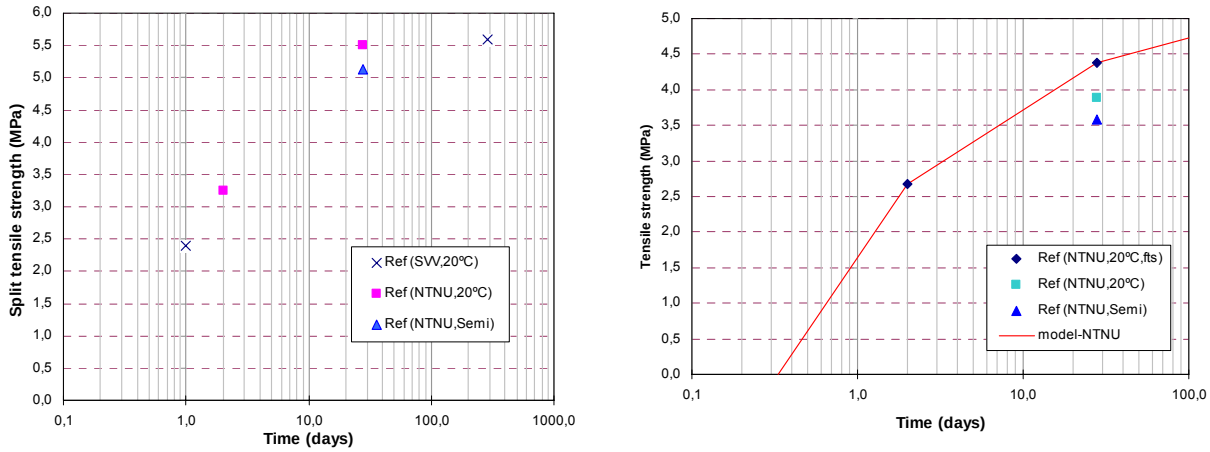

Figure A.12 Mechanical properties of reference concrete

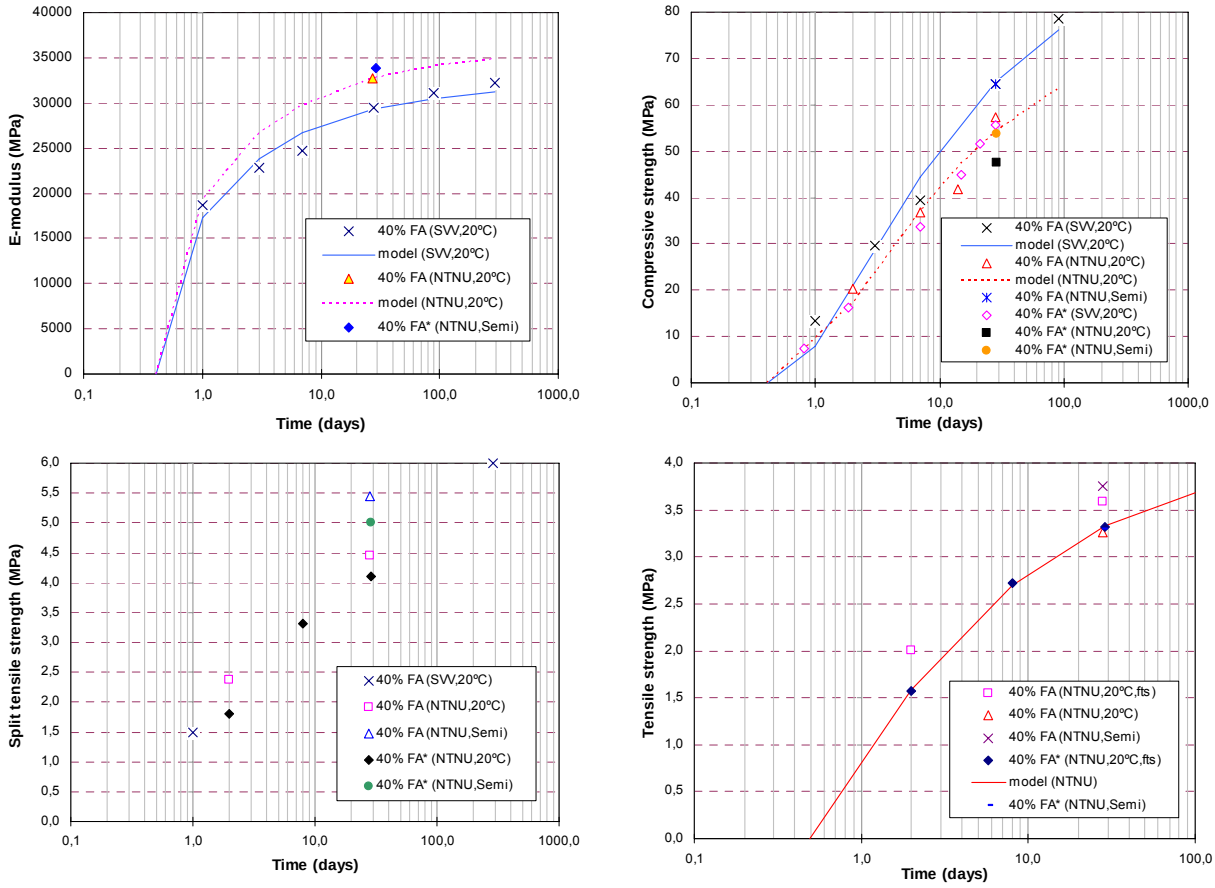

Figure A.13 Mechanical properties of 40% FA and 40% FA* concretes

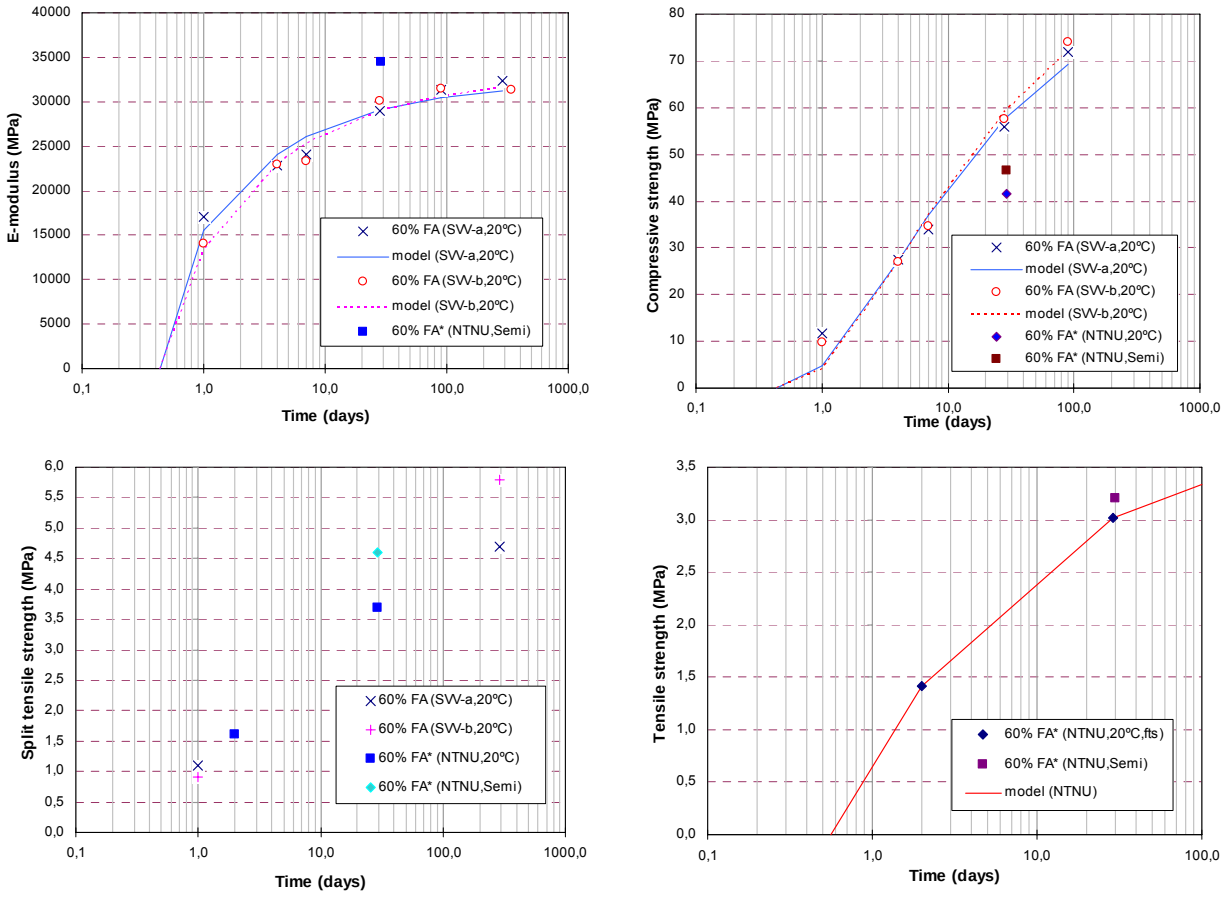

Figure A.14 Mechanical properties of 60% FA and 60% FA* concretes

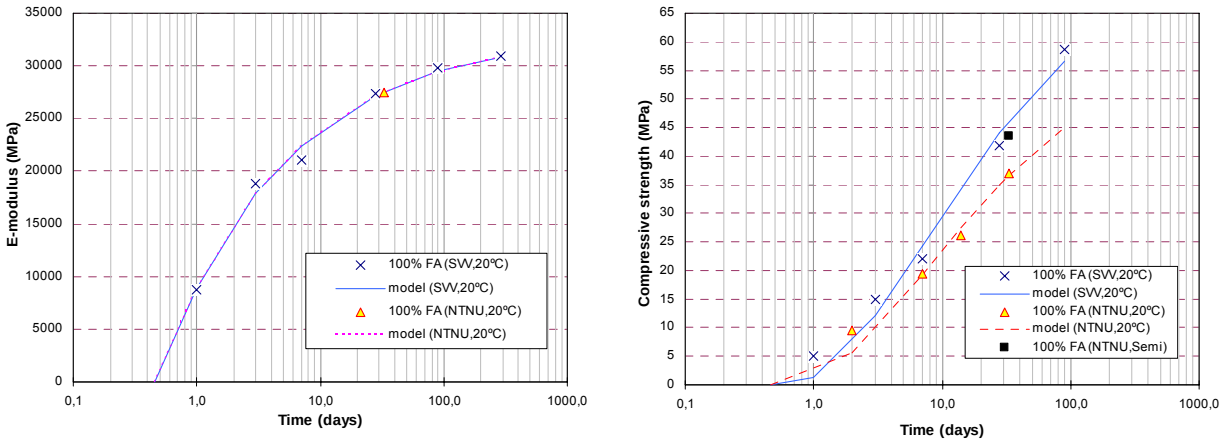

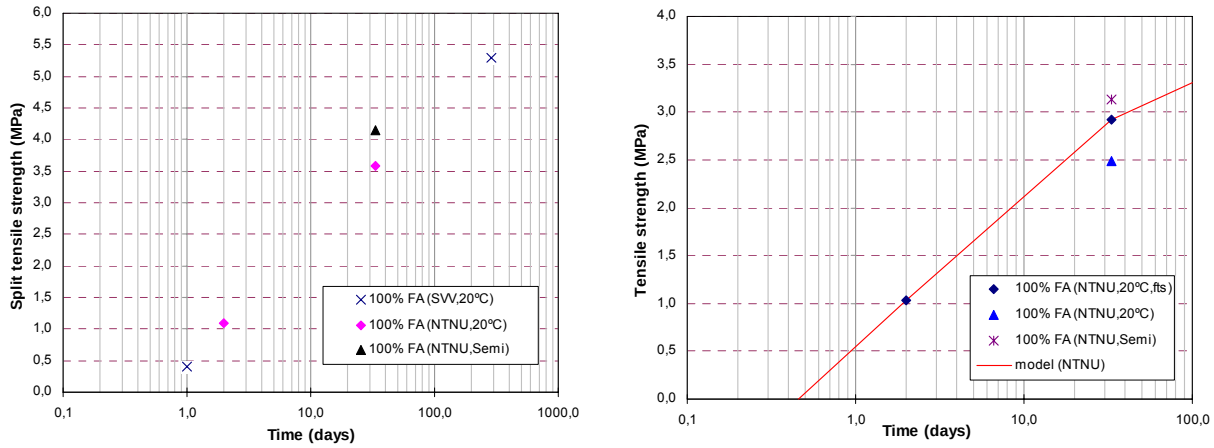

Figure A.15 Mechanical properties of 100% FA concrete

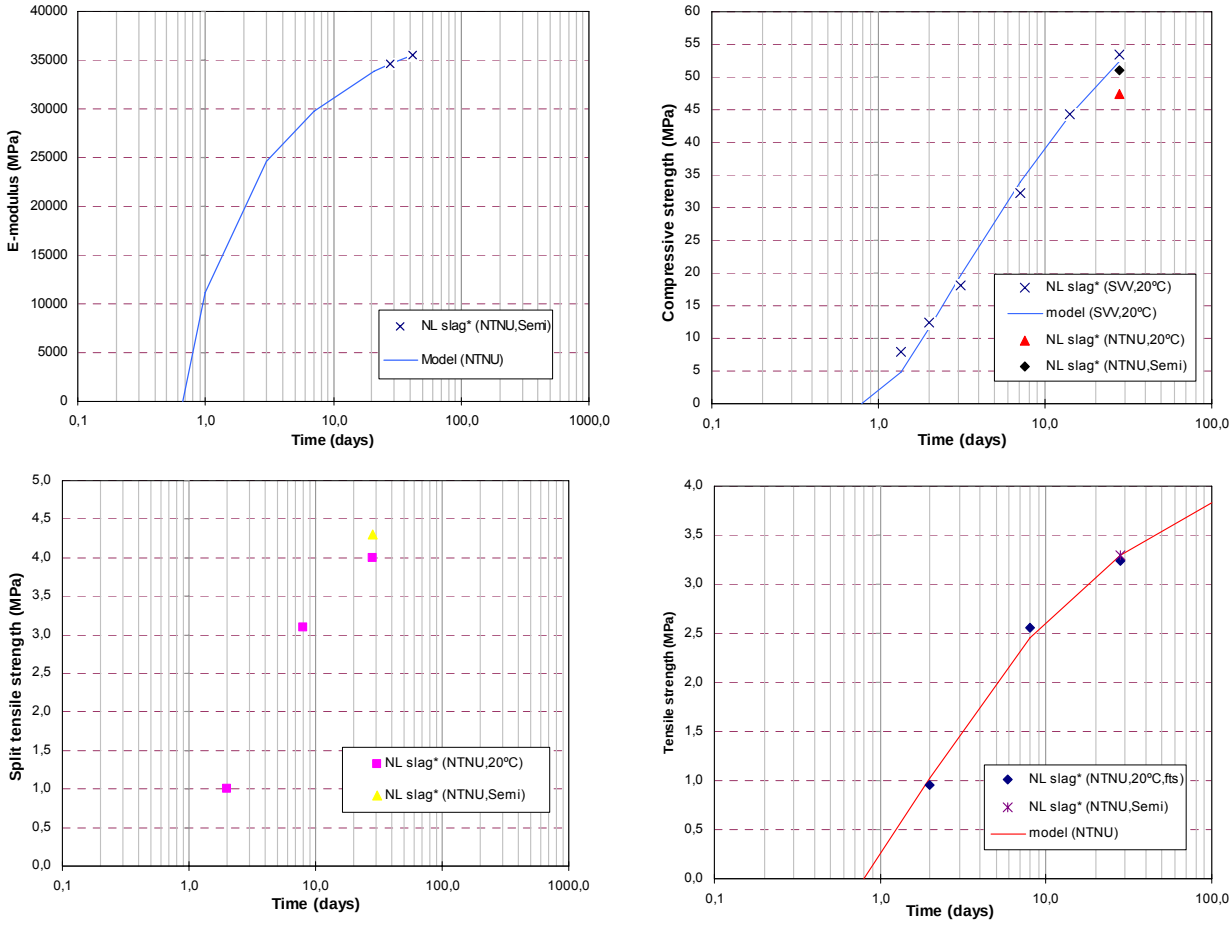

Figure A.16 Mechanical properties of NL slag* concrete

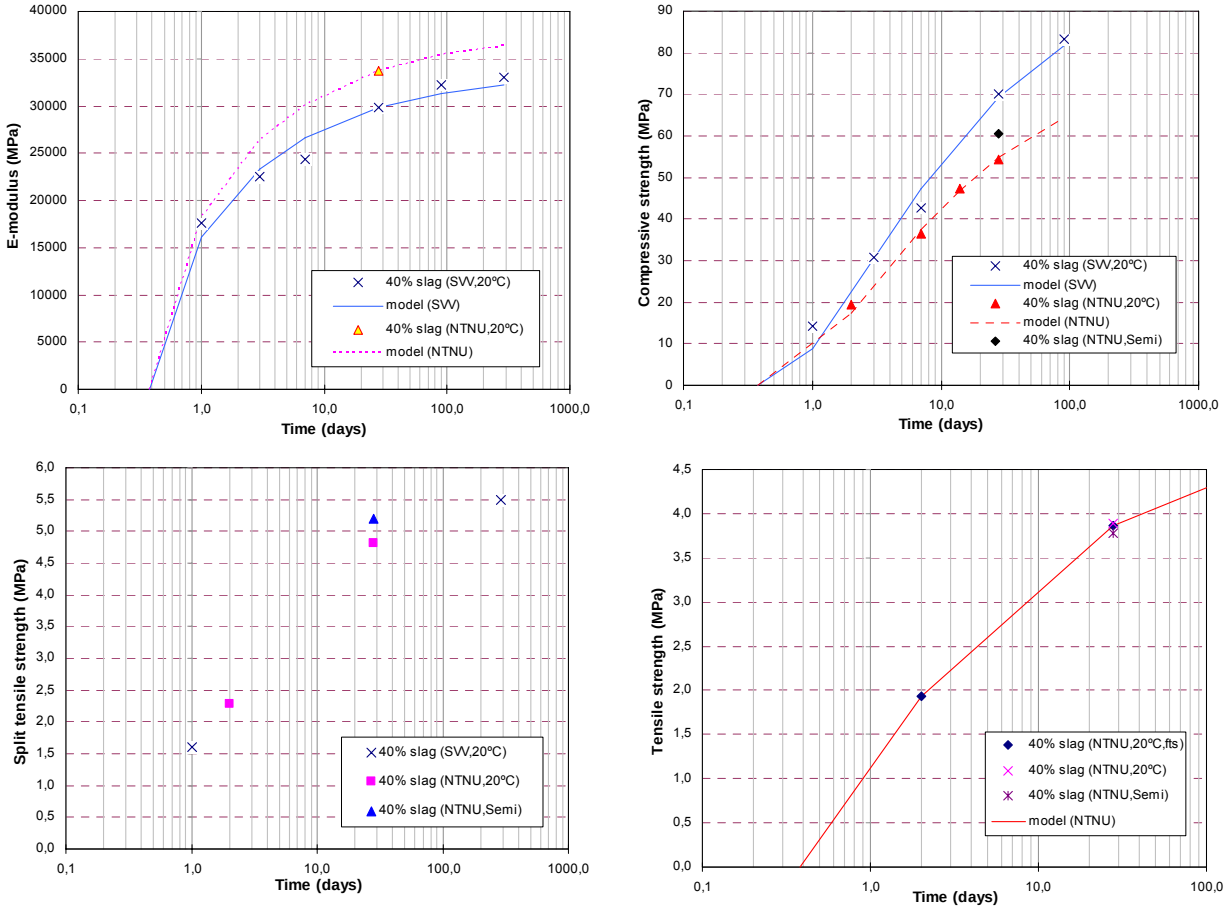

Figure A.17 Mechanical properties of 40% slag concrete

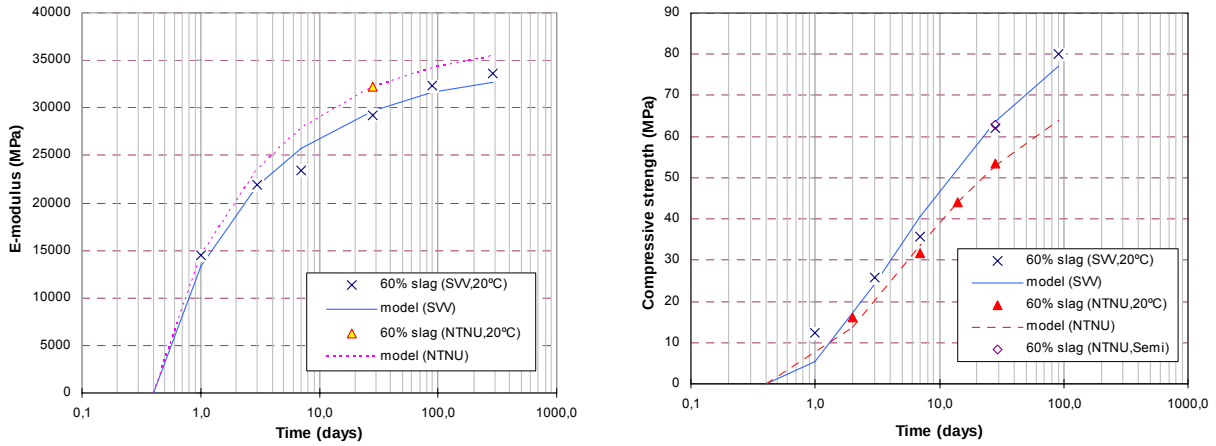

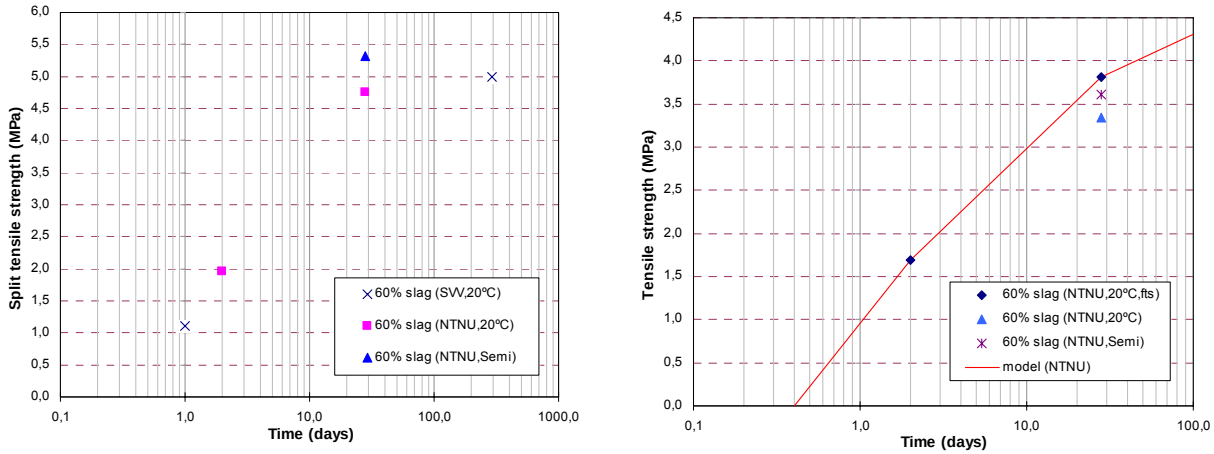

Figure A.18 Mechanical properties of 60% slag concrete

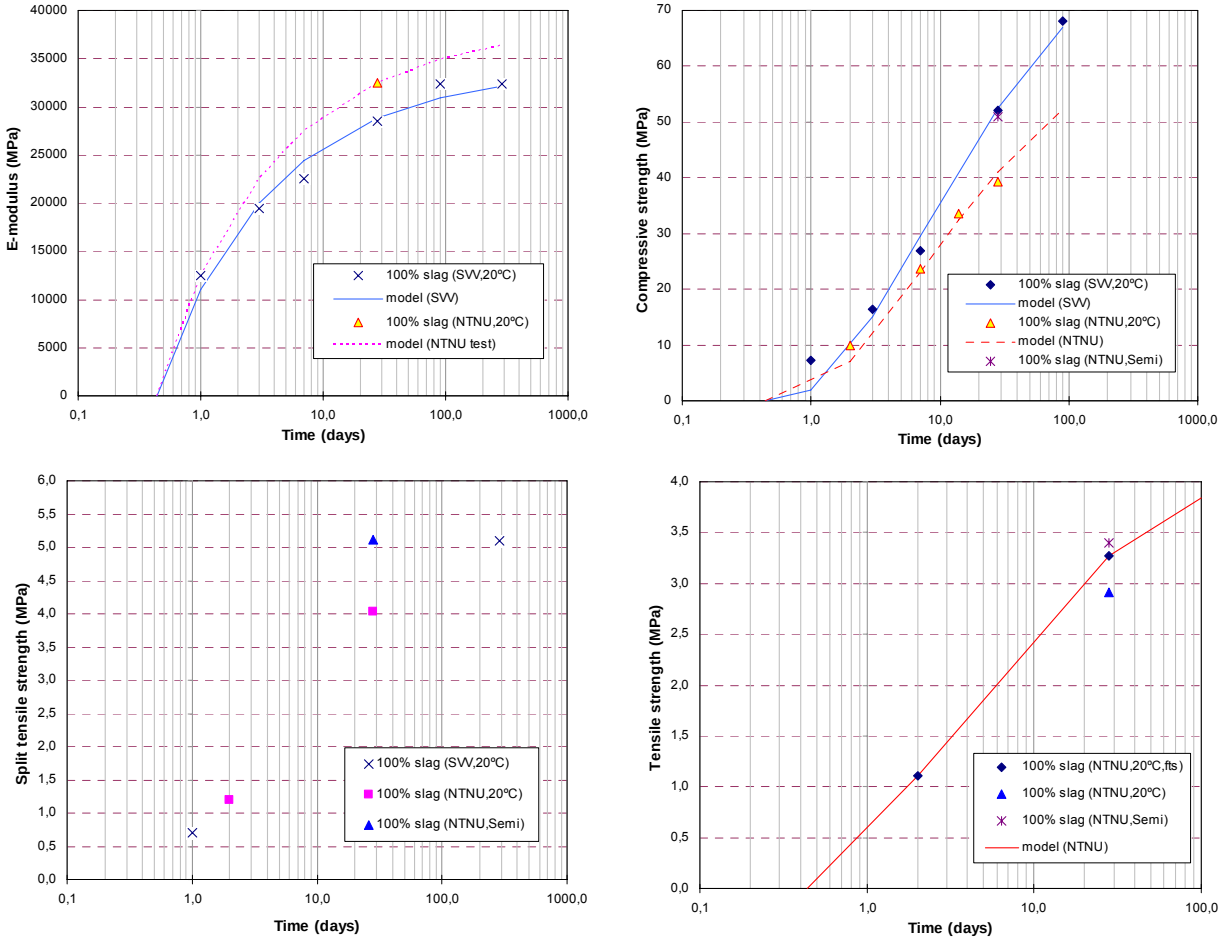

Figure A.19 Mechanical properties of 100% slag concrete

Table A.8 Parameters for mechanical properties

Concrete	f_{c28} (MPa) (20ºC)	f_{t28} (MPa)	E_{c28} (MPa)	s	n_t	n_E	$t_{0,eq}$ (hours)
Ref-0,45 (SVV)	76,09		31084,0	0,256		0,312	
Ref-0,45 (NTNU)	62,92	3,88	34980,0	0,256	0,629		8,0
40% BFS (SVV)	69,41		29867,0	0,366		0,298	
40% BFS (NTNU)	54,80	3,89	33715,0	0,366	0,604		9,1
60% BFS (SVV)	63,71		29738,6	0,430		0,322	
60% BFS (NTNU)	52,83	3,34	32190,0	0,430	0,601		9,6
100%BFS (SVV)	52,48		28827,7	0,549		0,291	
100%BFS (NTNU)	41,00	2,91	32505,0	0,549	0,618		10,5
40% FA (SVV)	64,84		29317,5	0,362		0,251	
40% FA (NTNU)	54,16	3,26	32736,0	0,362	0,491		9,8
60% FA (SVV-a)	57,56		29091,8	0,418		0,251	
60% FA (SVV-b)	59,07		28939,3	0,446		0,289	
60% FA (NTNU)				0,418			10,5
100% FA (SVV)	44,04		27188,4	0,564		0,325	
100% FA (NTNU)	34,97	2,85	27120,0	0,564	0,560		11,0
40% FA* (SVV)	53,49			0,356			
40% FA* (NTNU)	47,20	3,31	33846(semi)	0,362	0,623		11,8
60% FA* (SVV)	43,27			0,373			
60% FA* (NTNU)	41,20	3,20	34438(semi)	0,418	0,533		13,5
SV40 (SVV)	80,91		31704,8	0,197		0,421	
SV40* (SVV)	64,98			0,238			
SV40* (NTNU)	65,11	3,86	32414(semi)	0,197	0,722		8,0
NL slag* (SVV)	52,50			0,408			
NL slag* (NTNU)	47,40	3,30	35500(21,semi)	0,408	0,767		19,0

Appendix B: Creep data

Compressive creep tests

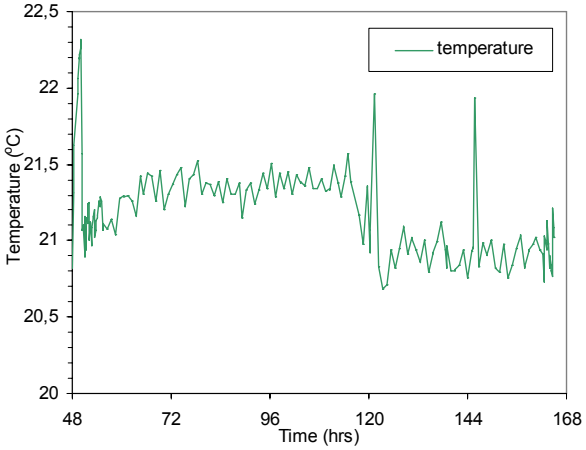

1) Temperature in room

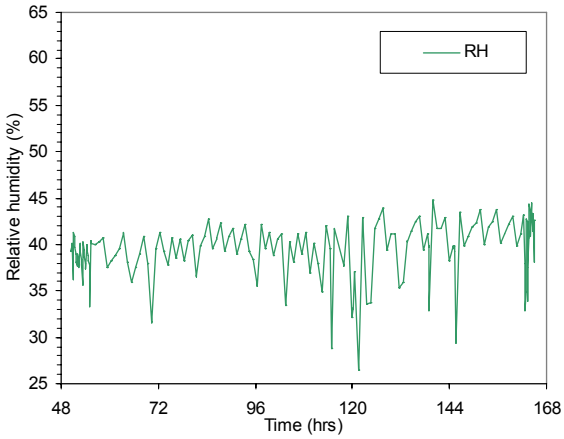

2) Relative humidity in room

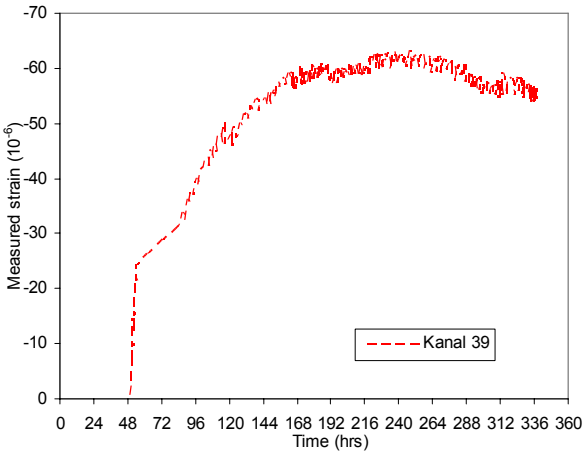

3) Load-independent strain (Dummy specimen)

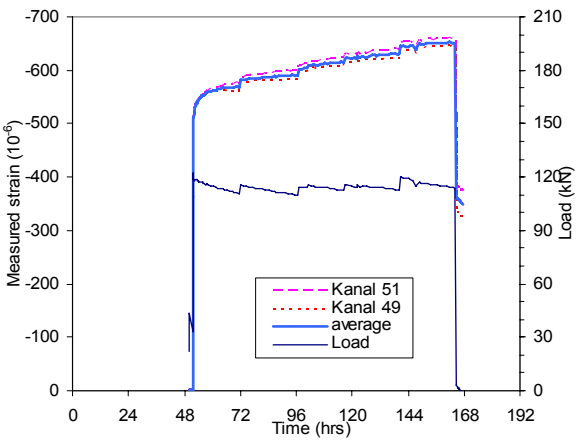

4) Load and measured strain (load at 50 hours)

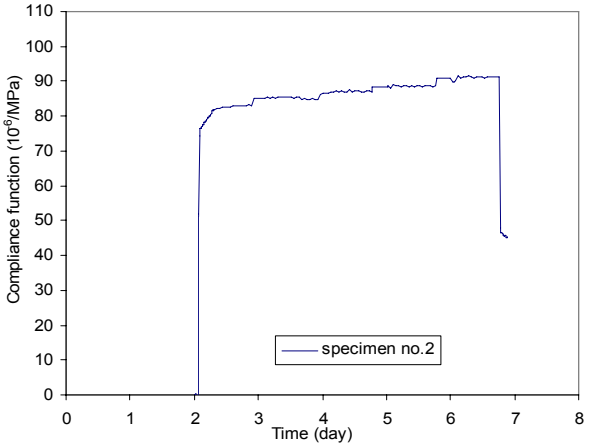

5) Creep compliance

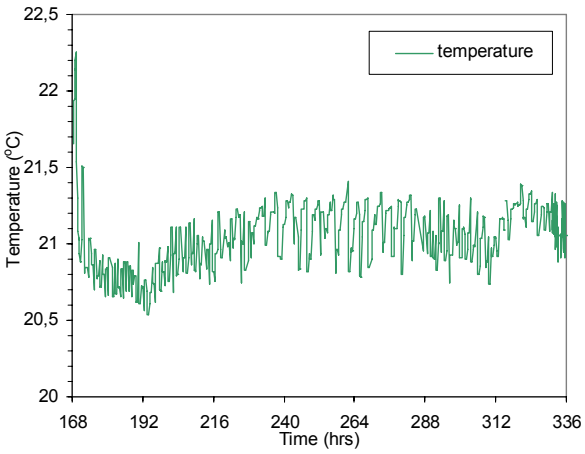

6) Temperature in room

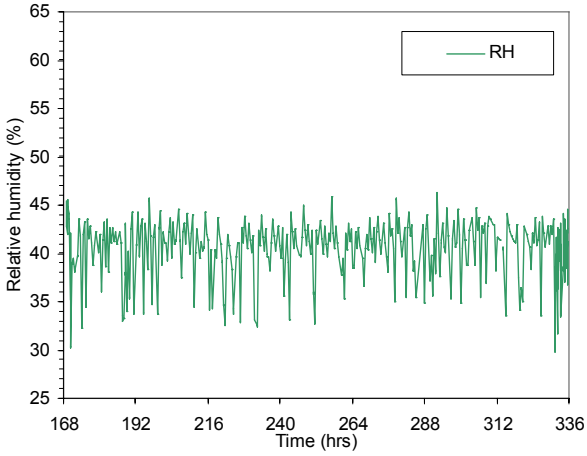

7) Relative humidity in room

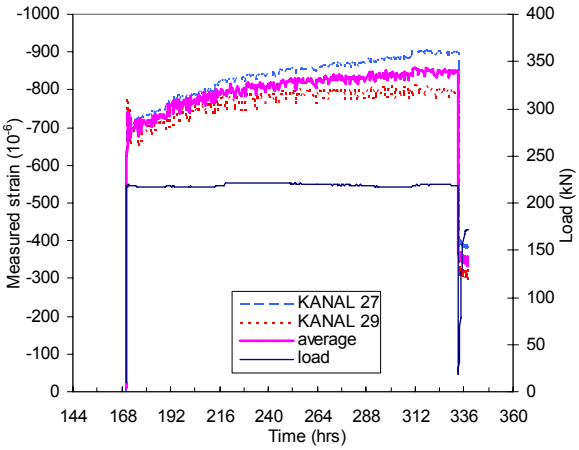

8) Load and measured strain (load at 170 hours)

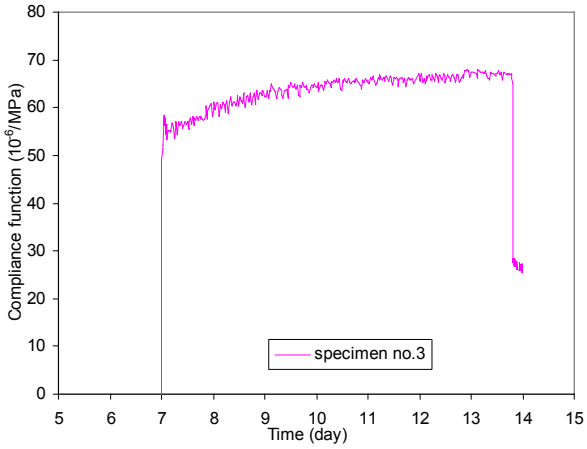

9) Creep compliance

Figure B.1 Compressive creep test on 2 and 7-old concrete (40% BFS)

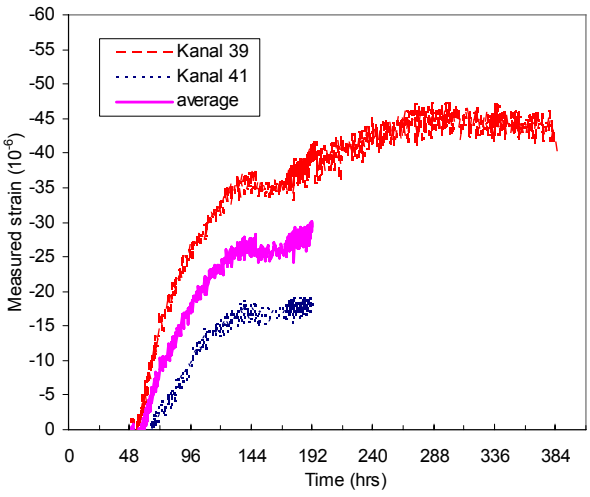

1) Load-independent strain (Dummy specimen)

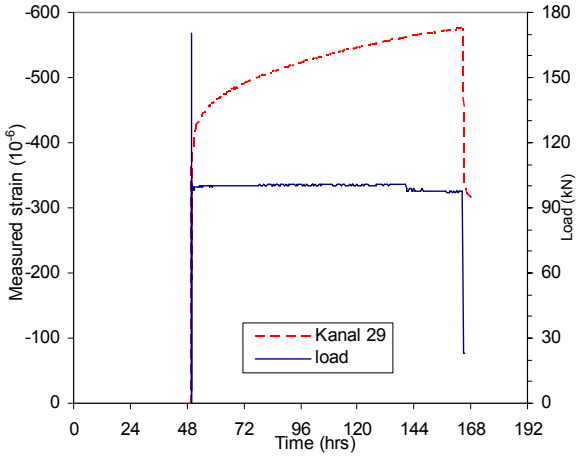

2) Load and measured strain (load at 50 hours)

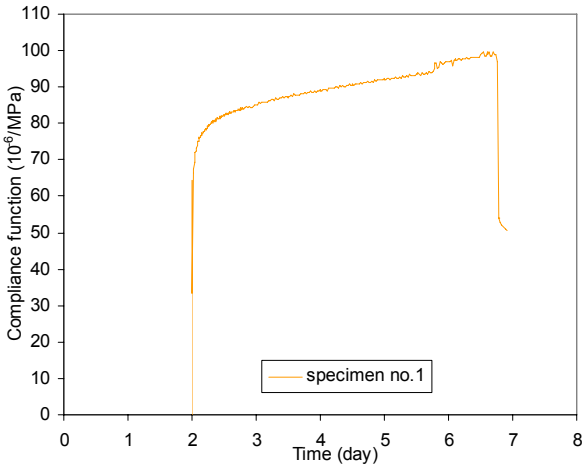

3) Creep compliance

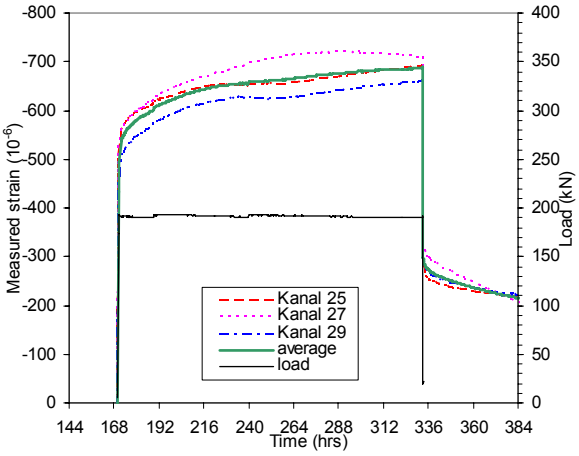

4) Load and measured strain (load at 170 hours)

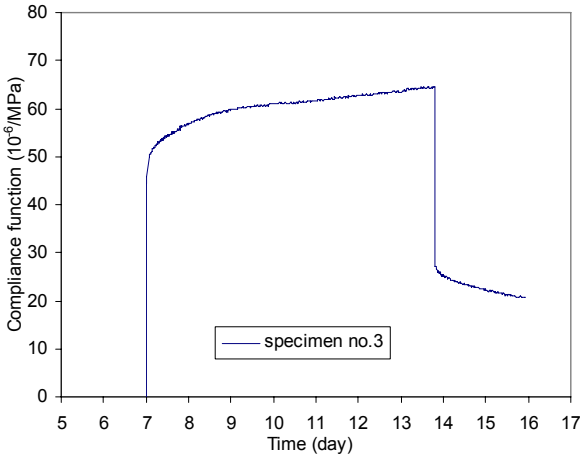

5) Creep compliance

Figure B.2 Compressive creep test on 2 and 7-old concrete (60% BFS)

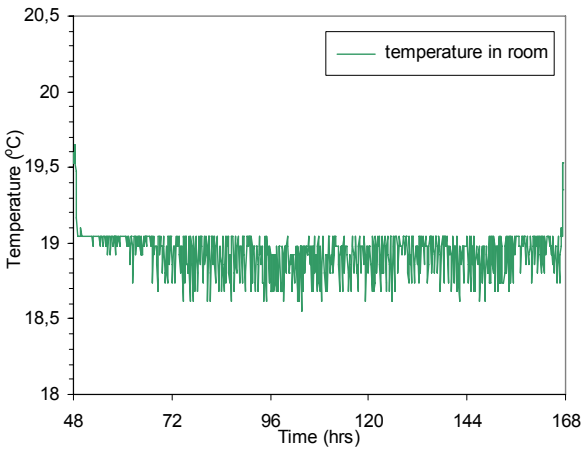

1) Temperature in room

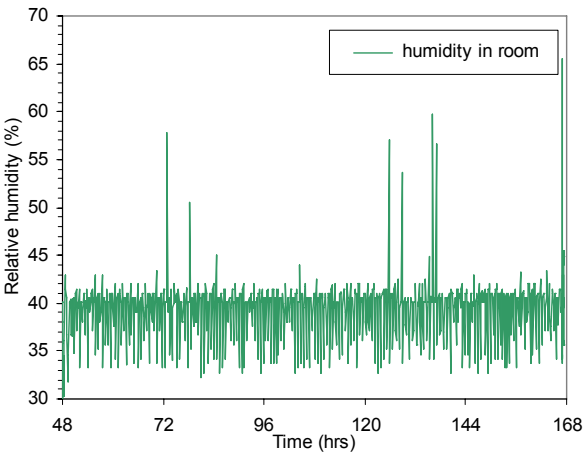

2) Relative humidity in room

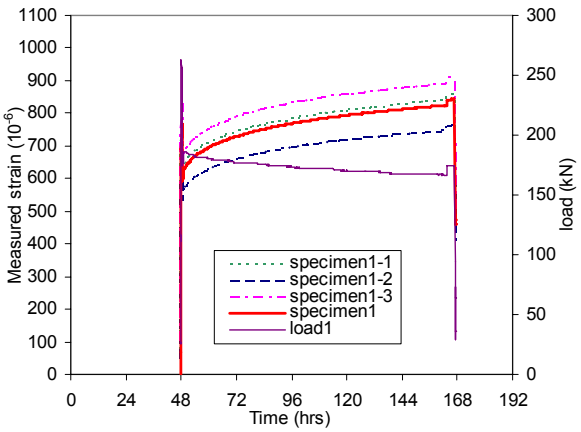

3) Load and measured strain (specimen no.1)

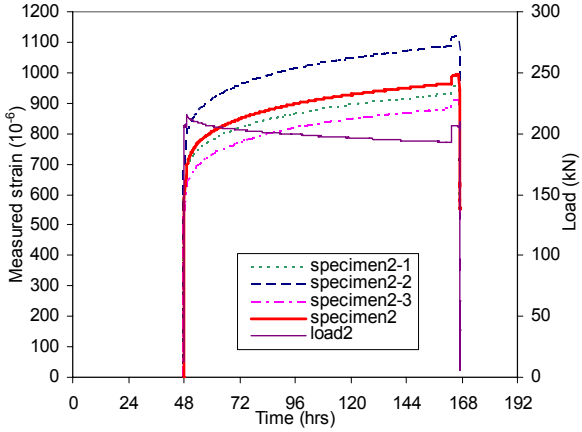

4) Load and measured strain (specimen no.2)

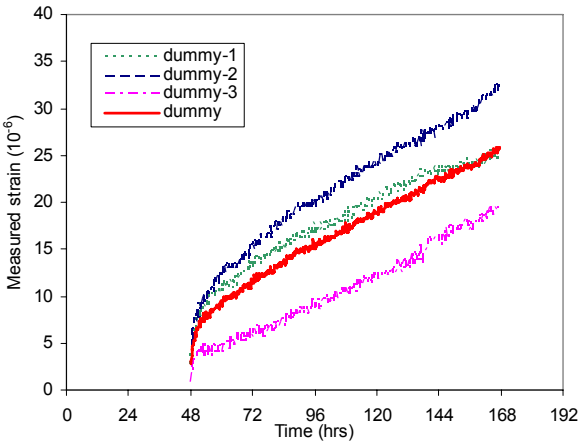

5) Load-independent strain (Dummy specimen)

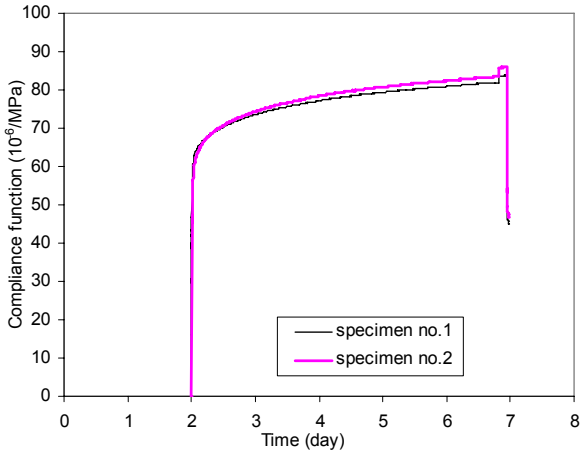

6) Creep compliance

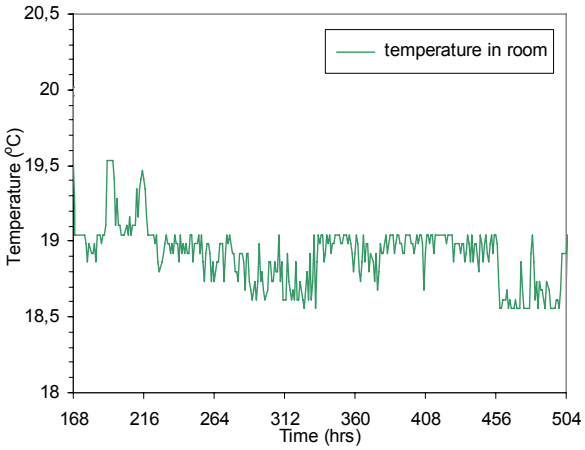

7) Temperature in room

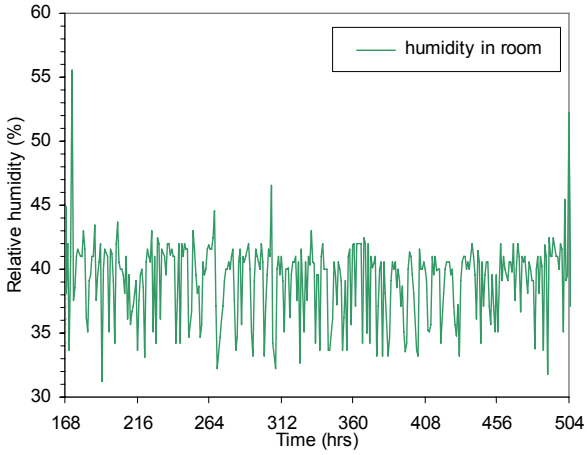

8) Relative humidity in room

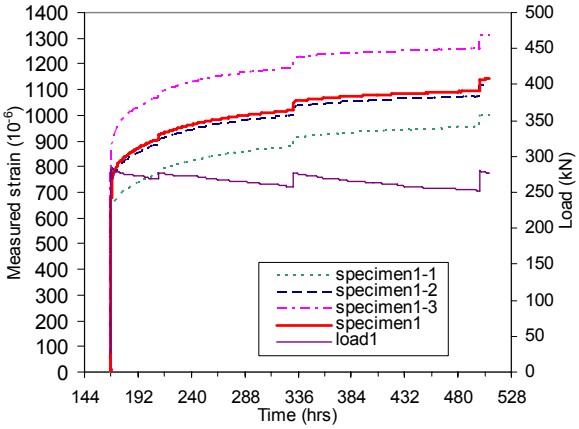

9) Load and measured strain (specimen no.1)

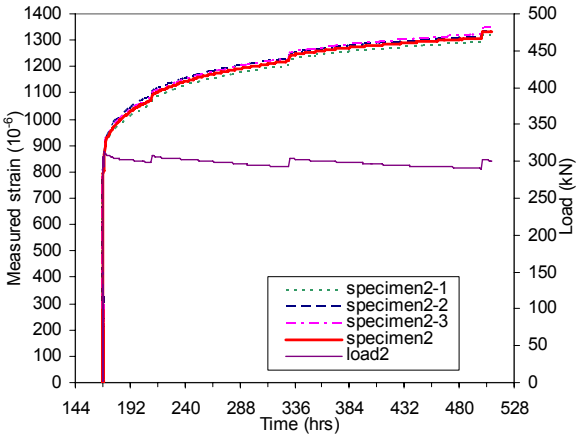

10) Load and measured strain (specimen no.2)

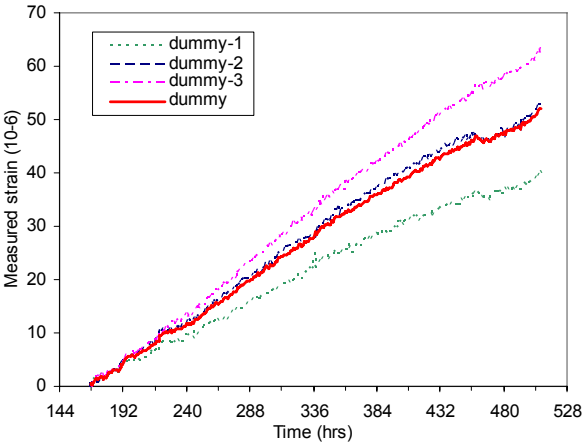

Load-independent strain (Dummy specimen)

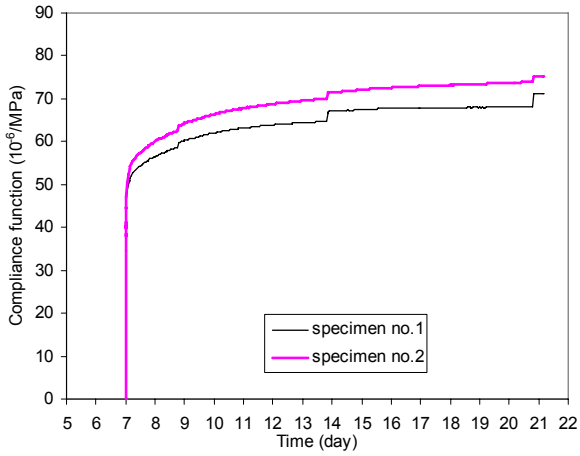

11) Creep compliance

Figure B.3 Compressive creep test on 2 and 7-old concrete (Basic 5*)

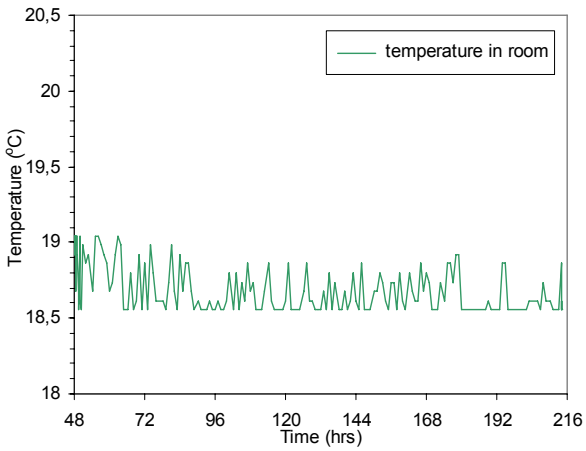

1) Temperature in room

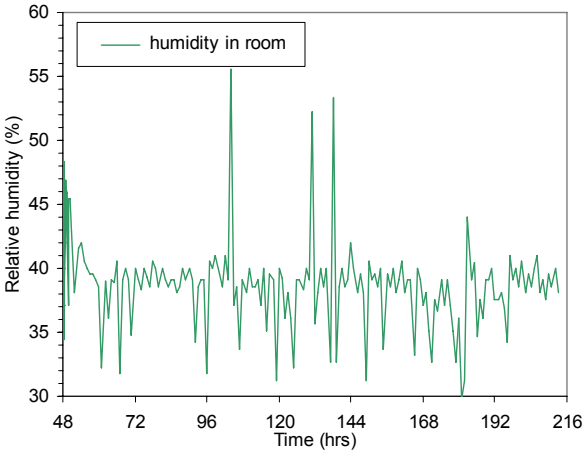

2) Relative humidity in room

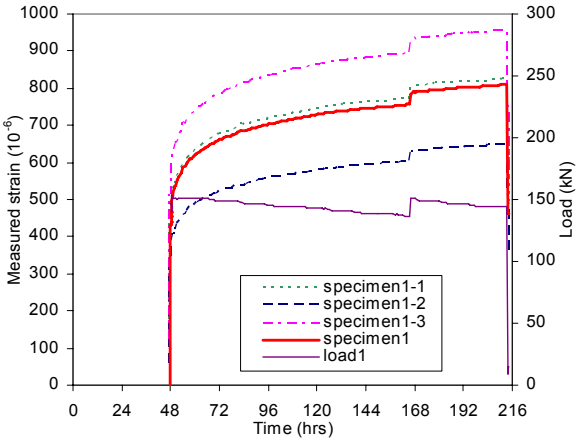

3) Load and measured strain (specimen no.1)

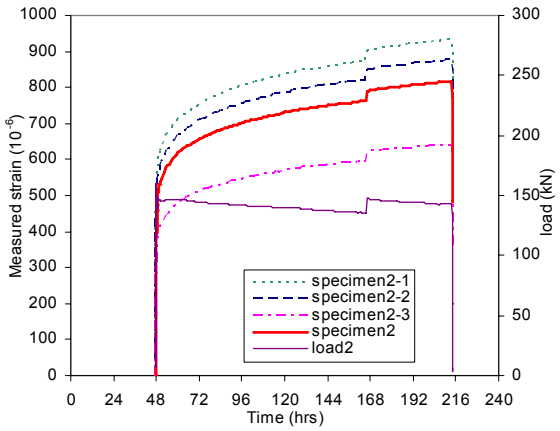

4) Load and measured strain (specimen no.2)

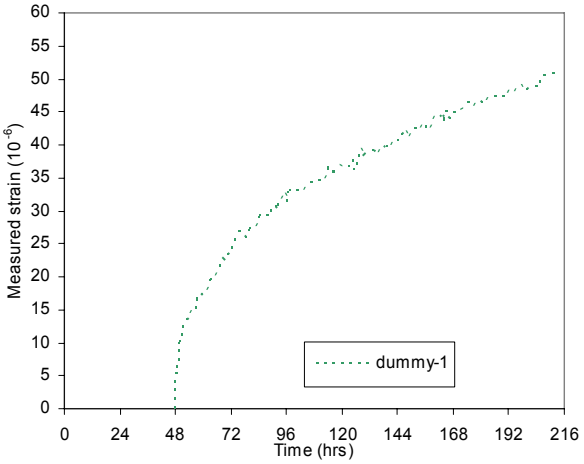

5) Load-independent strain (Dummy specimen)

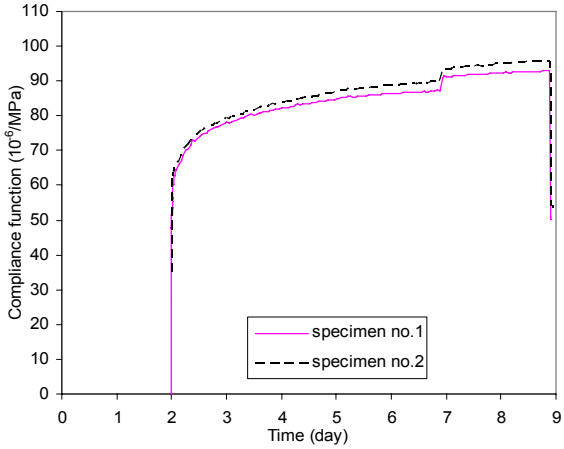

6) Creep compliance

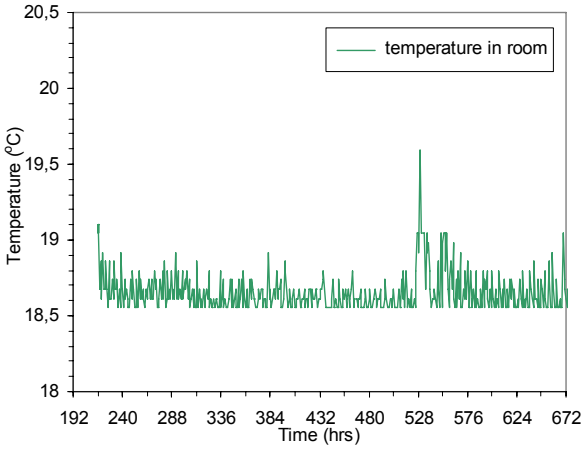

7) Temperature in room

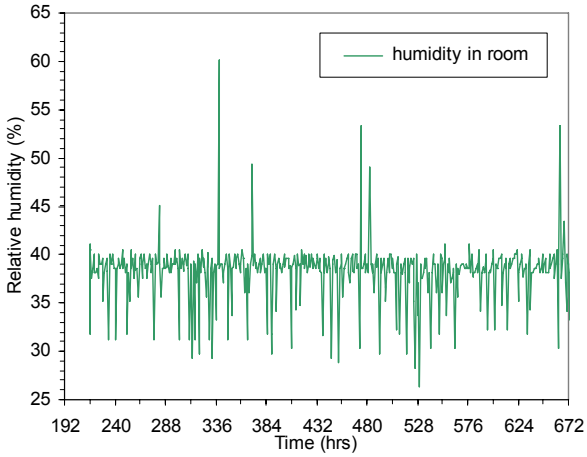

8) Relative humidity in room

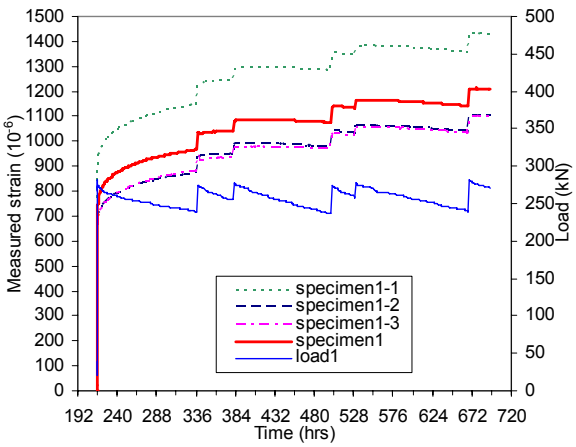

9) Load and measured strain (specimen no.1)

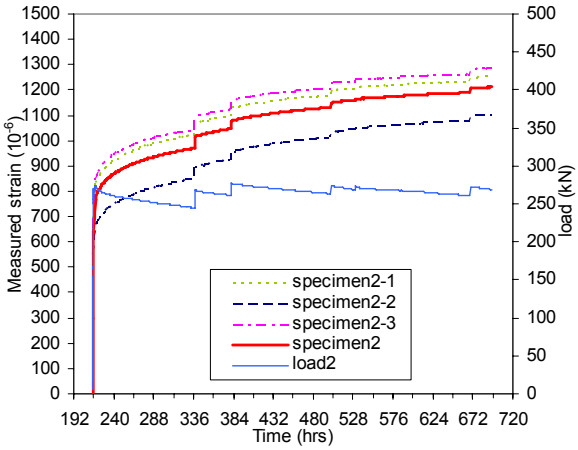

10) Load and measured strain (specimen no.2)

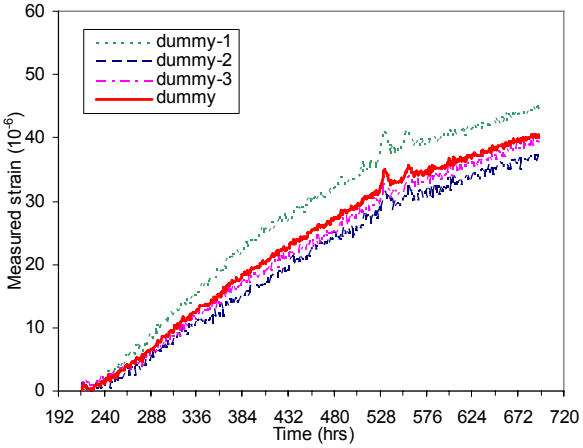

11) Load-independent strain (Dummy specimen)

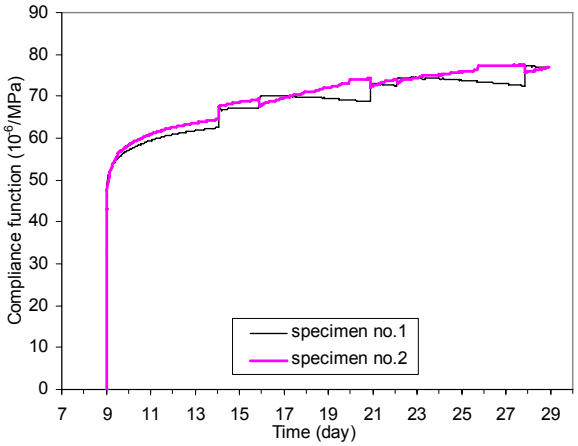

12) Creep compliance

Figure B.4 Compressive creep test on 2 and 9-old concrete (SV 40*)

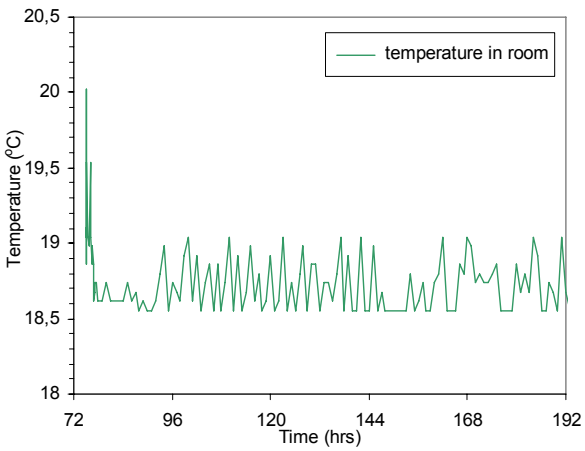

1) Temperature in room

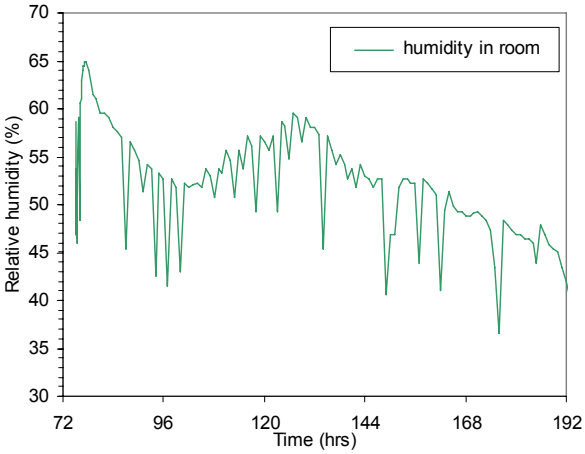

2) Relative humidity in room

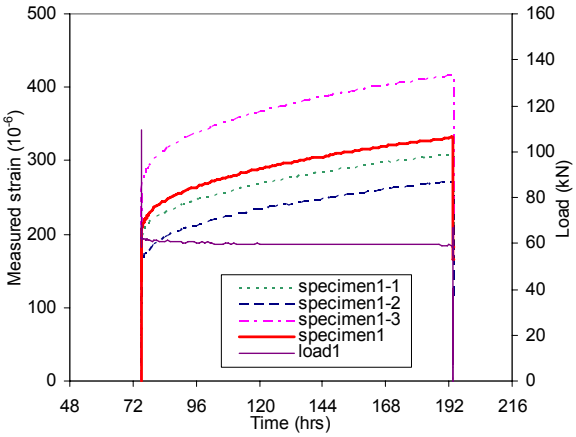

3) Load and measured strain (specimen no.1)

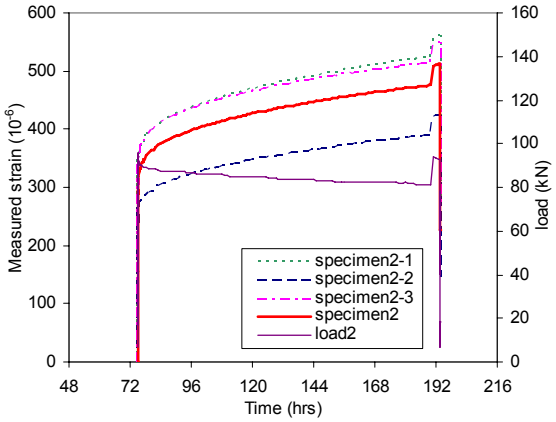

4) Load and measured strain (specimen no.2)

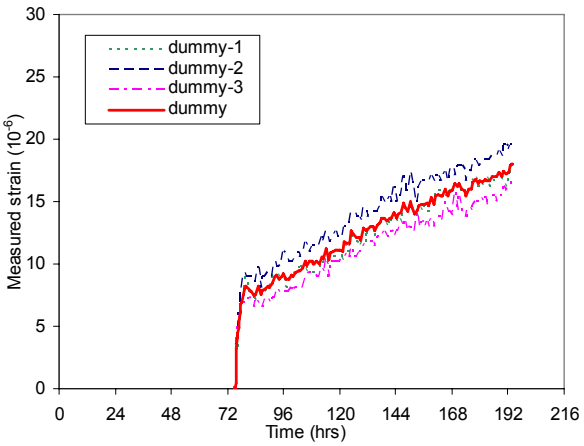

5) Load-independent strain (Dummy specimen)

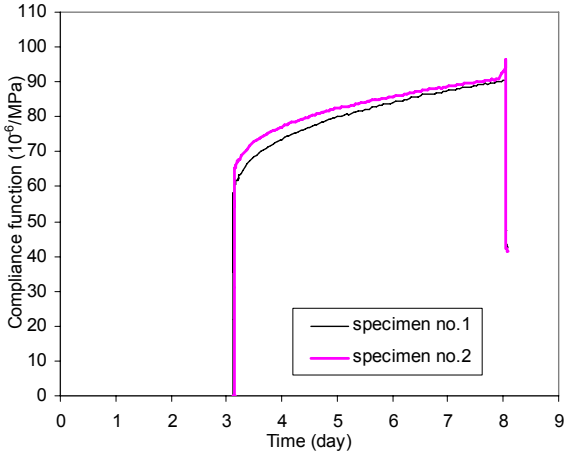

6) Creep compliance

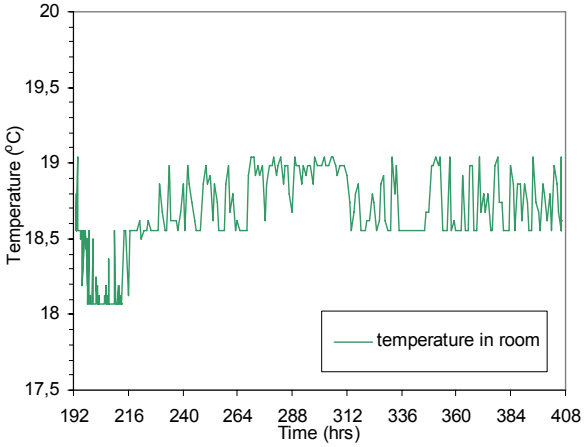

7) Temperature in room

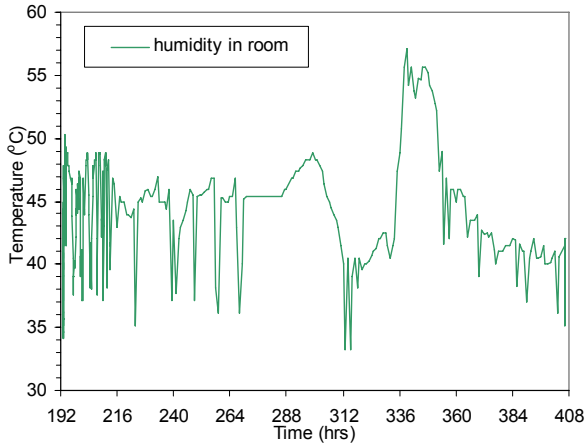

8) Relative humidity in room

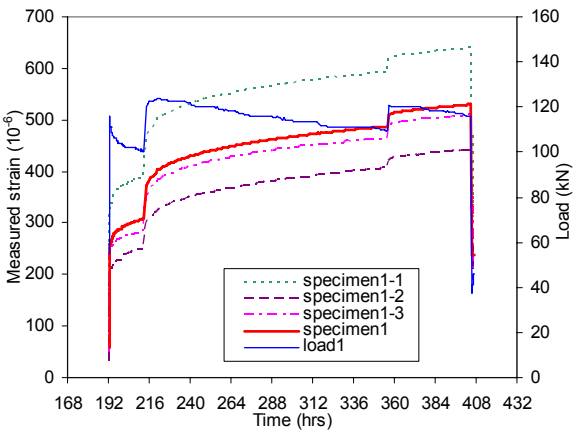

9) Load and measured strain (specimen no.1)

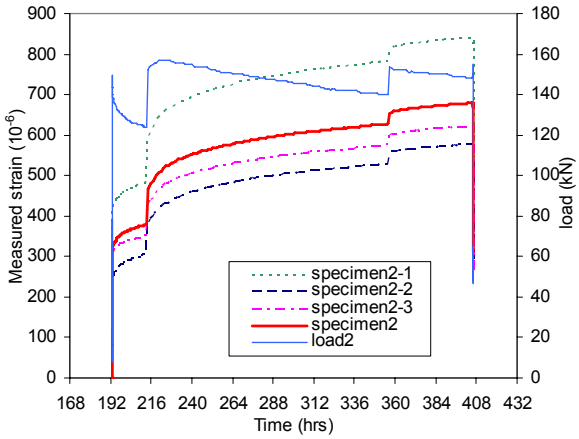

10) Load and measured strain (specimen no.2)

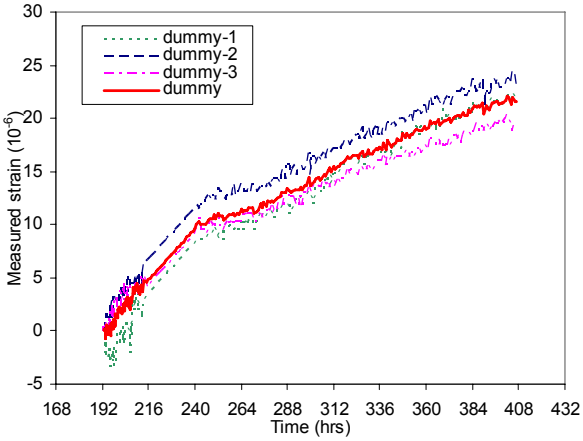

11) Load-independent strain (Dummy specimen)

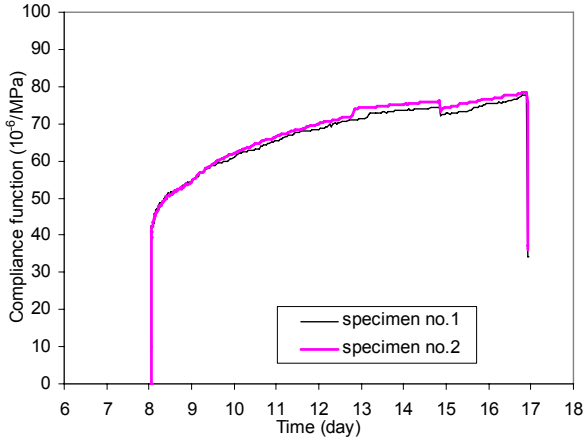

12) Creep compliance

Figure B.5 Compressive creep test on 3 and 8-old concrete (40% FA*)

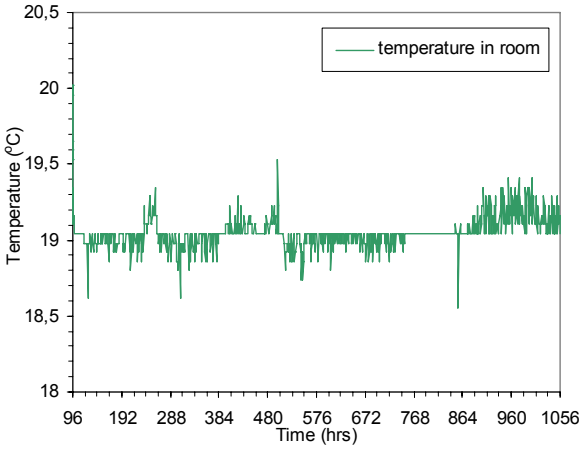

1) Temperature in room

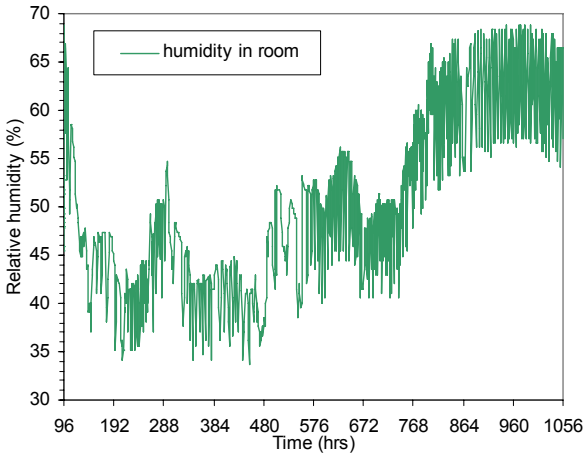

2) Relative humidity in room

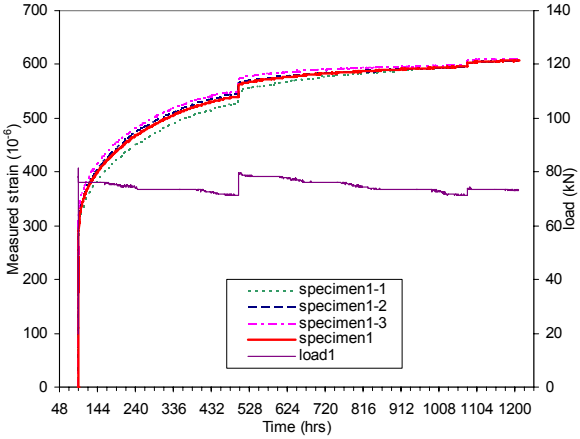

3) Load and measured strain (specimen no.1)

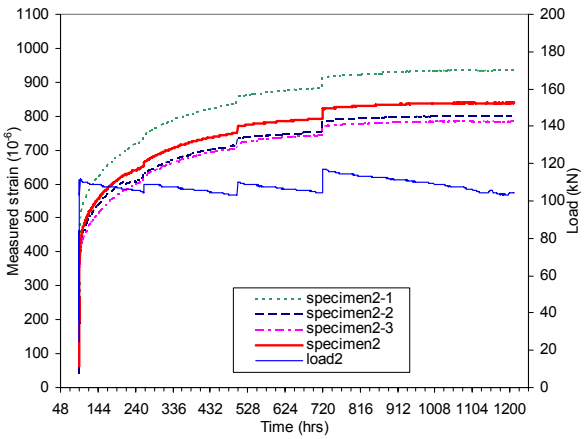

4) Load and measured strain (specimen no.2)

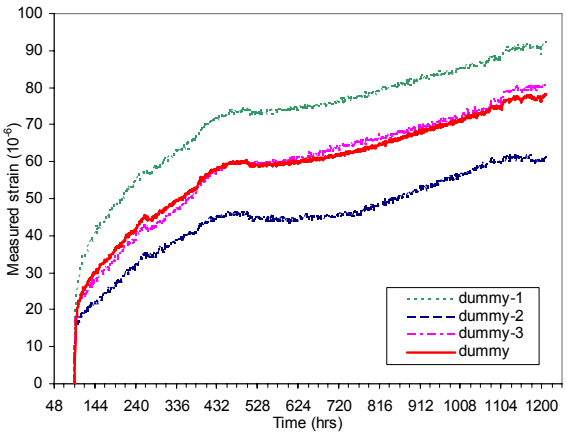

5) Load-independent strain (Dummy specimen)

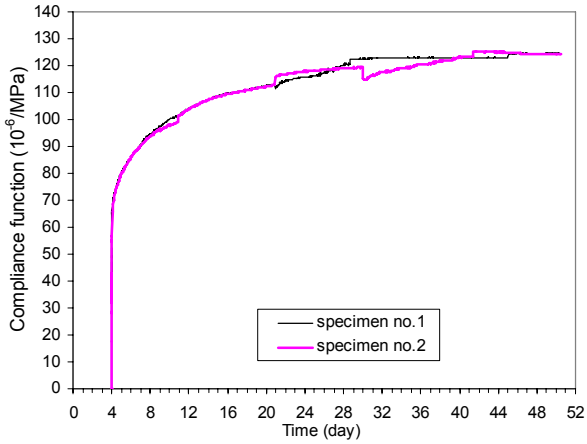

6) Creep compliance

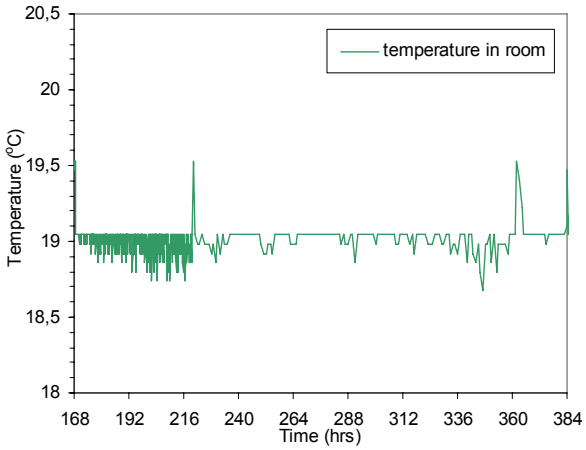

7) Temperature in room

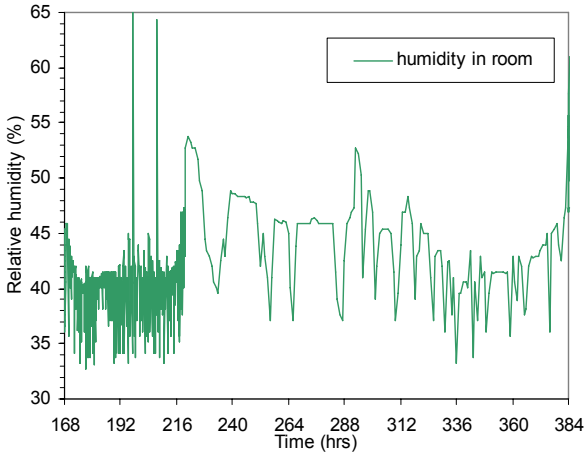

8) Relative humidity in room

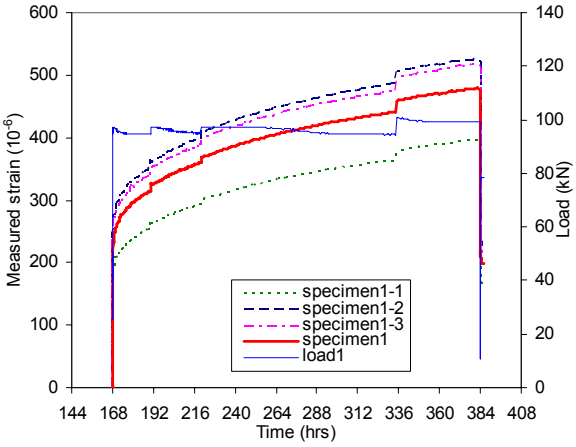

9) Load and measured strain (specimen no.1)

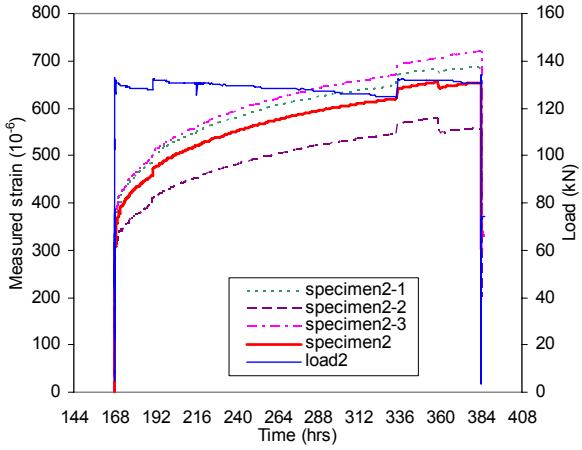

10) Load and measured strain (specimen no.2)

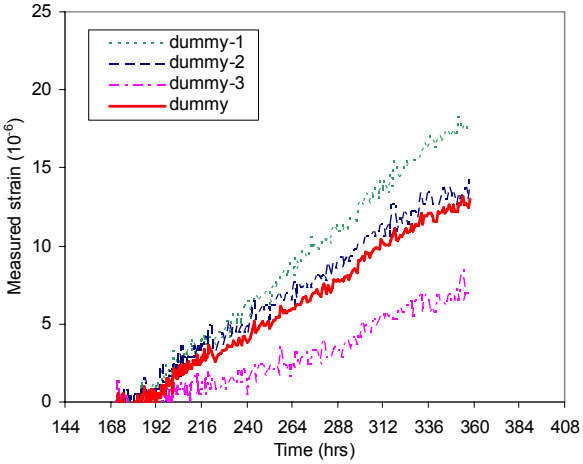

11) Load-independent strain (Dummy specimen)

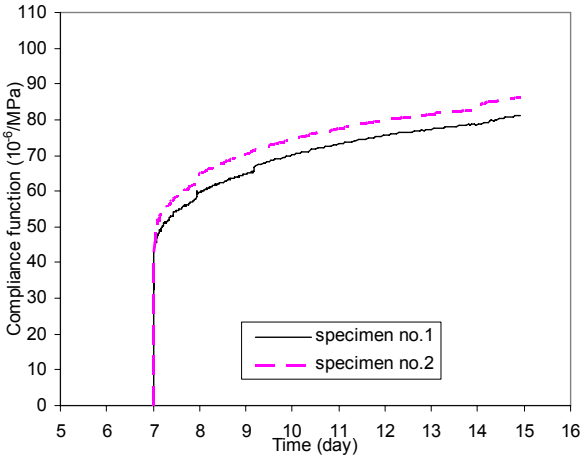

12) Creep compliance

Figure B.6 Compressive creep test on 4 and 7-old concrete (60% FA*)

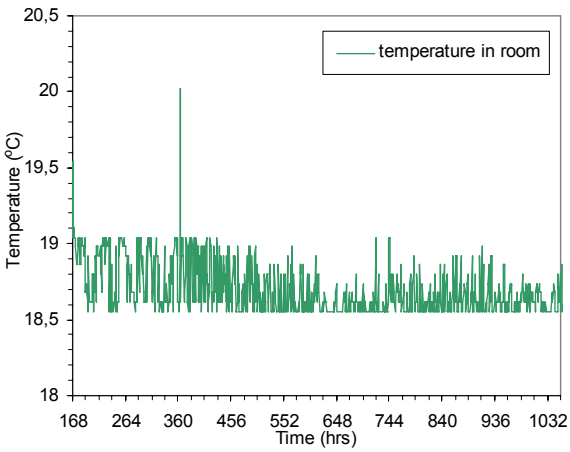

1) Temperature in room

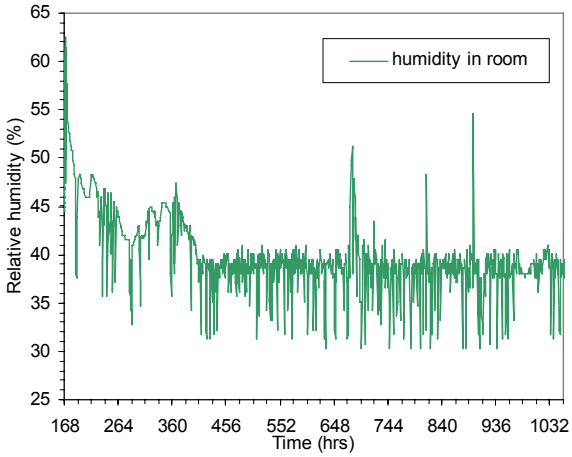

2) Relative humidity in room

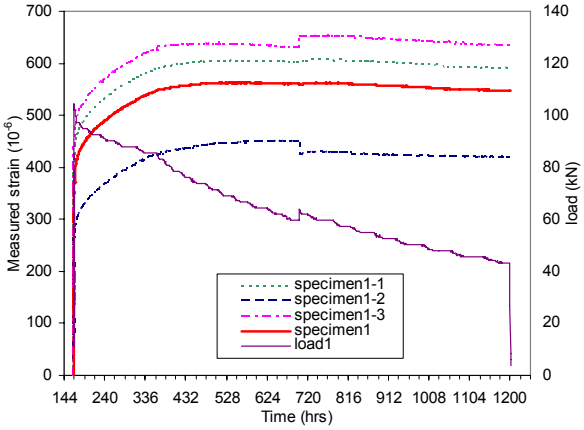

3) Load and measured strain (specimen no.1)

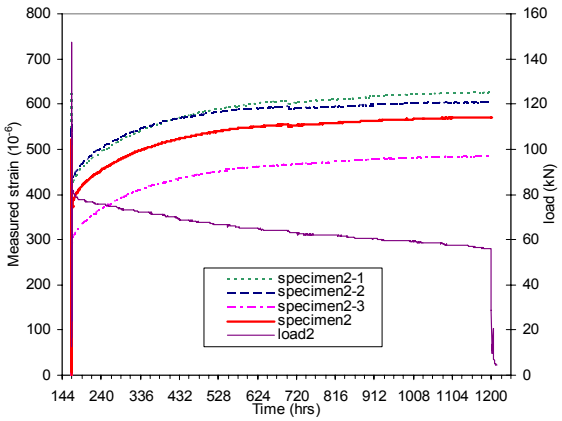

4) Load and measured strain (specimen no.2)

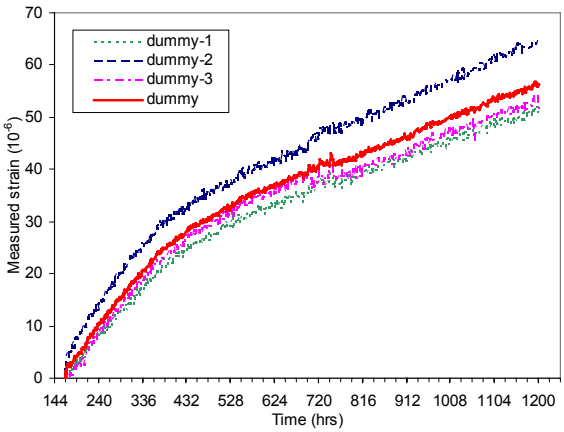

5) Load-independent strain (Dummy specimen)

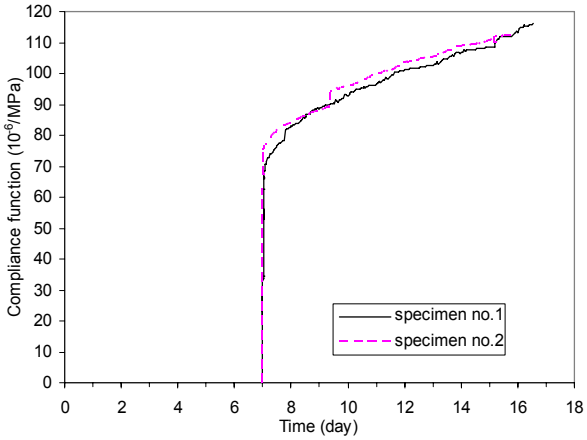

6) Creep compliance

Figure B.7 Compressive creep test on 7-old concrete (100% FA)

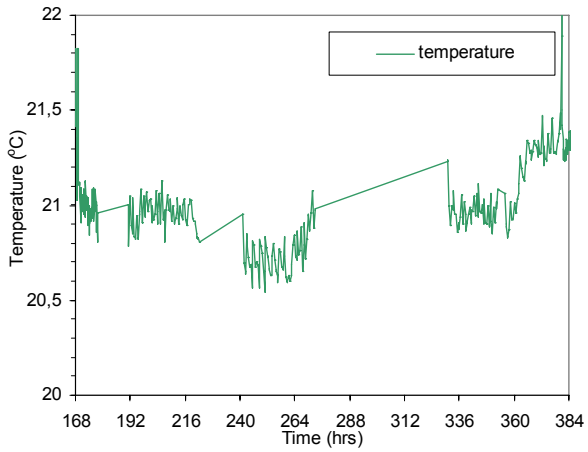

1) Temperature in room

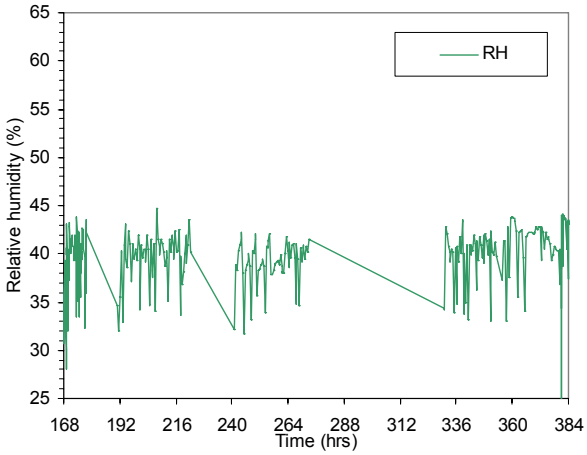

2) Relative humidity in room

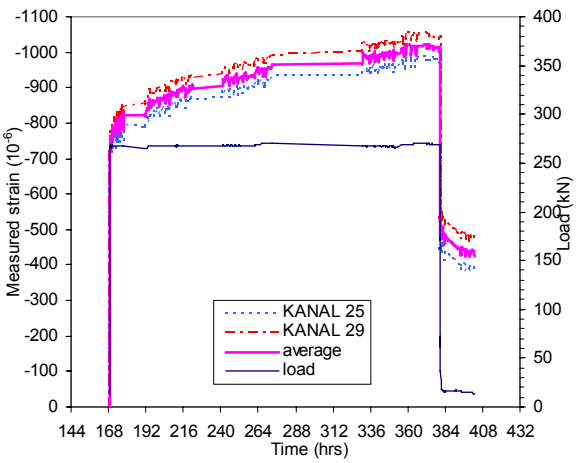

3) Load and measured strain (specimen no.2)

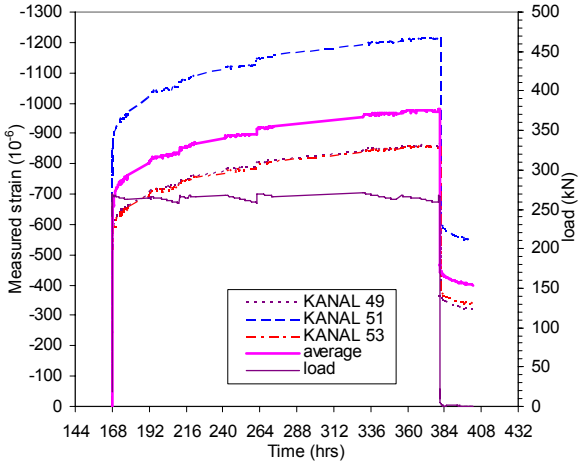

4) Load and measured strain (specimen no.3)

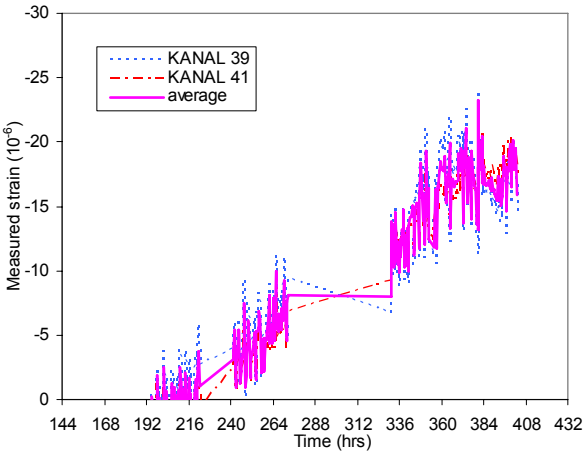

5) Load-independent strain (Dummy specimen)

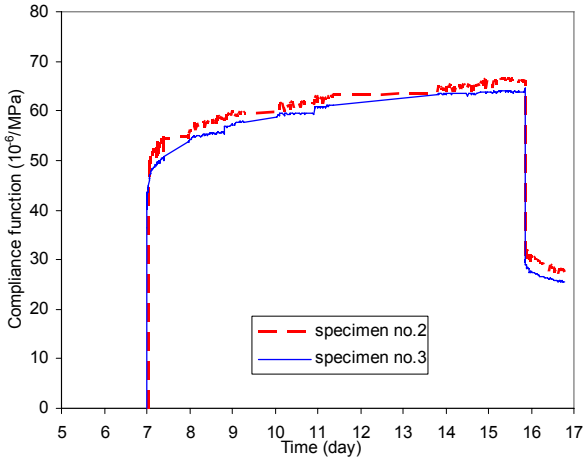

6) Creep compliance

Figure B.8 Compressive creep test on 7-old concrete (reference)

Tensile creep tests

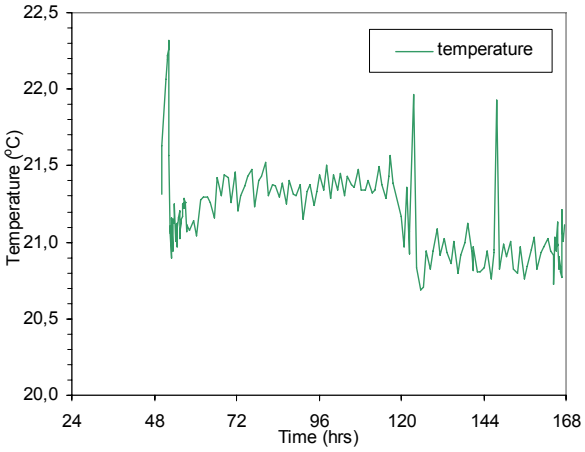

1) Temperature in room

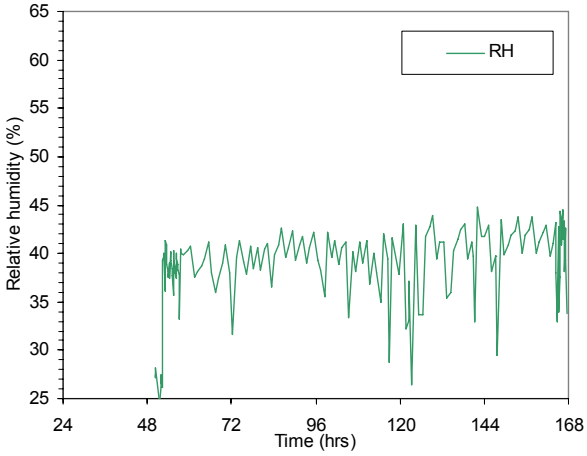

2) Relative humidity in room

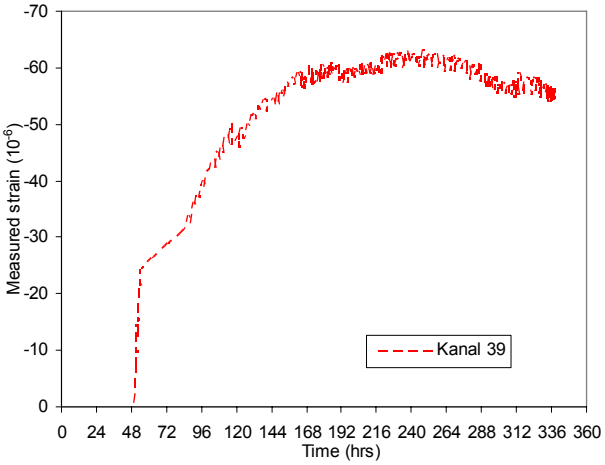

3) Load-independent strain (Dummy specimen)

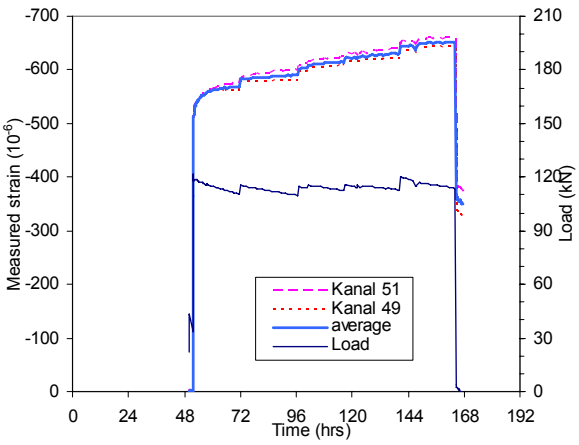

4) Load and measured strain (load at 48 hours)

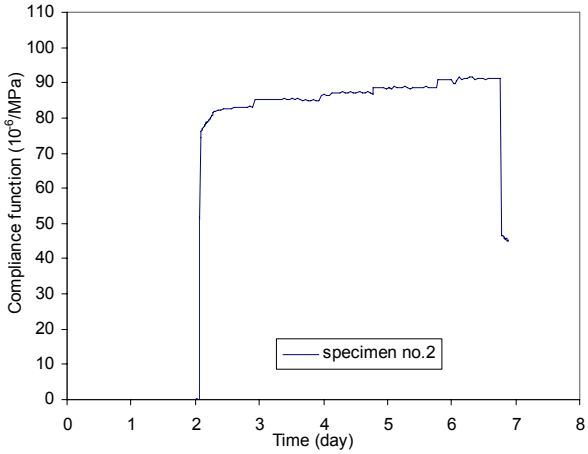

5) Creep compliance

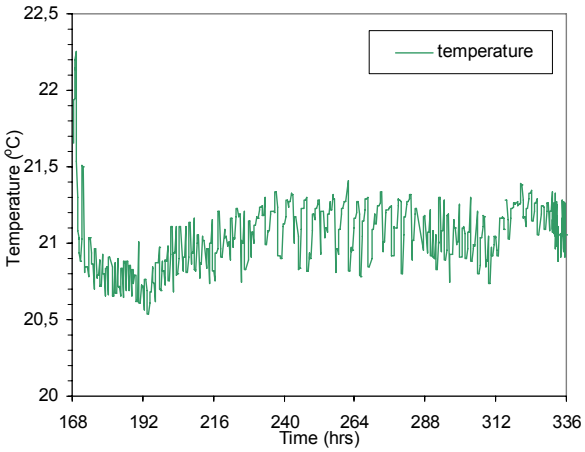

6) Temperature in room

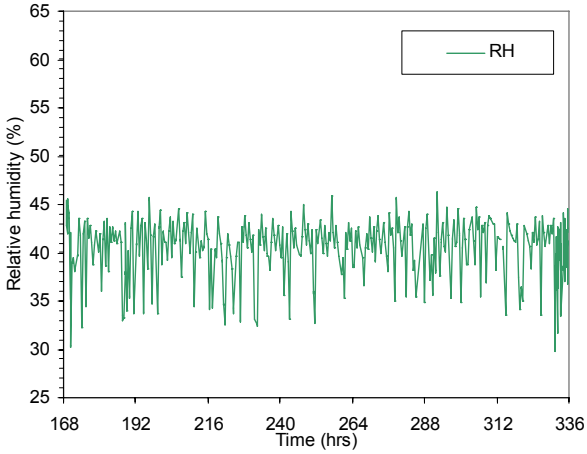

7) Relative humidity in room

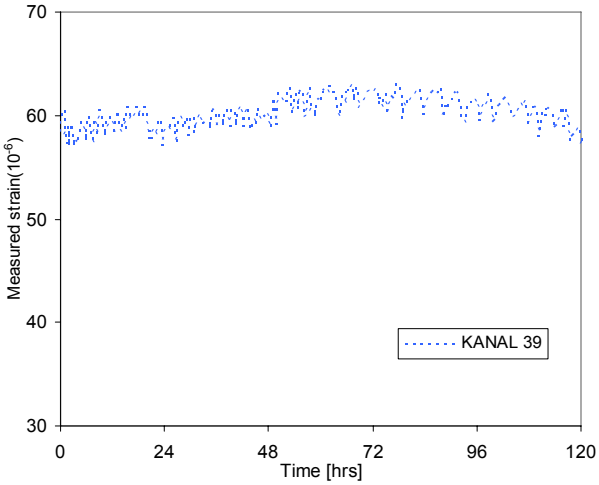

8) Load-independent strain (Dummy specimen)

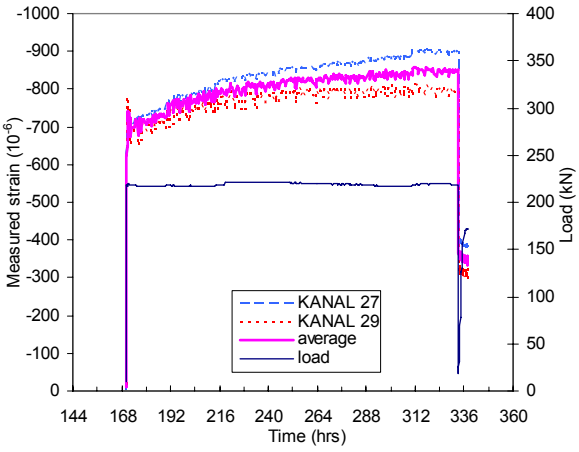

Load and measured strain (load at 168 hours)

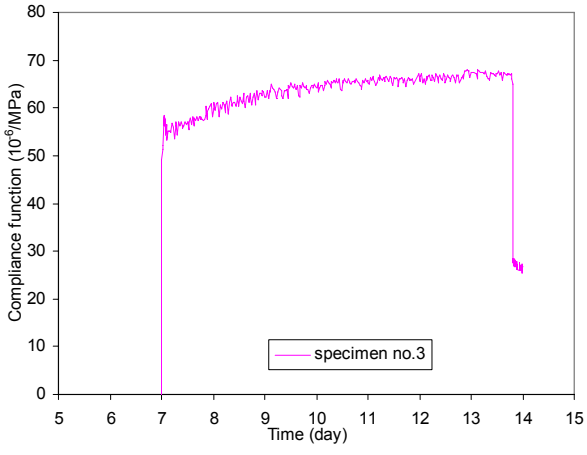

9) 10) Creep compliance

Figure B.9 Tensile creep test on 2 and 7-old concrete (40% BFS)

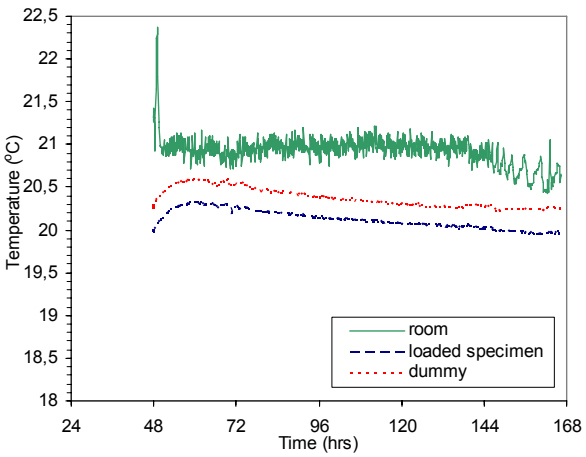

1) Temperature in room

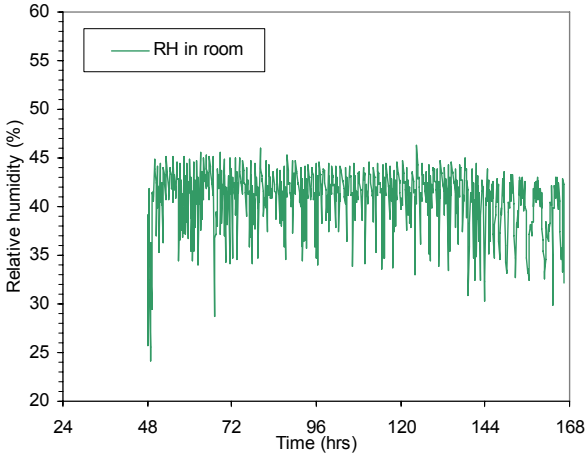

2) Relative humidity in room

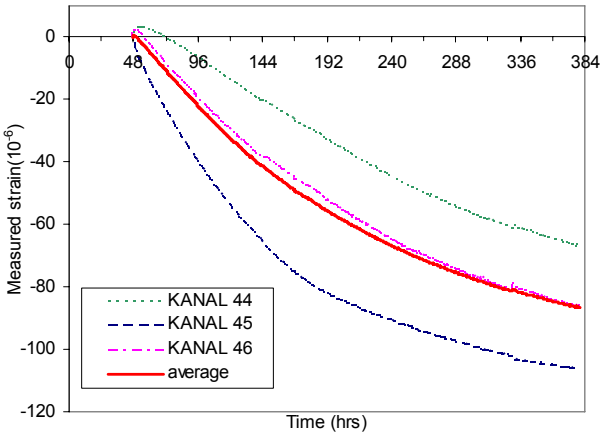

3) Load-independent strain (Dummy specimen)

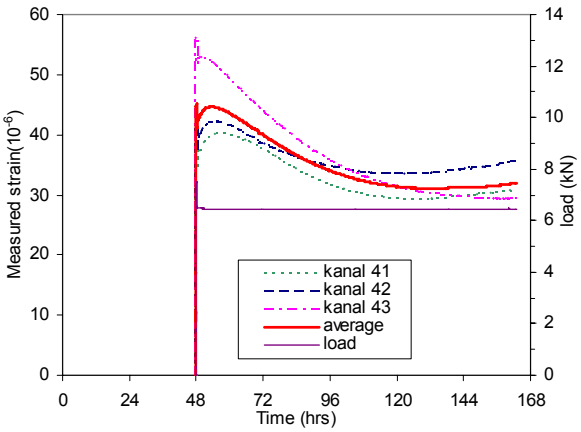

4) Load and measured strain (load at 48 hours)

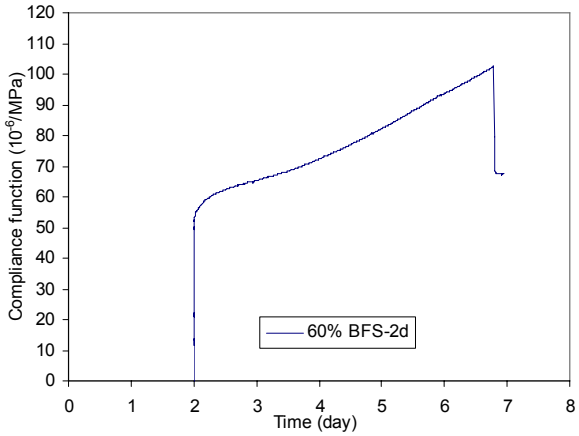

5) Creep compliance

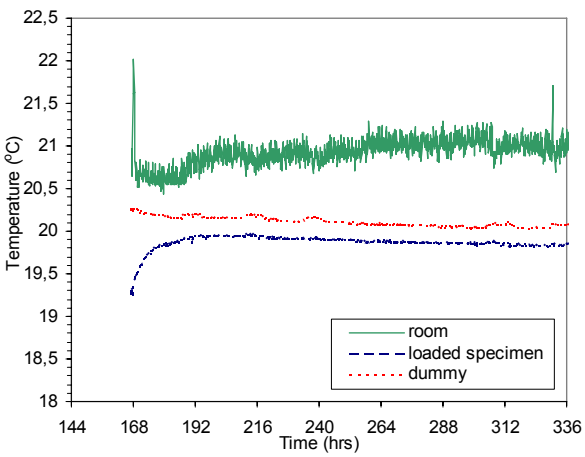

6) Temperature in room

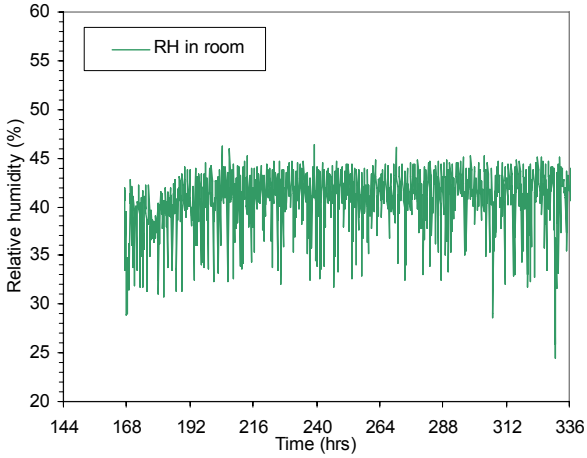

7) Relative humidity in room

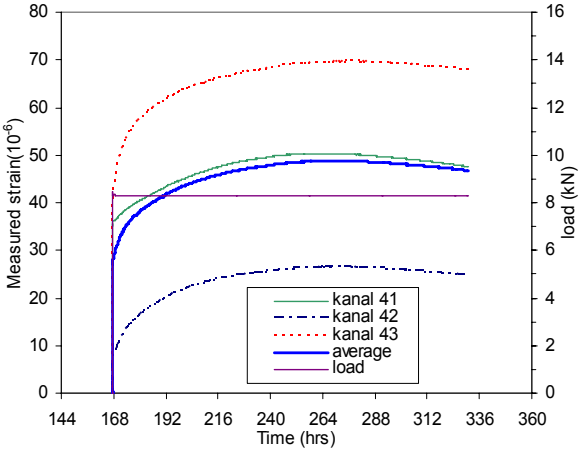

8) Load and measured strain (load at 167 hours)

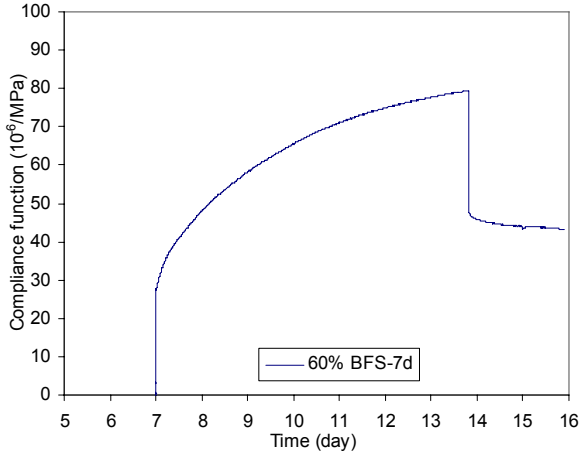

9) Creep compliance

Figure B.10 Tensile creep test on 2 and 7-old concrete (60% BFS)

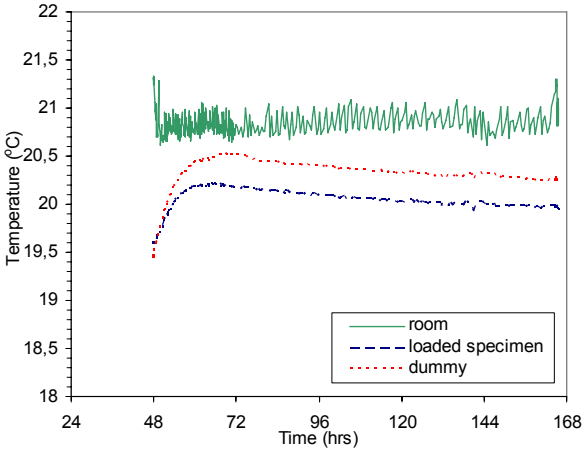

1) Temperature in room

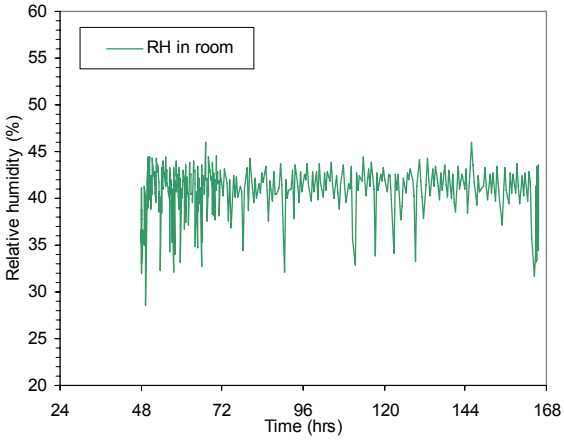

2) Relative humidity in room

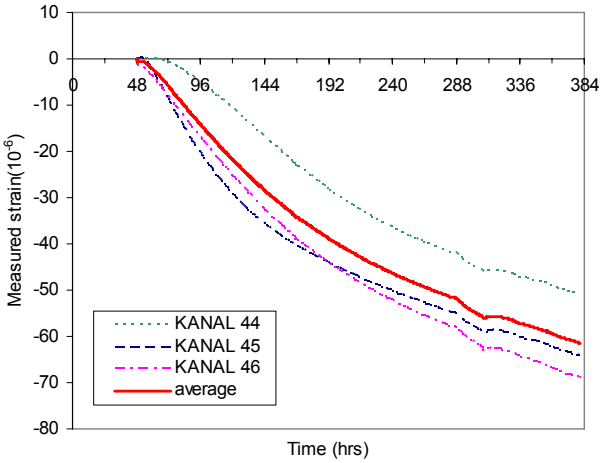

3) Load-independent strain (Dummy specimen)

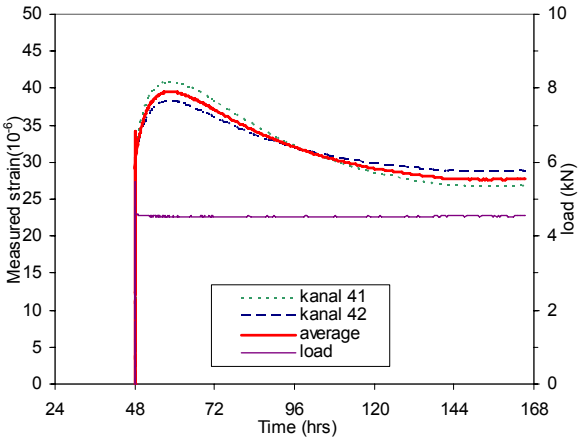

4) Load and measured strain (load at 48 hours)

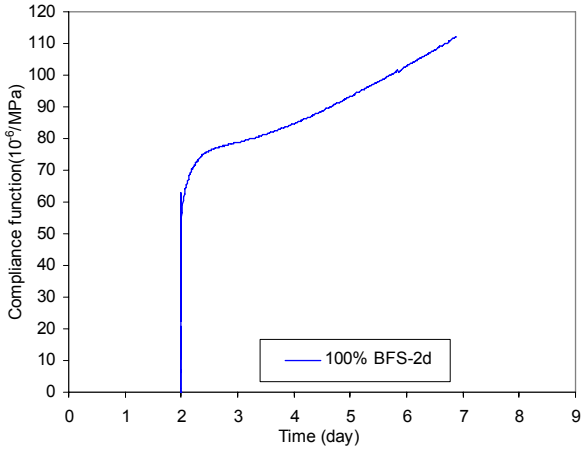

5) Creep compliance

Figure B.11 Tensile creep test on 2 old concrete (100% BFS)

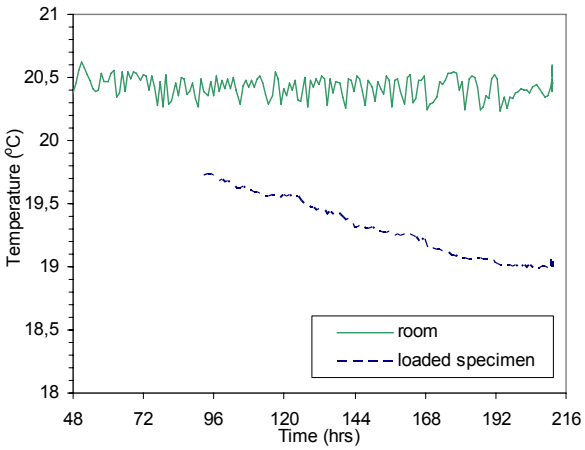

1) Temperature in room

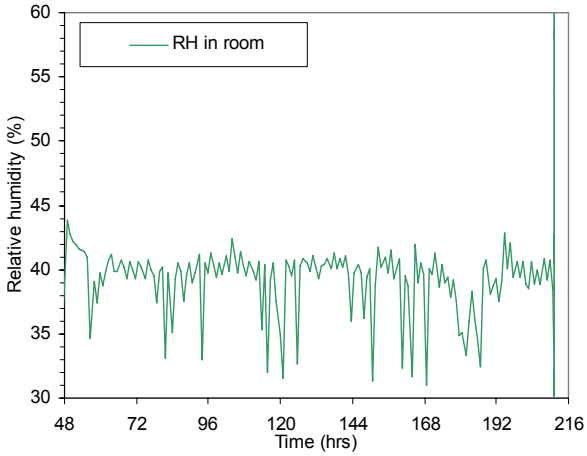

2) Relative humidity in room

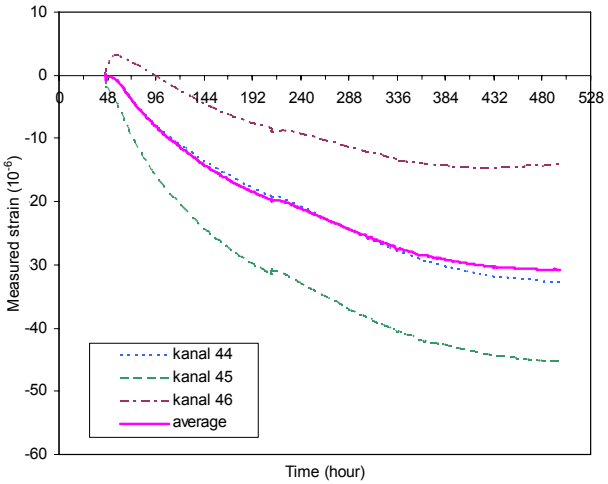

3) Load-independent strain (Dummy specimen)

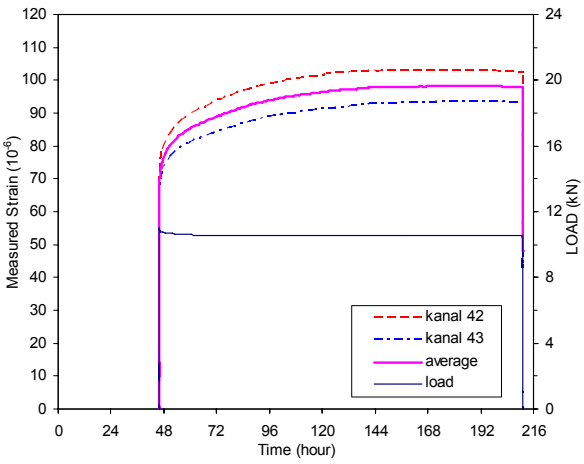

4) Load and measured strain (load at 46 hours)

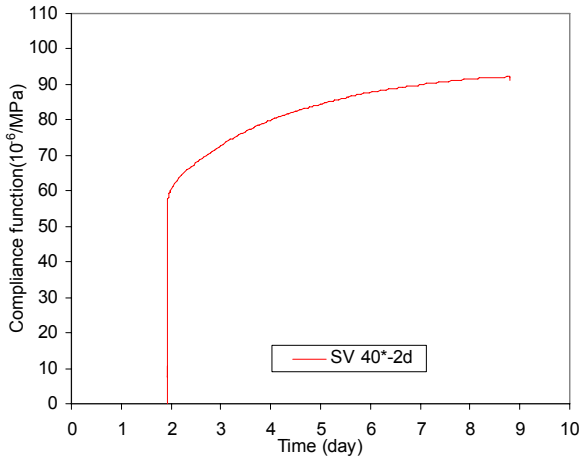

5) Creep compliance

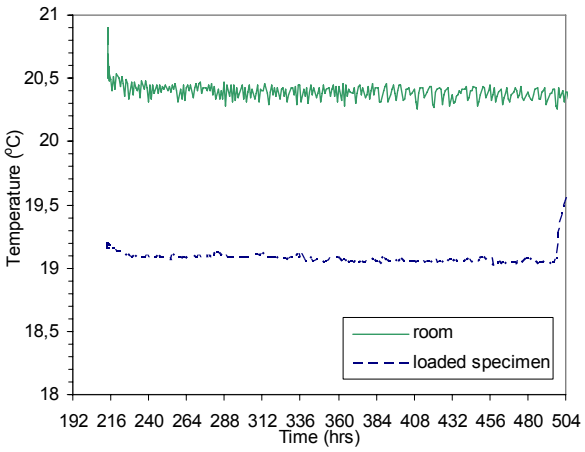

6) Temperature in room

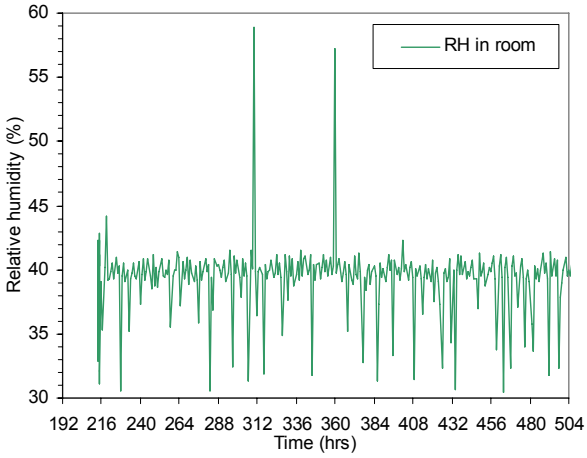

7) Relative humidity in room

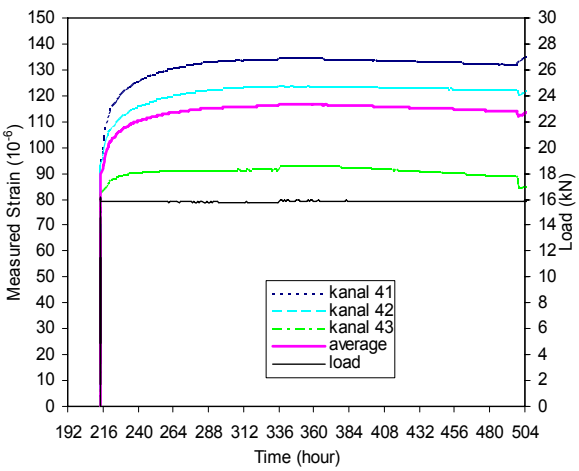

8) Load and measured strain (load at 214 hours)

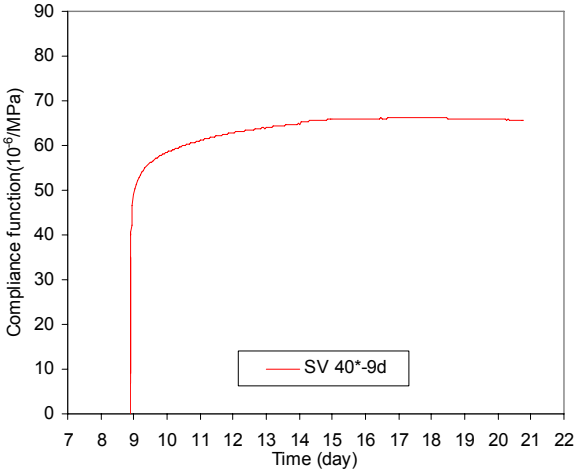

9) Creep compliance

Figure B.12 Tensile creep test on 2 and 7-old concrete (SV 40*)

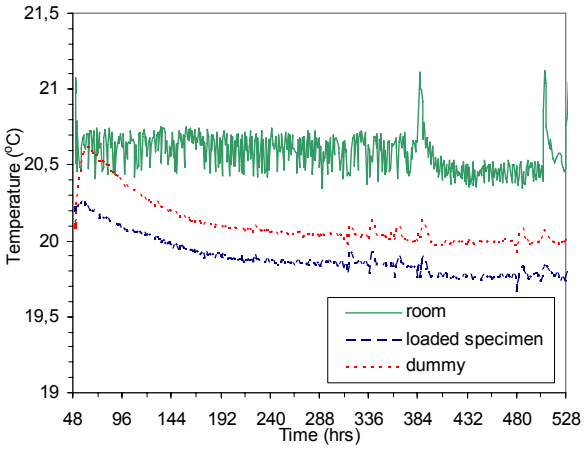

1) Temperature in room

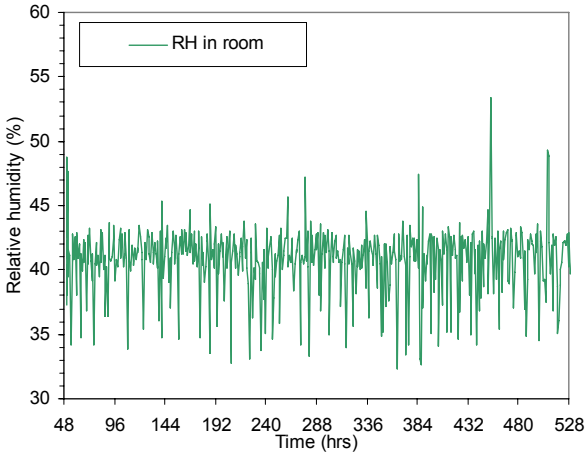

2) Relative humidity in room

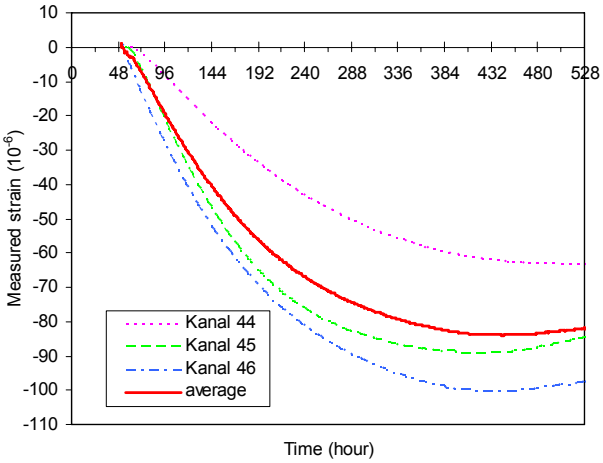

3) Load-independent strain (Dummy specimen)

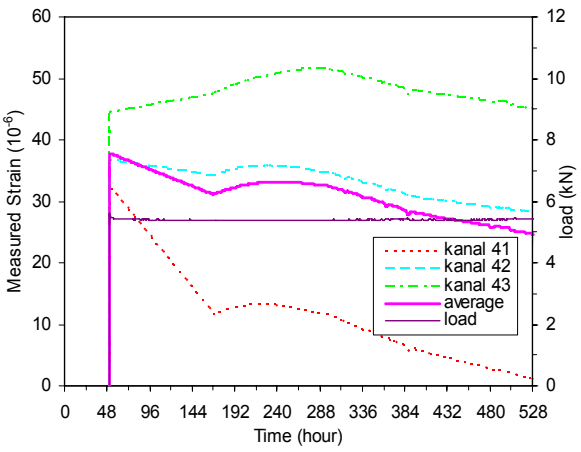

5) Load and measured strain (load at 51 hours)

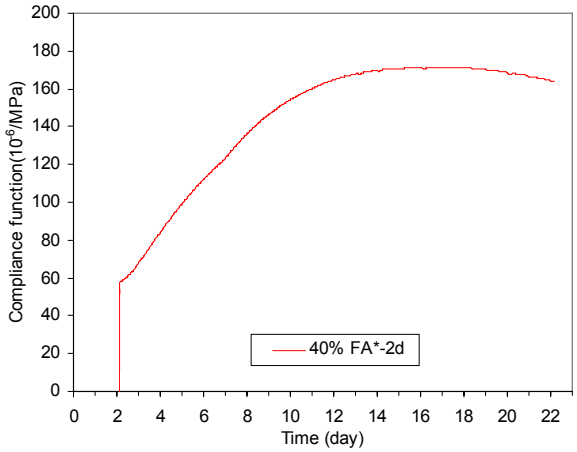

6) Creep compliance

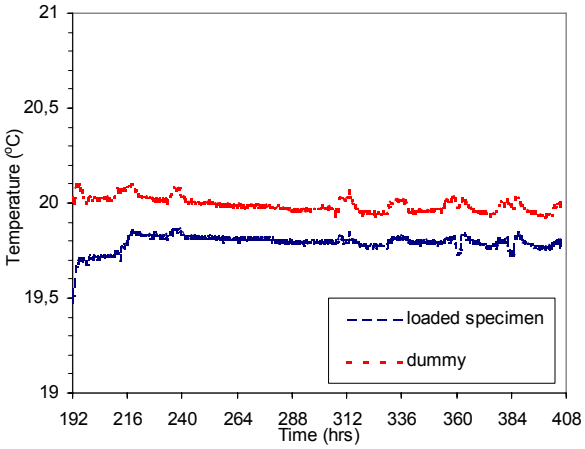

7) Temperature in room

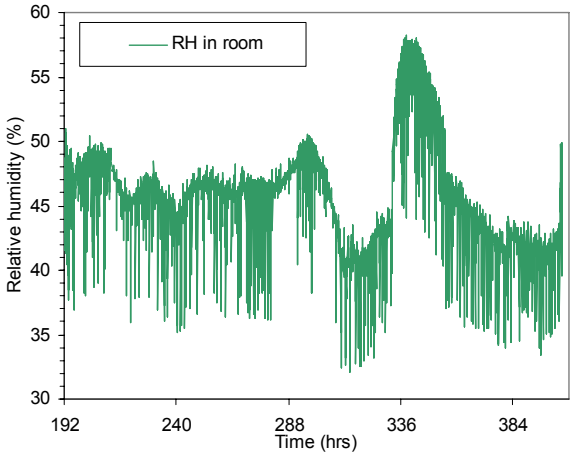

8) Relative humidity in room

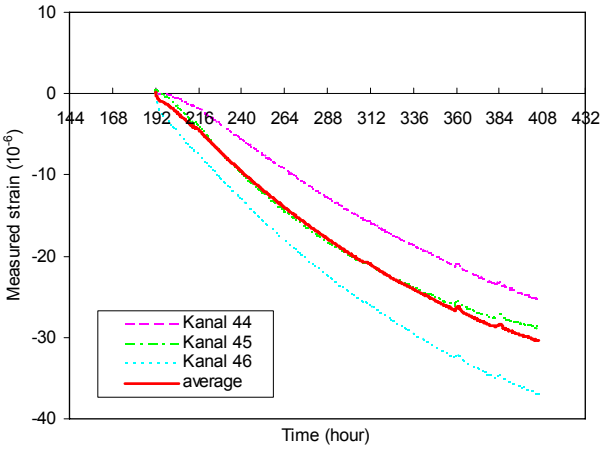

9) Load-independent strain (Dummy specimen)

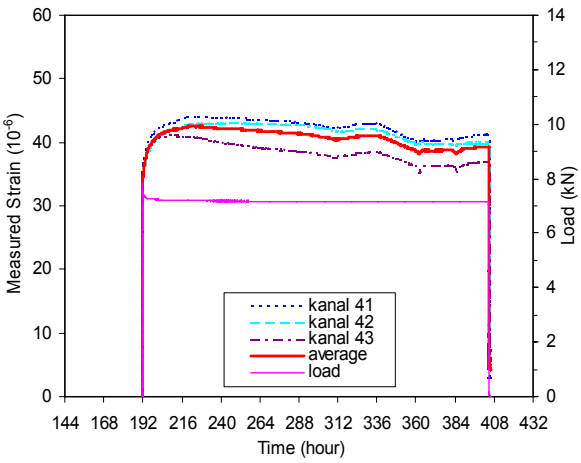

Load and measured strain (load at 192 hours)

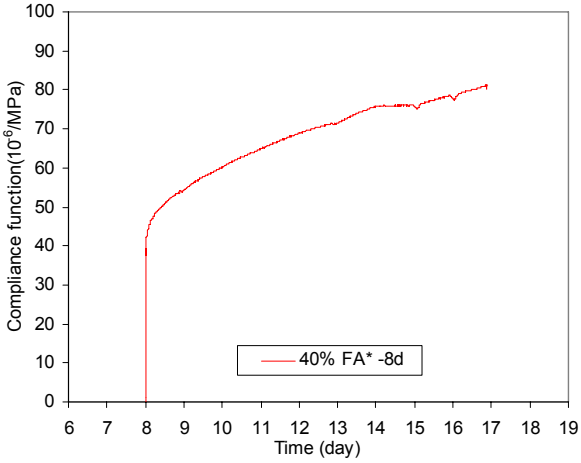

10) 11) Creep compliance

Figure B.13 Tensile creep test on 2 and 8-old concrete (40% FA*)

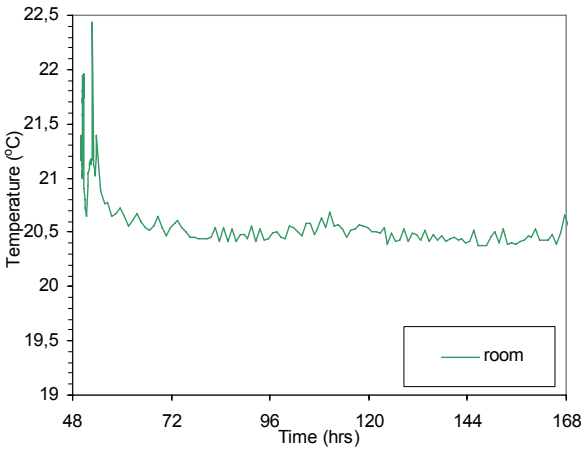

1) Temperature in room

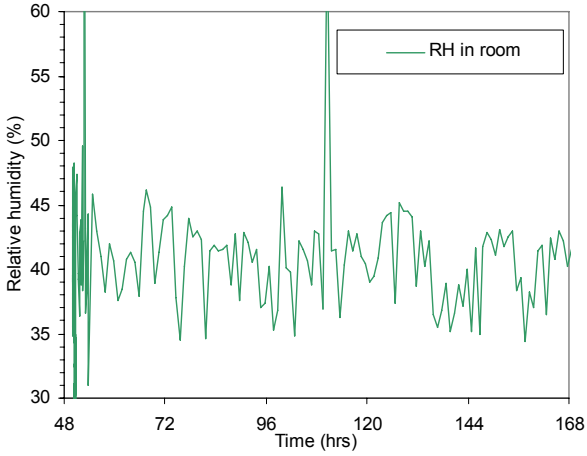

2) Relative humidity in room

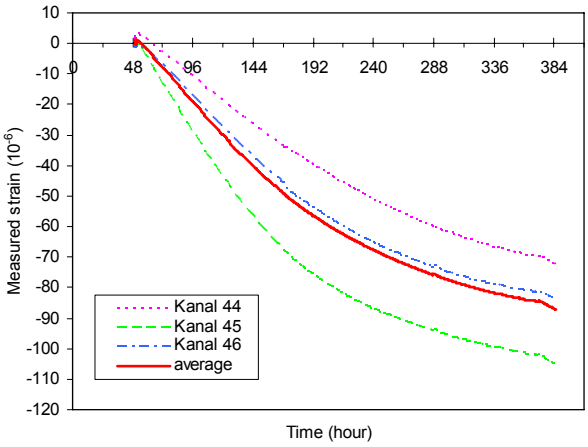

3) Load-independent strain (Dummy specimen)

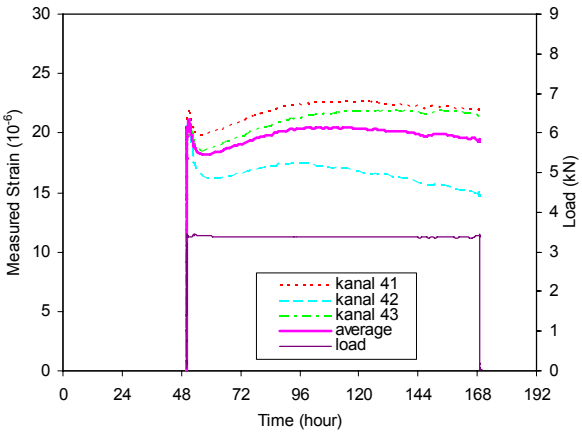

4) Load and measured strain (load at 51 hours)

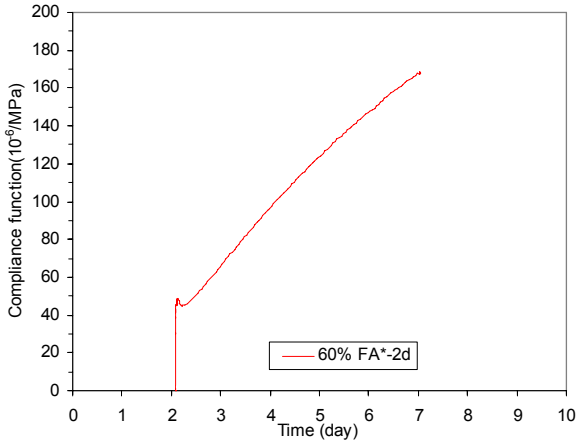

5) Creep compliance

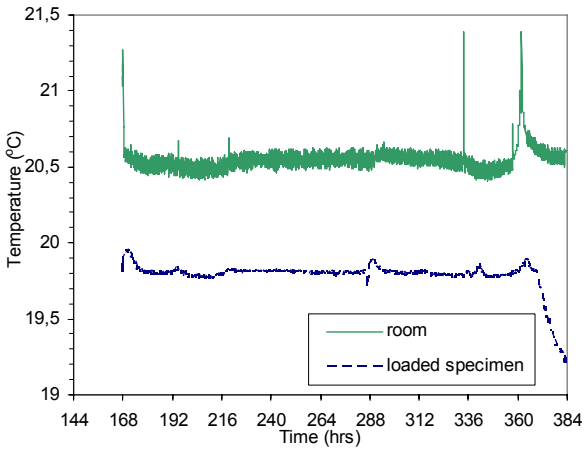

6) Temperature in room

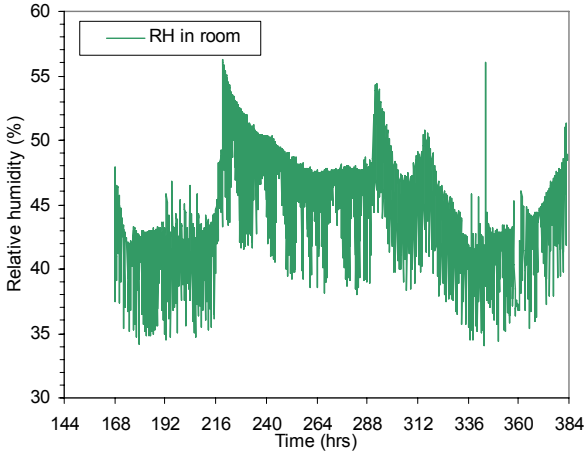

7) Relative humidity in room

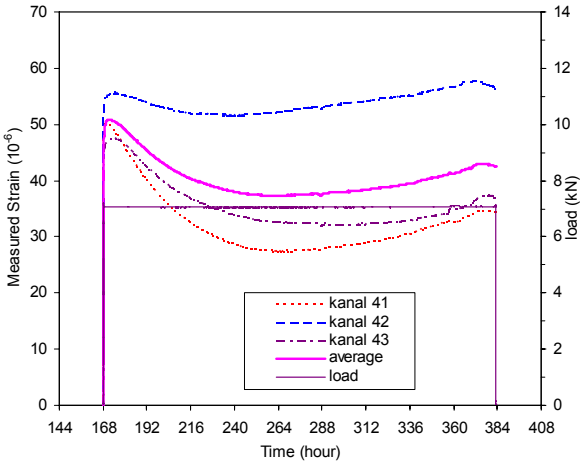

8) Load and measured strain (load at 168 hours)

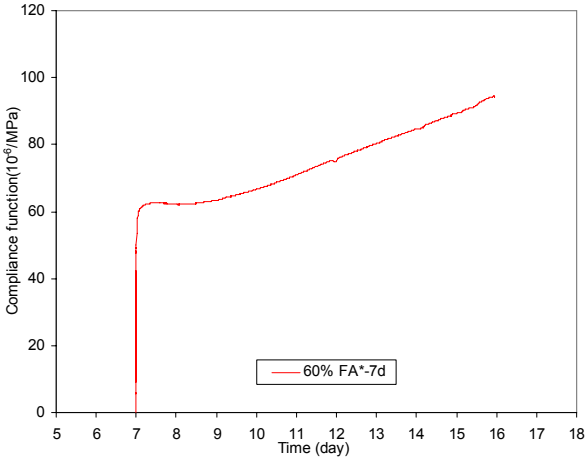

9) Creep compliance

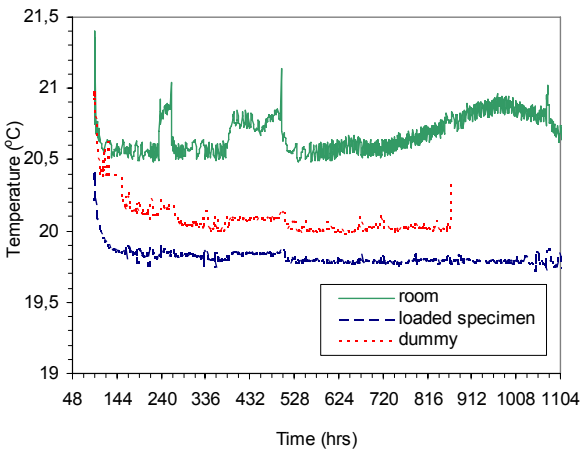

10) Temperature in room

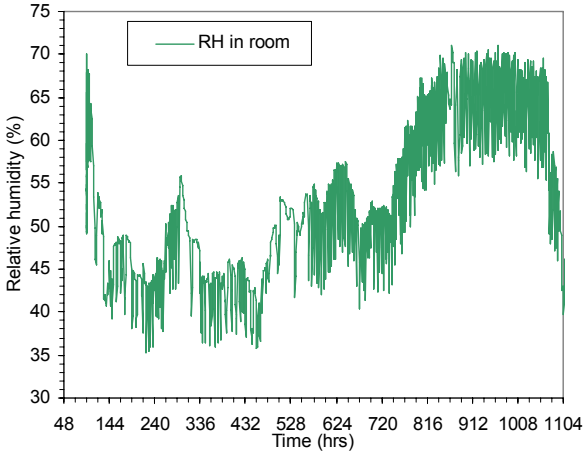

11) Relative humidity in room

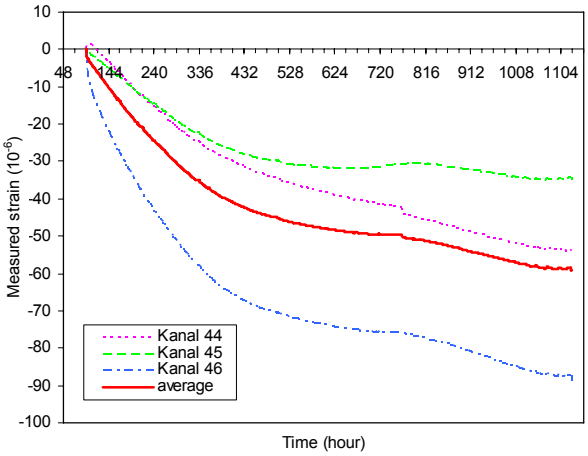

12) Load-independent strain (Dummy specimen)

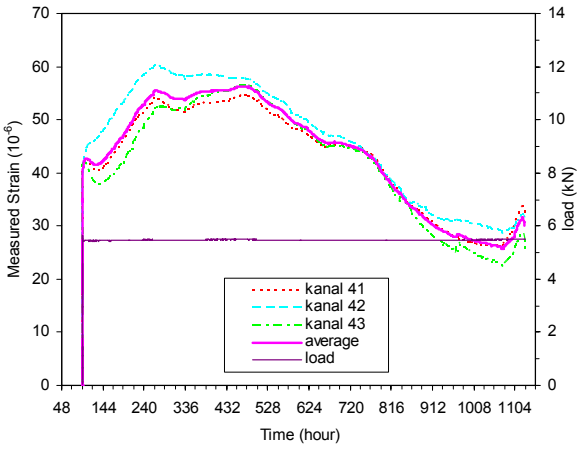

Load and measured strain (load at 96 hours)

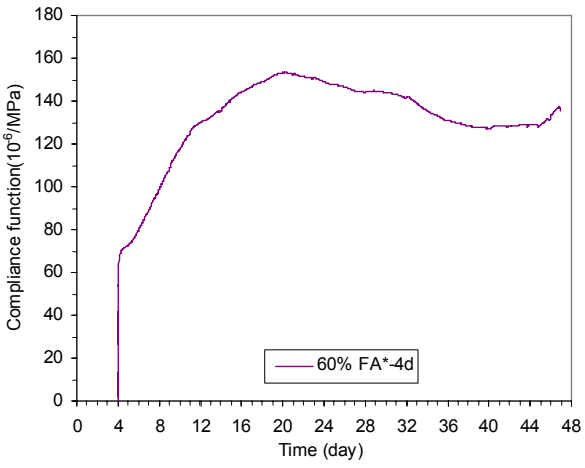

13) 14) Creep compliance

Figure B.14 Tensile creep test on 2, 4 and 7-old concrete (60% FA*)

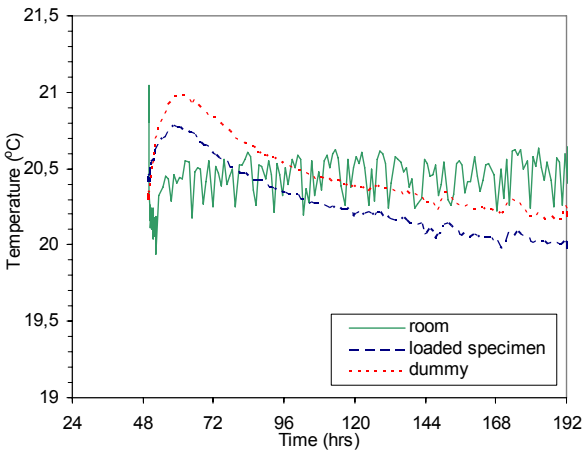

1) Temperature in room

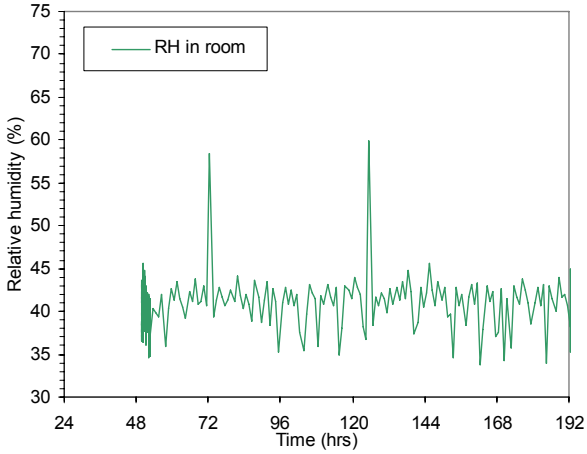

2) Relative humidity in room

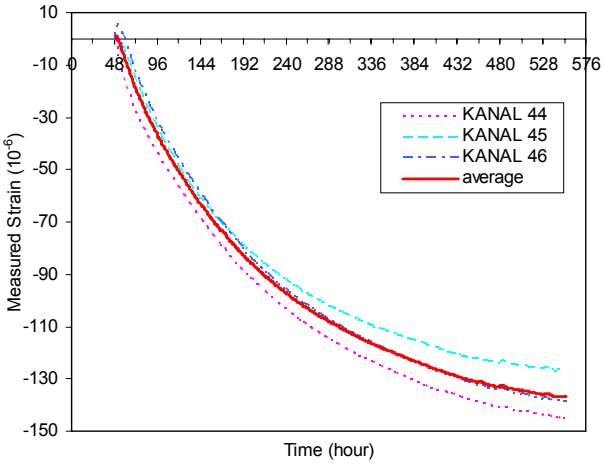

3) Load-independent strain (Dummy specimen)

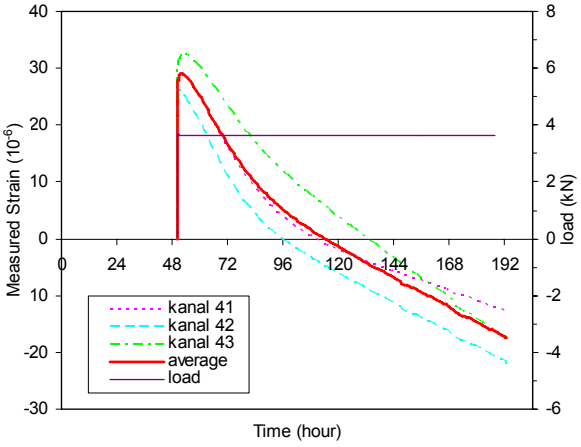

4) Load and measured strain (load at 54 hours)

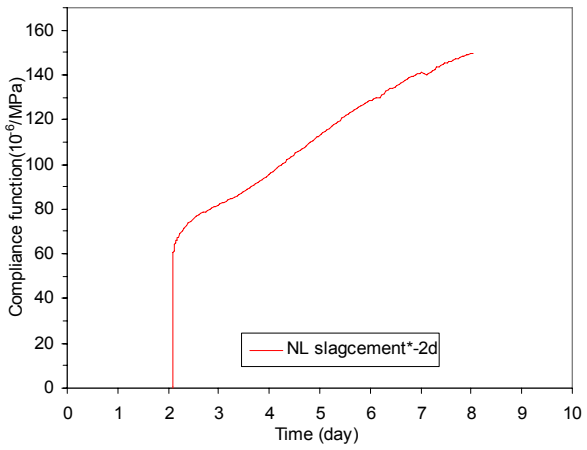

5) Creep compliance

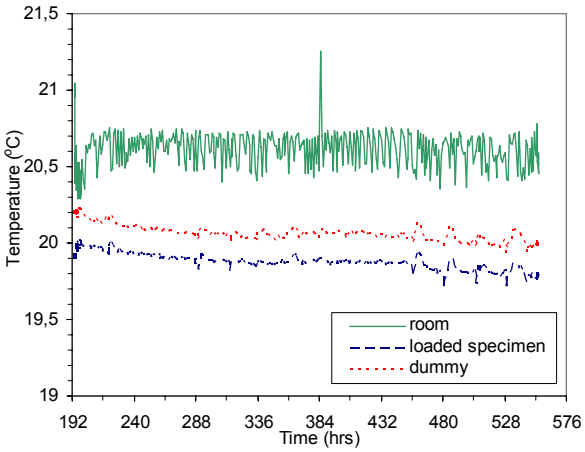

6) Temperature in room

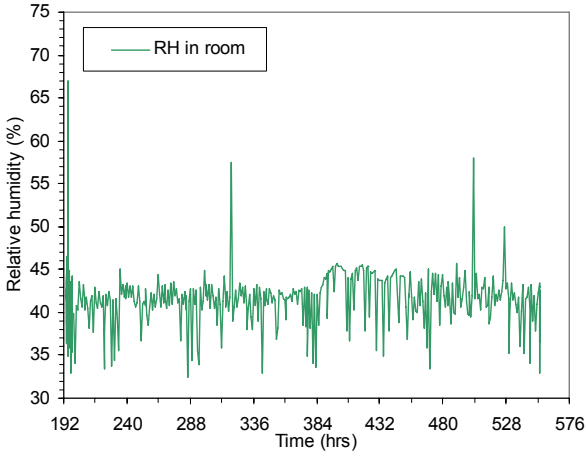

7) Relative humidity in room

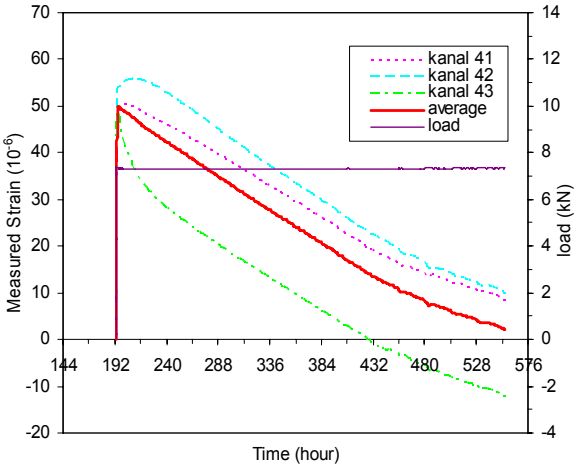

8) Load and measured strain (load at 194 hours)

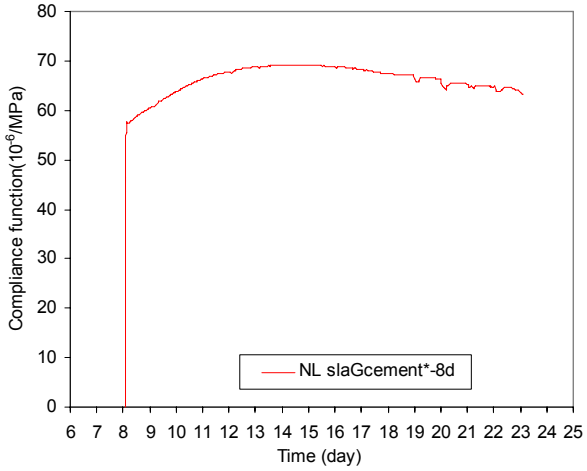

9) Creep compliance

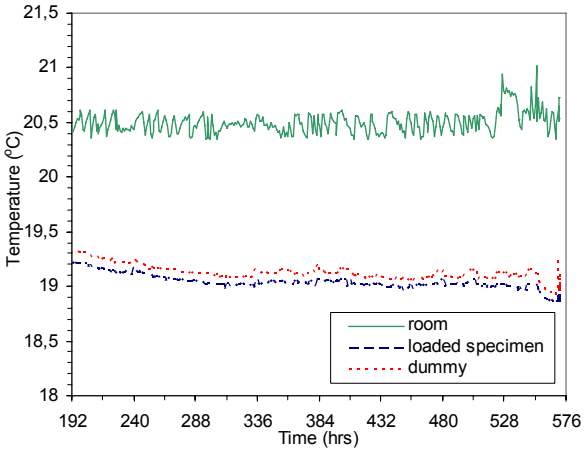

10) Temperature in room

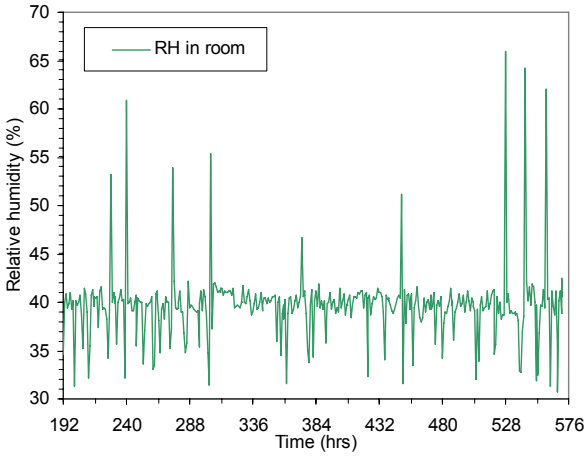

11) Relative humidity in room

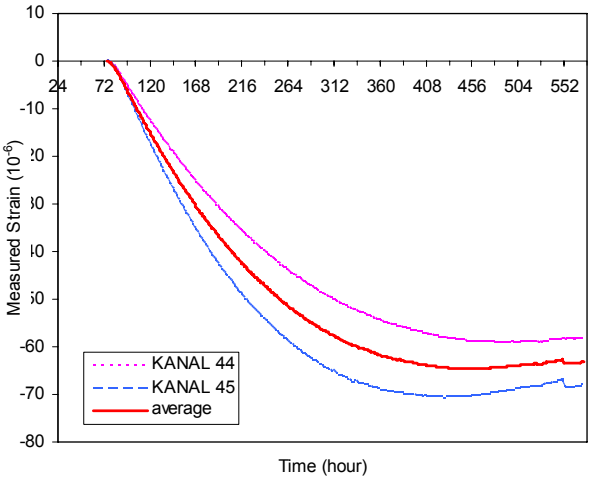

12) Load-independent strain (Dummy specimen)

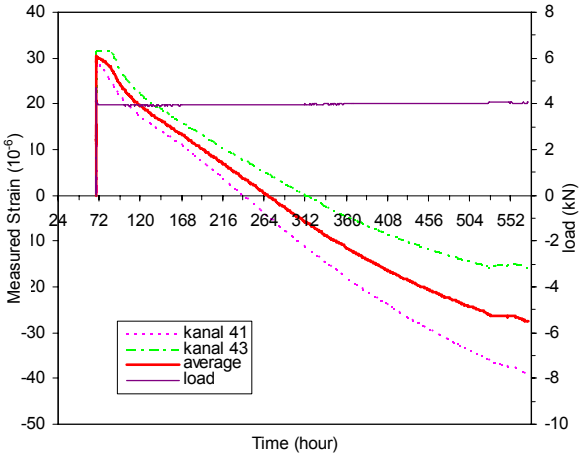

13) Load and measured strain (load at 69 hours)

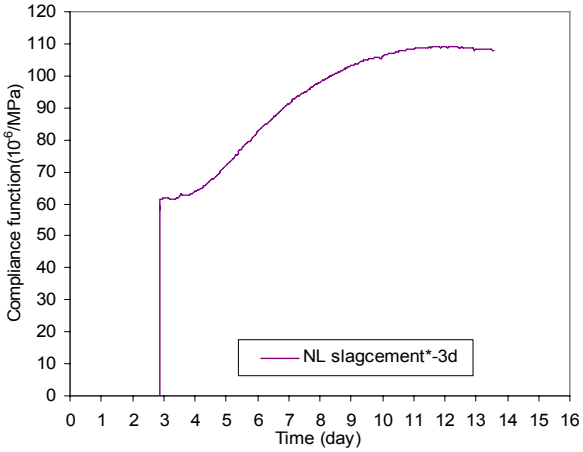

14) Creep compliance

Figure B.15 Tensile creep test on 2, 3 and 8-old concrete (NL slag*)

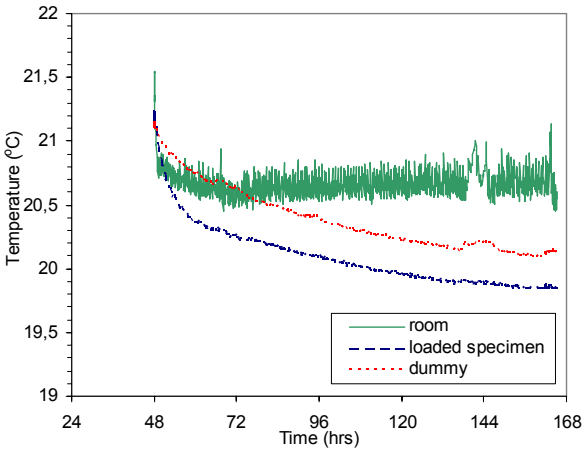

1) Temperature in room

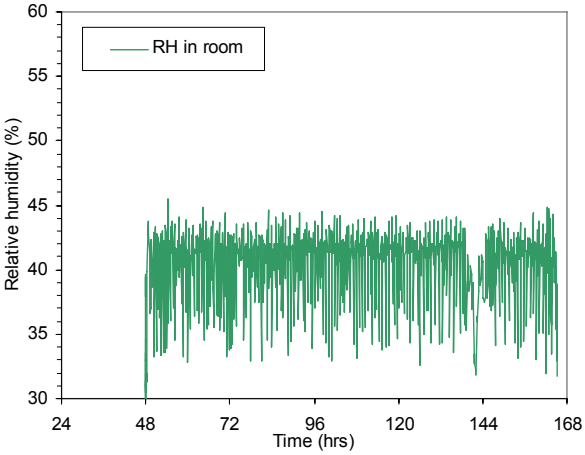

2) Relative humidity in room

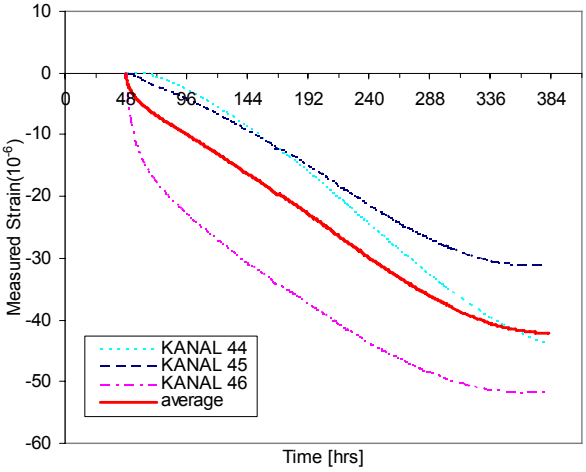

3) Load-independent strain (Dummy specimen)

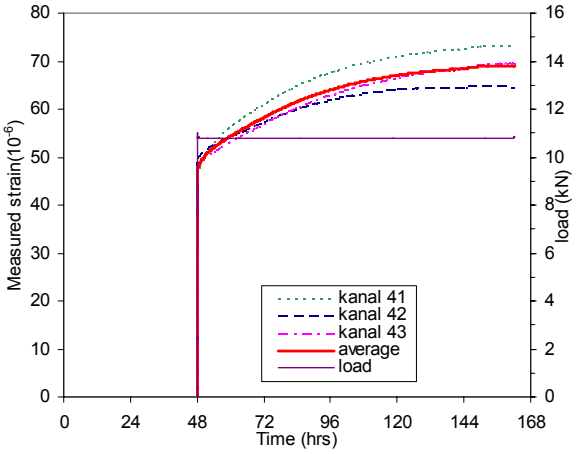

4) Load and measured strain (load at 48 hours)

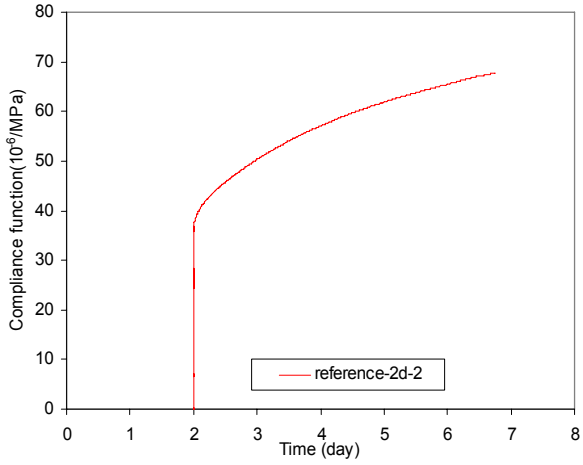

5) Creep compliance

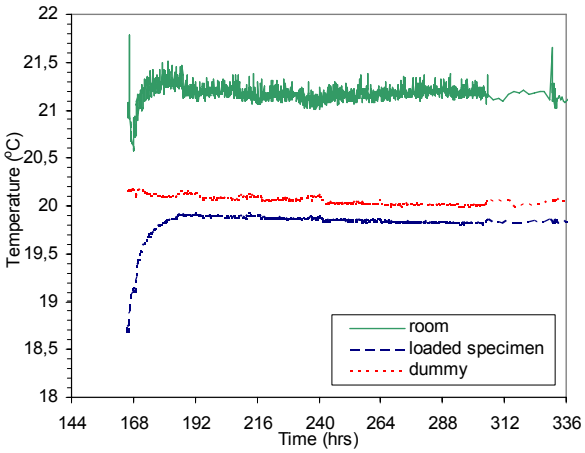

6) Temperature in room

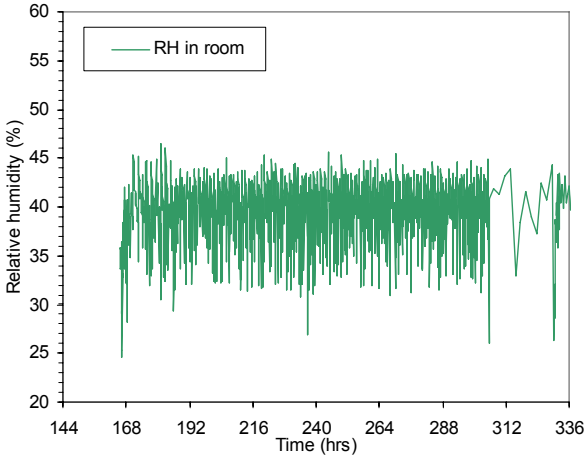

7) Relative humidity in room

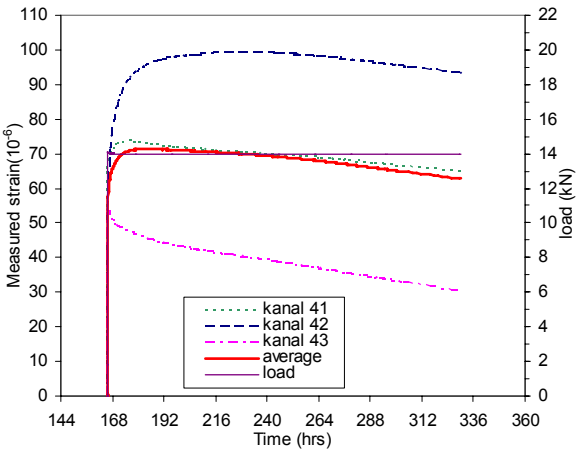

Load and measured strain (load at 166 hours)

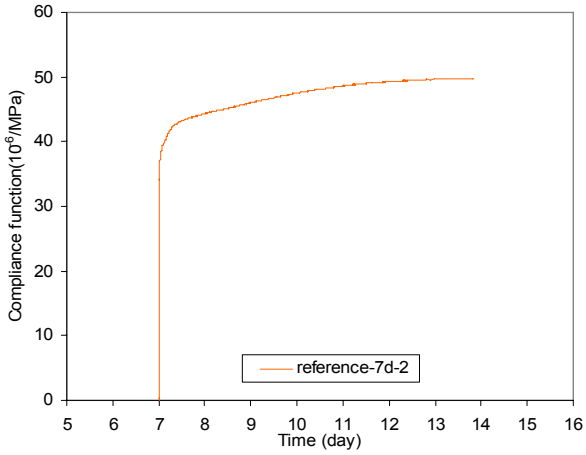

8) 9) Creep compliance

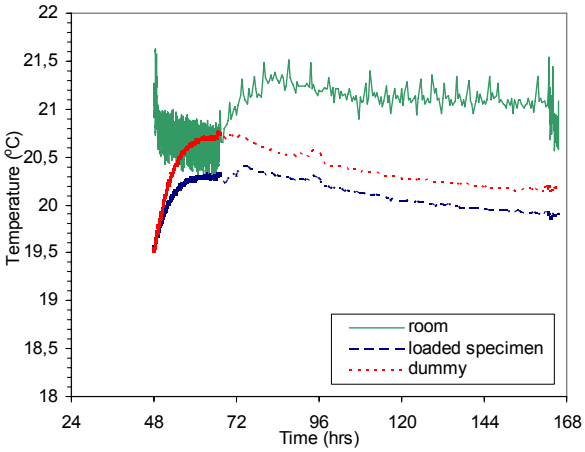

10) Temperature in room

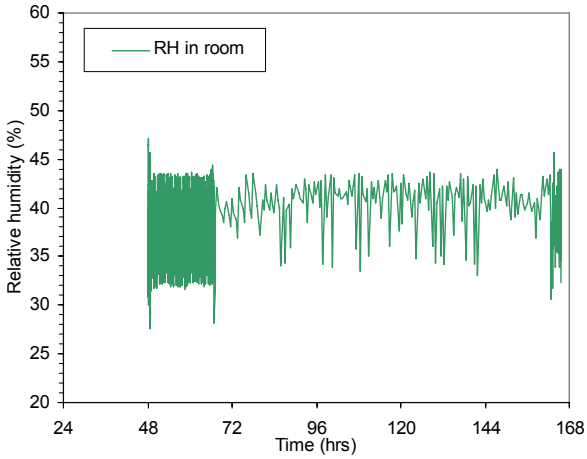

11) Relative humidity in room

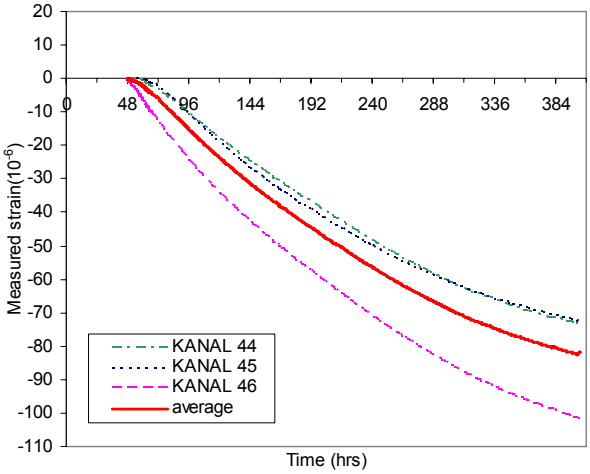

12) Load-independent strain (Dummy specimen)

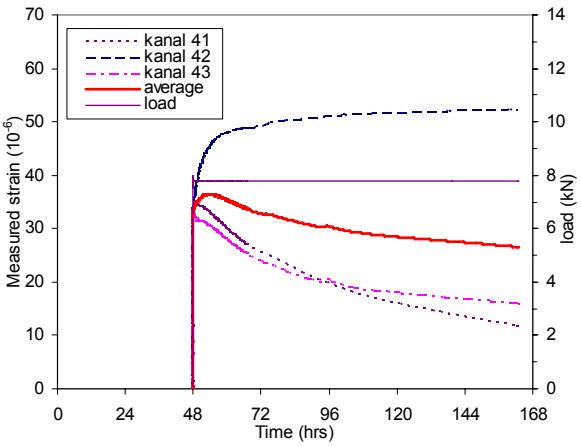

13) Load and measured strain (load at 48 hours)

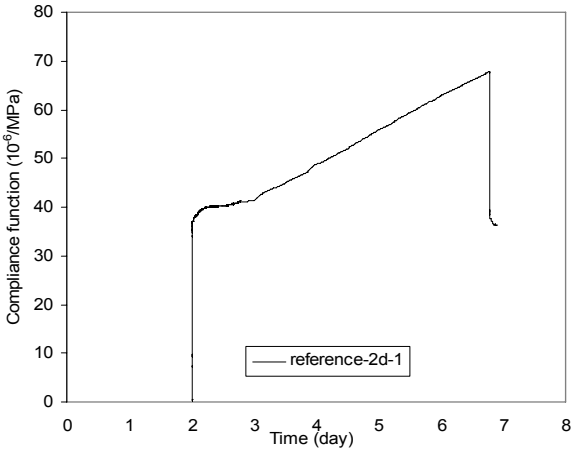

14) Creep compliance

Figure B.16 Tensile creep test on 2 and 7-old concrete (Reference)

Appendix C: Test results of Dilation Rig and TSTM

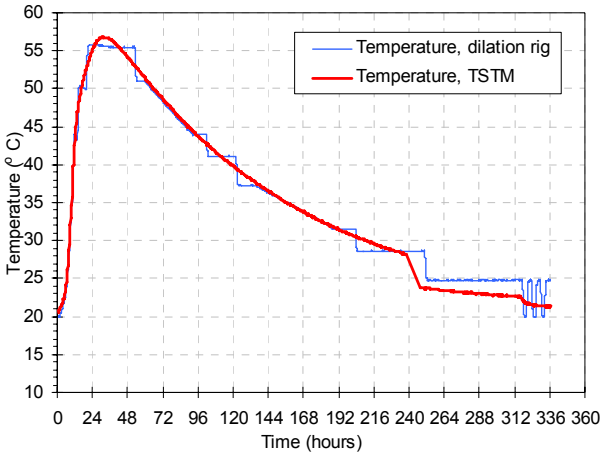

a) Temperature in dilation rig and TSTM

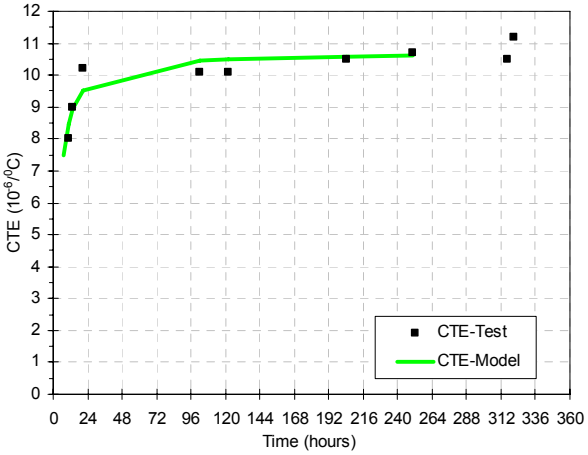

b) Calculated CTE and model

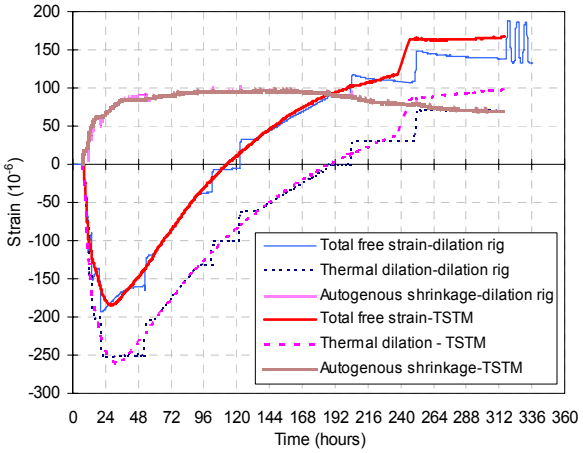

c) Separation of TD and AD

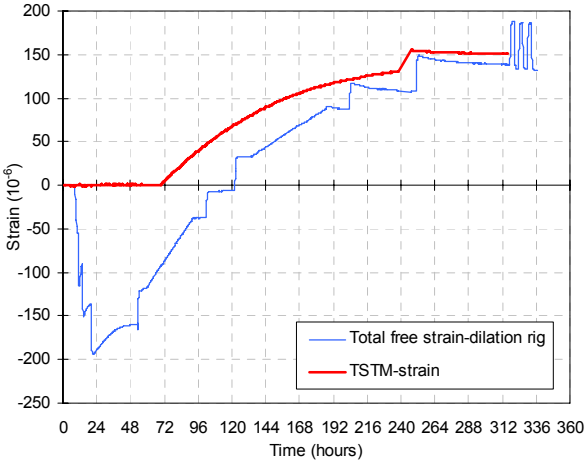

d) Measured strain in dilation rig and TSTM

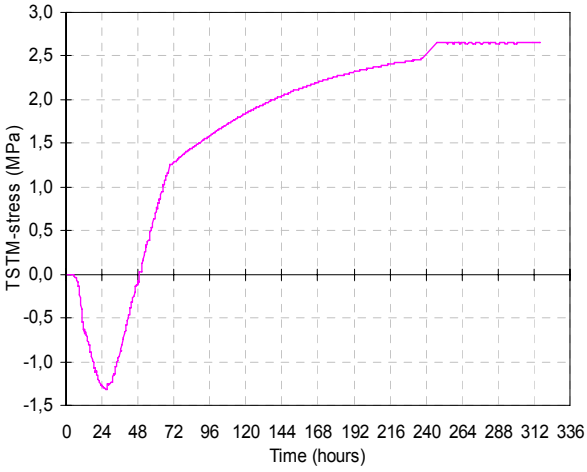

e) Restraint stress in TSTM

Figure C.1 Volume change and restraint stress (Reference concrete)

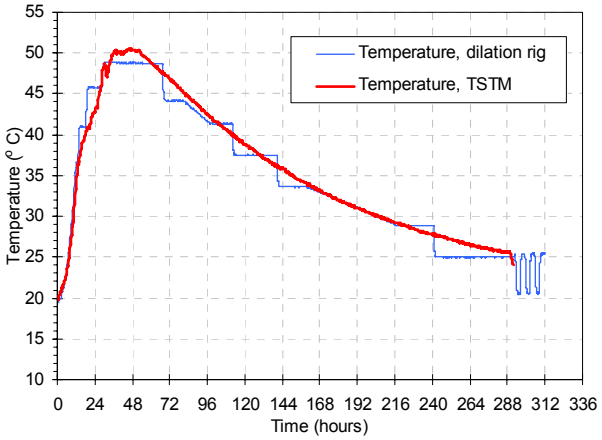

a) Temperature in dilation rig and TSTM

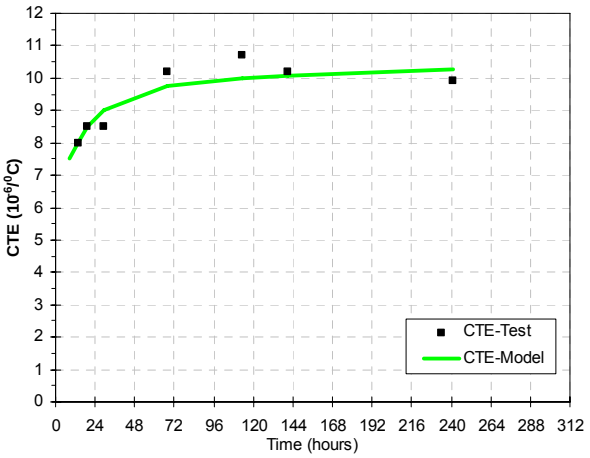

b) Calculated CTE and model

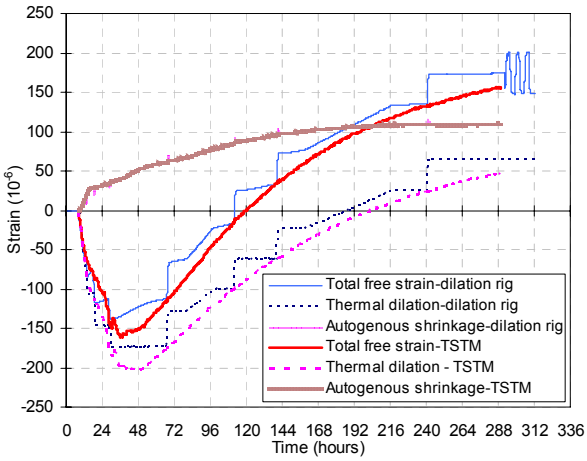

c) Separation of TD and AD

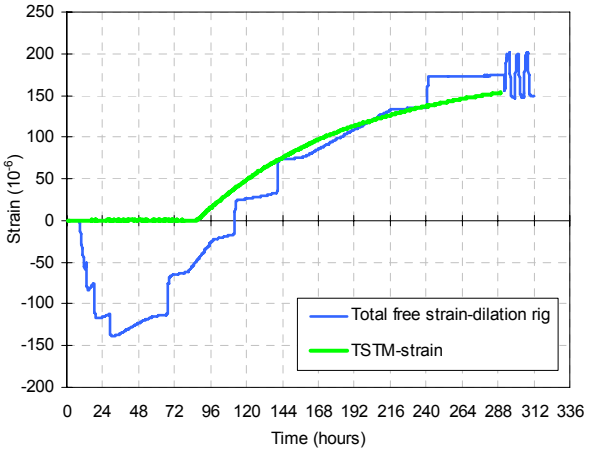

d) Measured strain in dilation rig and TSTM

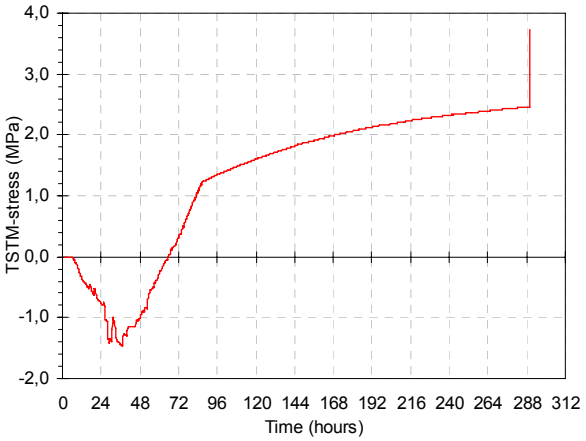

e) Restraint stress in TSTM

Figure C.2 Volume change and restraint stress (40% BFS)

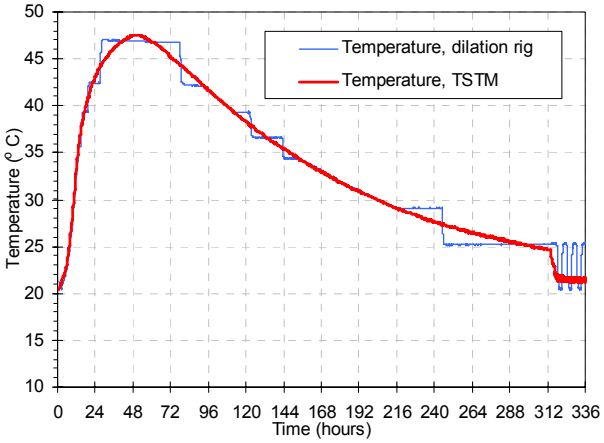

a) Temperature in dilation rig and TSTM

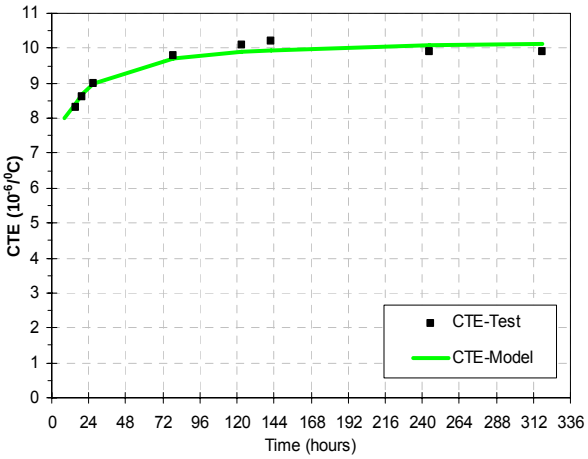

b) Calculated CTE and model

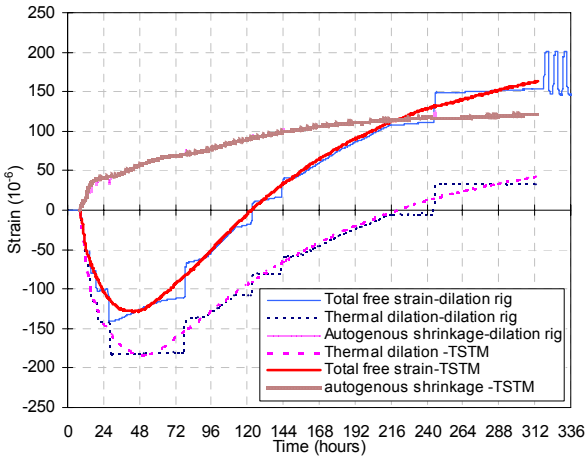

c) Separation of TD and AD

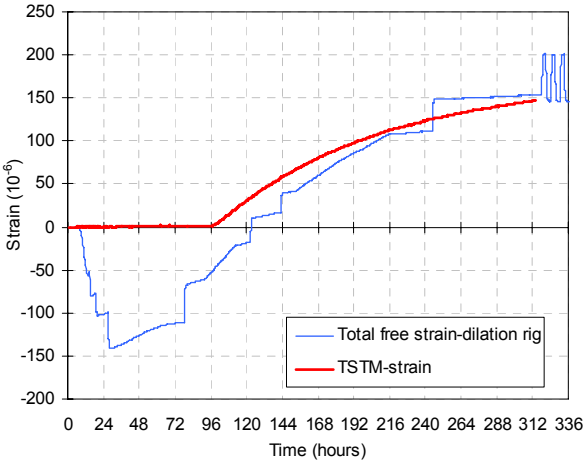

d) Measured strain in dilation rig and TSTM

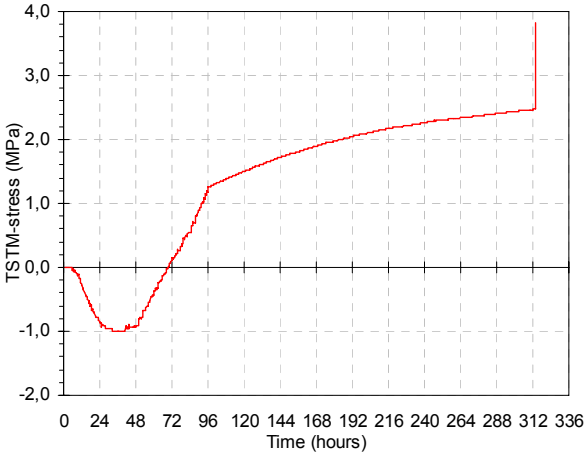

e) Restraint stress in TSTM

Figure C.3 Volume change and restraint stress (60% BFS)

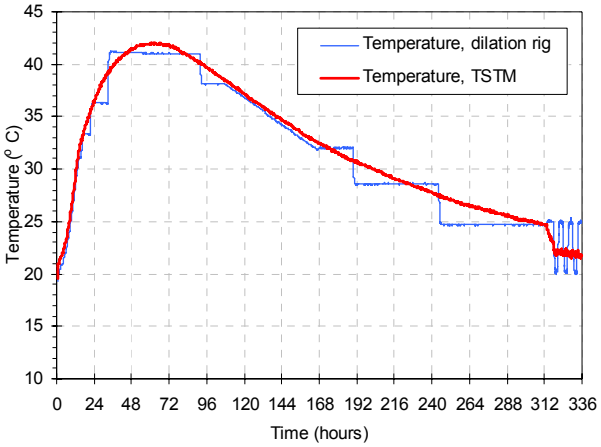

a) Temperature in dilation rig and TSTM

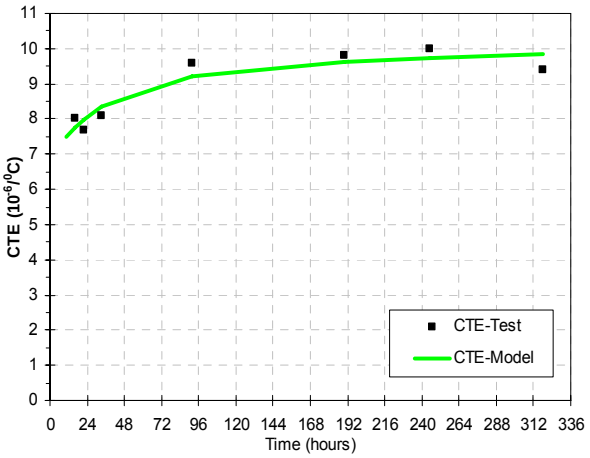

b) Calculated CTE and model

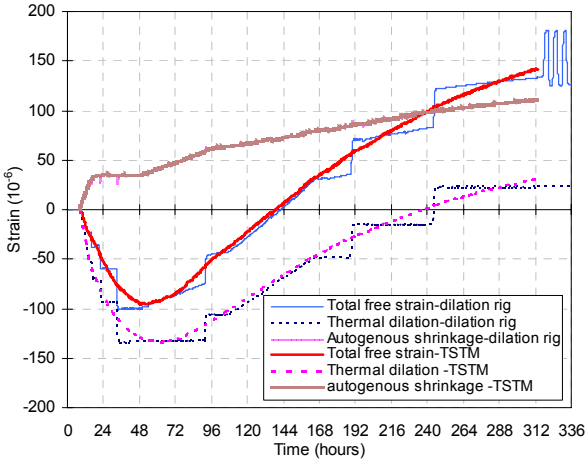

c) Separation of TD and AD

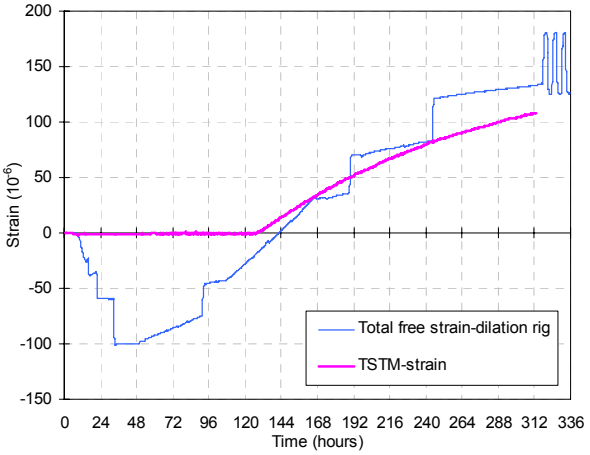

d) Measured strain in dilation rig and TSTM

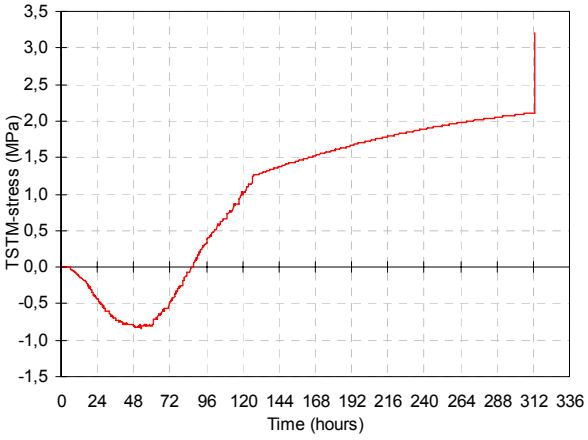

e) Restraint stress in TSTM

Figure C.4 Volume change and restraint stress (100% BFS)

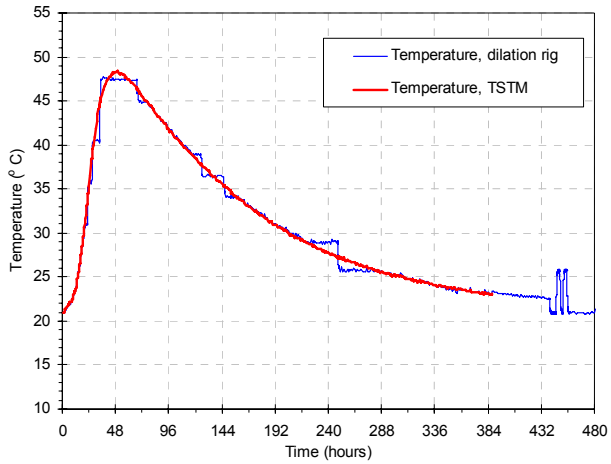

a) Temperature in dilation rig and TSTM

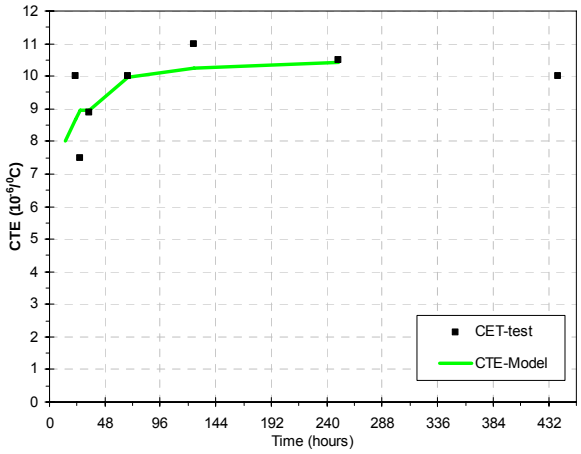

b) Calculated CTE and model

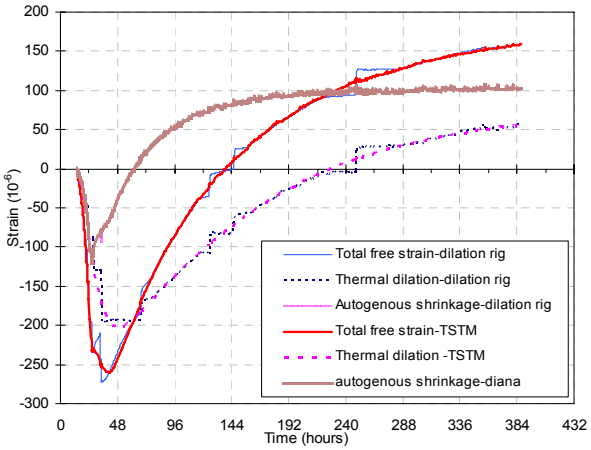

c) Separation of TD and AD

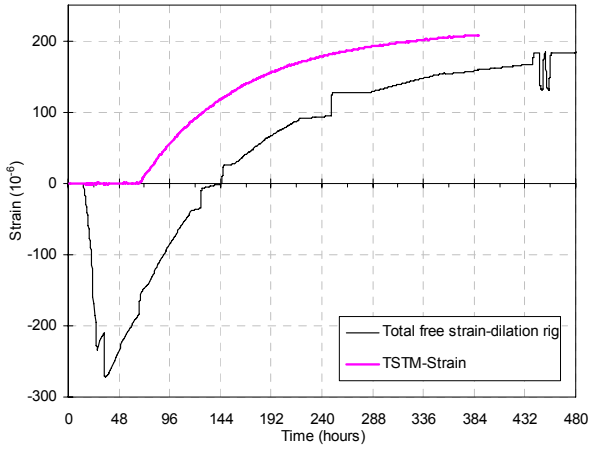

d) Measured strain in dilation rig and TSTM

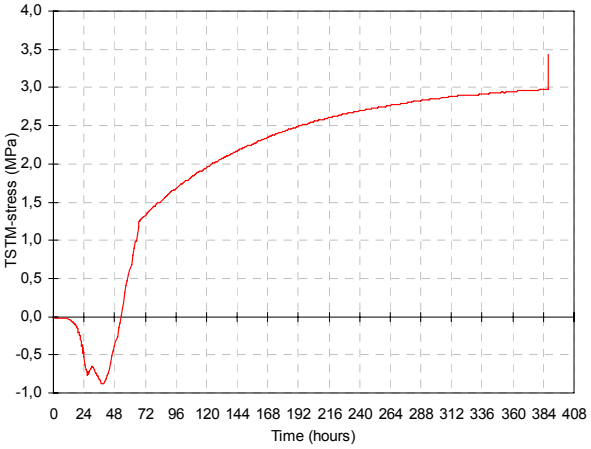

e) Restraint stress in TSTM

Figure C.5 Volume change and restraint stress (NL slag*)

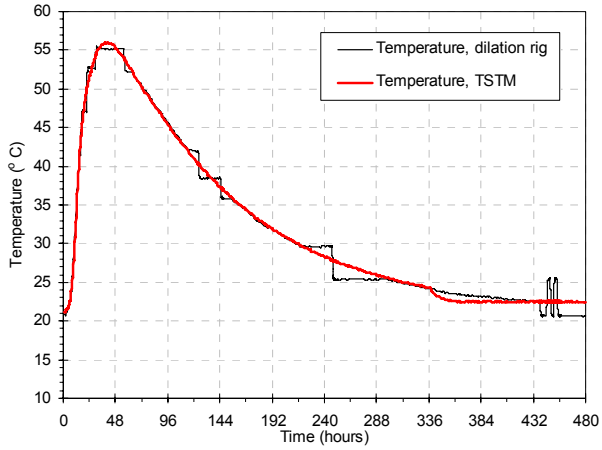

a) Temperature in dilation rig and TSTM

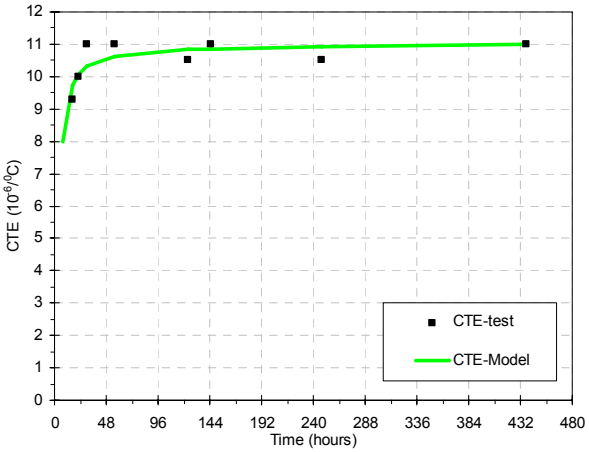

b) Calculated CTE and model

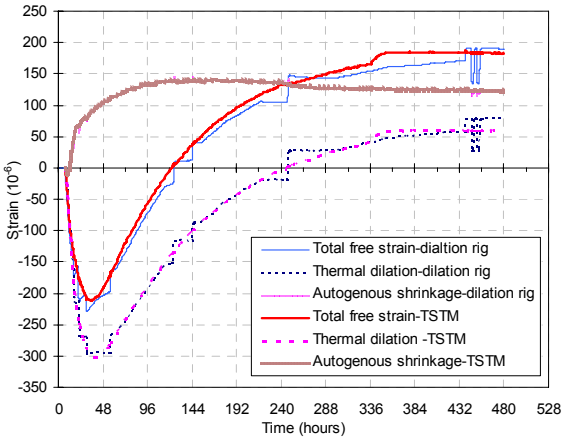

c) Separation of TD and AD

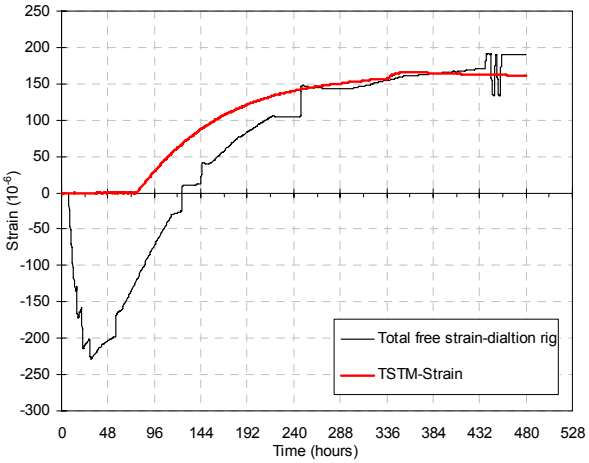

d) Measured strain in dilation rig and TSTM

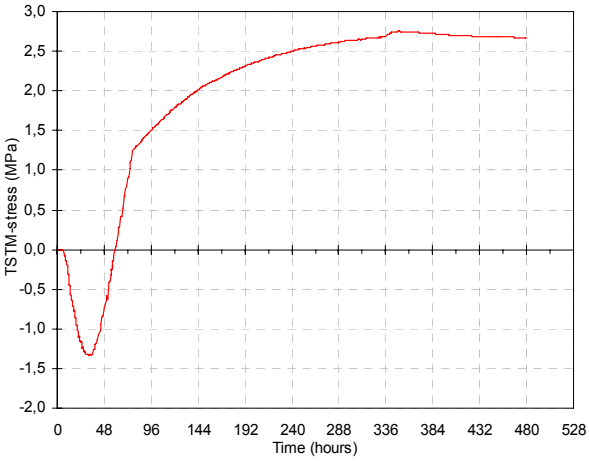

e) Restraint stress in TSTM

Figure C.6 Volume change and restraint stress (SV 40*)

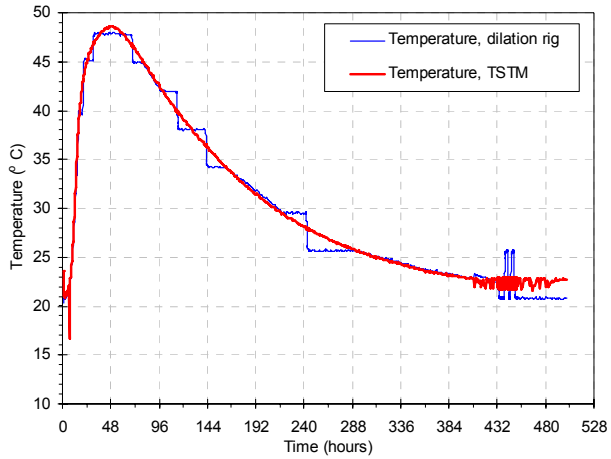

a) Temperature in dilation rig and TSTM

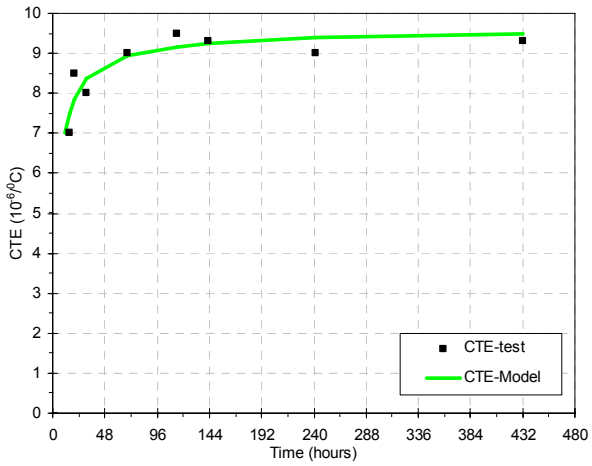

b) Calculated CTE and model

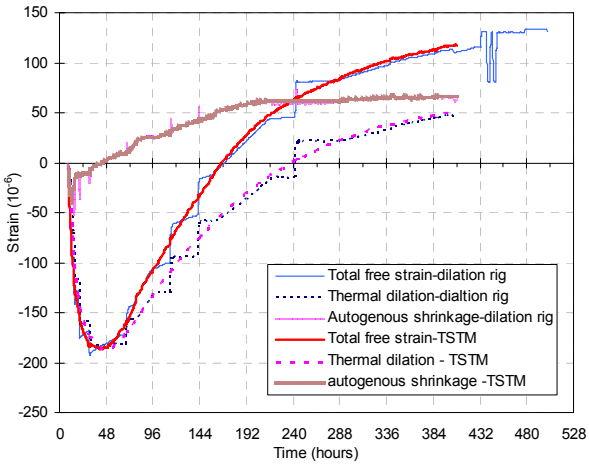

c) Separation of TD and AD

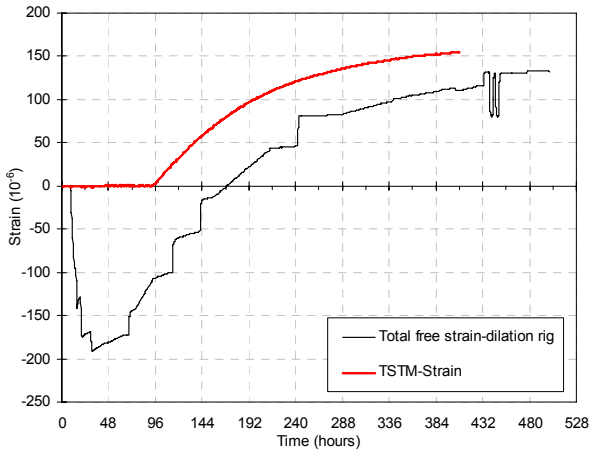

d) Measured strain in dilation rig and TSTM

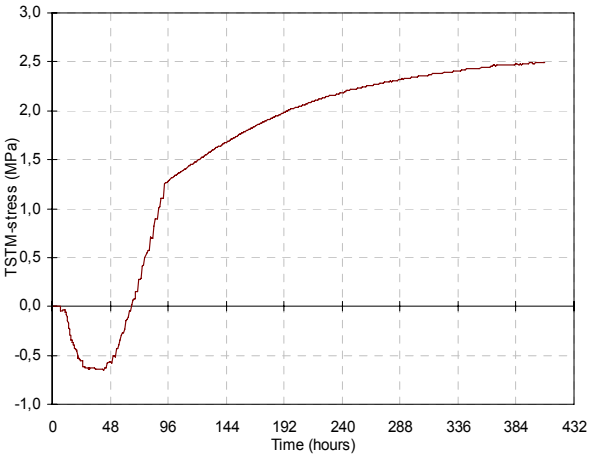

e) Restraint stress in TSTM

Figure C.7 Volume change and restraint stress (40% FA*)

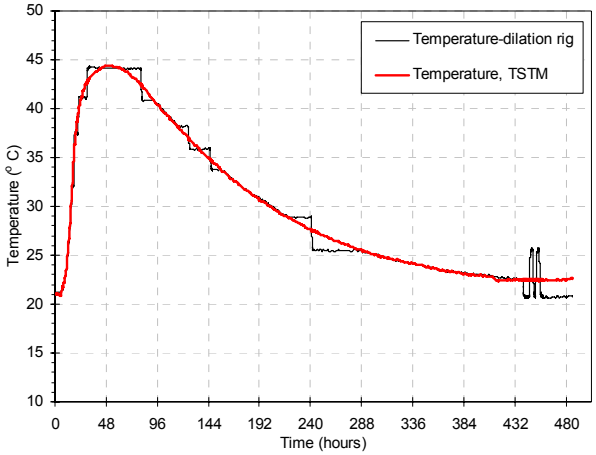

a) Temperature in dilation rig and TSTM

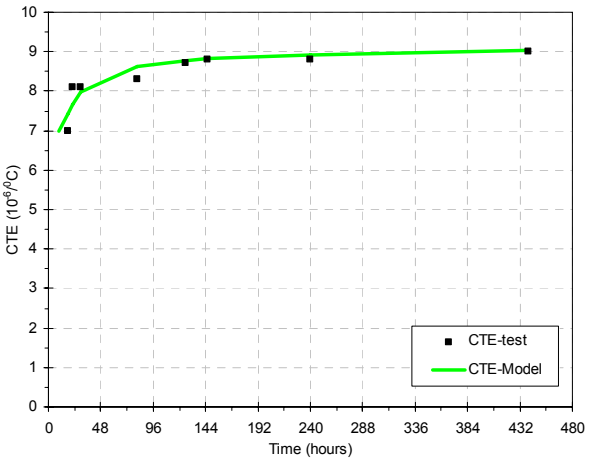

b) Calculated CTE and model

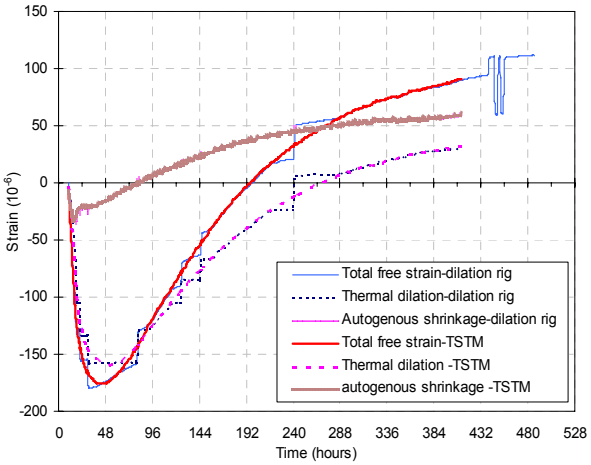

c) Separation of TD and AD

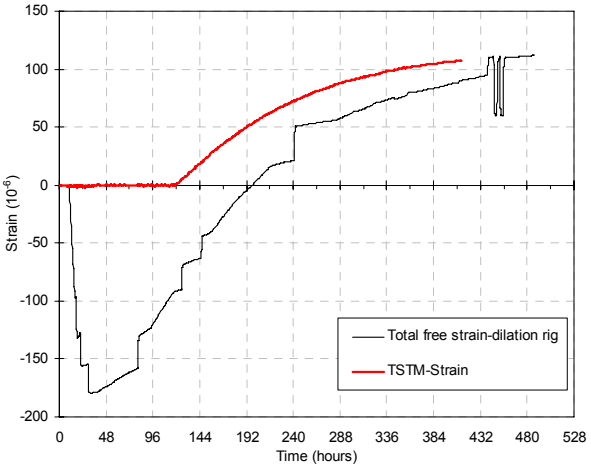

d) Measured strain in dilation rig and TSTM

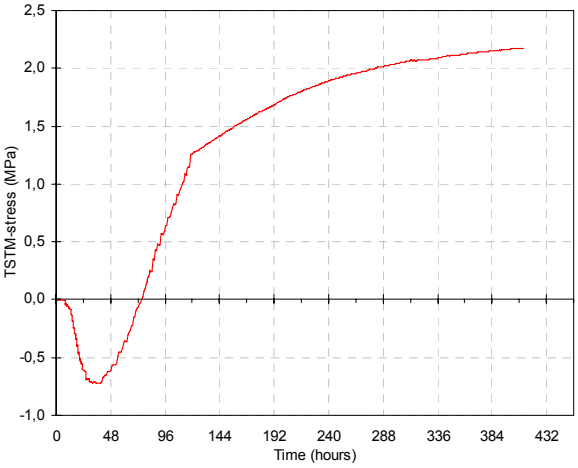

e) Restraint stress in TSTM

Figure C.8 Volume change and restraint stress (60% FA*)

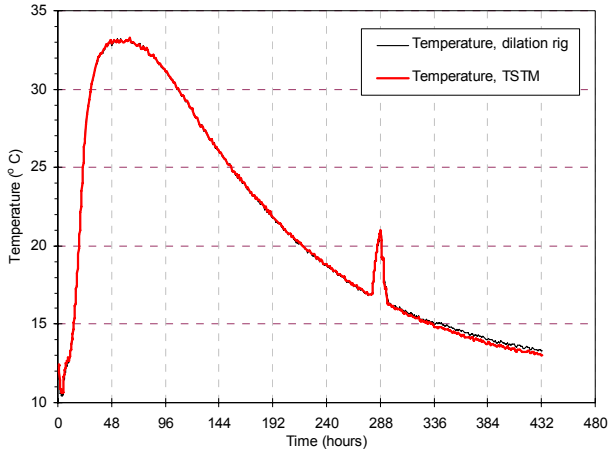

a) Temperature in dilation rig and TSTM

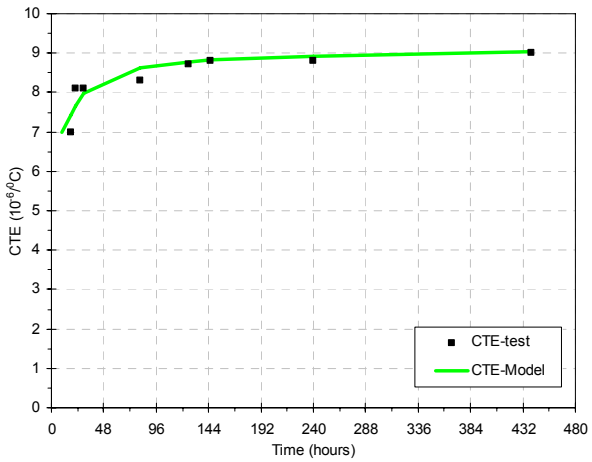

b) Calculated CTE and model

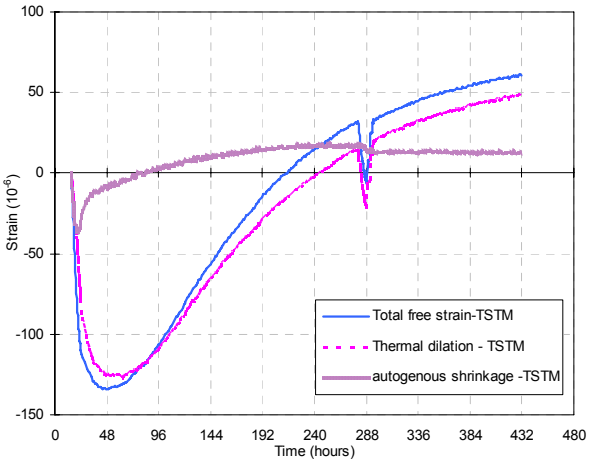

c) Separation of TD and AD

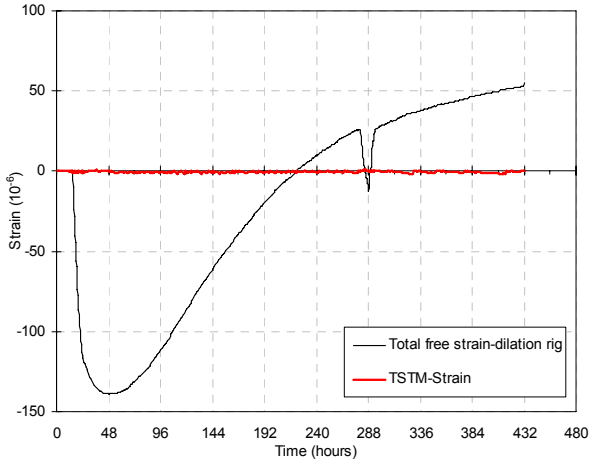

d) Measured strain in dilation rig and TSTM

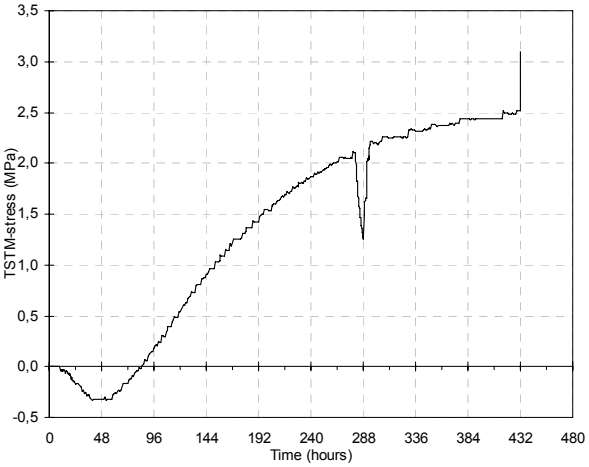

e) Restraint stress in TSTM

Figure C.9 Volume change and restraint stress (60% FA*-initial temperature 11ºC)

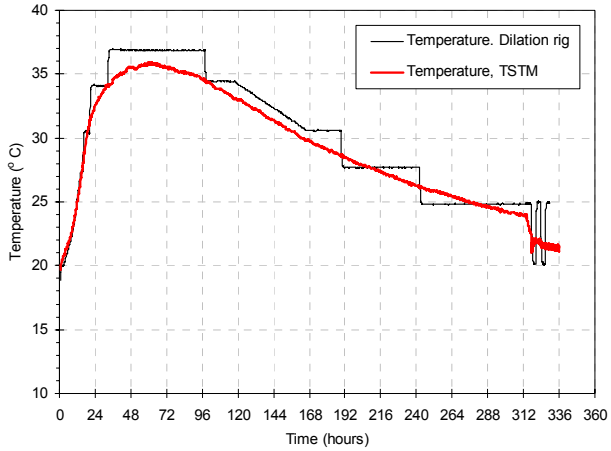

a) Temperature in dilation rig and TSTM

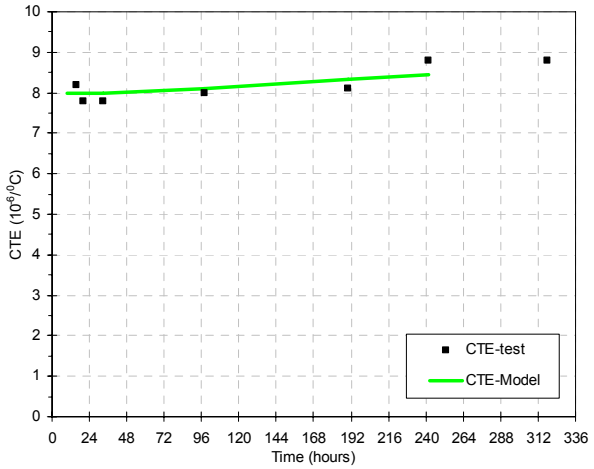

b) Calculated CTE and model

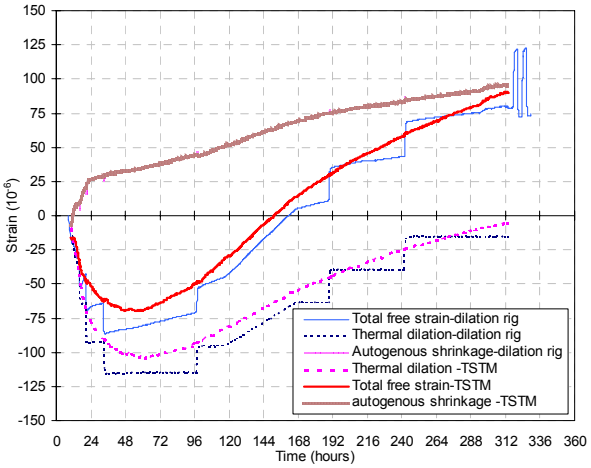

c) Separation of TD and AD

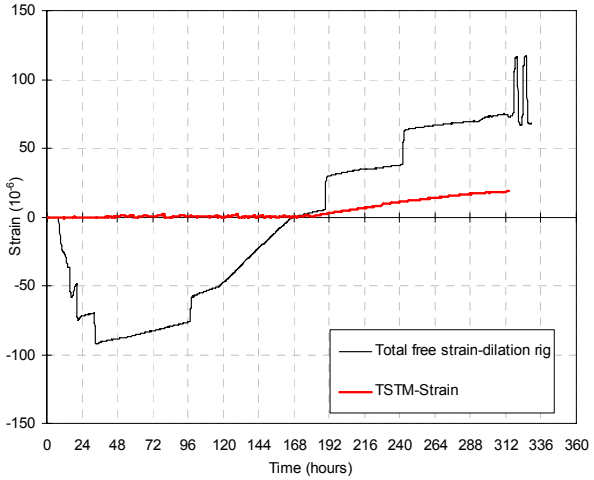

d) Measured strain in dilation rig and TSTM

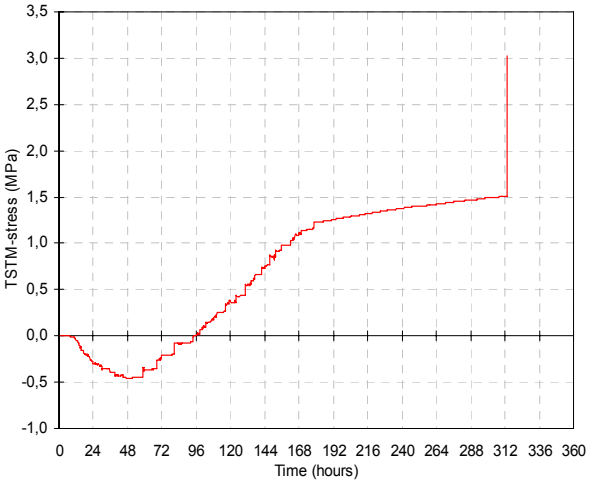

e) Restraint stress in TSTM

Figure C.10 Volume change and restraint stress (100% FA)

DEPARTMENT OF STRUCTURAL ENGINEERING
NORWEGIAN UNIVERSITY OF SCIENCE AND TECHNOLOGY
N–7491 TRONDHEIM, NORWAY
Telephone: +47 73 59 47 00 Telefax: +47 73 59 47 01

"Reliability Analysis of Structural Systems using Nonlinear Finite Element Methods",
C. A. Holm, 1990:23, ISBN 82-7119-178-0.

"Uniform Stratified Flow Interaction with a Submerged Horizontal Cylinder",
Ø. Arntsen, 1990:32, ISBN 82-7119-188-8.

"Large Displacement Analysis of Flexible and Rigid Systems Considering Displacement-Dependent Loads and Nonlinear Constraints", K. M. Mathisen, 1990:33, ISBN 82-7119-189-6.

"Solid Mechanics and Material Models including Large Deformations",
E. Levold, 1990:56, ISBN 82-7119-214-0, ISSN 0802-3271.

"Inelastic Deformation Capacity of Flexurally-Loaded Aluminium Alloy Structures",
T. Welo, 1990:62, ISBN 82-7119-220-5, ISSN 0802-3271.

"Visualization of Results from Mechanical Engineering Analysis",
K. Aamnes, 1990:63, ISBN 82-7119-221-3, ISSN 0802-3271.

"Object-Oriented Product Modeling for Structural Design",
S. I. Dale, 1991:6, ISBN 82-7119-258-2, ISSN 0802-3271.

"Parallel Techniques for Solving Finite Element Problems on Transputer Networks",
T. H. Hansen, 1991:19, ISBN 82-7119-273-6, ISSN 0802-3271.

"Statistical Description and Estimation of Ocean Drift Ice Environments",
R. Korsnes, 1991:24, ISBN 82-7119-278-7, ISSN 0802-3271.

“Properties of concrete related to fatigue damage: with emphasis on high strength concrete”,
G. Petkovic, 1991:35, ISBN 82-7119-290-6, ISSN 0802-3271.

"Turbidity Current Modelling",
B. Brørs, 1991:38, ISBN 82-7119-293-0, ISSN 0802-3271.

"Zero-Slump Concrete: Rheology, Degree of Compaction and Strength. Effects of Fillers as Part Cement-Replacement",
C. Sørensen, 1992:8, ISBN 82-7119-357-0, ISSN 0802-3271.

"Nonlinear Analysis of Reinforced Concrete Structures Exposed to Transient Loading",
K. V. Høiseth, 1992:15, ISBN 82-7119-364-3, ISSN 0802-3271.

"Finite Element Formulations and Solution Algorithms for Buckling and Collapse Analysis of Thin Shells", R. O. Bjærum, 1992:30, ISBN 82-7119-380-5, ISSN 0802-3271.

"Response Statistics of Nonlinear Dynamic Systems",
J. M. Johnsen, 1992:42, ISBN 82-7119-393-7, ISSN 0802-3271.

"Digital Models in Engineering. A Study on why and how engineers build and operate digital models for decisison support", J. Høyte, 1992:75, ISBN 82-7119-429-1, ISSN 0802-3271.

"Sparse Solution of Finite Element Equations",
A. C. Damhaug, 1992:76, ISBN 82-7119-430-5, ISSN 0802-3271.

"Some Aspects of Floating Ice Related to Sea Surface Operations in the Barents Sea",
S. Løset, 1992:95, ISBN 82-7119-452-6, ISSN 0802-3271.

"Modelling of Cyclic Plasticity with Application to Steel and Aluminium Structures",
O. S. Hopperstad, 1993:7, ISBN 82-7119-461-5, ISSN 0802-3271.

"The Free Formulation: Linear Theory and Extensions with Applications to Tetrahedral Elements with Rotational Freedoms", G. Skeie, 1993:17, ISBN 82-7119-472-0, ISSN 0802-3271.

"Høyfast betongs motstand mot piggdekkslitasje. Analyse av resultater fra prøving i Veisliter'n",
T. Tveter, 1993:62, ISBN 82-7119-522-0, ISSN 0802-3271.

"A Nonlinear Finite Element Based on Free Formulation Theory for Analysis of Sandwich Structures", O. Aamlid, 1993:72, ISBN 82-7119-534-4, ISSN 0802-3271.

"The Effect of Curing Temperature and Silica Fume on Chloride Migration and Pore Structure of High Strength Concrete", C. J. Hauck, 1993:90, ISBN 82-7119-553-0, ISSN 0802-3271.

"Failure of Concrete under Compressive Strain Gradients",
G. Markeset, 1993:110, ISBN 82-7119-575-1, ISSN 0802-3271.

"An experimental study of internal tidal amphidromes in Vestfjorden",
J. H. Nilsen, 1994:39, ISBN 82-7119-640-5, ISSN 0802-3271.

"Structural analysis of oil wells with emphasis on conductor design",
H. Larsen, 1994:46, ISBN 82-7119-648-0, ISSN 0802-3271.

"Adaptive methods for non-linear finite element analysis of shell structures",
K. M. Okstad, 1994:66, ISBN 82-7119-670-7, ISSN 0802-3271.

"On constitutive modelling in nonlinear analysis of concrete structures",
O. Fyrileiv, 1994:115, ISBN 82-7119-725-8, ISSN 0802-3271.

"Fluctuating wind load and response of a line-like engineering structure with emphasis on motion-induced wind forces",
J. Bogunovic Jakobsen, 1995:62, ISBN 82-7119-809-2, ISSN 0802-3271.

"An experimental study of beam-columns subjected to combined torsion, bending and axial actions", A. Aalberg, 1995:66, ISBN 82-7119-813-0, ISSN 0802-3271.

"Scaling and cracking in unsealed freeze/thaw testing of Portland cement and silica fume concretes", S. Jacobsen, 1995:101, ISBN 82-7119-851-3, ISSN 0802-3271.

"Damping of water waves by submerged vegetation. A case study of laminaria hyperborea", A. M. Dubi, 1995:108, ISBN 82-7119-859-9, ISSN 0802-3271.

"The dynamics of a slope current in the Barents Sea", Sheng Li, 1995:109, ISBN 82-7119-860-2, ISSN 0802-3271.

"Modellering av delmaterialenes betydning for betongens konsistens", Ernst Mørtsell, 1996:12, ISBN 82-7119-894-7, ISSN 0802-3271.

"Bending of thin-walled aluminium extrusions", Birgit Søvik Opheim, 1996:60, ISBN 82-7119-947-1, ISSN 0802-3271.

"Material modelling of aluminium for crashworthiness analysis", Torodd Berstad, 1996:89, ISBN 82-7119-980-3, ISSN 0802-3271.

"Estimation of structural parameters from response measurements on submerged floating tunnels", Rolf Magne Larssen, 1996:119, ISBN 82-471-0014-2, ISSN 0802-3271.

“Numerical modelling of plain and reinforced concrete by damage mechanics”, Mario A. Polanco-Loria, 1997:20, ISBN 82-471-0049-5, ISSN 0802-3271.

“Nonlinear random vibrations - numerical analysis by path integration methods”, Vibeke Moe, 1997:26, ISBN 82-471-0056-8, ISSN 0802-3271.

“Numerical prediction of vortex-induced vibration by the finite element method”, Joar Martin Dalheim, 1997:63, ISBN 82-471-0096-7, ISSN 0802-3271.

“Time domain calculations of buffeting response for wind sensitive structures”, Ketil Aas-Jakobsen, 1997:148, ISBN 82-471-0189-0, ISSN 0802-3271.

"A numerical study of flow about fixed and flexibly mounted circular cylinders", Trond Stokka Meling, 1998:48, ISBN 82-471-0244-7, ISSN 0802-3271.

“Estimation of chloride penetration into concrete bridges in coastal areas”, Per Egil Steen, 1998:89, ISBN 82-471-0290-0, ISSN 0802-3271.

“Stress-resultant material models for reinforced concrete plates and shells”, Jan Arve Øverli, 1998:95, ISBN 82-471-0297-8, ISSN 0802-3271.

“Chloride binding in concrete. Effect of surrounding environment and concrete composition”, Claus Kenneth Larsen, 1998:101, ISBN 82-471-0337-0, ISSN 0802-3271.

“Rotational capacity of aluminium alloy beams”,
Lars A. Moen, 1999:1, ISBN 82-471-0365-6, ISSN 0802-3271.

“Stretch Bending of Aluminium Extrusions”,
Arild H. Clausen, 1999:29, ISBN 82-471-0396-6, ISSN 0802-3271.

“Aluminium and Steel Beams under Concentrated Loading”,
Tore Tryland, 1999:30, ISBN 82-471-0397-4, ISSN 0802-3271.

"Engineering Models of Elastoplasticity and Fracture for Aluminium Alloys",
Odd-Geir Lademo, 1999:39, ISBN 82-471-0406-7, ISSN 0802-3271.

"Kapasitet og duktilitet av dybelforbindelser i trekonstruksjoner",
Jan Siem, 1999:46, ISBN 82-471-0414-8, ISSN 0802-3271.

“Etablering av distribuert ingeniørarbeid; Teknologiske og organisatoriske erfaringer fra en norsk ingeniørbedrift”, Lars Line, 1999:52, ISBN 82-471-0420-2, ISSN 0802-3271.

“Estimation of Earthquake-Induced Response”,
Símon Ólafsson, 1999:73, ISBN 82-471-0443-1, ISSN 0802-3271.

“Coastal Concrete Bridges: Moisture State, Chloride Permeability and Aging Effects”
Ragnhild Holen Relling, 1999:74, ISBN 82-471-0445-8, ISSN 0802-3271.

”Capacity Assessment of Titanium Pipes Subjected to Bending and External Pressure”,
Arve Bjørset, 1999:100, ISBN 82-471-0473-3, ISSN 0802-3271.

“Validation of Numerical Collapse Behaviour of Thin-Walled Corrugated Panels”,
Håvar Ilstad, 1999:101, ISBN 82-471-0474-1, ISSN 0802-3271.

“Strength and Ductility of Welded Structures in Aluminium Alloys”,
Miroslaw Matusiak, 1999:113, ISBN 82-471-0487-3, ISSN 0802-3271.

“Thermal Dilation and Autogenous Deformation as Driving Forces to Self-Induced Stresses in High Performance Concrete”,
Øyvind Bjøntegaard, 1999:121, ISBN 82-7984-002-8, ISSN 0802-3271.

“Some Aspects of Ski Base Sliding Friction and Ski Base Structure”,
Dag Anders Moldestad, 1999:137, ISBN 82-7984-019-2, ISSN 0802-3271.

"Electrode reactions and corrosion resistance for steel in mortar and concrete",
Roy Antonsen, 2000:10, ISBN 82-7984-030-3, ISSN 0802-3271.

"Hydro-Physical Conditions in Kelp Forests and the Effect on Wave Damping and Dune Erosion. A case study on Laminaria Hyperborea",
Stig Magnar Løvås, 2000:28, ISBN 82-7984-050-8, ISSN 0802-3271.

"Random Vibration and the Path Integral Method",
Christian Skaug, 2000:39, ISBN 82-7984-061-3, ISSN 0802-3271.

"Buckling and geometrical nonlinear beam-type analyses of timber structures",
Trond Even Eggen, 2000:56, ISBN 82-7984-081-8, ISSN 0802-3271.

”Structural Crashworthiness of Aluminium Foam-Based Components”,
Arve Grønsund Hanssen, 2000:76, ISBN 82-7984-102-4, ISSN 0809-103X.

“Measurements and simulations of the consolidation in first-year sea ice ridges, and some aspects of mechanical behaviour”, Knut V. Høyland, 2000:94, ISBN 82-7984-121-0, ISSN 0809-103X.

”Kinematics in Regular and Irregular Waves based on a Lagrangian Formulation”,
Svein Helge Gjøsund, 2000-86, ISBN 82-7984-112-1, ISSN 0809-103X.

”Self-Induced Cracking Problems in Hardening Concrete Structures”,
Daniela Bosnjak, 2000-121, ISBN 82-7984-151-2, ISSN 0809-103X.

"Ballistic Penetration and Perforation of Steel Plates",
Tore Børvik, 2000:124, ISBN 82-7984-154-7, ISSN 0809-103X.

"Freeze-Thaw resistance of Concrete. Effect of: Curing Conditions, Moisture Exchange and Materials", Terje Finnerup Rønning, 2001:14, ISBN 82-7984-165-2, ISSN 0809-103X

Structural behaviour of post tensioned concrete structures. Flat slab. Slabs on ground",
Steinar Trygstad, 2001:52, ISBN 82-471-5314-9, ISSN 0809-103X.

"Slipforming of Vertical Concrete Structures. Friction between concrete and slipform panel",
Kjell Tore Fosså, 2001:61, ISBN 82-471-5325-4, ISSN 0809-103X.

"Some numerical methods for the simulation of laminar and turbulent incompressible flows",
Jens Holmen, 2002:6, ISBN 82-471-5396-3, ISSN 0809-103X.

“Improved Fatigue Performance of Threaded Drillstring Connections by Cold Rolling”,
Steinar Kristoffersen, 2002:11, ISBN: 82-421-5402-1, ISSN 0809-103X.

"Deformations in Concrete Cantilever Bridges: Observations and Theoretical Modelling",
Peter F. Takâcs, 2002:23, ISBN 82-471-5415-3, ISSN 0809-103X.

"Stiffened aluminium plates subjected to impact loading",
Hilde Giæver Hildrum, 2002:69, ISBN 82-471-5467-6, ISSN 0809-103X.

"Full- and model scale study of wind effects on a medium-rise building in a built up area",
Jónas Thór Snæbjørnsson, 2002:95, ISBN82-471-5495-1, ISSN 0809-103X.

“Evaluation of Concepts for Loading of Hydrocarbons in Ice-infested water”,
Arnor Jensen, 2002:114, ISBN 82-417-5506-0, ISSN 0809-103X.

”Numerical and Physical Modelling of Oil Spreading in Broken Ice”,
Janne K. Økland Gjøsteen, 2002:130, ISBN 82-471-5523-0, ISSN 0809-103X.

”Diagnosis and protection of corroding steel in concrete”,
Franz Pruckner, 20002:140, ISBN 82-471-5555-4, ISSN 0809-103X.

“Tensile and Compressive Creep of Young Concrete: Testing and Modelling”,
Dawood Atrushi, 2003:17, ISBN 82-471-5565-6, ISSN 0809-103X.

“Rheology of Particle Suspensions. Fresh Concrete, Mortar and Cement Paste with Various Types of Lignosulfonates”,
Jon Elvar Wallevik, 2003:18, ISBN 82-471-5566-4, ISSN 0809-103X.

“Oblique Loading of Aluminium Crash Components”, Aase Reyes, 2003:15, ISBN 82-471-5562-1, ISSN 0809-103X.

“Utilization of Ethiopian Natural Pozzolans”, Surafel Ketema Desta, 2003:26,
ISSN 82-471-5574-5, ISSN:0809-103X.

“Behaviour and strength prediction of reinforced concrete structures with discontinuity regions”, Helge Brå, 2004:11, ISBN 82-471-6222-9, ISSN 1503-8181.

“High-strength steel plates subjected to projectile impact. An experimental and numerical study”, Sumita Dey, 2004:38, ISBN 82-471-6281-4 (elektr. Utg.), ISBN 82-471-6282-2 (trykt utg.), ISSN 1503-8181.

“Alkali-reactive and inert fillers in concrete. Rheology of fresh mixtures and expansive reactions.”
Bård M. Pedersen, 2004:92, ISBN 82-471-6401-9 (trykt utg.), ISBN 82-471-6400-0 (elektr. utg.), ISSN 1503-8181.

“On the Shear Capacity of Steel Girders with Large Web Openings”. Nils Christian Hagen, 2005:9 ISBN 82-471-6878-2 (trykt utg.), ISBN 82-471-6877-4 (elektr. utg.), ISSN 1503-8181.

”Behaviour of aluminium extrusions subjected to axial loading”. Østen Jensen, 2005:7, ISBN 82-471-6872-3 (elektr. utg.) , ISBN 82-471-6873-1 (trykt utg.), ISSN 1503-8181.

”Thermal Aspects of corrosion of Steel in Concrete”. Jan-Magnus Østvik, 2005:5, ISBN 82-471-6869-3 (trykt utg.) ISBN 82-471-6868 (elektr.utg), ISSN 1503-8181.

”Mechanical and adaptive behaviour of bone in relation to hip replacement.” A study of bone remodelling and bone grafting. Sébastien Muller, 2005:34, ISBN 82-471-6933-9 (trykt utg.) (ISBN 82-471-6932-0 (elektr.utg), ISSN 1503-8181.

“Analysis of geometrical nonlinearities with applications to timber structures”. Lars Wollebæk, 2005:74, ISBN 82-471-7050-5 (trykt utg.), ISBN 82-471-7019-1 (elektr. Utg.), ISSN 1503-8181.

“Pedestrian induced lateral vibrations of slender footbridges”, Anders Rönnquist, 2005:102, ISBN 82-471-7082-5 (trykt utg.), ISBN 82-471-7081-7 (elektr.utg.), ISSN 1503-8181.

“Initial Strength Development of Fly Ash and Limestone Blended Cements at Various Temperatures Predicted by Ultrasonic Pulse Velocity”, Tom Ivar Fredvik, 2005:112, ISBN 82-471-7105-8 (trykt utg.), ISBN 82-471-7103-1 (elektr.utg.), ISSN 1503-8181.

“Behaviour and modelling of thin-walled cast components”, Cato Dørum, 2005:128, ISBN 82-471-7140-6 (trykt utg.), ISBN 82-471-7139-2 (elektr. utg.), ISSN 1503-8181.

“Behaviour and modelling of selfpiercing riveted connections”, Raffaele Porcaro, 2005:165, ISBN 82-471-7219-4 (trykt utg.), ISBN 82-471-7218-6 (elektr.utg.), ISSN 1503-8181.

”Behaviour and Modelling og Aluminium Plates subjected to Compressive Load”, Lars Rønning, 2005:154, ISBN 82-471-7169-1 (trykt utg.), ISBN 82-471-7195-3 (elektr.utg.), ISSN 1503-8181

”Bumper beam-longitudinal system subjected to offset impact loading”, Satyanarayana Kokkula, 2005:193, ISBN 82-471-7280-1 (trykt utg.), ISBN 82-471-7279-8 (elektr.utg.), ISSN 1503-8181.

“Control of Chloride Penetration into Concrete Structures at Early Age”, Guofei Liu, 2006:46, ISBN 82-471-7838-9 (trykt utg.), ISBN 82-471-7837-0 (elektr. utgave), ISSN 1503-8181.

“Modelling of Welded Thin-Walled Aluminium Structures”, Ting Wang, 2006:78, ISBN 82-471-7907-5 (trykt utg.), ISBN 82-471-7906-7 (elektr.utg.), ISSN 1503-8181.

”Time-variant reliability of dynamic systems by importance sampling and probabilistic analysis of ice loads”, Anna Ivanova Olsen, 2006:139, ISBN 82-471-8041-3 (trykt utg.), ISBN 82-471-8040-5 (elektr.utg.), ISSN 1503-8181.

“Fatigue life prediction of an aluminium alloy automotive component using finite element analysis of surface topography”. Sigmund Kyrre Ås, 2006:25, ISBN 82-471-7791-9 (trykt utg.), ISBN 82-471-7791-9 (elektr.utg.), ISSN 1503-8181.

”Constitutive models of elastoplasticity and fracture for aluminium alloys under strain path change”, Dasharatha Achani, 2006:76, ISBN 82-471-7903-2 (trykt utg.), ISBN 82-471-7902-4 (elektr.utg.), ISSN 1503-8181.

“Simulations of 2D dynamic brittle fracture by the Element-free Galerkin method and linear fracture mechanics”, Tommy Karlsson, 2006:125, ISBN 82-471-8011-1 (trykt utg.), ISBN 82-471-8010-3 (elektr.utg.), ISSN 1503-8181.

“Penetration and Perforation of Granite Targets by Hard Projectiles”, Chong Chiang Seah, 2006:188, ISBN 82-471-8150-9 (printed ver.), ISBN 82-471-8149-5 (electronic ver.) ISSN 1503-8181.

“Deformations, strain capacity and cracking of concrete in plastic and early hardening phases”, Tor Arne Hammer, 2007:234, ISBN 978-82-471-5191-4 (trykt utg.), ISBN 978-82-471-5207-2 (elektr.utg.) ISSN 1503-8181.

“Crashworthiness of dual-phase high-strength steel: Material and Component behaviour”, Venkatapathi Tarigopula, 2007:230, ISBN 82-471-5076-4 (trykt utg.) ISBN 82-471-5093-1 (elektr.utg.) ISSN 1503-8181.

“Fibre reinforcement in load carrying concrete structures”, Åse Lyslo Døssland, 2008:50, ISBN 978-82-471-6910-0 (trykt utg.), ISBN 978-82-471-6924-7 (elektr.utg.), ISSN 1503-8181.

“Low-velocity penetration of aluminium plates”, Frode Grytten, 2008:46, ISBN 978-82-471-6826-4 (trykt utg.) ISBN 978-82-471-6843-1 (elektr. Utg.) ISSN 1503-8181.

“Robustness studies of structures subjected to large deformations”, Ørjan Fylling, 2008:24, ISBN 978-82-471-6339-9 (trykt utg.) ISBN 978-82-471-6342-9 (elektro.utg.) ISSN 1503-8181.

“Constitutive modelling of morsellised bone”,Knut Birger Lund, 2008:92, ISBN 978-82-471-7829-4 (trykt utg.) ISBN 978-82-471-7832-4 (elektro.utg.) ISSN 1503-8181.

“Experimental Investigations of Wind Loading on a Suspension Bridge Girder”, Bjørn Isaksen, 2008:131, ISBN 978-82-471-8656-5 (trykt utg.) ISBN 978-82-471-8673-2 (elektro.utg.) ISSN 1503-8181.